# New Oligopyridine Ligands for Transition Metal Complexes and Their Applications

## Inauguraldissertation

zur
Erlangung der Würde eines Doktors der Philosophie
Vorgelegt der
Philosophisch-Naturwissenschaftlichen Fakultät
der Universität Basel

von
Peter Kopecky

Genehmigt von der Philosophisch-Naturwissenschaftlichen Fakultät der Universität Basel auf Antrag der Herren Professoren

Prof. Dr. E. C. Constable

PD Dr. D. Häussinger

Basel, den 22.05.2012

Prof. Dr. M. Spiess

Dekan

creative commons

**Namensnennung-Keine kommerzielle Nutzung-Keine Bearbeitung 2.5 Schweiz**

---

## Sie dürfen:

das Werk vervielfältigen, verbreiten und öffentlich zugänglich machen

## Zu den folgenden Bedingungen:

**Namensnennung**. Sie müssen den Namen des Autors/Rechteinhabers in der von ihm festgelegten Weise nennen (wodurch aber nicht der Eindruck entstehen darf, Sie oder die Nutzung des Werkes durch Sie würden entlohnt).

**Keine kommerzielle Nutzung**. Dieses Werk darf nicht für kommerzielle Zwecke verwendet werden.

**Keine Bearbeitung**. Dieses Werk darf nicht bearbeitet oder in anderer Weise verändert werden.

- Im Falle einer Verbreitung müssen Sie anderen die Lizenzbedingungen, unter welche dieses Werk fällt, mitteilen. Am Einfachsten ist es, einen Link auf diese Seite einzubinden.
- Jede der vorgenannten Bedingungen kann aufgehoben werden, sofern Sie die Einwilligung des Rechteinhabers dazu erhalten.
- Diese Lizenz lässt die Urheberpersönlichkeitsrechte unberührt.



Quelle: http://creativecommons.org/licenses/by-nc-nd/2.5/ch/ Datum: 3.4.2009

## *Acknowledgements*

First of all, I thank my supervisors Prof. Dr. Edwin C. Constable and Prof. Dr. Catherine E. Housecroft for welcoming me in their group and entrusting me with this inspiring PhD project. During the last three and a half years, they did a great job helping, advising and supporting me. Since the very beginning, they encouraged me and transmitted their passion for chemistry. All the way, while also giving me a lot of freedom in my work.

I thank PD Dr. Daniel Häussinger for being my co-referee and co-examiner. Of course I have to thank him for recording countless NMR spectra on his 600 MHz NMR machine, his excellent expertise and for the many discussions that we had.

I would also like to thank all the supporting staff of the Department of Chemistry, particularly Dr. Nadig for recording EI- and FAB-MS spectra and for his kind advice and Marcus Hauri for the supply of materials essential for survival. Jason Price, Pirmin Rösel, Ralph Schmitt, Gabriel Schneider and Sven Brauchli are thanked for recording the endless ESI-MS spectra. I'd like to thank Jaroslav Padevet for his help and advice with the 500 MHz NMR machine. Biljana Bozic-Weber and Liselotte Siegfried are thanked for the preparation and measurements of the solar cells.

Big thanks go to the current and former members of the Constable/Housecroft group for providing such a diverse working environment: Beatrice Erismann for managing all administrative issues and treating me with kind coffee breaks. Ana Hernandez Redondo for starting the Dye Sensitized Solar Cells project and Stephan Graber the Light Emitting Electrochchemical Cells project, I am also grateful for his help in the beginning of my thesis. Raphael Wyss is thanked for his efforts in exploring the imine condensation on a $[Ru(bpy)_3]^{2+}$ complex. Great thanks to Markus Neuburger and Jennifer Zampese for always measuring and resolving my crystal structures despite the "ugly" crystals. I'd like to thank Iain Wright who eventually managed to teach me electrochemistry even though he hates me. I have to thank Guoqi Zhang who was able to use my "accidental" ligand and prepare some coordination polymers which resulted in a nice publication. I am grateful to have found many friends who accepted me for who I am although I seem to look angry all the time and I am not Swiss…I hope that these friendships will continue. Emma Dunphy I have to thank for the time we spent as office neighbours and the time she took to help me with photophysics. This eventually resulted in a friendship accompanied by many activities outside the lab.

I'd like to thank Dr. Henk Bolink and his coworkers for preparing the LEC devices.

I thank Aicha, Niamh Murray and Iain for proof reading, and a special thanks to Prof. C. Housecroft who contributed a great deal to make this manuscript worth reading.

My special thanks go to my parents for encouraging and supporting me through all my studies. Moc vám děkuji!

Finally, I'd like to thank Aicha for always being there for me, despite me often being unfriendly, for her big help finishing my thesis and for always leading me back on the right track!

# *Abstract*

This thesis concerns the synthesis of polypyiridine ligands, their use for preparation of transition metal complexes and finally, the application of the transition metal complexes for Dye Sensitized Solar Cells (DSCs) and Light Emitting Electrochemical Cells (LECs).

***Chapter 1*** gives a short introduction of the ligands, the metal complexes which were involved in this work, as well as, their applications.

***Chapter2*** defines the objectives of this work.

***Chapter 3*** describes the synthetic approaches to new polypyridine ligands with either the classical KRÖHNKE method or with less used and for some substituents not reported methods. These include direct coupling of lithium organyls or the Jahng reaction, followed by the discussion of their characterization and properties.

***Chapter 4*** describes the synthesis of homoleptic copper(I) complexes and their characterization. Difficulties with NMR experiments and the reason thereof are discussed in detail along with electrochemical experiments. Their use in the preparation of DSCs is given at the end of this chapter.

***Chapter 5*** regards the synthesis and characterization of novel iridium(III) complexes, as well as, the results for some LECs devices.

***Chapter 6*** shows the results obtained with novel ruthenium(II) complexes based on new bpy or tpy ligands, respectively.

Parts of this work have been published:

B. Bozic-Weber, E. C. Constable, C. E. Housecroft, P. Kopecky M. Neuburger, J. A. Zampese, *Dalton Trans.* **2011**, *40(46)*, 12584.

E. C. Constable, C. E. Housecroft, P. Kopecky, M. Neuburger, J. A. Zampese, G. Zhang, *CrystEngComm* **2012**, *14(2)*, 446.

E. C. Constable, C. E. Housecroft, N. Hostettler, P. Kopecky, M. Neuburger, J. A. Zampese, *Dalton Trans*. **2012**, *41*, 2890.

## *List of abbreviations*

| | |
|---|---|
| Å | Ångström |
| Ac | acetyl |
| AcPy | 2-acetyl-pyridine |
| Ar | aryl |
| AM | air mass |
| BBFO+ | broad band fluorine observation probe |
| $[BMIM]^+$ | 1-butyl-3-methylimidazolium |
| Bpy | 2,2'-bipyridine |
| btphen | (2,9-di-p-tolyl-1,10-phenanthroline) |
| btphen | (2,9-bis(3,5-di-tert-butyl-4-methoxyphenyl)-1,10-phenanthroline) |
| *n*-Bu | *n*-butyl |
| *t*-Bu | *tert*-butyl |
| °C | degree Celsius |
| calc. | calculated |
| cd | candela |
| cm | centimetre |
| COSY | correlation spectroscopy |
| Cp | cyclopentadienyl |
| CV | cyclic voltammetry (cyclic voltammograms) |
| $\delta$ | chemical shift [ppm] |
| $\Delta/\Lambda$ | descriptors of the configuration for chiral complexes |
| 2-D | two dimensional |
| D | deuterium (number of deuterium atoms in a solvent: solvent-$d_n$) |
| dm | decimetre |
| DMF-DMA | *N*,*N*-dimethylformamide dimethylacetal |
| dmdaabpy | 6,6'-dimethyl-4,4'-diacrylic acid-2,2'-bipyridine |
| dmdbybpy | 6,6'-dimethyl-4,4'-dibenzoic acid-2,2'-bipyridine |
| dmdcabpy | 6,6'-dimethyl-4,4'-dicarboxylic acid-2,2'-bipyridine |
| dmdpabpy | 6,6'-dimethyl-4,4'-diphosphonic acid-2,2'-bipyridine |
| dmphen | (2,9-dimethyl-1,10-phenanthroline) |
| DMSO | dimethyl sulfoxide |
| dpa | di-2-pyridylamine |
| dpdcabpy | 6,6'-diphenyl-4,4'-dicarboxylic acid-2,2'-bipyridine |
| dpdbabpy | 6,6'-diphenyl-4,4'-dibenzoic acid-2,2'-bipyridine |
| dppe | bis(diphenylphosphine)ethane |
| dpphen | (2,9-diphenyl-1,10-phenanthroline) |

| | |
|---|---|
| DSC | dye sensitized solar cell |
| dtfmphen | (2,9-ditrifluoromethyl-1,10-phenanthroline) |
| E | standard half-cell potential |
| EA | elemental analysis |
| $\varepsilon_{max}$ | molar absorption coefficient |
| EI | electron impact |
| en | ethylene diamine |
| eq | equivalent |
| EQE | external quantum efficiencies |
| ESI | electron spray ionization |
| Et | ethyl |
| $E_{tot}$ | total emitted energy |
| eV | electron volt |
| EXSY | exchange spectroscopy |
| FAB | fast bombardment |
| FF | fill factor of the cell |
| FTO | fluorine doped tin oxide |
| FTIR | Fourier-transform infrared spectroscopy |
| g | gram |
| G | global |
| h | hour |
| $\eta$ | overall conversion efficiency from solar to electrical energy for a photovoltaic device |
| HMBC | heteronuclear multiple bond correlation |
| HMQC | heteronuclear multiple quantum coherence |
| HOMO | highest occupied molecular orbital |
| Hz | hertz |
| IR | infrared; for the IR spectra with w for weak, s for strong, m for medium |
| iTMC | ionic transition metal complex |
| ITO | indium tin oxide |
| *J* | coupling constant |
| $J_{SC}$ | photocurrent density measured at short-circuit |
| K | Kelvin |
| $\lambda_{em}$ | emission wavelength |
| $\lambda_{ex}$ | excitation wavelength |
| $\lambda_{abs}$ | absorption wavelength |
| LC | ligand centred transition |

| | |
|---|---|
| LEC | light emitting electrochemical cell |
| LED | light emitting diode |
| LUMO | lowest unoccupied molecular orbital |
| m | metre or minute |
| M | $mol*L^{-1}$ |
| MALDI-TOF | matrix assisted laser desorption/ionisation-time of flight |
| MBI | 1-methylbenzimidazole |
| MC | metal centered transition |
| Me | methyl |
| mg | milligram |
| Mg | megagram |
| MHz | megahertz |
| mL | millilitre |
| MLCT | metal-to-ligand charge transfer |
| mm | millimetre |
| mmol | millimol |
| µmol | micromol |
| 3-MPN | 1-butyl-3-methylimidazolium iodide |
| MS | mass spectrometry |
| mV | millivolt |
| *m/z* | mass to charge ratio |
| $\nu$ | frequency in $cm^{-1}$ or Hz |
| N3 | $[Ru(4,4'\text{-}(dicarboxylicacid)\text{-}2,2'\text{-}bipyridine)_2(SCN)_2]$ |
| N719 | $[Ru(4,4'\text{-}(dicarboxylicacid)\text{-}2,2'\text{-}bipyridine)_2(SCN)_2][TBA]_2$ |
| NIR | near infrared |
| nm | nanometre |
| NN | NN-ligand |
| ns | nanosecond |
| NMR | nuclear magnetic resonance, with the signals being identifed as s for singlet, d for doublet, t for triplet, q for quartet, br for broad signal |
| NOESY | nuclear Overhauser enhancement spectroscopy |
| OLED | organic light emitting devices |
| $P_{IN}$ | intensity of the incident light |
| pbpy | 6'-phenyl-2,2'-bipyridine |
| PEDOT | poly(3,4-ethylenedioxythiophene) |
| Ph | phenyl |
| PLC | preparative layer chromatography |

| | |
|---|---|
| PLQE | photo luminescence quantum efficiency |
| PMMA | Poly(methyl-2-methylpropenoat)/Polymethylmethacrylat |
| POP | bis[2-(diphenylphosphino)phenyl]ether |
| PP | bisphosphine ligand |
| PPI | 1-(2-oxo-2-(pyridin-2-yl)ethyl)pyridin-1-ium;<br>pyridinium salt of 2-acetylpyridine |
| ppm | parts per million |
| ppy | 2-phenyl-pyridine |
| PSS | poly(styrene sulfonic acid) |
| py | pyridine |
| rt | room temperature |
| c-Si | crystalline silicon |
| a-Si | amorphous Si |
| $t_{1/2}$ | time to reach half of the maximum brightness (lifetime) |
| TBA | *tert*-butylammonium |
| $TBAPF_6$ | *tert*-butylammonium hexafluoridophosphate |
| TDP | *N,N*'-di-m-tolyl-*N,N*'-diphenylbenzidine, often called tetraphenyldiamine |
| TEMPO | (2,2,6,6-tetramethyl-piperidin-1-yl)oxyl |
| TFA | trifluoroacetic acid |
| THF | tetrahydrofuran |
| thmpy | 2-methyl-6-thienyl-pyridine |
| thPhbpy | 6'-thien-2-yl-2,2'-bipyridine |
| TLC | thin layer chromatography |
| iTMC | ionic transition-metal complex |
| TMS | tetra methyl silylane |
| TOCSY | total correlation spectroscops, sometimes it is also referred to as HOHAHA (homonuclear Hartmann Hahn) |
| $t_{on}$ | turn-on time, the time to reach the maximum luminance of the LEC device |
| TPI | 1-(2-oxo-2-(thiophen-2-yl)ethyl)pyridin-1-ium,<br>pyridinium salt of 2-acetylthiophene |
| tpy | 2,2':6',2''-terpyridine |
| TW | tera watt |
| UV | ultraviolet |
| V | volt |
| vis | visible |
| $V_{OC}$ | open-circuit photovoltage |
| vol. | volume |

| | |
|---|---|
| *vs.* | *versus* |
| VT-NMR | variable temperature NMR |
| wt% | weight % |

# *Table of contents*

## *General Experimental Part*

*Infrared* spectra were recorded on a Shimadzu FTIR 8400 S Fourier-transform spectrophotometer with solid samples on a Golden Gate ATR.

*$^{1}H$ and $^{13}C$ NMR* spectra were recorded on Bruker AM 400 or DRX 500 spectrometers, or using a Bruker Avance III 600 MHz with BBFO+ smart probe, 5 mm, z-gradient; chemical shifts are with respect to residual solvent peaks (TMS $\delta$ 0 ppm). $^{77}$Se NMR spectra were recorded on a Bruker Avance III NMR spectrometer operating 600.13 MHz proton frequency; the instrument is equipped with a 5-mm broadband direct observe probe (BBFO+); $^{77}$Se chemical shifts were referenced externally, relative to selenophene in $CD_2Cl_2$ at a shift of $\delta$605 ppm. (All measurements on the 600 MHz NMR machine were carried out by PD Dr. D. Häussinger)

*Crystal structure determination*: Data were collected on a Bruker-Nonius KappaAPEX diffractometer, with data reduction, solution and refinement using the programs APEX2[1], SIR92[2] and CRYSTALS,[3] or on a Stoe IPDS diffractometer with data reduction, solution and refinement using Stoe IPDS software[4] and SHELXL97.[5] ORTEP figures were drawn using Ortep-3 for Windows[6], and structures were analysed with the program Mercury v. 2.3.[7,8]

Solution UV/vis spectroscopic measurements were recorded using an Agilent 8453 spectrophotometer or a Varian Cary 5000 spectrophotometer. Emission spectra were recorded on a Shimadzu 5301PC spectrofluorophotometer.

EI and electrospray (ESI) *mass spectra* were recorded on Finnigan MAT 95, Finnigan MAT LCT or LCQ mass spectrometers. (EI-MS were measured by Dr. P. Nadig; ESI-MS were done by Dr. J. Price, Dr. P. Rösel, R. Schmitt, G. Schneider and S. Brauchli)

*Electrochemical measurements* were carried out using a CHI 900B with glassy carbon working and platinum auxiliary electrodes; a silver wire was used as a pseudo-reference electrode. Solvent HPLC grade acetonitrile and 0.1 M [$^{n}Bu_4N$][$PF_6$] was used as supporting electrolyte. $Cp_2Fe$ was used as external reference before each experiment.

The *microanalyses* were performed with a Leco CHN-900 microanalyser by W. Kirsch.

*Microwave reactions* were carried out in a Biotage Initiator$^{TM}$ 8 reactor. Absolute solvents were used for all reactions (ACROS crown capped bottles). Starting materials were purchased from ACROS Organics, Sigma-Aldrich, Fluorochem or Fisher Scientific and were used without further purification.

# Chapter 1

# 1 Introduction

## 1.1 Polypyridine Ligands in Coordination Chemistry

About 120 years ago there was an important discovery by Fritz BLAU.[9] He was investigating metal salts of picolinic acid and their reactivities. While performing a dry distillation of copper picolinate he obtained the now well known and widely used 2,2'-bipyridine (bpy), one of six possible isomers.

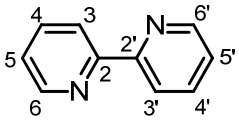


**Figure 1-1** 2,2'-Bipyridine in the preferred trans conformation.

Since then it has been extensively studied and used for various applications. The enormous interest in this compound can be explained by its ability to act as a bidentate chelating ligand which can form complexes with various metals different in size and charge and these exhibit very robust redox stability. Moreover, bpy offers the possibility for further substitution and functionalization leading to a vast number of derivatives which have been used as attractive building blocks for supra- and macromolecular chemistry as well as analytical and photochemistry.[10] Not only their chelating properties have been investigated, but also in medicinal chemistry, e.g. 2,2':6',2''-terpyridine was found to be active against some cancer cells.[11] There are even some natural products which have a bpy core, such as camptothecin or lavendamycin (Figure 1-2), the latter having antibiotic effects and even anti proliferative properties for many cancer cells.[12]

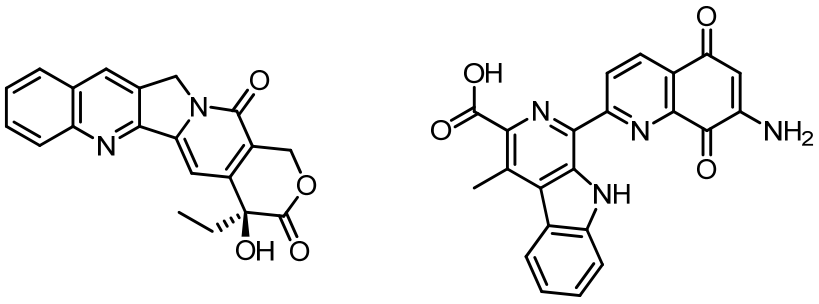


*Camptothecin* *Lavendamycin*

**Figure 1-2** 2,2'-Bipyridine based natural products.

Due to this importance there are uncountable reports for preparation which have been reviewed in 1984 by L. A. SUMMERS[13] and later in 1996 updated by P. J. STEEL.[14] Not to forget are the contributions from our group which resulted in a review in 1989.[15] Probably the most appealing summary can be found in A. P. SMITH and C. L. FRASER's book chapter from Comprehensive Coordination Chemistry.[16] The parent compound bpy and simple

symmetrically substituted derivatives could be synthesized from early on by homo coupling methods, e.g. ULLMANN reaction using a halopyridine in the presence of a metal ($Cu^0$ or $Ni^0$). The preparation of more complex or asymmetrically substituted bpy's was introduced by KRÖHNKE in 1950's by the reaction between pyridinium salts of ketones and unsaturated ketones followed by the treatment with ammonium acetate to form a new pyridine ring with various substituents. Since the development of transition metal catalyzed crosscoupling reactions, such as STILLE, SUZUKI or NEGISHI, etc., which involve the reaction between halopyridines and organometalic pyridines. These methods could be successfully applied for the synthesis of polypyridine ligands containing various functional groups in nearly all imaginable substitution patterns.

It is known, that thiophene has the ability to tune the electronic properties of bpy.[17] Another interesting feature of 6'-thien-2-yl-2,2'-bipyridine (thPhbpy) is that it can furthermore behave as a *N*-, *N*,*N*-, *N*,*N*,*S*- or even *N*,*N*,*C*-donor ligand. This behaviour depends very much on the metal-ions involved. There are few examples with ruthenium where thPhbpy acts as a *N*,*N*,*S*-donor.[18] The complexation of coinage metals, such as Pt, Pd and Au, yield very often cyclometalated species. An interesting dependence found here is the regioselectivity of the cyclometalation, giving monomeric species with Pt and Pd, and a dimer if Au is involved (see Figure 1-3).[19]

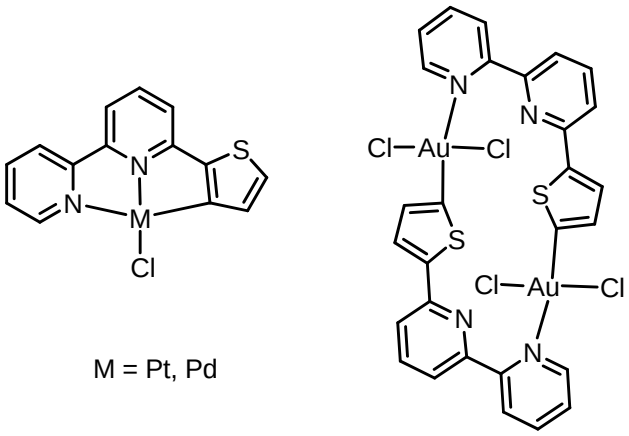


**Figure 1-3** Metal dependent regioselectivity of cyclometalation.

Nevertheless, being the focus for some reactions, the ligand thPhbpy has never been used for the complexation of iridium(III) nor copper(I) complexes to the best of our knowledge. The interest here was to see, whether the introduction of the sulphur in these systems might bring some new and interesting properties in the envisioned metal complexes and for the resulting devices, such as Light Emitting Electrochemical Cells (LECs) or Dye Sensitized Solar Cells (DSCs) based on their corresponding complexes.

For the purpose of this work, only bpy ligands with substituents in 4'- and 6'-position are focused upon. Therefore the synthesis for only these derivatives will be explained.

## 1.2 Synthetic Approaches for 6-R-bipyridines

There are different synthetic routes available in the literature. One of the easiest, cheapest and most versatile approaches is the KRÖHNKE methodology (Scheme 1-1).

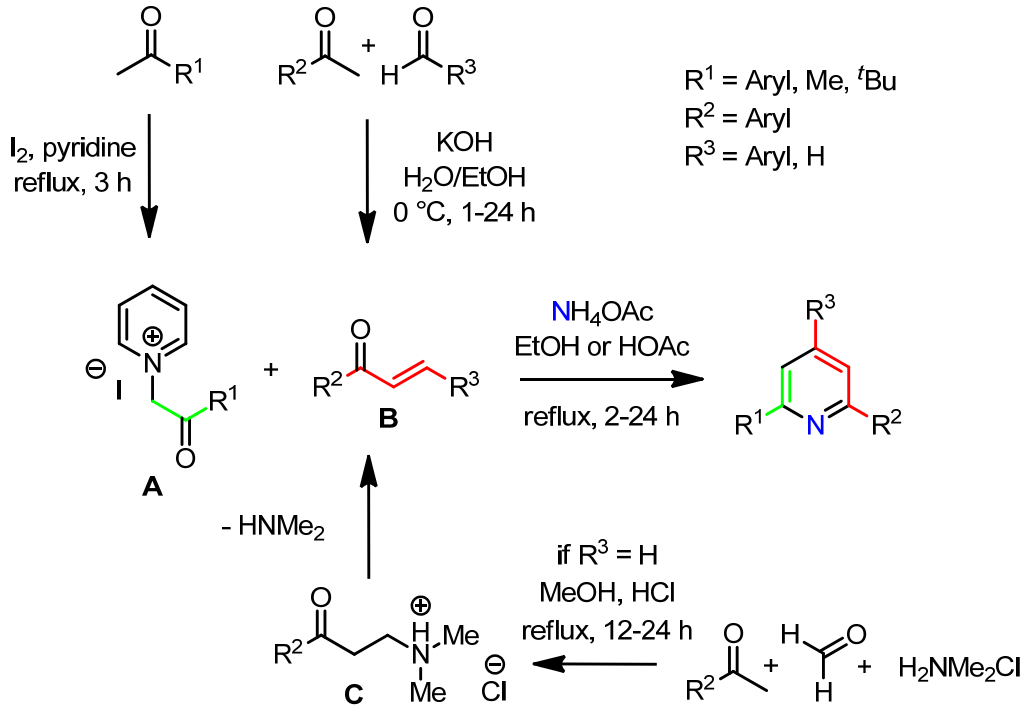


**Scheme 1-1** Synthesis of precursors and pyridines *via* KRÖHNKE methodology.

This very useful reaction was developed in 1930 by Professor Fritz KRÖHNKE and has since steadily been developed and improved, which resulted in a review in 1976.[20] It describes the synthesis of pyridines decorated with various substituents and shows many detailed examples. Even though, most of the chemists working with polypyridines are very likely to use this type of reaction, the original work is almost never cited. The KRÖHNKE reaction is a one pot, multi component synthesis, where a ketone, activated as a pyridinium salt, reacts with an α,β-unsaturated ketone in a MICHAEL-type reaction, to give a 1,5-diketone. With ammonium acetate as the source of $NH_3$, the MICHAEL product can then undergo an imine condensation and a ring closure. The final step bears the elimination of pyridinium halide to give a newly formed pyridine. This method has a few advantages compared to other conventional methods for pyridine synthesis like HANTZSCH[21] or TSCHITSCHIBABIN.[22] The pyridinium salt of the ketone has a higher oxidation state then the parent compound and a dehydrogenation reaction is not required anymore. In the TSCHITSCHIBABIN reaction, half of the ketone is used up to oxidize the pyridine (see Scheme 1-2) and the yield can never exceed 50 %.[23] In contrast, the KRÖHNKE reaction can yield the product in up to 95 %. Furthermore, with the KRÖHNKE method, substituted pyridines, bi-, ter-, and up to septipyridines can be prepared from simple building blocks, the pyridinium salts (**A**) and the vinyl ketones (**B**) or MANNICH bases (**C**). Compared to the HANTZSCH synthesis, where the products are always

symmetrical, the substituents of the KRÖHNKE product can differ from each other and unsymmetrical products are accessible. Another big advantage is the stability of all starting materials so that there is no need for carrying out the reaction under inert conditions. Without any doubt one can say that the KRÖHNKE reaction is the method of choice if polypyridines are needed.

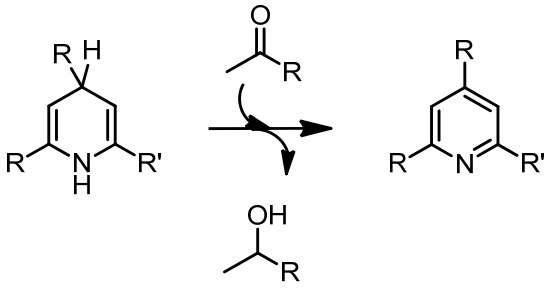

**Scheme 1-2** Reduction of the ketone (TSCHITSCHIBABIN).

A different approach, which comes immediately in mind, not only because of the recent NOBEL PRIZE award, is of course the direct substitution of bipyridine *via* Pd-catalysed C-C cross coupling, e.g. SUZUKI coupling.[24] Certainly, the yields of these reactions are excellent but a multistep synthesis of the bipyridine precursor (**A**) is required and for most substituents, the boronic acid ester precursor (**B**) has to be synthesized as well (Scheme 1-3) because they are usually not commercially available.

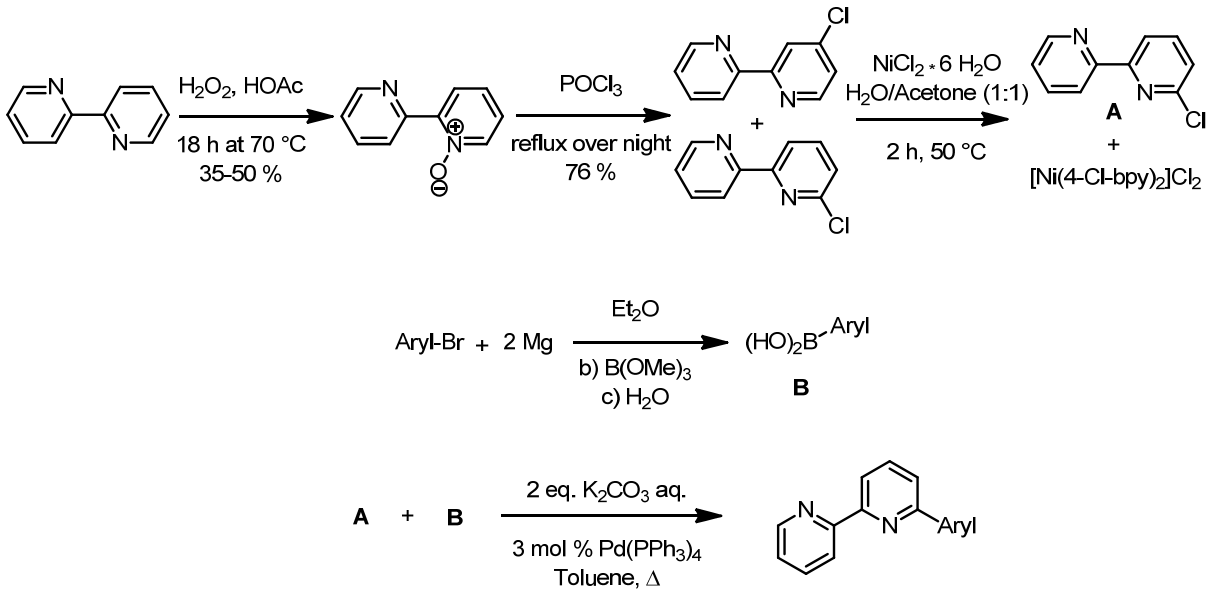

**Scheme 1-3** Synthesis pathway to 6'-substituted 2,2'-bpy *via* SUZUKI cross coupling.

The alternative to the Pd catalysed reaction is the direct coupling of unsubstituted bpy with Li-organyls. This approach works quite well for simple substituents, such as methyl or phenyl and was first introduced by SAUVAGE and co-workers in 1982.[25] For convenience of a one pot

reaction, the use of relatively cheap and commercially available starting materials, this brings enormous time saving.

## 1.3 Applications of coordination compounds

As mentioned above, bpy is a very versatile and robust chelating ligand and forms stable complexes with many metals. This work focused on complexes of ruthenium(II), copper(I) and iridium(III), and their applications.

DSCs are one subject in our group. The main goal here is the replacement of ruthenium dyes as sensitizers with compounds containing earth abundant metals such as Cu or Zn. For better understanding there will be a short description of ruthenium sensitized devices followed by copper based solar cells and the state of the art precedent to this work.

### 1.3.1 Ruthenium

Coordination compounds containing ruthenium, particularly Ru(II) polypyridine complexes, are the group of transition metal complexes which have been studied most intensively from a photochemical point of view. It is an exceptional combination of chemical stability, redox properties, luminescence emission, excited-state lifetime and excited-state reactivity which led many researchers to pursue these types of compounds. Ruthenium polypyridine complexes are good at absorbing visible light; they have relatively intense and long-lived luminescence, and can undergo reversible redox processes in both the ground and excited states. The prototype compound $[Ru(bpy)_3]^{2+}$ has certainly been studied at length and widely used in research laboratories during the last 30 years. Ru(II) polypyridine complexes have contributed a great deal to the development of all branches of photochemistry and photophysics, electrochemistry, electro-generated chemiluminescence, and electron and energy transfer. They are also favoured for the preparation and investigation of supramolecular assemblies as light-harvesting antennae or luminescent sensors, etc. 20 years ago GRÄTZEL *et al.* published a photovoltaic device with a ruthenium dye as sensitizer for mesoporous $TiO_2$ with conversion efficiencies around 7 %.[26] Since then the number of investigated dyes and devices increased nearly exponentially. It is therefore only natural that there are several exhaustive reviews dealing with Ru(II) polypyridine.[27]

#### 1.3.1.1 Structure and Bonding

The bipyridine ligands are usually colourless compounds which have σ-donor orbitals localized on the nitrogen atoms and the π–orbitals are more or less delocalized on the aromatic rings. The metal centre $Ru^{2+}$ is a $d^6$ system displaying an octahedral coordination sphere binding three bpy ligands. The structure of the prototype compound $[Ru(bpy)_3]^{2+}$ is shown in Figure 1-4.

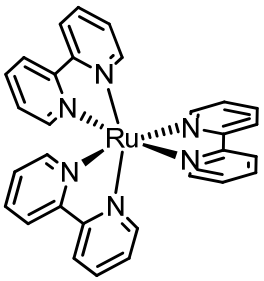


**Figure 1-4** Structure of $[Ru(bpy)_3]^{2+}$.

### 1.3.1.2 Absorption Spectrum and Excited States

Figure 1-5 displays the absorption spectrum of $[Ru(bpy)_3]^{2+}$ and the proposed assignments.[27] Most intense are the high energy bands which are ligand centred (LC) at 185 nm (not shown in the figure) and 285 nm. They result from spin-allowed LC $\pi \rightarrow \pi^*$ transitions. The two remaining less intense bands at 240 and 450 nm originate from spin-allowed metal-to-ligand charge transfer (MLCT) $d \rightarrow \pi^*$ transitions. The shoulders at 322 and 344 nm are speculated to be metal-centred (MC) transitions.

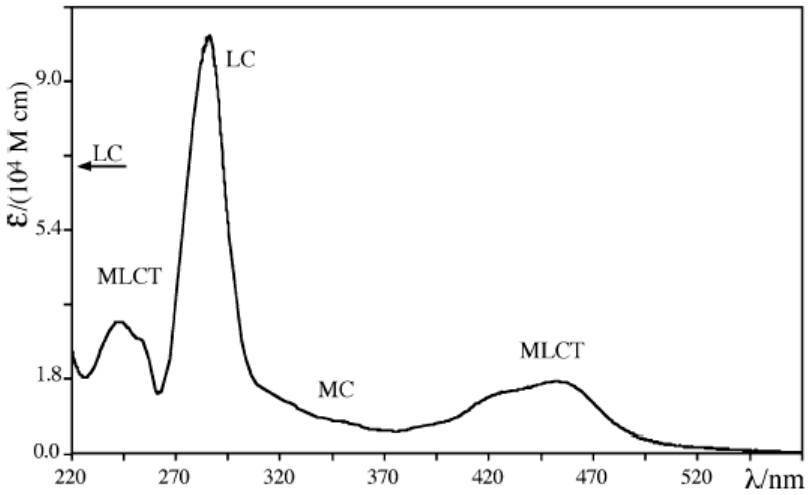


**Figure 1-5** Electronic absorption spectrum of $[Ru(bpy)_3]^{2+}$ in alcoholic solution.[27]

Figure 1-6 shows a simplified molecular orbital diagram to describe the most important transitions in $[Ru(bpy)_3]^{2+}$. A single-configuration one-electron description of the excited state in octahedral symmetry allows a promotion of an electron from a πM metal orbital to the $\pi^*_L$ ligand orbitals which results in MLCT excited states. MC excited states are possible when an electron is promoted from πM to σ∗M orbitals.

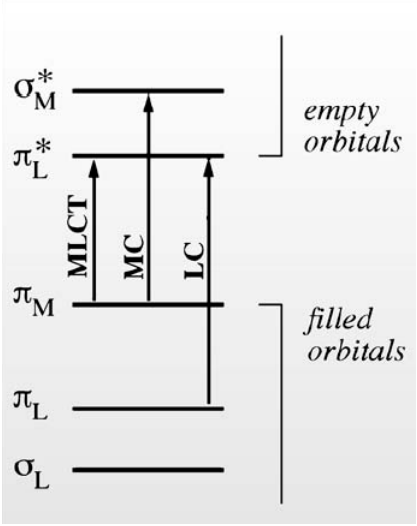


**Figure 1-6** Simplified molecular orbital diagram for Ru(II) polypyridine complexes in octahedral symmetry showing the three types of electronic transitions occurring at low energies.[27]

LC excited states can be obtained by promoting an electron from $\pi_L$ to $\pi^*_L$. It is established that all these excited states may have singlet or triplet multiplicity, respectively, although spin–orbit coupling due to the heavy metal centre causes large singlet–triplet mixing, predominantly in MC and MLCT excited states.

#### 1.3.1.3 Emission properties

In $d^6$ octahedral complexes the MC excited states are strongly displaced compared to the ground-state geometry and metal–ligand vibration coordinates. Therefore MC excited states usually undergo fast radiationless dissipation to the ground state and/or ligand dissociation reactions (Figure 1-7) and no luminescence emission can be observed.

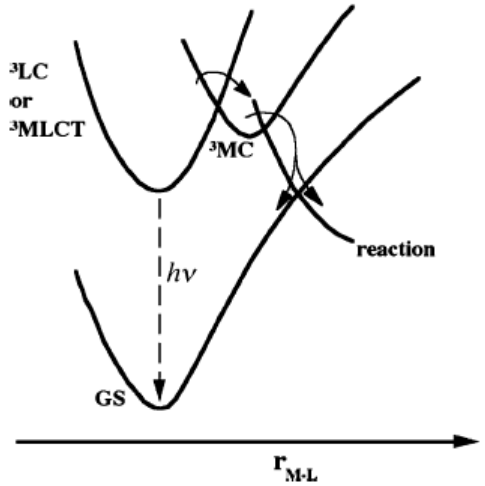


**Figure 1-7** Possible pathways for excited electron.[27]

On the other hand, LC and MLCT excited states are usually similar in geometry and bond distances to the ground state. Relaxation can then result in photon emission.

The properties of the excited state in a $[Ru(bpy)_3]^{2+}$ depend very much on the orbital nature of its lowest excited state. The energy positions of the MLCT and LC excited states depend

on the ligand field strength, the redox properties of metal and ligands, and intrinsic properties of the ligands. It is therefore possible to vary the emissive properties by the introduction of functionalized ligands.[27] The design of complexes with desired properties is possible at least to a certain degree.

#### 1.3.1.4 Quenching of the $^3$MLCT Excited State: Energy and Electron Transfer Processes

The possibility of using the long-lived excited state of $[Ru(bpy)_3]^{2+}$ as an energy donor in energy transfer processes is a reason for the early interest in its photochemistry. Hundreds of bimolecular excited-state reactions of $[Ru(bpy)_3]^{2+}$ and of its derivatives have been studied in detail. The most common energy transfers are summarized in the diagram shown in Figure 1-8.

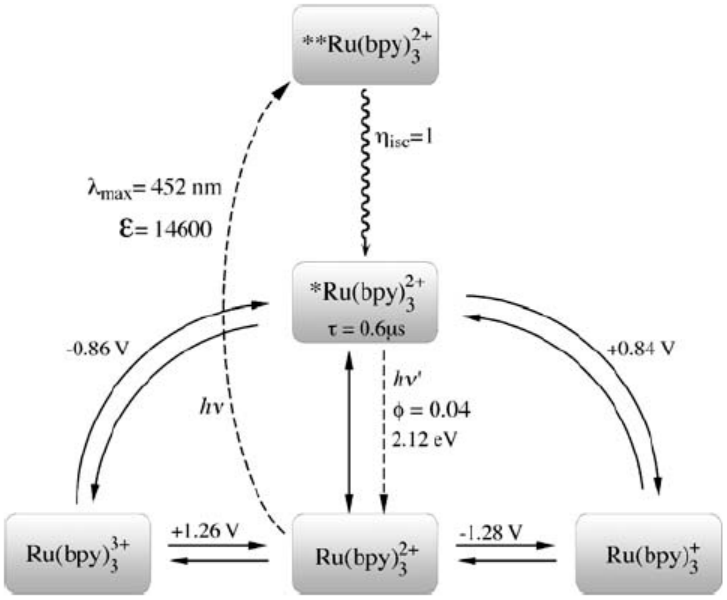


**Figure 1-8** Energy and electron transfer processes of $[Ru(bpy)_3]^{2+}$. $^{**}[Ru(bpy)_3]^{2+}$ indicates higher-energy spin-allowed excited states and $^{*}[Ru(bpy)_3]^{2+}$ indicates the lowest spin-forbidden excited state ($^3$MLCT). Reported potentials are in aqueous solution *vs.* SCE.[27]

The lowest $^3$MLCT excited state of $[Ru(bpy)_3]^{2+}$ lives long enough to encounter other solute molecules and possesses suitable properties to play the role of energy donor, electron donor, or electron acceptor.

### 1.3.2 Dye Sensitized Solar Cells (DSCs)

#### 1.3.2.1 General: Sun and Solar Cells

The demand for energy is growing worldwide and there is a great need for economically feasible and renewable energy. In the year 2000 the average global energy consumption rate was 13 TW. The assumed value for global energy consumption in 2050 is around 30 TW.[28,29]

It is acknowledged that solar energy has the one of the largest potentials to satisfy future needs.[30] The estimated global solar potential value is 600 TW and with 10 % efficient solar farms, about 60 TW of power could be supplied. The sun emits light similar to a black body at 5760 K with a range of wavelengths from the ultraviolet (UV) and visible (vis) to the infrared (IR). The atmosphere has a big influence on the wavelength spectrum. UV light is filtered out by ozone. Water and $CO_2$ then absorb mainly in the infrared causing dips in the solar spectrum at 900, 1100, 1400, and 1900 nm ($H_2O$) and at 1800 and 2600 nm ($CO_2$). For measurements of solar cells the AM 1.5 G solar radiation spectrum is used as shown in Figure 1-9.

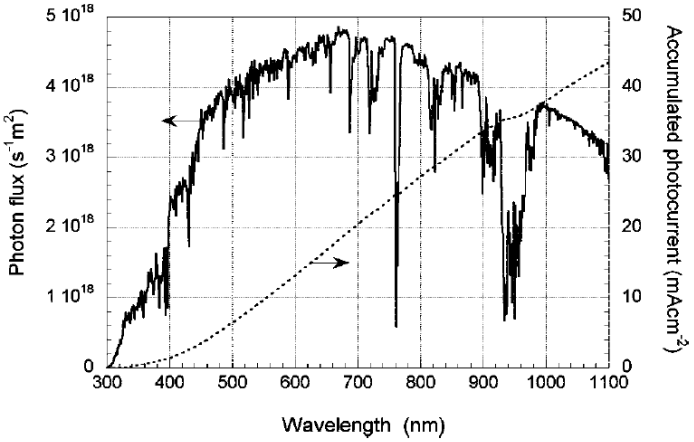


**Figure 1-9** Photon flux of the AM 1.5 G spectrum at 1000 W $m^{-2}$ (AM: air mass = 1/cos φ, φ = angle of sun elevation, usually 42°; G: global) and calculated photocurrent.[28]

The overall conversion efficiency, η, from solar to electrical energy for a photovoltaic device is given by the photocurrent density measured at short-circuit ($J_{sc}$), the open-circuit photovoltage ($V_{oc}$), the fill factor of the cell (FF), and the intensity of the incident light ($P_{in}$).

$$\eta = \frac{J_{SC} V_{OC} FF}{P_{in}}$$

The fill factor can be between 0 and less than 1 and expresses the ratio of the maximum power ($P_{max}$) of the solar cell per unit area divided by the $V_{oc}$ and $J_{sc}$ given by

$$FF = P_{max}/(J_{SC} V_{OC})$$

The maximum power is obtained as the product of the photocurrent and photovoltage at the voltage where the power output of the cell is maximal.

The research area of photovoltaics has been developing over the last few decades, the first successful experiments being made in the Bell Laboratories in 1940. There are now many types of solar cell including semiconductor materials such as crystalline silicon (c-Si), amorphous Si (a-Si), galliumarsenide (GaAs) or cadmiumselenide (CdSe).[31] Solar cells based on c-Si are well developed and used all over the world. They can reach efficiencies as high as

25 % being only slightly below the theoretically feasible value of 29 %.[32] Figure 1-10 shows the state of the art silicon based solar cell which consist of a c-Si layer between two electrodes with thin oxide layers.

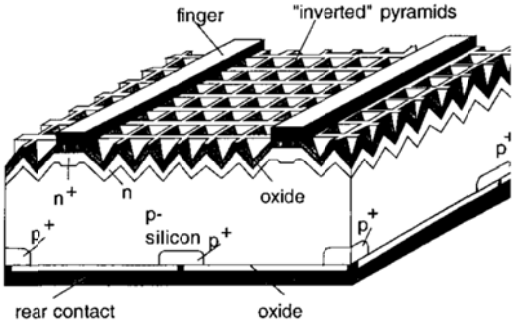


**Figure 1-10** c-Si based solar cell.[32]

The advantages of silicon as a material are its non-toxicity and high abundance in the Earth's crust; the main disadvantage is the high production costs of pure single crystalline silicon (CZOCHALSKI process)[33] which is not environmentally friendly. a-Si based solar cell are significantly better in consideration of the same facts but so far they suffer from lower efficiencies. Better results give solar cells based on III-V semiconductors such as GaAs or InP but these materials are highly toxic and carcinogen. Table 1-1 compares inorganic solar cells.

| Module classification | Efficiency [%] | Area [$cm^2$] | $V_{OC}$ [V] | $I_{SC}$ [A] | ff |
|---|---|---|---|---|---|
| Si (crystalline) | 22.7 | 778 | 5.6 | 3.9 | 0.80 |
| Si (multicrystalline) | 15.3 | 1017 | 14.6 | 1.4 | 0.79 |
| Si (thin-film polycrystalline) | 8.2 | 661 | 25.0 | 0.3 | 0.68 |
| CIGSS | 13.4 | 3459 | 31.2 | 2.2 | 0.69 |
| CdTe | 10.7 | 4874 | 26.2 | 3.2 | 0.62 |
| a-Si/a-SiGe/a-SiGe (tandem) | 10.4 | 905 | 4.4 | 3.3 | 0.66 |

**Table 1-1** Overview of best modules of inorganic solar cells; AM1.5 G (1000 $W/m^2$) at 25 °C (a-Si = amorphous silicon/hydrogen alloy, a-SiGe = amorphous silicon/germanium/hydrogen alloy).[31]

DSCs are a considerable alternative for photovoltaic devices. DSCs use $TiO_2$ as semiconductor which is also non-toxic and feasible but it is a wide-band gap semiconductor (3 eV) which needs UV energy for charge separation and this is not available as mentioned above. In order to use the available photons in the visible and infrared region, sensitizing of the semiconductor with dyes which can absorb these photons and are then able to inject electrons to the $TiO_2$ is necessary. Today it is safe to say that ruthenium(II) polypyridine complexes/dyes initiated and contributed a great deal to the development of dye-sensitized solar cells. Even though the principle of dye sensitized semiconductors goes back to 1960 and attempts to prepare DSCs have been made,[34] they never attained much attention due to their low efficiencies (< 1 %). The main problem was the belief that only semiconductors with smooth surfaces could be used, similar to silicon based solar cells. Only the use of a mesoporous electrode sintered from titania nanoparticles, which increased the surface area

able to adsorb the dye molecules, increased the conversion efficiencies to 7 %. In the course of the last 20 years these values reached the mark of 12 %.[35]

### 1.3.2.2 Architecture and operational principles of DSCs

A DSC consists of relatively few components and a schematic view of the setup and the principle of how the cell operates is shown in Figure 1-11. Typically, the configuration is the following: The main component is the semiconductor, a mesoporous layer of $TiO_2$ nanoparticles. $TiO_2$ is a stable and nontoxic oxide and is often used as a white pigment in paint, sun blocker or food. It occurs naturally in three crystal forms: rutile, anatase and brookite; rutile being the thermodynamically most stable form. But for DSCs anatase is preferred due to higher band gap (3.2 *vs.* 3.0 eV for rutile) and therefore higher conduction band energy. This results in higher Fermi level and $V_{OC}$.

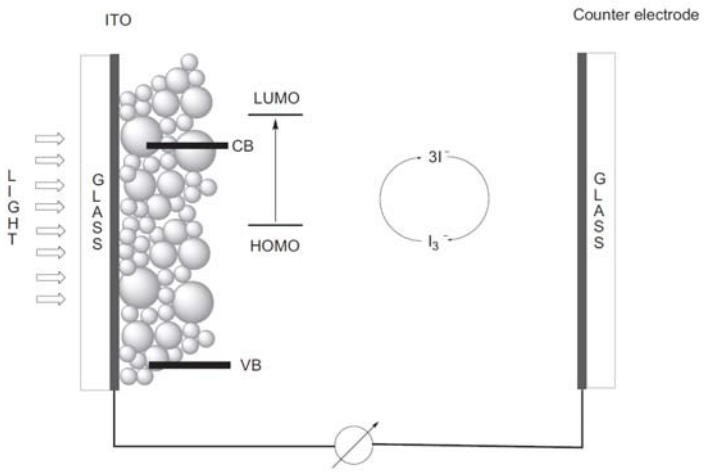


**Figure 1-11** Schematic set up of a DSC.

Usually, 10 µm layers of anatase nanoparticles (10-30 nm in diameter) are sintered on a transparent conducting oxide; typically fluorine doped tin oxide (FTO). The resulting porosity of these films is 50-60 % which offers a much bigger surface area about factor 1000 compared to single crystalline films. Thus much more dye particles can be attached to the semiconductor in a monolayer fashion. Nowadays there are manifold dyes under investigation such as metal free organic molecules, porphyrins and phthalocyanines but ruthenium polypyridine complexes were investigated in the first place and are still the most studied dyes. Independent of the nature of the dye it should fulfil the following requirements:

- The absorption spectrum of the photosensitizer should cover the whole visible region and if possible a part of the near-infrared (NIR);
- The photosensitizer needs anchoring groups, such as -COOH, $-H_2PO_3$, $-SO_3H$, which can form covalent bonds to the semiconductor surface;

- To allow an efficient electron transfer between a dye in its excited state and the conduction band of the semiconductor, the latter should be lower in energy (n-type DSC). n-Type DSCs are possible when the excited state level of the dye is higher than the conduction band of the semiconductor so that electrons from exited dye molecules can be injected in the semiconductor;
- To allow the regeneration of the photo sensitizer, its oxidized state level has to be more positive than the redox potential of the electrolyte;
- Furthermore the dye should be photo stable, and electrochemical and thermal stability are also needed.

The photo sensitization process is generally described as the following: The adsorbed dye can absorb photons with wavelengths in the visible or near infrared region. An electron gets promoted in the LUMO of the dye, which should be localized near the semiconductor (preferably on the anchoring ligand), this electron can be injected to the conduction band of the semiconductor if this process is faster than the relaxation processes of the excited dye. The dye is then restored to its ground state by electron transfer from the electrolyte. The standard electrolyte which is usually used and gives the best results for DSCs is an organic solvent (acetonitrile) containing the iodide/triiodide redox system. $I^-$ ions are oxidized by the excited dye and form $I_3^-$ ions which then diffuse through the electrolyte to the cathode. The cathode is coated with a thin layer of platinum catalyst, which is able to reduce $I_3^-$ to $I^-$ and completes the regenerative cycle. Even though electrolytes based on $I^-/I_3^-$ give the best efficiencies and are the preferred choice they have the drawback of being corrosive and not suitable for all dyes. Other systems have been investigated, such as $Co^{2+}/Co^{3+}$ polypyridine complexes or $SCN^-/(SCN)_3^-$ and organic systems based on TEMPO and TDP. The last component of a DSC is the counter electrode, usually consisting of transparent and conducting tin oxide (FTO) on a glass substrate. Although FTO is a very poor counter electrode with a very high charge transfer resistance ($10^6\ \Omega\ cm^{-2}$ in a standard iodide/triiodide electrolyte) it can be functionalized by thermal deposition of a thin layer of Pt (5 $\mu$g $cm^{-2}$) so that it still remains transparent and the charge transfer resistances drops to values lower than $1\ \Omega\ cm^{-2}$. There are other, less often used materials, such as carbon counter electrode (e.g. graphite/carbon black mixture), conducting polymers as Poly(3,4-ethylenedioxythiophene) (PEDOT) doped with toluenesulfonate anions, and recently cobalt sulfide.[28]

Illumination of DSCs generates voltage which is dependent on electrochemical potential of the electron at the two contacts; usually this results from the difference between the Fermi level of the semiconductor and the redox potential of the electrolyte.

Figure 1-12 depicts the basic electron transfer processes and the potentials for a state-of-the-art device based on the **N3** (one of the best Ru-dyes) dye adsorbed on $TiO_2$ with $I^-/I_3^-$ as redox couple in the electrolyte.

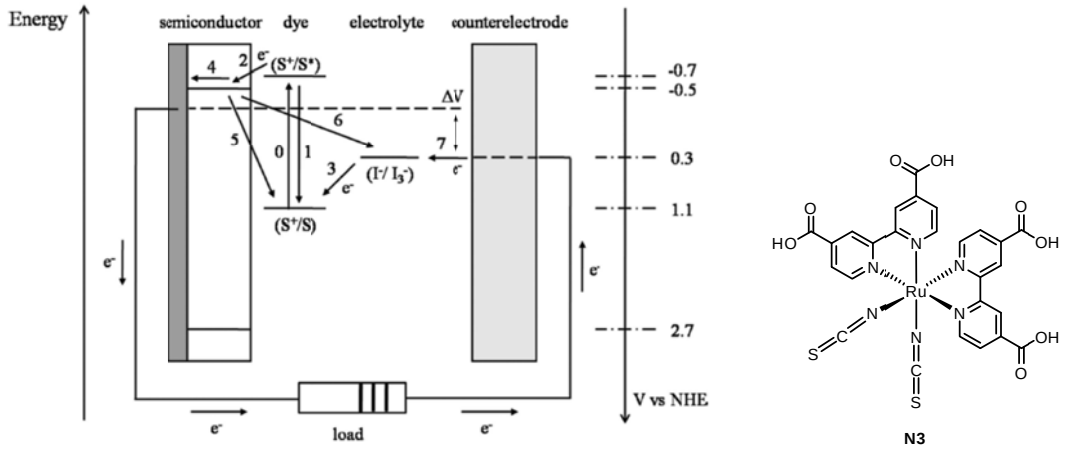


**Figure 1-12** Simple energy level diagram of a DSC based on the **N3** dye.

The desired electron transfer processes (processes 2, 3, 4, and 7) compete with the reactions where the electrons are lost for the photovoltaic process. These are in detail: the direct recombination of the excited dye which can be suppressed by longer excited state lifetimes (1); the electrons injected into $TiO_2$ can undergo back reactions (5 and 6) with either oxidized dyes or acceptors in the electrolyte (e.g. $I_3^-$).[28]

Many alternatives for all components in conventional DSCs have been investigated. Our group explores the dye component, in particular metal complexes with earth abundant metals which could replace the expensive ruthenium. Copper(I) bipyridine complexes exhibit similar behaviour in their photochemical and photophysical properties and are a reasonable alternative. In the following sections these will be explained.

### 1.3.3 Copper

Copper is a metal with a long history and has been used for at least 10000 years. The process for isolating it from ores such as malachite or azurite ($Cu_nCO_3(OH)_2$, n = 2 or 3) seems to have been developed independently in several parts of the world since several centuries B.C.. Preparation of bronze alloys (Cu/Sn-alloy) made a universal material for objects of utility or weapons and the widespread use was responsible for the naming of a whole period of civilization between 2500 and 600 B.C.: the Bronze Age. *Aes Cyprium*, was the roman name for bronze because most of the ores were imported from the island of Cyprus. It was later simplified to *cuprum* and then eventually anglicised into *copper*. Pure copper is mainly produced from naturally occurring sulfides by smelting and electrolytic refining. Its most appreciated properties are thermal and electrical conductivity and it is used for all kinds of power transmission and generation. There is only a fixed resource on the Earth's crust and

the demand for copper is increasing steadily. This results in the increase of its price, while in 1999 one pound of copper could be purchased for $0.60 only, today the price is 7 times higher ($4.18 in April 2012).[36,37]

This work focuses on 6'-substituted 2,2'-bipyridine ligands and their homoleptic, and cationic Cu(I) complexes which show a rich photophysical behaviour. The substituent in the 6'-position is needed to stabilize the Cu(I)-complex against nucleophilic attacks and their oxidation to $Cu^{2+}$ by $O_2$.[38] The photophysical properties of copper(I) complexes with NN-type ligands (NN indicates a chelating imine ligand, typically 1,10-phenanthroline or 2,2'-bipyridine) have been intensively studied and are known to be critically dependent upon ligand substitution little is known about the influence on their effectiveness as photosensitisers.

#### 1.3.3.1 Chemical Properties

Copper is a transition metal, it is the first row element in group 11 followed by silver and gold and is also referred to as coinage metal. Copper has eleven valence electrons and it is energetically more favoured to fill the 3*d* shell fully with ten electrons, the 4*s* shell contains the last remaining one. Except for the possibility to adopt +1 oxidation state, copper has nothing in common with alkaline metals. The filled *d* shell shields the *s* electron somewhat from the nuclear charge, resulting in a higher first ionization enthalpy of Cu than that of the alkaline metals. Also the heat of sublimation and the melting point of Cu are also much higher than those of the alkalis. Copper has a noble character exhibiting a positive electrochemical potential, it is not corroded by acids, except by strongly oxidizing ones such as $HNO_3$ and $H_2SO_4$. In solution Cu can adopt two common oxidation states: +1 and +2. $Cu^+$ is able to disproportionate to $Cu^0$ and $Cu^{2+}$. This equilibrium is very much dependent on the nature of ligands. The $d^{10}$ configuration results in a symmetric localization of the electronic charge, and a tetrahedral coordination of the ligands around the metal is favoured (Figure 1-13).

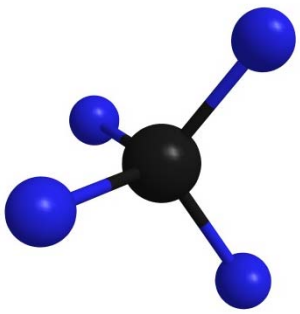

**Figure 1-13** Tetrahedral coordination environment typical of Cu(I) complexes (Cu black, N blue).

The full *d* also prevents *d-d* MC transitions in Cu(I) compounds. In contrast, these transitions can be observed for $d^9$ Cu(II) complexes which are responsible for the relatively intense absorption bands in the visible spectral window and the blue or green colour of Cu(II) compounds. Unfortunately, excited states of copper(II) complexes are rather short lived and deactivate *via* ultrafast non-radiative processes which renders them far less interesting than Cu(I) complexes from the photophysical point of view. Copper(I) cationic complexes can show luminescence originating from MLCT states, as long as empty $\pi$ orbitals are easily accessible on the ligands. The MLCT transitions are possible due to the low oxidation potential of Cu(I) and they are similar to those of $d^6$ metals like Ru(II) bipyridines[27] and Ir(III) phenylpyridine[39] complexes. This fact makes Cu(I) compounds interesting alternatives to Ru and Ir compounds from economical and environmental points of view.[40]

### 1.3.3.2 Ground State Geometry

$Cu(NN)_2^+$ complexes generally exhibit distorted tetrahedral geometries. The distortions from $D_{2d}$ symmetry are caused by intra- and intermolecular, as well as by $\pi$-stacking interactions. It has been shown that in solid state the geometry is mainly dictated by packing forces and counter anions. The main distortion can be expressed through the deviation of the dihedral angle $\theta$ between the two diimine ligands from ideal 90° (Figure 1-14). For example, for [Cu(**dmphen**)$_2$][X] this angle flattens from 88° for X = $BF_4^-$ to 73° if X = picrate.

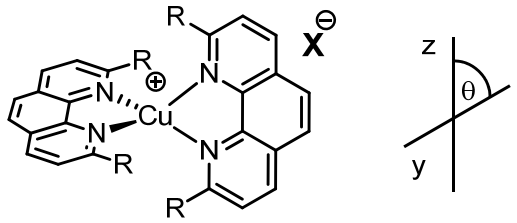


R = Me (**dmphen**), $CF_3$ (**dtfmphen**), Ph (**dpphen**)

**Figure 1-14** Tetrahedral geometries for [Cu(L)$_2$][X] complexes; Ligands: **dmphen** = 2,9-dimethyl-1,10-phenanthroline, **dtfmphen** = 2,9-ditrifluoromethyl-1,10-phenanthroline, **dpphen** = 2,9-diphenyl-1,10-phenanthroline); $X^-$ see text.

If the anion is not varied the dependence on the substituent can be observed. For example, the dihedral angles between the two phenanthroline planes in [Cu(**dmphen**)$_2$][$PF_6$], [Cu(**dtfmphen**)$_2$][$PF_6$] and [Cu(**dpphen**)$_2$][$PF_6$] are 79.4, 87.5 and 79.8°. These results show that already small substituents such as -$CH_3$ cause significant geometric distortion. Bulkier $CF_3$ groups force a more rigid quasi-tetrahedral arrangement in [Cu(**dtfmphen**)$_2$][$PF_6$]. In the case of [Cu(**dpphen**)$_2$][$PF_6$], the distortion is influenced by intramolecular $\pi$-$\pi$ stacking interactions between phenyl rings and phenanthroline cores of the other ligand. The electronic absorption spectra are sensibly dependant on the geometry and are therefore tuneable by the alteration of the substituents on the NN-ligands.[37]

### 1.3.3.3 Absorption Spectra

Figure 1-15 shows the absorption spectra of three homoleptic complexes of 2,9-disubstituted phenanthrolines in dichloromethane solution, $[Cu(\mathbf{dmphen})_2]^+$, $[Cu(\mathbf{btphen})_2]^+$, and $[Cu(\mathbf{bdtbmpphen})_2]^+$. The ligands have either alkyl or aryl substituents (see Figure 1-15).

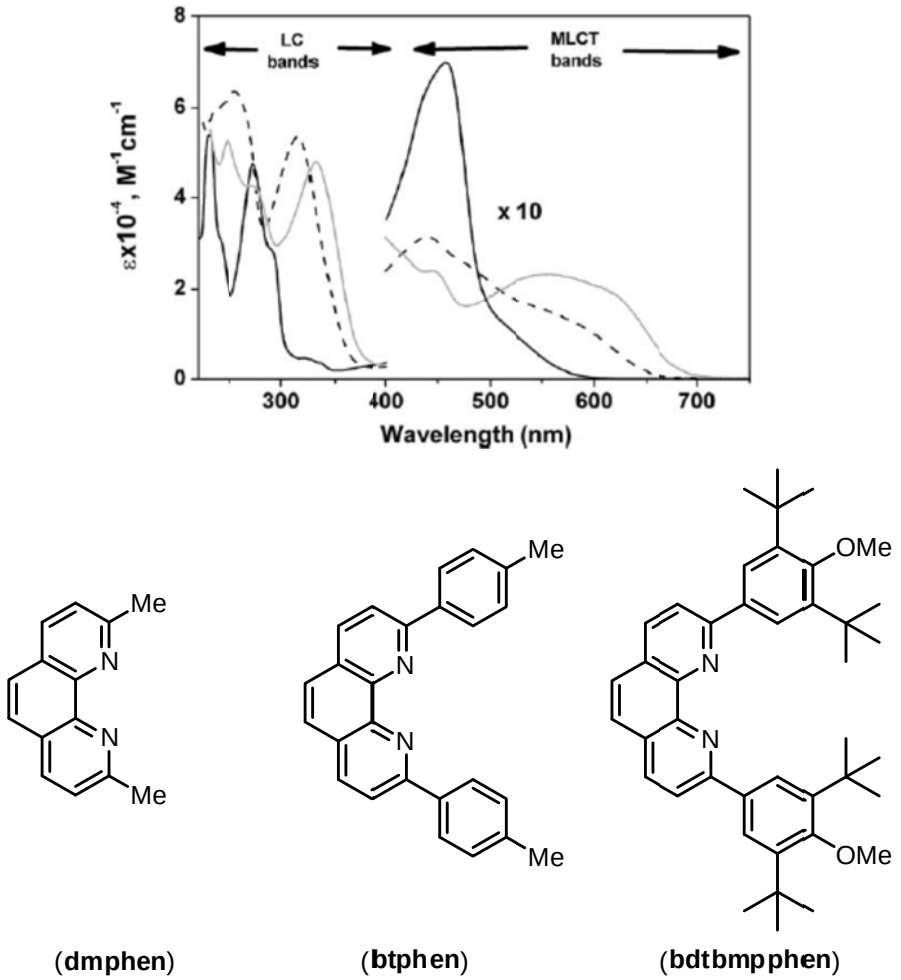


**Figure 1-15** Absorption spectra of $[Cu(\mathbf{dmphen})_2]^+$ (full black line) $[Cu(\mathbf{btphen})_2]^+$ (dashed line) $[Cu(\mathbf{bdtbmpphen})_2]^+$ (full grey line) in $CH_2Cl_2$ at room temperature; Ligands: **dmphen** = 2,9-dimethyl-1,10-phenantroline, **btphen** = 2,9-di-p-tolyl-1,10-phenanthroline, **btphen** = 2,9-bis(3,5-di-tert-butyl-4-methoxyphenyl)-1,10-phenanthroline.

The UV part of the spectra show typical intense bands which can be assigned to LC $\pi-\pi$ transitions of the phenanthroline ligands with molar absorption coefficients ($\varepsilon$) being in the order of 50000-60000 $M^{-1}cm^{-1}$. In the visible spectral range the bands are much weaker than those in the UV with $\varepsilon$ values usually lower than 10000 $M^{-1}cm^{-1}$, these have been assigned to MLCT. McMillin et al.[41] and others[42] have devoted a lot of work to the exploration of the absorption spectra of many mononuclear Cu(I)-bis(phenanthroline) complexes. They could identify at least three MLCT bands in the vis region. They are termed band I (above 500 nm), band II (maximum around 430-480 nm, the most common), and band III (390-420 nm, often hidden by the onset of band II). Spectral intensities are very much related to the symmetry

of the complex ($D_{2d}$ *vs.* $D_2$, Figure 1-16) which is dependent on the distortion from the tetrahedral geometry (see above).

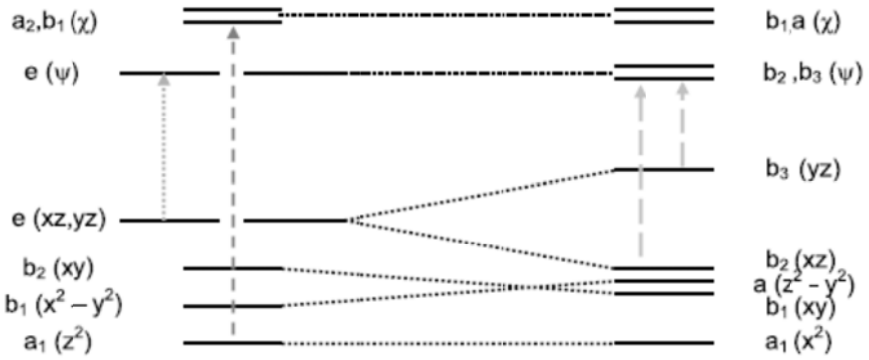


**Figure 1-16** Schematic orbital splitting diagrams for $[Cu(NN)_2]^+$. Left, $D_{2d}$ symmetry; right, $D_2$ symmetry. Grey arrows represent the transitions leading to bands I (--), band II (…), and band III (- - -).

A detailed discussion will not be repeated here and can be found elsewhere.[37] Just the trend should be clarified: the more the $[Cu(NN)_2]^+$ complex is distorted from ideal tetrahedral geometry the smaller the band gap gets and the transitions move to lower energies, see Figure 1-16.

#### 1.3.3.4 Excited State Distortion

When $[Cu(NN)_2]^+$ is excited by light an electron is promoted to the LUMO and the metal centre changes its formal oxidation state from Cu(I) to Cu(II).[40] The Cu(I) MLCT excited complex undergoes further flattening compared to its ground state and its geometry resembles more that of ground state Cu(II)-bisphenanthroline complexes. In this excited state flattened tetrahedral structure a fifth coordination site is made available for the Cu(II) $d^9$ ion, that can be filled by nucleophilic species such as solvent molecules and counterions. The intermediate species thus obtained is termed a "pentacoordinated exciplex".[41] Figure 1-17 depicts schematically the photoinduced formation of the exciplex, which had been proposed by McMillin and coworkers 20 years ago based on classical photochemical experiments on series of $[Cu(NN)_2]^+$ complexes with increasingly nucleophilic counter anions.[43] This has later been nicely confirmed by light-initiated time-resolved X-ray absorption spectroscopy (LITR-XAS).[44]

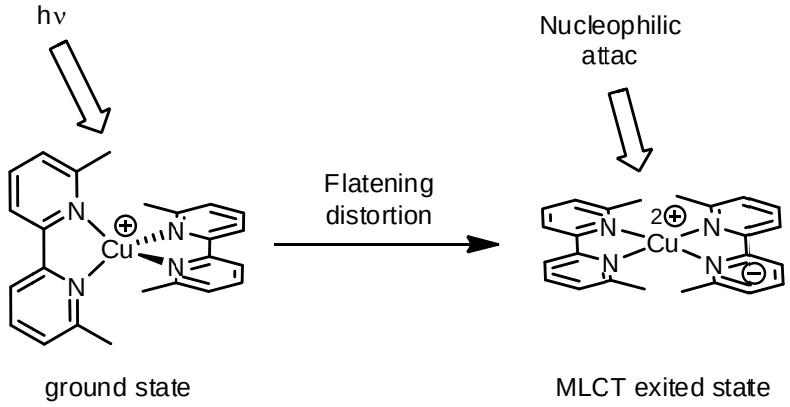


**Figure 1-17** Flattening distortion and faciliated nucleophilic attack by solvent, counterion, or other molecules following light excitation in Cu(I)-bipyridines.

### 1.3.3.5 Emissive Excited State(s) and Luminescence Spectra

In 1980 McMillin and Blaskie reported for the first time luminescence from $[Cu(NN)_2]^+$ complexes in solution.[45] Luminescence from $[Cu(NN)_2]^+$ complexes can be observed in poorly electron donor solvents, usually dichloromethane. The emission bands are wide with values for $\lambda_{ex}$ between 680 and 740 nm, with rather low quantum yields ($\Phi_{em}$ $10^{-3}$-$10^{-4}$).[40] Excited state lifetimes in dichloromethane solution depend on the degree of excited state distortion and the shielding of the exciplex quenching. For example, when excited into the MLCT band region, $[Cu(\mathbf{dmphen})_2]^+$ emits around 700 nm with an excited state lifetime of 54 ns in air-equilibrated dichloromethane. The spectrum is shown in Figure 1-18.

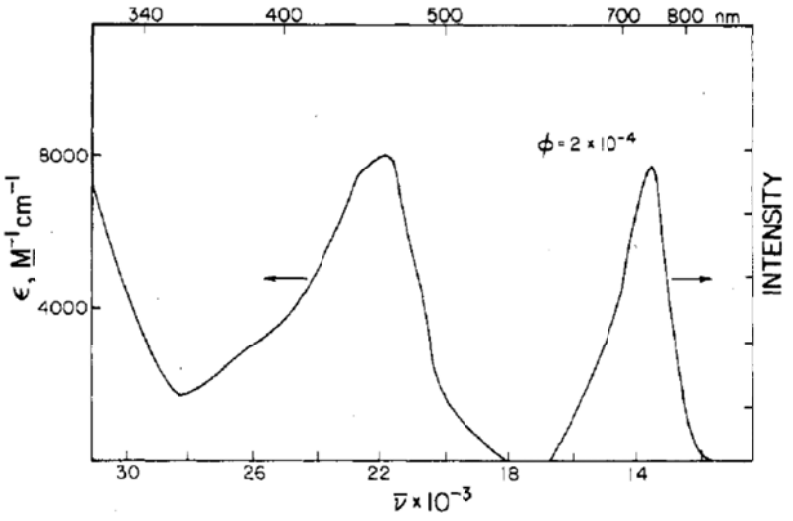


**Figure 1-18** Absorption spectrum (left, MLCT) and emission spectrum (right) of $[Cu(\mathbf{dmphen})_2]^+$ in $CH_2Cl_2$.[45]

### 1.3.3.6 Heteroleptic Cu(I) complexes

It is established that heteroleptic Cu(I) complexes show improved luminescent properties. This suggests that the excited states may possess longer lifetimes and are more stable against thermal dissipation. Longer excited state lifetimes might also be preferable for

application in DSCs for electron injection into $TiO_2$. The preparation of heteroleptic complexes, such as $[Cu(NN)(PP)]^+$ (PP stands for bisphosphine ligand, e.g. POP = bis[2-(diphenylphosphino)phenyl]ether or dppe = bis(diphenylphosphine)ethane, see Figure 1-19) is fairly easy by successive ligand addition.[46]

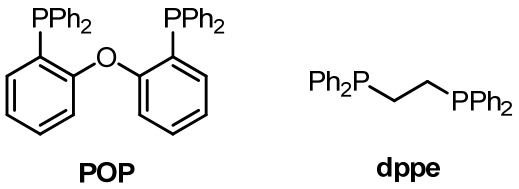


**Figure 1-19** Bisphosphine ligands.

On the other hand, the preparation of heteroleptic $[Cu(NN)(N'N')]^+$ complexes poses some difficulties. The reactions often yield mixtures of both homoleptic complexes ($[Cu(NN)_2]^+$, $[Cu(N'N')_2]^+$) and the heteroleptic complex. The equilibrium can be shifted in favour of the heteroleptic complex by careful choice of the substituents in $\alpha,\alpha'$-position of the diimine ligands. With bulky substituents the formation of one homoleptic complex can be prevented.[47]

### 1.3.3.7 State of the art in our laboratory

In previous work, A. Hernandez REDONDO investigated DSCs with Cu(I) dyes as photosensitizers.[48] Several homoleptic $[Cu(NN)_2]^+$ complexes bearing anchoring groups, such as carboxylic acids or phosphonic acids, were prepared and it was demonstrated that they are indeed able to produce a photo current.[49] The studied ligands are depicted in Figure 1-20. Their corresponding $[Cu(L)_2]^+$ (for L see Figure 1-20) complexes were applied to DSC. The usual preparation was the following: on a FTO coated glass substrate a paste of $TiO_2$ nano particles was doctor bladed, followed by drying and sintering (430 °C). The substrate was immersed into a solution of the copper dye for several hours (usually 3 h); a second glass substrate was coated with few drops of 5 mM $H_2[PtCl_6]$ isopropanol solution, the solvent was left to evaporate and sintering at ca. 380 °C for 15 minutes yielded the Pt counter electrode; both substrates were sandwiched together and a drop of electrolyte (0.5 M LiI, 0.05 M $I_2$ and 0.5 M 1-methylbenzimidazole (MBI) in 1-buthyl-3-methylimidazolium iodide (3-MPN)) was deposited between the two layers. The cells were illuminated with AM 1.5 G light and the I/V-curves were recorded. The best overall efficiencies could be observed for $[Cu(L)_2]^+$ with L = dmdcabpy ($\eta$ = 0.4 %) and dmdaabpy ($\eta$ = 0.9 %).

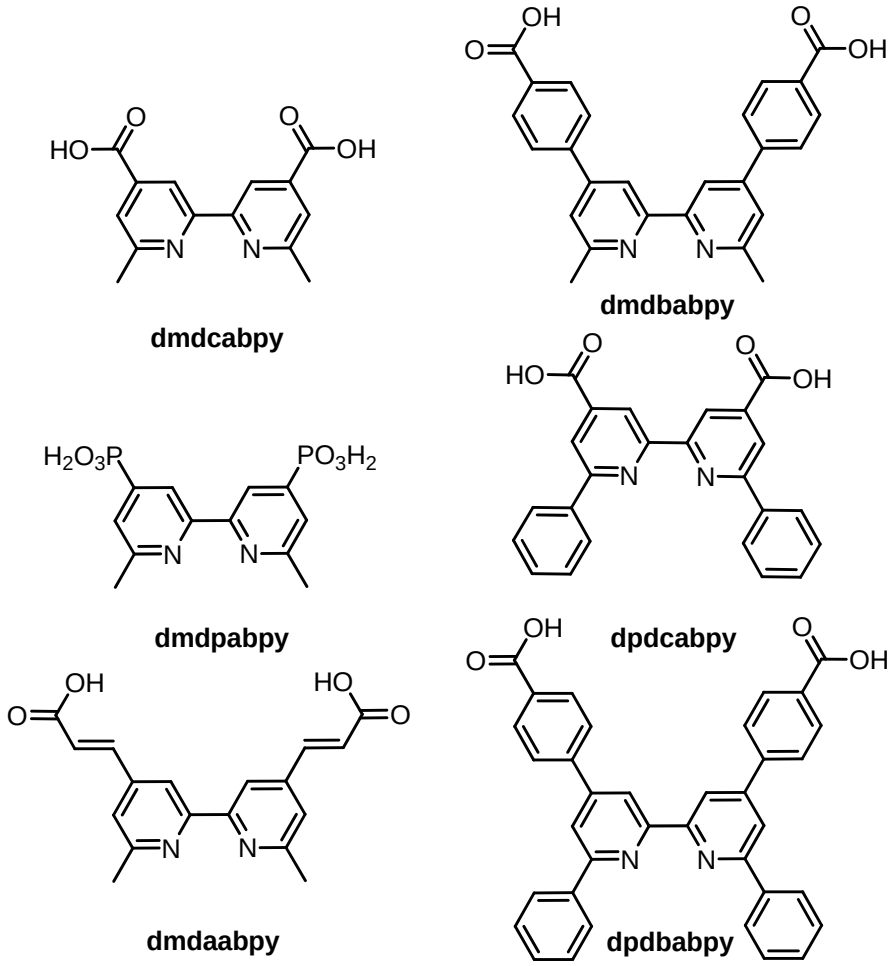


**Figure 1-20** Anchoring ligands; **dmdcabpy** = 6,6'-dimethyl-4,4'-dicarboxylic acid-2,2'-bipyridine, **dmdpabpy** = 6,6'-dimethyl-4,4'-diphosphonic acid-2,2'-bipyridine, **dmdaabpy** = 6,6'-dimethyl-4,4'-diacrylic acid-2,2'-bipyridine, **dmdbybpy** = 6,6'-dimethyl-4,4'-dibenzoic acid-2,2'-bipyridine, **dpdcabpy** = 6,6'-diphenyl-4,4'-dicarboxylic acid-2,2'-bipyridine, **dpdbabpy** = 6,6'-diphenyl-4,4'-dibenzoic acid-2,2'-bipyridine.[48]

The preparation of heteroleptic copper(I) complexes with simple substituents is not trivial, see above. But the kinetic lability of copper(I) comlexes[50] was used to prepare the heteroleptic species directly on the semiconductor surface by a solid support reaction.[48,51] Typically, the glass substrate with the $TiO_2$ semiconductor was immersed for 3 h into an alcoholic solution of the desired anchoring ligand, then the same substrate was dipped into an alcoholic solution of an appropriate homoleptic $[Cu(NN)_2]^+$ complex to allow the ligand exchange reaction (Figure 1-21). After 20 h the substrate was emerged and washed with ethanol. Succesful exchange could be observed by the red colouration of the semiconductor and proved by UV/vis reflectance spectra. Maximal voltage and current were determined under illumination and the highest efficiency (1.4 %) could be observed for [Cu(**dmdpbpy**)(**dpdbabpy**)]$^+$, see Figure 1-22.

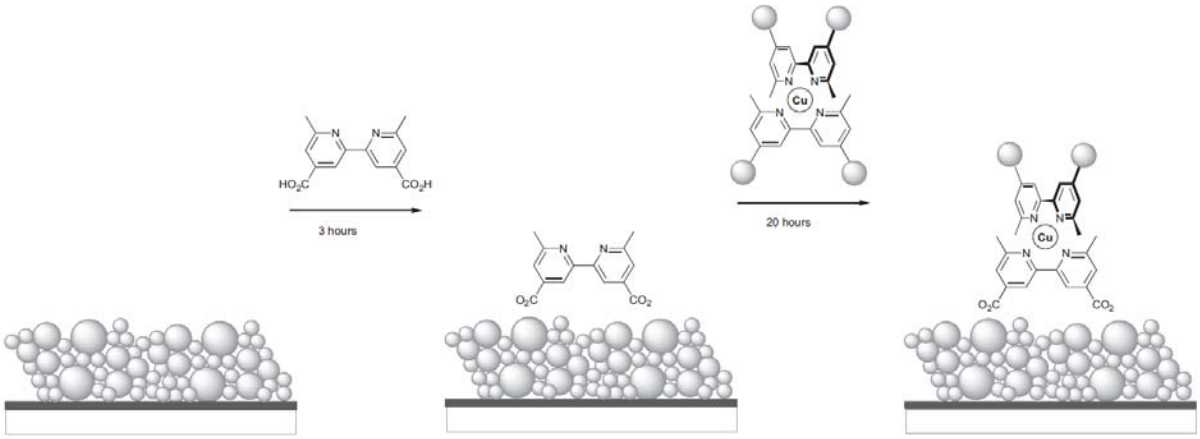


**Figure 1-21** Sequence of the sensitization of $TiO_2$: immersion into a solution of the anchoring ligand followed by immersion into a solution of the homoleptic copper dye (ligand exchange reaction).

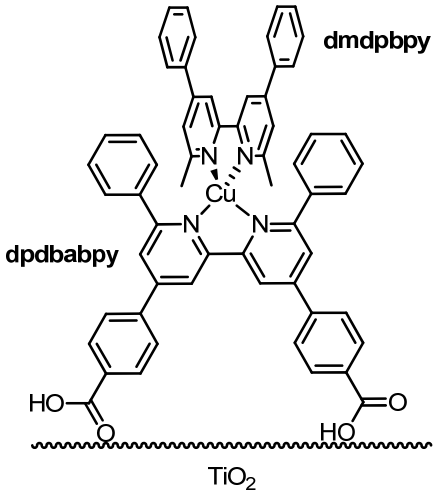


**Figure 1-22** Heteroleptic copper(I)-complex on $TiO_2$ surface; ligands: **dmdpbpy** = 6,6'-dimethyl-4,4'-diphenyl-2,2'-bipyridine, **dpdbabpy** = 6,6'-diphenyl-4,4'-dibenzoic acid-2,2'-bipyridine.

These findings should be confirmed, namely the reproducibility of the exchange reaction on the titania surface should be established and the family of heteroleptic copper(I) complexes should be enlarged. Several asymmetric bpy ligands were synthesized, their corresponding $[Cu(NN)_2]^+$ prepared and tested in DSCs. The results will be presented in section 4.1.3.

### 1.3.4 Iridium

Iridium is the heaviest metal in group 9. It is quite rare and its natural occurrence is $10^{-7}$ % in the earth crust. It is rarer than, for example, Ru ($10^{-6}$ %) or Au ($4x10^{-7}$ %) which makes it quite expensive. This and the fact that the polypyridine complexes were elusive for long time to chemists, made them less attractive and less investigated than the analogous Ru or Os compounds. An appealing characteristic is the longlived excited state of Ir(III) complexes, which originate from MLCT- and LC-transitions and strong spin-orbit coupling allows for

intersystem crossing to energetically similar triplet states which permit the formation of emissive, mixed (triplet) excited states.[39]

#### 1.3.4.1 Ir(III) coordination centre

The Ir(III) cation is a $5d^6$ centre and the electronic properties of its polypyridine complexes are very similar to those of other well-known octahedral complexes, e.g**,** Ru(II) ($4d^6$), Os(II), and Re(I) (latter both $5d^6$).[52] The situation concerning orbital and state energies for electronic transitions is similar for all $d^6$ metals and was already explained before (see section 1.3.1). The only exception is that due to relativistic effects the heavy Ir exhibits strong spin-orbit coupling. This can be expressed with the spin-orbit coupling constants of the metal centres ($\zeta$ = 431 (Fe), 1042 (Ru), 3381 (Os), 3909 (Ir) $cm^{-1}$) and facilitates inter system crossing from singlet to triplet states, the latter being phosphorescent. The outstanding emissive properties and the tunability of the emission wavelength make Iridium complexes attractive for light emitting devices.

#### 1.3.4.2 Light Emitting Electrochemical Cells (LECs)

Conventional inorganic light emitting devices (LED) consist of doped semiconductor materials resulting in a p-n junction. The current can flow easily from the anode (p-side) to cathode (n-side), but not in the opposite direction. Charge-carriers, electrons and holes have different potentials. When an electron meets a hole, it falls into a lower energy level yielding an energy release in the form of a photon (see Figure 1-23).

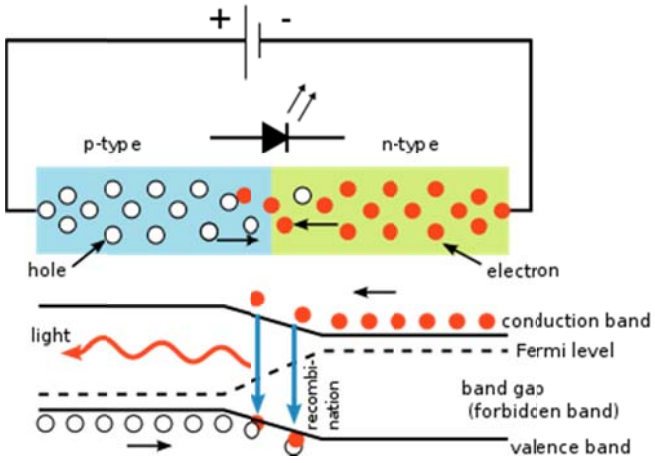


**Figure 1-23** Schematic representation of a LED.

The wavelength of the emitted photon depends on the band gap between the materials forming the p-n junction. Suitable materials for LEDs have a direct band gap with energies corresponding to near-infrared (NIR), visible, or near-ultraviolet light. The first devices were made with gallium arsenide with emissions in the NIR and red region of visible light.

Compared to conventional inorganic LEDs, the ones using organic semiconductors show some advantages such as processability (e.g., thin films), transparency, and the potential for lower-cost and large-area devices. Thus, they are becoming an alternative to established inorganic technology as their efficiencies and stabilities have improved dramatically over the last years.[53] Unfortunately, there are some drawbacks. Todays stable and efficient organic light-emitting devices (OLEDs) consist of a multi-stack of small molecular-weight materials or polymeric materials (PLEDs), respectively, that need air-sensitive injection layers or metals for efficient electron injection. The preparation of these devices requires high vacuum conditions and then rigorous encapsulation to avoid degradation of the electron-injecting layers. A different type of electroluminescent device is the LEC, which displays a much more straightforward architecture and does not depend on air-sensitive materials for electron injection. This simplifies their preparation and makes them more cost efficient than OLEDs. A comparative picture of both devices is shown in Figure 1-24.

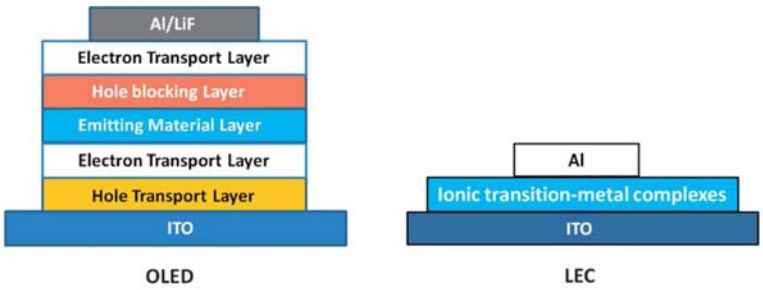


**Figure 1-24** Simplistic scheme of device architectures for OLED (left) and LEC (right).[54]

In its simplest form, a LEC consists of a single active layer composed of an ionic transition-metal complex (iTMC) sandwiched between two electrodes. The mobile ions enable the formation of ionic junctions which lower the barrier for electron and hole injection, which makes these devices independent of the work function of the electrode. In this research $[Ru(bpy)_3]^{2+}$ has been widely studied but mainly as a model compound. Earth abundant metals, such as Cu are also under investigation. Due to the reasons explained above Ir(III) complexes are much more favoured. A wide variety of colours, and efficiencies as high as 36 lm $W^{-1}$ have been reported for iridium(III) iTMCs.[55] For practical application, however, there is still one important obstacle, their very low lifetimes (minutes to a few days).[56] The low lifetimes of iTMC-based electroluminescent devices have been related to the intrinsic instability of the iTMC under working conditions, mainly due to participation of water molecules which destroy the active complexes. The use of more hydrophobic complexes significantly increased the device lifetime.[57]

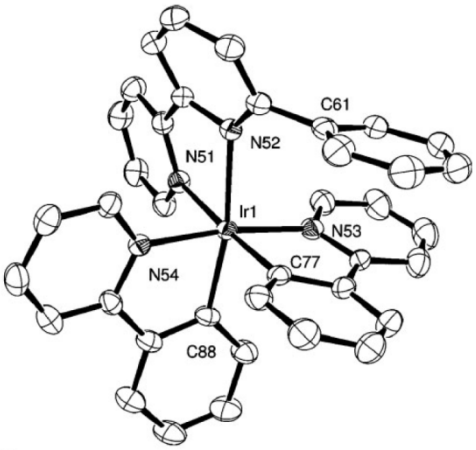


**Figure 1-25** Solid state structure of $[Ir(ppy)_2(\mathbf{pbpy})]^+$; ligands: ppy = 2-phenyl-pyridine, pbpy = 6'-phenyl-2,2'-bipyridine.

Another solution to this problem is the use of π-π-interactions, which are known to have an influence on the photophysical properties of iTMC.[58] Two former members of our group were able to develop a supramolecularly caged ionic iridium(III) complex $[Ir(ppy)_2(\mathbf{pbpy})][PF_6]$ (see Figure 1-25). The lifetime of a simple electroluminescent device was more than 3000 hours at an average luminance of 200 cd $m^{-2}$ while operating at a driving voltage of 3 V, which was a huge improvement compared to the parent complex $[Ir(ppy)_2(bpy)][PF_6]$ without a phenyl group on the bpy ligand. Furthermore, the device turn-on time was of a few seconds and the device was suitable for first applications. Following these findings, the substituents of **pbpy** should be altered, to see if the lifetimes could be further improved or/and the emission wavelengths changed. These results will be explained in section 5.1.3.

# Chapter 2

# 2 Objectives of this work

The work for this PhD consists of two major projects: LECs and DSCs. The initial aim of the former project was the synthesis of 6'-thienyl-2,2'-bipyridine (L) as a ligand for the iridium(III) complex $[Ir(ppy)_2(L)][PF_6]$. A homologue complex where L = 6'-phenyl-2,2'-bpy showed promising results for LEC devises in terms of stability. The question was whether the incorporation of a heteroaromatic substituent could improve other properties, such as emission wavelength for example, while the device stability is maintained. To enlarge the scope, the synthesis of homolog bpy ligands with different hetero atoms in the substituent was envisioned.

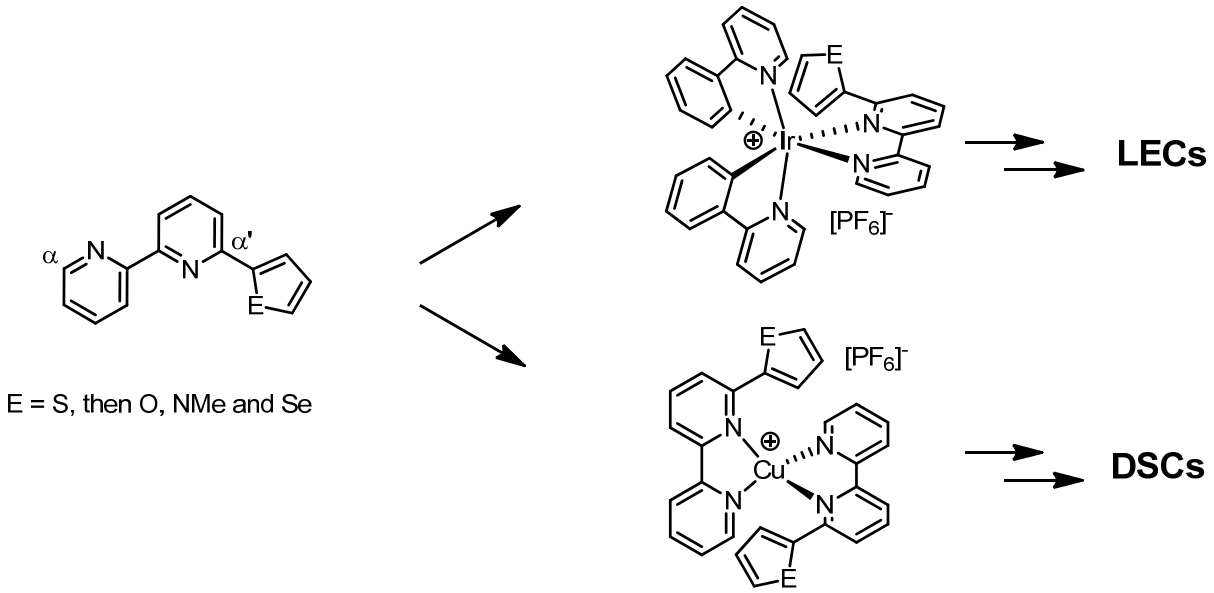


**Figure 2-1** Choice of ligands and target molecules.

The idea behind the latter project is a relatively simple one. In the field of photovoltaic devices, the concept of dye sensitized solar cells evolved very much in the past two decades. When this work was started, the best dye was still a ruthenium(II) polypyridine complex which reaches efficiencies above 11 %. Even though the amount of dye needed for one device is very low, once mass production was carried out, there would be a vast demand for the precious metal and the costs for these devices would be quite high. Therefore, among a few others, the group of Profs. Constable/Housecroft searches for earth abundant metal derivatives. It has been established that copper(I) bpy complexes exhibit similar photophysical properties to those of ruthenium(II). Copper is earth abundant and even though its price has increased in the past decade due to higher demand, it is still much cheaper than ruthenium. Since copper(I) is labile towards oxidation to copper(II), at least one substituent in an α position of the bpy ligand is necessary in order to diminish nucleophilic attack of $H_2O$ or solvent molecules. This fact is somewhat unfortunate because it makes the use of ligands developed for ruthenium(II) complexes, unusable. New ligands

for copper(I) complexes have to be designed and synthesized. Heteroleptic copper(I) complexes are better suited for this application but are more difficult to isolate. In a previous work, Ana Hernandez Redondo first investigated homoleptic copper(I) complexes with carboxylic acid containing bpy ligands which did not yield satisfying results. Later, she was able to establish the preparation of heteroleptic copper(I) complexes directly on the surface of the $TiO_2$ semiconductor *via* a ligand exchange reaction. With this method, it was possible to prepare a DSC device which achieved a conversion efficiency above 1 % (Figure 2-2) which was a tremendous improvement compared to the use of homoleptic copper(I) complexes.

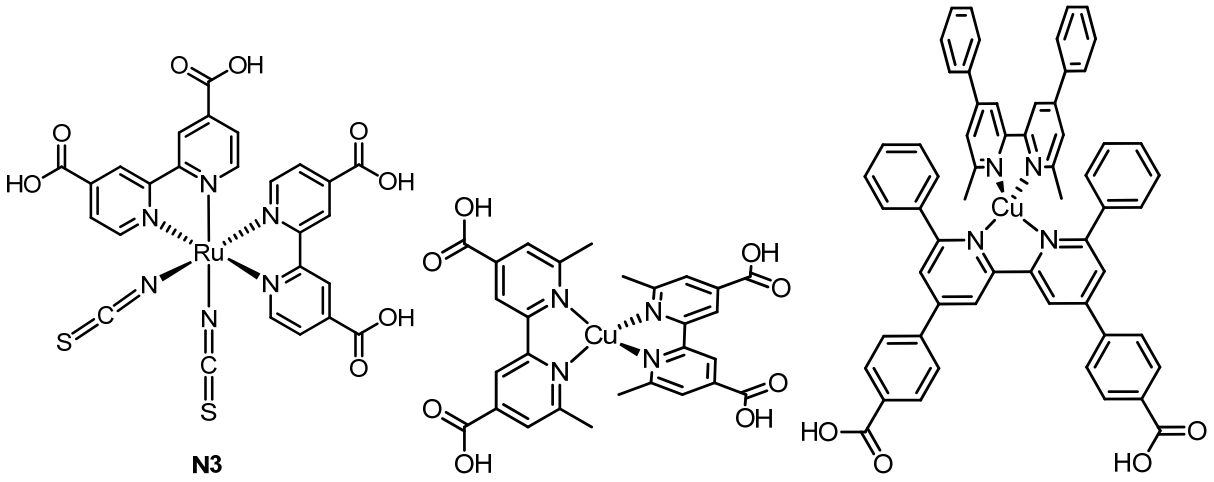


**Figure 2-2** Dyes for DSCs: (left) best ruthenium(II) dye; evolution of copper dyes in Constable/Housecroft laboratory: (middle) homoleptic copper(I) dye; (right) heteroleptic copper(I) dye.

One aim of this thesis was to prepare 6'-R-bpy ligands where R is a (hetero) aromatic ring and see whether this functionalization makes the copper(I) dye molecules stable enough or even could improve the efficiency of the DSCs. Further demand on the bpy ligands is a simple synthesis which allows for an easy access if possible in high yield and without the need of inert atmosphere condition. This should then be followed by the preparation of DSCs devices and evaluation of their results. The effects of different substituents in the α-position should be investigated and the possible substitution in other positions envisioned.

After a diploma thesis in the field of pure inorganic chemistry, the objectives of the practical work included improvement of organic synthetic skills, as well as, the preparation of coordination compounds. The enlargement of analytical skills includes techniques such as: UV/vis and emission spectroscopy, electrochemistry and NMR. The knowledge of the corresponding software should be acquired as well.

Additionally, the work included the supervision of student's practical courses in the first and second semester, as well as supervision of Masters and project students, which helped to develop teaching skills, assertivenes and to repeat some basic chemical knowledge.

Since the work was carried out in an English speaking group, oral language knowledge would be improved along with writing skills.

The main goal was to reach the maturity of an independent researcher.

# Chapter 3

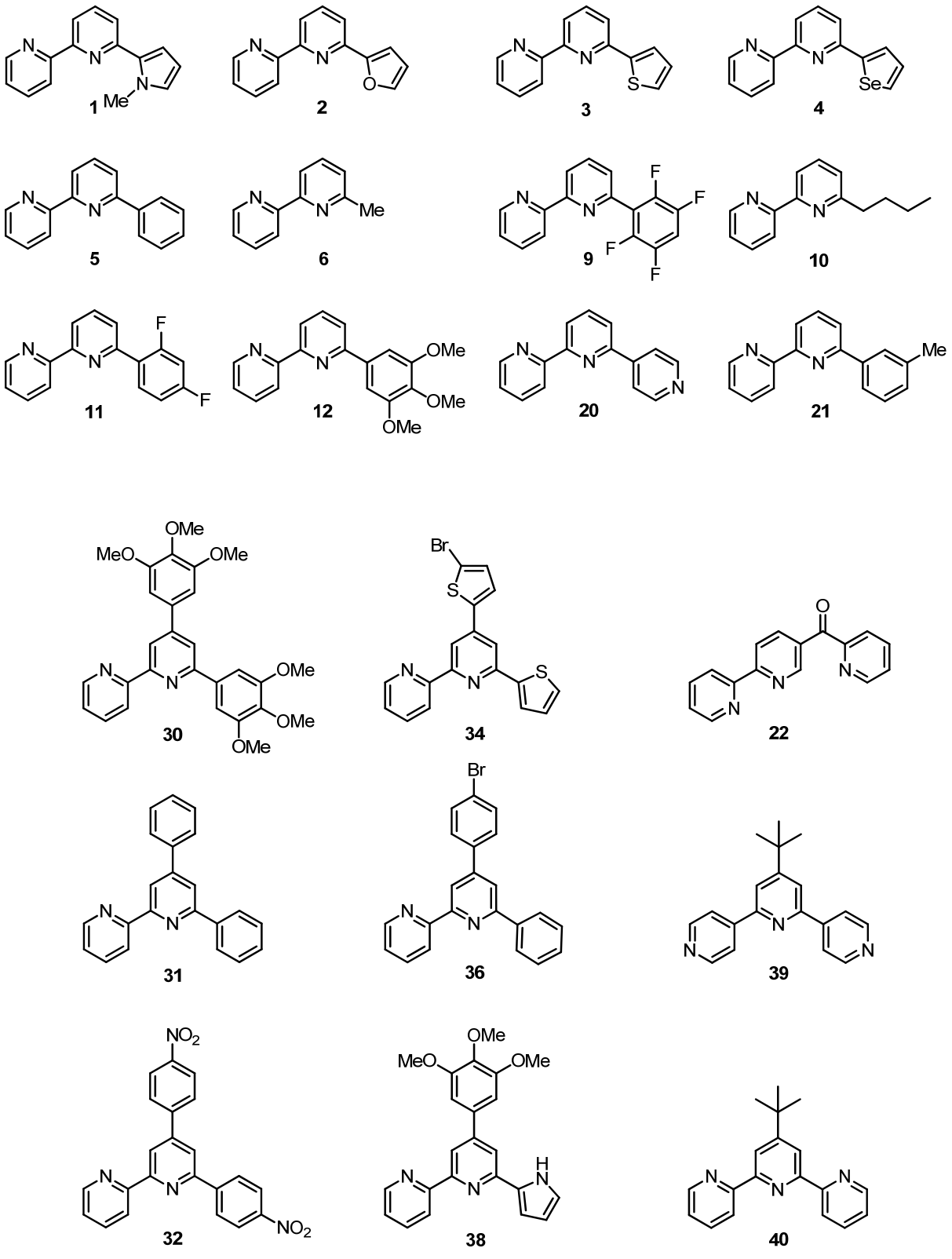


**Figure 2-3** Overview of relevant ligands

# 3 Polypyridine Ligands

An overview of all relevant ligands is given in **Figure 2-3** (see page 32) before this chapter. For more convenient reading it is possible to pull the leaflet out.

## 3.1 Target Molecules

The starting point for this work was the preparation of 6'-thiophen-2-yl-2,2'-bipyridine (**3**), (Figure 3-1). The particular interest for this ligand has been explained in detail, see section 1.1. It has been prepared previously by various groups, including the CONSTABLE group, and has been studied as a chelating ligand mainly for ruthenium(II) complexes.

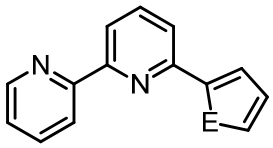


E = NMe (**1**), O (**2**), S (**3**), Se (**4**)

**Figure 3-1** Envisioned ligands.

Furthermore, the analogous ligand **2** bearing a furan substituent has been studied only little and to the best of our knowledge, ligands 6'-(*N*-methylpyrrol-2-yl)-2,2'-bipyridine (**1**) and 6'-(selenophen-2-yl)-2,2'-bipyridine (**4**) had not been reported at all. The idea behind the preparation of this series was to investigate whether the substitution of the hetero atom in the five membered rings has an influence on the properties of the ligands and their metal complexes.

In the course of this work the need for bpy ligands with different substituents evolved which led to the introduction of alkyl substituents (methyl and *n*-butyl) as well as aromatic substituents bearing further functional groups changing their electronic properties or the symmetry (see Figure 3-2).

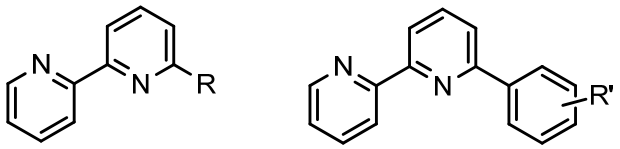


R = Me, *n*-Bu  R = H, OMe, Me, F, ect.

**Figure 3-2** Further target molecules.

Their preparation and properties will be described in the following sections.

## 3.2 Results and Discussion

### 3.2.1 Synthesis

#### 3.2.1.1 Ligand 2 *via* KRÖHNKE synthesis

Ligand **2** has been prepared by a standard procedure, following the KRÖHNKE methodology, (Scheme 3-1). As mentioned in the previous section, to obtain 2,6-substituted pyridines, the precursor for the reaction has to be a MANNICH base, in this case the 1-(furan-2-yl)-3-*N*,*N*-dimethylamin-propan-1-one (**7**). This has been prepared by reacting 1-(furan-2-yl)-ethan-1-one with an excess of paraformaldehyde and *N*,*N*-dimethylamine hydrochloride and catalytic amounts of hydrochloric acid in refluxing ethanol or it can also be carried out under microwave conditions (reaction path a, Scheme 3-1). The product can be precipitated with acetone and usually used without further purification in the next step. The second precursor, the KRÖHNKE salt 1-(2-oxo-2-(pyridin-2-yl)ethyl)pyridin-1-ium iodide (**8**) can be prepared *via* an ORTHOLEVA-KING reaction (pathway b, Scheme 3-1).[59] Herein, the 2-acetylpyridine reacts directly with iodine and pyridine to give **8**.

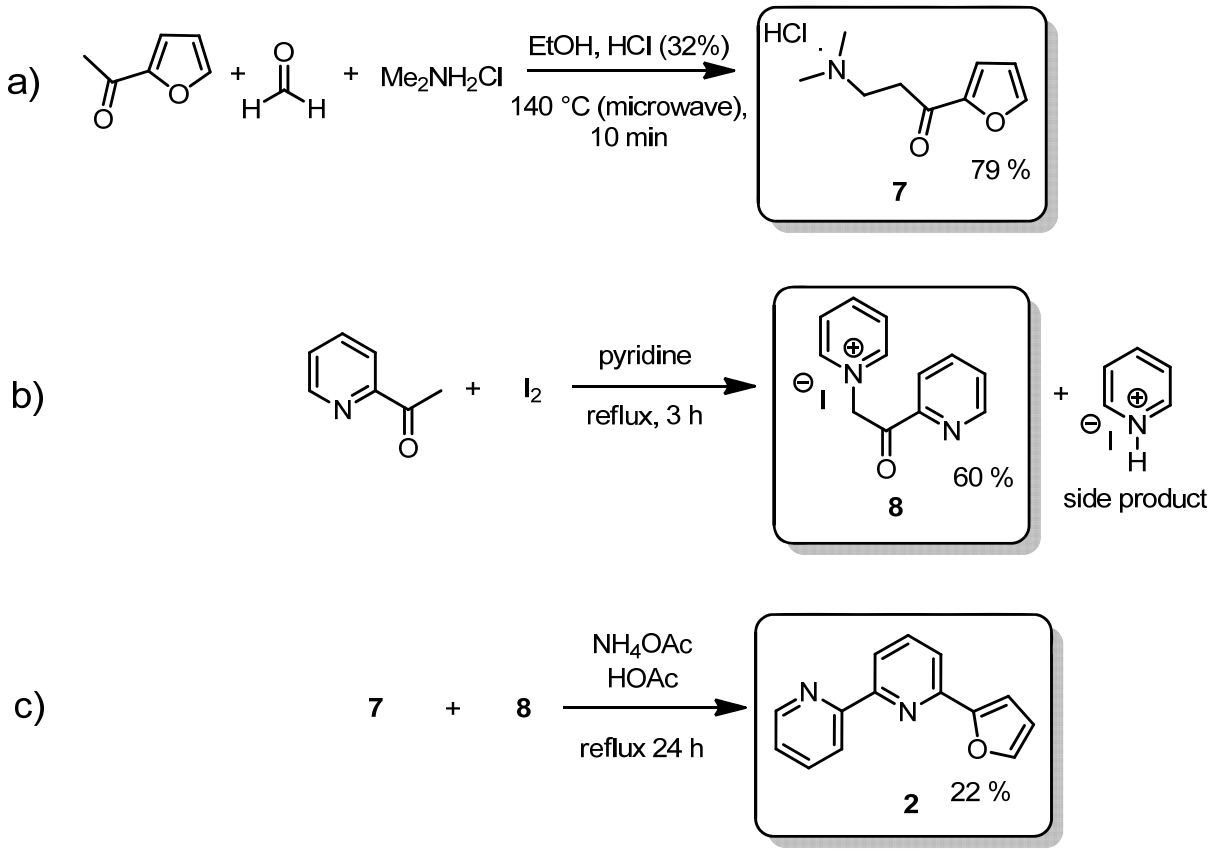


**Scheme 3-1** Preparation of ligand **2** *via* KRÖHNKE methodology.

There are some crucial tricks which improve the yield tremendously which are usually not mentioned in the literature. The iodine has to be dissolved in warm pyridine prior to use, to avoid the formation of unfavoured triiodide salts. Secondly, prolonged reaction times do not

necessarily improve the yields; rather the opposite is the case. As mostly, reactions involving a pyridine moiety behave slightly different and/or cause troubles. In the case of **8**, rather shorter reaction time is advantageous (< 3 h), otherwise the separation from the side product and purification become difficult. With both starting materials at hand the KRÖHNKE reaction was carried out which gave the desired product with a yield of only 22 % (pathway c, Scheme 3-1). The overall yield after three steps is then 10 % and comparable to the one pot synthesis *via* direct coupling, see next section. This method requires the preparation of two starting materials, since they are not commercially available and with the final reaction it consists of three steps, which can be time consuming. Depending on experience of the chemist it can take up to two weeks to obtain the final product. Thus, a shorter, easier and cheaper method would be desirable.

### 3.2.1.2 Preparation by direct lithiation reactions

The synthesis of the other ligands with hetero aromatic substituents was attempted by the direct coupling of bpy with an organolithium reagent. Methyl lithium and phenyl lithium are commercially available and the preparation of the ligands 6'-phenyl-2,2'-bipyridine (**5**) and 6'-methyl-2,2'-bipyridine (**6**) could be reproduced without any difficulties and in good yields, 60-80 % (Scheme 3-2).[25,60]

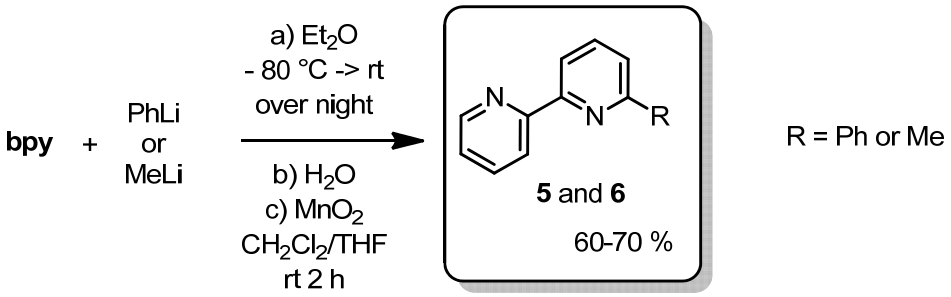


**Scheme 3-2** Direct coupling with PhLi and MeLi.

While 2-thienyl lithium is commercially available from conventional suppliers, the *N*-methyl-pyrrole derivative can be purchased only from specialized manufacturer and 2-selenoyl-derivative cannot be bought at all. Therefore, these precursors were prepared *in situ*. Usually, the corresponding hetero aromatic compound was diluted in tetrahydrofuran at low temperature, then a slight excess of *n*-butyl lithium was added. After one hour the bpy was added directly in one portion and the reaction mixture was allowed to slowly warm up to ambient temperature and then stirred for additional 10-12 h, usually overnight. The reaction was then quenched with water followed by a rearomatization with $MnO_2$ (Scheme 3-3). The yields turned out to be modest but considering the time saving and the cheap starting materials they are acceptable. It is possible that the first step of the reaction, the lithiation of the hetero aromatic ring, is the limiting factor in the sequence. Since the yield of

the intermediate has not been determined and unreacted bpy could always have been recovered the real conversion rates are a bit higher. This type of reaction could be applied successfully to a small series to obtain ligands **1**, **3** and **4**. The reaction has not been optimized since it yielded enough material to proceed with following complexation reactions.

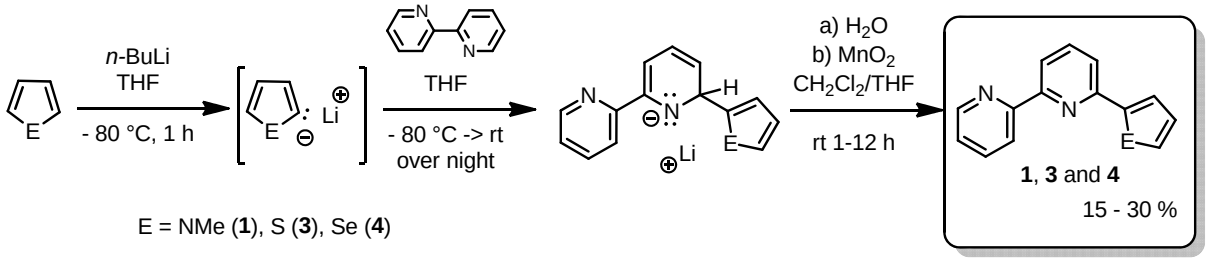


**Scheme 3-3** Synthesis of **1**, **3** and **4** *via* direct coupling with Li-organyls

This method of the direct coupling has been attempted for other substrates as well, unfortunately with not much success.

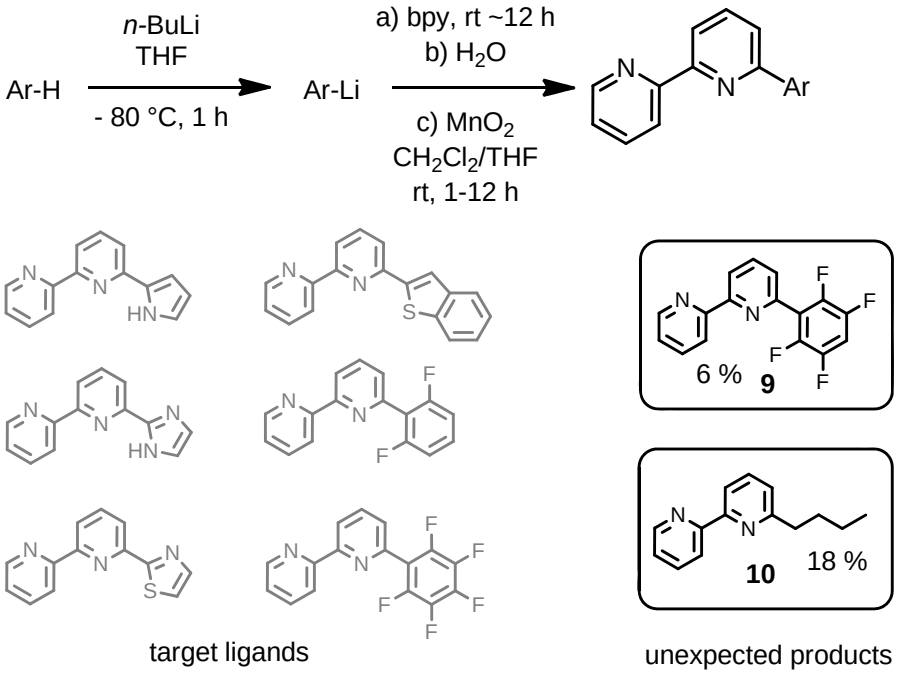


**Scheme 3-4** Unsuccessful direct coupling *via* Li-organyls (ligands **9** and **10** as unexpected products).

Various aromatic compounds have been used for this reaction such as pyrrole, imidazole, benzo[b]thiophene, 1,3-difluorobenzene and 1,2,3,4,5-pentafluorobenzene but in each case, no desired product could be obtained. Only the reaction with pentafluorobenzene yielded some useful material in a poor yield and not the expected product. The lithiation of the starting material proceeded only under the elimination of LiF and the resulting lithiated compound is probably quite stable and less reactive than the hetero aromatic homologues. The isolated product was to our surprise the 6'-(2,3,5,6-tetrafluorophenyl)-2,2'-bipyridine (**9**). Another unexpected product was obtained when attempted to lithiate thiazole. Under

the standard conditions the lithiation does not proceed fast enough or at all since non of the desired product could be isolated, and the reaction mixture contained still enough *n*-BuLi to lithiate the bpy directly. It is even imaginable that the thiazole acts as a promoter. The major product observed was the 6'-*n*-butyl-2,2'-bipyridine (**10**) in a low yield of 18 %. The fact that the reaction with pyrrole was not successful, led to the use of *N*-methylpyrrole for the direct lithiation, see above. These findings confirm the fact, that this method is not versatile, at least not as a one pot reaction. Maybe if the lithiated intermediates would be isolated, the yields might be improved.

#### 3.2.1.3 Exploring the JAHNG reaction

For the investigation of the electronic donating or withdrawing effects, respectively, of functionalized phenyl-bipyridines, it was intended to prepare 6'-(2,4-difluorophenyl)-2,2'-bipyridine (**11**) and 6'-(2,3,4-trismethoxyphenyl)-2,2'-bipyridine (**12**). Since **11** could not be obtained by the direct method it was intended to prepare it via KRÖHNKE methodology. Unfortunately, the preparation of the MANNICH base caused difficulties and could not be obtained under standard procedures. An alternative route was then sought.

The preparation of 2,2':6',2''-terpyridine (tpy) is carried out in our group frequently but it is neither trivial nor possible under KRÖHNKE conditions. The MANNICH base of 2-acetylpyridine (**C**) cannot be easily isolated due to its reactivity towards itself. It undergoes the elimination of dimethylamine and the vinyl ketone reacts then in an intramolecular MICHAEL reaction to give the indolizinol (**D**), which, in the presence of ammonia, reacts further to give the blue azacyanine (**E**), as shown in Scheme 1-1.[61]

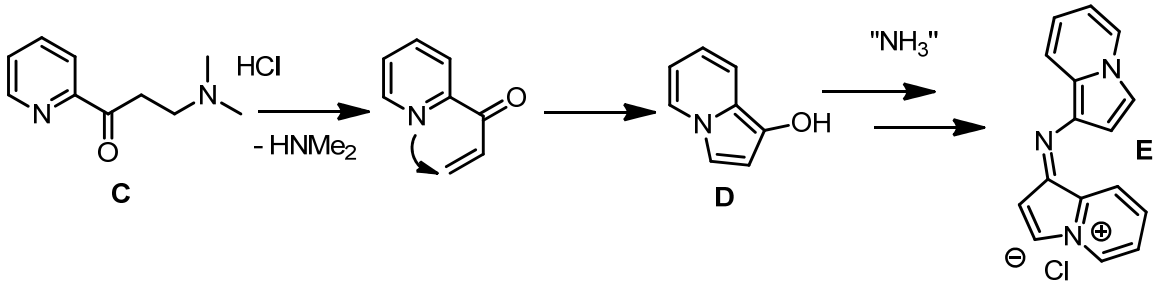


**Scheme 3-5** Auto condensation of 1-(pyrid-2-yl)-3-*N*,*N*-dimethylaminepropan-1-one.

Convenient syntheses have been introduced, first by POTTS *et al*. in 1982 where he prepares the tpy in three steps via the dithioacetal (**F**), followed by a reduction of the resulting 4'-(methylthio)-2,2':6',2''-terpyridine with $NiCl_2/NaBH_4$ to give the desired product in overall yield of 23 %.[62] Nine years later then, JAMESON published an improved synthesis with two steps only and an augmented total yield of 47 %.[63] The intermediate in this method is the enaminone (**13**). (Scheme 3-6)

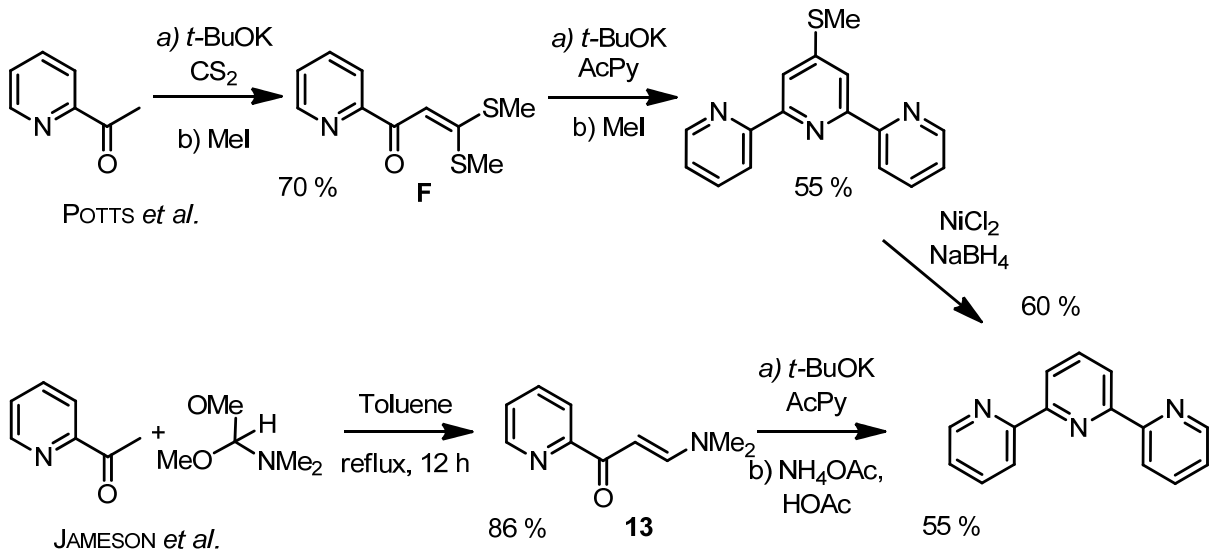


**Scheme 3-6** Comparison of POTTS and JAMESON syntheses of tpy.

Compound **13** can be prepared by reacting 2-acetylpyridine and *N*,*N*-dimethylformamide dimethylacetal (DMF-DMA) in toluene using azeotropic distillation of methanol in the course of 2 to 3 h. The yields are good to excellent between 60 and 95 %.[64] There are many examples of this reaction with various conditions, altering the reagent, solvents or adding a catalyst, etc.[65] However, in our opinion the best conditions reported so far are using aryl ketones with DMF-DMA under microwave irradiation, without any solvent within 10 min at high temperatures. The isolation of the product can sometimes be difficult but the yields are usually very good to excellent. Since the reaction is carried out without any solvent, the scale can be as big as 100-150 mmol and the time saving is quite remarkable. With these reactions at hand it was quite easy to prepare different enaminones within a few days (see Scheme 3-7).

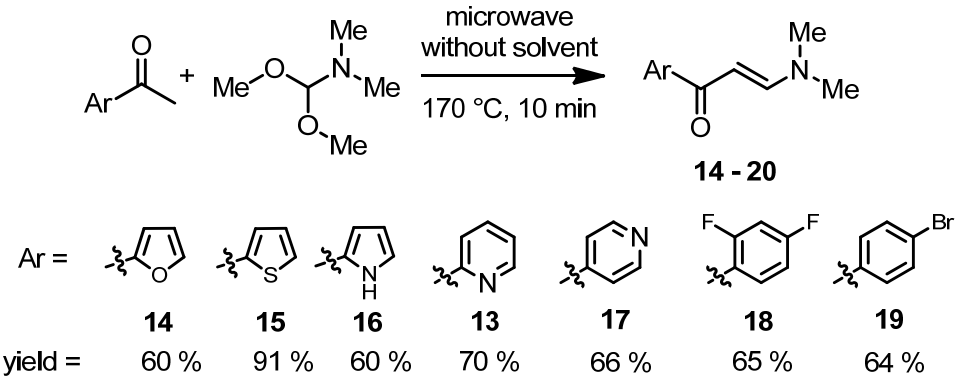


**Scheme 3-7** Microwave assisted preparation of enaminones.

The idea was to introduce these to an altered JAMESON synthesis to obtain bpy ligands, which were not accessible with any other route with fewer steps. It was only later that we discovered that this idea has already been realized by JAHNG and co-workers but luckily enough, only with different substituents.[66] Nevertheless, *via* this method we were able to prepare some new 6'-Ar-2,2'-bipyridine ligands in two steps and for our purposes reasonable

yields. The second step is a multistep and multicomponent reaction consisting of *in situ* preparation of an enolate which reacts then in a MICHAEL condensation with a 1-aryl-3-dimethylamine vinyl ketone followed by an elimination of dimethylamine to give a 1,5-bisarylpentane-1,5-diol. This reacts further upon addition of ammonium acetate in two cascade imine condensations to give the ring closure and a following oxidation yields the desired product, a 2,6-bisaryl-pyridine. This reaction is possible in two ways: either the enaminone of the desired substituent reacts with the enolate of 2-acetylpyridine (pathway **i**, Scheme 3-8) or enaminone **13** reacts with the enol of the aryl ketone (pathway **ii**, Scheme 3-8).

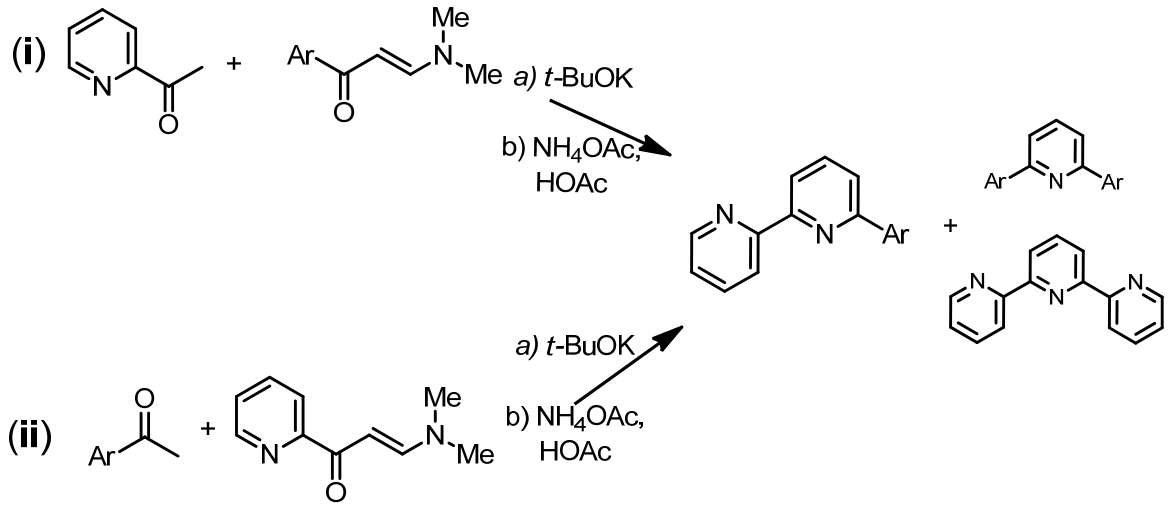


**Scheme 3-8** Pathways of the JAHNG reaction.

A minor disadvantage of this reaction is the reversibility of the MICHAEL addition which causes scrambling of the substituents and besides the desired 6'-Ar-2,2'-bpy also 2,6-bisAr-pyridine and the tpy can be isolated. For example, in the case of ligand **11** (see Scheme 3-9), 2-acetylpyridine is used as C-H active component and 1-(2',4'-difluorophenyl)-3-(*N*,*N*-dimethylamine)-prop-2-ene-1-one (**18**) as MICHAEL acceptor. The desired product was obtained but only in a poor yield of 14 %. The 2,6-bis(2,'4'-difluorophenyl)-pyridine (3 %) could be isolated as a minor side product, and the major product was 2,2':6',2''-terpyridine in 20 % yield or 40 % in relation to 2-acetylpyridine, respectively. Even though, the reaction time was shorter than usual, 30 min for the generation of the enolate instead of 2 h and 1 h for the MICHAEL condensation instead of 14 h, the formation and then decomposition of the 1,5-diketone was very fast, probably due to the activation by means of the electron withdrawing effect of the fluorine substituents on the phenyl ring.

This problem of scrambling during the reaction was not mentioned in the literature before, even though, we used the same conditions, it was never possible to avoid this.[66] For the purpose of our group this inconvenience can be turned into an advantage, since the tpy ligand is needed very often.

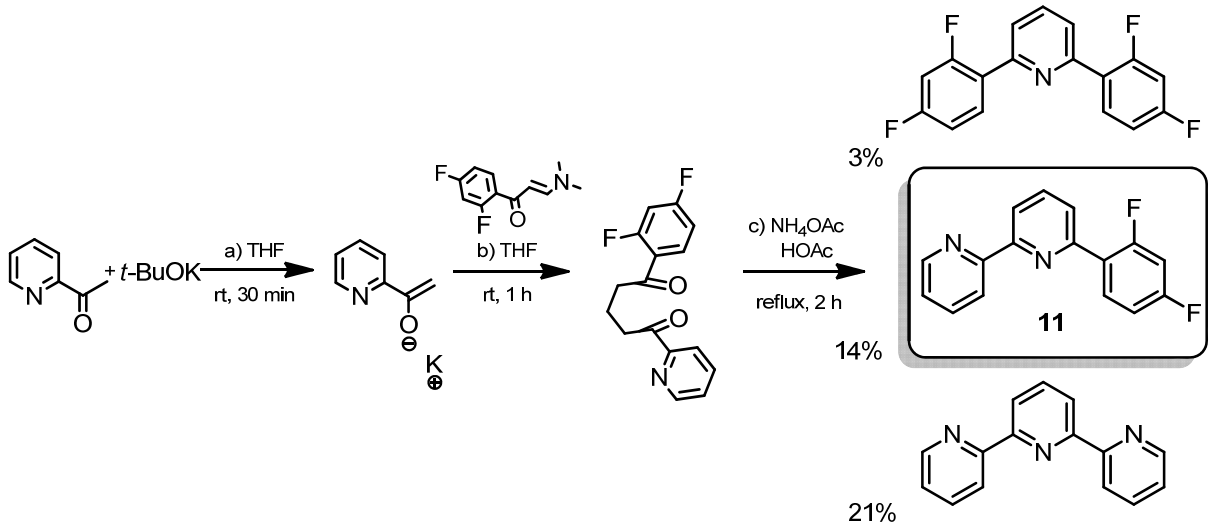


**Scheme 3-9** Preparation of ligand **11** *via* JAHNG reaction.

A few ligands which could not have been synthesized *via* the direct coupling method were then obtained with the JAHNG reaction. The products and their yields are summarized in Table 3-1. The distribution cannot be predicted; nevertheless Table 3-1 suggests that pathway **ii** is preferable if the amount of tpy should be minimal.

| Ar | 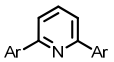 | 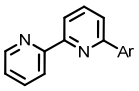 | 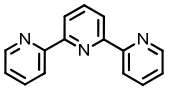 |
|---|---|---|---|
|  | 0% | (**20**) 51% | 20% |
| 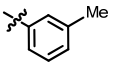 | 4% | (**21**) 45% | 0% |
| 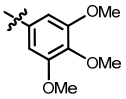 | 4% | (**12**) 14% | 18% |
| 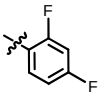 | 3% | (**11**) 14% | 40% |

**Table 3-1** Product distributions and yields for the JAHNG reaction.

If the phenyl substituent of the bpy ligand bears further electron donating as well as withdrawing substituents, which influence the electronic properties dramatically, the yield of the desired product drops below 20 % and the amount of tpy increases. This observation is independent of the reaction path chosen (Scheme 3-8). The formation of the 2,6-disubstituted pyridine is always lower than 5 %. The ligands 6'-(pyrid-4-yl)-2,2'-bipyridine (**20**) and 6'-(*m*-tolyl)-2,2'-bipyridine (**21**) could be obtained in good yields of 51 and 45 %, respectively, and the formation of tpy are low. These values are comparable with the yields reported in the literature before.[66] Maybe this is the reason why the scrambling was not considered.

### 3.2.1.4 Ligand 22 *via* auto condensation of 13

The JAHNG reaction yielded an unexpected product as well. In the two cases where 2-acetyl pyrrole or 1-acetyl imidazole were applied for this reaction no desired product could be obtained. Instead, the 5'-(2-pyridinoyl)-2,2'-bipyridine (**22**) was isolated in low yields (3-10 %, Scheme 3-10).

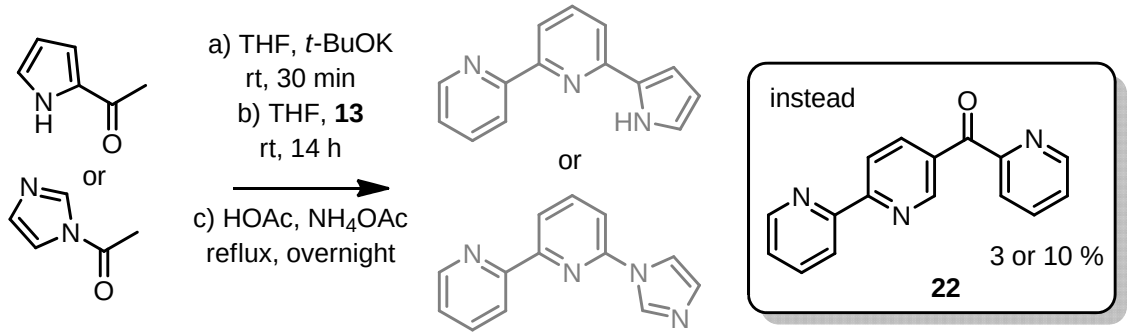


**Scheme 3-10** Unsuccessful JAHNG reactions.

This reaction has been described in the literature before.[67] In the presence of ammonium acetate two equivalents of enaminone (**13**) can condense with each other to give **22**. A possible mechanism could be MICHAEL type reaction of an enamine with **13** followed by an intramolecular imine condensation, as proposed in Scheme 3-11.

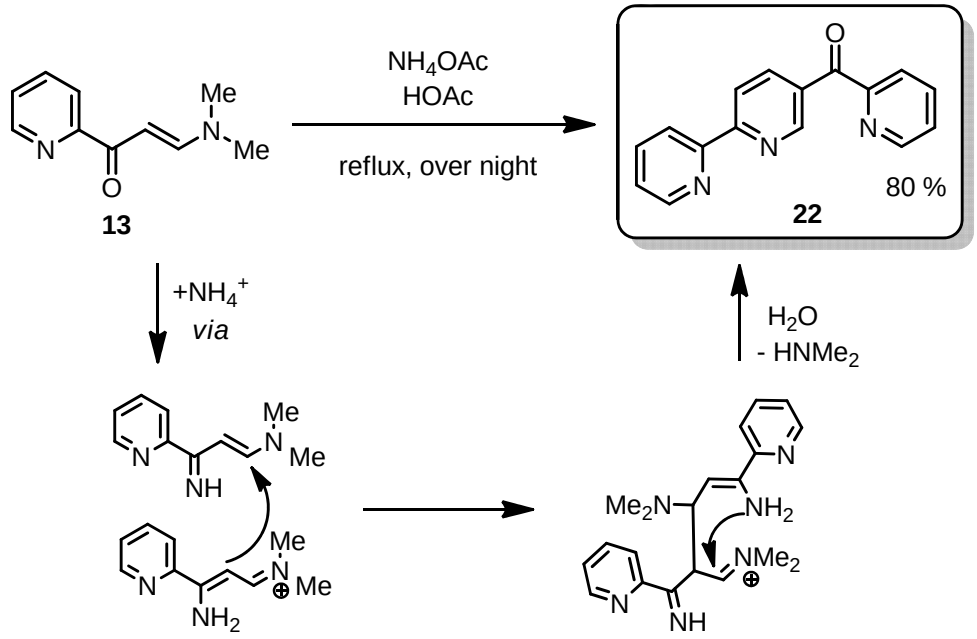


**Scheme 3-11** Preparation of ligand **21**with proposed mechanism.

The procedure could be reproduced without any difficulties and the desired product was obtained in very good yield of 80 %. Even though, this ligand was not intended it presents a very interesting ligand. Its metal complexes were not reported and it should be possible to further functionalize this ligand at the carbonyl function. A few reactions have been carried out and will be presented in section 6.1.

### 3.2.1.5 4',6'-Bis substituted 2,2'-bpy ligands via Kröhnke reaction

In the course of this work, a few bpy ligands with substituents in 6'- as well as 4'-position were also prepared. These ligands were formed by standard KRÖHNKE reactions where a chalcone was reacted with PPI (**8**) and $NH_4OAc$ in ethanol to yield the expected products.

The chalcones for the KRÖHNKE reaction were prepared by standard CLAISEN-SCHMIDT condensation or under slightly modified conditions, respectively (Scheme 3-12).

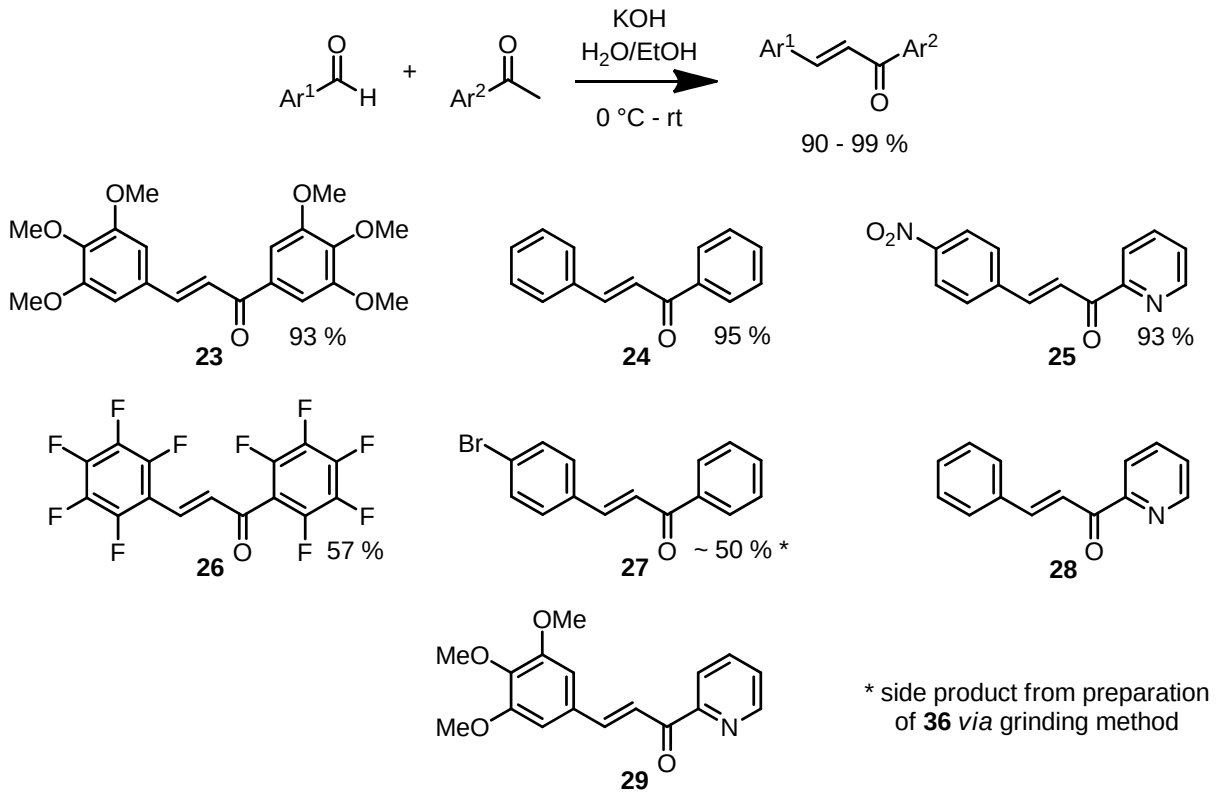


**Scheme 3-12** Preparation of chalcones **23**-**29**.

Chalcone **23** was obtained by reacting 3,4,5-*tris*methoxyacetophenone and 3,4,5-*tris*methoxybenzaldehyde in ethanol/water (1:2) mixture adding potassium hydroxide as base. The water in this mixture lowers the solubility of the product, which leads to its precipitation and draws the reaction equilibrium to the product side. Usually, aldol condensation reactions are quite fast (0.5-1 h) but in this case the electron releasing effect of the three methoxy groups deactivates both the ketone and the aldehyde, so that the reaction time had to be prolonged to 24 h to obtain **23** in 93 % yield. The treatment of **23** with **8** yielded the desired ligand, 4',6'-*bis*(3,4,5-*tris*methoxyphenyl)-2,2'-bipyridine (**30**) in a moderate yield of 56 %, the overall yield being then 31 % after three steps.

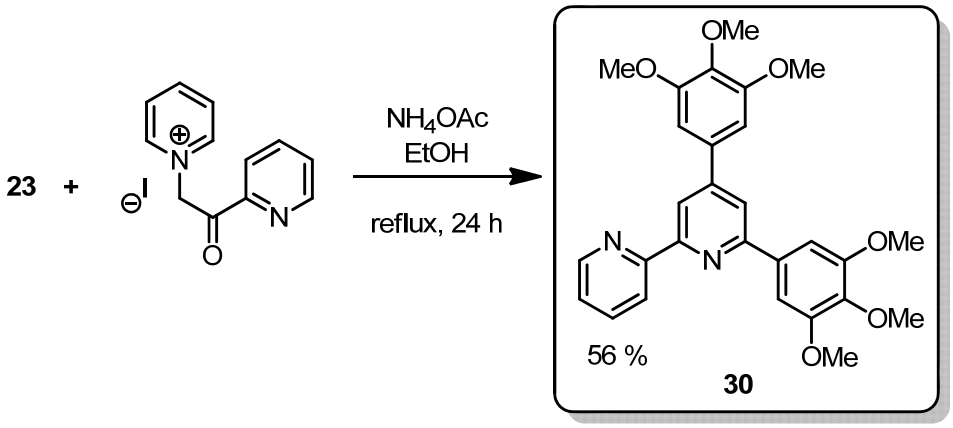


**Scheme 3-13** Synthesis of 4',6'-*bis*(3,4,5-*tris*methoxyphenyl)-2,2'-bipyridine (**30**).

The parent compound, namely the 4',6'-diphenyl-2,2'-bipyridine (**31**) was prepared in the same manner without any drawbacks in a lower yield of 38 % and an overall yield of 22 %. More problematic was the preparation of a chalcone with electron withdrawing substituents. The 1,3-bis(2',3',4',5',6'-pentafluorophenyl)-prop-2-ene-1-one **26** could be prepared under standard conditions but even though a longer reaction time (16 h) was applied, the product could be isolated in only moderate 57 % yield (Scheme 3-14). Unfortunately, the KRÖHNKE reaction with **26** was unsuccessful very likely due to the easy substitution of the fluorine in the 4'-position even with mild nucleophiles, such as ethanol.[68] This might explain also the somewhat lower yield of the previous aldol condensation (Scheme 3-14).

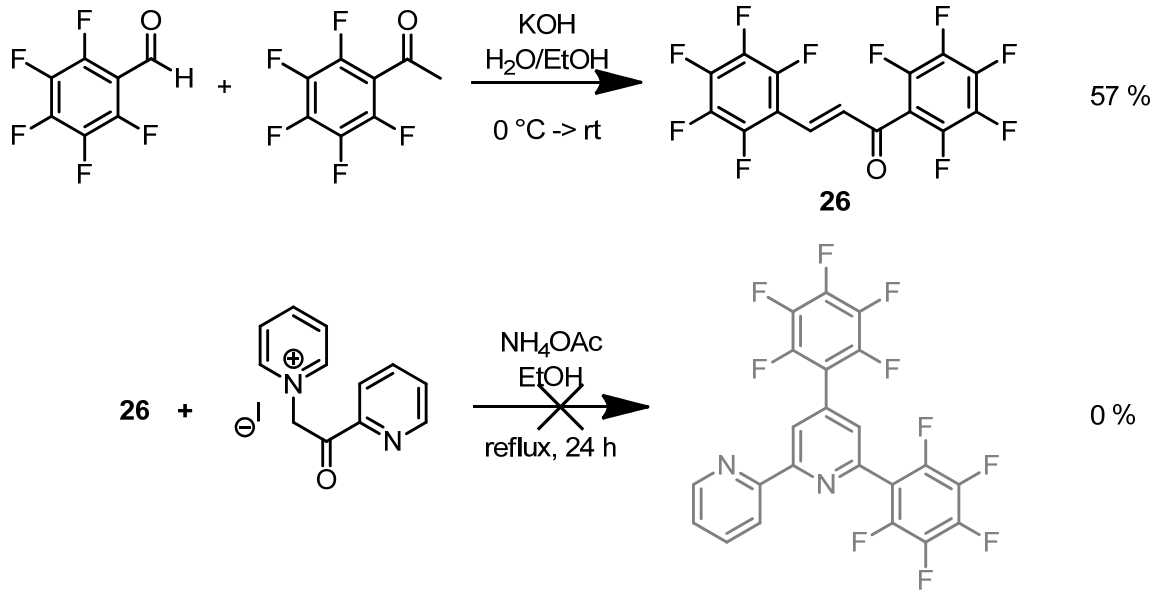


**Scheme 3-14** Synthetic approach to 4',6'-*bis*(2,3,4,5,6-pentafluorophenyl)-2,2'-bipyridine.

Alternatively, 1,3-*bis*(4'-nitrophenyl)-prop-2-ene-1-one (**G**, Scheme 3-15) was targeted but all attempts failed. The ketone is very reactive and the in situ prepared enol reacted with itself, yielding a black tar, or if the aldehyde was present, the product of a tandem aldol condensation – MICHAEL addition, the 1,3,5-*tris*(*p*-nitrophenyl)-pentane-1,5-dione (**H**) was

isolated. Tests of different reaction conditions, i.e. different temperatures and slow addition of the enolate to the aldehyde or using solid alox as mild base, were all unsuccessful (Scheme 3-15).[69,70]

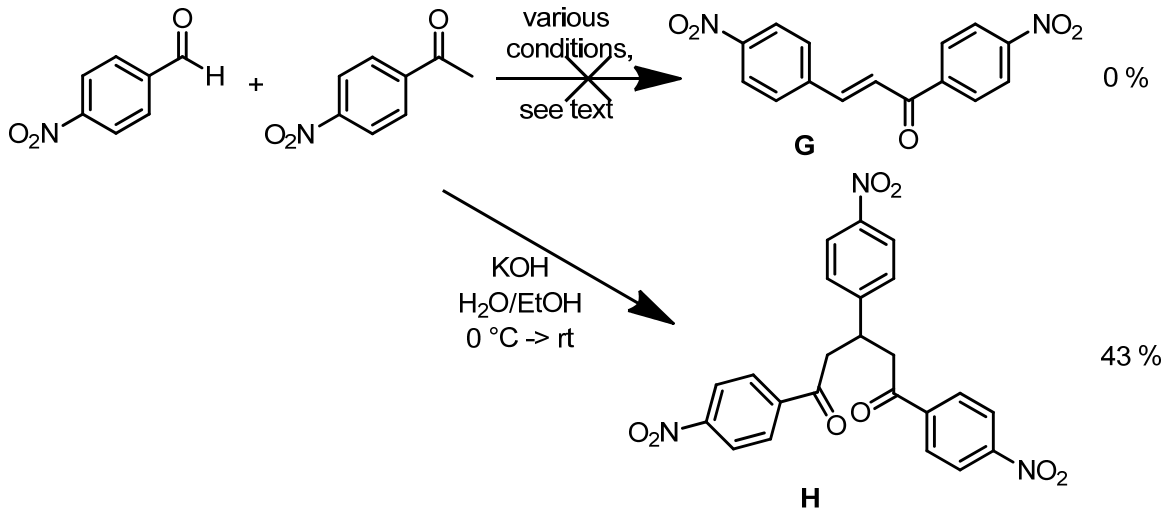


**Scheme 3-15** Synthetic approach to 4',6'-*bis*(*p*-nitrophenyl)-2,2'-bipyridine.

Eventually, it was possible to isolate the 1-(pyrid-2-yl)-3-(4'-nitrophenyl)-prop-2-ene-1-one (**25**) using anhydrous conditions. The enolate of 2-acetylpyridine was prepared using one fold excess of potassium *tert*-butoxide as base and was added slowly to a tetrahydrofuran solution of *p*-nitrobenzaldehyde. The desired product precipitated immediately. After filtration and washing with water, **25** was obtained in an excellent yield of 98 %. To prepare ligand **32** *via* the KRÖHNKE reaction, the pyridinium salt of *p*-nitroacetophenone had to be synthesized. This was achieved by the ORTOLEVA-KING reaction, by treatment of the ketone with iodine in pyridine as solvent for 3 h at reflux to give **33** in a good yield of 81 %. Ligand **32** was then prepared by a slightly modified KRÖHNKE synthesis reacting chalcone **25** and pyridinium salt **33** in ethanol at reflux for 24 h. The desired product was obtained in a good yield of 65 % This ligand was reported very recently by KOOHMAREH and coworker.[71] They claim to have prepared the 1,3-bis(*p*-nitrophenyl)-prop-2-en-1-one under standard conditions for CLAISEN-SCHMIDT condensations. However, this was impossible to reproduce, very likely due to the high reactivity of *p*-nitroacetophenone **J** (see above). The overall yield improved to 51 % compared to 27 % being reported before. The characterization of the product of KOOMAREH was poor and not convincing and ligand **32** could not be found elsewhere in the literature.

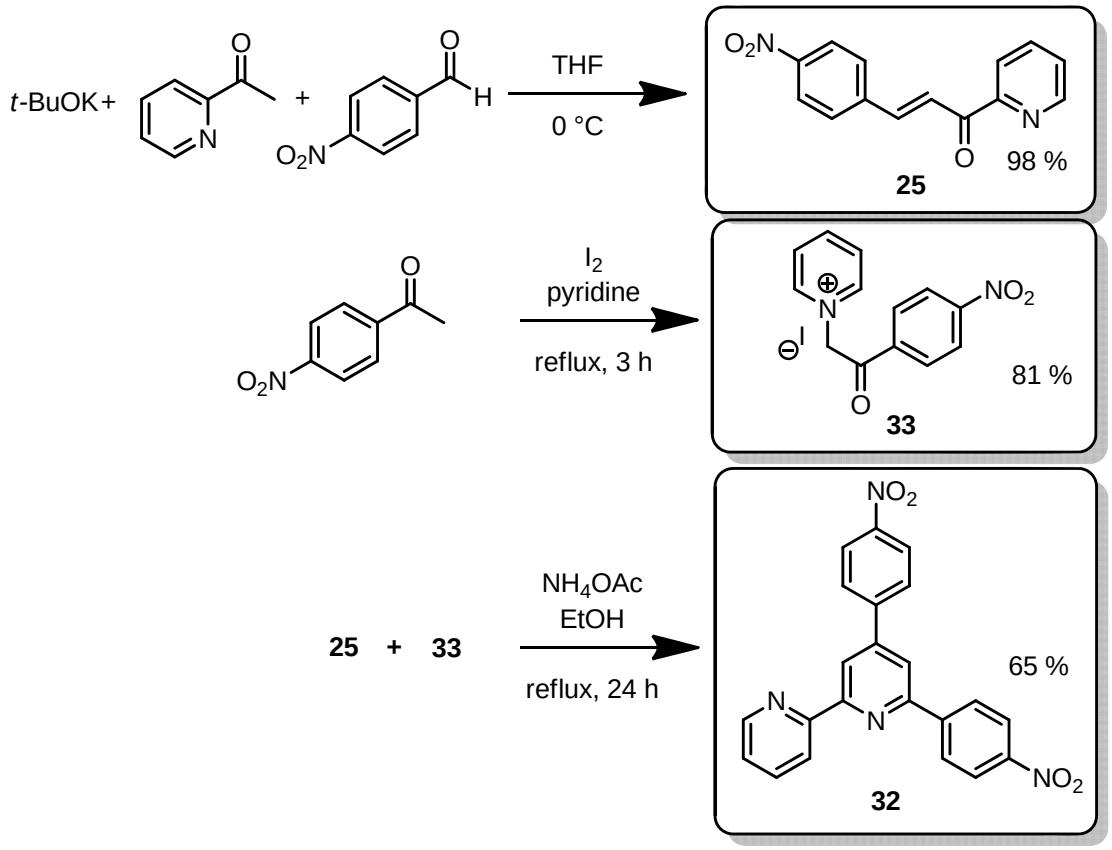


**Scheme 3-16** Synthesis of 4',6'-bis(*p*-nitrophenyl)-2,2'-bipyridine.

Two further ligands were prepared bearing a bromine function in order to allow the possibility of further substitution of these ligands. Ligand **34** 4'-(4-bromothiophen-2-yl)-6'-(thiophen-2-yl)-2,2'-bipyridine was prepared under standard Kröhnke conditions from chalcone **28** and the pyridinium salt of 2-acetylthiophene (**35**, **TPI**) to give the desired product in 43 %.

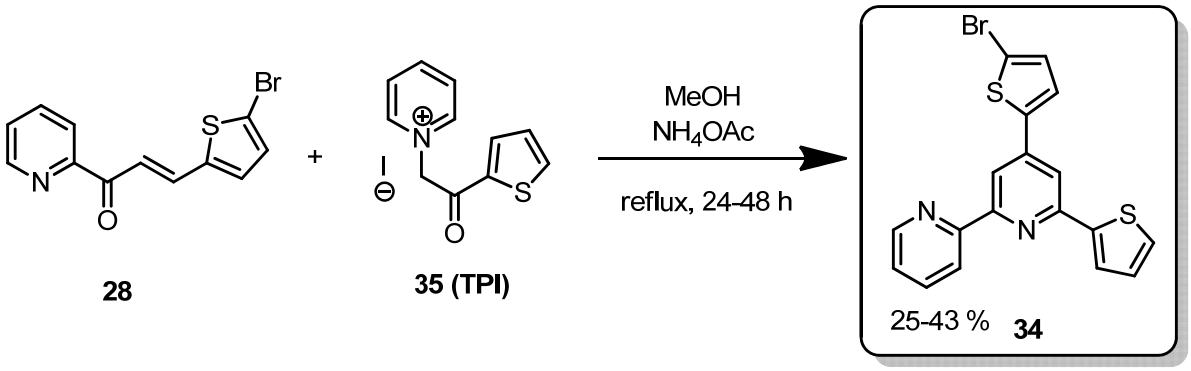


**Scheme 3-17** Synthesis of 4'-(4-bromothiophen-2-yl)-6'-(thiophen-2-yl)-2,2'-bipyridine (**34**).

Ligand **36** 4'-(4-bromophenyl)-6'-(phenyl)-2,2'-bipyridine was obtained using the "grinding" method.[72] One equivalent of each of acetophenone and 4-bromobenzaldehyde, and two equivalents of sodium hydroxide were combined using a mortar and pestle until a yellow powder formed (ca. 10 min). Then one equivalent of each 2-acetylpyridine and sodium hydroxide were added and ground for a further 10 minutes The powder was transferred to a

suspension of ammonium acetate in glacial acetic acid and heated to reflux for 2 h, then continued to stir at room temperature over the weekend. The crude product was precipitated with addition of water and was purified by column chromatography. This reaction was carried out as a test reaction and the grinding was not performed very thoroughly and was applied for short times only, which explains the low yield of 10 %.

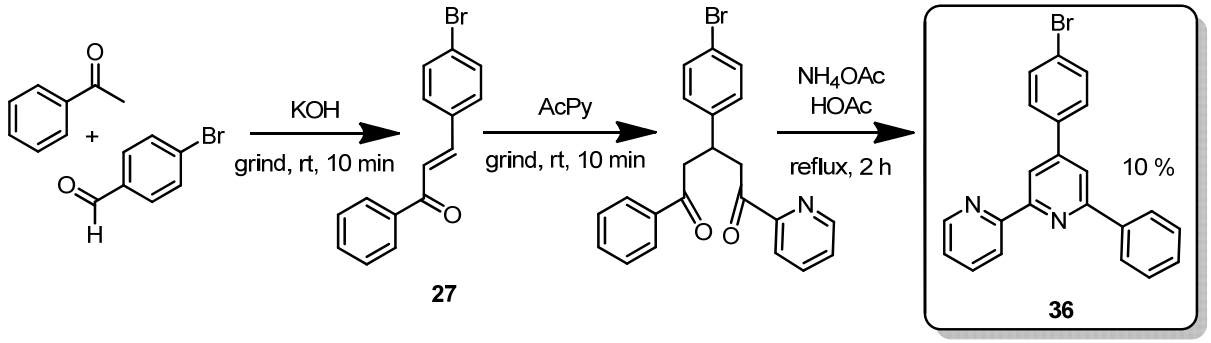


**Scheme 3-18** Synthesis of 4'-(4-bromophenyl)-6'-phenyl-2,2'-bipyridine (**36**).

Ligand **34** was prepared with the intention of further functionalization on the backbone of this ligand, meaning coupling *via*, e.g, HARTWIG-BUCHWALD reaction with various amines, such as carbazole (**I**), thiophenazine (**J**) or 2,5-bis(thiophen-2-yl)-pyrrole (**K**) to introduce chromophores or antennae, respectively, which might have been useful for copper(I) complexes and their applications in DSCs (Scheme 3-19) by enhancing the absorptive properties.

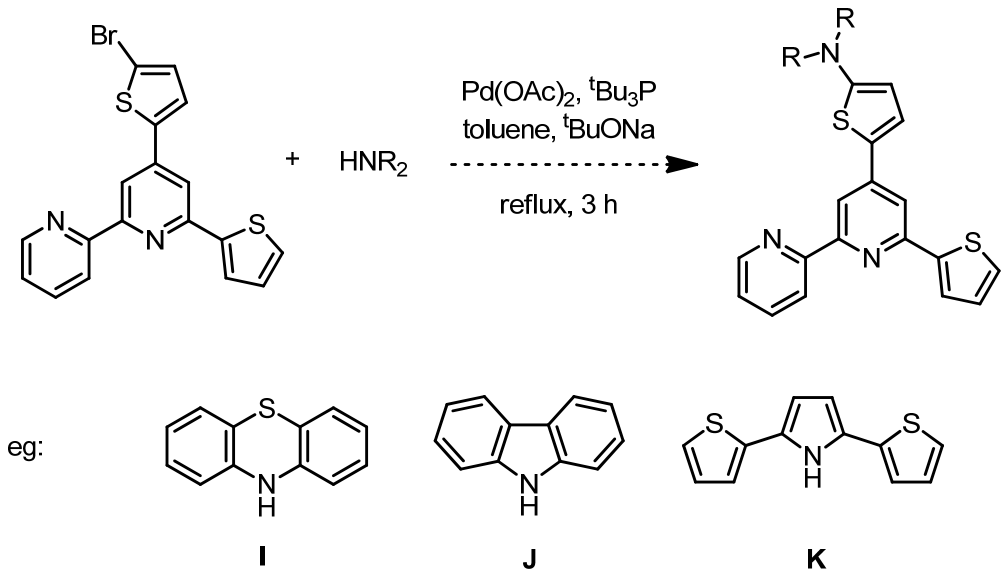


**Scheme 3-19** Envisioned derivatization of ligand **34**.

For comparison, ligand **36** was synthesized to see the influence of the sulfur atoms in the aromatic rings. Unfortunately, there was not enough time at the end of this thesis to pursue the idea further.

Various attempts to prepare 6'-(pyrrol-2-yl)-2,2'-bipyridine by KRÖHNKE, JAHNG or direct coupling reactions failed. It is easier to prepare a chalcone bearing a pyridyl substituent than

a MANNICH base. From the first approach there was still the pyridinium salt of 2-acetylpyrrole (**37**). In a second reaction chalcone **29** was prepared by a standard aldol condensation in a rather low yield of 37 %. The KRÖHNKE reaction produced the 4'-(3,4,5-trismethoxyphenyl)-6'-(pyrrol-2-yl)-2,2'-bipyridine **38** also in a lower yield of 30 %.

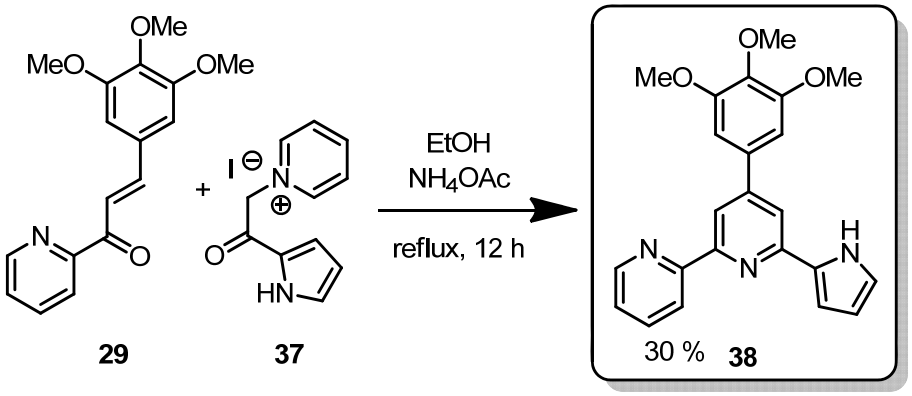


**Scheme 3-20** Synthesis of 4'-(3,4,5-*tris*methoxyphenyl)-6'-(pyrrol-2-yl)-2,2'-bipyridine (**38**).

This ligand is quite interesting since the pyrrole moiety could be deprotonated and this could lead to neutral metal complexes, which might find some application in OLEDs.

#### 3.2.1.6 4'-*tert*-Butyl terpyridines

In an attempt to prepare a chalcone with a non-aromatic substituent a test reaction was carried out using 4-acetylpyridine and pivalic aldehyde under standard CLAISEN-SCHMIDT condensation conditions. The desired product did not precipitate as expected but the reaction mixture turned red immediately. This colour change is usually an indication that the chalcone reacts further with still present enolate to give the MICHAEL adduct, a 1,5-diketone which in alkaline conditions is a deep red potassium salt. In our group there is an interest for divergent terpyridine ligands as building blocks for coordination polymers. So, instead of disposing of the unwanted diketone, a second equivalent of 4-acetylpyridine was added and after stirring overnight at room temperature, the mixture was treated with aqueous ammonium hydroxide and in the course of 8 h under reflux a yellow precipitate formed which could be isolated in 22 % yield and identified as 4'-*tert*-Bu-4,2':6',4''-terpyridine (**39**, Scheme 3-21). Coordination polymers are not the subject of this thesis but Dr. G. ZHANG was able to prepare such compounds using ligand **39** and we were able to publish these. The results will not be described here, since it was not subject of this thesis.[73]

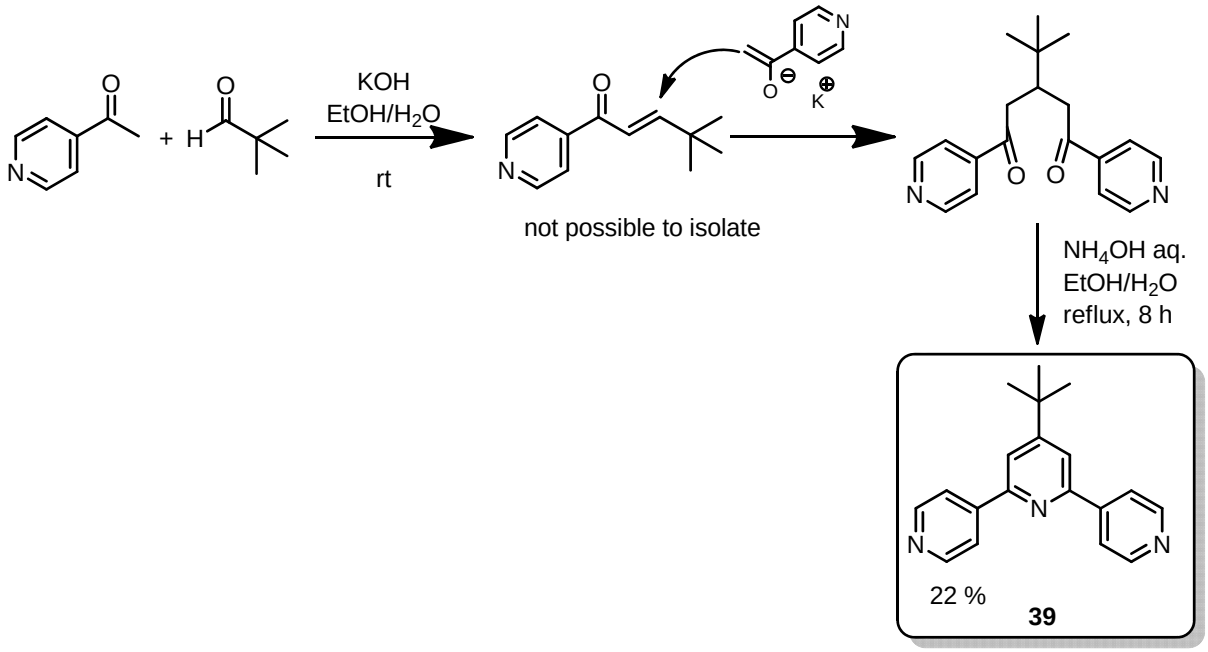


**Scheme 3-21** Synthesis of 4'-*t*-Bu-4,2':6',4''-terpyridine.

Even more surprising was the fact, that the convergent homologue, namely the 4'-*tert*-Bu-2,2':6',2''-terpyridine (**40**) was not published before either. Although the *tris* substituted derivative 4,4',4''-*t*-$Bu_3$tpy is now a well established ligand and is commercially available, its *mono* substituted homologue **40** had not been reported in the open literature.[74] Therefore, its synthesis was first carried out under the same conditions as ligand **39** (Scheme 3-22). But with this method only a poor yield of 12 % could be achieved.

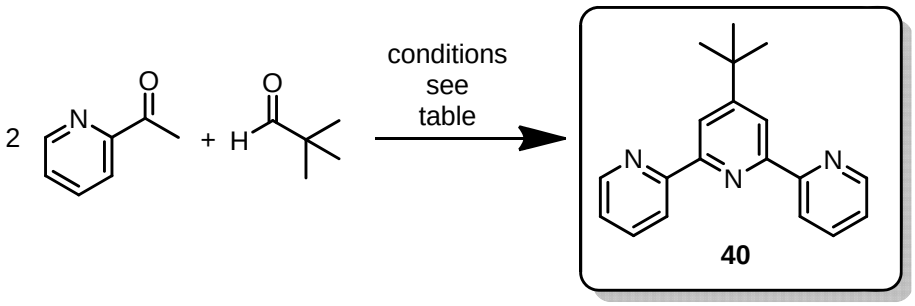


| conditions | | | | | | | |
|---|---|---|---|---|---|---|---|
| entry | | base | "$NH_3$" | solvent | T | t [h] | yield [%] |
| 1 | a) | KOH | | EtOH/ $H_2O$ | rt | 12 | - |
| | b) | | $NH_4OH$ | same | reflux | 22 | 12* |
| 2 | a) | KO*t*Bu | | THF | rt | 12 | |
| | b) | | $NH_4OAc$ | THF/ HOAc | reflux | 5 | 65** |

**Scheme 3-22** Syntheses of 4'-*t*-Bu-2,2':6',2''-terpyridine (**40**); a) aldol condensation + MICHAEL addition; b) imine condensation + ring closure + oxidation; *) column necessary; **) filtration through $Al_2O_3$.

With slightly modified conditions the yield could be improved to 65 %. In this case 2-acetylpyridine was treated with potassium *tert*-butoxide in tetrahydrofuran to prepare the corresponding enolate then pivalic aldehyde was added and stirred overnight at room

temperature. Then ammonium acetate in glacial acid was added and this mixture was stirred at reflux for 5 h. The crude product could be easily purified by filtering through alox.[75]

Some test reactions were carried out to explore the possibility of the combination of the Jahng and Kröhnke strategies. A model enaminone was used as a Michael acceptor and was refluxed with PPI in ethanol in the presence of excess ammonium acetate. This might give direct access to 4'-*N*,*N*-dimethylamino substituted bipyridines in only three steps. There are not many examples for such bpy derivatives in the literature.[76] As for 4'-*N*,*N*-dimethyl amino-6'-aryl 2,2'-bipyridine there were no reports whatsoever. It seems that there is a reason why such a reaction has never been reported! Unfortunately, none of the test reactions worked and led mostly to decomposition of the starting materials.

In conclusion, it can be stated that during this work twelve new and, to the best of our knowledge, unreported ligands could be synthesized. In particular, six new 6'-Ar-2,2'-bpy, four new 4',6'-bis(Ar)$_2$-2,2'-bpy and two new 4'-*t*-Bu-terpyridines. Some of them were prepared by conventional KRÖHNKE methodology, especially the 4',6'-*bis*substituted bipyridines. Secondly, the direct coupling of bpy with organolithium reagents was known before but could be applied for simple hetero aromatic compounds, such as *N*-methyl pyrrole, furan, thiophene and selenophen. It was therefore possible to expand the scope of this reaction. Thirdly, the "JAHNG" reaction was applied successfully to new substituents and the scope of this reaction could be enlarged as well. An overview of all ligands relevant for this work is given in the leaflet before this chapter (see page 32).

## 3.3 Properties

### 3.3.1 Characterization

All new ligands were characterized by standard techniques. First of all the molecular weight was confirmed by electron impact mass spectroscopy (EI-MS). The molecular structure was proved by solution nuclear magnetic resonance spectroscopy (NMR). For the assignment of all observed signals 2-D techniques, such as COSY, HMQC and HMBC were carried out. The compounds show relatively simple spectra which are easily assigned. The unsymmetrical 6'-R-bpy ligands exhibit two three-spin-systems and one four-spin-system. A typical $^{1}$H NMR spectrum of a mono substituted bpy ligand shows seven proton and ten $^{13}$C signals for the bpy moiety along with the appropriate signal of the substituent. Examples of $^{1}$H NMR spectra for ligands **1**-**4** and the assignment of the individual signals are depicted in Figure 3-3.

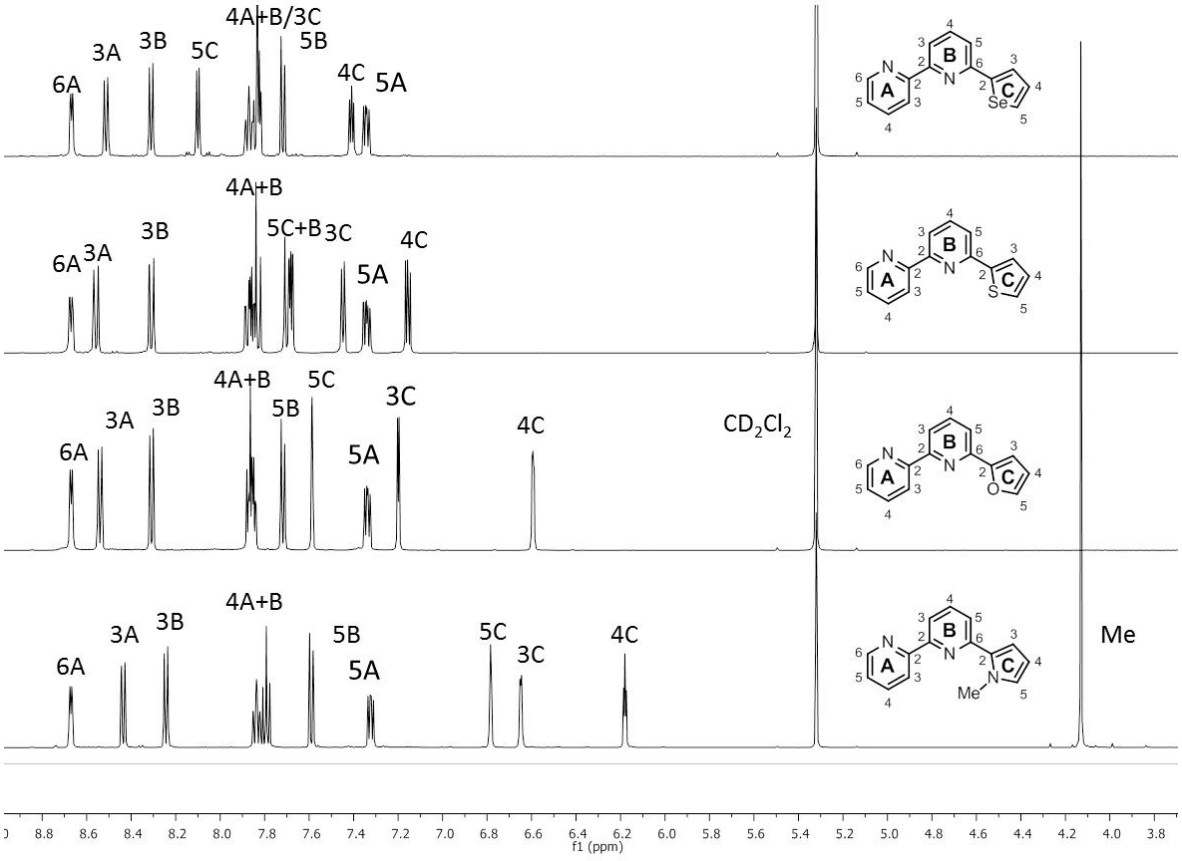


**Figure 3-3** Room temperature $^{1}$H NMR of $CD_2Cl_2$ solutions of 6'-R-bpy ligands **1**-**4**.

An additional substituent in the 4'-position of the bpy moiety differs from the previous spectra in missing out the signal for $H^{4B}$ and in having additional signals originating from the substituent. Figure 3-4 shows the $^{1}$H NMR spectra of ligands **30**-**32**. Even though, the two substituents in one ligand are the same, they have slightly different environments which result in different shifts. The substituents in 6'-position are shifted to lower field, compared

to the substituent in 4'-position, due to its proximity to the nitrogen atom, which has a deshielding effect.

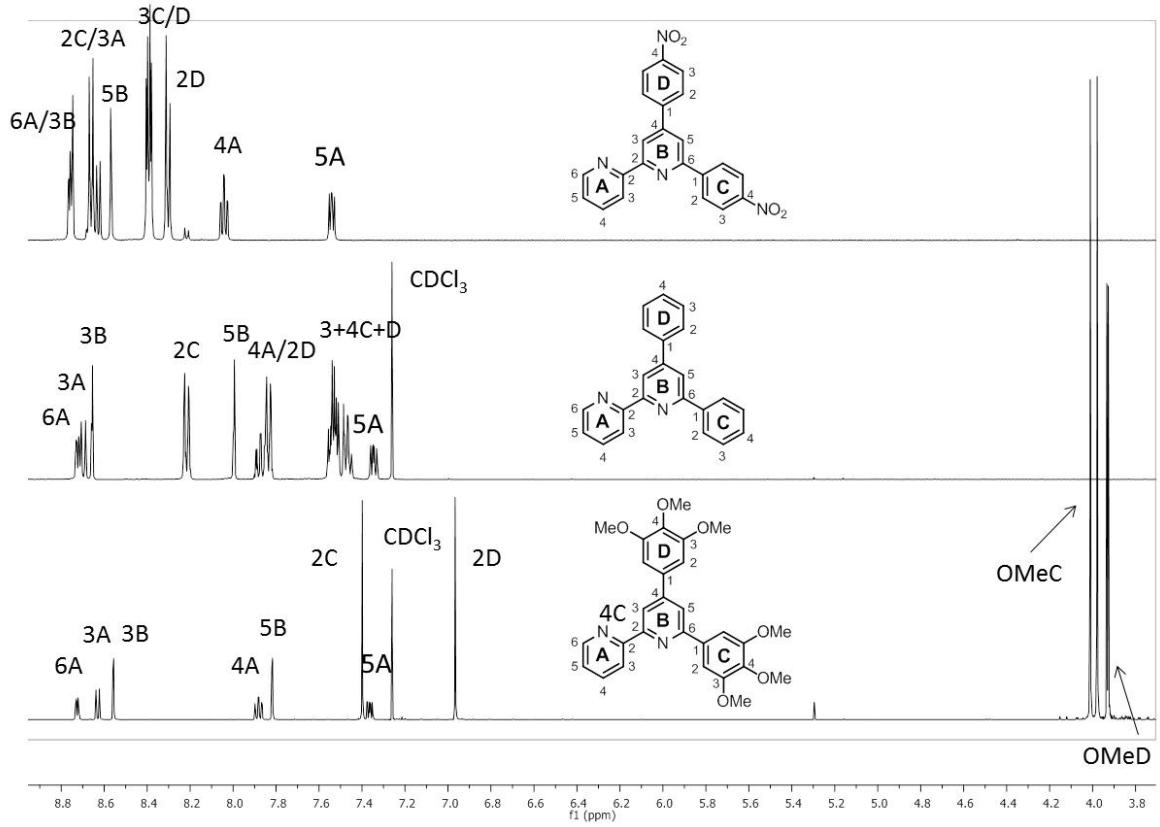


**Figure 3-4** Room temperature $^{1}$H NMR of $CD_2Cl_2$ solutions of (new) 4',6'-$R_2$-bpy ligands (**30**-**32**).

Additionally, the compositions of the ligands were confirmed by IR and elemental analysis.

## 3.3.2 Solid state structures

### 3.3.2.1 Ligand 1

Single crystals of **1** were grown by slow evaporation of a hexane solution of the ligand. The compound crystallizes in the triclinic *P*–1 space group with the asymmetric unit containing two independent, but structurally similar, molecules (A and B). Figure 3-5 shows the molecular structure of molecule A. The bpy domain adopts the expected *trans*-configuration with the two rings in each unit deviating slightly from planarity (angles between the least squares planes in independent molecules A and B are 14.14(8) and 5.79(8)°, respectively). The pyrrole ring lies close to the bpy plane (angles between the least squares planes of rings containing atoms N2 and N3, and corresponding rings in molecule B, are 3.19(9) and 11.62(9)$^{o}$). The orientation of the pyrrole ring is such that the methyl substituent faces the lone pair of atom N2 (Figure 3-5), and similarly in the second independent molecule. The methyl H atoms are too distant from N2 for there to be weak C–H...N interactions.

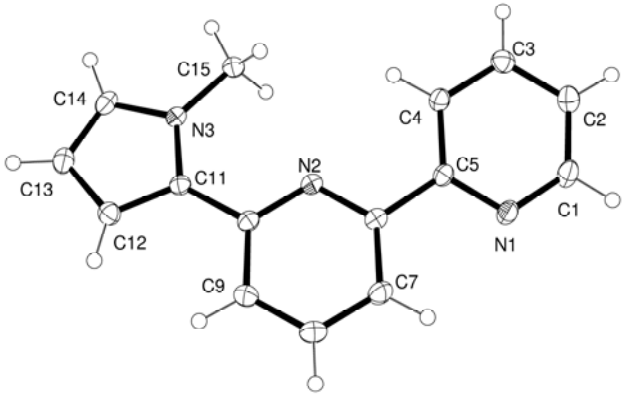


**Figure 3-5** Structure of one (molecule A) of two independent molecules of **3**; ellipsoids plotted at 40 % probability level. Selected bond lengths and angles: N1-C1 1.338(2), N1-C5 1.347(2), N2-C6 1.3460(19), N2-C10 1.341(2), N3-C11 1.3866(19), N3-C14 1.372(2), N3-C15 1.460(2) Å; C11-N3-C14 109.00(13), C11-N3-C15 128.76(13), C14-N3-C15 122.20(14)°.

Thus, the preference for the observed orientation is presumably associated with minimizing repulsive H...H interactions while maintaining an approximately planar molecular geometry to optimize intermolecular interactions. The crystal packing is such that pairs of molecules A associate through face-to-face $\pi$-stacking across an inversion centre, and similarly for pairs of molecules B.[77] The centroid...plane distances are 3.37 and 3.30 Å, for A and B, respectively. Molecules further assemble into ribbons through weak $CH_{pyrrole}...N_{bpy}$ hydrogen bonds (C14H141...N1' = 2.62, C14...N1' = 3.579(2) Å, C14–H141...N1' = 176°, corresponding parameters for molecules B are C29H291...N4' = 2.69, C29...N4' = 3.655(2) Å, C29-H291...N4' = 175°). The two sets of ribbons are approximately orthogonal to one another (Figure 3-6).

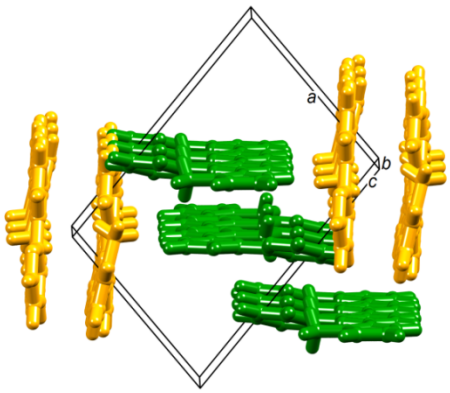


**Figure 3-6** Part of the packing diagram for **1**. Ribbons of molecules A and B are shown in green and orange, respectively.

#### 3.3.2.2 Ligands 2 and 3

Despite various attempts with different solvent systems and crystal growing methods (e.g., slow evaporation, layering, diffusion) it was not possible to obtain single crystals of ligand **2** suitable for crystal structure determination. Even though this ligand has been known for

some time, its crystal structure has not been reported. Ligand **3** on the other hand has been reported several times, as has its solid state structure.[78]

#### 3.3.2.3 Ligand 4

Crystals of ligand **4** suitable for X-ray diffraction grew overnight by evaporation of a diethyl ether solution of the compound, and Figure 3-7 depicts the structure. The molecule is planar (angles between the least squares planes of the rings containing N1/N2 and N2/Se1 are 3.4(3) and 5.2(3) $^{o}$) and fully ordered.

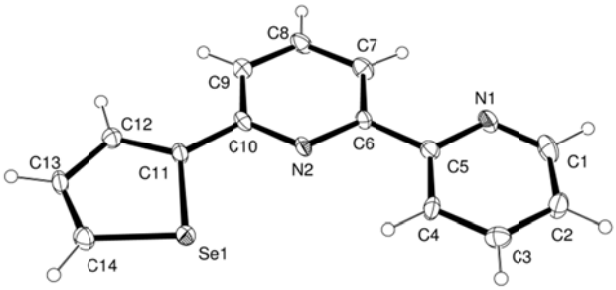


**Figure 3-7** Structure of **4**; ellipsoids plotted at 30 % probability level. Selected bond lengths and angles: C11-Se1 1.864(7), C14-Se1 1.866(7), C1-N1 1.333(9), C5-N1 1.340(8), C6-N2 1.359(6), C10-N2 1.328(8) Å; C5-N1-C1 116.8(6), C6-N2-C10 118.3(5), C14-Se1-C11 86.3(3)°.

The bpy domain is in the expected *trans*-configuration. The orientation of the selenium-containing heterocycle results in a Se1...N2 separation of 2.982(5) Å (compare the sum of the van der Waals radii of 3.54 Å). The observed separation is shorter than intramolecular Se...N contacts observed in related molecules: 3.490(2) Å in 2-((mesitylselanyl)methyl)quinoline,[79] 3.406(2) Å in 1,3-bis(2-pyridylmethyl)triselane,[79] and 3.448(4) Å in 2,6-bis((phenylselanyl)methyl)pyridine.[80] Significantly, **4** adopts an analogous conformation to **3** in which the S...N separation in the solid state is 2.895(3) Å. Both **4** and its sulphur analogue[78] crystallize in the space group *Pna*$2_1$ with similar cell dimensions, and the molecular packing in the two compounds is essentially the same involving C-H...$\pi$ and C-H...N interactions. Despite the planarity of ligand **4**, there is no face-to-face $\pi$-stacking.

### 3.3.2.4 Ligand 12

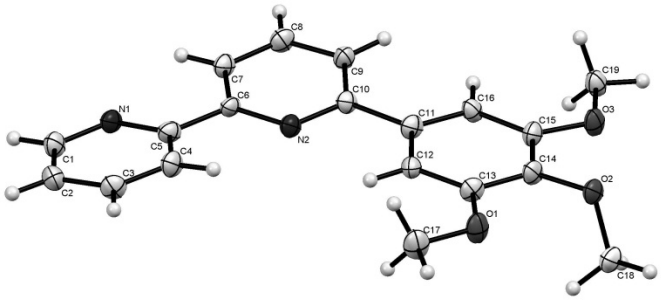


**Figure 3-8** Solid state structure of **12**, ellipsoids plotted at 50 % probability level. Selected bond lengths and angles: C1-N1 1.342(5), C5-N1 1.343(4), C6-N2 1.352(4), C10-N2 1.346(4) Å; C5-N1-C1 117.9(3), C6-N2-C10 118.6(3), C13-O1-C17 117.5(3), C14-O2-C18 112.6(3), C15-O3-C19 116.9(3), N1-C5-C6-N2 = 169.6(3), N2-C10-C11-C12 6.3(4), C12-C13-O1-C17 0.9(5), C15-C14-O2-C18 101.0(4), C16-C15-O3-C19 1.0(5)°.

Suitable crystals for X-ray structure determination of ligand **12** were obtained by slow evaporation of a diethyl ether solution. The compound crystallizes as colourless needles in the monoclinic space group $P2_1/c$ (Figure 3-8). The bpy moiety shows the expected *trans* configuration being twisted from planarity by 10.3(3)° and the phenyl substituent by 6.3(4)°. Two of three methoxy substituents (3- and 5-positions) are in plane with the phenyl ring, while the third in the 4-position is nearly perpendicular to the ring (80.9(4)°). The packing is dictated by hydrogen bonds with O…H distances being in the range of 2.519(2)-2.676(2) Å (C…(H)…O separation being between 3.245(4)-3.542(4) Å). Short distances can be observed between N1 and of each molecule and two H atoms of two adjacent ligands, the separation being 2.599(3) Å (N1…H'(C19)) and 2.609 Å (N1…H''(C18)) (the N…C separations being 3.489(4)/3.407(4) Å). These values are typical for hydrogen bonds observed in solid state structures.[81] σ-π-edge to head interactions between C2 and H(C2') (2.686(4) Å) of two pyridine rings. All these results in sheets of molecules, two of these alternatively beining oriented nearly perpendicular to each other (Figure 3-9).

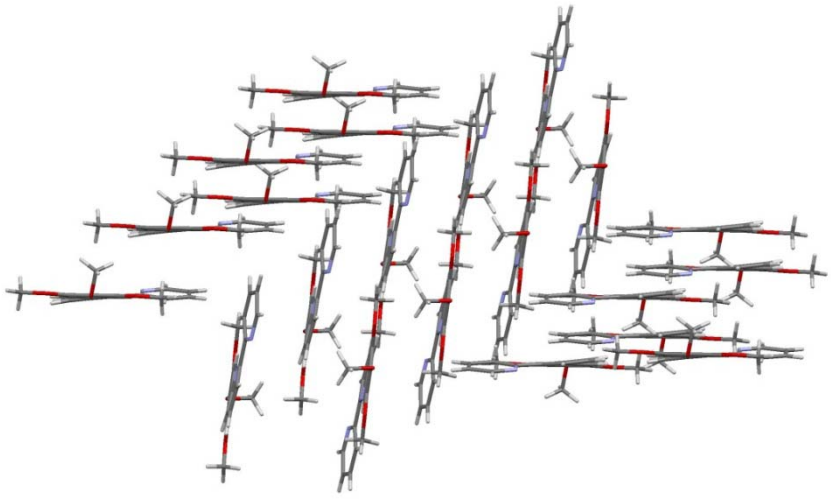

**Figure 3-9** Packing of ligand **12**.

### 3.3.2.5 Ligand 30

Slow evaporation of a dichloromethane/diethyl ether solution of ligand **30** yielded colourless needles and its solid state structure was determined by X-ray crystallography (Figure 3-11).

Compound **30** crystallizes in the same monoclinic space group $P2_1/c$ as its parent compound 6'-(trismethoxyphenyl)-2,2'-bipyridine (**12**). The bpy domain is in the expected *trans* configuration and deviates from perfect planarity with a dihedral angle of 174.4(2)° but the pyridine ring is also twisted and the angle between the least square planes being 14°. The trismethoxyphenyl substituents are twisted out of plane by 14.5(3) or 32.2(3)°, respectively, to avoid repulsive interactions of the hydrogen atoms of the central pyridine ring and the phenyl substituents. The methyl substituents on the phenyl substituents are all not in plane with the phenyl substitutents and subtend different dihedral angles ranging from 2.6(3) to 16.4(3)° in the 3,5-positions of the phenyl rings and 80.8(2)/81.3(2)° in the 4-positions. The same compound crystallizes as a polymorph if a diethyl ether solution is used for the crystal growing process instead of a dichloromethane/diethyl ether mixture (see above).

It crystallizes in the triclinic space group *P*-1. The molecular structure is similar to the previous one but the phenyl substituents are more twisted (31.07(9)/34.65(9)° *vs.* 14.5(3)/32.2(3)°) and the oxygen atoms of the methoxy substituents in the 4-positions on the phenyl rings are less distorted from a trigonal geometry (114.47(7)/116.03(6) *vs.* 112.1(1)/111.7(1)°).

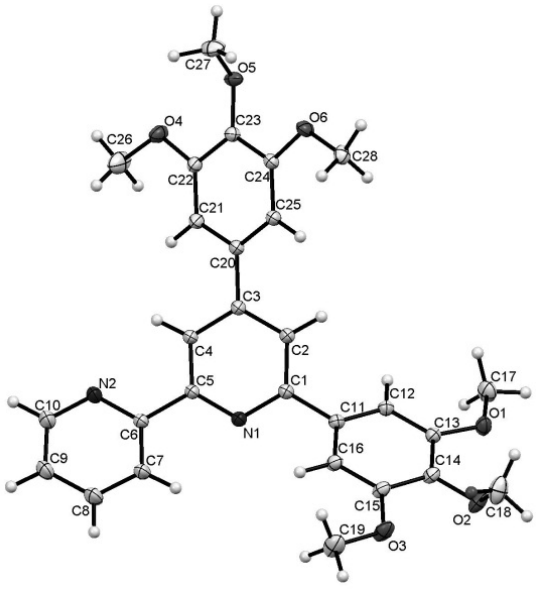


**Figure 3-10** Solid state structure of **30** polymorph b, ellipsoids plotted at 50 % probability level. Selected bond lengths and angles: C1-N1 1.3531(8), C5-N1 1.3473(9), C6-N2 1.350(1), C10-N2 1.3489(8) Å; C5-N1-C1 118.14(6), C6-N2-C10 117.78(7), C13-O1-C17 117.41(6), C14-O2-C18 114.47(7), C15-O3-C19 116.98(7), C22-O4-C26 116.99(7), C23-O5-C27 116.03(6), C24-O6-C28 117.01(6), N1-C5-C6-N2 174.54(6), C2-C1-C11-C12 31.07(9), C2-C3-C20-C25 34.65(9), C12-C13-O1-C17 9.2(1), C15-C14-O2-C18 73.62(9), C22-C23-O5-C27 78.66(9)°.

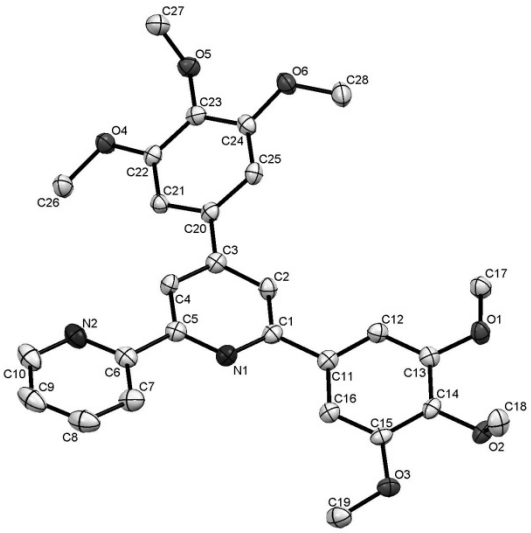


**Figure 3-11** Solid state structure of **30** polymorph a, hydrogen atoms are omitted for clarity reasons, ellipsoids plotted at 50 % probability level. Selected bond lengths and angles: C1-N1 = 1.348(2), C5-N1 = 1.348(3), C6-N2 1.339(3), C10-N2 1.346(2) Å; C5-N1-C1 118.3(2), C6-N2-C10 118.2(2), C13-O1-C17 117.0(1), C14-O2-C18 112.1(1), C15-O3-C19 117.6(1), C22-O4-C26 116.5(1), C23-O5-C27 111.7(1), C24-O6-C28 = 117.3(1), N1-C5-C6-N2 174.4(2), N1-C1-C11-C16 14.5(3), C2-C3-C20-C25 31.8(3), C12-C13-O1-C17 16.4(3), C15-C14-O2-C18 80.8(2), C22-C23-O5-C27 81.3(2)°.

The packing is dominated by hydrogen bonds between O5/O6 of one molecule and H(C9) (2.4570(5) and 2.6338(6) Å) of the next unit. Two of these chains are connected *via* hydrogen bonds between N2 and H(C17) so that they are rotated about a $C^2$ axis this being perpendicular to the central pyridine ring. π-π-stacking here seems not very important, the closest, observed distance between two aromatic rings is 3.9 Å which is rather long.[77]

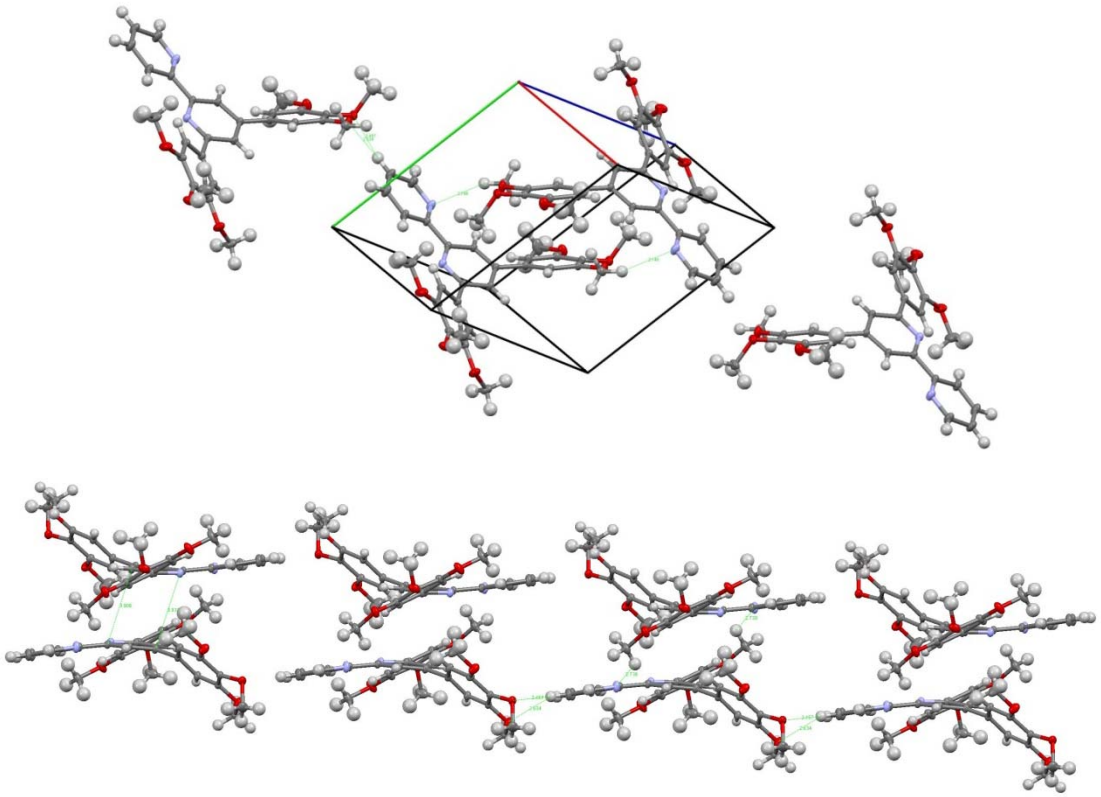

**Figure 3-12** Packing of ligand **30** polymorph b.

### 3.3.2.6 Ligand 32

Only low quality crystals of **32** were obtained by slow evaporation of a dichloromethane solution of the compound, correspondingly, that is why the final R value is rather high, at 11 %. This ligand crystallizes in the monoclinic space group P21/c as do ligands **12** and **30** (polymorph a).

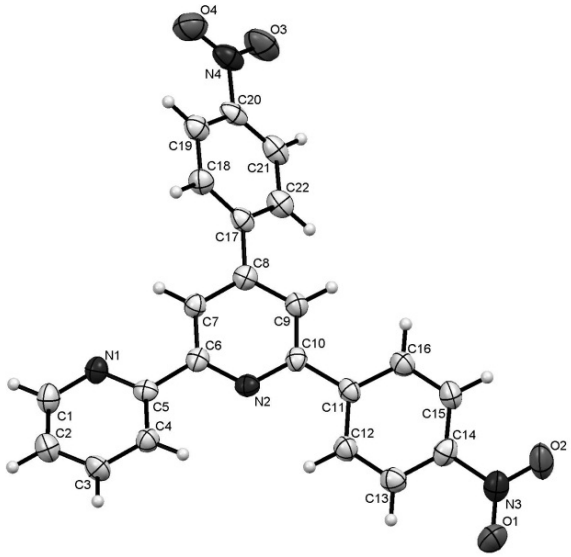


**Figure 3-13** Solid state structure of ligand **32**, ellipsoids plotted at 50 % probability level. Selected bond lengths and angles: C1-N1 1.336(8), C5-N1 1.348(7), C10-N2 1.338(8), C14-N3 1.465(8), C20-N4 1.48(1) Å; C5-N1-C1 117.5(5), C6-N2-C10 119.8(5), N1-C5-C6-N2 166.6(5), C9-C10-C11-C12 14.0(9), C7-C8-C17-C18 37.3(9)°.

The molecular structure is very similar to that of ligand **30** (polymorph a). Again, the bpy domain favours the *trans*-configuration with a dihedral angle of 166.6(5)° which is smaller than for all other ligands described here. However, the pyridine ring is not twisted out of the plane as in the other structures. The two remaining *p*-nitrophenyl substituents are twisted as well with dihedral angles of 14.0(9)/37.3(9)°, which are comparable with the ones observed in ligand **30** (polymorph a). The oxygen atoms of the nitro groups form weak hydrogen bonds. Oxygen O3 interacts with H(C12) and O4 with H(C4) with bond lengths 2.558(6) and 2.527(7) Å so that chains of molecules are formed (Figure 3-14).

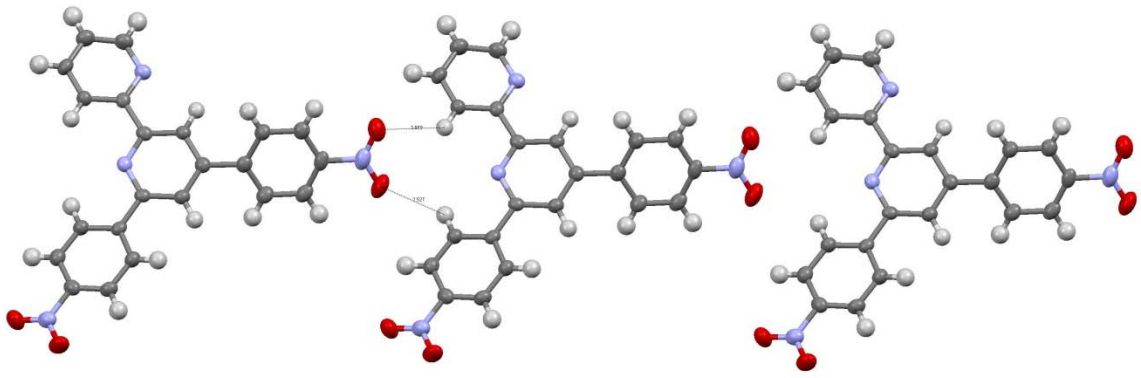

**Figure 3-14** Hydrogen bonded chains of ligand **32** molecules.

The central pyridine ring forms π-π-contacts to two *p*-nitrophenyl substituents above and under with distances around 3.4 Å which causes the chains to form zig-zag pattern, as shown in Figure 3-15. The angles between the zig-zag chains are with 34.1° comparable to the twist of the *p*-nitrophenyl substituent in the 4'-position of the ligand and can be held responsible for this aggregation.

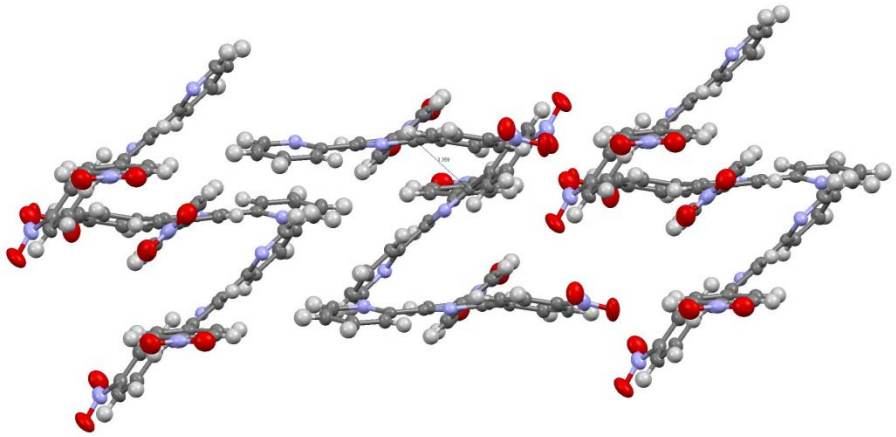

**Figure 3-15** Packing of ligand **32**.

These zig-zag chains are linked with each other *via* hydrogen bonds between from O2 of one molecule to H'(C21) of a second molecule (2.384(7) Å) and between the same oxygen atom and H(C13) a third ligand. In addition, a face to edge σ-π-bond between H(C1) and C5 (2.878(6) Å) of another ligand can be observed. This results in the zig-zag chains being interlocked with each other (Figure 3-15).

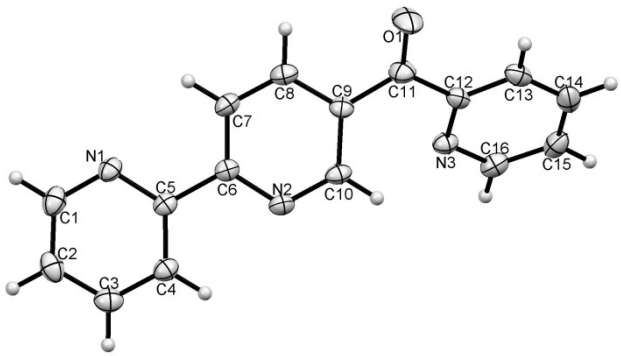


**Figure 3-16** Structure of **22**; ellipsoids plotted at 50 % probability level. Selected bond lengths and angles: C1-N1 1.347(3), C5-N1 1.364(3), C6-N2 1.360(3), C10-N2 1.351(3), C12-N3 1.349(2), C16-N3 1.326(3) Å; C5-N1-C1 118.4(2), C6-N2-C10 119.1(2), C12-N3-C16 116.8(2), C9-C11-C12 119.8(2), C9-C11-O1 120.8(2), N1-C11-C12-N3 178.6(2)°.

Suitable crystals of ligand **22** for X-ray diffraction were obtained by slow evaporation of an *n*-hexane solution of **22** (Figure 3-16). The ligand crystallizes in the monoclinic space group $P2_1/c$. The molecule deviates from planar alignment. The bpy domain is in the expected *trans* configuration and is nearly planar with a dihedral angle of 178.6(2)°. The pyridine moiety linked *via* the carbonyl function is twisted from the plane by a dihedral angle of

46.5(2)°. Carbon atom C11 is nearly perfectly trigonal planar as expected with angles being between 119.4(2)-120.8(2)°. The bond lengths of N3/C12 (1.349(2) Å) and N3/C16 (1.326(3) Å) are only marginal shorter than the of the bpy moiety. The nitrogen N3 undergoes hydrogen interactions to H(C10) the distance being 2.566(2) Å. The C=O bond is with 1.222 Å similar to the bond length in for example acetone (1.230 Å). The packing is dominated by weak hydrogen bonds N3'…H(C10) and O1'…H(C3) (2.745(2) and 2.714(2) Å) with a contributions of π-stacking, the centroid-centroid distances of all three pyridyl rings of two distinct molecules being 3.8 Å.

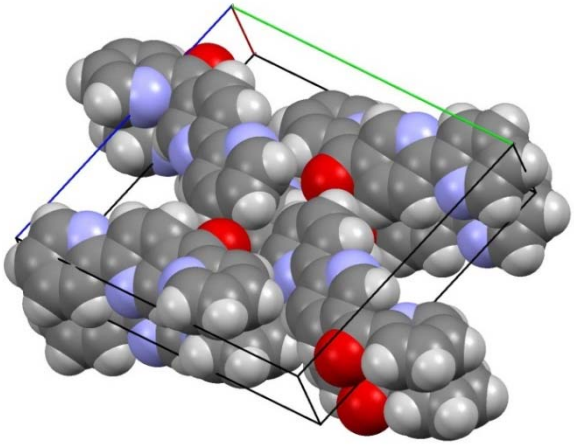

**Figure 3-17** Packing of ligand **22**.

Crystals of ligand **40** suitable for X-ray diffraction grew overnight from a diethyl ether solution of the compound (Figure 3-18). The three pyridine rings adopt the expected *trans,trans*-configuration. The *tert*-butyl group is ordered in contrast to the disordered substituents observed in the complexes discussed later. The tpy domain in ligand **40** deviates from planarity, with angles between the least squares planes of rings containing N1/N2 and N2/N3 being 24.84(8) and 14.47(8)°.

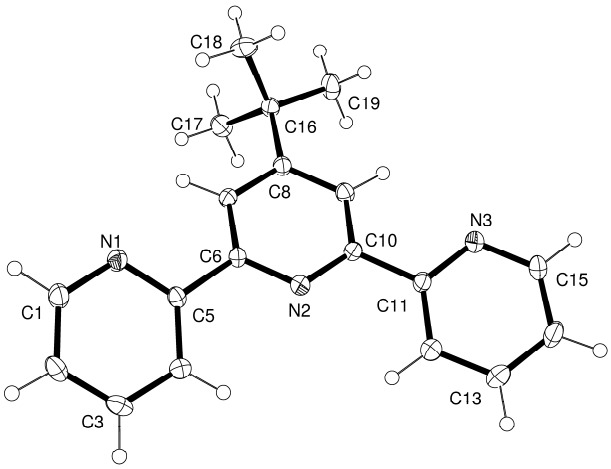


**Figure 3-18** ORTEP representation of ligand **40** with ellipsoids plotted at 40 % probability level. Selected bond parameters: N1-C1 1.337(2), N1-C5 1.348(2), N2-C6 1.348(2), N2-C10 1.340(2), N3-C11 1.343(2), N3-C15 1.340(2), C1-C2 1.382(3), C8-C16 1.532(2) Å; C1-N1-C5 117.48(15), C6-N2-C10 117.15(14), C11-N3-C15 117.30(17)°.

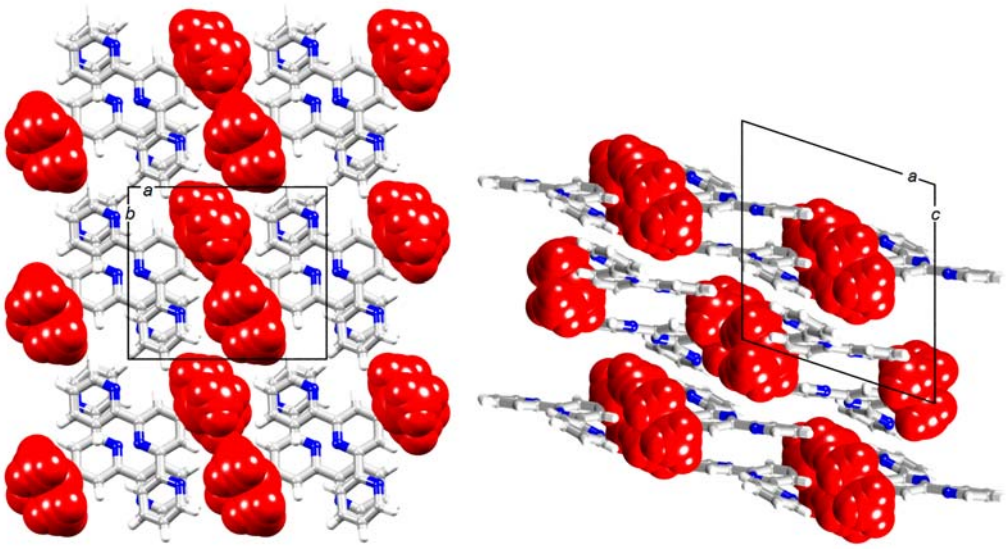


**Figure 3-19** Packing of molecules in ligand **40** viewing the unit cell (a) down the c-axis, and (b) down the b-axis. The *t*-Bu groups are shown in space-filling representation.

As shown in Figure 3-19, molecules of ligand **40** pack with alternating tpy and *tert*-butyl domains, and centrosymmetric pairs of molecules are potentially arranged to permit face-to-face π-stacking between the rings containing atoms N1 and N3. However, efficient interactions are prevented by the presence of the sterically demanding *tert*-butyl groups (Figure 3-19). The dominant packing forces are between *tert*-butyl CH and tpy units in adjacent molecules: non-classical CH...N hydrogen bonds (C17-H173...N1' 2.72, C17...N1' 3.74(2) Å, C17–H173...N1' 147°) and rather weak CH...π interactions (CH...centroid of ring with N1' 3.5 Å, distance of H to plane of ring being 2.7 Å).[82]

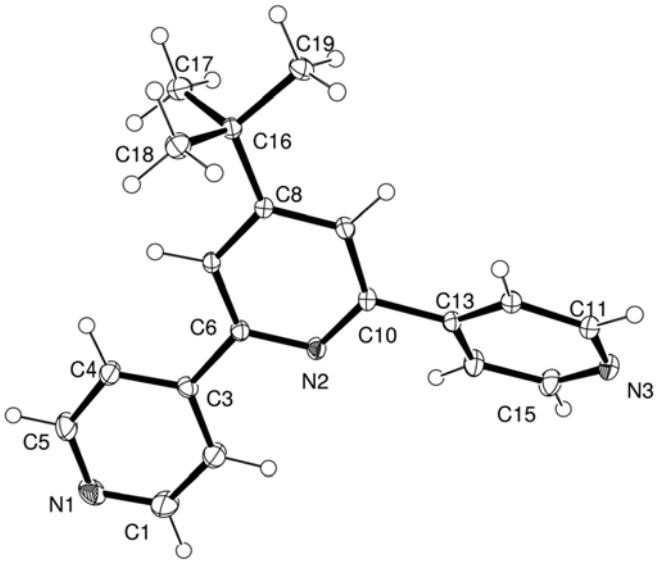


**Figure 3-20** Structure of ligand **39** (ellipsoids plotted at 40 % probability level). Selected bond parameters: N1-C1 1.333(2), N1–C5 1.327(2), N2–C6 1.3479(18), N2–C10 1.3411(18), N3–C11 1.339(2), N3-C15 1.339(2), C8–C16 1.528(2), C16–C17 1.536(2), C16–C18 1.534(2), C16–C19 1.5310(19) Å; C1-N1–C5 115.17(14), C6-N2-C10 17.35(12), C11–N3–C15 115.96(13)°.

Single crystals suitable for X-ray analysis were grown overnight by evaporation of a diethyl ether solution of ligand **39**. The molecular structure is depicted in Figure 3-20. Selected bond lengths and angles are given in the figure caption. The only feature of note is the non-planarity of the 4,2':6',4''-tpy domain; the angles between the least squares planes of the rings containing N1/N2 and N2/N3 are 7.45(9) and 31.83(9)°. The origin of the twist of the pyridine ring containing N3 is the close proximity of the *t*-Bu group of a neighbouring molecule. This is highlighted in Figure 3-21 with space-filling representations of the two *t*Bu units (see figure caption). The crystal packing is further supported by C–H/N contacts (C4-H41…N3' 2.543(1), C4/N3' 3.484(2) Å).

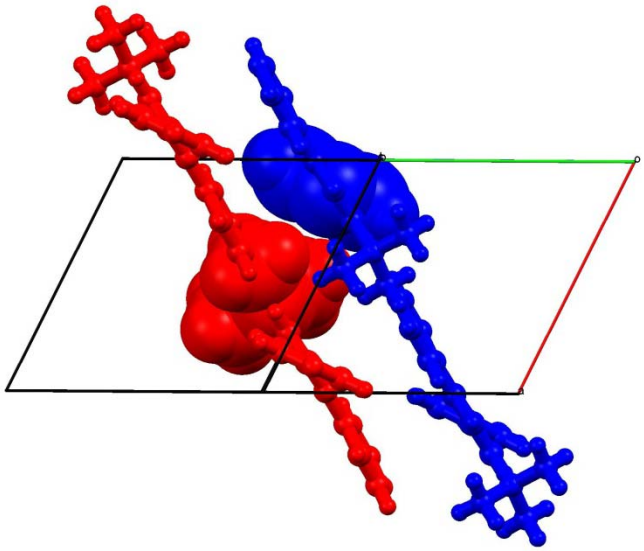

**Figure 3-21** Packing of molecules of ligand **39** illustrating (a) the origin of the nonplanarity of the 4,2':6',4'-tpy with *t*-Bu (red) and py ring containing N3 (blue space-filling representation).

### 3.3.3 $^{77}$Selenium NMR

Ligand **4** was synthesized to expand the family of heterocyclic ligands in this work (Figure 3-1). But it has also another advantage: the $^{77}$Se isotope is NMR active. The element selenium has six natural isotopes: $^{74}$Se (0.87 %), $^{76}$Se (9.02 %), $^{77}$Se (7.58 %), $^{78}$Se (23.52 %), $^{80}$Se (49.82 %), $^{82}$Se (9.19 %). One of them,$^{77}$Se, has a nuclear spin number I = ½ and it is possible to record high-resolution NMR spectra. Its receptivity relative to $^{1}$H is 5.4*10$^{-4}$ and is comparable to that of $^{13}$C. Each type of selenium compound has a characteristic chemical shift range (Figure 3-22).[83]

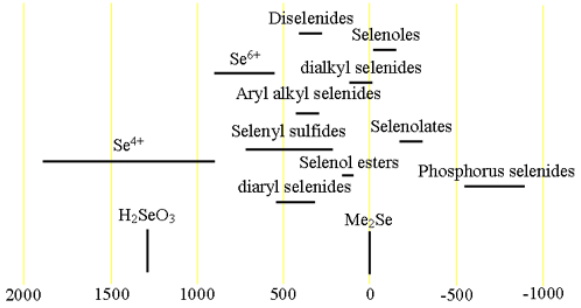


**Figure 3-22** Spectral range of Selenium compounds.[84]

The range is quite big and spans over 3000 ppm (from -1000 to 2000 ppm). Changes in structure and environments cause quite dramatic shifts. Thus, the idea was that it could be used as a kind of NMR probe, to see whether there is a significant interaction between the hetero atom and the metal centre of complexes. To avoid the use of $Me_2Se$ as reference which is volatile, odoriferous and quite toxic, we decided to use selenophen (starting material for ligand **4**) instead. The $^{1}$H NMR spectrum of the reference is shown in Figure 3-23.

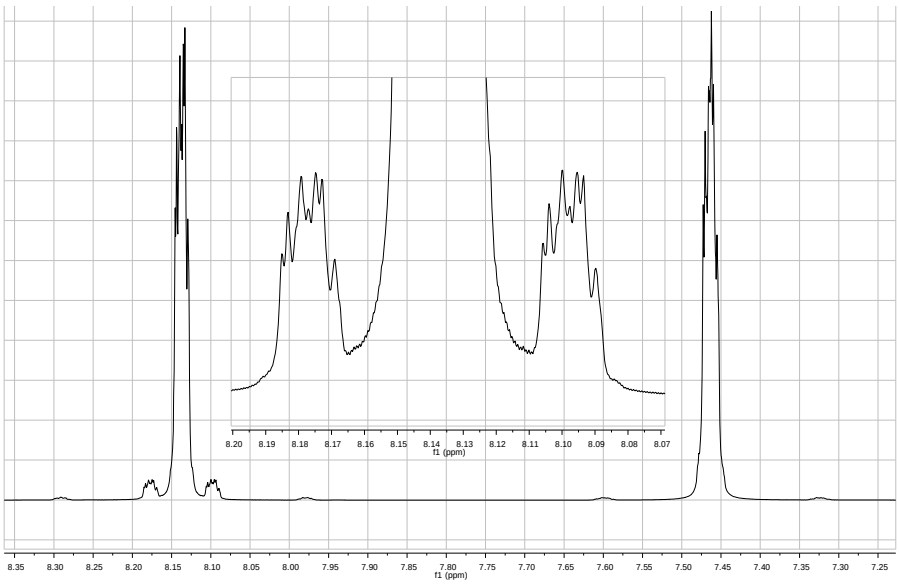


**Figure 3-23** 600 MHz $^{1}$H NMR spectrum of selenophen ($C_4H_4Se$).

Selenium shows coupling to other nuclei and satellites appear in $^{1}H$ or $^{13}C$ spectra. The selenium satelites show the same fine structure as the vicinal proton signal which for the selenophene can be described as a spectrum of higher order. It is similar to to other five membered hetero aromatic cycles, such as furane or thiophene which show an AA'XX' spin system. From the 1H NMR spectrum of selenophene the coupling constant $^{2}J$ (Se,H$^{2}$) shows a typical value of 48 Hz (see Figure 3-23). Other couplings cannot be deduced. The $^{77}Se$ NMR spectra were recorded directly as well as using the two dimensional HMBC method. The signal of selenophen was set to $\delta$ 605 ppm as external reference.[83] Figure 3-23 shows the HMBC spectrum of the reference compound selenophen. Here too, the $^{2}J$ (Se,H$^{2}$) can be observed the $^{3}J$ (Se,H$^{3}$) is too small and cannot be resolved.

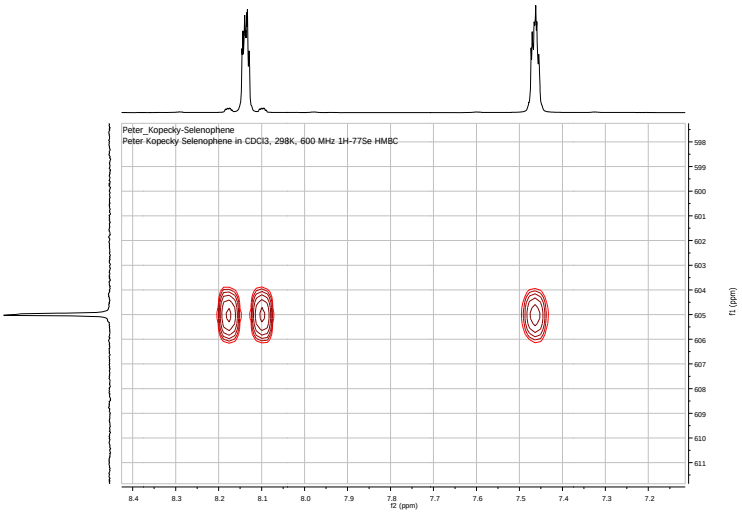


**Figure 3-24** 600 MHz HMBC spectrum of Selenophen.

The chemical shift of the 6'-(selenophen-2-yl)-2,2'-bipyridine (**4**) was then determined using the same procedure. The $^{1}H$ NMR spectrum is depicted in Figure 3-25.

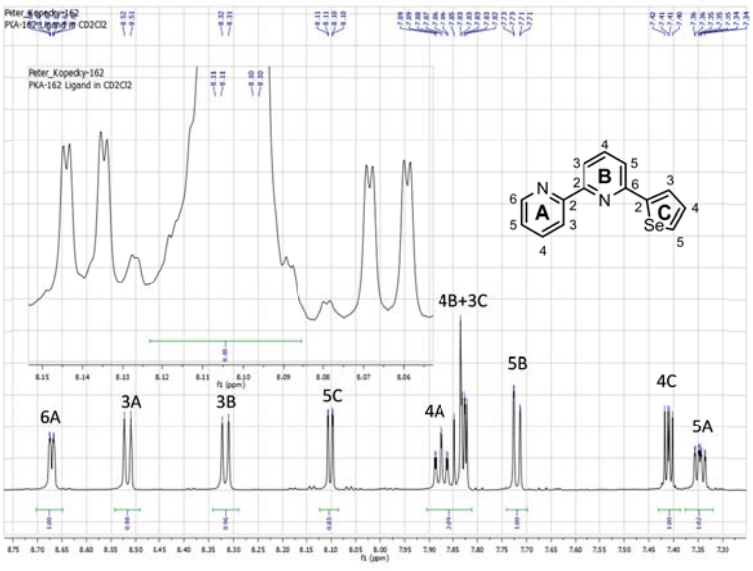


**Figure 3-25** 600 MHz $^{1}H$ NMR spectrum of ligand **4**.

The $^{1}$H NMR, as well as the HMBC spectrums show a $^{2}J$ (Se,$H^{5C}$) coupling with a similar value to the reference compound selenophene of 46 Hz. Here the three spin system is of first order and can be described as AMX. The fine structure shows the couplings: $^{3}J$ ($H^{5C}$,$H^{4C}$) = 6 Hz and $^{4}J$ ($H^{5C}$,$H^{3C}$) = 1 Hz. The $^{3}J$ (Se,$H^{3/4C}$) couplings are again to small to resolve so that protons $H^{3C}$ and $H^{4C}$ do not show any satellites.

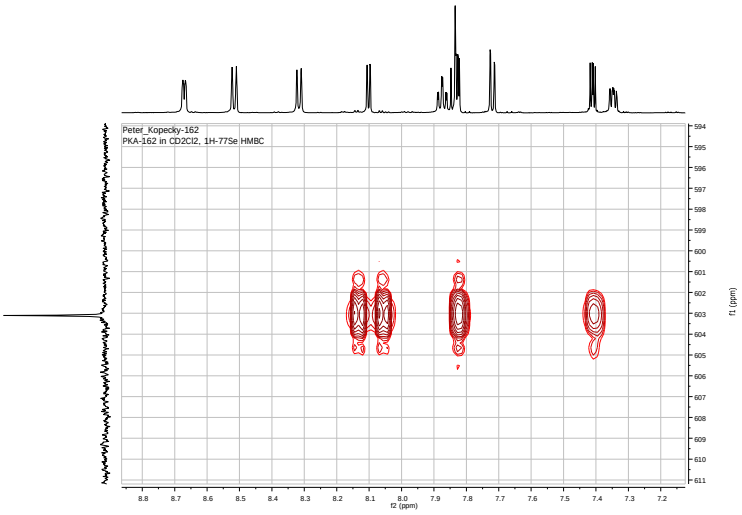


**Figure 3-26** 600 MHz HMBC of ligand **4**.

Figure 3-26 shows the $^{1}$H-$^{77}$Se HMBC spectrum of ligand **4**. The chemical shift is $\delta$603 ppm and therefore only slightly different than the reference compound selenophen. Obviously, the substitution of a hydrogen atom with a bipyridine molecule does not change the environment or electronic properties of the heteroaromatic ring very much. Nevertheless, if the selenium atom would coordinate to a metal centre the shift should change quite drastically. The complexation of compound **4** and the effect to the NMR spectra will be described in next chapter.

### 3.3.4 Electronic Absorptions and Emission

All of these ligands absorb in the UV region of the spectral range which can be attributed to excitation of an electron from HOMO to LUMO ($\pi$-$\pi$*-transitions). The relaxations of the excited states for most of the ligands result in fluorescence and they show emissions in the near UV or even in the blue region of visible light. For comparison with metal complexes in the following chapters and to preserve the possibility to exclude any emissions which might originate from ligands, the absorption and emission spectra for all ligands were recorded.

#### 3.3.4.1 Ligands 1-4

The first group of ligands investigated were ligands **1**-**4**, the 2,2'-bipyridine ligand bearing a five membered, heteroaromatic ring as substituent in the 6'-position (Figure 3-1). The observed spectra are shown in Figure 3-27. The absorption maxima do not depend very

much on the hetero atom containing substituent and they differ only slightly in value for ligands **1**-**4**. The values are summarized in Table 3-2.

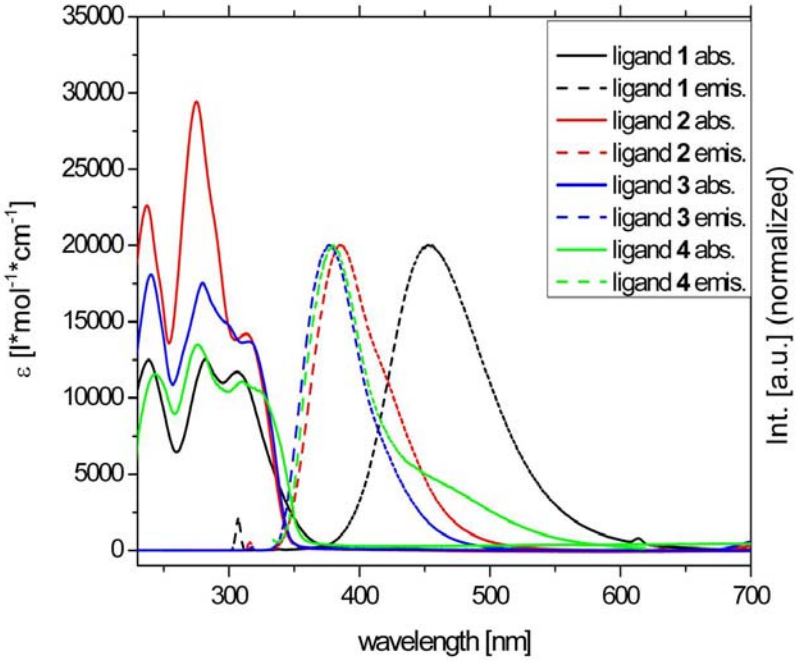


**Figure 3-27** Absorption (solid) and emission (dashed) spectra of ligands **1**-**4**.

An anomaly in this series is the twice as high ε value for the furan derivative **2**. A look at the emissions for these ligands shows a similar situation. Again three compounds have similar values and one is strongly shifted, here far to the visible region (453 nm). The oxygen containing compound **2** emits at 386 nm. Relative to this, the S and Se containing ligands **3** and **4** are both blue shifted to 377 and 380 nm, respectively. The biggest shift is exhibited by the *N*-methyl pyrrole containing ligand (**1**) which is red shifted to 453 nm. Even though the absorptions of all four ligands are quite similar, the emissions are different and show a noticeable trend of growing emission energy with increasing atomic number of the hetero atom: N, O, S, Se. This result is not in line with the energies for calculated HOMO-LUMO gaps ($E = \frac{h*c}{\lambda} \approx \frac{1240.6}{\lambda/nm}$): N (3.35 eV), O (3.52 eV), S (3.51 eV), Se (3.42 eV).

### 3.3.4.2 Ligands 5, 6, 10-12, 20 and 21

Figure 3-28 shows the absorption and emission spectra of the remaining 6'-R-bpy ligands. The influence of the substituents on the electronic transitions of the bpy ligands is the following. Ligands **6** (black) and **10** (green) show very similar absorption spectra and differ only slightly in intensity, the butyl substituted being lower. The emission on the other hand is different. While the methyl substituted bpy emits at 334 nm the emission of the *n*-butyl derivative is shifted 24 nm to lower energy.

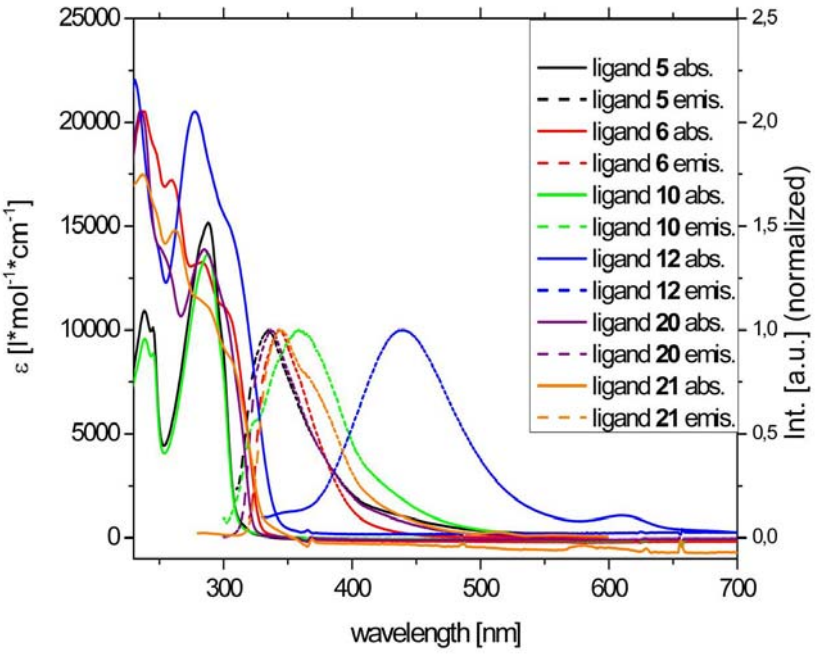


**Figure 3-28** Absorption (solid) and emission (dashed) spectra of ligands **5**, **6**, **10**, **12**, **20** and **21**.

A similar situation can be observed for ligand **5** (red) and **21** (orange). These two ligands differ only in one methyl group in *meta* position on the phenyl substituent of the bpy. Therefore no big difference can be observed. Their absorption spectra are nearly exactly the same and the emission of ligand **21** is only 2 nm red shifted compared to phenyl bpy (**5**). In the case where the substituent is 4-pyridyl (**20**, purple), the absorption spectrum is comparable to phenyl bpy (**5**), suggesting that the substitution of a carbon atom in the aromatic substituent by nitrogen does not have a big effect. An effect can again be observed for the emission. Ligand **20** emits at 337 nm, which is comparable to the value of methyl bpy (**6**). The only ligand which stands out is ligand **12** (blue) where the phenyl substituent carries three additional methoxy groups and suffers from strong electron donating effect. This results in a remarkable bathochromic shift for the emission of 100 nm to $\lambda_{abs}$ = 440 nm.

Another exception in this ligand family is the 6'-(2,4-difluorophenyl)-2,2'-bipyridine (**11**) which exhibits several emission maxima dependent on the excitation wavelength and is therefore depicted in a separate graph (Figure 3-29). The excitation spectra are shown in a separate graph (see Figure 3-30).

Figure 3-29 shows the emission spectra at different excitation wavelengths. It shows that at higher energies ($\lambda_{ex}$ = 237 and 245 nm) only one emission is observed at 360/380 nm. A second emission could be detected at 400/420 nm for excitations with lower energy wavelengths ($\lambda_{ex}$ = 305/340/370 nm). If the sample is irradiated with $\lambda_{ex}$ = 290 nm both emissions could be observed. Interestingly, the excitation spectra are the same for all emission wavelengths (see Figure 3-30). The reason for this behaviour remains unclear. A

possible explanation could be the formation of excimers (excited dimer).[85] Proof may be obtained by conducting emission experiments with varying concentrations. With higher concentration the lower energy emission of the supposed excimer should increase in intensity.

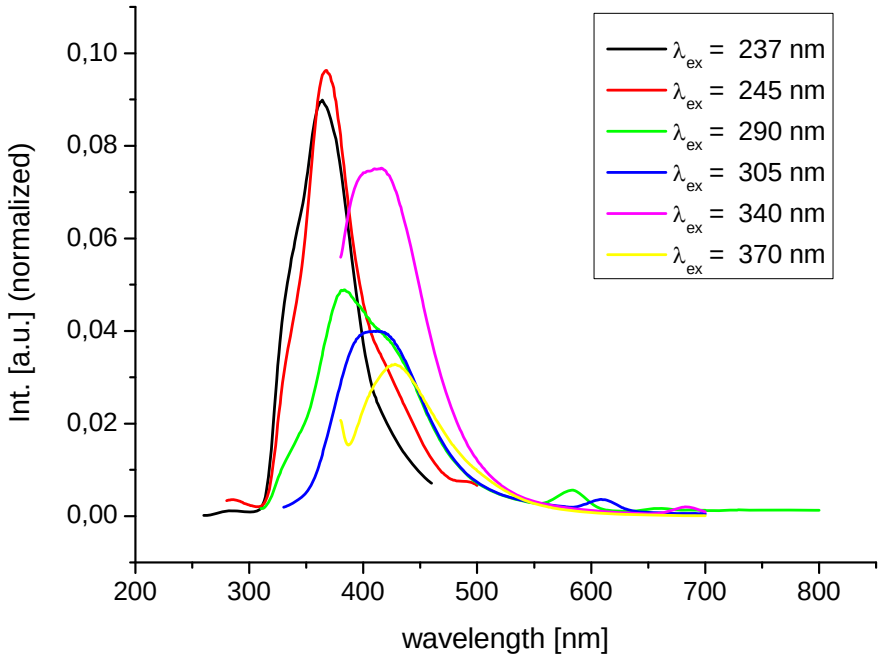


**Figure 3-29** Emission spectra of ligand **11**.

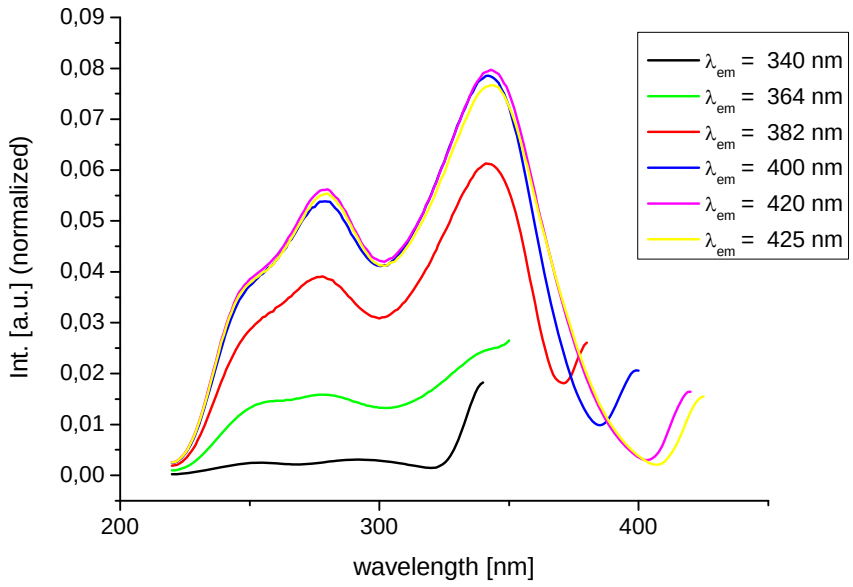


**Figure 3-30** Exitaction spectra of ligand **11**.

### 3.3.4.3 Ligand 22

Ligand **22** contains three nitrogen atoms from which one remains available after ligation to a metal centre. Sometimes changes in absorption, as well as emission were observed for metal complexes. For comparison reasons, protonation with TFA was carried out for the free ligand

and the electronic spectra were recorded for both the neutral and the protonated ligand. The results are shown in Figure 3-31. The ligand shows a main transition at 303 nm and a second one appears as a shoulder at 285 nm with extinction coefficients around 14000 $dm^3$ $mol^{-1}$ $cm^{-1}$. Upon protonation the main transition shifts to higher wavelength as expected but only marginally by 10 nm. However, the emission remains unaffected after protonation. Protonation experiments for Ru(II) and Ir(III) complexes containing ligand **22** were carried out as well and will be described in sections 6.1.2.3 and 5.1.2.4 .

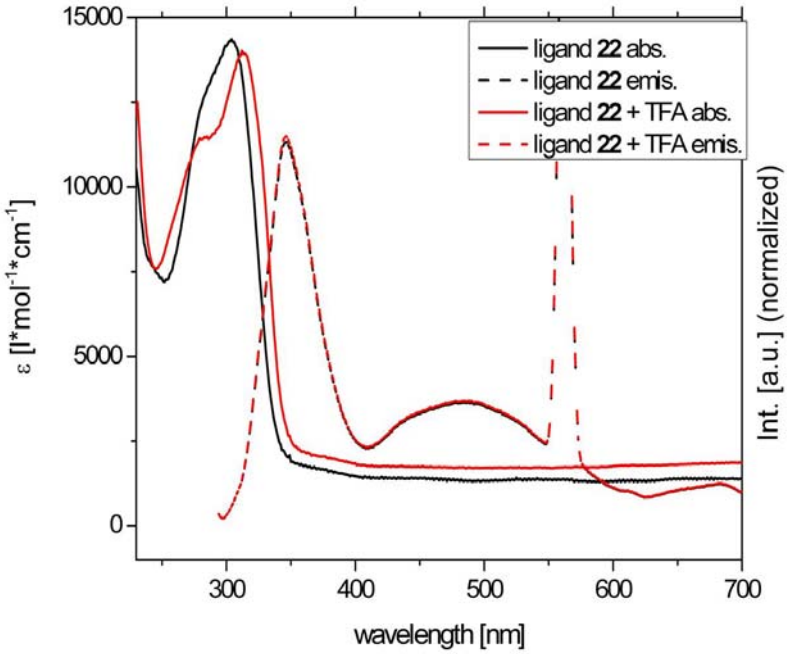


**Figure 3-31** Absorption (solid) and emission (dashed) spectra of ligand **22**; neat compound (black) and protonated with TFA (red).

### 3.3.4.4 Ligands 30-32, 34 and 38

Figure 3-32 shows the absorption and emission spectra of ligands **30**-**32**, 4',6'-bis phenyl substituted 2,2'-bipyridines with various decoration of the phenyl rings. These substituents are: methoxy groups, hydrogen atoms or nitro groups, respectively. This small family of ligands was prepared to see the effect on absorption and emission by variation of the electronic properties of the substituents, neutral (**31**), electron donating (**30**) or withdrawing (**32**), respectively, and later then the consequences on their corresponding metal complexes, especially Ir(III) (see section 5.1.2.4). The parent compound **31** (4',6'-diphenyl-2,2'-bipyridine) exhibits a main absorption at 257 nm and a less intense band at 312 nm. Both, compounds **30** and **32** show bathochromic shifts with similar values, 285 nm for the methoxy derivative and 289 nm for the nitro compound. The determination of the onsets of the lowest energy absorption shows that the substitution of phenyl rings with electron donating and withdrawing substituents lowers the HOMO-LUMO gap in both cases (Table 3-2). Usually, electron withdrawing substituents tend to stabilize HOMO by removing electron

density and electron donating groups should have the opposite effect. But it seems that in these cases the LUMO is affected as well. The substitution has a bigger effect on the emissive properties of the ligands. While the parent compound (**31**) emits at 356 nm, the emission of ligand **32** is only slightly red shifted (367 nm) with a second signal at 428 nm, lower in intensity, and ligand **30** shows a single emission at 442 nm which is shifted 85 nm relative to ligand **31**.

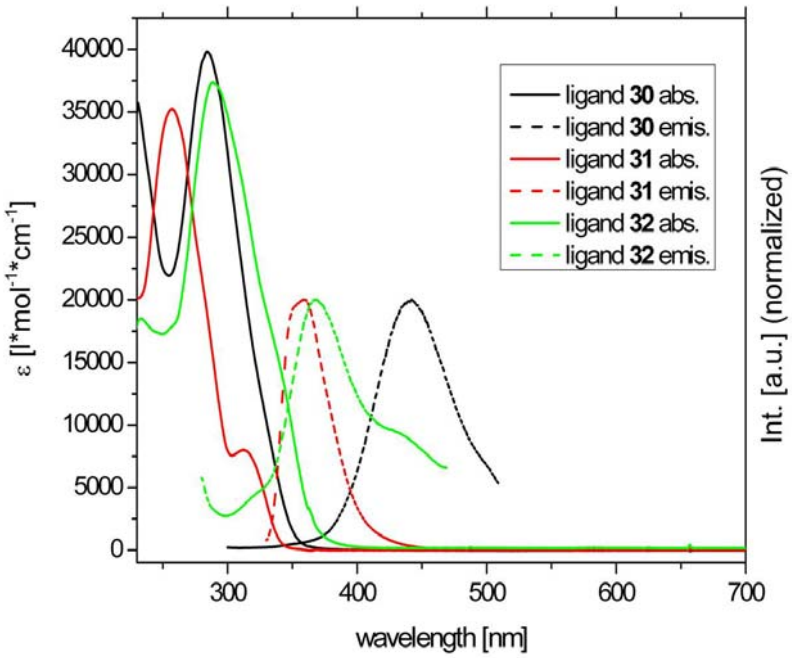


**Figure 3-32** Absorption (solid) and emission (dashed) spectra of ligands **30**-**32**.

The next small series consists of three 4',6'-disubstituted 2,2'-bpy ligands bearing two different substituents. Ligand **36** is known and has been reported in the literature several times. Therefore only two of them are shown in Figure 3-33. Ligand **34** has an additional 5-bromothiophenyl substituent in the 4'-position compared to ligand **3**. The absorption maximum is at 306 nm and the calculated HOMO-LUMO gap is 3.22 eV, which is lower than for ligand **3**. The emission is shifted 12 nm to lower energy. This is being consistent with the bigger conjugated π-system. Ligand **38** bears an unsubstituted pyrrole in 6'-position, in comparison to ligand **1**, and a 3,4,5-trismethoxyphenyl substituent in the 4'-position, comparable to ligand **30**. The absorption spectrum shows two transitions at 286 and 304 nm which are similar for both ligands. The absorption was observed at 436 nm and is therefore blue shifted relative to both ligand **1** (453 nm) and **30** (442 nm).

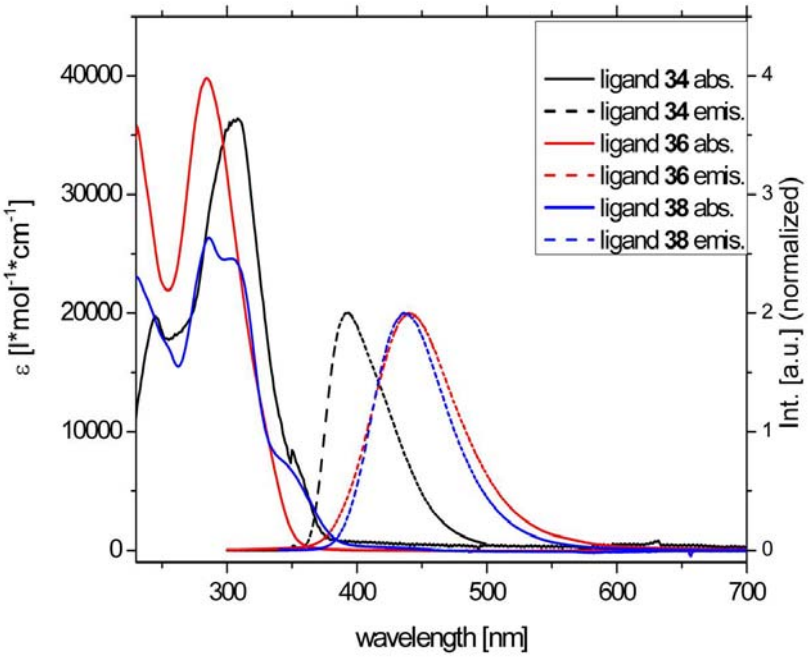


**Figure 3-33** Absorption (solid) and emission (dashed) spectra of ligands **34** and **38**.

### 3.3.4.5 Ligands 39 and 40

The last graph shows the electronic spectra for the two isomeric 4'-*tert*-butyl terpyridine ligands. Figure 3-34 shows the influence of the position of the nitrogen atoms on the absorption and emission. The absorption spectra are very similar differing mainly in intensity. The first emission maximum is the same for both ligands (337 nm) but the second transition is shifted 16 nm for ligand **40** and 40 nm for ligand **39**. The signals for the convergent tpy ligand are much sharper than for the other isomer.

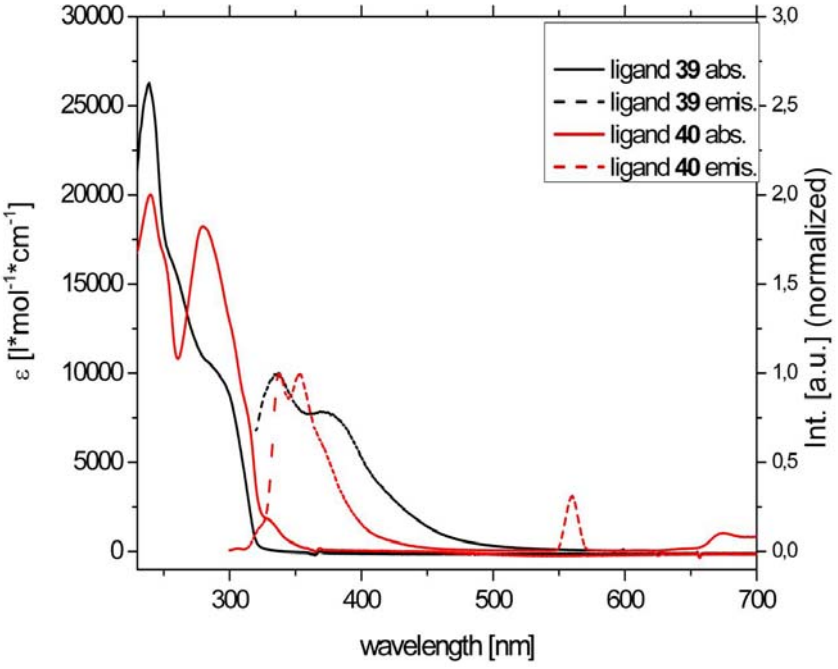


**Figure 3-34** Absorption (solid) and emission (dashed) spectra of ligands **39** and **40**.

The spectroscopic data of all ligands introduced in this section are summarized in Table 3-2.

| ligand | $\lambda_{abs}$ [nm] ($\varepsilon$ [l mol$^{-1}$ cm$^{-1}$ 10$^3$]) | $\lambda_{em}$ [nm] | HOMO-LUMO gap |
|---|---|---|---|
| **1** | 239 (12.5)/282 (12.6)/ 307 (11.7) | 453 | 3.35 eV |
| **2** | 237 (22.6)/ 275 (29.4)/ 313 (14.3) | 386 | 3.52 eV |
| **3** | 243 (11.6)/ 276 (13.4)/ 311 (11.0)/ 325 (10.5) | 380 | 3.51 eV |
| **4** | 242 (18.1)/ 280 (17.5)/ 299 (15.0)/ 316 (13.8) | 377 | 3.42 eV |
| **5** | 237 (20.5)/ 256 (17.2)/ 282 (13.2)/ 300 (11.2) | 343 | 3.67 eV |
| **6** | 238 (10.9)/ 245 (10.1)/ 288 (15.1) | 334 | 3.82 eV |
| **10** | 237 (9.6)/ 245 (8.9)/ 288 (13.7) | 359 | 3.86 eV |
| **11** | 237 (26.2)/ 289 (15.7) | 367/413* | 3.67 eV |
| **12** | 231 (22.0)/ 277 (20.5)/ 302 (15.4) | 439 | 3.44 eV |
| **20** | 236 (20.6)/ 253 (13.3)/ 285 (13.9) | 337 | 3.76 eV |
| **21** | 237 (17.5)/ 253 (13.8)/ 286 (13.8) | 345 | 3.57 eV |
| **22** | 283 (12.9)/ 304 (14.3) | 346/485 | 2.99 eV |
| **30** | 285 (39.6) | 442 | 3.41 eV |
| **31** | 257 (35.3)/ 312 (8.0) | 356 | 3.58 eV |
| **32** | 289 (37.3) | 367/428 | 3.24 eV |
| **34** | 244 (19.5)/ 308 (36.4) | 392 | 3.18 eV |
| **38** | 286 (26.3)/ 304 (24.5)/ 343 (7.5) | 438 | 3.10 eV |
| **39** | 239 (26.2)/ 257 (16.4)/ 289 (10.3) | 337/374 | 3.79 eV |
| **40** | 240 (20.1)/ 250 (16.8)/ 281 (18.3) | 337/352 | 3.47 eV |

**Table 3-2** Spectroscopic data of ligands **1**-**6**, **10**-**12**, **20**-**22**, **30**-**32**, **34**, **38**-**40**.

### 3.3.5 Electrochemistry

Electrochemistry experiments were performed for some 6'-substituted bpy ligands, especially for these with hetero aromatic substituents. Most of the ligands can be reduced at lower potentials (ca. -2 Volt) and the S and Se containing ligands can be oxidized.

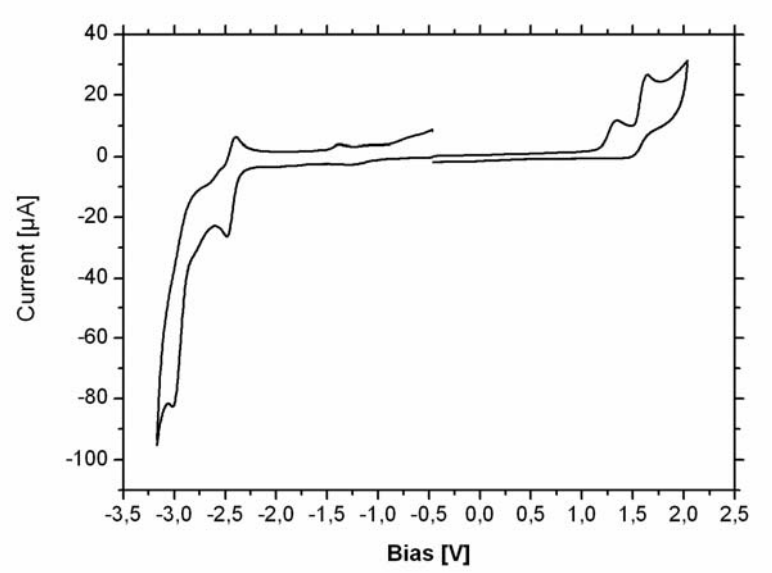


**Figure 3-35** CV of ligand **3** (*vs*. $Fc/Fc^{+}$).

Figure 3-35 shows as an exemple the cyclic voltametry spectrum of ligand **3**. It exhibits an irreversible oxidation at 1.3 and another at 1.9 V. The reduction of the ligand occurs at -2.4 V. The remaining data are summarized in Table 3-3.

| Ligand | 1st $ox^{irr}$ [V] | 1st $red^{qr}$ E/2 [V] | HOMO [eV] | LUMO [eV] | gap [eV] |
|---|---|---|---|---|---|
| 2 | 1.36 | -2.44 | -5.82 | -2.51 | 3.31 |
| 3 | 1.34 | -2.44 | -5.96 | -2.44 | 3.52 |
| 4 | 1.72 | -2.42 | -6.28 | -2.47 | 3.81 |
| 40 | - | $-2.59^{irr}$ | - | -2.48 | 3.81 |

**Table 3-3** Electrochemical data for ligands **2**-**4** and **40**; irr, irreversible; qr, quasi reversible.

## 3.4 Experimental

### 3.4.1 Precursor

#### 3.4.1.1 3-(dimethylamino)-1-(furan-2-yl)propan-1-one hydrochloride (7)

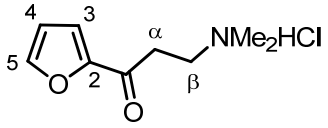


2-Acetylfuran (2.20 g, 20.0 mmol, 1.0 eq), paraformaldehyde (1.80 g, 60.0 mmol, 3.0 eq) and dimethylamine hydrochloride (1.96 g, 24.0 mmol, 1.2 eq) were dissolved in MeOH (50 ml). After addition of catalytic amounts of HCl (1.0 ml, 32 wt%) the resulting solution was stirred under reflux overnight. The solvent was evaporated and the resulting solid recrystallized from EtOH. Cooling to 273 K and cool filtration yielded white crystals ( 2.5 g, 12.3 mmol, 61.4 %), $^{1}$H-NMR: (400 MHz, $CDCl_3$) $\delta$ 7.62 (s, 1 H, $H^5$), 7.35 (d, *J* 3.6, 1 H, $H^4$), 6.57 (s, 1 H, $H^3$), 3.64 – 3.38 (m, 4 H, $H^{\alpha+\beta}$), 2.81 (d, *J* 4.9, 6 H, $H^{Me}$). Analytical data match those published.[86]

#### 3.4.1.2 1-(2-oxo-2-(pyridin-2-yl)ethyl)pyridin-1-ium (8)

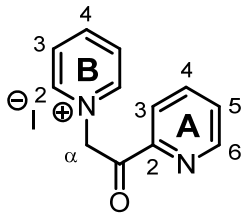


Iodine (5.08 g, 20.0 mmol, 1 eq) was dissolved in dry, hot pyridine (50.0 ml), with at least 10 min stirring at 100° C. Then 2-acetylpyridine (2.42 g, 20.0 mmol, 1 eq) was added to the mixture over 5 m and was stirred for 2 h under reflux. After cooling the crude product was isolated by filtering and was washed with big amount of $Et_2O$/EtOH (9:1) to give a grey powder (4.7g). This was dissolved in ~100 ml boiling EtOH containing 5 wt% activated charcoal and filtered hot over Celite®. Out of this solution yellow plate like crystals formed (3.5 g, 10.7 mmol, 54 %). The mother liquid was evaporated to give dirty yellow crystals which were again dissolved in hot EtOH, until yellow micro crystals precipitated (0.5 g, 1.5 mmol, 8 %). $^{1}$H NMR (400 MHz, MeOD-$d_3$) $\delta$ (ppm) 8.94 (d, *J* 5.6 Hz, 2 H, $H^{2B}$), 8.81 (dd, *J* 4.8, 0.9 Hz, 1 H, $H^{6A}$), 8.72 (t, *J* 7.9 Hz, 1 H, $H^{4B}$), 8.21 (t, *J* 7.1 Hz, 2 H, $H^{3B}$), 8.13 (dt, *J* 7.8, 1., $H^{3A}$), 8.06 (td, *J* 7.7, 1.7 Hz, 1 H, $H^{4A}$), 7.73 (ddd, *J* 7.5, 4.8, 1.3 Hz, 1 H, $H^{5A}$), 6.53 (s, 2 H, $H^{\alpha}$). Analytical data match those published.[64]

### 3.4.1.3 (*E*)-1-(Pyrid-2-yl)-3-*N*,*N*-dimethylaminoprop-2-en-1-one (13)

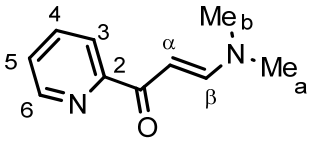


To a 10 ml microwave vial 2-acetylpyridine (2.26 g, 18.7 mmol, 1 eq) and DMF-DMA (2.23 g, 18.7 mmol, 1 eq) were added and stirred at 170 °C for 10 m The brown residue was extracted several times with hot hexane. After removal of the solvent **13** was obtained as green crystals (2.67 g, 15.2 mmol, 81 %). Analytical data match those published.[65]

### 3.4.1.4 (*E*)-1-(Furan-2-yl)-3-*N*,*N*-dimethylaminoprop-2-en-1-one (14)

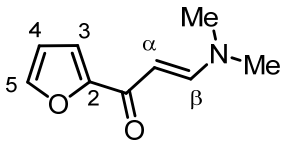


To a 5 ml microwave vial 2-acetylfuran (1.10 g, 10.0 mmol, 1 eq) and DMF-DMA (1.19 g, 10.0 mmol, 1 eq) were added and stirred at 170 °C for 10 m The brown residue was extracted several times with hot hexane. After removal of the solvent **14** was obtained as yellow crystals (1.31 g, 7.9 mmol, 79 %). Analytical data match those published.[65]

### 3.4.1.5 (*E*)-1-(Thiophen-2-yl)-3-*N*,*N*-dimethylaminoprop-2-en-1-one (15)

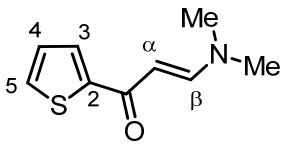


To a 5 ml microwave vial 2-acetylthiophene (1.26 g, 10.0 mmol, 1 eq) and DMF-DMA (1.19 g, 10.0 mmol, 1 eq) were added and stirred at 170 °C for 10 m Additon of pentane to the brown residue initiated precipitation of the product. After filtration **15** was obtained as yellow crystals (1.65 g, 9.1 mmol, 91 %). Analytical data match those published.[65]

### 3.4.1.6 (*E*)-1-(1H-Pyrrol-2-yl)-3-*N*,*N*-dimethylaminoprop-2-en-1-one (16)

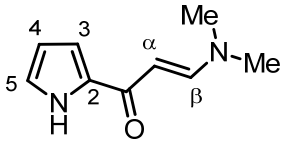


To a 5 ml microwave vial 2-acetylpyrrole (1.00 g, 9.2 mmol, 1 eq) and DMF-DMA (1.09 g, 9.2 mmol, 1 eq) were added and stirred at 150 °C for 13 m The reaction yielded green/black crystals. After washing with $Et_2O$ **16** was obtained as green crystals (0.92 g, 5.6 mmol, 60 %). Analytical data match those published.[65]

### 3.4.1.7 (*E*)-1-(Pyrid-4-yl)-3-*N*,*N*-dimethylaminoprop-2-en-1-one (17)

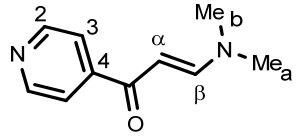


DMF-DMA (1.19 g, 10.0 mmol, 1.0 eq) and 4-acetylpyridine (1.21 g, 10.0 mmol, 1.0 eq) were mixed in a 20 ml microwave vial without any solvent and stirred for 10 min at 165 °C to yield a black oil. This was diluted with a few ml MeOH and extracted several times with hot hexane. Solvent was removed from the combined hexane fractions to yield (**17**) as yellow crystals (1.16 g, 6.6 mmol, 66 %). $^{1}$H NMR (500 MHz, $CDCl_3$) $\delta$ (ppm) 8.67 (dd, *J* 4.4, 1.7 Hz, 2 H, $H^2$), 7.84 – 7.78 (br d, *J* 12.3 Hz, 1 H, $H^{\beta}$), 7.65 (dd, *J* 4.5, 1.6 Hz, 2 H, $H^3$), 5.62 (d, *J* 12.3 Hz, 1 H, $H^{\alpha}$), 3.16 (s, 3 H, $H^{NMe}{}_a$), 2.93 (s, 3 H, $H^{NMe}{}_b$); $^{13}$C NMR (126 MHz, $CDCl_3$) $\delta$ (ppm) 186.84 ($C^{C=O}$), 155.22 ($C^4$), 150.27 ($C^2$), 122.87 ($C^{\beta}$), 121.16 ($C^3$), 91.62 ($C^{\alpha}$), 45.22 ($C^{Me}{}_a$), 37.31 ($C^{Me}{}_b$); EI-MS *m/z*: 176.1 $[M]^+$ (38 %, calc. 176.1), 159.1 $[M\text{-}OH]^+$(60 %), 98.1 $[M\text{-}py]^+$ (100 %); EA: calc. for $C_{10}H_{12}N_2O$, C 68.16 %, H 6.86 %, N 15.90 %, found C 68.08 %, H 6.75 %, N 15.71 %. All analytical data match those published.[87,65]

### 3.4.1.8 (*E*)-1-(2,4-Difluorophenyl)-3-*N*,*N*-dimethylaminoprop-2-en-1-one (18)

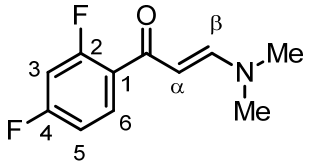


DMF-DMA (1.19 g, 10.0 mmol, 1.0 eq) and 4-acetylpyridine (1.56 g, 10.0 mmol, 1.0 eq) were mixed in a 20 ml microwave vial without any solvent and stirred for 10 min at 160 °C to yield a brown oil. This was diluted with a few ml of MeOH and extracted several times with hot hexane. The combined hexane fractions were freed of solvent to yield (**18**) as yellow crystals (1.15 g, 5.5 mmol, 55 %). $^{1}$H NMR (500 MHz, $CDCl_3$) $\delta$ (ppm) 7.88-7.67 (m, 2 H, $H^{3+\alpha}$), 6.90 (td, *J* 8.3, 2.4 Hz, 1 H, $H^5$), 6.79 (ddd, *J* 11.1, 8.8, 2.5 Hz, 1 H, $H^6$), 5.60 (dd, *J* 12.3, 2.2 Hz, 1 H, $H^{\alpha}$), 3.13 (s, 3 H, $H^{NMe}{}_b$), 2.89 (s, 3 H, $H^{NMe}{}_a$); $^{13}$C NMR (126 MHz, $CDCl_3$) $\delta$ (ppm) 184.53 ($C^{C=O}$), 164.21 (dd, *J* 251.1, 12.4 Hz, $C^2$), 161.12 (dd, *J* 250.2, 12.4 Hz, $C^4$), 154.55 ($C^{\beta}$), 132.30 (dd, *J* 9.9, 4.7 Hz, $C^3$), 125.64 (dd, *J* 14.2, 3.8 Hz, $C^1$), 111.58 (dd, *J* 20.9, 3.5 Hz, $C^5$), 104.23 (dd, *J* 28.0, 25.2 Hz, $C^6$), 96.43 ($C^{\alpha}$), 45.23 ($C^{Me}{}_b$), 37.42 ($C^{Me}{}_a$); $^{19}$F NMR (376 MHz, $CDCl_3$) $\delta$(ppm) -107.16 (s, 1 F, $F^{C4}$), -107.95 (br s, 1 F, $F^{C2}$); EI-MS *m/z*: 211.1 $[M]^+$ (37 %, calc. 211.1), 194.1 $[M\text{-}OH]^+$(100 %), 141.1 $[M\text{-}C_4H_8N]^+$ (35 %), 98.1 $[M\text{-}C_6H_3F_2]^+$ (45 %); EA: calc. for $C_{11}H_{11}N_1OF_2$, C 62.55 %, H 5.25 %, N 6.63 %, found C 62.49 %, H 5.42 %, N 6.68 %.

### 3.4.1.9 (*E*)-1-(4-Bromophenyl)-3-*N*,*N*-dimethylaminoprop-2-en-1-one (19)

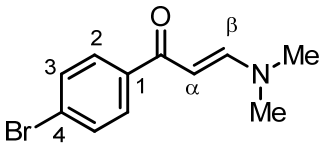


To a 5 ml microwave vial 4-bromoacetophenone (3.83 g, 20.0 mmol, 1 eq) and DMF-DMA (2.38 g, 20.0 mmol, 1 eq) were added and stirred at 150 °C for 10 m The resulting brown oil was treated with diethyl ether and a yellow precipitate formed. This was filtered off, washed with little $Et_2O$ and **19** was obtained as yellow powder (3.23 g, 12.7 mmol, 64 %). Analytical data match those published.[65]

### 3.4.1.10 (*E*)-1,3-Bis(trimethoxyphenyl)-prop-2-ene-1-one (23)

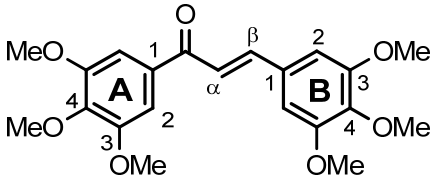


3,4,5-Trimethoxyacetophenone (2.15 g, 10.0 mmol, 1.0 eq) and 3,4,5-trimethoxybenzaldehyde (1.96 g, 10.0 mmol, 1.0 eq) were dissolved in 50 ml EtOH, then KOH (1.12 g, 20.0 mmol, 2.0 eq), dissolved in 50 ml $H_2O$, was added. The solution turned yellow immediately. Water was added slowly until the product started to precipitate (~ 200 ml). This suspension was stirred (TLC control: after 10, 60 min starting material still present) for additional 24 h. The solid was filtered off, washed with water and $Et_2O$. Compound **23** was obtained as a pale yellow powder (3.62 g, 9.3 mmol, 93 %) and was used without further purification in the next step. $^1$H-NMR (400 MHz, $CDCl_3$) $\delta$ (ppm) 7.72 (d, *J* 15.6 Hz, 1 H, $H^{\alpha}$), 7.32 (d, *J* 15.6 Hz, 1 H, $H^{\beta}$), 7.25 (2 H, s, $H^{2A}$), 6.86 (2 H, s, $H^{B2}$), 3.95 (6 H, s, $H^{OMe_a{}^A}$), 3.94 (3 H, s, $H^{OMe_b{}^A}$), 3.92 (6 H, s, $H^{OMe_a{}^B}$), 3.90 (3 H, s, $H^{OMe_b{}^B}$); $^{13}$C NMR (101 MHz, $CDCl_3$) $\delta$ (ppm) 189.60 ($C^{C=O}$), 153.67 ($C^{3A}$), 153.32 ($C^{3B}$), 145.12 ($C^{\alpha}$), 133.77 ($C^{4A}$), 130.53 ($C^{4B}$), 121.49 ($C^{\beta}$), 106.45 ($C^{2A}$), 105.94 ($C^{2B}$), 61.14 ($C^{OMe_b{}^{A+B}}$), 56.66 ($C^{OMe_a{}^A}$), 56.45 ($C^{OMe_a{}^B}$); EI-MS *m/z*: 388.2 $[M]^+$ (100 %, calc. 388.2), 373.1 $[M\text{-}Me]^+$ (42 %), 357.1 $[M\text{-}MeO]^+$ (30 %) 354.1 $[M\text{-}Me_2O]^+$ (11 %). All analytical data match those published.[88]

### 3.4.1.11 (*E*)-1,3-Di(phenyl)-prop-2-ene-1-one (24)

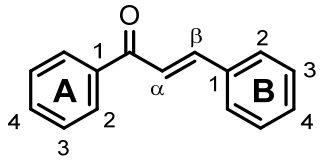


Acetophenone (1.20 g, 10.0 mmol, 1.0 eq) and benzaldehyde (1.06 g, 10.0 mmol, 1.0 eq) were dissolved in 50 ml EtOH then KOH (1.12 g, 20.0 mmol, 2.0 eq), dissolved in 50 ml $H_2O$, was added. The solution turned yellow immediately. Water was added slowly until the product started to precipitate (~ 200 ml). This suspension was stirred 2 h. The solid was filtered off, washed with water and little $Et_2O$. Compound **24** was obtained as a pale yellow powder (1.83 g, 8.8 mmol, 88 %) and was used without further purification in the next step. All analytical data match those published.[89]

### 3.4.1.12 (*E*)-1-(*p*-Nitrophenyl)-3-(pyrid-2-yl)-prop-2-ene-1-one (25)

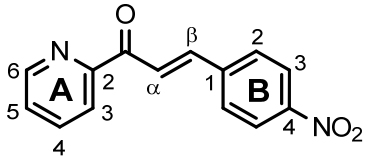


Potassium *tert*-butoxide (2.31 g, 20.0 mmol, 2.0 eq) was suspended in THF (20 ml), then 2-acetylpyridine (1.25 g, 10.0 mmol, 1.0 eq) was added and a yellow suspension formed immediately. This was added slowly to a THF solution of *p*-nitrobenzaldehyde (1.53 g, 10.0 mmol, 1.0 eq) at 0 °C to form a red suspension. After 30 min the precipitate was filtered off, washed with $H_2O$ and dried in a desiccator. **25** was obtained as a yellow powder (2.5 g, 9.8 mmol, 98 %) and was pure enough to be used for the following step. $^1$H-NMR (500 MHz, $CDCl_3$) $\delta$ (ppm) 8.76 (d, *J* 4.4 Hz, 1 H, $H^{6A}$), 8.43 (d, *J* 16.1 Hz, 1 H, $H^{\alpha}$), 8.27 (d, *J* 8.7 Hz, 2 H, $H^{3B}$), 8.20 (d, *J* 7.8 Hz, 1 H, $H^{3A}$), 7.92 (d, *J* 16.1 Hz, 1 H, $H^{\beta}$), 7.91 (td, *J* 7.8, 1.6 Hz, 1 H, $H^{4A}$) , 7.86 (d, *J* 8.7 Hz, 2 H, $H^{2B}$) , 7.53 (dd, *J* 7.0, 5.1 Hz, 1 H, $H^{5A}$); $^{13}$C NMR (101 MHz, $CDCl_3$) $\delta$ (ppm) 189.09 ($C^{C=O}$), 153.72 ($C^{2A}$), 149.11 ($C^{6A}$), 148.69 ($C^{4B}$), 141.45 ($C^{1B}$), 141.42 ($C^{\beta}$), 137.37 ($C^{4A}$), 129.39 ($C^{2B}$), 127.50 ($C^{5A}$), 124.95 ($C^{\alpha}$), 124.27 ($C^{3B}$), 123.24 ($C^{3A}$); EI-MS *m/z*: 254.1 $[M]^+$ (100 %, calc. 254.1); EA: calc. for $C_{14}H_{11}N_2O_4$, C 63.87 %, H 4.21 %, N 10.64 %, found C 63.96 %, H 4.20 %, N 10.61 %. All analytical data match those published.[90]

### 3.4.1.13 (*E*)-1,3-*bis*(2,3,4,5,6-Pentafluorophenyl)-prop-2-ene-1-one (26)

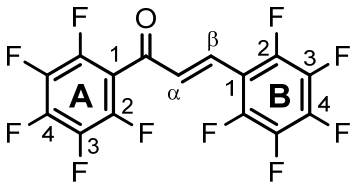

2,3,4,5,6-Pentafluoroacetophenone (2.10 g, 10.0 mmol, 1.0 eq) and 2,3,4,5,6-pentafluorobenzaldehyde (1.96 g, 10.0 mmol, 1.0 eq) were dissolved in 50 ml EtOH then KOH (1.12 g, 20.0 mmol, 2.0 eq), dissolved in 50 ml $H_2O$, was added. The solution turned yellow immediately. Water was added slowly until the product started to precipitate (~ 200 ml). This suspension was stirred (TLC control: after 10, 60 min still educts present) for additional 16 h. The solid was filtered off, washed with water and $Et_2O$. Compound **26** was obtained as a pale yellow powder (2.17 g, 5.7 mmol, 57 %) and was used without further purification in the next step. All analytical data match those published.[91]

### 3.4.1.14 (*E*)-1-(pyrid-2-yl)-3-(5-Bromothiophenyl)-prop-2-ene-1-one (28)

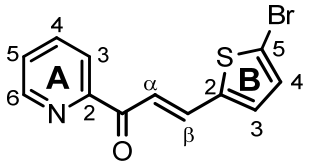

2-Acetylpyridine (1.21 g, 10.0 mmol, 1.0 eq) and 5-bromothiophenol carbaldehyde (1.91 g, 10.0 mmol, 1.0 eq) were dissolved in 50 ml EtOH then KOH (1.12 g, 20.0 mmol, 2.0 eq), dissolved in 50 ml $H_2O$, was added. The solution turned yellow immediately. Water was added slowly until the product started to precipitate (~ 200 ml). This suspension was stirred 2 h. The solid was filtered off, washed with water and $Et_2O$. Compound **28** was obtained as a pale yellow powder (2.29 g, 7.8 mmol, 78 %) and was used without further purification in the next step. All analytical data match those published.[92]

### 3.4.1.15 (*E*)-1-(pyrid-2-yl)-3-(3,4,5-trismethoxyphenyl)-prop-2-ene-1-one (29)

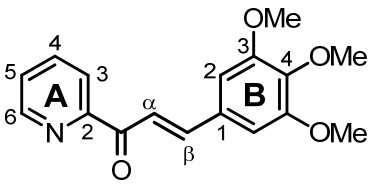

2-Acetylpyridine (1.21 g, 10.0 mmol, 1.0 eq) and 3,4,5-trimethoxybenzaldehyde (1.96 g, 10.0 mmol, 1.0 eq) were dissolved in 50 ml EtOH then KOH (1.12 g, 20.0 mmol, 2.0 eq),

dissolved in 50 ml $H_2O$, was added. The solution turned yellow immediately. Water was added slowly until the product started to precipitate (~ 200 ml). This suspension was stirred (TLC control: after 10, 60 min still educts present) for additional 10 h. The solid was filtered off, washed with water and $Et_2O$. Compound **29** was obtained as a pale yellow powder (1.10 g, 3.7 mmol, 37 %) and was used without further purification in the next step. All analytical data match those published.[93]

### 3.4.1.16 1-(2-(*p*-Nitrophenyl)-2-oxoethyl) pyridinium iodide (33)

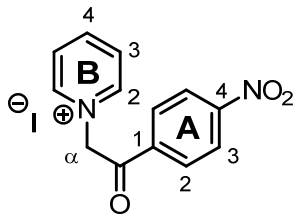


A solution of $I_2$ (5.21 g, 20.5 mmol, 1.03 eq) in 8 ml dry pyridine was added to a solution of *p*-nitroacetophenone (3.41 g, 20 mmol, 1.0 eq) in 5 ml dry pyridine and was then stirred for 6 h at 80 °C. After 2 h too much black precipitate formed which indicated that there was not enough solvent. More pyridine was added (10 ml). After an hour the precipitate was filtered off, washed with $Et_2O$/EtOH (9:1) and recrystallized from EtOH to give dark yellow crystals (6.0 g, 16.2 mmol, 81.0 %). $^1$H NMR (500 MHz, $CD_3CN$) $\delta$ (ppm) 8.71 (dd, *J* 6.7, 1.3 Hz, 2 H, $H^{2B}$), 8.65 (1 H, tt, *J* 7.9, 1.3, $H^{4B}$), 8.42 (2 H, m; $H^{2A}$), 8.26 (2 H, m, $H^{3B}$), 8.15 (1 H, dd, *J* 7.8, 6.8 Hz, $H^{3B}$), 6.34 (2 H, s, $H^{\alpha}$), $^{13}$C NMR (101 MHz, $CD_3CN$) $\delta$ (ppm) 190.33 ($C^{C=O}$), 152.34 ($C^{4A}$), 148.02 ($C^{4B}$), 147.10 ($C^{2B}$), 138.97 ($C^{1A}$), 130.79 ($C^{2A}$), 129.16 ($C^{3B}$), 125.20 ($C^{3A}$), 67.69 ($C^{\alpha}$), ESI-MS *m/z*: 254.1 $[M]^+$ (100 %, calc. 254.1). All analytical data match those published.[94]

### 3.4.1.17 1-(2-oxo-2-(thiophen-2-yl)ethyl)pyridin-1-ium (37)

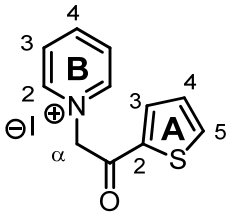


Iodine (5.08 g, 20.0 mmol, 1 eq) was dissolved in dry and hot pyridine (50.0 ml), at least 10 min stirring at 100° C. Then 2-acetyl thiophene (2.52 g, 20.0 mmol, 1 eq) was added to the mixture over 5 m and was stirred for 5 h under reflux. After cooling the crude product was isolated by filtering and was washed with big amount of $Et_2O$/EtOH (9:1) to give a grey powder (5.0g). This was dissolved in ~100 ml boiling EtOH containing 5 wt% activated charcoal and filtered hot over Celite®. Out of this solution yellow plate like crystals formed (4.4 g, 13.3 mmol, 65 %). $^1$H NMR (500 MHz, $CDCl_3$) 8.58 (d, *J* 6.0 Hz, 2 H, $H^{2B}$), 8.11 (t, *J* 7.8,

0.9 Hz, 1 H, $H^{4B}$), 7.62 (t, *J* 6.6 Hz, 2 H, $H^{3B}$), 7.55 (d, *J* 3.8 Hz, 1 H, $H^{5A}$), 7.42 (d, *J* 4.8 Hz, 1 H, $H^{3A}$), 6.75 (t, *J* 4., $H^{4A}$), 5.95 (s, 2 H, $H^{a}$).[64]

## 3.4.2 Ligands

### 3.4.2.1 6'-(*N*-Methylpyrrol-2-yl)-2,2'-bipyridine (1)

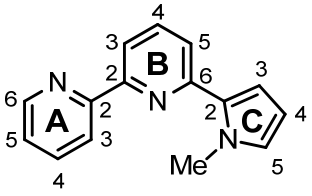


1-Methylpyrrole (2.03 g, 25.0 mmol) was added to dry THF (20 ml) and the solution was cooled to 223 K. *n*-BuLi (18.8 ml, 1.6 M) was added and the reaction mixture was stirred for 1 h and then warmed to 273 K. 2,2'-Bipyridine (3.51 g, 22.5 mmol) was added and the red suspension was allowed to warm to room temperature after which it was stirred for 12 h. The reaction mixture was quenched with water and the organic layer removed. The aqueous layer was extracted three times with $CH_2Cl_2$. An excess of $MnO_2$ was added to the combined $CH_2Cl_2$ layers and the resulting black suspension was stirred at room temperature overnight. After drying over $MgSO_4$, the mixture was filtered and the filtrate collected. Solvent was removed *in vacuo*, and the product purified by column chromatography (silica M60, pentane/ethyl acetate 95:5 changing to 9:1). **1** was isolated as a white crystalline solid (0.907 g, 15.4%). $^1$H NMR (500 MHz, $CD_2Cl_2$) $\delta$ (ppm) 8.67 (dd, *J* 4.7, 0.7 Hz, 1 H, $H^{6A}$), 8.44 (d, *J* 7.9 Hz, 1 H, $H^{3A}$), 8.24 (d, *J* 7.8 Hz, 1 H, $H^{3B}$), 7.84 (t, *J* 7.7 Hz, 1 H, $H^{4A}$), 7.79 (t, *J* 7.8 Hz, 1 H, $H^{4B}$), 7.59 (d, *J* 7.8 Hz, 1 H, $H^{5B}$), 7.32 (m, 1 H, $H^{5A}$), 6.79 (m, 1 H, $H^{5C}$), 6.65 (m, 1 H, $H^{3C}$), 6.18 (t, *J* 3.2 Hz, 1 H, $H^{4C}$), 4.13 (s, 3 H, $H^{Me}$); $^{13}C\{^1H\}$ NMR (126 MHz, $CD_2Cl_2$) $\delta$ (ppm) 156.9 ($C^{2A}$), 155.4 ($C^{2B}$), 152.6 ($C^{6B}$), 149.6 ($C^{6A}$), 137.8 ($C^{4B}$), 137.4 ($C^{4A}$), 132.2 ($C^{2C}$), 127.0 ($C^{5C}$), 124.2 ($C^{5A}$), 121.8 ($C^{5B}$), 121.3 ($C^{3A}$), 117.9 ($C^{3B}$), 111.4 ($C^{3C}$), 108.1 ($C^{4C}$), 37.9 ($C^{Me}$); IR (solid, $\nu$/cm$^{-1}$) 2964 (w), 2937 (w), 2358 (w), 2331 (w), 1580 (m), 1566 (m), 1556 (m), 1456 (m), 1435 (m), 1157 (w), 1097 (w), 775 (w), 721 (w), 530 (s); UV/vis ($CH_2Cl_2$, 1.0*10$^{-5}$ mol dm$^{-3}$) $\lambda_{max}$/nm 237 ($\varepsilon$/dm$^3$ mol$^{-1}$ cm$^{-1}$ 18300), 281 (18700), 303 (17000); emission ($\lambda_{ex}$ = 282 nm) $\lambda_{em}$ = 457 nm; EI MS:*m/z* 235.1 $[M]^+$ (calc. 235.1), 234.1 $[M-H]^+$ (base peak, calc. 234.1); EA: calc. for $C_{15}H_{13}N_3$ C 76.57 %, H 5.57 %, N 17.86 %. found C 76.54 %, H 5.64 %, N 17.88 %.

### 3.4.2.2 6'-(Furan-2-yl)-2,2'-bipyridine (2)

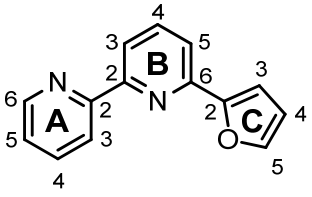

In 20 ml HOAc **8** (1.63 g, 5.0 mmol, 1.0 eq), the Mannich base **7** (1.02 g, 5.0 mmol, 1.0 eq) and $NH_4OAc$ (3.85 g, 50.0 mmol, 10 eq) were suspended and stirred under reflux for 8 h and overnight at room temperature. The solvent was evaporated to give a black residue which was suspended in $H_2O$ and the pH was adjusted to ~8. The aqueous phase was extracted into $CH_2Cl_2$ (~3 x 30 ml). The combined organic layers were washed with diluted NaOH solution (~1 M) and water then dried over $MgSO_4$. The solid was filtered off and the solvent was evaporated to give a brown residue. The crude product was purified by column chromatography ($SiO_2$, $CH_2Cl_2$/MeOH 1:0-96:4) The desired product was obtained in the first major fraction as a yellow solid (250.0 mg, 1.13 mmol, 23 %). $^1$H NMR (400 MHz, $CD_2Cl_2$) $\delta$ (ppm 8.67 (d, *J* 4.7 Hz, 1 H, $H^{6A}$), 8.54 (d, *J* 8.0 Hz, 1 H, $H^{3A}$), 8.31 (s, *J* 8.1 Hz, 1 H, $H^{3B}$), 7.89-7.81 (m, 2 H, $H^{4A+B}$), 7.72 (d, 8.1 Hz, 1 H, $H^{5B}$), 7.59 (d, 1.0 Hz, 1 H, $H^{5C}$), 7.34 (ddd, *J* 7.4, 4.8, 1.0 Hz, 1 H, $H^{5A}$), 7.20 (d, *J* 3.3 Hz, 1 H, $H^{3C}$), 6.59 (dd, *J* 3.4, 1.8 Hz, 1 H, $H^{4C}$); $^{13}$C NMR (101 MHz, $CD_2Cl_2$) $\delta$ 156.44 ($C^{2A}$), 156.30 ($C^{2B}$), 154.64 ($C^{6B}$), 149.66 ($C^{6A}$), 149.29 ($C^{2C}$), 143.88 ($C^{5C}$), 138.14 ($C^{4B}$), 137.37 ($C^{4A}$), 124.41 ($C^{5A}$), 121.48 ($C^{3A}$), 119.63 ($C^{3B}$), 118.84 ($C^{5B}$), 112.58 ($C^{4C}$), 109.09 ($C^{3C}$); UV/vis ($CH_2Cl_2$, 1.0*10$^{-5}$ mol dm$^{-3}$) $\lambda_{max}$/nm 239 ($\varepsilon$/dm$^3$ mol$^{-1}$ cm$^{-1}$ 22300), 277 (29000), sh 290 (21000), 318 (13400); emission ($\lambda_{ex}$ = 317 nm) $\lambda_{em}$ = 378 nm. All other analytical data match those previously reported.[66]

### 3.4.2.3 6'-(Thiophen-2-yl)-2,2'-bipyridine (3)

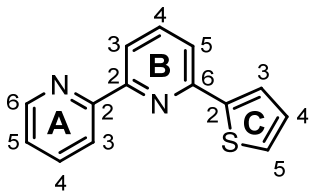


**Method 1**

*n*-BuLi (1.6 M in hexane, 11 mmol, 6.3 ml) was added to a solution of thiophene (0.80 ml, 10.0 mmol) in THF (20 ml) at 223–233 K. The yellow solution was stirred for 1 h, after which time bpy (1.56 g, 10.0 mmol) was added. The reaction mixture turned red immediately. The suspension was allowed to warm to room temperature and was then stirred for 12 h. After quenching the reaction with $H_2O$, the organic layer was separated and the aqueous phase extracted 3 times with $CH_2Cl_2$. The organic layers were combined and an excess of $MnO_2$ was added. The black suspension was stirred at room temperature overnight and was then dried over $MgSO_4$. The solids were separated by filtration, the solvent removed *in vacuo*, and the product purified by column chromatography (silica M60, $CH_2Cl_2$ changing to $CH_2Cl_2$/MeOH 99:1–97:3). Compound **3** was obtained as a brown oil as the 1st major fraction, and after recrystallization from hexane, **3** was isolated as white crystals (220 mg, 10 %). The 2$^{nd}$ major

fraction was identified as 4-(thiophen-2-yl)-2,2'-bipyridine **41** (260 mg, 12 %). Spectroscopic data for **2** were in agreement with those published.

**Method 2**

2-Acetylthiophene (1.26 g, 10 mmol) was added to a solution of *t*ert-BuOK (2.24 g, 20 mmol) in dry THF (30 ml). The mixture was stirred for 2 h at room temperature during which time it turned yellow. 1-(Pyridin-2-yl)-3-*N*,*N*-dimethylamino-prop-2-en-1-one **13** (1.76 g, 10 mmol) was added and the reaction mixture was stirred for 14 h during which time it became deep red. Excess solid $NH_4OAc$ and HOAc (25 ml) were added and the mixture was stirred under reflux for 2 h to give a black solution. The solvents were removed in *vacuo* and the black residue was suspended in$H_2O$ and the pH adjusted to 8 by adding solid $K_2CO_3$. The aqueous phase was extracted several times with $CH_2Cl_2$, the organic phases were combined and dried over $MgSO_4$. After removing the solvent under reduced pressure, the resulting black oil was dissolved in toluene and filtered through Celite®. The solvent was evaporated to give a brown paste which was passed through a column ($SiO_2$ 60 µ, 18 cm, hexanes/EtOAc) to give two products, 2,6-bis(thiophen-2-yl)-pyridine **42** as the 1$^{st}$ major fraction (245 mg, 10 % or 20 % relative to 2-acetylthiophene, respectively) and compound **3** as the 2$^{nd}$ major fraction (430 mg, 18 %). $^1$H NMR (400 MHz, $CD_2Cl_2$) $\delta$ (ppm) 8.67 (ddd, *J* 4.8, 1.6, 0.8 Hz, 1 H, $H^{6A}$), 8.56 (d, *J* 8.0 Hz, 1 H, $H^{3A}$), 8.31 (dd, *J* 7.8, 0.8 Hz, 1 H, $H^{3B}$), 7.91-7.80 (m, 2 H, $H^{4A+B}$), 7.70 (dd, *J* 7.9, 0.8 Hz, 1 H, $H^{5B}$), 7.68 (dd, *J* 3.7, 1.1 Hz, 1 H, $H^{5C}$), 7.45 (dd, *J* 5.1, 1.1 Hz, 1 H, $H^{3C}$), 7.34 (ddd, *J* 7.5, 4.8, 1.2 Hz, 1 H, $H^{5A}$), 7.16 (dd, *J* 5.0, 3.7 Hz, 1 H, $H^{4C}$); $^{13}$C NMR (101 MHz, $CD_2Cl_2$) $\delta$ (ppm) 156.25 ($C^{2A}$), 156.12 ($C^{2B}$), 152.34 ($C^{2C}$), 149.63 ($C^{6A}$), 145.84 ($C^{6B}$), 138.22 ($C^{4B}$), 137.44 ($C^{4A}$), 128.62 ($C^{4C}$), 128.18 ($C^{3C}$), 125.13 ($C^{5C}$), 124.44 ($C^{5A}$), 121.54 ($C^{3A}$), 119.55 ($C^{3B}$), 119.10 ($C^{5A}$); UV/vis ($CH_2Cl_2$, 1.0*10$^{-5}$ mol dm$^{-3}$) $\lambda_{max}$/nm 242 ($\varepsilon$/dm$^3$ mol$^{-1}$ cm$^{-1}$ 17900), 282 (17300), 301 (14700), 319 (13500); emission ($\lambda_{ex}$ = 315 nm) $\lambda_{em}$ = 373 nm. Spectroscopic data for **2** were in agreement with those published.[95,96]

### 3.4.2.4 6'-(Selenophen-2-yl)-2,2'-bipyridine (4)

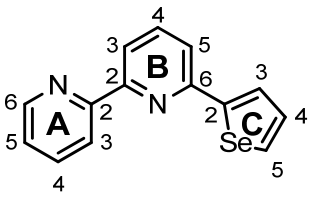


*n*-BuLi (1.6 M in hexanes, 1.6 ml, 2.6 mmol) was added to a solution of selenophen (190 µl, 2.2 mmol) in THF (12 ml) at 190 K. The pale yellow solution was stirred for 1 h, after which **bpy** (310 mg, 2.0 mmol) was added. The reaction mixture slowly turned red. The suspension was allowed to warm to room temperature and then was stirred for 12 h during which time it became deep red. After quenching the reaction with $H_2O$, the organic layer was separated

and the aqueous phase was extracted 3 times with $CH_2Cl_2$. The organic layers were combined and an excess of $MnO_2$ was added. The black suspension was stirred at room temperature overnight, and dried over $MgSO_4$. The precipitate was removed by filtration and the filtrate collected. After solvent removal in *vacuo*, the product was purified by column chromatography (silica M60, pentane/ethylacetate 95:5 to 9:1). Compound **4** was isolated as an yellow solid (160 mg, 28 %). $^1$H NMR (500 MHz, $CD_2Cl_2$) $\delta$ (ppm) 8.67 (d, *J* 4.1 Hz, 1 H, $H^{A6}$), 8.51 (d, *J* 7.9 Hz, 1 H, $H^{A3}$), 8.31 (d, *J* 7.8 Hz, 1 H, $H^{B3}$), 8.10 (d, *J* 5.6 Hz, 1 H,$H^{C5}$), 7.87 (t, *J* 7.7 Hz, 1 H,$H^{A4}$), 7.83 (m, 2 H,$H^{4B+3C}$), 7.72 (d, *J* 7.8 Hz, 1 H,$H^{5B}$), 7.41 (m, 1 H, $H^{4C}$), 7.34 (m, 1 H, $H^{5A}$); $^{13}$C{$^1$H} NMR (101 MHz, $CD_2Cl_2$) $\delta$ 156.2 ($C^{2A/2B}$), 156.1 ($C^{2A/2B}$), 153.7 ($C^{2C}$), 152.7 ($C^{6B}$), 149.6 ($C^{6A}$), 138.2 ($C^{4B}$), 137.5 ($C^{4A}$), 133.4 ($C^{5C}$), 131.4 ($C^{4C}$), 126.7 ($C^{3C}$), 124.5 ($C^{5A}$), 121.5 ($C^{3A}$), 119.7 ($C^{3B}$), 118.1 ($C^{5B}$); $^{77}$Se{$^1$H} NMR (114 MHz, $CD_2Cl_2$) $\delta$(ppm) 603.1; IR (solid, $\nu$/cm$^{-1}$) 3049 w, 2922 w, 2851 w, 1580 w, 1562 s, 1541 w, 1454 w, 1423 s, 1265 w, 1225 w, 1151 w, 1092 w, 1078 w, 1045 w, 989 w, 968 w, 912 w, 847 w, 824 w, 771 s, 735 s, 704 s, 677 s, 648 w; UV/vis ($CH_2Cl_2$, 1.0*10$^{-5}$ mol dm$^{-3}$) $\lambda_{max}$/nm 241 ($\varepsilon$/dm$^3$ mol$^{-1}$ cm$^{-1}$ 11500), 275 (13500), 312 (11000); (weak) emission ($\lambda_{ex}$ = 275 nm) $\lambda_{em}$ = 369 nm; ESI MS: *m/z* 309.0 [M + Na]$^+$ (base peak, calc. 309.0), 287.3 [M + H]$^+$ (calc. 287.0); EA: calc. for $C_{14}H_{10}N_2Se$ C 58.96 %, H 3.53 %, N 9.82%, found C 58.89 %, H 3.57 %, N 9.68 %.

### 3.4.2.5 6'-Methyl-2,2'-bipyridine (6)

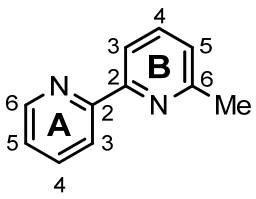


MeLi (1.6 M in $Et_2O$, 50.0 ml, 75.0 mmol, 1.5 eq) was added to a solution of bpy (7.80 g, 50.0 mmol, 1.0 eq) in THF (110 ml) at 190 K. The pale yellow solution was stirred for 1 h at the same temperature. The reaction mixture slowly turned red, was allowed to warm to room temperature and was then stirred for 18 h during which time it became deep red. After quenching the reaction with $H_2O$, the organic layer was separated and the aqueous phase was extracted 3 times with $CH_2Cl_2$. The organic layers were combined and an excess of $MnO_2$ was added. The black suspension was stirred at room temperature overnight, and dried over $MgSO_4$. The precipitate was removed by filtration and the filtrate collected. After solvent removal in *vacuo*, the product was purified by column chromatography (silica M60, pentane/$Et_2O$ 9:1 to 1:1). Compound **6** was isolated in the first major fraction as an off white solid (3.40 mg, 40 %). Minor fractions were observed containing 6,6'-dimethyl-2,2'-bipyridine (380 mg, 4 %). $^1$H NMR (500 MHz, $CDCl_3$) $\delta$ (ppm) 8.59 (d, *J* 4.6 Hz, 1 H, $H^{A6}$), 8.32 (d, *J* 8.0 Hz, 1 H, $H^{A3}$), 8.09 (d, *J* 8.0 Hz, 1 H, $H^{3B}$), 7.71 (t, *J* 7.7 Hz, 1 H,$H^{4A}$), 7.61 (t, *J* 7.7 Hz, 1 H, $H^{4B}$), 7.20 (dd, *J* 7.5, 4.9 Hz, 1 H, $H^{5A}$), 7.08 (d, *J* 7.6 Hz, 1 H, $H^{5B}$), 2.55 (s, 1 H, $H^{Me}$); UV/vis

($CH_2Cl_2$, 1.0*$10^{-4}$ mol $dm^{-3}$) $\lambda_{max}$/nm 238 ($\varepsilon$/$dm^3$ $mol^{-1}$ $cm^{-1}$ 10900), 245 (10100), 288 (15100); emission ($\lambda_{ex}$ = 315 nm) $\lambda_{em}$ = 337 nm. All other analytical data match those previously reported.[25]

### 3.4.2.6 6'-(2,3,5,6-Tetrafluorophenyl)-2,2'-bipyridine (9)

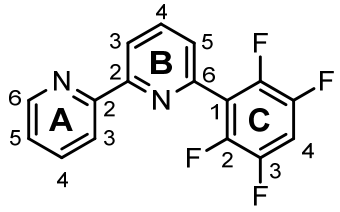


*n*-BuLi (1.6 M in hexanes, 20.0 ml, 30.0 mmol, 1.3 eq) was added to a solution of 1,2,3,4,5-pentafluorobenzene (4.20 g, 25.0 mmol, 1.1 eq) in THF (40 ml) at 200 K. The pale yellow solution was stirred for 1 h, after which **bpy** (3.51 g, 22.5 mmol, 1.0 eq) was added. The reaction mixture slowly turned red. The suspension was allowed to warm to room temperature and then was stirred for 12 h during which time it became deep red. After quenching the reaction with $H_2O$, the organic layer was separated and the aqueous phase was extracted 3 times with $CH_2Cl_2$. The organic layers were combined and an excess of $MnO_2$ was added. The black suspension was stirred at room temperature overnight, and dried over $MgSO_4$. The precipitate was removed by filtration and the filtrate collected. After solvent removal in *vacuo*, the product was purified by column chromatography (silica M60, pentane/ethylacetate 95:5 to 9:1). Compound **9** was isolated as an yellow solid (210 mg, 5 % or 10 % relative to recovered bpy). $^1$H NMR (500 MHz, $CDCl_3$) $\delta$ (ppm) 8.79 (d, *J* 2.1 Hz, 1 H, $H^{6A}$), 8.71 (d, *J* 4.5 Hz, 1 H, $H^{3A}$), 8.56 (d, *J* 8.2 Hz, 1 H, $H^{3B}$), 8.47 (d, *J* 8.0 Hz, 1 H, $H^{4A}$), 7.95 (dd, *J* 8.1, 1.8 Hz, 1 H, $H^{4B}$), 7.85 (td, *J* 7.8, 1.8 Hz, 2 H, $H^{5A}$), 7.35 (dd, *J* 7.5, 4.9 Hz, 1 H,$H^{5B}$), 7.14 (m, 1 H, $H^{4C}$); $^{13}$C{$^1$H} NMR $^{13}$C NMR (151 MHz, $CDCl_3$) $\delta$ (ppm) 163.5 (dd, *J* 251.2, 12.1 Hz, $C^{4C}$), 161.1 (dd, *J* 252.9, 12.0 Hz, $C^{2C}$), 155.5 ($C^{2A}$), 152.0 ($C^{6B}$), 148.4 ($C^{6A}$), 138.1 ($C^{2B}$), 137.8 ($C^{4A+B}$), 132.5 (dd, *J* 9.6, 4.5 Hz $C^{6C}$), 124.6 (d, *J* 10.0 Hz $C^{5B}$), 124.2 ($C^{5A}$), 123.7 (d, *J* 11.0 Hz $C^{1C}$), 121.8 ($C^{3A}$), 120.2 ($C^{3B}$), 112.1 (dd, *J* 21.0, 3.6 Hz $C^{5C}$), 104.6 (dd, *J* 27.1, 25.3 Hz $C^{3C}$); EI MS: *m*/*z* 304.1 $[M]^+$ (base peak, calc. 304.1); IR (solid, $\nu$/$cm^{-1}$) 3049 w, 2922 w, 2851 w, 1580 w, 1562 s, 1541 w, 1454 w, 1423 s, 1265 w, 1225 w, 1151 w, 1092 w, 1078 w, 1045 w, 989 w, 968 w, 912 w, 847 w, 824 w, 771 s, 735 s, 704 s, 677 s, 648 w.

### 3.4.2.7 6'-*n*-Butyl-2,2'-bipyridine (10)

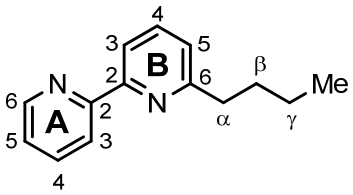


To a THF solution (10 ml) of thiazole (1.28 g, 15.0 mmol, 1.1 eq) *n*-BuLi (1.6 M in hexanes, 13.9 ml, 19.5 mmol, 1.3 eq) was added over 10 m The first clear solution turned yellow then to a green suspension. After stirring this mixture at 190 K for an hour bpy (2.13 g, 13.6 mmol, 1.0 eq) was added and the mixture turned deep red immediately. It was then allowed to warm up to room temperature and was stirred overnight. The reaction was quenched by addition of $H_2O$. The organic layer was separated and the aqueous phase was extracted 3 times with $CH_2Cl_2$. The organic layers were combined and an excess of $MnO_2$ was added. The black suspension was stirred at room temperature overnight, and dried over $MgSO_4$. The precipitate was removed by filtration and the filtrate collected. After solvent removal in *vacuo*, the product was purified by column chromatography (silica M60, pentane/$Et_2O$ 9:1 to 2:8). Compound **10** was isolated as a yellow oil (516 mg, 18 % or 39 % relative to recovered bpy) in the first major fraction. The second major fraction obtained the starting material bpy (1.19 g, 66 %). $^1$H NMR (500 MHz, $CD_2Cl_2$) $\delta$ (ppm) 8.64 (ddd, *J* 4.8, 1.9, 1.0 Hz, 1 H, $H^{A6}$), 8.45 (dt, *J* 8.0, 1.1 Hz, 1 H, $H^{3A}$), 8.20 (dd, *J* 7.8, 1.0 Hz, 1 H, $H^{3B}$), 8.10 (ddd, *J* 8.1, 7.7, 1.0 Hz, 1 H,$H^{4A}$), 7.72 (t, *J* 7.7 Hz, 1 H, $H^{4B}$), 7.30 (ddd, *J* 7.5, 4.8, 1.2 Hz, 1 H, $H^{5A}$), 7.17 (dd, *J* 7.7, 1.0 Hz, 1 H, $H^{5B}$), 2.87-2.82 (m, 2 H, $H^{\alpha}$), 1.82-1.74 (m, 2 H, $H^{\beta}$), 1.48-1.38 (m, 2 H, $H^{\gamma}$), 0.97 (t, *J* 7.4 Hz, 3 H, $H^{Me}$); $^{13}$C{HMQC/HMBC} NMR (500 MHz, $CD_2Cl_2$) $\delta$ 156.2 ($C^{A2/B2}$), 156.1 ($C^{2A/2B}$), 153.7 ($C^{2C}$), 152.7 ($C^{6B}$), 149.40 ($C^{6A}$), 137.28 ($C^{4B}$), 136.97 ($C^{4A}$), 133.4 ($C^{5C}$), 131.4 ($C^{4C}$), 126.7 ($C^{3C}$), 123.83 ($C^{5A}$), 122.94 ($C^{5B}$), 121.18 ($C^{3A}$), 118.27 ($C^{3B}$), 38.23 ($C^{\alpha}$), 32.14 ($C^{\beta}$), 22.66 ($C^{\gamma}$) , 14.04 ($C^{Me}$); EI-MS *m/z*: 212.1 $[M]^+$ (100 %, calc. 212.1); UV/vis ($CH_2Cl_2$, 1.0 x $10^{-4}$ mol $dm^{-3}$) $\lambda_{max}$/nm 237 ($\varepsilon$/$dm^3$ $mol^{-1}$ $cm^{-1}$ 9600), 245 (8900), 288 (13700); emission ($\lambda_{ex}$ = 314 nm) $\lambda_{max}$ = 359 nm.

### 3.4.2.8 6'-(2,4-Difluorophenyl)-2,2'-bipyridine (11)

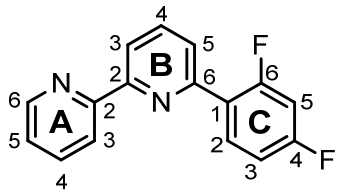


Fresh *t*ert-BuOK (1.06 g, 9.46 mmol, 2.0 eq) was dissolved in 20 ml dry THF at ambient temperature. Then 2-acetylpyridine (0.53 ml, 4.73 mmol, 1.0 eq) was added, the solution turned yellow quickly, during 30 min a precipitate formed and the suspension turned slightly

pink. Then a solution of 1-(2,4-difluorophenyl)-3-*N*,*N*-dimethylamine-prop-2-ene-1-one (1.0 g, 4.73 mmol, 1.0 eq) in 5 ml THF was added and the suspension turned red immediately. This mixture was stirred for a further 30 min. Then $NH_4OAc$ (20 eq, 7.70 g, 100 mmol), dissolved in HOAc (20 ml), was added and the dark solution was stirred for 2 h at reflux. The solvents were reduced on a rotary evaporator, the black residue was suspended in $H_2O$ and solid $K_2CO_3$ was added until the $CO_2$ evolution deceased. The aqueous phase was extracted several times into $CH_2Cl_2$, the combined organic phases were dried over $MgSO_4$ and the solvent was evaporated to give the crude product as a dark solid. This was passed through a column ($SiO_2$, pentane/$Et_2O$ 1:1). The desired product was collected as the second major fraction as an off white powder (175.0 mg, 0.6 mmol, 14 %). $^1$H NMR (600 MHz, $CDCl_3$) $\delta$ (ppm) 8.73 (d, *J* 4.2 Hz, 1 H, $H^{6A}$), 8.56 (d, *J* 8.0 Hz, 1 H, $H^{3A}$), 8.44 (d, *J* 7.8 Hz, 1 H, $H^{3B}$), 8.21 (m, 1 H, $H^{6C}$), 7.90 (t, *J* 7.8 Hz, 2 H, $H^{4A+B}$), 7.81 (dd, *J* 7.8, 1.4 Hz, 1 H, $H^{5B}$), 7.39 (t, *J* 5.5 Hz, 1 H, $H^{5A}$), 7.03 (td, *J* 8.2, 2.3 Hz, 1 H, $H^{5C}$), 6.92 (m, 1 H, $H^{3C}$); $^{13}$C NMR (151 MHz, $CDCl_3$) $\delta$ (ppm) 163.5 (dd, *J* 251.2, 12.1 Hz, $C^{4C}$), 161.1 (dd, *J* 252.9, 12.0 Hz, $C^{2C}$), 155.5 ($C^{2A}$), 152.0 ($C^{6B}$), 148.4 ($C^{6A}$), 138.1 ($C^{2B}$), 137.8 ($C^{4A+B}$), 132.5 (dd, *J* 9.6, 4.5 Hz $C^{6C}$), 124.6 (d, *J* 10.0 Hz $C^{5B}$), 124.2 ($C^{5A}$), 123.7 (d, *J* 11.0 Hz $C^{1C}$), 121.8 ($C^{3A}$), 120.2 ($C^{3B}$), 112.1 (dd, *J* 21.0, 3.6 Hz $C^{5C}$), 104.6 (dd, *J* 27.1, 25.3 Hz $C^{3C}$); EI-MS *m/z*: 268.1 $[M]^+$ (100 %, calc. 268.1); IR (solid, $\nu$/cm$^{-1}$) 3094 (w), 3051 (w), 2920 (w), 2851 (w), 1733 (w), 1717 (w), 1622 (s), 1601 (s), 1593 (s), 1582 (s), 1573 (s), 1562 (s), 1558 (s), 1543 (m), 1504 (s), 1474 (m), 1454 (s), 1438 (m), 1425 (s), 1397 (s), 1385 (s), 1320 (m), 1298 (m), 1288 (m), 1265 (s), 1224 (m), 1162 (m), 1137 (s), 1113 (s), 1100 (s), 1086 (s), 1050 (m), 1038 (m), 990 (m), 966 (s), 941 (m), 927 (w), 916 (m), 897 (w), 870 (m), 843 (s), 836 (s), 829 (m), 816 (s), 808 (m), 793 (w), 772 (s), 733 (s), 713 (s), 699 (m), 694 (m), 687 (w), 664 (w), 650 (m), 645 (s), 637 (s), 622 (s), 611 (m), 605 (m); UV/vis ($CH_2Cl_2$, 5.0 x 10$^{-5}$ mol dm$^{-3}$) $\lambda_{max}$/nm 237 ($\varepsilon$/dm$^3$ mol$^{-1}$ cm$^{-1}$ 26200), 280 (15000), 291 (15800); emission $\lambda_{max}$ ($\lambda_{ex}$) = 363 (237), 367 (245), 382/ 410 (290), br 410 (305), 403/413 (340), 428 (370) nm.

### 3.4.2.9 6'-(3,4,5-Trimethoxyphenyl)-2,2'-bipyridine (12)

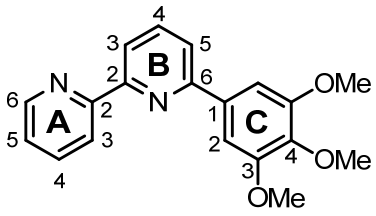


This ligand was prepared by the same procedure as ligand **11** using 3,4,5-trismethoxyacetophenone (2.15 g, 10.0 mmol, 1 eq) and **13** (1.76 g, 10.0 mmol, 1 eq) and was obtained as an off white powder (440 mg, 1.4 mmol, 14 %). $^1$H NMR (500 MHz, $CDCl_3$) $\delta$ (ppm) 8.70 (ddd, *J* 4.7, 1.8, 0.9 Hz, 1 H, $H^{6A}$), 8.58 (dt, *J* 7.9, 1.0 Hz, 1 H, $H^{3A}$), 8.37

(dd, *J* 7.8, 0.9 Hz, 1 H, $H^{3B}$), 7.88 (t, *J* 7.9 Hz, 1 H, $H^{4B}$), 7.86 (td, *J* 7.9, 1.9 Hz, 1 H, $H^{4A}$), 7.72 (dd, *J* 7.9, 1.0 Hz, 1 H, $H^{5B}$) 7.38 (s, 2 H, $H^{2C}$), 7.33 (ddd, *J* 7.5, 4.8, 1.2 Hz, 1 H, $H^{5A}$), 3.921 (s, 6 H, $H^{OMe}{}_a$), 3.917 (s, 3 H, $H^{OMe}{}_b$); $^{13}$C NMR (HMQC/HMBC 500 MHz, $CDCl_3$) $\delta$ (ppm) 156.2 ($C^{2A}$), 155.6 ($C^{2B}$), 153.5 ($C^{6B}$), 149.2 ($C^{6A}$), 139.6 ($C^{4C}$), 138.6 ($C^{3C}$), 137.7 ($C^{4B}$), 136.9 ($C^{4A}$) , 135.1 ($C^{1C}$), 123.7 ($C^{5A}$), 121.3 ($C^{3A}$), 120.2 ($C^{5B}$), 119.4 ($C^{3B}$), 104.4 ($C^{2C}$), 60.9 ($C^{OMe}{}_b$), 56.2 ($C^{OMe}{}_a$); ESI-MS *m/z*: 323.2 $[MH]^+$ (100 %, calc. 322.1); IR (solid, $\nu$/$cm^{-1}$) 3022 (w), 3008 (w), 2973 (m), 2943 (m), 2920 (m), 2865 (w), 2836 (m), 2358 (w), 2354 (w), 2321 (w), 1674 (s), 1668 (m), 1653 (m), 1647 (m), 1636 (w), 1587 (s), 1569 (m), 1558 (m), 1539 (w), 1501 (m), 1464 (m), 1450 (s), 1436 (m), 1409 (s), 1355 (s), 1330 (s), 1245 (m), 1217 (s), 1175 (s), 1145 (m), 1125 (s), 1094 (s), 1035 (w), 1027 (m), 993 (s), 980 (s), 888 (s), 857 (s), 825 (s), 808 (m), 798 (m), 777 (s), 751 (m), 673 (m), 654 (s), 637 (m), 608 (s), 602 (m), UV/vis ($CH_2Cl_2$, 5.0 x $10^{-5}$ mol $dm^{-3}$) $\lambda_{max}$/nm 231 ($\varepsilon$/$dm^3$ $mol^{-1}$ $cm^{-1}$ 22000), 278 (20500), sh 299 (15500); emission ($\lambda_{ex}$ = 278 nm) $\lambda_{max}$ = 437 nm. 2,2':6',2''-Terpyridine was obtained as a minor side product (209 mg, 0.9 mmol, 9 %).

### 3.4.2.10 2,2':6',4''-Terpyridine (20)

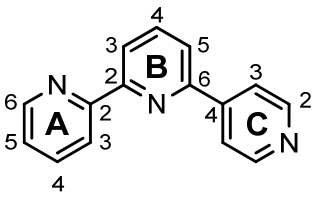


Fresh *t*ert-BuOK (1.12 g, 10.0 mmol, 2.0 eq) was dissolved in 20 ml dry THF at ambient temperature. Then 2-acetylpyridine (1.21 g, 5.0 mmol, 1 eq) was added, the solution turned yellow quickly, during 30 min a precipitate formed and the suspension turned slightly pink. Then a solution of **17** (1.76 g, 5.0 mmol, 1 eq) in 5 ml THF was added and the suspension turned red immediately. This mixture was stirred for a further 30 min and left over night (~ 10 h) at rt without stirring. Then $NH_4OAc$ (20 eq, 7.70 g, 100 mmol), dissolved in HOAc (20 ml), was added and the dark solution was stirred for 2 h at reflux. The solvents were reduced on a rotary evaporator, the black residue was suspended in $H_2O$ and solid $K_2CO_3$ was added until the $CO_2$ evolution deceased. The aqueous phase was extracted several times into $CH_2Cl_2$, the combined organic phases were dried over $MgSO_4$ and the solvent was evaporated to give the crude product as a dark solid. This was passed through a column ($Al_2O_3$, pentane/$Et_2O$ 1:1). The desired product was collected as the second major fraction (627.0 mg, 2.7 mmol, 54 %). $^1$H-NMR (500 MHz, $CDCl_3$) $\delta$ (ppm) 8.74 (dd, *J* 4.6, 1.6 Hz, 2 H, $H^{2C}$), 8.69 (d, *J* 4.7 Hz, 1 H, $H^{6A}$), 8.59 (d, *J* 8.0 Hz, 1 H, $H^{3A}$), 8.47 (d, *J* 7.8 Hz, 1 H, $H^{3B}$), 8.02 (dd, *J* 4.5, 1.6 Hz, 2 H, $H^{3C}$), 7.93 (t, *J* 7.8 Hz, 1 H, $H^{4B}$), 7.85 (dt, *J* 7.7, 1.7 Hz, 1 H, $H^{4A}$), 7.82 (d, *J* 7.8 Hz, 1 H, $H^{5B}$), 7.33 (ddd, *J* 7.4, 4.8, 0.9 Hz, 1 H, $H^{5A}$); UV/vis ($CH_2Cl_2$, 1.0 x $10^{-4}$ mol $dm^{-3}$) $\lambda_{max}$/nm 236 ($\varepsilon$/$dm^3$ $mol^{-1}$ $cm^{-1}$ 20600), 253 (13300), 285 (13900); emission

($\lambda_{ex}$ = 306 nm) $\lambda_{max}$ = 337 nm. The first minor fraction contained 2,2':6',2''-tpy (120 mg, 1.0 mmol, 10 %, or 20 % in respect to 2-acetylpyridine). The analytical data are in agreement with those previously reported.[66,97]

### 3.4.2.11 6''-(*m*-Tolyl)-2,2'-bpy (21)

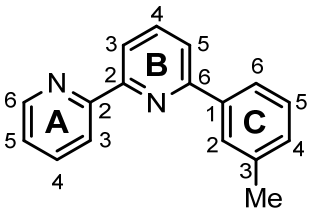


This ligand was prepared by the same procedure as above but *m*-tolylacetophenone was used as the C-H acid component and **13** as $\alpha,\beta$-unsaturated carbonyl. The crude product was purified by column chromatography ($SiO_2$, pentane/$Et_2O$ 9:1 – 2:3). The first major fraction yielded the product as an off white powder (1.10 g, 45 %). The very first minor fraction gave the 2,6-Bis(m-tolyl)pyridine (0.11 g, 4 %) as side product but no 2,2':6',2''-tpy was isolated. $^1$H NMR (500 MHz, $CDCl_3$) $\delta$ (ppm) 8.68 (ddd, *J* 4.7, 1.9, 0.9 Hz, 1 H, $H^{6A}$), 8.62 (dt, *J* 7.8, 1.1 Hz, 1 H, $H^{3A}$), 8.34 (dd, *J* 7.8, 1.0 Hz, 1 H, $H^{3B}$), 7.95 (m, 1 H, $H^{2C}$), 7.91 (dm, *J* 7.8 Hz 1 H, $H^{6C}$), 7.87 (t, *J* 7.8 Hz 1 H, $H^{4B}$), 7.83 (dt, *J* 7.8, 1.8 Hz 1 H, $H^{4A}$), 7.75 (dd, *J* 7.8, 1.8 Hz 1 H, $H^{5B}$), 7.38 (t, *J* 7.6 Hz 1 H, $H^{5C}$), 7.31 (ddd, *J* 7.4, 4.8, 1.2 Hz 1 H, $H^{5A}$), 7.24 (dm, *J* 7.7 Hz 1 H, $H^{4C}$) 2.46 (s, 3 H, Me); $^{13}$C NMR (HMBC/HMQC 500 MHz, $CDCl_3$) $\delta$ (ppm) 156.6 ($C^{6B}$), 156.1 ($C^{2A}$), 154.7 ($C^{2B}$), 149.1 ($C^{6A}$), 139.3 ($C^{1C}$), 138.0 ($C^{3C}$), 137.6 ($C^{4B}$), 137.0 ($C^{4A}$), 129.8 ($C^{4C}$), 128.7 ($C^{5C}$), 127.7 ($C^{2C}$), 124.1 ($C^{6C}$), 123.8 ($C^{5A}$), 121.4 ($C^{3A}$), 120.5 ($C^{5B}$), 119.3 ($C^{3B}$), 21.6 ($C^{Me}$); EI-MS *m/z*: 246.1 $[M]^+$ (100 %, calc. 246.1); IR (solid, $\nu$/cm$^{-1}$) 3051 (w), 3018 (w), 3012 (w), 3002 (w), 2955 (w), 2919 (w), 2857 (w), 2360 (m), 2321 (w), 2313 (w), 1700 (m), 1653 (m), 1607 (w), 1580 (s), 1560 (s), 1555 (m), 1506 (w), 1490 (w), 1472 (m), 1456 (m), 1447 (m), 1427 (s), 1420 (m), 1319 (w), 1287 (w), 1280 (w), 1258 (w), 1191 (w), 1156 (w), 1102 (w), 1084 (w), 1041 (w), 990 (w), 826 (w), 770 (s), 745 (w), 697 (w), 668 (m), 643 (m), 618 (m), 602 (m); UV/vis ($CH_2Cl_2$, 5.0 x 10$^{-5}$ mol dm$^{-3}$) $\lambda_{max}$/nm 238 ($\varepsilon$/dm$^3$ mol$^{-1}$ cm$^{-1}$ 22000), 261 (19000), 285 (14600), sh 301 (11900); emission ($\lambda_{ex}$ = 262 nm) $\lambda_{max}$ = 346 nm.

### 3.4.2.12 5'-(2-Pyridinoyl)-2,2'-bpy (20)

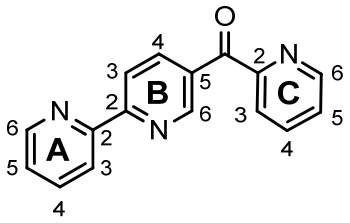


Ligand **20** was prepared following a slightly modified procedure from the literature.[67] The vinyl ketone **13** (1.76 g, 10 mmol, 2.0 eq) and an excess of $NH_4OAc$ (100 mmol, 7.7 g, ~10 eq)

were dissolved in 30 ml HOAc and stirred at reflux over night. The solvent was evaporated, the black residue suspended in $H_2O$ and pH 8 was adjusted by adding solid $K_2CO_3$. The aqueous phase was extracted several times into $CH_2Cl_2$ and the combined organic layers were dried over $MgSO_4$. After removing the solvent under reduced pressure the resulting black oil was dissolved in toluene and filtered through Celite®. The solvent was evaporated to give a brown paste which was recrystallized from pentane to yield white and crystalline fibers (1.064 g, 4.07 mmol, 80.14 %). $^1$H NMR (500 MHz, $CDCl_3$) $\delta$ (ppm) H 9.40 (1 H, s, $H^{6B}$), 8.74 (d, *J* 4.1 Hz, 1 H, $H^{6C}$), 8.70 (d, *J* 4.0 Hz, 1 H, $H^{6A}$), 8.58 – 8.52 (m, 2 H, $H^{3+4B}$), 8.49 (d, *J* 8.0 Hz, 1 H, $H^{3A}$), 8.15 (d, *J* 7.8 Hz, 1 H, $H^{3C}$), 7.93 (td, *J* 7.7, 1.7 Hz, 1 H, $H^{4C}$), 7.83 (td, *J* 7.8, 1.7 Hz, 1 H, $H^{4A}$), 7.52 (dd, *J* 7.0, *J* 5.3 Hz, 1 H, $H^{5C}$), 7.34 (dd, *J* 6.9, 5.3 Hz, 1 H, $H^{5A}$); $^{13}$C NMR (126 MHz, $CDCl_3$) $\delta$ (ppm) 192.18 ($C^{C=O}$), 159.01 ($C^{2B}$), 155.45 ($C^{2A}$), 154.45 ($C^{2C}$), 152.19 ($C^{6B}$), 149.63 ($C^{6A}$), 148.89 ($C^{6C}$), 139.55 ($C^{4B}$), 137.52 ($C^{4C}$), 137.25 ($C^{4A}$), 131.86 ($C^{5B}$), 127.04 ($C^{5C}$), 124.81 ($C^{3C}$), 124.64 ($C^{5A}$), 122.19 ($C^{3A}$), 120.5 ($C^{3B}$); EI-MS *m/z*: 261.2 $[M]^+$ (100 %, calc. 261.2), 233 $[M\text{-}CO]^+$ (71 %), 184 $[M\text{-}py]^+$ (40 %), 155 $[M\text{-}py\text{-}CO]^+$ (66); IR (solid, $\nu$/cm$^{-1}$) 3007 (w), 2972 (w), 2943 (w), 2920 (w), 2837 (w), 2654 (w), 2457 (w), 2359 (w), 1981 (w), 1717 (w), 1674 (m), 1653 (m), 1639 (w), 1585 (s), 1549 (m), 1504 (m), 1450 (m), 1435 (m), 1408 (s), 1373 (m), 1356 (s), 1331 (s), 1319 (s), 1290 (m), 1244 (m), 1217 (s), 1175 (m), 1124 (s), 1094 (s), 1063 (m), 1026 (m), 993 (s), 980 (m), 947 (m), 933 (m), 889 (m), 858 (s), 825 (s), 795 (m), 777 (m), 744 (m), 694 (w), 654 (m), 609 (m) cm$^{-1}$.; UV/vis ($CH_2Cl_2$, 5.0 x 10$^{-5}$ mol dm$^{-3}$) $\lambda_{max}$/nm 228 ($\varepsilon$/dm$^3$ mol$^{-1}$ cm$^{-1}$ 10500), 282 (12900), 300 (14200); emission $\lambda_{em}$ ($\lambda_{ex}$) = 349, sh 450, 500 (286); EA: calc. for $C_{16}H_{11}N_3O_*{}^1/_4\ H_2O$) C 72.30, H 4.36, N 15.81, found C 72.78, H 4.46, N 15.75.

### 3.4.2.13 4',6'-Bis(3,4,5-trimethoxyphenyl)-2,2'-bpy (30)

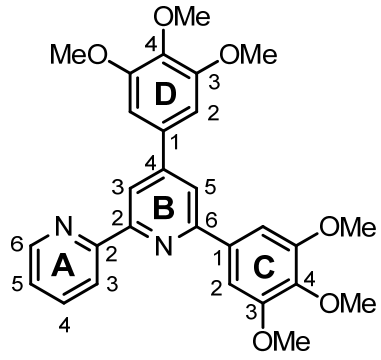


In 25 ml EtOH were suspended **8** (0.98 g, 3.0 mmol, 1.0 eq), the chalcone **10** (1.17 g, 3.0 mmol, 1.0 eq) and $NH_4OAc$ (4.00 g, 51.9 mmol, 17 eq) and stirred under reflux. The yellow suspension turned black over the course of 3 h (TLC: 3 h, showed no starting materials but 3 spots, very likely diketone present; 24 h, only two spots and little ketone). The solvent was evaporated to give a black residue which was suspended in $H_2O$ and the pH was adjusted to ~8. The aqueous phase was extracted into $CH_2Cl_2$ (~3 x 30 ml). The

combined organic layers were washed with diluted NaOH solution (~1 M) and water then dried over $MgSO_4$. The solid was filtered off and the solvent was evaporated to give a brown residue. The crude product was passed through a column ($SiO_2$, pentane/$Et_2O$ 2:1-1:4, then $CH_2Cl_2$/MeOH 1:0-96:4) The desired product was obtained in the first major fraction as a yellow solid (814 mg, 1.67 mmol, 56 %). $^1$H NMR (500 MHz, $CDCl_3$) $\delta$ (ppm) 8.73 (ddd, *J* 4.8, 1.8, 0.9 Hz, 1 H, $H^{6A}$), 8.63 (dt, *J* 8.0, 1.1 Hz, 1 H, $H^{3A}$), 8.56 (d, *J* 1.6 Hz, 1 H, $H^{3B}$), 7.88 (td, *J* 8.0, 1.8 Hz, 1 H, $H^{4A}$), 7.82 (d, *J* 1.6 Hz, 1 H, $H^{5B}$), 7.40 (s, 2 H, $H^{2C}$), 7.36 (ddd, *J* 7.5, 4.8, 1.2 Hz, 1 H, $H^{5A}$), 6.97 (s, 2 H, $H^{2D}$), 4.01 (s, 6 H, $H^{OMe_a{}^C}$), 3.98 (s, 6 H, $H^{OMe_a{}^D}$), 3.933 (s, 3 H, $H^{OMe_b{}^C}$), 3.927 (s, 3 H, $H^{OMe_b{}^D}$), 4.01 (s, 6 H, $H^{OMe_a{}^D}$); $^{13}$C NMR (HMQC/HMBC 500 MHz, solvent$_3$) $\delta$ (ppm) 157.0 ($C^{6B}$), 156.1 ($C^{2A}$), 156.0 ($C^{2B}$), 150.7 ($C^{4B}$), 149.3 ($C^{6A}$), 139.3 ($C^{4C}$), 138.9 ($C^{4D}$), 136.9 ($C^{4A}$), 135.3 ($C^{1C}$), 135.2 ($C^{3C}$), 134.7 ($C^{1+3D}$), 123.9 ($C^{5A}$), 121.5 ($C^{3A}$), 118.6 ($C^{5B}$), 117.6 ($C^{3B}$), 104.6 ($C^{2C}$), 104.5 ($C^{2D}$), 60.9 ($C^{OMe_b{}^{C+D}}$), 56.4 ($C^{OMe_a{}^D}$), 56.3 ($C^{OMe_a{}^C}$); EI-MS *m/z*: 488.2 $[M]^+$ (100 %, calc. 488.2); IR (solid, $\nu$/cm$^{-1}$) 3000 (m), 2939 (m), 2843 (w), 2825 (w), 2362 (m), 2333 (m), 1700 (m), 1653 (m), 1583 (s), 1545 (s), 1505 (s), 1456 (s), 1398 (m), 1383 (s), 1326 (s), 1245 (s), 1233 (s), 1201 (m), 1186 (m), 1167 (m), 1121 (s), 1092 (s), 1032 (m), 998 (s), 962 (m), 919 (w), 900 (w), 888 (m), 851 (m), 827 (s), 799 (s), 761 (m), 729 (m), 683 (s), 668 (s), 657 (s), 625 (m), 618 (s); UV/vis ($CH_2Cl_2$, 5.0 x 10$^{-5}$ mol dm$^{-3}$) $\lambda_{max}$/nm 233 ($\varepsilon$/dm$^3$ mol$^{-1}$ cm$^{-1}$ 35300), 285 (39600); emission $\lambda_{max}$ ($\lambda_{ex}$) = 440 (283) nm.

### 3.4.2.14 4',6'-Diphenyl-2,2'-bpy (31)

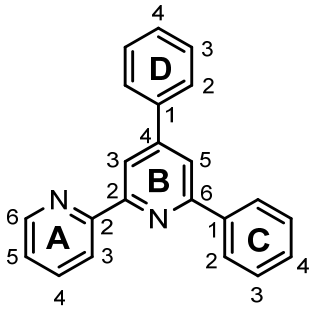


In 50 ml EtOH **8** (0.82 g, 2.5 mmol, 1.0 eq), the chalcone **6** (0.52 g, 2.5 mmol, 1.0 eq) and $NH_4OAc$ (5.78 g, 75.0 mmol, 30 eq) were suspended and stirred under reflux. The yellow/orange suspension turned dark. (TLC: 3 h, showed no starting materials but 3 spots, very likely diketone present; 24 h, only two spots and little ketone) The solvent was evaporated to give a black residue which was suspended in $H_2O$ and the pH was adjusted to ~8. The aqueous phase was extracted into $CH_2Cl_2$ (~3 x 30 ml). The combined organic layers were washed with diluted NaOH solution (~1 M) and water then dried over $MgSO_4$. The solid was filtered off and the solvent was evaporated to give a brown residue. The crude product was passed through a column ($SiO_2$, pentane/$Et_2O$ 2:1-1:4). The desired product was obtained in the first and major fraction and was isolated as a yellow solid (290 mg,

0.94 mmol, 38 %). The spectroscopic data matched those reported.[98] UV/vis ($CH_2Cl_2$, 5.0 x $10^{-5}$ mol $dm^{-3}$) $\lambda_{max}$/nm 220 ($\varepsilon$/$dm^3$ $mol^{-1}$ $cm^{-1}$ 22100), 257 (35400), 312 (8200); emission $\lambda_{max}$ ($\lambda_{ex}$) = 351/361 (312) nm.

### 3.4.2.15 4',6'-Bis(*p*-nitrophenyl)-2,2'-bpy (32)

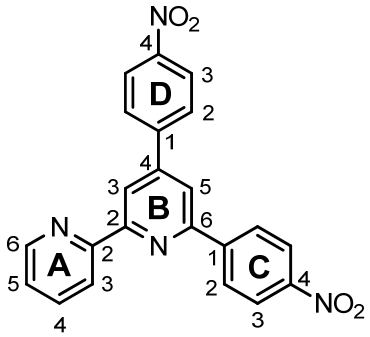


In 50 ml EtOH were suspended **12** (0.82 g, 2.5 mmol, 1.0 eq), the chalcone **11** (0.52 g, 2.5 mmol, 1.0 eq) and $NH_4OAc$ (6.24 g, 81.0 mmol, 30 eq) and stirred under reflux. The yellow/orange suspension turned dark (TLC: 3 h, showed no starting materials but 3 spots, very likely diketone present; 24 h, only two spots and little ketone). The solvent was evaporated to give a black residue. This was suspended in $H_2O$ and the pH was adjusted to ~8. The aqueous phase was extracted into $CH_2Cl_2$ (~ 3 x 30 ml). The combined organic layers were washed with diluted NaOH sol. (~1 M) and water and then dried over $MgSO_4$. The solid was filtered off and the solvent was evaporated to give a brown residue. The crude product was passed through a column ($SiO_2$, pentane/$Et_2O$ 2:1-1:4). The desired product was obtained in the first and major fraction and was isolated as a yellow solid (702.0 mg, 1.76 mmol, 65 %). $^1$H NMR (500 MHz, DMSO-$d_6$) $\delta$ (ppm) 8.76 (ddd, *J* 4.7, 1.8, 0.9 Hz, 1 H, $H^{6A}$), 8.75 (d, *J* 1.6 Hz, 1 H, $H^{3B}$), 8.69 – 8.64 (m, 2 H, $H^{2C}$), 8.63 (dt, *J* 8.0, 1.1 Hz, 1 H, $H^{3A}$), 8.57 (d, *J* 1.6 Hz, 1 H, $H^{5B}$), 8.41 – 8.36 (m, 4 H, $H^{3D+C}$), 8.32 – 8.27 (m, 2 H, $H^{2D}$), 8.04 (td, *J* 7.7, 1.8 Hz, 1 H, $H^{4A}$), 7.54 (ddd, *J* 7.4, 4.8, 1.2 Hz, 1 H, $H^{5A}$); $^{13}$C NMR (HMQC/HMBC 500 MHz, DMSO-$d_6$) $\delta$ (ppm) 155.8 ($C^{2A+B}$), 150.8 ($C^{6A}$), 149.4 ($C^{4C+D}$), 149.3 ($C^{6B}$), 145.2 ($C^{1C+D}$), 140.0 ($C^{4A}$), 138.9 ($C^{4B}$), 130.2 ($C^{2D}$), 129.7 ($C^{2C}$), 126.2 ($C^{5A}$), 125.5 ($C^{3C+D}$), 122.4 ($C^{3A}$), 121.1 ($C^{5B}$), 119.5 ($C^{3B}$); EI-MS *m/z*: 398.1 $[M]^+$ (100 %, calc. 398.1); IR (solid, $\nu$/$cm^{-1}$) 3113 (w), 3088 (w), 3064 (w), 2947 (w), 2850 (w), 2451 (w), 2361 (w), 1593 (s), 1581 (s), 1567 (m), 1548 (s), 1505 (s), 1496 (s), 1488 (s), 1471 (m), 1432 (m), 1419 (m), 1393 (m), 1384 (m), 1342 (s), 1286 (m), 1264 (m), 1248 (m), 1223 (w), 1150 (w), 1125 (w), 1105 (s), 1091 (m), 1081 (m), 1051 (w), 1036 (w), 1008 (m), 991 (m), 973 (w), 958 (w), 906 (w), 858 (s), 848 (s), 836 (s), 825 (s), 811 (s), 793 (s), 753 (s), 746 (s), 737 (s), 711 (s), 691 (s), 660 (s), 640 (s), 613 (s); UV/vis ($CH_2Cl_2$, 5.0 x $10^{-5}$ mol $dm^{-3}$) $\lambda_{max}$/nm 234 ($\varepsilon$/$dm^3$ $mol^{-1}$ $cm^{-1}$ 18600), 291 (37300); (weak) emission $\lambda_{max}$ ($\lambda_{ex}$) = 366 (233), 380 + 436 (340) nm; EA: calc. for $C_{22}H_{14}N_4O_4$, C 66.33 %, H 3.54 %, N 14.06 %, found C 65.87 %, H 3.65 %, N 14.08 %.

### 3.4.2.16 4'-(5-Bromothiophen-2-yl)-6'-(thiophen-2-yl)-2,2'-bpy (34)

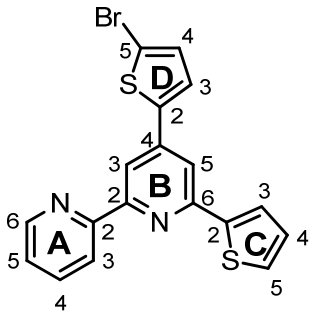


The vinyl ketone **7** (294.2 mg, 1.0 mmol, 1.0 eq), **37** (331.2 mg, 1.0 mmol, 1.0 eq) and ammonium acetate (~1 g, 13 mmol, 13 eq) were suspended in methanol (15 ml) and the resulting reaction mixture was stirred for 40 h at reflux (until TLC showed no further progress). The solvent was removed under reduced pressure, the black residue suspended in $H_2O$ and the pH was adjusted to ~8 by adding solid $K_2CO_3$. The dark green solution was extracted several times into $CH_2Cl_2$. The combined organic layers were dried over $MgSO_4$, the solid was filtered off and the solvent was evaporated to give a dark green and crystalline solid. The crude product was purified by short column chromatography ($SiO_2$, 2.5x5 cm, $CH_2Cl_2$/MeOH 1:0 – 8:2). The desired product was obtained as the first major fraction and was isolated as a pale yellow solid (171.0 mg, 0.43 mmol, 43 %). $^1$H NMR (500 MHz, $CDCl_3$) $\delta$ (ppm) 8.68 (d, *J* 4.2 Hz, 1 H, $H^{6A}$), 8.56 (d, *J* 7.9 Hz, 1 H, $H^{3A}$), 8.43 (d, *J* 1.3 Hz, 1 H, $H^{3B}$), 7.85 (td, *J* 7.8, 1.6 Hz, 1 H, $H^{4A}$), 7.70 (d, *J* 1.3 Hz, 1 H, $H^{5A}$), 7.68 (d, *J* 3.8 Hz, 1 H, $H^{5C}$), 7.42 (d, *J* 4.2 Hz, 1 H, $H^{3C}$), 7.41 (d, *J* 3.8 Hz, 1 H, $H^{4D}$), 7.33 (dd, *J* 6.9, 5.3 Hz, 1 H, $H^{5A}$), 7.14 (dd, *J* 4.9, 3.8 Hz, 1 H, $H^{4C}$), 7.11 (d, *J* 3.8 Hz, 1 H, $H^{3D}$); $^{13}$C (126 Hz, $CDCl_3$) $\delta$ (ppm) 156.60 ($C^{2B}$), 155.63 ($C^{2A}$), 152.87 ($C^{2C}$), 149.23 ($C^{6A}$), 145.05 ($C^{6B}$), 143.15 ($C^{4B}$), 142.51 ($C^{2D}$), 137.20 ($C^{4A}$), 131.45 ($C^{3D}$), 128.29 ($C^{5C}$), 128.15 ($C^{4C}$), 126.10 ($C^{4D}$), 125.05 ($C^{3C}$), 124.32 ($C^{5A}$), 121.74 ($C^{3A}$), 115.17 ($C^{3B}$), 114.54 ($C^{5B}$), 114.47 ($C^{5D}$); EI-MS *m/z*: 398.0/400.0 $[M]^+$ (78/84 %, calc. 398.0/400.0), 319.0 $[M\text{-}Br]^+$ (100 %); IR (solid, $\nu$/$cm^{-1}$) 3107 (w), 3061 (w), 2966 (w), 2923 (w), 2855 (w), 2360 (m), 2358 (m), 2337 (w), 1717 (w), 1684 (w), 1653 (w), 1648 (w), 1636 (w), 1595 (m), 1582 (s), 1567 (s), 1558 (m), 1544 (s), 1528 (m), 1522 (m), 1506 (m), 1472 (m), 1450 (m), 1439 (m), 1428 (m), 1412 (m), 1398 (m), 1362 (w), 1306 (w), 1284 (w), 1260 (w), 1237 (w), 1227 (w), 1204 (w), 1113 (w), 1076 (w), 1065 (w), 1045 (m), 1039 (m), 999 (w), 984 (m), 963 (m), 882 (m), 853 (s), 832 (m), 822 (m), 783 (s), 752 (m), 741 (s), 690 (s), 668 (s), 646 (m), 626 (m), 617 (m), 601 (s); UV/vis ($CH_2Cl_2$, 5.0 x $10^{-5}$ mol $dm^{-3}$) $\lambda_{max}$/nm 243 ($\varepsilon$/$dm^3$ $mol^{-1}$ $cm^{-1}$ 20400), 304 (37000), 348 (9100); emission $\lambda_{max}$ ($\lambda_{ex}$) = 395 (310) nm; EA: calc. for $C_{18}H_{11}N_2S_2Br$, C 54.14 %, H 2.78 %, N 7.02 %, found C 54.39 %, H 3.03 %, N 6.80 %.

### 3.4.2.17 4'-(4-Bromophenyl)-6'-(phenyl)-2,2'-bpy (36)

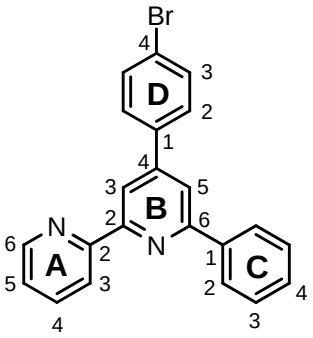


Acetophenone (2.4 g, 20.0 mmol, 1 eq), benzaldehyde (3.7 g 20.0 mmol) and NaOH (s) (1.6 g, 40.0 mmol, 2 eq) were combined using a mortar and pestle, and the yellow medium was aggregated until a yellow powder formed (ca. 10 min). Then 2-acetylpyridine (1 eq., 7.28 ml, 20 mmol, 1 eq) and NaOH (s) (0.8 g, 20.0 mmol, 1 eq) were mixed together using a mortar and pestle until a yellow powder was formed (ca. 10 min). The powder was transferred to a suspension of ammonium acetate (5 g, excess) in glacial acetic acid (25 ml, ca. 100 %) and heated to reflux for 2 h then stirred at room temperature over the weekend. An off-white precipitate formed. The crude product was precipitated out of solution *via* the addition of water (10 ml), collected and washed with water and ethanol. The crude material was purified by column chromatography ($SiO_2$, pentane/$Et_2O$ 2:1-1:4). Compound **36** was obtained in the second major fraction (800 mg, 2.1 mmol, 10 %). The first major fraction yielded unreacted chalcone (2.0 g, 9.6 mmol, 48 %). $^1$H NMR (500 MHz, $CDCl_3$) $\delta$ (ppm) 8.71 (ddd, *J* 4.8, 1.9, 0.9 Hz, 1 H, $H^{6A}$), 8.66 (dt, *J* 8.0, 1.1, 1.1 Hz, 1 H, $H^{3A}$), 8.57 (d, *J* 1.5 Hz, 1 H, $H^{3B}$), 8.18 (dd, *J* 8.3, 1.3 Hz, 2 H, $H^{2C}$), 8.00 (dd, *J* 8.4, 1.3 Hz, 1 H, $H^{4C}$), 7.92 (d, *J* 1.6 Hz, 1 H, $H^{5B}$), 7.86 (dt, *J* 7.8, 1,6 Hz, 1 H, $H^{4A}$), 7.68 (d, *J* 8.5 Hz, 2 H, $H^{3D}$), 7.63 (d, *J* 8.6 Hz, 2 H, $H^{2D}$), 7.55-7.42 (m, 2 H, $H^{3C}$), 7.34 (ddd, *J* 7.5, 4.8, 1.3 Hz, 1 H, $H^{5A}$). All analytical data match those previously published.[99]

### 3.4.2.18 4'-(3,4,5-Trimethoxyphenyl)-6'-(pyrrol-2-yl)-2,2'-bpy (38)

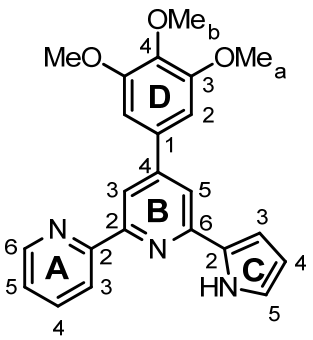


In 25 ml EtOH were suspended **37** (0.50 g, 1.5 mmol, 1.0 eq), the chalcone **29** (0.47 g, 1.5 mmol, 1.0 eq) and $NH_4OAc$ (3.6 g, 47.2 mmol, 30 eq) and stirred under reflux for 24 h. The solvent was evaporated to give a black residue which was suspended in $H_2O$ and the pH

was adjusted to ~8. The aqueous phase was extracted into $CH_2Cl_2$ (~3 x 30 ml). The combined organic layers were washed with diluted NaOH solution (~1 M) and water then dried over $MgSO_4$. The solid was filtered off and the solvent was evaporated to give a brown residue. The crude product was passed through a column ($SiO_2$, pentane/$Et_2O$ 2:1-1:4, then $CH_2Cl_2$/MeOH 1:0-96:4) The desired product was obtained in the first major fraction as a yellow solid (180 mg, 0.47 mmol, 30 %). $^1$H NMR (500 MHz, $CD_2Cl_2$) $\delta$ (ppm) 9.88 (s, 1 H, $H^{NH}$), 8.71 (ddd, *J* 4.8, 1.8, 0.9 Hz, 1 H, $H^{6A}$), 8.55 (dt, *J* 8.0, 1.0, 1.0 Hz, 1 H, $H^{3A}$), 8.40 (d, *J* 1.6 Hz, 1 H, $H^{3B}$), 7.88 (dt, *J* 7.9, 1.9 Hz, 1 H, $H^{4A}$), 7.76 (d, *J* 1.6 Hz, 1 H, $H^{5B}$), 7.37 (ddd, *J* 7.5, 4.8, 1.2 Hz, 1 H, $H^{5A}$), 6.99 (td, *J* 2.6, 1.4 Hz, 1 H, $H^{5C}$), 6.97 (s, 2 H, $H^{2D}$), 6.87 (ddd, *J* 3.7, 2.4, 1.4 Hz, 1 H, $H^{3C}$), 6.34 (dt, *J* 3.6, 2.6 Hz, 1 H, $H^{4C}$), 3.95 (s, 6 H, $H^{OMea}$), 3.85 (s, 3 H, $H^{OMeb}$); $^{13}$C NMR (HMQC/HMBC 500 MHz, $CD_2Cl_2$) $\delta$ (ppm) 156.41 ($C^{2A}$), 156.28 ($C^{2B}$), 154.17 ($C^{3D}$), 150.81 ($C^{6B}$), 150.56 ($C^{2C}$), 149.44 ($C^{6A}$), 139.48 ($C^{4D}$), 137.24 ($C^{4A}$), 134.79 ($C^{4B}$), 131.90 ($C^{1D}$), 124.32 ($C^{5A}$), 121.48 ($C^{3A}$), 120.23 ($C^{5C}$), 116.37 ($C^{5B}$), 116.32 ($C^{3B}$), 110.67 ($C^{4C}$), 107.91 ($C^{3C}$), 104.81 ($C^{2D}$), 60.75 ($C^{OMe_bD}$), 56.56 ($C^{OMe_aD}$); EI-MS *m/z*: 387.1 $[M]^+$ (100 %, calc. 387.2); IR (solid, $\nu$/cm$^{-1}$) 3000 (m), 2939 (m), 2843 (w), 2825 (w), 2362 (m), 2333 (m), 1700 (m), 1653 (m), 1583 (s), 1545 (s), 1505 (s), 1456 (s), 1398 (m), 1383 (s), 1326 (s), 1245 (s), 1233 (s), 1201 (m), 1186 (m), 1167 (m), 1121 (s), 1092 (s), 1032 (m), 998 (s), 962 (m), 919 (w), 900 (w), 888 (m), 851 (m), 827 (s), 799 (s), 761 (m), 729 (m), 683 (s), 668 (s), 657 (s), 625 (m), 618 (s); UV/vis ($CH_2Cl_2$, 5.0 x 10$^{-5}$ mol dm$^{-3}$) $\lambda_{max}$/nm 286 ($\varepsilon$/dm$^3$ mol$^{-1}$ cm$^{-1}$26300), 304 (24500), 343 (7500); emission ($\lambda_{ex}$ = 283 nm) $\lambda_{max}$ = 440 nm.

### 3.4.2.19 4'-*tert*-Butyl-4,2':6',4''-terpyridine (39)

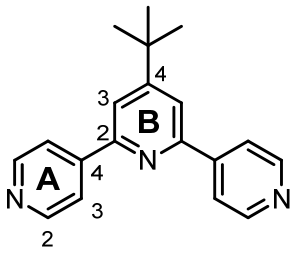


Solid KOH (1.12 g, 20 mmol) was added to a solution of 4-acetylpyridine (1.11 g, 10.0 mmol) and pivalaldehyde (0.861 g, 10.0 mmol) in EtOH/$H_2O$ (2:1 by vol., total vol. 30 ml) was then added. The mixture turned yellow and then red within a few minutes. A second equivalent of 4-acetyl-pyridine (1.11 g, 10.0 mmol) was then added. The mixture was stirred at room temperature overnight, after which time aqueous $NH_4OH$ (25 ml, 6.5 mol/ml) was added. The reaction mixture was stirred under reflux and after 1 h, a white precipitate started to form. After 8 h under reflux, the mixture was allowed to cool and the precipitate was collected by filtration, washed with $H_2O$ and dried in a desiccator. Compound **39** was isolated as a pale yellow solid (650 mg, 22 %). $^1$H NMR (500 MHz, $CDCl_3$) $\delta$ (ppm) 8.75 (d, *J* 6.1 Hz, 4 H, $H^{A2}$), 8.00 (d, *J* 6.2 Hz, 4 H, $H^{A3}$), 7.82 (s, 2 H, $H^{B3}$), 1.43 (s, 9 H, $H^{Me}$); $^{13}$C NMR

(126 MHz, $CDCl_3$) $\delta$ (ppm) 162.8 ($C^{B4}$), 155.0 ($C^{B2}$), 150.7 ($C^{A2}$), 146.7 ($C^{A4}$), 121.5 ($C^{A3}$), 118.2 ($C^{B3}$), 35.5 ($C^{CMe3}$) 30.9 ($C^{Me}$); EI MS: m/z 289.2 $[M]^+$ (calc. 289.2), 274.1 $[M–Me]^+$ (base peak, calc. 274.1), 233.1 $[M–Bu]^+$ (calc. 232.1); IR (solid, $cm^{-1}$) $\nu$ 3034 w, 2953 w, 2901w, 2864 w, 2363 w, 2330 w, 1701 w, 1684 w, 1653 w, 1593 s, 1558 w, 1541 w, 1402 w, 1362 w, 1321 w, 1252 w, 1202 w, 1138 w, 1065 w, 993 w, 962 w, 930 w, 895 w, 881 w, 827 s, 818 s, 750 w, 650 s, 631 s; UV/vis ($CH_2Cl_2$, 1.0 x $10^{-4}$ mol $dm^{-3}$) $\lambda_{max}$/nm 239 ($\varepsilon$/$dm^3$ $mol^{-1}$ $cm^{-1}$ 26200), 257 (16400), 289 (10300); emission ($\lambda_{ex}$ = 305 nm) $\lambda_{max}$ = 337/374 nm; EA: calc. for $C_{19}H_{19}N_3$ requires C 78.86 %, H 6.62 %, N 14.52% found C 78.83 %, H 6.65 %, N 14.20 %.

### 3.4.2.20 4'-*tert*-Butyl-2,2':6',2''-terpyridine (40)

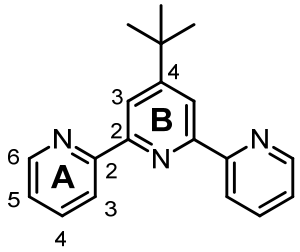


**Method 1**

2-Acetylpyridine (2.42 g, 20.0 mmol) was dissolved in EtOH (25 ml) and an aqueous solution (5 ml) of KOH (1.12 g, 20 mmol) was added, followed by pivalaldehyde (0.861 g, 10.0 mmol). The mixture turned yellow then red within minutes and was stirred at room temperature overnight. Aqueous $NH_4OH$ (32 % by wt., 25 ml) was then added to the deep red suspension and the reaction mixture was heated at reflux for 22 h. Removal of solvent in *vacuo* gave a dark oil. This was suspended in $H_2O$, the pH was adjusted to 8 and the mixture extracted several times with $CH_2Cl_2$. After separation, the combined organic layers were dried over $MgSO_4$, and then the solvent was removed under reduced pressure to give a brown solid. After column chromatography ($SiO_2$, pentane–ethyl acetate 1:1 changing to 1:9), compound **40** was isolated as a white powder (348 mg, 1.20 mmol, 12 %). See below for characterization.

**Method 2**

2-Acetylpyridine (606 mg, 5.0 mmol) was added to a solution of *t*ert-BuOK (561 mg, 5.0 mmol) in THF (25 ml). The mixture turned red immediately. Pivalaldehyde (215 mg, 2.5 mmol) was then added and the mixture was stirred at room temperature overnight. Solid $NH_4OAc$ (3.5 g, 50 mmol) dissolved in glacial HOAc (25 ml) was added to the deep red suspension and the resulting red solution was stirred for 5 h under reflux. Solvents were removed in *vacuo* to give a brown solid which was suspended in water and the pH was adjusted to 8. The crude product was extracted several times into $Et_2O$ (10 × 50 ml), and the combined organic layers were dried over $MgSO_4$. After removal of solvent under reduced

pressure, the crude product was isolated as a yellow solid. Purification by column (short, 5 × 5 cm) chromatography (alumina, pentane/$Et_2O$ 2:1) resulted in **40** being isolated as a white powder (472 mg, 1.63 mmol, 65.2 %). m.p. 140–142 °C. $^1$H NMR (400 MHz, $CD_3CN$) $\delta$ (ppm) 8.69 (d, *J* 4.7 Hz, 2 H, HA6), 8.64 (d, *J* 8.0 Hz, 2 H, $H^{A3}$), 8.53 (s, 2 H, $H^{B3}$), 7.93 (td, *J* 7.8, 1.7 Hz, 2 H, $H^{A4}$), 7.30 (ddd, *J* 7.4, 4.8, 1.0 Hz, 2 H, $H^{A5}$), 1.44 (s, 9 H, $^t$Bu); $^{13}$C NMR (101 MHz, $CD_3CN$) $\delta$ (ppm) 163.0 ($C^{B4}$), 156.7 ($C^{A2}$), 156.0 ($C^{B2}$), 150.0 ($C^{A6}$), 137.9 ($C^{A4}$), 124.8 ($C^{A5}$), 121.7 ($C^{A3}$), 118.5 ($C^{B3}$), 30.6 ($C^{Bu}$); $^1$H NMR (500 MHz, $CDCl_3$) $\delta$ (ppm) 8.69 (ddd, *J* 4.8, 1.8, 0.9 Hz, 2 H, $H^{A6}$), 8.60 (dd, *J* 8.0, 1.0 Hz, 2 H, $H^{A3}$), 8.48 (s, 2 H, $H^{B3}$), 7.82 (td, *J* 7.7, 1.8 Hz, 2 H, $H^{A4}$), 7.30 (ddd, *J* 7.5, 4.8, 1.2 Hz, 2 H, $H^{A5}$), 1.45 (s, 9 H, $^t$Bu); $^{13}$C NMR (126 MHz, $CDCl_3$) $\delta$ (ppm) 162.4 ($C^{B4}$), 156.9 ($C^{A2}$), 155.6 ($C^{B2}$), 149.3 ($C^{A6}$), 137.0 ($C^{A4}$), 123.8 ($C^{A5}$), 121.6 ($C^{A3}$), 118.3 ($C^{B3}$), 31.0 ($C^{Bu}$); EI MS: m/z 289.2 $[M]^+$ (calc. 289.2), 274.1 $[M\text{-}Me]^+$ (base peak, calc. 274.1), 233.1 $[M\text{-}Bu]^+$ (calc. 232.1); IR (solid, $\nu$/cm$^{-1}$) 3051 w, 2964 w, 2932 w, 2868 w, 2363 w, 2326 w, 1701 w, 1684 w, 1653 w, 1583 s, 1568 s, 1545 s, 1466 s, 1454 w, 1396 s, 1364 w, 1267 w, 1240 w, 1204 w, 1153 w, 1128 w, 1074 w, 1043 w, 991 w, 964 w, 935 w, 895 w, 881 w, 849 w, 791 s, 741 s, 685 s, 650 s, 623 s; UV/vis ($CH_2Cl_2$, 1.0×10$^{-5}$ mol dm$^{-3}$) $\lambda_{max}$/nm 219 ($\varepsilon$/dm$^3$ mol$^{-1}$ cm$^{-1}$ 18000) 240 (20000), 251sh (16000), 282 (18100), 312sh (8000); emission ($\lambda_{ex}$ = 282 nm) $\lambda_{em}$ = 339, 353 nm; EA: calc. for $C_{19}H_{19}N_3$ C 78.86 %, H 6.62 %, N 14.52 %, found C 78.33 %, H 6.83 %, N 14.24 %.

### 3.4.3 Crystal structure determinations

#### 3.4.3.1 Ligand 1

$C_{15}H_{13}N_3$, *M* = 235.29, colourless block, triclinic, space group *P*–1, *a* = 8.9873(7), *b* = 10.3479(7), *c* = 12.9086(10) Å, $\alpha$ = 98.400(4), $\beta$ = 99.933(4), $\gamma$ = 90.639(4)°, *U* = 1169.00(15) Å$^3$, *Z* = 4, $D_c$ = 1.337 Mg m$^{-3}$, $\mu$(Mo-K$_\alpha$) = 0.082 mm$^{-1}$, *T* = 123 K. Total 32162 reflections, 7705 unique, $R_{int}$ = 0.033. Refinement of 6116 reflections (325 parameters) with $I > 2\sigma(I)$ converged at final *R*1 = 0.0832 (*R*1 all data = 0.0923), *wR*2 = 0.0787 (*wR*2 all data = 0.1079), gof = 0.9314.

#### 3.4.3.2 Ligand 4

$C_{14}H_{10}N_2Se$, *M* = 285.21, colourless needle, orthorhombic, space group *Pna*2$_1$, *a* = 10.715(5), *b* = 19.191(8), *c* = 5.731(3) Å, *U* = 1178.4(9) Å$^3$, *Z* = 4, $D_c$ = 1.608 Mg m$^{-3}$, $\mu$(Mo-K$_\alpha$) = 3.162 mm$^{-1}$, *T* = 123 K. Total 19837 reflections, 2811 unique, $R_{int}$ = 0.092. Refinement of 1755 reflections (155 parameters) with $I > 2\sigma(I)$ converged at final *R*1 = 0.0458 (*R*1 all data = 0.0774), *wR*2 = 0.0421 (*wR*2 all data = 0.0805), gof = 1.102.

#

### 3.4.3.3 Ligand 12

$C_{19}H_{18}N_2O_3$, $M$ = 322.36, colourless needle, monoclinic, space group $P2_1/n$, $a$ = 13.308(12), $b$ = 5.258(5), $c$ = 22.320(2) Å, $\alpha$ = 90.00, $\beta$ = 95.99, $\gamma$ = 90.00°, $U$ = 1553.2(3) Å$^3$, $Z$ = 4, $D_c$ = 1.378 Mg m$^{-3}$, $\mu$(Mo-K$\alpha$) = 0.094 mm$^{-1}$, $T$ = 123 K, $\Theta_{max}$ = 26.372°. Total 12734 reflections, 3180 unique, $R_{int}$ = 0.092. Refinement of 2023 reflections (217 parameters) with $I$ >2$\sigma$ ($I$) converged at final $R$1 = 0.0696 ($R$1 all data = 0.1435), $wR$2 = 0.0723 ($wR$2 all data = 0.1286), gof = 1.043.

### 3.4.3.4 Ligand 22

$C_{16}H_{11}N_3O$, $M$ = 261.28, colourless needle, monoclinic, space group *P2(1)/c,* $a$ = 3.764(4), $b$ = 19.699(2), $c$ = 16.788(17) Å, $\alpha$ = 90.00, $\beta$ = 90.15, $\gamma$ = 90.00°, $U$ = 1244.6(2) Å$^3$, $Z$ = 4, $D_c$ = 1.394 Mg m$^{-3}$, $\mu$(Mo-K$\alpha$) = 0.710 mm$^{-1}$, $T$ = 123 K. Total 17340 reflections, 3344 unique, $R_{int}$ = 0.092. Refinement of 1696 reflections (181 parameters) with $I$ >2$\sigma$ ($I$) converged at final $R$1 = 0.0485 ($R$1 all data = 0.1171), $wR$2 = 0.0437 ($wR$2 all data = 0.0933), gof = 1.118.

### 3.4.3.5 Ligand 30

Polymorph a

$C_{28}H_{28}N_2O_6$, $M$ = 488.54, colourless needle, monoclinic, space group *P2(1)/c,* $a$ = 13.088(7), $b$ = 17.989(8), $c$ = 10.984(8) Å, $\alpha$ = 90.00, $\beta$ = 108.62, $\gamma$ = 90.00°, $U$ = 2451.0(3) Å$^3$, $Z$ = 4, $D_c$ = 1.324 Mg m$^{-3}$, $\mu$(Mo-K$\alpha$) = 0.711 mm$^{-1}$, $T$ = 123 K. Total 27283 reflections, 5624 unique, $R_{int}$ = 0.092. Refinement of 3375 reflections (235 parameters) with $I$ >2$\sigma$ ($I$) converged at final $R$1 = 0.0397 ($R$1 all data = 0.0842), $wR$2 = 0.0398 ($wR$2 all data = 0.0879), gof = 1.110.

Polymorph b

$C_{28}H_{28}N_2O_6$, $M$ = 488.54, colourless prisms, triclinic, space group *P-1,* $a$ = 10.599(2), $b$ = 11.030(2), $c$ = 12.225(3) Å, $\alpha$ = 96.34, $\beta$ = 108.94, $\gamma$ = 108.69°, $U$ = 1243.4(5) Å$^3$, $Z$ = 2, $D_c$ = 1.305 Mg m$^{-3}$, $\mu$(Mo-K$\alpha$) = 0.092 mm$^{-1}$, $T$ = 123 K. Total 43182 reflections, 11963 unique, $R_{int}$ = 0.023. Refinement of 9173 reflections (325 parameters) with $I$ >2$\sigma$ ($I$) converged at final $R$1 = 0.0403 ($R$1 all data = 0.0766), $wR$2 = 0.0469 ($wR$2 all data = 0.0766), gof = 1.054.

### 3.4.3.6 Ligand 32

$C_{22}H_{14}N_4O_4$, $M$ = 498.37, yellow blocks, monoclinic, space group *P2(1)/c,* $a$ = 20.196(8), $b$ = 7.019(16), $c$ = 13.309(6) Å, $\alpha$ = 90.00, $\beta$ = 106.79, $\gamma$ = 90.00°, $U$ = 1806.3(11) Å$^3$, $Z$ = 4, $D_c$ = 1.465 Mg m$^{-3}$, $\mu$(Mo-K$\alpha$) = 0.104 mm$^{-1}$, $T$ = 123 K. Total 17964 reflections, 3189 unique, $R_{int}$ = 0.1149. Refinement of 3189 reflections (273 parameters) with $I$ >2$\sigma$ ($I$) converged at final $R$1 = 0.1076 ($R$1 all data = 0.1260), $wR$2 = 0.3111 ($wR$2 all data = 0.3266), gof = 1.070.

### 3.4.3.7 Ligand 39

$C_{19}H_{19}N_3$, M = 289.38, colourless plate, triclinic, space group *P*-1, *a* = 9.0269(9), *b* = 10.1440(10), *c* = 10.6092(11) Å$^3$, $\alpha$ = 62.324(6), $\beta$ = 65.248(6), $\gamma$ = 70.093(6)°, *U* = 768.30(14) Å$^3$, *Z* = 2, $D_c$ = 1.251 Mg m$^{-3}$, m(Mo-Ka) = 0.075 mm$^{-1}$, *T* = 123 K. Total 15909 reflections, 4475 unique (Rint = 0.032). Refinement of 2812 reflections (199 parameters) with $I > 3\sigma$ (*I*) converged at final *R*1 = 0.0439 (*R*1 all data = 0.0723), *wR*2 = 0.0621 (*wR*2 all data = 0.1785), gof = 1.103.

### 3.4.3.8 Ligand 40

$C_{19}H_{19}N_3$, *M* = 289.38, colourless block, monoclinic, space group $P2_1/n$, *a* = 12.2325(14), *b* = 10.0731(11), *c* = 13.1592(14) Å, $\beta$ = 108.435(5)°, *U* = 1538.3(3) Å$^3$, *Z* = 4, $D_c$ = 1.249 Mg m$^{-3}$, $\mu$(Mo-K$_\alpha$) = 0.075 mm$^{-1}$, *T* = 173 K. Total 19659 reflections, 5342 unique, $R_{int}$ = 0.052. Refinement of 2802 reflections (199 parameters) with $I > 2\sigma$ (*I*) converged at final *R*1 = 0.0476 (*R*1 all data = 0.1008), *wR*2 = 0.0506 (*wR*2 all data = 0.1260), gof = 1.1300.

# Chapter 4

# 4 Copper Complexes

## 4.1 Results and Discussion

An overview of all relevant ligands is given in Figure 4-62 (see page 165) at the end of this chapter.

### 4.1.1 Preparation

All copper(I) complexes were prepared in the same manner, following a standard literature procedure. The precursor $[Cu(NCMe)_4][PF_6]$ was prepared following a literature procedure[100] and the synthesis of the ligands was described in chapter 3. Then, two equivalents of the appropriate ligand were mixed with $[Cu(NCMe)_4][PF_6]$ in acetonitrile at room temperature and the reaction were monitored by thin layer chromatography; each was complete within two hours (Scheme 4-1). The complexes were isolated in yields between 60 and 99 % as red solids.


R = see leaflet at the end of this chapter

**Scheme 4-1** Synthesis of Copper(I) complexes.

In addition, a series of copper(II) complexes with bpy ligands, bearing a hetero aromatic substituent (**2**-**4**), were prepared. The reason for doing this is the following: Copper(I) bpy complexes containing heteroaromatic rings exhibit quite severe broadening of the $^1$H-NMR spectra. This is in contrast to copper(I) bpy complexes with simple substituents, such as Me, Ph or *n*Bu, which show well resolved signals (for details see section 4.1.2.4). The idea was to see whether the broadening could originate from partially oxidized species. The complexes were prepared following one procedure with two different copper(II) precursors (see Scheme 4-2).

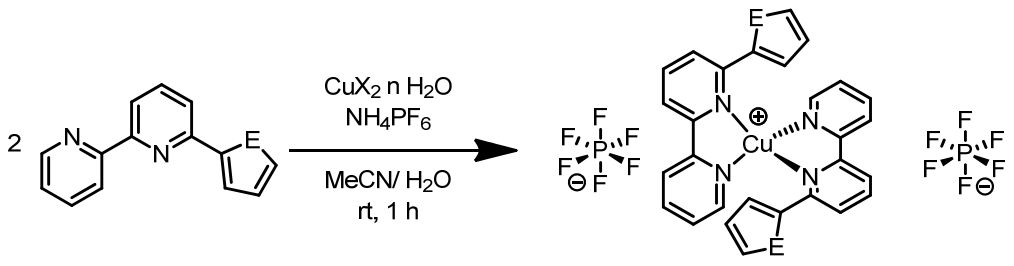


E = O, S, Se  $X^-$ = $Cl^-$, $NO_3^-$  n = 2, 3

**Scheme 4-2** Synthesis of copper(II) complexes.

For the same reasons a series of Ag(I) complexes was prepared with the same ligands (**2**-**4**). The preparation is very similar to that of copper(I) complexes. Two equivalents of the appropriate ligand were mixed with $AgPF_6$ or $AgBF_4$, respectively, dissolved in $CH_2Cl_2$ and stirred for 2 hours. After filtration and solvent removal, the crude materials were recrystallized by slow evaporation of a $CH_2Cl_2$ solution to yield the desired compounds as pale yellow crystals (see Scheme 4-3).

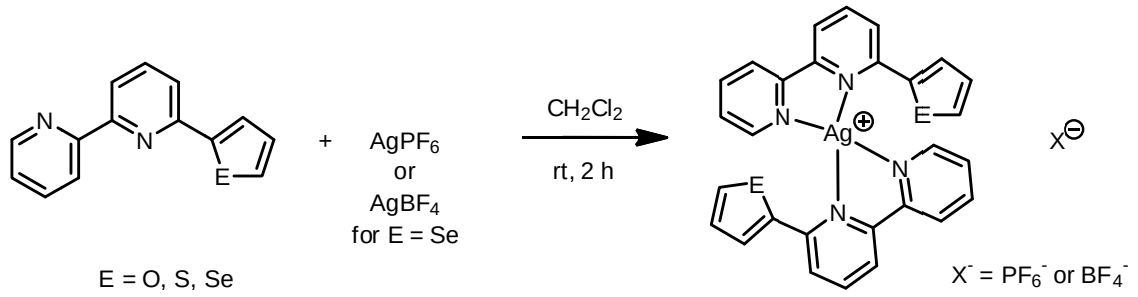


**Scheme 4-3** Synthesis of silver(I) complexes.

For some of the compounds the solid state structures were determined (see section 4.1.2.1) and the results of the NMR experiments will be discussed in section 4.1.2.4.

### 4.1.2 Characterization

The characterization of the complexes was carried out by Electrospray Ionization mass spectrometry (ESI-MS) from an ethanolic solution (< $10^{-6}$ mol $dm^{-3}$) of the compound. The mass spectrum of each complex exhibited a peak envelope corresponding to $[M\text{-}PF_6]^+$ with an isotope distribution matching that simulated.

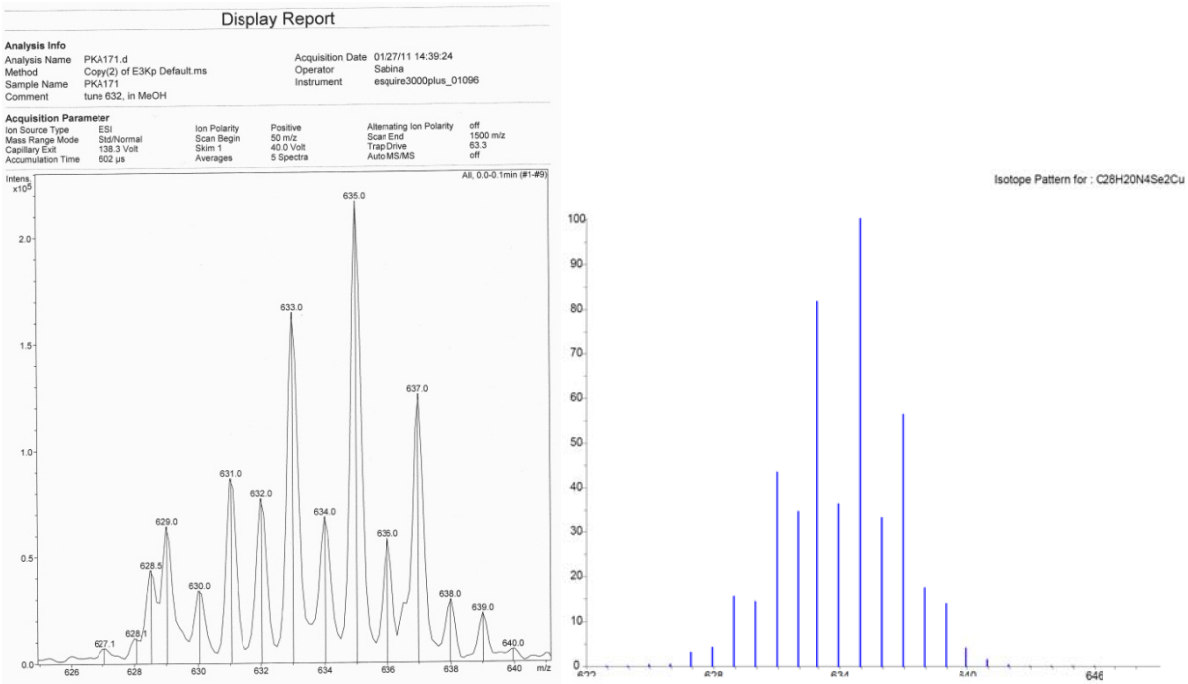


**Figure 4-1** The peak envelope of $[Cu(\mathbf{4})_2]^+$ in the ESI-MS of $[Cu(\mathbf{4})_2][PF_6]$ (left); simulated spectrum for the same composition (right).

As a representative example the ESI-MS spectrum of $[Cu(\mathbf{4})_2][PF_6]$ is shown in Figure 4-1, showing the expected isotope distribution dominated by isotopes of Cu and Se.

The characterization by NMR turned out to be somewhat difficult for the complexes containing heteroaromatic or bulky substituents. While complexes where the bpy ligands contain a rather simple substituent, such as methyl, *n*-butyl or phenyl showed sharp and well resolved spectra, the first mentioned complexes exhibited broad signals and it was impossible to obtain $^{13}C$- or 2-D NMR-spectra. Many experiments were carried out to understand the solution behaviour of these new complexes and these studies will be presented in section 4.1.2.4.

The IR spectra of the complexes were recorded and showed all the characteristic bands slightly shifted to higher energies compared to the free ligand, but most importantly the strong absorption of $[PF_6]^-$ could be observed at $\nu$ = 830 $cm^{-1}$.

UV/vis spectra showed the characteristic ligand based absorption bands (LC) in the UV region, and very low intensity MLCT bands between 430 and 550 nm characteristic for copper(I) complexes. For details see section 4.1.2.2.

The complexes show unusual electrochemical behaviour, which, to the best of our knowledge, not not been reported in the literature before, not even for similar compounds. The only exception is one report by Piero ZANELLO in 1991, where he investigated the electrochemical behaviour of $[Cu^{(I)}(Hdpa)][ClO_4]$ (Hdpa = di-2-pyridylamine).[101] Therefore, we devoted some time for these investigations and the results will be summarized in section 4.1.2.3., along with spectroelectrochemical experiments.

### 4.1.2.1 Solid State Structures

Single crystals of complexes containing a heteroaromatic substituent, namely $[Cu(\mathbf{1})_2][PF_6]$, $[Cu(\mathbf{2})_2][PF_6]$, $[Cu(\mathbf{3})_2][PF_6]$ were grown by recrystallization from ethanol, by layering a $CHCl_3$ solution of the compound with toluene, and from a dichloromethane/diethyl ether solution kept at 2 °C, respectively. All three complexes crystallize without solvent, and the structures and packing can therefore be directly compared. Figure 4-2, Figure 4-3 and Figure 4-4 illustrate the structures of the $[Cu(\mathbf{1})_2]^+$, $[Cu(\mathbf{2})_2]^+$ and $[Cu(\mathbf{3})_2]^+$ cations. Several crystal growth experiments were carried out in the attempt to determine the structure of $[Cu(\mathbf{4})_2][PF_6]$ but only crystals of poor quality could be obtained, where problems with twinning yielded a poorly refined structure (R = 25 %). Nevertheless, the preliminary data are shown in Figure 4-5 and selected bond parameters are summarized in Table 4-1 for all four complexes. $[Cu(\mathbf{1})_2][PF_6]$ and $[Cu(\mathbf{2})_2][PF_6]$ crystallize in monoclinic space groups *C*2/*c* and $P2_1/c$, respectively, and the two ligands in each of $[Cu(\mathbf{2})_2]^+$ and $[Cu(\mathbf{3})_2]^+$ are related by a 2-fold axis passing through atom Cu1. $[Cu(\mathbf{3})_2][PF_6]$ crystallizes in the triclinic *P*-1 space group

and one of the two ligands suffers from a 2-fold rotational disorder of the thienyl substituent. This has been modelled over two positions with fractional occupancies of 0.869(2) and 0.131(2). Only the major occupancy site is considered in Figure 4-4 and Table 4-1. The hexafluoridophosphate anion in each structure is ordered.

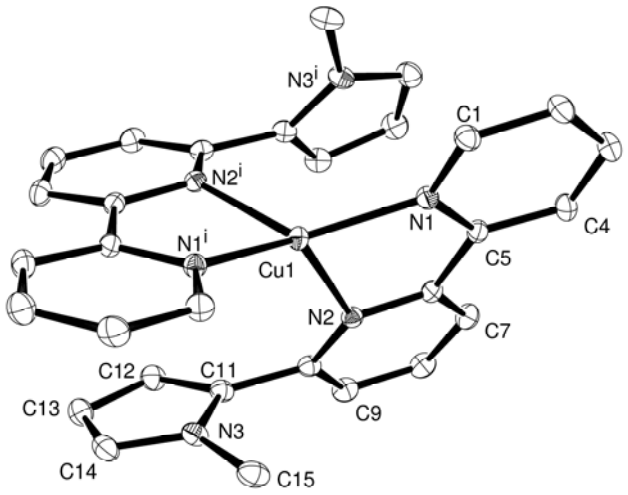


**Figure 4-2** Structure of the $[Cu(\mathbf{1})_2]^+$ cation in $[Cu(\mathbf{1})_2][PF_6]$ with H atoms omitted (ellipsoids plotted at 40 % probability level).

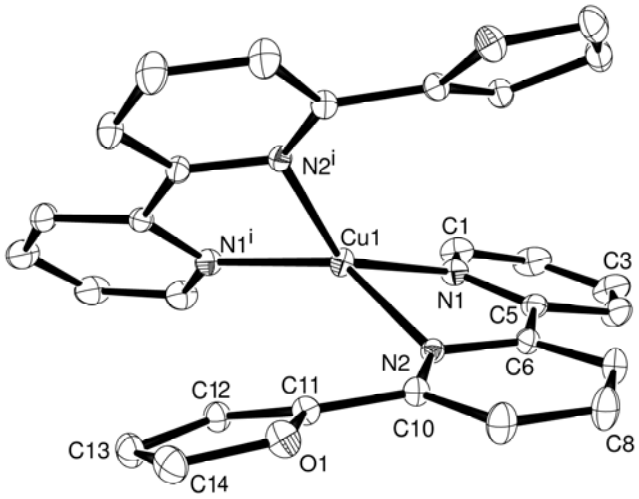


**Figure 4-3** Structure of the $[Cu(\mathbf{2})_2]^+$ cation in $[Cu(\mathbf{1})_2][PF_6]$ with H atoms omitted (ellipsoids plotted at 40 % probability level).

Inspection of the bond distances in Table 4-1 shows that the Cu1-N2 bond in $[Cu(\mathbf{2})_2][PF_6]$ is noticeably longer (2.200(2) Å) than the remaining Cu-N bonds, all of which are close to 2.0 Å. The elongation is associated with a deformation of the corresponding bpy ligand away from planarity: the angle between the least squares planes of the two rings in this copper-bound bpy is 27.16(14)° compared to 16.36(13)° for the second bpy in $[Cu(\mathbf{2})_2]^+$, 14.62(4)° in $[Cu(\mathbf{1})_2]^+$, 8.54(4)° in $[Cu(\mathbf{3})_2]^+$ 7.03(4)° and in $[Cu(\mathbf{4})_2]^+$. As a result of these structural changes, each thienyl substituent in the $[Cu(\mathbf{2})_2]^+$ cation engages in face-to-face $\pi$-stacking

with the central pyridine ring of the second ligand, the thienyl centroid...pyridine plane separations being 3.55 and 3.58 Å.

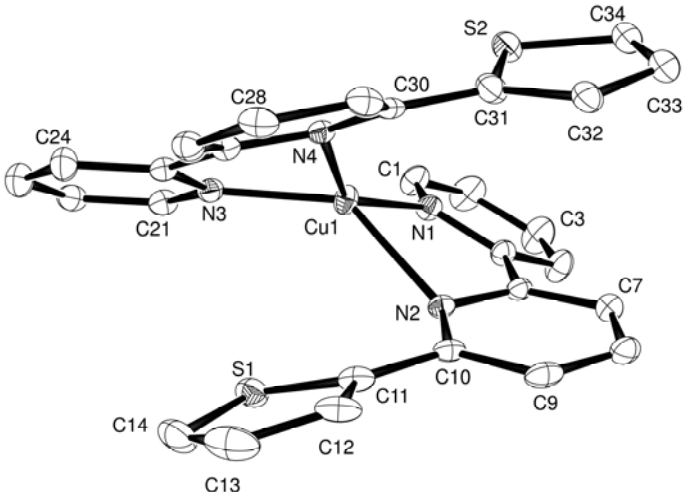


**Figure 4-4** Structure of the $[Cu(\mathbf{3})_2]^+$ cation in $[Cu(\mathbf{3})_2][PF_6]$ with H atoms omitted (ellipsoids plotted at 40 % probability level). The ring containing atom S2 is disordered and only the major occupancy site is illustrated.

$[Cu(\mathbf{4})_2][PF_6]$ crystallizes in the monoclinic space group $P2_1/n$ and was able to confirm the gross structural features of the cation. The copper(I) ion is in a flattened tetrahedral environment with Cu–N bond distances in the range ≈ 1.9 to 2.0 Å. Both selenophen-2-yl substituents are rotationally disordered over two positions, but in each ring, one position is dominant. Considering only the major occupancy sites, the orientation of one of the heterocyclic rings permits a short Cu...Se contact of ≈ 3.2 Å. Furthermore, compared to all other complexes the bpy moieties deviate only a little from planarity but the substituents are more twisted.

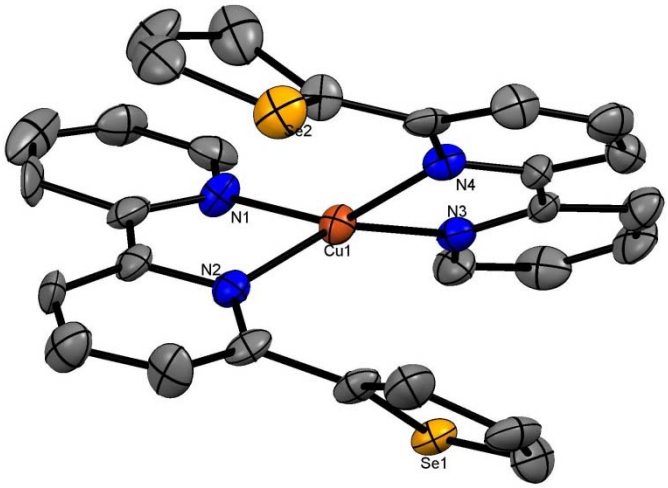


**Figure 4-5** Structure of the $[Cu(\mathbf{4})_2]^+$ cation in $[Cu(\mathbf{4})_2][PF_6]$ with H atoms omitted (ellipsoids plotted at 30 % probability level).

The angles between the least square planes of the substituents and the central pyridine ring are 41.21 and 33.04° and allow a face to face π-stacking between the substituent and the second central pyridine ring with selenophenyl centroid...pyridine centroid distances of 3.6 or 3.8 Å, respectively. It can be speculated that these motifs are dependent on the bulkiness of the ring. $[Cu(\mathbf{1})_2][PF_6]$ and $[Cu(\mathbf{4})_2][PF_6]$ show similar molecular structures, which differ from $[Cu(\mathbf{2})_2][PF_6]$ and $[Cu(\mathbf{3})_2][PF_6]$. The Se atoms are quite sterically demanding and could be compared to the dimensions of methyl groups.[102]

| | $[Cu(1)_2][PF_6]$ | $[Cu(2)_2][PF_6]$ | $[Cu(3)_2][PF_6]$ [a] | $[Cu(4)_2][PF_6]$ |
|---|---|---|---|---|
| | Atom X = N3 | atom X = O1 | atom X = S1, S2 | Atom X = Se1, Se2 |
| **Bond distance /Å** | | | | |
| **Cu1-N1** | 1.9918(6) | 2.0046(6) | 1.980(2) | 1.932 |
| **Cu1-N2** | 2.0758(6) | 2.0932(5) | 2.200(2) | 1.973 |
| **Cu1-N3/N1$^i$** | 1.9918(6) | 2.0046(6) | 2.006(2) | 1.957 |
| **Cu1-N4/N2$^i$** | 2.0758(6) | 2.0932(5) | 2.095(2) | 2.018 |
| **C11-X** | 1.3800(10) | 1.3759(8) | 1.720(3) | 1.882 |
| **C14-X** | 1.3713(11) | 1.3690(10) | 1.712(3) | 1.757 |
| **C31-X** | | | 1.7111(6) | 1.829 |
| **C34-X** | | | 1.7001(4) | 1.737 |
| | | | | |
| **Bond angle / deg** | | | | |
| **N1-Cu1-N2** | 81.43(2) | 81.05(2) | 80.41(8) | 82.72 |
| **N1-Cu1-N3/N1$^i$** | 134.50(4) | 124.53(4) | 128.44(9) | 105.61 |
| **N2-Cu1-N3/N1$^i$** | 129.55(2) | 137.70(2) | 133.10(8) | 151.48 |
| **N1-Cu1-N4/N2$^i$** | 129.55(2) | 137.70(2) | 143.07(9) | 144.63 |
| **N2-Cu1-N4/N2$^i$** | 101.79(3) | 102.26(3) | 94.74(8) | 106.28 |
| **N3/N1$^i$-Cu1-N4/N2$^i$** | 81.43(2) | 81.05(2) | 80.97(9) | 82.91 |
| **C11-X-C14** | 108.77(7) | 106.59(6) | 92.14(16) | 84.87 |
| **C31-X-C34** | | | 92.690(9) | 85.75 |

**Table 4-1** Selected bond parameters for the homoleptic copper(I) complexes with L = **1**-**4**. In each of $[Cu(\mathbf{1})_2]^+$ and $[Cu(\mathbf{2})_2]^+$, the two ligands are related by a 2-fold axis

The extent of inter-ligand π-stacking within each cation is illustrated in Figure 4-6. In $[Cu(\mathbf{2})_2][PF_6]$, each furyl group is twisted 16.36(4)° with respect to the plane of the pyridine ring to which it is attached, but as Figure 4-6b shows, the mutual twisting of the heterocyclic rings within the ligands does not result in inter-ligand stacking within the $[Cu(\mathbf{2})_2]^+$ cation. We have already noted that in $[Cu(\mathbf{3})_2]^+$, both thienyl substituents are involved in intra-cation face-to-face interactions (Figure 4-6c).

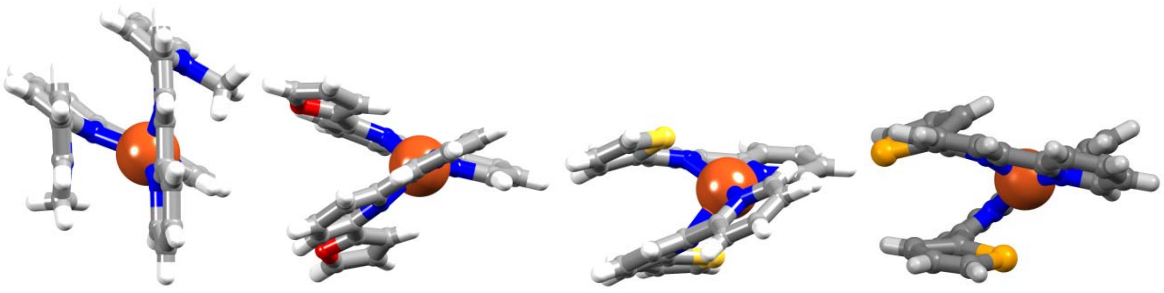

a) b) c) d)

**Figure 4-6** Representations of the (a) $[Cu(\mathbf{1})_2]^+$, (b) $[Cu(\mathbf{2})_2]^+$, and (c) $[Cu(\mathbf{3})_2]^+$ (d) $[Cu(\mathbf{4})_2]^+$ cations, illustrating the inter-ligand face-to-face π-interactions.

However, the most effective intramolecular aryl embrace is achieved in $[Cu(\mathbf{1})_2]^+$, despite the presence of the *N*-methyl substituents. Each pyrrolyl unit twists 54.87(4)° out of the plane of the central pyridine ring in coordinated **1**. The ligand attains a conformation that permits a face-to-face $\pi$-interaction between the pyrrolyl domain of one ligand and the central pyridine ring of the other: the interplane angle is 2.8° and the pyrrolyl centroid...pyridine plane separation is 3.46 Å. There is a trend within this series; the bigger the heteroatom in substituent ring of the bpy ligand (or in the case of the nitrogen containing N-methyl-pyrrole ring a sterically demanding substituent on the ring), the more pronounced is the intermolecular $\pi$-stacking. The crystal packing in all four complexes involves extensive cation...anion CH...F contacts and some degree of inter-cation $\pi$-stacking, although in $[Cu(\mathbf{2})_2][PF_6]$ this is rather inefficient.

Single crystals of $[Cu(\mathbf{5})_2][PF_6]$, $[Cu(\mathbf{6})_2][PF_6]$ and $[Cu(\mathbf{21})_2][PF_6]$ were grown from dichloromethane solutions of the complexes layered with diethyl ether. Both $[Cu(\mathbf{5})_2][PF_6]$ and $[Cu(\mathbf{21})_2][PF_6]$ crystallize in the monoclinic space group *C*2/*c* even though $[Cu(\mathbf{21})_2][PF_6]$ crystallizes with a solvent molecule (toluene) in contrast to $[Cu(\mathbf{5})_2][PF_6]$ which is solvent free. In contrast, $[Cu(\mathbf{6})_2][PF_6]$ crystallized in the triclinic spacegroup *P*-1. The structures of the $[Cu(\mathbf{5})_2]^+$ $[Cu(\mathbf{6})_2]^+$ and $[Cu(\mathbf{21})_2]^+$ cations are depicted in Figure 4-7, Figure 4-8 and Figure 4-9, and bond parameters for the metal coordination spheres are listed in the figure captions.

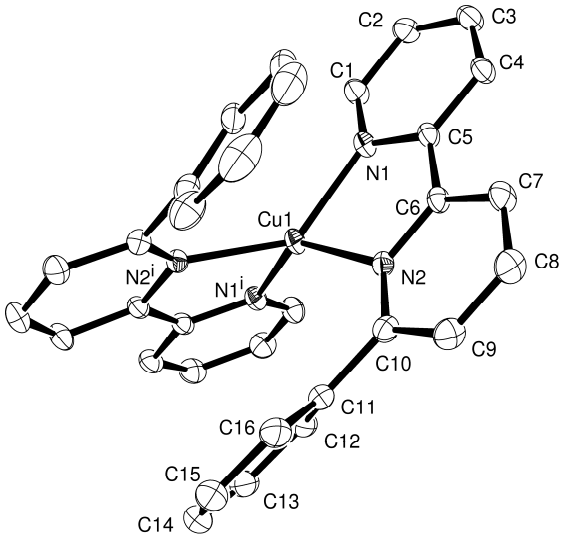


**Figure 4-7** Structure of the $[Cu(\mathbf{5})_2]^+$ cation in $[Cu(\mathbf{5})_2][PF_6]$ with H atoms omitted (ellipsoids plotted at 30 % probability level). Selected bond parameters: Cu1-N1 2.0278(14), Cu1-N2 2.0530(14) Å; N1-Cu1-N2 80.82(6), N1-Cu1-N1i 119.11(8), N1-Cu1-N2i 135.29(6), N1i-Cu1-N2i 80.82(6), N2-Cu1-N2i 114.09(8)°.

The copper(I) coordination sphere in $[Cu(\mathbf{6})_2]^+$ is close to tetrahedral, with the angle between the two bpy domains being 87.31(3)° (Figure 4-11a). In contrast, Figure 4-11 b and c illustrate significant flattening of the ligand arrangement, the corresponding angle being 65.47(2)° for $[Cu(\mathbf{5})_2]^+$ and a smaller angle of 47.9° is observed for $[Cu(\mathbf{21})_2]^+$. The difference

originates in intra-cation arene stacking in $[Cu(\mathbf{5})_2]^+$ as well as in $[Cu(\mathbf{21})_2]^+$. The phenyl substituent of one ligand **5** (twisted 45.02(10)° with respect to the bpy unit) lies over the pyridine ring containing N2 of the second ligand. Although there is a face-to-face π-interaction (centroid to ring distance = 3.66 Å), it is not optimal since the planes of the two rings subtend an angle of 10.8° with one another. A similar situation can be found for the $[Cu(\mathbf{21})_2]^+$ cation but here the π-stacking is more pronounced (centroid to ring distance = 3.44 Å) and the angle between the two planes is with 4.9° only half as big as for $[Cu(\mathbf{5})_2]^+$.

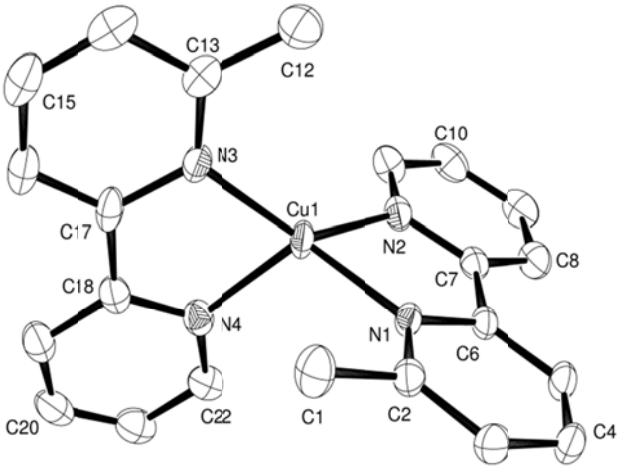


**Figure 4-8** Structure of the $[Cu(\mathbf{6})_2]^+$ cation in $[Cu(\mathbf{6})_2][PF_6]$ with H atoms omitted (ellipsoids plotted at 30 % probability level). Selected bond parameters: Cu1-N3 1.996(2), Cu1-N2 1.998(2), Cu1-N4 2.044(2), Cu1-N1 2.0443(18) Å; N3-Cu1-N2 137.88(9), N3-Cu1-N4 81.64(9), N2-Cu1-N4 116.07(9), N3-Cu1-N1 126.69(8), N2-Cu1-N1 81.78(8), N4-Cu1-N1 115.82(8)°.

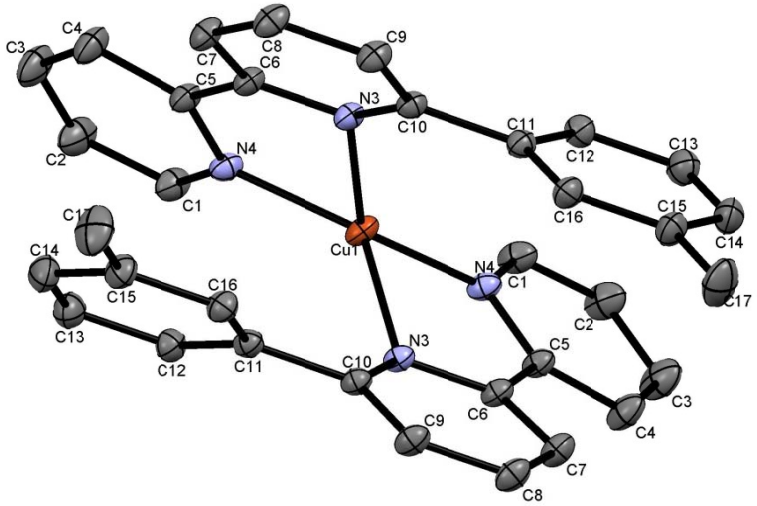


**Figure 4-9** Structure of the $[Cu(\mathbf{21})_2]^+$ cation in $[Cu(\mathbf{21})_2][PF_6]_*$(Toluene) with H atoms omitted (ellipsoids plotted at 50 % probability level). Selected bond parameters: Cu1-N3 2.0984(6), Cu1-N4 1.9851(6) Å; N3-Cu1-N4 81.54(3), N3-Cu1-N3 97.05(3), N4-Cu1-N3 132.36(3), N4-Cu1-N4 133.14(4)°.

The crystal packing in [Cu(**5**)$_2$][PF$_6$] is dominated by C–H…F contacts rather than π-stacking interactions. The same is true for [Cu(**21**)$_2$][PF$_6$], but since it crystallizes with solvent molecules, face-to-edge π-stacking between the toluene ring and H(C14) of the cation is involved to some degree (ring to H distance = 3.0 Å). In contrast, the packing in [Cu(**6**)$_2$][PF$_6$] involves efficient face-to-face π-stacking between centrosymmetric pairs of cations, involving bpy domains containing atoms N3/N4 and N3'/N4' (inter-plane separation = 3.4 Å). Extension of the π-stacking between bpy units of adjacent cations involving N3/N4 and N3''/N4'' (inter-plane distance = 3.3 Å) results in the propagation of chains slicing diagonally through the unit cell.

Single crystals of [Cu(**12**)$_2$][PF$_6$] could be obtained by slow evaporation of an acetonitrile solution of the compound and the molecular structure of the cation [Cu(**12**)$_2$]$^+$ is shown in Figure 4-10, the dimensions and angles of the coordination centre are listed in the caption. The structure of [Cu(**12**)$_2$]$^+$ is discussed separately because it crystallizes with solvent molecules (acetonitrile) in a different space group (monoclinic; *Cc*).

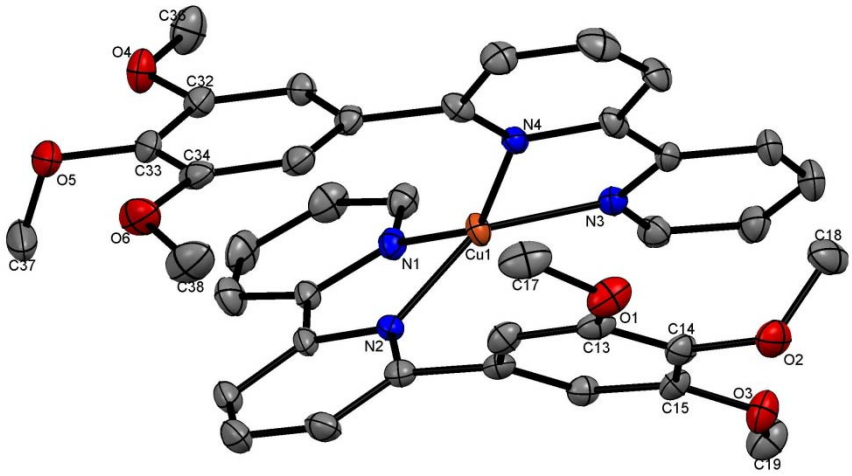


**Figure 4-10** Structure of the [Cu(**12**)$_2$]$^+$ cation in [Cu(**12**)$_2$][PF$_6$]$_*$(MeCN) with H atoms omitted (ellipsoids plotted at 25 % probability level). Selected bond parameters: Cu1-N2 1.949(4), Cu1-N3 1.963(4), Cu1-N1 1.977(4), Cu1-N4 1.999(4) Å; N2-Cu1-N3 145.78(16), N2-Cu1-N1 83.65(17), N3-Cu1-N1 108.71(16), N2-Cu1-N4 105.54(16), N3-Cu1-N4 83.18(16), N1-Cu1-N4 144.35(16)°.

Nevertheless, the molecular structure is related to the two previous described ([Cu(**5**)$_2$]$^+$ and [Cu(**21**)$_2$]$^+$). Here too, the two bpy moieties are flattened from the optimal tetrahedral symmetry, with an angle between the two ligands of 52.05°. This is again caused by intermolecular π-interactions of the substituent of one bpy ligand between the central pyridine ring of the second ligand. The tris(methoxy)phenyl substituent is twisted from the plane in which the bpy moiety lies, spanning an angle of 49.49 and 50.49°, respectively, and the distance between the two being 3.54 Å. Therefore, the π-interactions are less pronounced than in [Cu(**21**)$_2$]$^+$ but more than in [Cu(**5**)$_2$]$^+$. The packing in [Cu(**12**)$_2$]$^+$ involves

intermolecular π-interactions between a tris(methoxy)phenyl substituent of one molecule and the external pyridine ring of the next molecule, the distance between the phenyl centroid and the bpy plane being 3.58 Å. This results in zig-zag chains, which in turn are connected through the anions *via* F…H distances (2.4-2.7 Å).

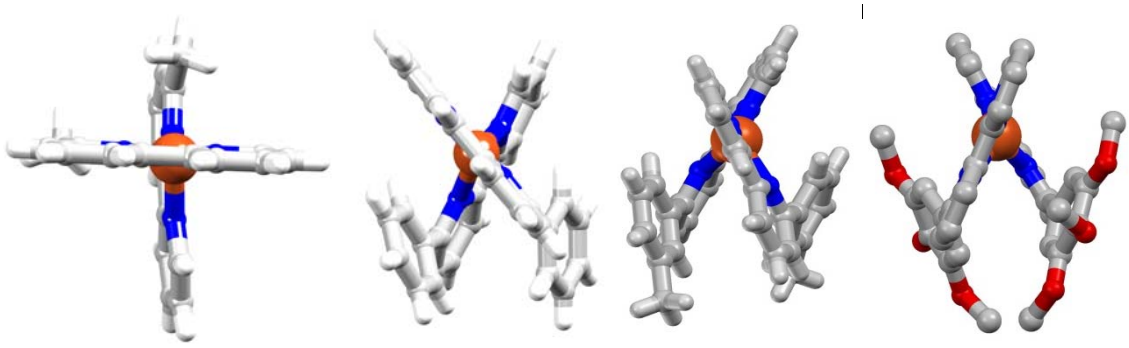


**Figure 4-11** Comparison of the coordination spheres in (a) $[Cu(\mathbf{6})_2]^+$ (b) $[Cu(\mathbf{5})_2]^+$ (c) $[Cu(\mathbf{21})_2]^+$ and (d) $[Cu(\mathbf{12})_2]^+$ in the hexafluoridophosphate salts.

Copper complexes with 4',6'-disubstituted bpy ligands were prepared and for some of them single crystals could be obtained. Single crystals of $[Cu(\mathbf{30})_2][PF_6]$ were grown by slow evaporation of a acetonitrile solution of the compound. It crystallizes in the monoclinic space group *C*2/*c* with solvent molecules. Approximately 11 % of the acetonitrile molecules are disordered, as well as all of the $[PF_6]^-$ anions. The molecular structure of the cation $[Cu(\mathbf{30})_2]^+$ is comparable to $[Cu(\mathbf{12})_2]^+$ as well as to $[Cu(\mathbf{5})_2]^+$. It is depicted in Figure 4-12, with the bond parameter and angle of the coordination sphere given in the caption.

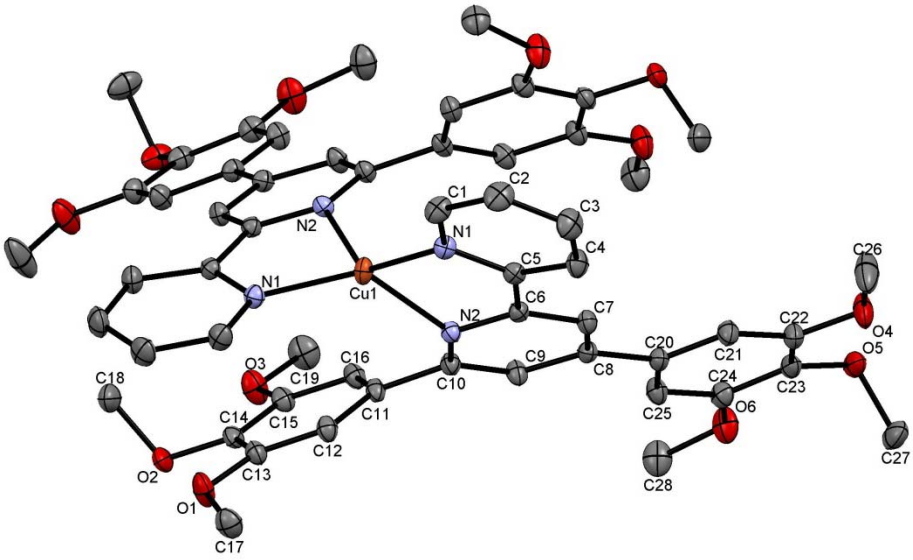


**Figure 4-12** Structure of the $[Cu(\mathbf{30})_2]^+$ cation in $[Cu(\mathbf{30})_2][PF_6]_*(MeCN)$ with H atoms omitted (ellipsoids plotted at 50 % probability level). Selected bond parameters: Cu1-N1 1.9767(12), Cu1-N2 2.0727(12) Å; N1-Cu1-N1 133.83(7), N1-Cu1-N2 81.83(5), N1-Cu1-N2 129.56(5), N2-Cu1-N2 101.79(7)°.

The coordination sphere is, too, distorted from tetrahedral geometry. The angle between the two bpy moieties is 42.08° smaller than the above described. Only the tris(methoxy)phenyl substituent in the 4'-position is in plane with the central pyridine ring. The second pyridine ring (15.54°) and the second phenyl ring are twisted (3.74°). The deviation from planarity of the bpy moiety results again in an elongation of the Cu-N2 bonds of ~0.1 Å compared to $[Cu(\mathbf{12})_2]^+$. The π-interactions are of the same originate as mentioned before and result in 3.5 Å distance between the phenyl substituent of one ligand and the central pyridine ring of the second ligand. The packing is dictated by intermolecular p-π-interactions between C14 and O2 of two cations, as well as by weak hydrogen bonds between O6/O5 and HC17 (2.9/2.6 Å) and a contribution from F…H contacts (2.6 Å), which result in a zig-zag pattern (Figure 4-13).

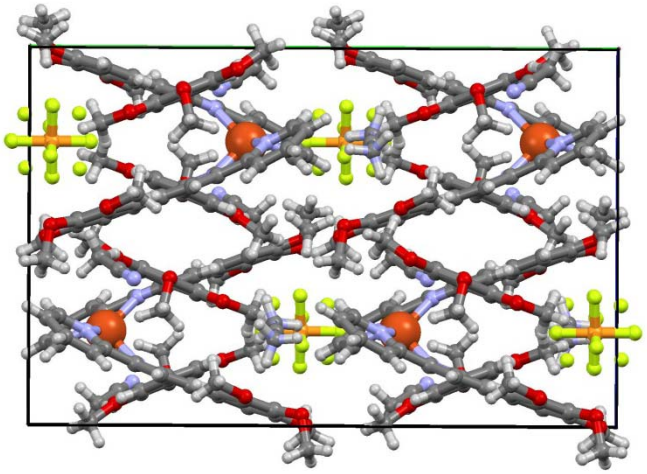

**Figure 4-13** Packing pattern of $[Cu(\mathbf{30})_2][PF_6]$.

All attempts to obtain crystalline material of $[Cu(\mathbf{31})_2][PF_6]$ failed, so that unfortunately this structure cannot be compared to the parental and unsubstituted derivative. Single crystals of the nitro derivative were obtained by slow evaporation of a dichloromethane solution of $[Cu(\mathbf{32})_2][PF_6]$ as dark red blocks. The compound crystallizes in the monoclicnic space group $P2_1/c$, but only a poor data set could be obtained and the preliminary structure (R1 = 0.196) is shown in Figure 4-14, the bond parameters and angles are listed in the caption. It can be clearly seen that the molecular structure is very similar to that previously described. Again, the copper atom exhibits a four-coordinate geometry which is tremendously distorted from an optimal tetrahedral geometry. The angle between the two bpy planes is the smallest (29.67°) of all complexes described here. The intercationic π-interactions result in distances of 3.4 and 3.5 Å between nitrophenyl substituent in 4'-position of one ligand (centroid) and the central pyridine ring of the second ligand (plane). The phenyl rings are slightly twisted from planarity with the bpy ligand (4.1 and 11.7°).

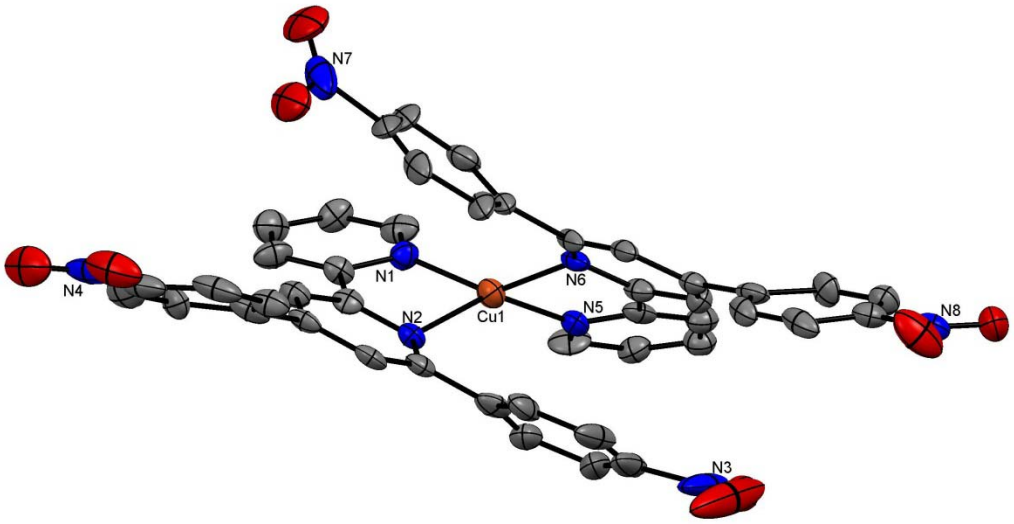


**Figure 4-14** Structure of the $[Cu(\mathbf{32})_2]^+$ cation in $[Cu(\mathbf{32})_2][PF_6]$ with H atoms omitted (ellipsoids plotted at 25 % probability level). Selected bond parameters: Cu1-N1 1.984(11), Cu1-N5 2.037(13), Cu1-N6 2.046(13), Cu1-N2 2.069(10) Å; N1-Cu1-N5 113.8(5), N1-Cu1-N6 142.3(5), N5-Cu1-N6 82.1(5), N1-Cu1-N2 82.2(5), N6-Cu1-N2 106.4(4), N5-Cu1-N2 142.3(4)°.

The packing in $[Cu(\mathbf{32})_2][PF_6]$ is dominated by intermolecular π-π–interactions (3.4-3.6 Å) resulting in columns of cations. These in turn are connected *via* hydrogen bonds (2.1-2.5 Å) between the oxygen atoms of the nitro groups and hydrogen atoms of neighbouring cations. Furthermore, the packing is supported by F…H distances (2.4 Å) between the cations and anions. The packing motif is depicted in Figure 4-15.

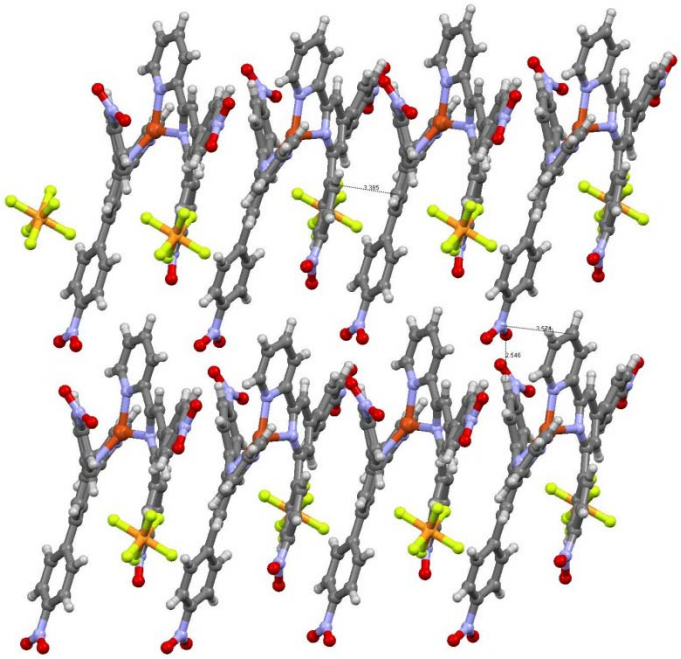

**Figure 4-15** Packing pattern of $[Cu(\mathbf{32})_2][PF_6]$.

Figure 4-16 shows the preliminary structure of $[Cu(\mathbf{36})_2][PF_6]$. Suitable single crystals could be obtained from slow evaporation of a dichloromethane solution of the compound as red

plates. The measurement yielded only a poor data set (R = 0.1712) but again the molecular structure could be confirmed.

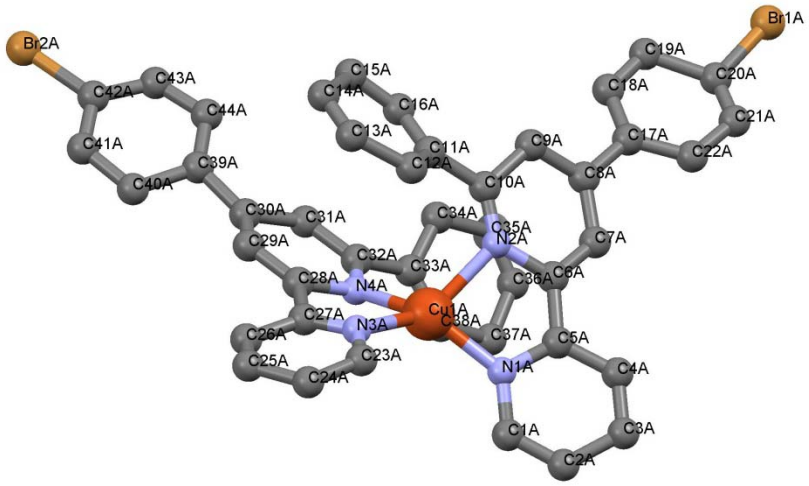


**Figure 4-16** Structure of the $[Cu(\mathbf{36})_2]^+$ cation in $[Cu(\mathbf{36})_2][PF_6]$ with H atoms omitted. Selected bond parameters: Cu1A-N1A 1.968(13), Cu1A-N4A 2.007(11), Cu1A-N3A 2.058(11), Cu1A-N2A 2.106(11) Å; N1A-Cu1A-N4A 134.4(4), N1A-Cu1A-N3A 122.3(4), N4A-Cu1A-N3A 82.8(4), N1A-Cu1A-N2A 83.2(4), N4A-Cu1A-N2A 102.6(4), N3A-Cu1A-N2A 138.5(4)°.

The compound crystallizes in the orthorhombic space group $P2_12_12_1$ with solvent molecules (dichloromethane). A distorted tetrahedral coordination sphere of the copper metal centre is again the result of intermolecular π-interactions of the phenyl substituent with the central pyridine ring of the second bpy ligand (3.58 and 3.65 Å). In this case the planes are nearly parallel, the interplane angle being the smallest (1.2°) of all molecules presented. Nevertheless, the π-stacking is less pronounced than in $[Cu(\mathbf{1})_2][PF_6]$ or $[Cu(\mathbf{21})_2][PF_6]$. The angle between the two bpy planes is 38.5° a bit smaller than the one observed for $[Cu(\mathbf{30})_2][PF_6]$ (43.1°). The packing is dictated by intermolecular π-interactions (3.3-3.7 Å), Br…H distances (2.8-3.0 Å) as well as by F…H (2.3-2.7 Å) bonds.

An interesting exception within the $[Cu(\mathbf{Rbpy})_2][PF_6]$ complexes, where R is an aromatic substituent on the bpy ligand, is the next compound. Suitable single crystals of $[Cu(\mathbf{34})_2][PF_6]$ could be obtained by recrystallization from ethanol as red plates. The compound crystallizes in the triclinic space group *P*-1 with solvent molecules which are distorted, the structure is depicted in Figure 4-17. Interestingly, there are no intermolecular π-interactions whatsoever. The coordination sphere of the copper is only slightly distorted from the optimal tetrahedral geometry. So it can be speculated whether there are interactions between the sulphur atoms and the metal centre to some degree. Indeed, if a second coordination sphere is considered, the geometry around the copper can be described as a distorted octahedral. The Cu…N bond lengths are in the expected range of 2.032-2.054 Å and the Cu…S are somewhat longer with 2.99 or 3.06 Å, respectively. These values are slightly longer than the sum of the van der Waals radius of S and the ionic radius of six coordinated

$Cu^+$ (1.8+0.91 = 2.71 Å).[102] The ligands themselves are more or less planar except the substituents in the 6'-positions which are twisted, the interplane angles being 19.83 and 22.76°, respectively. Both bpy moieties subtend an angle of 74.40°. This value is only 13° smaller than the nearly perpendicular angle in $[Cu(\mathbf{6})_2][PF_6]$ but twice as big as in $[Cu(\mathbf{36})_2][PF_6]$ (38.5°) where the substituents do not bear hetero atoms. Compared to $[Cu(\mathbf{3})_2][PF_6]$, which has no substituent in the 4'-position, the flattening of the tetrahedron is much less pronounced: 74.4 *vs.* 35.9°.

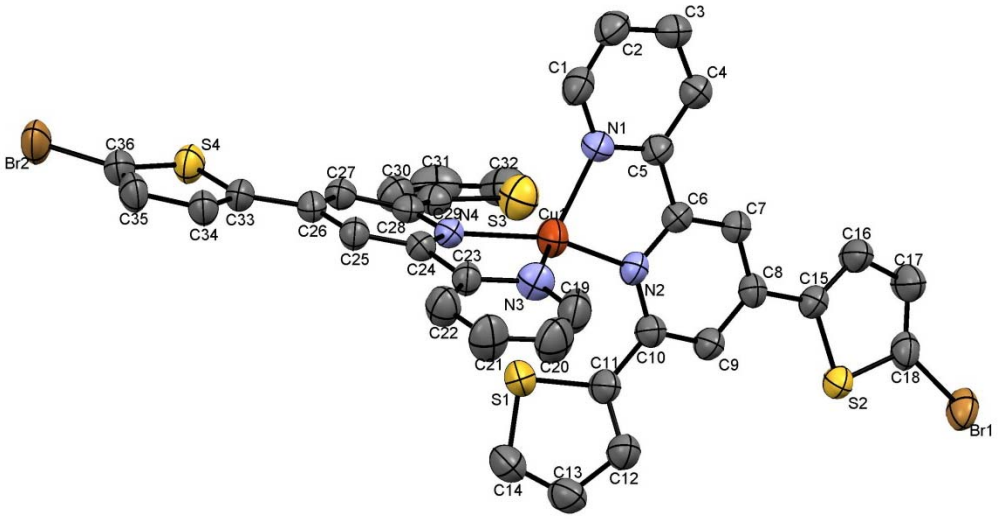


**Figure 4-17** Structure of the $[Cu(\mathbf{34})_2]^+$ cation in $[Cu(\mathbf{34})_2][PF_6]$ with H atoms omitted (ellipsoids plotted at 50 % probability level). Selected bond parameters: Cu1-N2 2.032(5), Cu1-N1 2.032(5), Cu1-N3 2.034(5), Cu1-N4 2.054(5), Cu1-S1' 3.06(2), Cu1-S3 2.992(3) Å; N2-Cu1-N1 82.8(2), N2-Cu1-N3 118.1(2), N1-Cu1-N3 121.2(2), N2-Cu1-N4 141.7(2), N1-Cu1-N4 113.4(2), N3-Cu1-N4 84.1(2), S3-Cu1-N4 73.8(2), S3-Cu1-N2 76.4(2), S3-Cu1-N1 78.0(2), S3-Cu1-S1' 97.1(5), S1'-Cu1-N3 70.1(5), S1'-Cu1-N4 83.8(5), S1'-Cu1-N2 76.5(5), S3-Cu1-N3 155.7(2), S1'-Cu1-N1 159.3(5)°.

The packing is dominated by cation anion interactions with F…H distances being 2.55 Å. To some small degree intermolecular π-stacking can be observed between an external pyridine ring of one cation and the bromothiophenyl substituent of a second molecule, the distances between the centroids being 3.75 Å.

To see whether the observed Cu…S distances correspond to interactions, a test reaction with a *N,S*-donor ligand was carried out. The product was not very stable and the characterization is poor. Nevertheless, it was possible to obtain a single crystal and a preliminary structure (R = 0.147) of a $[Cu(N,S)_2][PF_6]$ complex. The ligand used is 2-methyl-6-thiophen-2-yl-pyridine. In this case the copper metal has only two nitrogen atoms available and therefore has no choice but to saturate its coordination sphere with the sulfur atoms. The molecular structure of the cation is depicted in Figure 4-18. The coordination geometry is one of a strongly distorted tetrahedron and should rather be described as "butterfly" structure. The two nitrogen atoms coordinate to the copper metal and their arrangement is nearly linear

with the angle N-Cu-N being 164.1(3) . The Cu…N distances are 1.926(8) and 1.937(8) Å and the Cu…S separation are with 2.730(3) and 2.810(4) Å the shortest here observed.

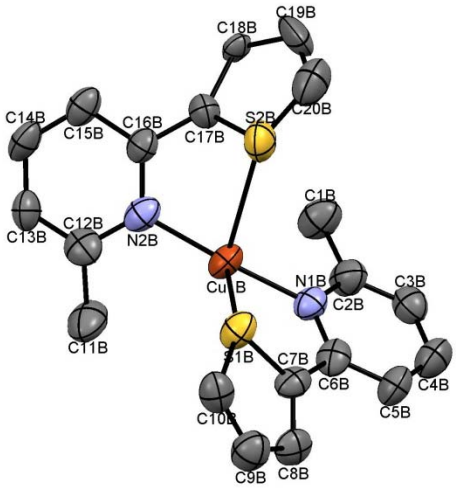


**Figure 4-18** Structure of the $[Cu(thmpy)_2]^+$ cation in $[Cu(thmpy)_2][PF_6]$ with H atoms omitted (ellipsoids plotted at 50 % probability level). Selected bond parameters: Cu1-N1 1.926(8), Cu1-N2 1.937(8), Cu1-S1 2.730(3), Cu1-S2 2.810(4) Å; N1-Cu1-N2 164.1(3), N1-Cu1-S1 81.1(2), N2-Cu1-S1 114.8(3), N1A-Cu1A-S2 99.2(2), N2-Cu1-S2 81.9(2), S1-Cu1-S2 95.28(11)°.

For comparison reasons and to obtain supporting NMR experiments (see section 4.1.2.4), a series of copper(II) complexes have been prepared with ligands **2**-**4** and crystals were grown for solid state structure determination. Figures Figure 4-20Figure 4-22 andFigure 4-23 show the molecular structures of the cations $[Cu(L)_2]^{2+}$ (L = **2**, **3** and **4**). Suitable crystals were obtained by slow evaporation of a dichloromethane solution of $[Cu(\mathbf{2})_2][PF_6]_2$ or acetonitrile solutions of $[Cu(\mathbf{3})_2][PF_6]_2$ and $[Cu(\mathbf{4})_2][PF_6]_2$, respectively, as black blocks. All compounds crystallize in the orthorhombic space group *Pbcn* with solvent molecules. In all compounds the asymmetric units contain half of the metal atom with one ligand, one $[PF_6]^-$ anion and one solvent molecule; for the two latter compounds the acetonitrile molecules are disordered; and the other half is produced by symmetry operations. Therefore, the copper atom has the oxidation state of 2+, and usually this prefers coordination geometries such as square planar, trigonal pyramidal or octahedral. A possible structure, one could expect would be of octahedral geometry, if the ligand could act as *N,N,O*(*S,Se*) donor, comparable to $[Cu(tpy)_2]^+$.[103] The structure of $[Cu(tpy)_2]^{2+}$ and the proposed structure of $[Cu(L)_2]^{2+}$, L being ligand **2**, **3** or **4**, are shown in Figure 4-19. While $[Cu(\mathbf{2})_2][PF_6]_2$, where the heteroaromatic substituents on the bpy ligands contain oxygen atoms, seems to adopt the expected structure (Figure 4-20), $[Cu(\mathbf{3})_2][PF_6]_2$ and $[Cu(\mathbf{4})_2][PF_6]_2$ on the other hand (substituents bear S or Se heteroatoms, respectively), do not exhibit the proposed conformation but the coordination sphere around the copper(II) metal is distorted tetrahedral and the hetero atoms of the substituents point away from the metal centre (Figure 4-22 and Figure 4-23).

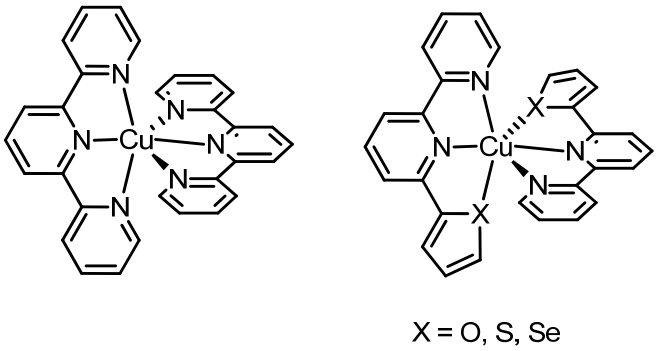


**Figure 4-19** Molecular structure of $[Cu(tpy)_2]^{2+}$ (left) and proposed structure of $[Cu(L)_2]^{2+}$ (L = **2**, **3** or **4**) (right).

This situation can be explained by the HSAB theory (Hard and Soft Acids Bases) in that manner that copper(II) is harder than copper(I) with its higher charge and smaller radius and therefore oxygen is the better counterpart than sulphur or selenenium. Unfortunately, $[Cu(\mathbf{2})_2][PF_6]_2$ crystallizes with dichloromethane and the two other compounds with acetonitrile so that they cannot be compared without doubts. Nevertheless, the molecular structure of $[Cu(\mathbf{2})_2]^{2+}$ (Figure 4-20) clearly shows a distorted tetrahedral coordination geometry of the four nitrogen atoms around the metal centre, the angle between the two bpy planes being 54.4°. Each bpy ligand is planar with the furanyl substituent being twisted from this plane at an angle of 33.76° and the oxygen atom pointing towards the copper.

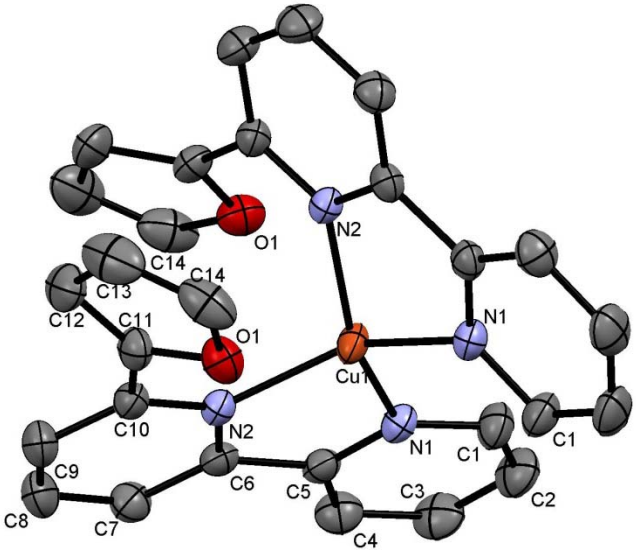


**Figure 4-20** Structure of the $[Cu(\mathbf{2})_2]^{2+}$ cation in $[Cu(\mathbf{2})_2][PF_6]_2$ with H atoms omitted (ellipsoids plotted at 50 % probability level). Selected bond parameters: Cu1-N1-1.955(3), Cu1-N2 1.976(3), Cu1-O1 2.875(3) Å; N1-Cu1-N1 105.68(16), N1-Cu1-N2 146.59(11), N1-Cu1-N2 82.86(11), N2-Cu1-N2 107.96(15), O1-Cu1-N2 68.12(9), O1-Cu1-N2 70.00(9), O1-Cu1-N1 87.4(1), O1-Cu1-N1 141.1(1), O1-Cu1-O1 105.16(7)°.

The Cu…N distances are with 1.955(3) and 1.976(3) Å as expected and the distances to the oxygen atoms amount to 2.875(3) Å which can be interpreted as a weak interaction. The coordination sphere can be described as strongly distorted square planar with two weak Cu…O interactions in the second coordination sphere as indicated in Figure 4-21. The

supposed octahedral geometry does not seem to be stable for ligand **2**, which is consistent with the oxygen atom in the furanyl substituent being only a weak donor.

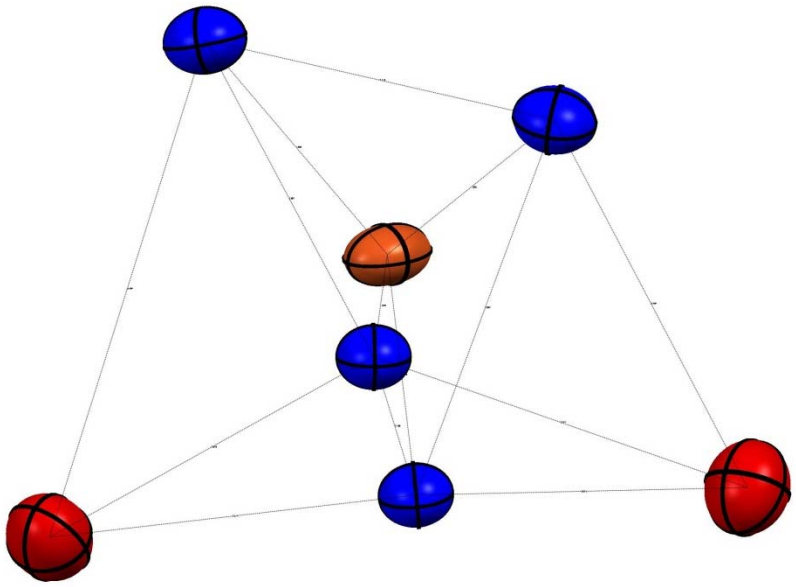

**Figure 4-21** Distorted square planar coordination environment capped with two oxygen atoms of [Cu(**2**)$_2$][PF$_6$]$_2$.

To some degree there is intermolecular π-stacking involved. It is the same nature as described before ([Cu(**2**)$_2$][PF$_6$]) and even though the furanyl plane of one bpy ligand and the pyridine ring of the second ligand subtend an angle of 25.0°, the furanyl centroid and pyridyl plane separation being 3.31 Å. This is far more effective than in the copper(I) species (3.67 Å). On the other hand, no intermolecular π-interaction can be observed and the packing is dominated by cation-anion interactions (F…H distances 2.46-2.63 Å), as well as by solvent-cation interactions, the Cl…H separations being 2.89 Å.

The two structures containing the heavier chalcogen atoms can be compared directly with each other and they are indeed very similar and differ from [Cu(**2**)$_2$][PF$_6$]$_2$ only by the orientation of the substituents on the bpy ligands. Both, [Cu(**3**)$_2$][PF$_6$]$_2$ and [Cu(**4**)$_2$][PF$_6$]$_2$ exhibit a flattened tetrahedral coordination geometry, the angles between the two bpy planes being 57.37 and 57.78°, respectively. The Cu…N distances are nearly of the same value, 1.955(2)/1.977(2) and 1.9574(19)/1.9696(19)Å, respectively. As mentioned before, the heteroatoms of the substituent rings are oriented away from the metal centre and they point towards each other, the S…S separation being 3.526(7) Å and Se…Se 3.750(1) Å, both values are slightly smaller than the sum of two van der Waals radii (3.6 and 3.8 Å).[102] Both cations show similar intermolecular π-interactions as [Cu(**2**)$_2$][PF$_6$]$_2$. The substituents are twisted from the bpy planes (41.25 and 42.37°), these values are higher than these for the furanyl derivative but compared to each other nearly the same, which would support the interaction between the two chalcogen atoms. The intermolecular π-stacking is less pronounced than for [Cu(**2**)$_2$][PF$_6$]$_2$. Even though, the angle between the substituents and

the central pyridine ring of the second bpy are smaller (21.4 and 23.8°), separations between the substituent centroid and the pyridyl plane are longer (3.49 and 3.55 Å). The packing is dictated by cation-anion interactions, too, with F…H distances in the range or 2.5-2.7 Å for both compounds. Additionally, there are some hydrogen bonds between the solvent molecules (acetonitrile) with N…H separations of 2.45 and 2.47 Å, respectively. $[Cu(\mathbf{3})_2][PF_6]_2$ shows no inter cation $\pi$-stacking but for $[Cu(\mathbf{4})_2][PF_6]_2$ short distances between the selenoyl substituents of two distinct molecules can be observed (3.59 Å).

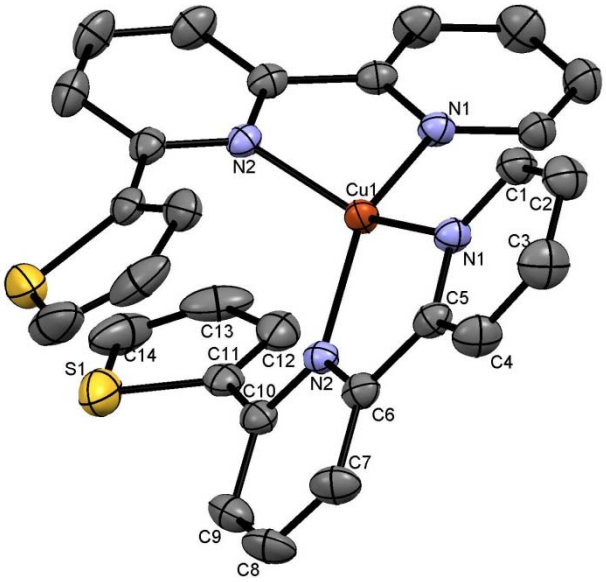


**Figure 4-22** Structure of the $[Cu(\mathbf{3})_2]^{2+}$ cation in $[Cu(\mathbf{3})_2][PF_6]_2$ with H atoms omitted (ellipsoids plotted at 50 % probability level). Selected bond parameters: Cu1-N1 1.955(2), Cu1-N2 1.977(2), Cu1-N2 1.977(2), S1-S1 3.536(7) Å; N1-Cu1-N1 105.15(12), N1-Cu1-N2 145.71(8), N1-Cu1-N2 82.64(8), N2-Cu1-N2 109.87(12)°.

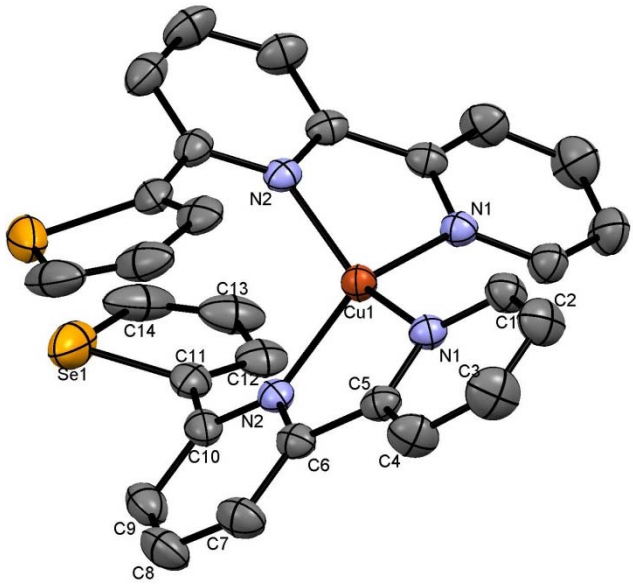


**Figure 4-23** Structure of the $[Cu(\mathbf{4})_2]^{2+}$ cation in $[Cu(\mathbf{4})_2][PF_6]_2$ with H atoms omitted (ellipsoids plotted at 30 % probability level). Selected bond parameters: Cu1-N1 1.9574(19), Cu1-N2 1.9696(19), Se1-Se1 3.750(1) Å; N1-Cu1-N1 105.14(11), N1-Cu1-N2 145.01(7), N1-Cu1-N2 82.80(8), N2-Cu1-N2 110.39(11)°.

The reactions of $Cu(NO_3)_2$ yielded small amounts of a side product or intermediate, the heteroleptic complexes $[Cu(L)_2NO_3][PF_6]$ (L = **3** and **4**), respectively, as green crystals. These crystals grew directly out of the reaction mixture on the top of the walls of the vial when the solvent was left to evaporate slowly. $[Cu(\mathbf{3})_2NO_3][PF_6]$ afforded a poor data set but they were good enough to determine a preliminary structure (R = 0.100) which is shown in Figure 4-24. The derivative $[Cu(\mathbf{4})_2NO_3][PF_6]$ (Figure 4-25) which contains the heavier Se atoms, yielded green crystals of better quality and a good data set. Both compounds crystallize in the monoclinic space group *P*-1 and show similar molecular structures which differ only in the heteroatom in the substituents on the bpy ligands. On going from S to Se the bond lengths at the coordination sphere increase as expected but the angles experience only small changes. The two bpy moieties and one nitro group are oriented so that the coordination sphere can be described as a distorted octahedron with the four nitrogen atoms being in the equatorial positions, one oxygen atom of the nitro group occupying one and the sulphur atom S1 the second apical position. The N…Cu bonds are in the range of 1.96 to 2.15 Å, the O…Cu separation is 2.190(4) Å and the distance between S1 and Cu is 3.529(2) Å. The sulphur atom (S2) of the second thienyl ring is oriented away from the metal centre and the ring engages rather in π-stacking with the N1 containing pyridyl ring, the thienyl centroid N1 distance being 3.33 Å. The packing is dominated by cation-anion interactions only with F…H distances in the range of 2.38-2.55 Å. The bond distances and angles of the coordination sphere are given in the caption of Figure 4-24.

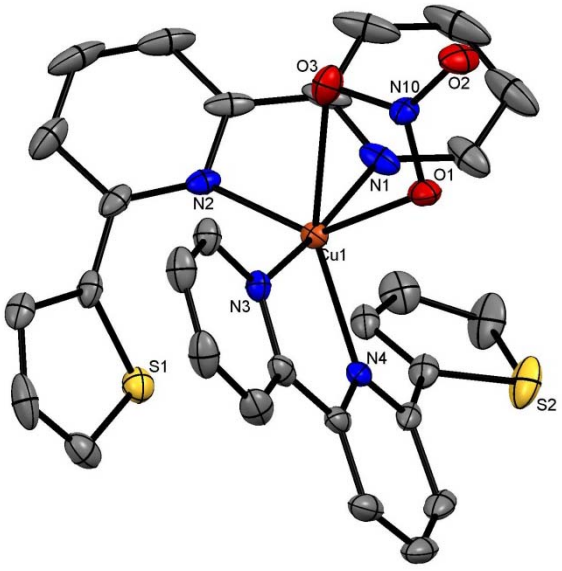


**Figure 4-24** Structure of the $[Cu(\mathbf{3})_2NO_3]^+$ cation in $[Cu(\mathbf{3})_2NO_3][PF_6]$ with H atoms omitted (ellipsoids plotted at 25 % probability level). Selected bond parameters: Cu1-N3 1.956(3), Cu1-N1 1.971(4), Cu1-N2 2.063(4), Cu1-N4 2.154(4), Cu1-O1 2.190(4), Cu1-S1 3.529(2) Å; N3-Cu1-N1 165.69(17), N3-Cu1-N2 101.07(16), N1-Cu1-N2 81.99(18), N3-Cu1-N4 79.96(16), N1-Cu1-N4 109.99(18), N2-Cu1-N4 124.60(14), N3-Cu1-O1 85.65(14), N1-Cu1-O1 83.24(16), N2-Cu1-O1 140.05(14), N4-Cu1-O1 95.33(14)°.

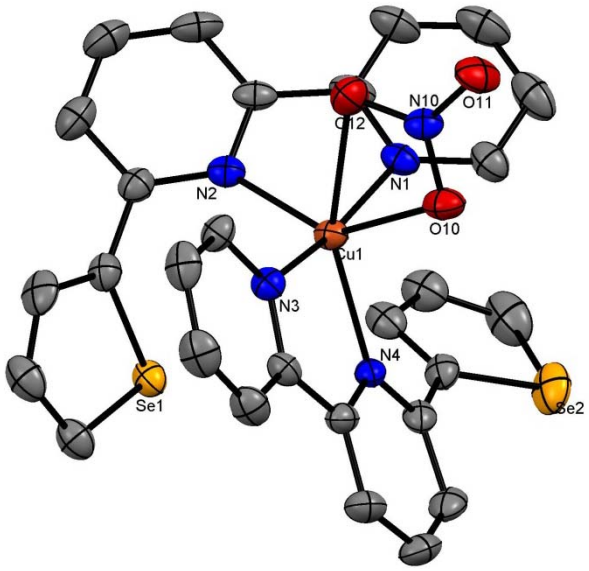


**Figure 4-25** Structure of the $[Cu(\mathbf{4})_2NO_3]^+$ cation in $[Cu(\mathbf{4})_2NO_3][PF_6]$ with H atoms omitted (ellipsoids plotted at 50 % probability level). Selected bond parameters: Cu1-N3 1.963(2), Cu1-N1 1.971(2), Cu1-N2 2.089(2), Cu1-N4 2.146(2), Cu1-O10 2.258(3), Cu1-Se1 3.643(2) Å; N3-Cu1-N1 165.14(11), N3-Cu1-N2 101.23(10), N1-Cu1-N2 80.10(10), N3-Cu1-N4 80.19(10), N1-Cu1-N4 111.05(11), N2-Cu1-N4 126.95(9), N3-Cu1-O10 85.86(10), N1-Cu1-O10 84.07(10), N2-Cu1-O10 140.84(9), N4-Cu1-O10-92.15(9)°.

Figure 4-25 shows the molecular structure of the cation $[Cu(\mathbf{4})_2NO_3]^+$ which is, as already mentioned, nearly identical with that of $[Cu(\mathbf{3})_2NO_3]^+$. The Cu…N bonds are slightly longer (1.96-2.26 Å) as are the Cu…O (2.258(3) Å) and the Cu…Se (3.643(2) Å) bonds. The $\pi$-interaction between the Se2 containing selenoyl ring and the N2 containing pyridyl ring results in a distance of 3.407 Å (selenyl centroid…N2 distance). Here too, the packing is dominated by anion-cation interactions with F…H separation being in the range of 2.36-2.56 Å.

In the series of silver(I) complexes single crystals could be obtained for all compounds except the furanyl derivative. The following three figures show the three monomeric compounds. In Figure 4-26 is depicted the molecular structure of $[Ag(\mathbf{3})_2][PF_6]$ and selected bond distances and angles are listed in the caption. There is some resemblance to the corresponding copper(I) complex ($[Cu(\mathbf{3})_2][PF_6]$). The compound crystallizes in the triclinic space group *P*-1 without any solvent molecule. The coordination sphere can be described as a strongly distorted tetrahedron. The bond lengths between Cu and N atoms are in the range of 2.24 to 2.52 Å and they are significantly longer than in $[Cu(\mathbf{3})_2][PF_6]$ as expected. The bpy domains are not planar with the angles between the least squares planes of the two pyridine rings of 26.1 and 29.4°. Smaller angles can be observed between the thienyl- and the central pyridine-rings (13.2/16.5°). The sulfur atoms are oriented towards the metal centre with the distances between them and Ag being 3.295(4)/3.405(5) Å. These values are very similar to those observed in $[Cu(\mathbf{3})_2][PF_6]$ (3.281(7)/3.453(8) Å) since the $Ag^+$ cation has a bigger radius and is softer than copper and in addition to this there is no disorder of the thienyl rings as is

observed for $[Cu(\mathbf{3})_2]^+$, it can be speculated that the S…Ag interaction is more pronounced in this case.

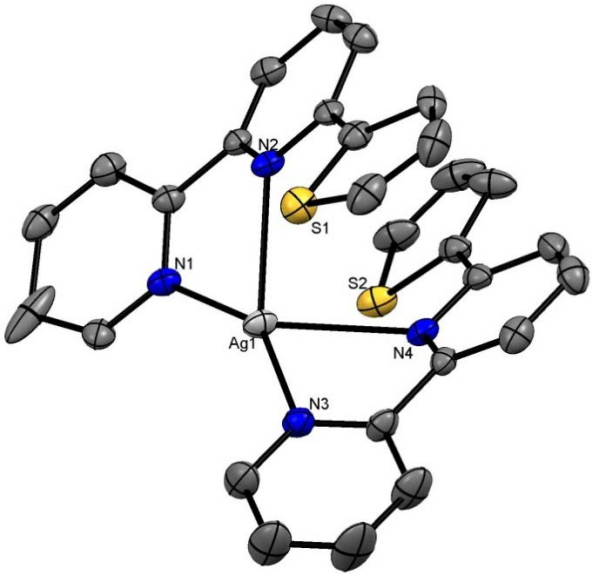


**Figure 4-26** Structure of the $[Ag(\mathbf{3})_2]^+$ cation in $[Ag(\mathbf{3})_2][PF_6]$ with H atoms omitted (ellipsoids plotted at 30 % probability level). Selected bond parameters: Ag1-N3 2.241(3), Ag1-N1 2.285(3), Ag1-N2 2.438(3), Ag1-N4 2.522(3), Ag1-S1 3.405 (8), Ag1-S2 3.281(7) Å; N3-Ag1-N1 153.88(10), N3-Ag1-N2 122.14(10), N1-Ag1-N2 71.83(11), N3-Ag1-N4 70.83(10), N1-Ag1-N4 105.81(11), N2-Ag1-N4 155.36(9)°.

The interligand π-stacking is of the same magnitude as in $[Cu(\mathbf{3})_2][PF_6]$. Here, both thienyl substituents lie above the central pyridine ring of the other ligand, the thienyl centroid to central pyridine ring distances being 3.57/3.62 Å (3.55 Å in $[Cu(\mathbf{3})_2][PF_6]$). The packing is dictated by weak inter cation π-interactions and anion-cation attraction, the F…H distances are in the range of 2.4 to 2.6 Å.

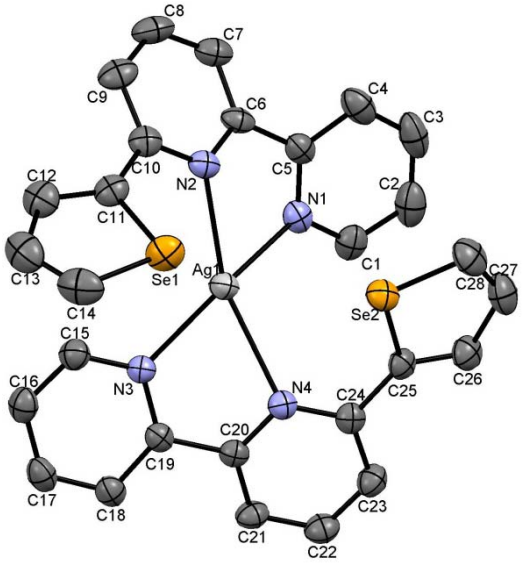


**Figure 4-27** Structure of the $[Ag(\mathbf{4})_2]^+$ cation in $[Ag(\mathbf{4})_2][PF_6]$ with H atoms omitted (ellipsoids plotted at 50 % probability level). Selected bond parameters: Ag1-N3 2.241(4), Ag1-N1 2.284(4), Ag1-N2 2.430(4), Ag1-N4 2.521(4), Ag1-Se1 3.453(1), Ag1-Se2 3.355(1), Se1-Se2 4.551(1) Å; N3-Ag1-N1 153.74(13), N3-Ag1-N2 122.24(13), N1-Ag1-N2 72.06(13), N3-Ag1-N4 70.72(12), N1-Ag1-N4 105.68(13), N2-Ag1-N4 155.23(11)°.

Figure 4-27 shows the molecular structure $[Ag(\mathbf{4})_2][PF_6]$. The compound crystallizes in the triclinic space group *P*-1. The coordination sphere is very much similar to that of $[Ag(\mathbf{3})_2][PF_6]$ with only slightly longer Cu…N bonds and the angles vary only in a few degrees. The interligand π-stacking is here not really noteworthy, the least square plane angles between the selenophenyl rings and the central pyridine rings of the opposite ligands being to big (23.2/34.0°). An interesting feature of this cation is that both selenophenyl substituents point towards each other with the Se…Se separation being 4.551(1) Å. This distance is 20 % longer than the sum of two van der Waals radii of selen (2r(Se) = 3.8 Å).[102] The distances of the Se atoms to Ag are with 3.453(1) and 3.355(1) Å, only 0.05 Å longer than the Ag…S distances in $[Ag(\mathbf{3})_2][PF_6]$. The molecular structure of $[Ag(\mathbf{4})_2]^+$ does not change upon replacement of the anion. Figure 4-28 shows the cation in the compound $[Ag(\mathbf{3})_2][BF_4]$. The structure is very much the same and the changes in bond lengths and angles are negligible. The intermolecular interactions are dominated by F…H distances between the cations and anions and are for both compounds in the range of 2.4 to 2.6 Å.

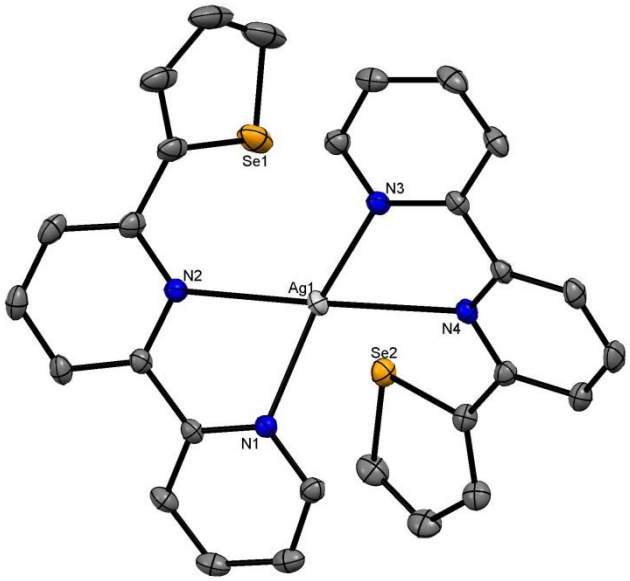


**Figure 4-28** Structure of the $[Ag(\mathbf{4})_2]^+$ cation in $[Ag(\mathbf{4})_2][BF_4]$ with H atoms omitted (ellipsoids plotted at 35 % probability level). Selected bond parameters: Ag1-N3 2.2403(19), Ag1-N1 2.2748(18), Ag1-N2 2.4850(19), Ag1-N4 2.5407(19), Ag1-Se1 3.3384(6), Ag1-Se2 3.4720(6), Se1-Se2 4.6484(7); N3-Ag1-N1 155.79(7), N3-Ag1-N2 119.48(7), N1-Ag1-N2 71.49(6), N3-Ag1-N4 69.84(7), N1-Ag1-N4 108.55(6), N2-Ag1-N4 157.88(6)°.

In the attempt to react $AgPF_6$ and ligand **3** in the ratio 1:1 single crystals could be obtained. Surprisingly, the observed structure suggests a metal to ligand ratio of 3:1. A weighting error cannot be completely excluded due to the fact that $AgPF_6$ is quite hygroscopic, which could explain the stoichiometric deficiency of the metal. Figure 4-29 shows the asymmetric part of the polymeric chain in $([Ag_3(\mathbf{3})_4][PF_6]_3)_n$ and the caption lists all important bond parameters. This compound crystallizes in the monoclinic space group *C*2/*c*. This compound finally demonstrates the ability of ligand **3** to act as an *N,N,S*-donor. The three Ag atoms are not

arranged linearly and subtend an angle of 165.19(3)°. The coordination sphere of Ag1 can be described as distorted octahedral. Ag1 is coordinated by one **3** with N1 and N2 being in the equatorial positions and S1 in the apical position. The two remaining equatorial positions are occupied by S2 and N4 from a second ligand **3**. The remaining pyridine ring from this ligand is twisted with the least square plane angle between the two pyridine rings being 46.6° and N3 coordinates to the next silver atom (Ag2). The second apical position of the Ag1 octahedron is occupied by Ag2 the metal-metal distance being 3.087(1) Å. The coordination geometry for Ag2 can be described as distorted octahedral, Ag1 and S4 being in the apical positions and the nitrogen atoms N3, N5, N6 and S3 in the equatorial. Finally, the coordination site of Ag3 can be described as distorted tetragonal pyramidal, here the atoms S3, S4, N7 and N8 occupy the positions in the square base and S1' the apical positions. The sulfur atoms S1 and S3 act as bridging atoms between Ag1/Ag3 and Ag3/Ag2, respectively. All S…Ag bonds are in the range of 2.54 and 3.14 Å and are consequently the shortest here observed. The distances between Ag3…S1 (2.639(2) Å) and Ag3…S3 (2.540(2) Å) are even shorter than the Cu…S distances observed in $[Cu(thmpy)_2][PF_6]$ (see Figure 4-18).

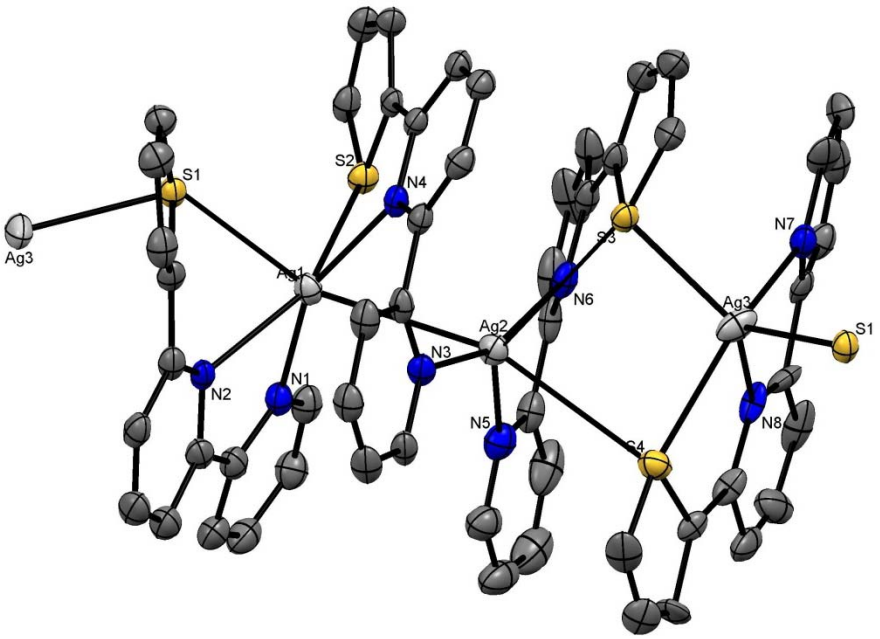


**Figure 4-29** Structure of the $[Ag_3(\mathbf{3})_4]^{3+}$ cation in $([Ag_3(\mathbf{3})_4][PF_6]_3)_n$ with H atoms omitted (ellipsoids plotted at 20 % probability level). Selected bond parameters: Ag1-N1 2.238(7). Ag1-N4 2.239(7), Ag1-N2 2.407(6), Ag1-S2 2.784(2), Ag1-Ag2 3.0868(10), Ag2-N3 2.231(6), Ag2-N5 2.270(8), Ag2-N6 2.407(6), Ag3-N8 2.456(10), Ag3-N7 2.522(13), Ag3-S3 2.5401(19), Ag3-S4 2.632(4), Ag3-S1 2.639(2), Ag3-S4' 2.717(7) Å; N1-Ag1-N4 153.3(2), N1-Ag1-N2 71.4(2), N4-Ag1-N2 125.2(2), N1-Ag1-S2 97.87(17), N4-Ag1-S2 75.08(15), N2-Ag1-S2 152.93(15), N3-Ag2-N5 125.4(3), N3-Ag2-N6 160.9(2), N5-Ag2-N6 72.5(3), N8-Ag3-N7 65.6(4), N8-Ag3-S3 127.8(2), N7-Ag3-S3 96.2(3), N8-Ag3-S4 79.9(3), N7-Ag3-S4 144.8(4), S3-Ag3-S4 99.90(10), N8-Ag3-S1 120.7(2), N7-Ag3-S1 110.3(3), S3-Ag3-S1 111.41(7), S4-Ag3-S1 92.70(10)°.

The packing is dominated by F…H distances and no inter cationic π-stacking can be observed. In Figure 4-30 is depicted the prolongation of the polymeric chain in $([Ag_3(\mathbf{3})_4][PF_6]_3)_n$.

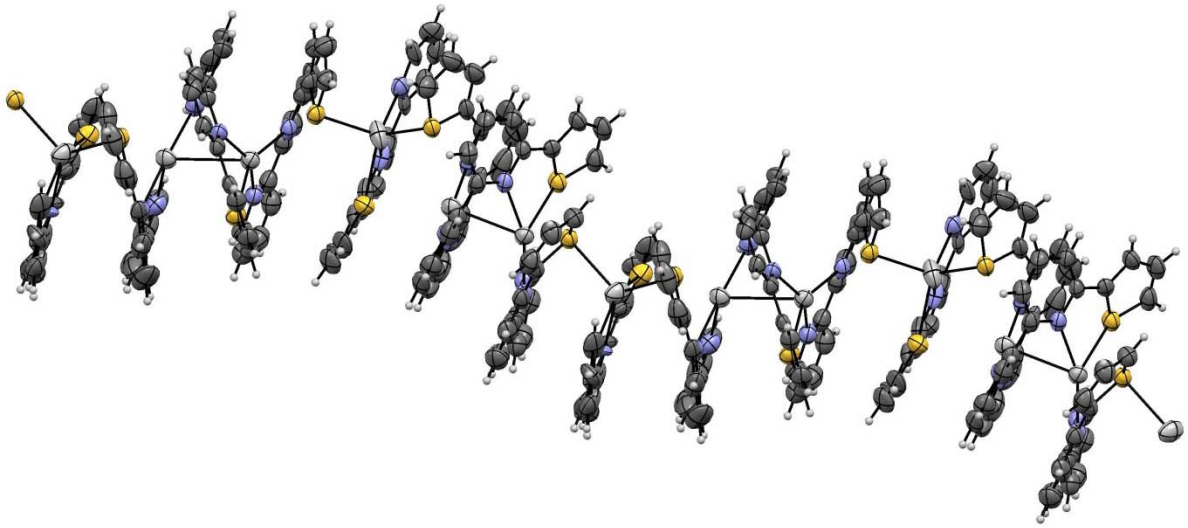

**Figure 4-30** Prolongation of the asymmetric unit of $[Ag_3(\mathbf{3})_4]^{3+}$

It is known that in thiophene, the sulfur atom is not a very good donor and coordination compounds where the thiophene is involved in short metal sulfur distances are rare. Upon a literature search only three exotic Ag(I) complexes were found, where the interactions seem to be of the same order.[104] One example is shown in Figure 4-31 where the short Ag…Ag distances (2.957(1) and 3.8519(9) Å) can be observed as well as short Ag…S separations (2.860(1) and 3.005(2) Å).

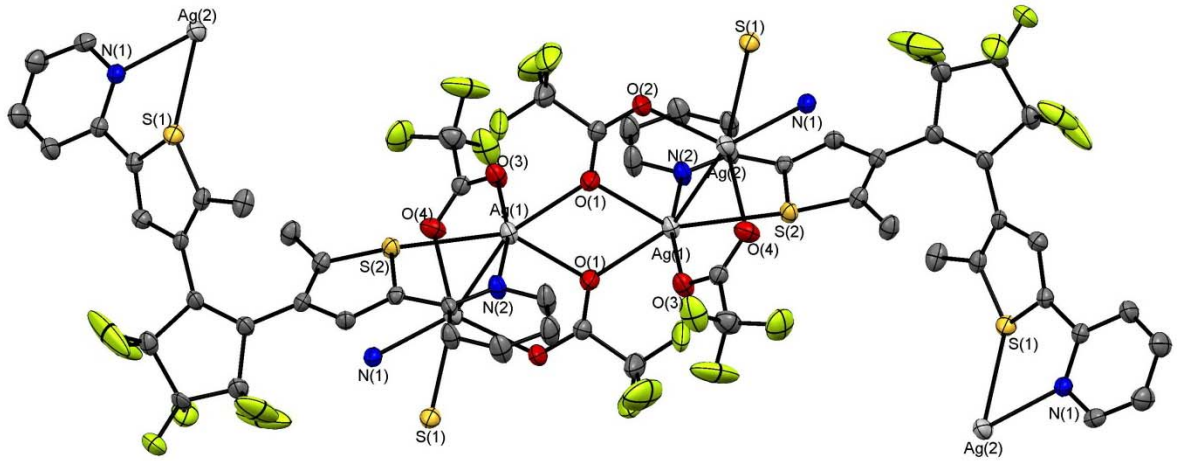


**Figure 4-31** Part of the structure of $[Ag_2(BM\text{-}2\text{-}PTP)(CF_3CO_2)]_n$. Selected bond parameter: Ag1-O1 2.433(3), Ag1-O1 2.494(4), Ag1-O3 2.234(3), Ag1-N2 2.248(4), Ag2-O2 2.242(3), Ag2-O4 2.345(3), Ag2-N1 2.297(4), Ag1-S2 2.860(1), Ag2-S1 3.005(2), Ag1-Ag2 2.957(1), Ag1-Ag1‘ (3.8519(9) Å; O1-Ag1-O1‘ 77.1(1), O1-Ag1-O3 93.9(1), O1-Ag1-N2 99.5(1), O1-Ag1-O3 95.9(1), O1-Ag1-N2 93.7(1), O3-Ag1-N2 164.9(1), O2-Ag2-O4 127.3(1), O2-Ag2-N1 126.3(1), O4-Ag2-N1 93.5(1), S2-Ag1-Ag2 64.07(2), S2-Ag1-O3 92.99(9), S2-Ag1-O1 140.25(7), S2-Ag1-N2 72.3(1), S1-Ag2-O4 156.51(8), S1-Ag2-N1 70.80(9), S1-Ag2-O2 76.0(1), S1-Ag2-Ag1 106.61(2)°. (BM-2-PTP = 1,2-bis(2’-methyl-5’-(2’’-pyridyl)-3’-thienyl)-perfluorocyclopentene)[104].

In conclusion, the above described solid state structures confirm the expected conformations for the copper(I) complexes. It could be shown that upon oxidation to $Cu^{2+}$ the structure does not change dramatically and it can be speculated that it is mainly dictated

by inter ligand interactions. Furthermore, for copper(II) complexes the substituents in 6'-position on the bpy ligand prevent the preferable square planar coordination of the two bpy moieties. If the substituent is a five membered heteroaromatic ring and the ligand may be regarded as a tridentate ligand, possible coordination could be observed for the furanyl derivative only.

There was some interest to see whether metal sulfur interactions are possible when the S atom is embedded in a thiophene ring. There are no examples in the literature, to the best of our knowledge. In this work it was possible to show some short distances which are only ~20 % longer than Cu…S bonds (2.3-2.4 Å) of thioethers.[105] For the softer $Ag^+$ it was possible to achieve short Ag…S bonds by lowering the metal to ligand ratio (3:4) which was not feasible for copper(I).

### 4.1.2.2 Electronic absorption spectroscopy

The electronic absorption spectra of dichloromethane solutions of $[CuL_2][PF_6]$ with L = **1**-**6** (Figure 4-32) exhibit high energy absorption bands arising from ligand-based $\pi^* \leftarrow \pi$ transitions. For each complex, two broad absorptions with values of $\varepsilon_{max}$ ranging from 1700 to 3800 $dm^3\ mol^{-1}\ cm^{-1}$ are observed around 400–435 nm and 513–550 nm and are assigned to MLCT transitions.

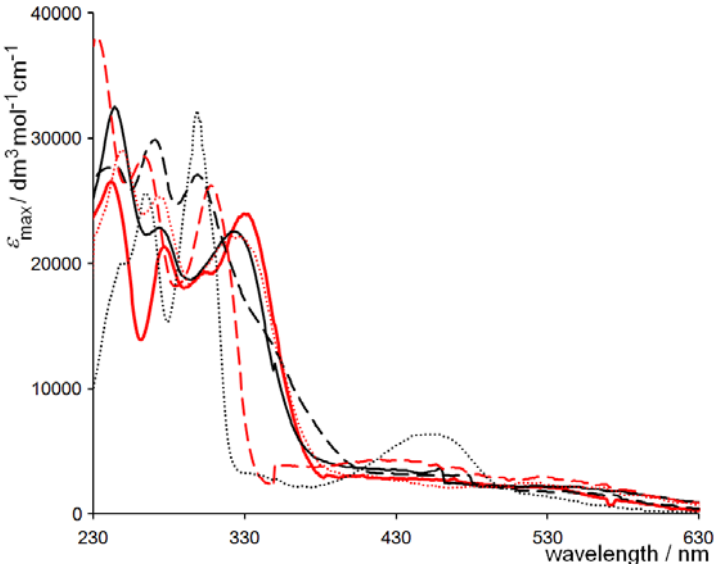


**Figure 4-32** Electronic absorption spectra of $CH_2Cl_2$ solutions of $[CuL_2][PF_6]$ for L = **1**-**6**. Key: Hashed black line, L = **1**; solid red line, L = **2**; solid black line, L = **3**; dotted red line, L = **4**; hashed red line, L = **5**; dotted black line L = **6**. See experimental section for solution concentrations.

Difficulties with the NMR spectra of copper(I) complexes led to investigations of the solvent influence on these compounds. Figure 4-33 shows the UV/vis spectra of $[Cu(\mathbf{3})_2][PF_6]$ in various solvents.

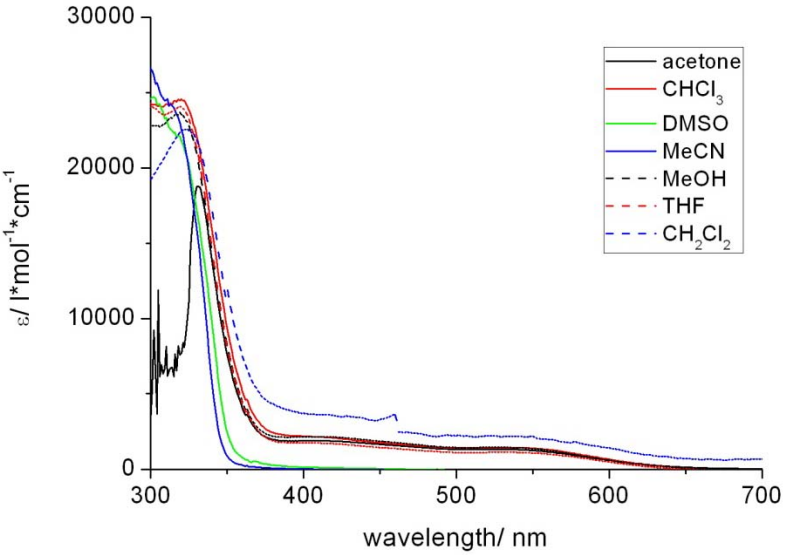


**Figure 4-33** Electronic absorption spectra of various solutions of $[Cu(3)_2][PF_6]$: Black solid line, acetone; red solid line, $CHCl_3$; green solid line, DMSO; blue solid line, MeCN; black hashed line, MeOH; red hashed line, THF; blue hashed line, $CH_2Cl_2$.

It becomes apparent that most solvents do not have any influence on the absorption spectrum. In acetone, chloroform, dichloromethane, methanol and tetrahydrofuran the LC transition (~330 nm) as well as the MLCT bands (410/550 nm) can be observed. There is no obvious shift to be seen and in dichloromethane, the absorption coefficients ($\varepsilon_{max}$) for the MLCT transitions are twice as high as for all other solvents. This cannot be a concentration error, since $\varepsilon_{max}$ is lower for the LC transitions in dichloromethane. On the other hand, strongly donating solvents as acetonitrile and dimethylsulfoxide are able to undergo a ligand exchange (see Scheme 4-4). At the low concentrations of the complex ($c = 10^{-5}$mol/L), the excess of solvent becomes so high that the equilibrium is shifted to the solvate complex ($[Cu(S)_4][PF_6]$) and free ligand.

$$[Cu(L)_2][PF_6] + \text{solvent (S)} \rightleftharpoons [Cu(S)_4][PF_6] + L$$

S = MeCN, DMSO

**Scheme 4-4** Ligand exchange reaction in acetonitrile or DMSO

This can be observed by quick decolourization of the acetonitrile and DMSO solutions and becomes apparent in the UV/vis spectrum where the MLCT bands are no longer observable. Furthermore, the LC bands exhibit a small hypsochromic shift (~1000 $cm^{-1}$) compared to the other solvents. These observations were later considered to explain the solution behaviour which is responsible for broadening of the NMR spectra (see section 4.1.2.4).

#### 4.1.2.3 Electrochemistry and Spectroelectrochemistry

For a better understanding of their unexpected behaviour, extensive electrochemical experiments have been conducted for copper(I) complexes with heteroaromatic substituents

on the bpy moieties. Figure 4-34 shows as an example the cyclic voltammogram of $[Cu(\mathbf{3})_2][PF_6]$ in acetonitrile ($10^{-4}$ mol $L^{-1}$) with $TBAPF_6$ (1 mM) as supporting electrolyte.

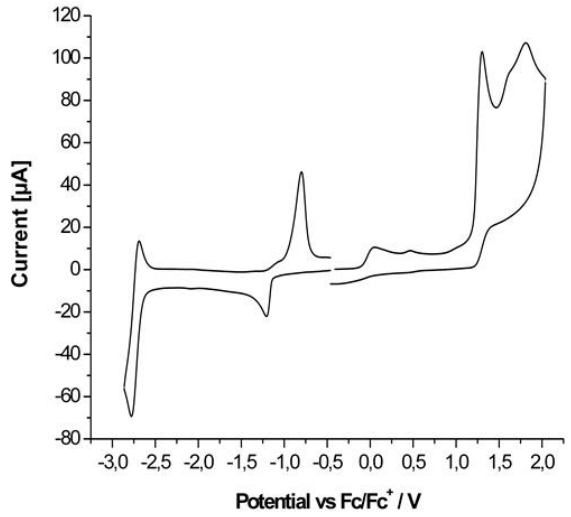


**Figure 4-34** CV of $[Cu(\mathbf{3})_2][PF_6]$ in MeCN ($10^{-4}$ mol $L^{-1}$) with $TBAPF_6$ (1 mM).

The first oxidation process can be assigned unambiguously to the oxidation of the metal centre: $Cu^+ \rightarrow Cu^{2+} + e^-$. This process is reversible, which is not obvious in the complete scan but can be clearly seen in Figure 4-35 where lower potentials were applied. The $E_{1/2}$ value of the oxidation is 0.01 V (*vs*. $Fc/Fc^+$) which corresponds to 0.65 V (*vs*. NHE) and is typical for $[Cu(NN)_2]^+$ cations.[106,107] At higher potentials, irreversible multi electron oxidation processes of the ligands occur. The potential values are similar to those observed for the free ligands.

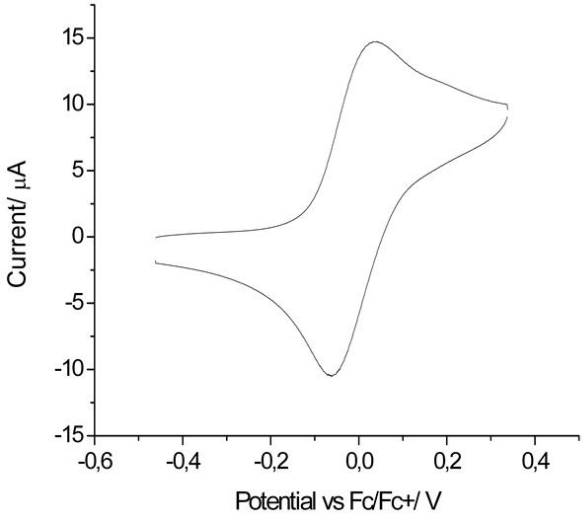


**Figure 4-35** CV of $[Cu(\mathbf{3})_2][PF_6]$ in MeCN ($10^{-4}$ mol $L^{-1}$) with $TBAPF_6$ (1 mM).

When negative potentials were applied, the first reduction was assigned to $Cu^+ + e^- \rightarrow Cu^0$. This process seems to be irreversible, thus we assume that copper(0) metal is plating on the electrode. It is very likely that the big oxidation peak at -0.69 V is caused by the stripping of plated $Cu^0$ from the electrode, since it is similar for all measured complexes (in the

range -0.54 V to -0.69) V).[101] At very low potential (-2.77 V), reduction of the ligand takes place which also seems to involve several electrons and can be described as quasi reversible. The potential in the complex is 290 mV lower than for the free ligand which is somewhat unexpected, as the ligand should become less electron rich upon coordination and therefore the reduction could be easier. When the values of all measured complexes are compared, it becomes apparent that the values of the ligand reductions are very similar with values in the range between -2.73 and -2.77 V (see Table 4-2). This shows clearly that the aromatic substituents do not affect the reduction potentials of the bpy. When considering the crystal structures (see section 4.1.2.1), one can see that the substituents are twisted from the plane of the bpy moiety and it can be assumed that the ligands are not fully conjugated which would explain the similar reduction values for different substituents. The only exceptions are $[Cu(\mathbf{1})_2][PF_6]$ which was measured against a Pt-electrode, so the deviation is within the error margin, and $[Cu(\mathbf{10})_2][PF_6]$ which shows the lowest potential (-2.88 V) but can be explained with the electron donating effect of the *n*-butyl substituent of the bpy.

The cyclic voltametry spectra of complexes with hetero aromatic substituents on the bpy ligands are overlaid in Figure 4-36.

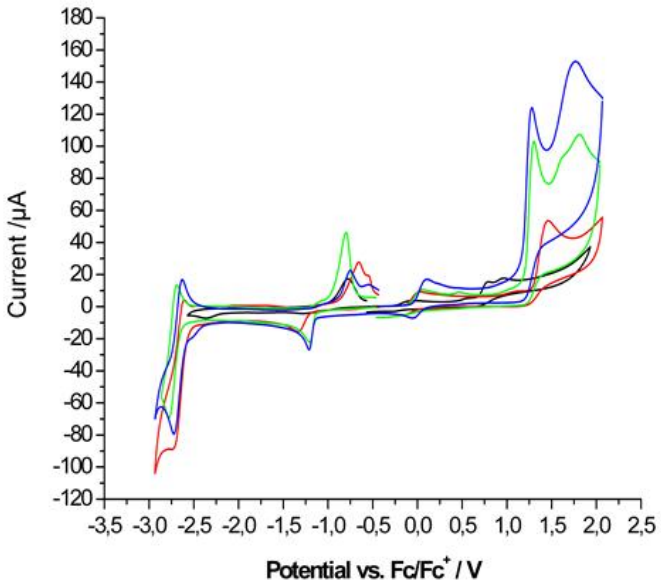


**Figure 4-36** CVs of $[Cu(L)_2][PF_6]$ in MeCN ($10^{-4}$ mol $l^{-1}$) with $TBAPF_6$ (1 mM); L = **1** (black), **2** (red), **3** (green), **4** (blue).

It shows at one glance that the copper oxidations are very similar and therefore do not depend much on the substitution of the ligands. The oxidations of the ligands are the same for thiophene and selenophen derivatives, the pyrrole compound is easier to oxidize and involves only one electron, the furanyl derivative on the other hand requires higher potential for being oxidized then the heavier chalchogen derivatives. The reductions to $Cu^0$ are similar for all compounds, as are the reductions of the ligands.

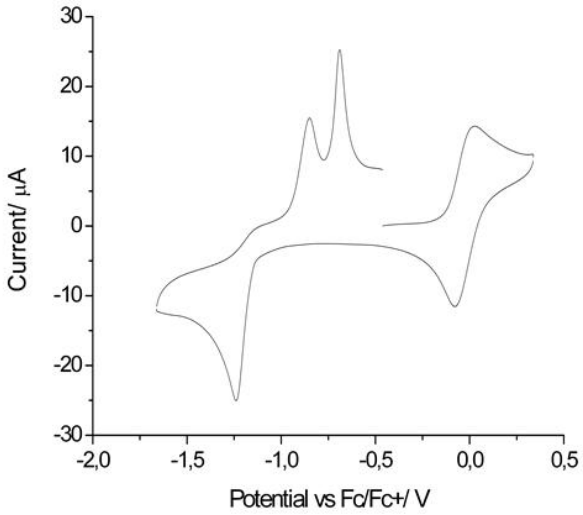


**Figure 4-37** CV of $[Cu(\mathbf{3})_2][PF_6]$ in MeCN ($10^{-4}$ mol $l^{-1}$) with $TBAPF_6$ (1 mM).

There seem to be more processes involved as soon as the metal centre is reduced to $Cu^0$. The spectra are reproducible but sometimes new peaks appear as can be seen in Figure 4-37. Therefore, experiments with several cycles were conducted and two examples are depicted in Figure 4-38. The spectrum is dependent on the sweep range of the cycle.

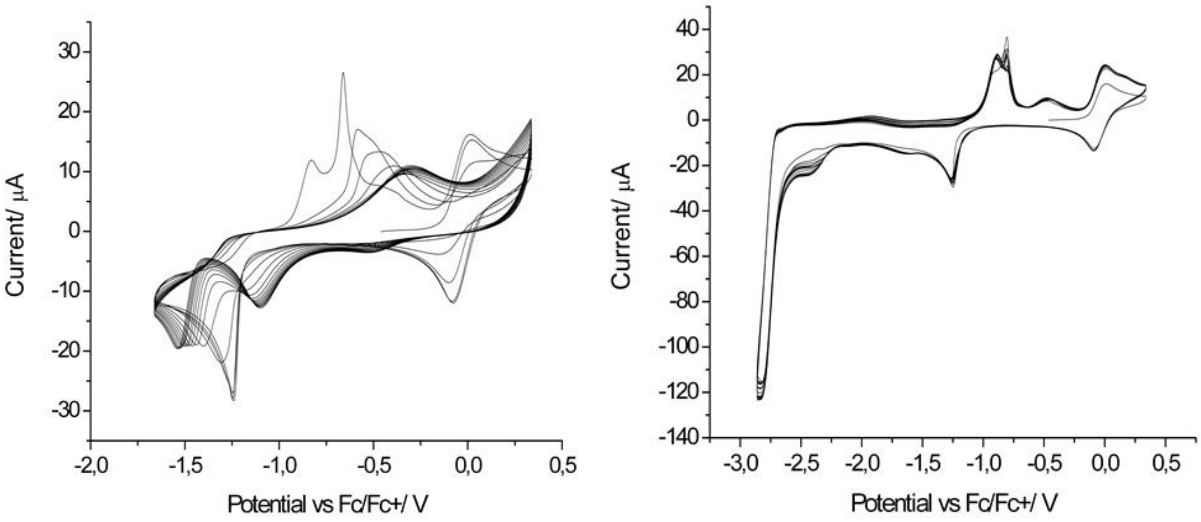


**Figure 4-38** CVs (15 cycles) of $[Cu(\mathbf{3})_2][PF_6]$ in MeCN ($10^{-4}$ mol $l^{-1}$) with $TBAPF_6$ (1 mM).

When the potential is not lower than -1.7 V, the first cycle is the same as observed before but with increasing number of cycles, the shape changes. The redox peak of $Cu^+/Cu^{2+}$ disappears. The first reduction shifts to higher potential and a second peak appears at lower potential. The two initial sharp oxidation peaks disappear and converge to a broad signal which is shifted to higher potential. It is very difficult to deduce what processes cause this behaviour. Thiophene is known to undergo electro induces polymerization reaction.[108] Furthermore, cyclovoltamograms with similar shapes and peaks at similar potentials were

observed and reported in literature for bisthienylpyridine compounds.[109] Therefore, a possible explanation might be that a reductive polymerization of the ligands occurs and the organic material deposits on the electrode. This hypothesis would be consistent with the disappearing of the copper based signals. The newly appearing signals may originate from the polymeric organic deposition. Even though polymerization of free ligands was not observed (see section 3.3.5), it is thinkable that the copper metal promotes the polymerization. Interestingly, when the sweep range is bigger the voltammograms do not change with increasing scans, and the compound seems to be stable. A better explanation might be that the compound suffers from the same transformation than for the shorter scan but the time elapsed between the reduction and the oxidation is longer (~20 s), so that new and fresh compound can diffuse to the electrode and the cyclic voltametry appears the same as for the previous scan. Yet another possibility may be that at lower potential, the polymeric ligands suffer from over reduction and are stripped from the electrode and go in solution, leaving a bare electrode for a next cycle. This would also explain the high current response at -2.7 V (Figure 4-38, right side).

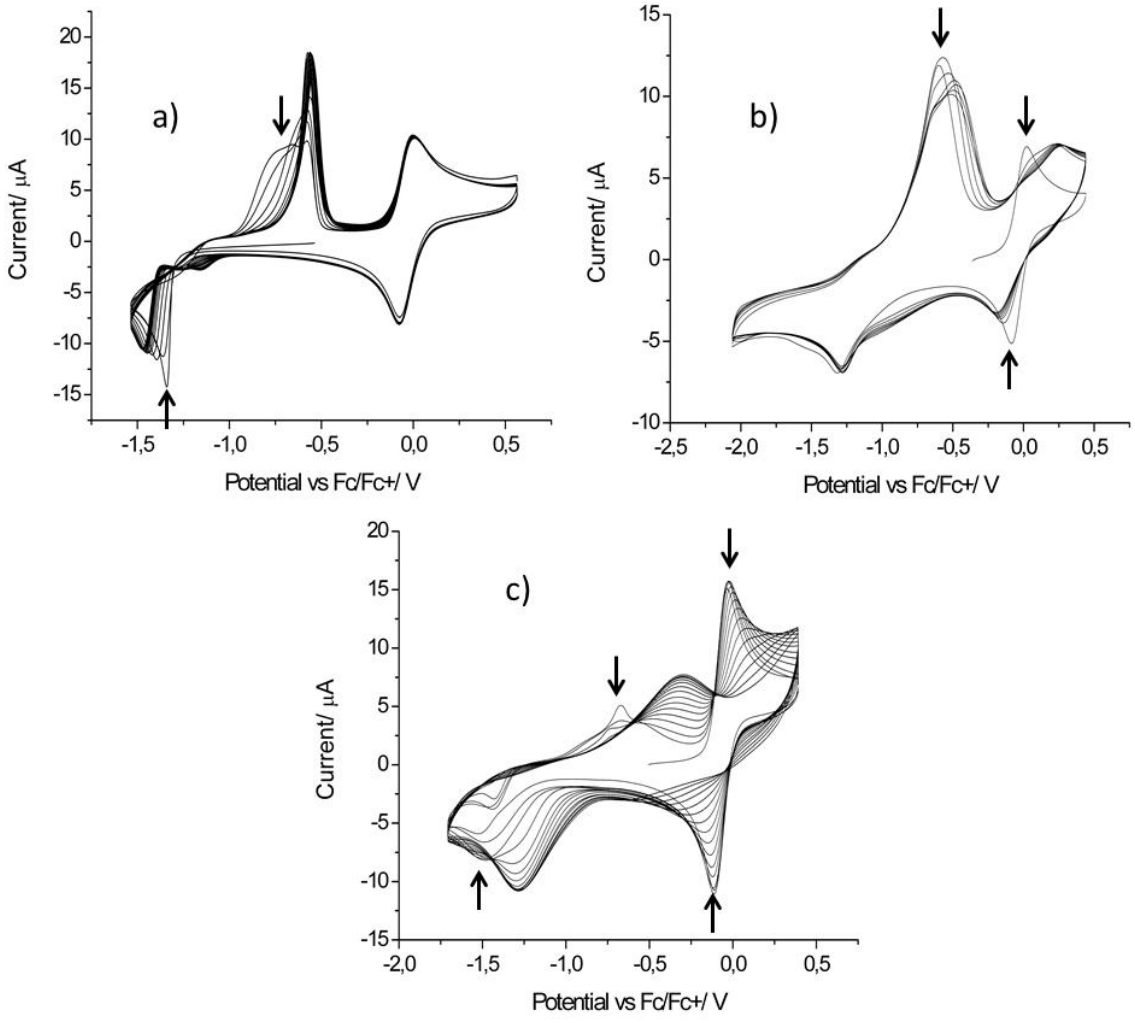


**Figure 4-39** CVs (15 cycles) of $[Cu(L)_2][PF_6]$ in MeCN ($10^{-4}$ mol $l^{-1}$) with $TBAPF_6$ (1 mM); a) L = **5**, b) L = **6**, c) L = **10**; starting positions are marked with arrows.

This dynamic behaviour seems to be dependent on the substitution on the bpy ligand. Figure 4-39 shows cycles of cyclic voltammograms of the three complexes without hetero aromatic substituent. It appears that while [Cu(**5**)$_2$][PF$_6$] seems to be stable even after the copper is being reduced to Cu$^0$. Unlike the thiophenyl derivative, ligand **5** seems to be stable towards reductive polymerization. The two complexes where the bpy ligands are substituted with aliphatic groups (Me, [Cu(**6**)$_2$][PF$_6$] and *n*Bu, [Cu(**10**)$_2$][PF$_6$]), are not.

| Complex | 1st ox. E/2 [mV] | ox [mV] | red [mV] | ΔE [mV] | 1st red$^{irr}$ [mV] | HOMO [eV] | LUMO [eV] | gap [eV] |
|---|---|---|---|---|---|---|---|---|
| [Cu(1)$_2$][PF$_6$] | -138 | -68 | -208 | 140 | -1277 | -4.54 | -3.64 | 0.90 |
| [Cu(2)$_2$][PF$_6$] | -23 | 28 | -73 | 101 | -1361 | -4.67 | -3.59 | 1.08 |
| [Cu(3)$_2$][PF$_6$] | -12 | 38 | -61 | 99 | -1137 | -4.66 | -3.70 | 0.96 |
| [Cu(4)$_2$][PF$_6$] | 49 | 99 | -2 | 101 | -1231 | -4.74 | -3.64 | 1.09 |
| [Cu(5)$_2$][PF$_6$] | 13 | 68 | -42 | 110 | -1331 | -4.67 | -3.57 | 1.10 |
| [Cu(6)$_2$][PF$_6$] | 16 | 63 | -31 | 94 | -1833 | -4.72 | -3.21 | 1.51 |
| [Cu(10)$_2$][PF$_6$] | -57 | -18 | -95 | 77 | -1501 | -4.65 | -3.52 | 1.13 |

**Table 4-2** Electrochemical data for [Cu(L)$_2$][PF$_6$]; L = **1**-**6** and **10**; irr, irreversible process.

Selected electrochemical data of the copper(I) complexes are summarized in Table 4-2.

A confirmation of the metal oxidation peak is accomplished by spectroelectrochemistry. Figure 4-40 shows the change of the electronic absorption spectra upon variation of the applied potential.

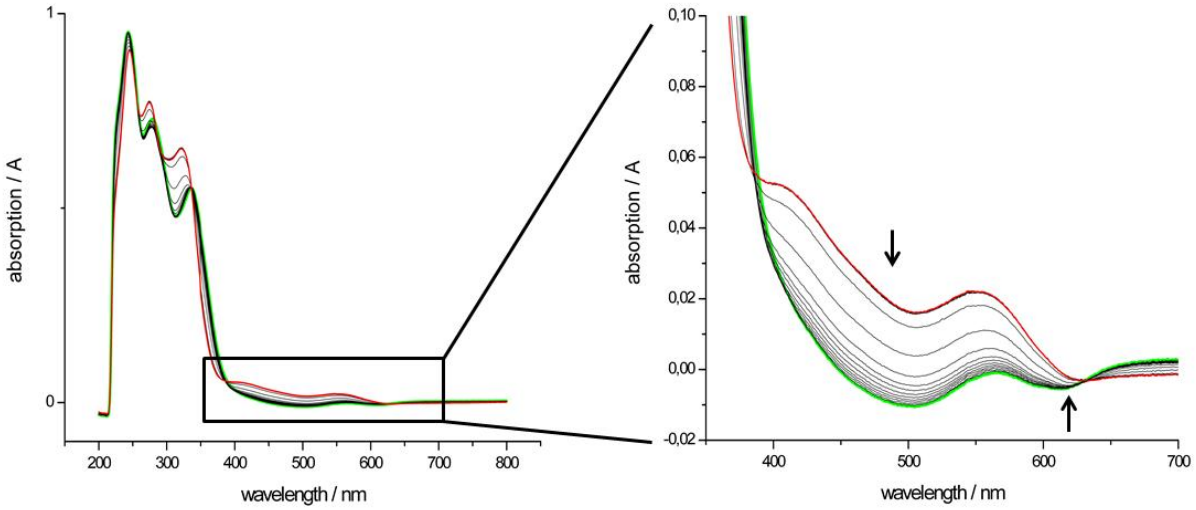


**Figure 4-40** Potential dependant absorption spectra of [Cu(3)$_2$][PF$_6$] in $CH_2Cl_2$ (~$10^{-5}$ mol $L^{-1}$) with $TBAPF_6$ (1 mM); potential 0(red)-1.5(green) V with 0.1 V steps; arrows indicate decrease or increase of bands, respectively.

When no voltage is applied, a spectrum can be observed which shows the typical MLCT bands for [Cu(**3**)$_2$][PF$_6$] (red curve in Figure 4-40). With increasing potential, these bands decrease. Then weak MLCT bands typical for copper(II) complexes start to appear and increase in intensity with increasing voltage (green curve in Figure 4-40). This spectrum cannot be compared to the spectrum of [Cu(**3**)$_2$][PF$_6$]$_2$, which was especially prepared for this purpose due to its insolubility in dichloromethane. Also, these experiments could not be carried out in acetonitrile since the copper(I) complexes are not stable in this donor solvent

at low concentrations (<$10^{-4}$ mol $l^{-1}$). Nevertheless, the observed spectra are comparable to similar complexes published by DE COLA in 2002.[107]

#### 4.1.2.4 NMR Spectroscopy

As mentioned above, the characterization with NMR spectroscopy proved somehow difficult. While $[CuL_2][PF_6]$ complexes with L = **5**, **6**, **10** and 6'-Cl-2,2'-bpy exhibit sharp and well resolved $^1$H NMR spectra (see Figure 4-41), all other complexes exhibit broadening of the signals. Figure 4-42 shows an example for a well resolved spectrum, the $^1$H NMR spectrum of $[Cu(\mathbf{10})_2][PF_6]$ and the assigned signals.

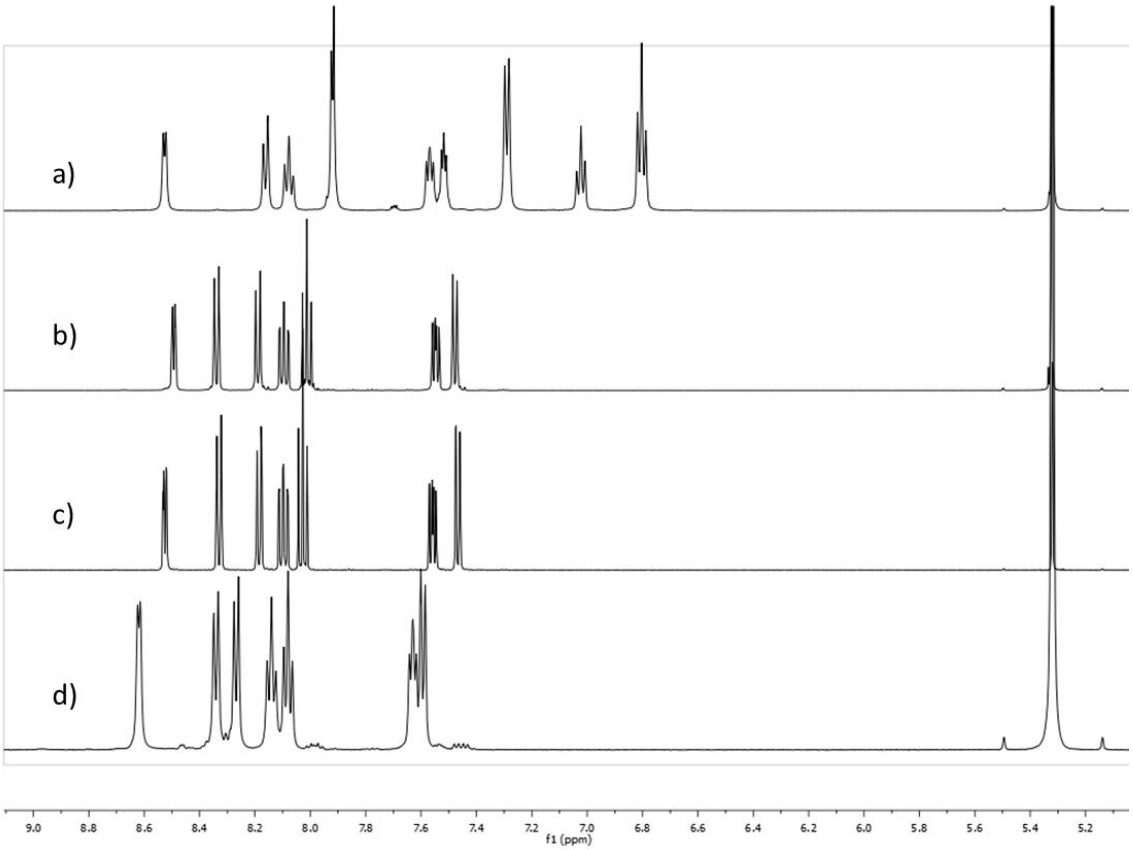


**Figure 4-41** Room temperature 500 $^1$H MHz NMR spectra ($\delta$9.0–5.3 ppm) of $CD_2Cl_2$ solutions of (a) $[Cu(\mathbf{5})_2][PF_6]$, (b) $[Cu(\mathbf{6})_2][PF_6]$, (c) $[Cu(\mathbf{10})_2][PF_6]$ and (d) $[Cu(6'\text{-Cl-bpy})_2][PF_6]$. The signal at $\delta$5.32 ppm arises from $CHDCl_2$ with the $^{13}$C satellites.

At room temperature, signals in the the $CD_2Cl_2$ solution $^1$H NMR spectra of $[Cu(L)_2][PF_6]$, (L = **1**-**4**, **12**, **20**, **21**, **30**, **31**, **34** and **36**), are broadened (Figure 4-43), in particular those of the thienyl derivative (Figure 4-43c).

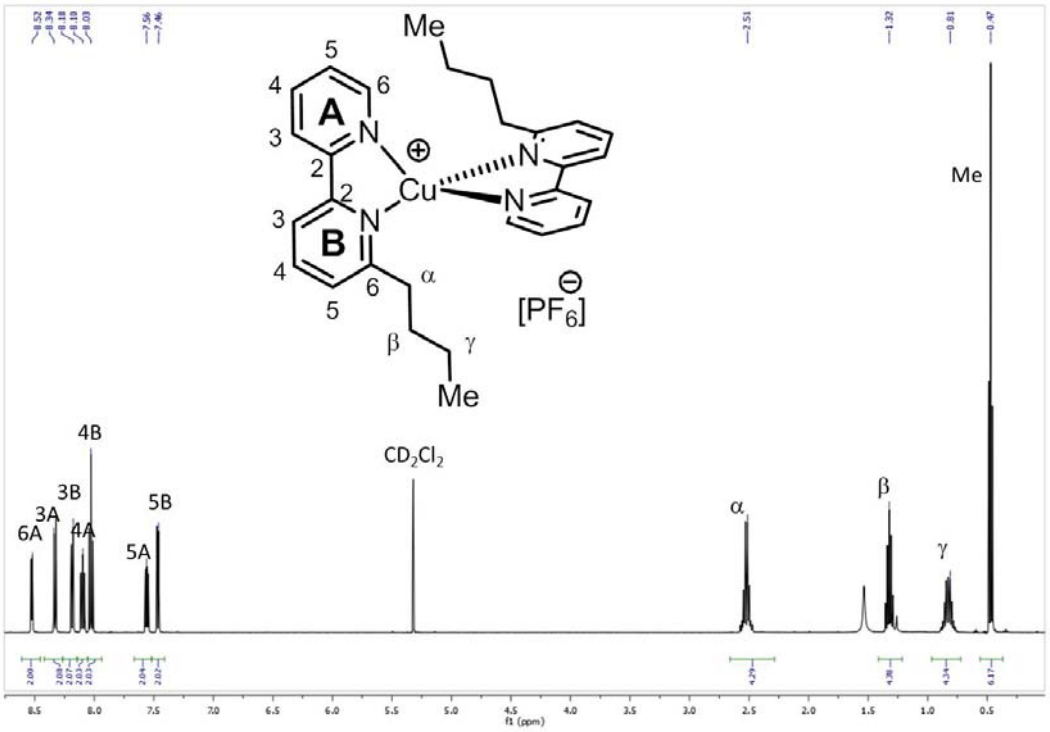


**Figure 4-42** 500 MHz Room temperature $^{1}$H NMR spectrum of [Cu(**10**)$_2$][PF$_6$] in $CD_2Cl_2$.

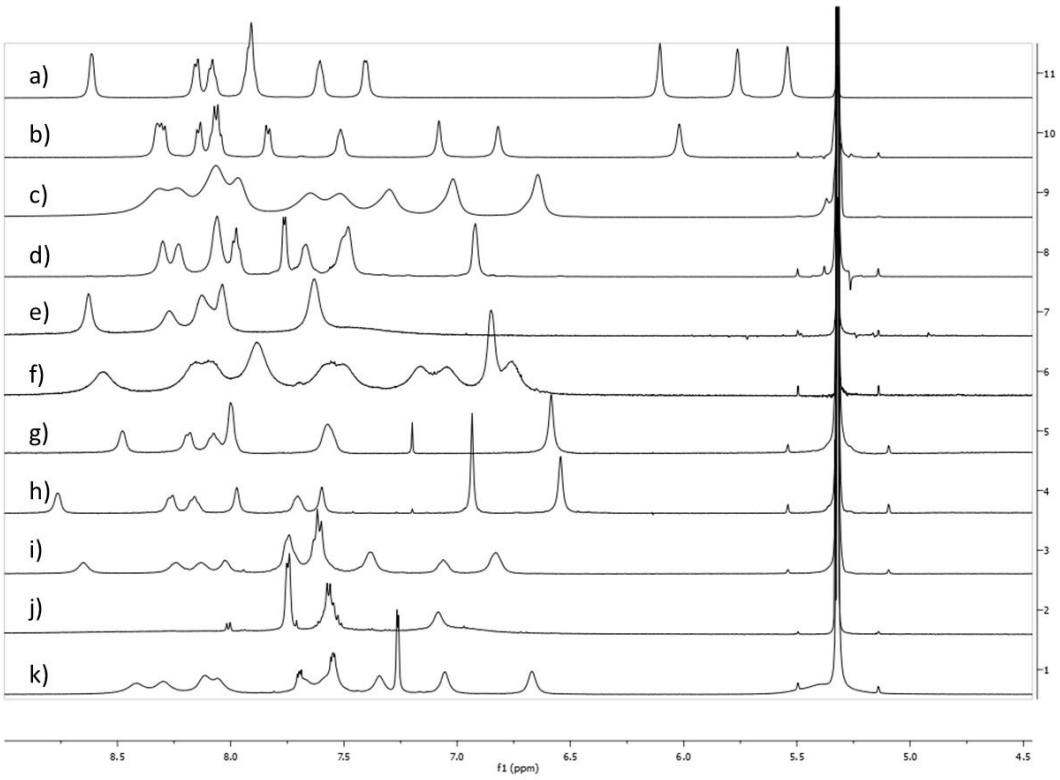


**Figure 4-43** Room temperature 500 MHz $^{1}$H NMR spectra ($\delta$9.0–4.5 ppm) of $CD_2Cl_2$ solutions of (a) [Cu(**1**)$_2$][PF$_6$], (b) [Cu(**2**)$_2$][PF$_6$], (c) [Cu(**3**)$_2$][PF$_6$], (d) [Cu(**4**)$_2$][PF$_6$], (e) [Cu(**20**)$_2$][PF$_6$], (f) [Cu(**21**)$_2$][PF$_6$], (g) [Cu(**12**)$_2$][PF$_6$], (h) [Cu(**30**)$_2$][PF$_6$], (i) [Cu(**31**)$_2$][PF$_6$], (j) [Cu(**34**)$_2$][PF$_6$] and (k) [Cu(**36**)$_2$][PF$_6$]. The signal at $\delta$5.32 ppm arises from $CDHCl_2$ with the $^{13}$C satellites from.

The spectra are better resolved at low temperatures. And thus could be fully assigned using 2-D techniques. In Figure 4-44 is shown the COSY-NMR spectrum of [Cu(**3**)$_2$][PF$_6$] at 228 K.

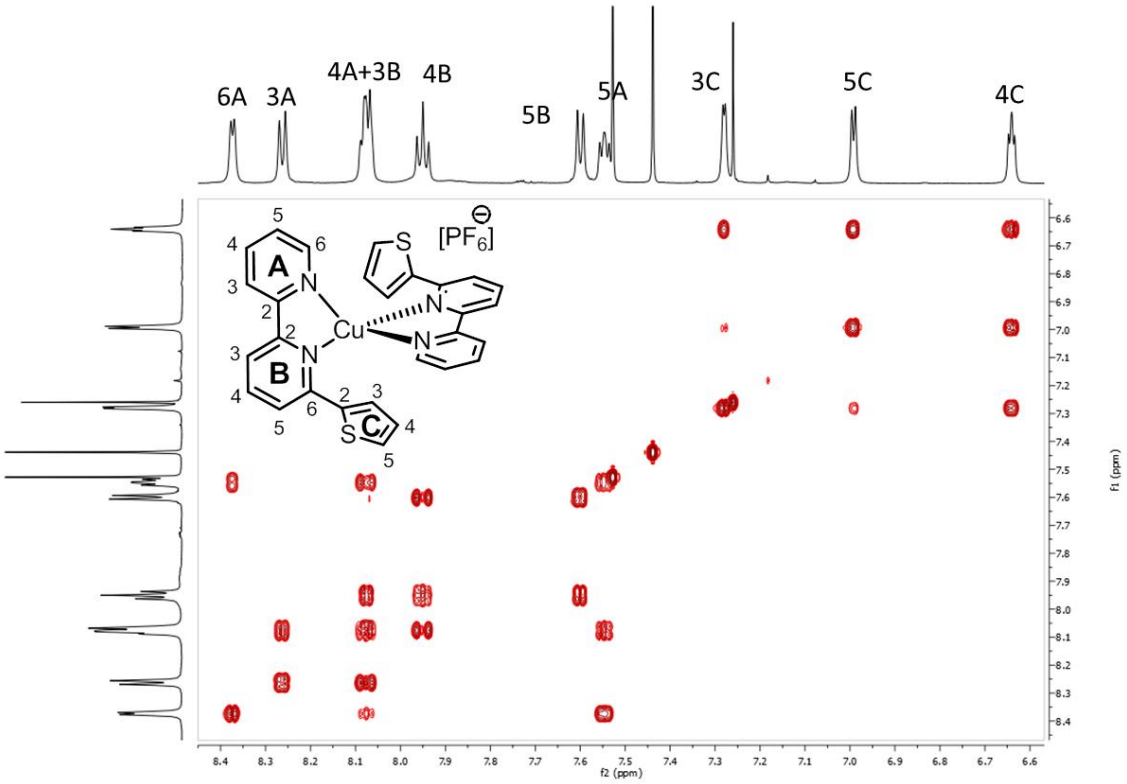


**Figure 4-44** Low temperature (228 K) 600 MHz COSY-NMR spectrum ($\delta$ 8.5–6.6 ppm) of a $CD_2Cl_2$ solution of [Cu(**3**)$_2$][$PF_6$].

In the beginning of this work, only complexes with ligands **1**-**6** were available. The first observations of the broadening of the signals were suggesting that it may arise from slow rotation of the hetero aromatic substituent about the $C_{bpy}$–$C_{substituent}$ bond, which might be caused either by bulkiness of the ring and/or by interactions between the hetero atom and the metal centre. The assumption of a hindered rotation of the substituents on the bpy moiety is not consistent with the observed low temperature $^1$H NMR spectra. If the broadening was caused by coalescence, there would be sets of signals for at least two distinct species at lower temperature. This is not the case and only one set of signals can be observed, which suggests that the broadening does not originate from a coalescence effect. To determine the reason for this phenomenon, new bpy ligands were prepared: For example, ligand **21** where the substitution of the phenyl substituent with a methyl group makes this ring asymmetrical around the rotation axis. This can be compared to the *N*-methyl pyrrole ligand (**1**) but does not contain a hetero atom in the substituent. Ligand **20** was meant to be symmetrical around the rotation axis and bearing a hetero atom which cannot coordinate to the same metal centre as the bpy moiety. Unfortunately, the nitrogen atom can be involved in coordination to a second metal centre which can result in several species in solution and the results for [Cu(**20**)$_2$][$PF_6$] are inconclusive. Furthermore, ligand **12** was synthesized; this contains three bulky methoxy groups on the phenyl substituent but it is symmetrical around the rotation axis. Also, ligands which were designed for

$[Ir(ppy)_2(L)][PF_6]$ (L = **30**-**32**) were used, as well as ligands **34** and **36** from an unfinished project. As can be seen in Figure 4-43, they all give broadened spectra which means that the nature of the substituent on the bpy as well as the introduction of a second substituent in the 4'-position promote the mechanism which causes this broadening.

The $^1$H Variable Temperature-NMR spectra of $[Cu(\mathbf{21})_2][PF_6]$ are shown as representative examples in Figure 4-45. The only difference to compound $[Cu(\mathbf{5})_2][PF_6]$ is a methyl substituent on the phenyl ring of the bpy moieties. Interestingly, this small change causes a significant difference in the $^1$H NMR spectrum. While the phenyl derivative gives a well resolved spectrum, the m-tolyl derivative shows quite broad signals. When the temperature is lowered, the signals sharpen and at 210 K, the spectrum is nearly as well resolved as the one of $[Cu(\mathbf{5})_2][PF_6]$ at room temperature.

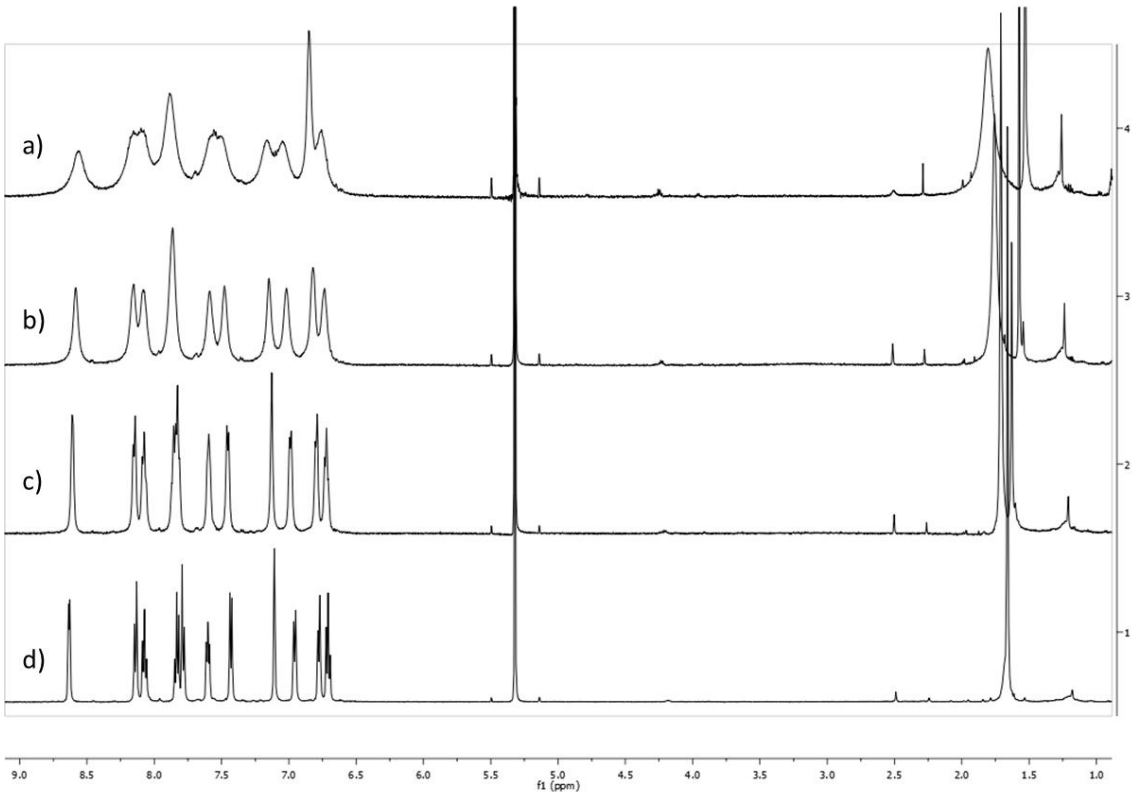


**Figure 4-45** VT 500 MHz NMR spectra ($\delta$ 9.0–1.0 ppm) of a $CD_2Cl_2$ solution of $[Cu(\mathbf{21})_2][PF_6]$, (a) 295 K (b) 270 K (c) 240 K and (d) 210 K.

To understand better what process(es) is/are causing the solution behaviour of the copper(I) complexes more experiments were conducted. For one, the influence of the solvent was investigated. As representative compounds were chosen the thiophenyl derivative $[Cu(\mathbf{3})_2][PF_6]$ and the simple complex $[Cu(\mathbf{6})_2][PF_6]$ containing methyl substituents on the bpy ligands. $^1$H NMR spectra were recorded in various solvents and the results are shown in Figure 4-46 ($[Cu(\mathbf{3})_2][PF_6]$) and in Figure 4-47 ($[Cu(\mathbf{6})_2][PF_6]$).

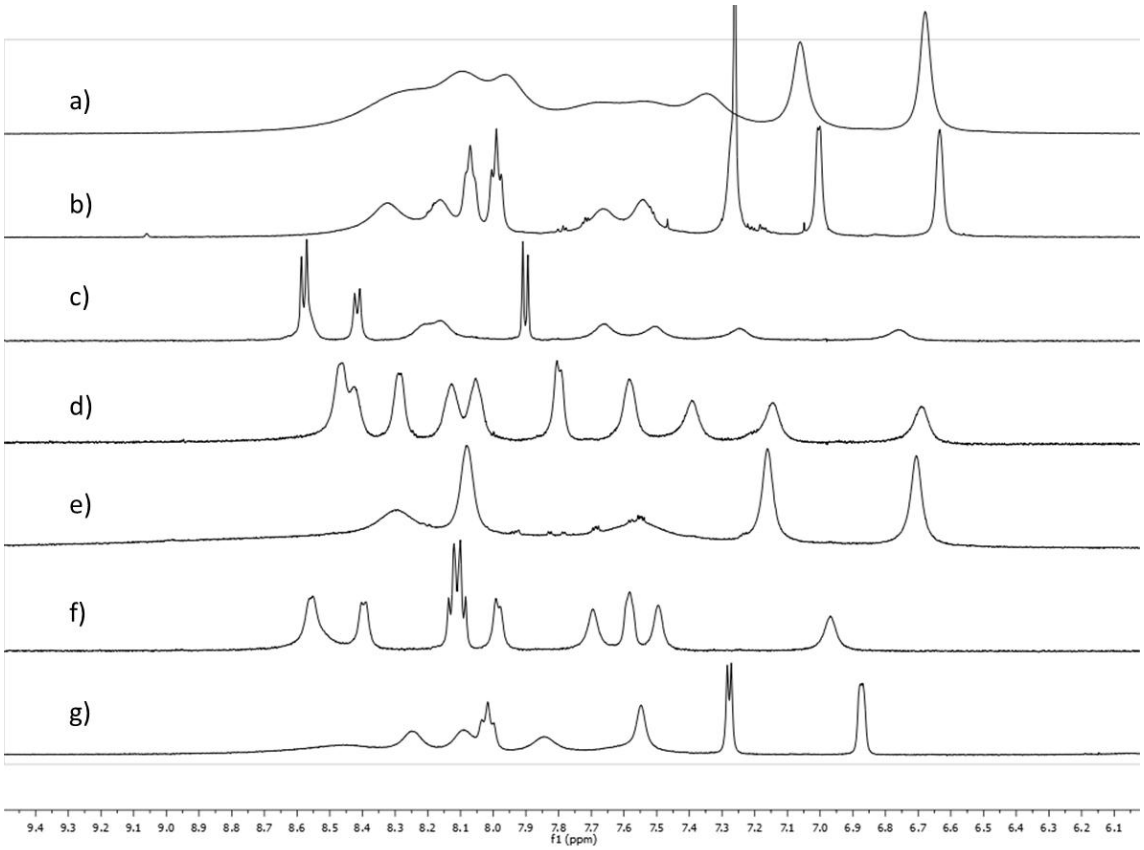


**Figure 4-46** Room temperature 500 MHz NMR spectra ($\delta$ 9.5–6.0 ppm) of [Cu(**3**)$_2$][PF$_6$] in various deuterated solvents: (a) $CD_2Cl_2$, (b) $CDCl_3$, (c) acetone-$d_6$, (d) MeOD-$d_3$, (e) THF-$d_8$, (f) DMSO-$d_6$ and (g) MeCN-$d_3$.

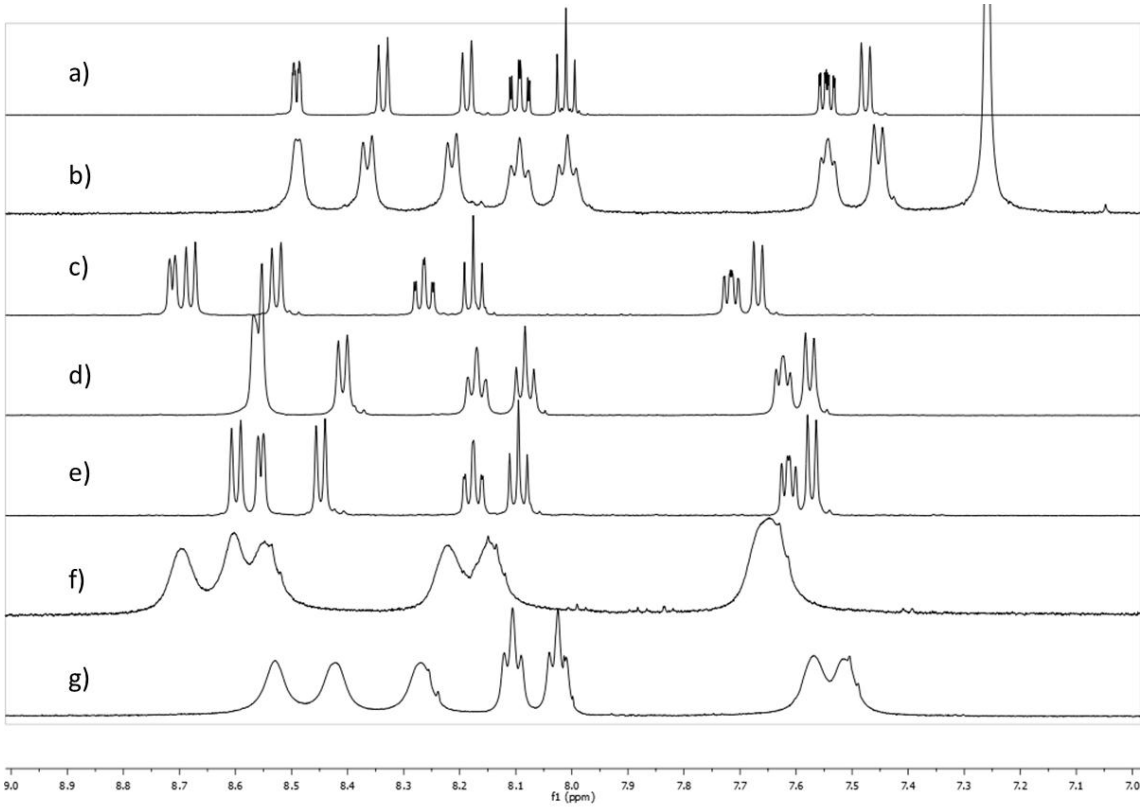


**Figure 4-47** Room temperature 500 MHz NMR spectra ($\delta$ 9.0–7.0 ppm) of [Cu(**6**)$_2$][PF$_6$] in various deuterated solvents: (a) $CD_2Cl_2$, (b) $CDCl_3$, (c) acetone-$d_6$, (d) MeOD-$d_3$, (e) THF-$d_8$, (f) DMSO-$d_6$, (g) MeCN-$d_3$.

The spectra are ordered with respect to the assumed donor ability of the solvents towards the copper(I) cation. For the thienyl derivative ([Cu(**3**)$_2$][PF$_6$]) all spectra obtained exhibit broadening of the signals as well as solvent specific shifts.

The reference compound ([Cu(**6**)$_2$][PF$_6$]) exhibits, as expected, sharp signals for most solvents. Surprisingly, in the good donor solvents acetonitrile and dimthylsulfoxide the spectra broaden as well. These results suggested that ligand exchange processes have to be involved. Indeed, it is known that copper(I) complexes are labile and they can undergo rapid ligand exchange processes (see also following section).

With the help of PD Dr. HÄUSSINGER NMR experiments were conducted to confirm the hypothesis: Following the work of Profs. SAUVAGE and LACOUR a racemic mixture of two diastereomeric complexes was prepared and low temperature EXSY-NMR measurements carried out which clearly showed exchange signals between the two diastereomers. In consequence, we were able to determine the exchange rate.

As already mentioned in the introduction, copper(I) complexes prefer to adopt a pseudo-tetrahedral geometry. With two identical symmetrical bidentate ligands, the coordination sphere is achiral with $D_{2d}$ symmetry. However, if two identical unsymmetrical bidentate ligands are used for the ligation, there are two chiral enantiomeric spiro entities possible which can be described as $\Delta/\Lambda$ configuration (Figure 4-48).[110,111]

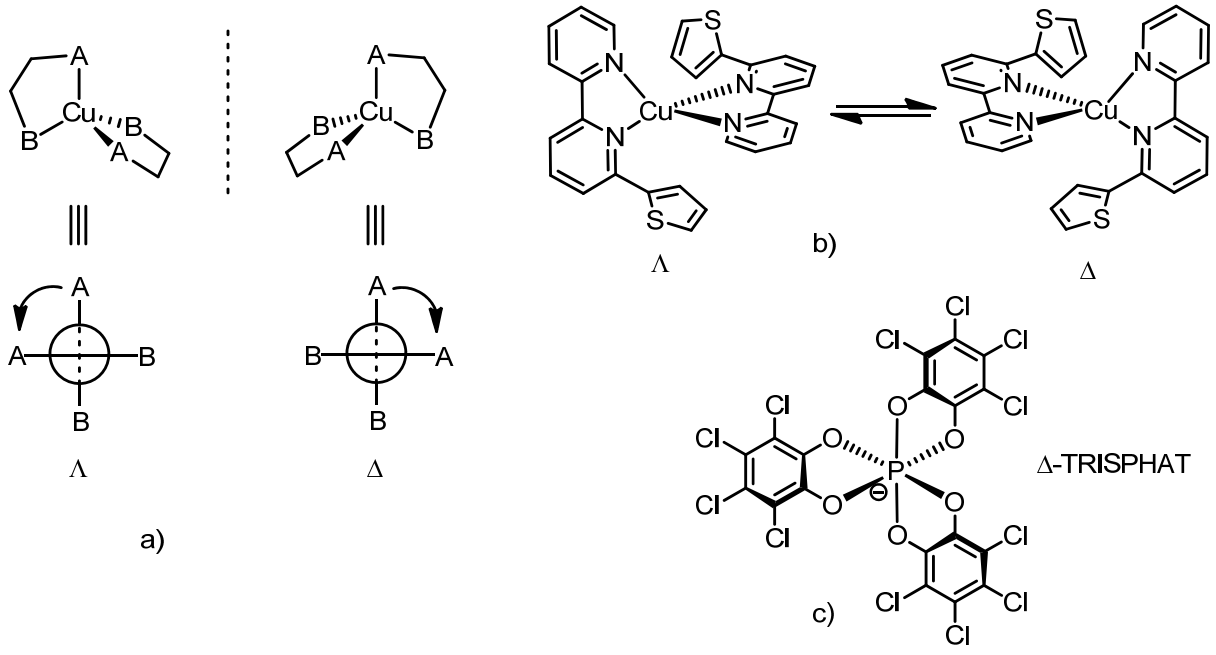


**Figure 4-48** a) Chiral spiro copper(I) complexes of $\Delta$ or $\Lambda$ configuration; b) configurational lability of Cu(I) complexes represented with [Cu(**3**)$_2$][PF$_6$]; c) $\Delta$ enantiomer of the tris(tetrachlorobenzenediolato)-phosphate anion ($\Delta$-TRISPHAT)[110].

The two enantiomers cannot be distinguished with NMR spectroscopy, but the introduction of a chiral anion results in two diastereomeric anion-cation pairs as shown in Figure 4-48b+c). The kinetic lability of the copper(I) complexes does not allow the differentiation at room temperature, however, if the temperature is lowered so that the racemization is slow enough, two separate sets of signals can be observed (see Figure 4-49).

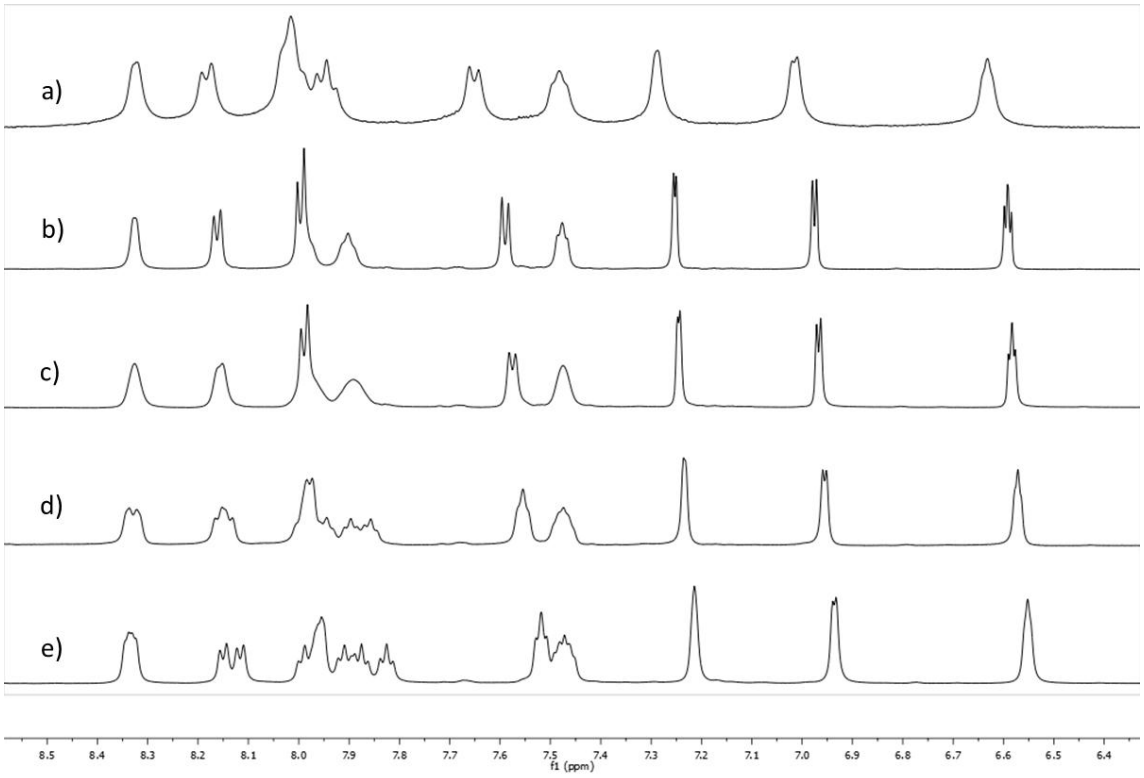


**Figure 4-49** VT 600 MHz NMR spectra ($\delta$ 8.6–6.4 ppm) of a $CD_2Cl_2$ solution of [Cu(**3**)$_2$][Δ-TRISPHAT], (a) 298 K (b) 248 K (c) 238 K, (d) 228 K and (e) 208 K.

In a first experiment [$NH_4$][Δ-TRISPHAT] was added directly to the NMR sample of [Cu(**3**)$_2$][$PF_6$] in a slight excess (1.1 eq). $^1$H NMR spectra were recorded at different temperatures. The results are shown in Figure 4-49 and reveal at least two processes. At room temperature the signals are slightly broadened but not as much as the pure $PF_6$-salt. This suggests an exchange process between the two anions. When the temperature is lowered to 248 K the signals sharpen and show the expected splitting. When lowered to 238 K the signals broaden again, which suggests this being the coalescence temperature. Lowering the temperature to 228 K the signals for the pyridine rings separate in two sets which is even more pronounced at 208 K. So, it could be demonstrated that this copper(I) complex is indeed chiral.

The first mentioned anion exchange process could be proved and eliminated by using a pure Δ-TRISPHAT salt of [Cu(**3**)$_2$]$^+$. As depicted in Figure 4-50, without $PF_6$ anions in solution the $^1$H NMR spectrum is much sharper at room temperature.

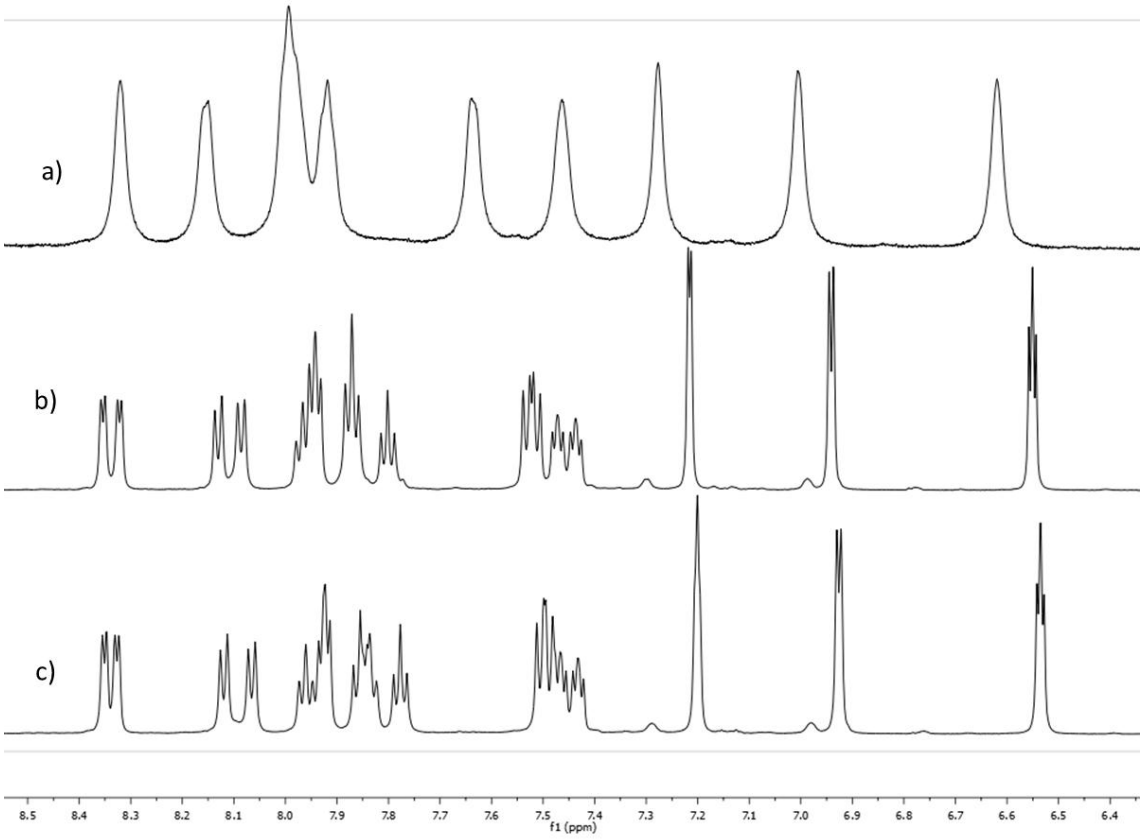


**Figure 4-50** VT 600 MHz NMR spectra ($\delta$ 9.0–1.0 ppm) of a $CD_2Cl_2$ solution of pure [Cu(**3**)$_2$][Δ-TRISPHAT], (a) 298 K (b) 220 K and (c) 208 K.

When the temperature is lowered, the $CD_2Cl_2$ solution of pure [Cu(**3**)$_2$][Δ-TRISPHAT] shows enantio-differentiation as well. But this time the resolution at 208 K was even better than in the previous experiment where the $[PF_6]^-$ anion was present. This suggests that the anion exchange process is proceeding even at this low temperature.

We then used the EXchange SpectroscopY (EXSY) to see whether there is an exchange between the two diastereomers. EXSY is essentially the same experiment as $^1$H-$^1$H NOESY (Nuclear Overhauser Effect SpectroscopY) but they are used for different purposes. NOESY is useful for determining which signals arise from protons that are close to each other and interact through space rather than through covalent bonds. A NOESY spectrum yields through space correlations *via* spin-lattice relaxation. On the other hand it also detects chemical and conformational exchange and is then called EXSY when used for this purpose.

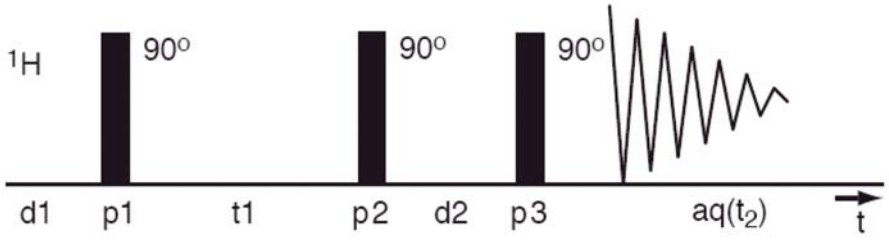


**Figure 4-51** Pulse sequence of a NOESY experiment; d1, relaxation delay; d2, mixing time; p, pulse; t1, evolution time; aq, acquisition

Figure 4-51 shows a typical NOESY pulse sequence. For quantitative NOESY, short mixing times (t) and long relaxation delays (d) are required. If there are two different conformations A and B which undergo chemical exchange reactions and an excited proton of A is present in B after the mixing time (d2), a cross peak between the two protons from two conformations is observable. Comparison of the cross-peak integrals yields the exchange ratio between the two species, and can be used to calculate the rate of exchange between A and B.

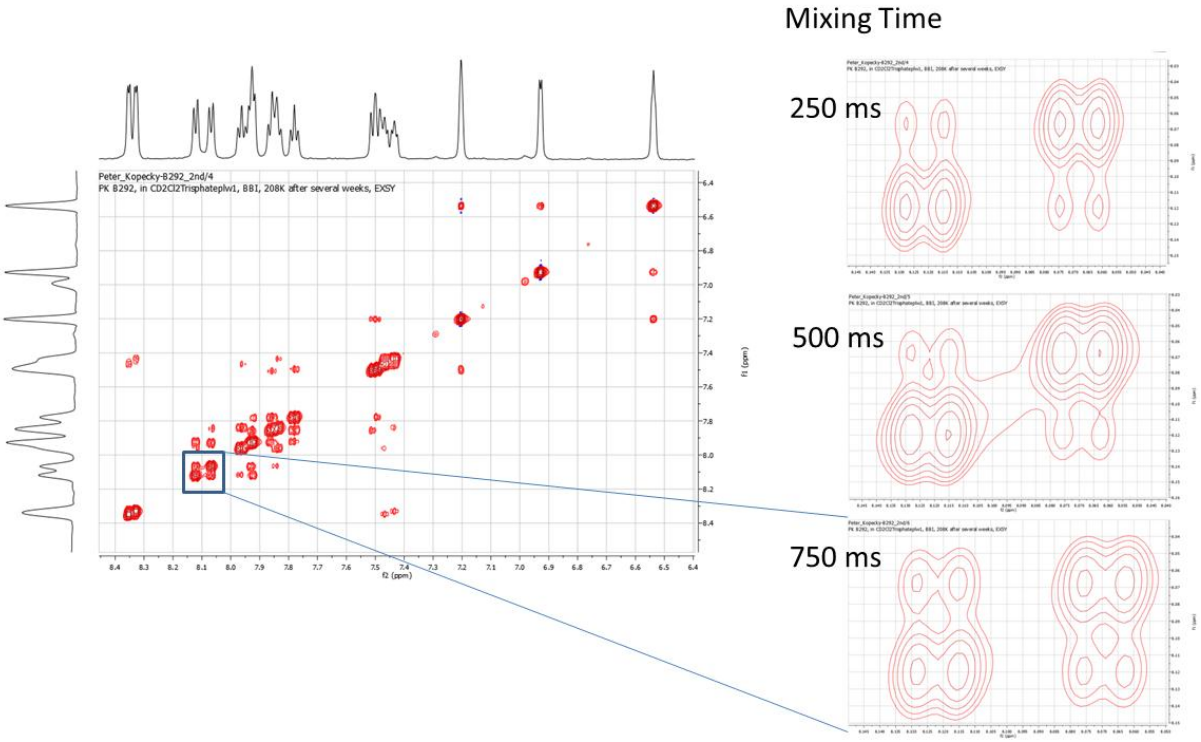


**Figure 4-52** 600 MHz EXSY NMR spectrum of [Cu(**3**)$_2$][Δ-TRISPHAT] at different mixing times.

In our experiment we were able to observe cross peaks between the two diastereomers. For the calculation of the exchange ratio we monitored the 3A-protons which show the biggest separation ($\Delta\delta_{[ppm]}$). As shown in Figure 4-52 there are cross peaks observable between the two species and with increasing mixing time the intensity of the cross peaks increases as well. A quantitative analysis yielded the exchange fraction which was then plotted against the mixing time. From this graph, the exchange rate k can be deduced directly from the slope of the graph and gives the value of $k \sim 0.5\ s^{-1}$ (see Figure 4-53). In other words, it takes approximately 2 seconds for a complete exchange. It is not possible to say how the exchange proceeds in detail. One possible pathway could be that one ligand dissociates completely and then coordinates again in the opposite conformation (Figure 4-54). A second possible change of the configuration could occur through a simple swinging of one ligand around a $C_2$ axis with a square planar transition state, but the bulky substituents in α-positions of the bpy moieties make this quite impossible. This leaves the possibility of that at least one N…Cu

bond has to dissociate then the bpy ligand rotates 180° and the N…Cu bond is restored again. Similar mechanisms were proposed by VAN KNOTEN.[112]

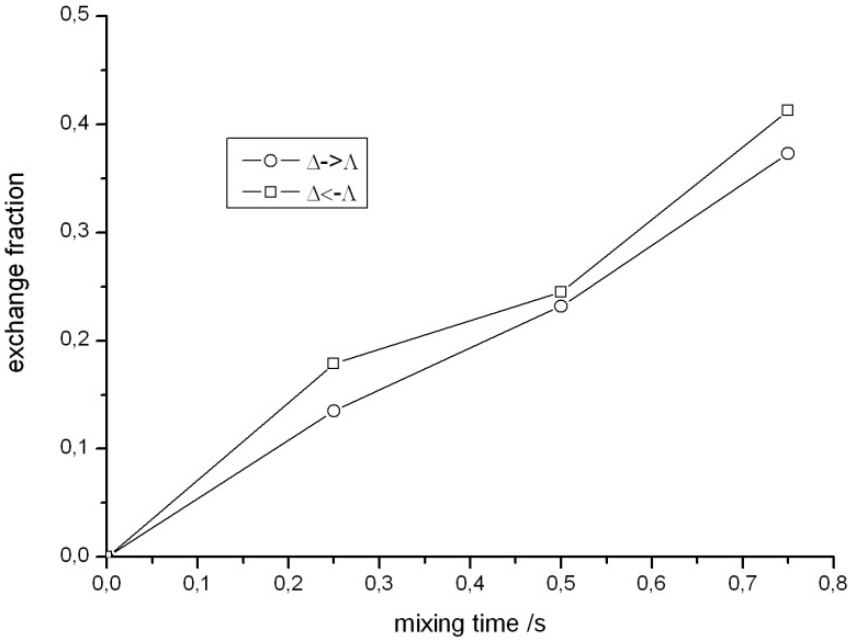


**Figure 4-53** EXSY NMR analysis for [Cu(**3**)$_2$][Δ-TRISPHAT].

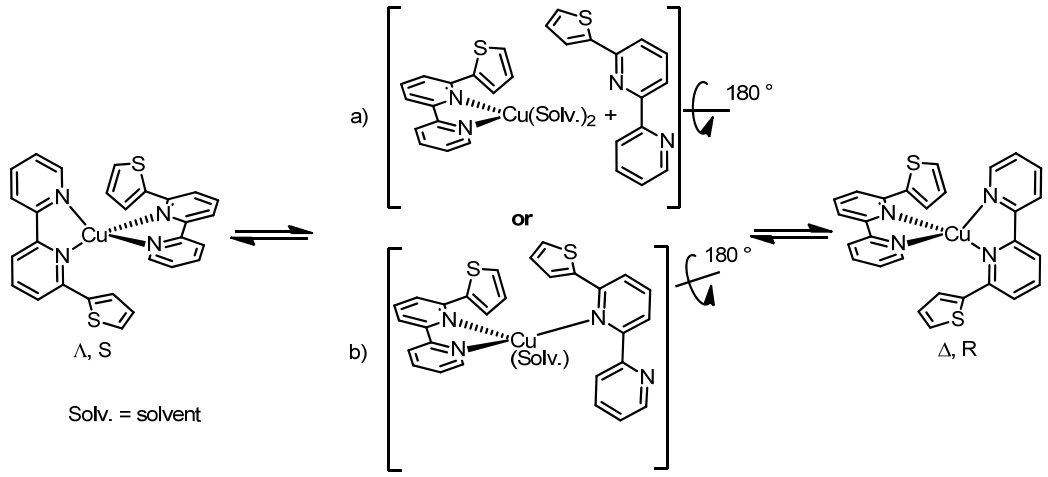


**Figure 4-54** Proposed exchange mechanism: a) complete dissociation of one ligand; b) partial dissociation.

A fact that has not been considered so far: Chlorinated solvents such as dichloromethane or chloroform but also the deuterated equivalent, tend to be slightly acidic due to decomposition. Therefore, in these solvents, $H^+$ as well as $Cl^-$ ions are present. Both are able to interact with the copper(I) bpy complexes. The $H^+$ can protonate free nitrogen atoms as soon as a Cu…N bond breaks, and at the same time the $Cl^-$ can very well act as a ligand to the metal centre. Apparently, these processes are very fast and do not influence the NMR spectra if the substituents on the bpy ligands are small and/or aliphatic. Aromatic and bulky substituents seem to slow these processes down which results in line broadening of the NMR spectra in chlorinated deutero solvents. The solvents which were used for all NMR

experiments were from sealed 1 ml ampules and were thought not to be acidic; this is however, not the case. If $CD_2Cl_2$ was passed through basic $Al_2O_3$ the observed NMR spectrum of [Cu(**3**)$_2$][$PF_6$] did not show strong line broadening.

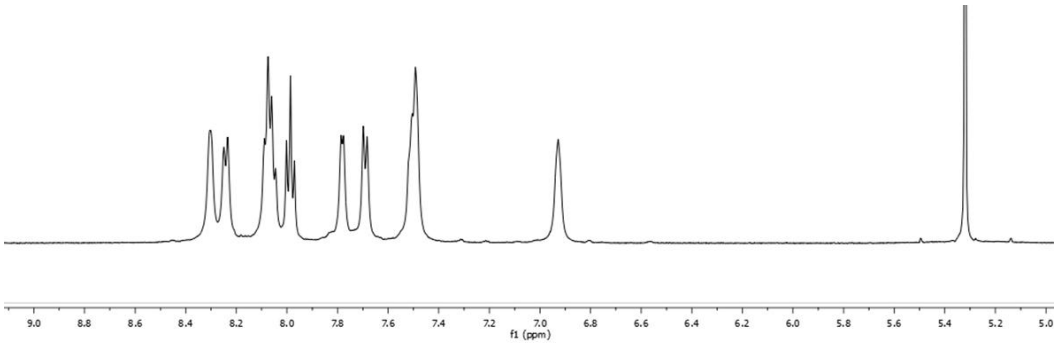


**Figure 4-55** Room temperature 400 MHz $^1$H NMR spectrum of [Cu(**3**)$_2$][$PF_6$] in acid free $CD_2Cl_2$ (basic alox filtration).

High temperature $^1$H NMR spectra were recorded for compound [Cu(**3**)$_2$][$PF_6$] in a $C_2D_2Cl_4$ solution and are shown in Figure 4-56. The compound seems to be stable up to 368 K. Again these experiments show that the broadening is not caused by coalescence, since at higher temperature the signals do not resolve. When the temperature is higher than 368 K the spectrum changes abruptly and only four signals can be observed.

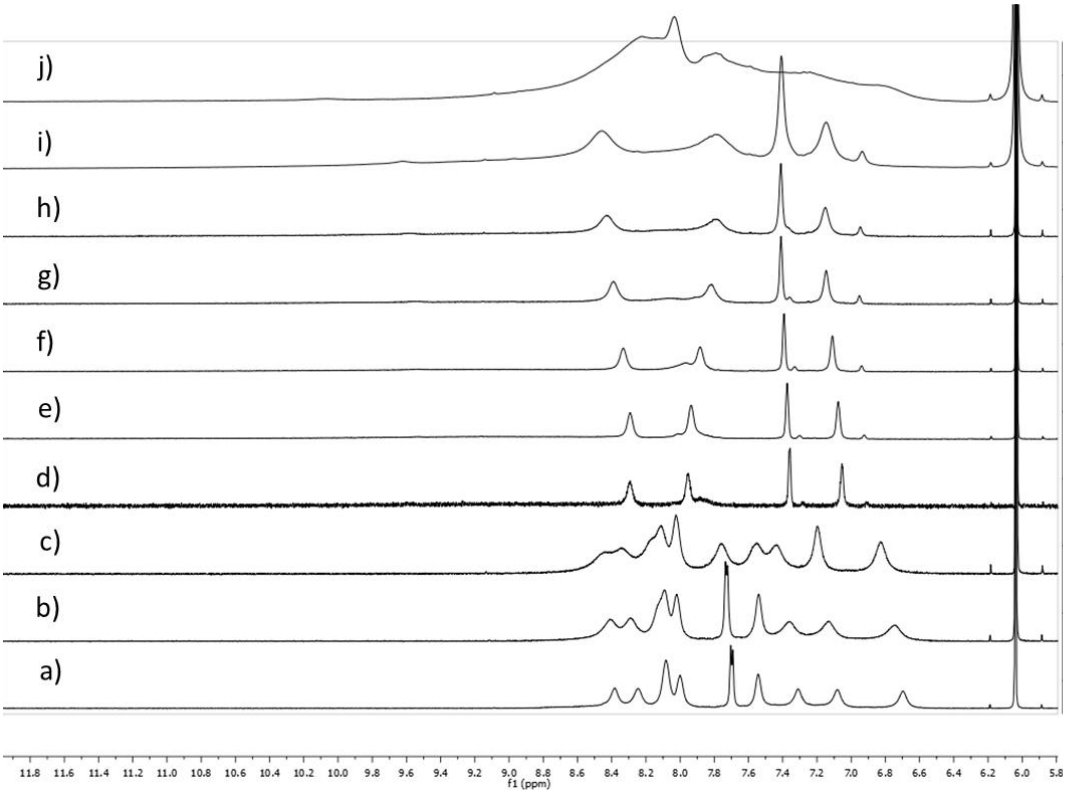


**Figure 4-56** High temperature 600 MHz $^1$H NMR of a $C_2D_2Cl_4$ solution of [Cu(**3**)$_2$][$PF_6$]; a) 298 K, b) 328 K, c) 358 K, d) 388 K, e) 398 K, f) 388 K, g) 378 K, h) 368 K, i) 358 K, j) 298 K.

These spectra look suspiciously similar to the of 2,2'-bpy and it is possible that at this elevated temperature ligand **3** undergoes a copper mediated cleavage of the thienyl substituent. The decomposition of the compound is revealed when the temperature is lowered back to 298 K and there it becomes clear that the two room temperature spectra are not superimposable.

A series of silver(I) compounds with ligands **2**-**4** was prepared, and the complexes [Ag(L)][X] (L = ligands **2**-**4**; X = $[PF_6]^-$ or $[BF_4]^-$) shall serve as model compounds. Figure 4-57 shows the $^1$H NMR spectra of the silver complexes and interestingly the $CD_2Cl_2$ solutions of the $PF_6$ salts show well resolved signals and no line broadening whatsoever.

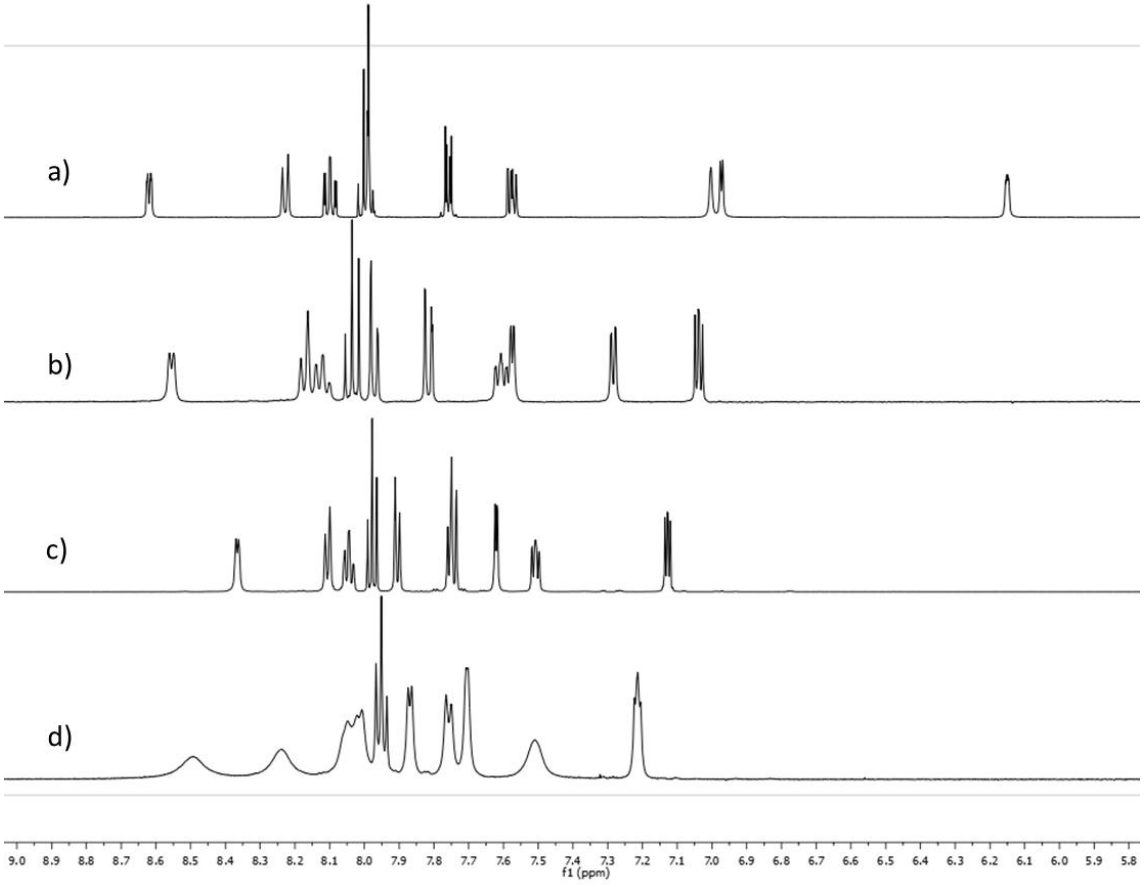


**Figure 4-57** Room temperature 500 MHz NMR spectra ($\delta$ 9.0–5.8 ppm) of $CD_2Cl_2$ solutions of a) [Ag(**2**)$_2$][$PF_6$], b) [Ag(**3**)$_2$][$PF_6$], c) [Ag(**4**)$_2$][$PF_6$] and d) [Ag(**4**)$_2$][$BF_4$].

However, in the presence of the smaller anion $BF_4^-$, the $^1$H NMR spectrum of [Ag(**4**)][$BF_4^-$] shows broadening of the pyridine proton signals, suggesting that there might be some exchange process between ligand and anion. Similar behaviour was also noticed for the copper(I) complexes (see above), where the $PF_6$-salt of $[Cu(\mathbf{3})]^+$ showed broader signals than the TRISPHAT salt. Nevertheless, it can be stated that the here investigated silver(I) complexes seem to be more stable in solution than the corresponding copper(I) complexes. It has to be noted that these observations stand in sharp contrast to the reports by VAN KNOTEN and co-workers. They investigated the dynamic behaviour of bis iminopyridine

complexes $[M(L)_2][SO_3CF_3]$ (M = $Cu^+$ or $Ag^+$; L = (*E*)-*N*-((6-methylpyridin-2-yl)methylene)-R-amine; R = Me, *c*-Hex, *i*-Pr or (S)-ChMePh) and stated the exact opposite, claiming that the silver complexes are less stable than the corresponding copper species.[112]

All the above mentioned results considered, we propose the following mechanism which might be responsible for the line broadening in the $^1$H NMR spectra of the copper(I) complexes (Scheme 4-5).

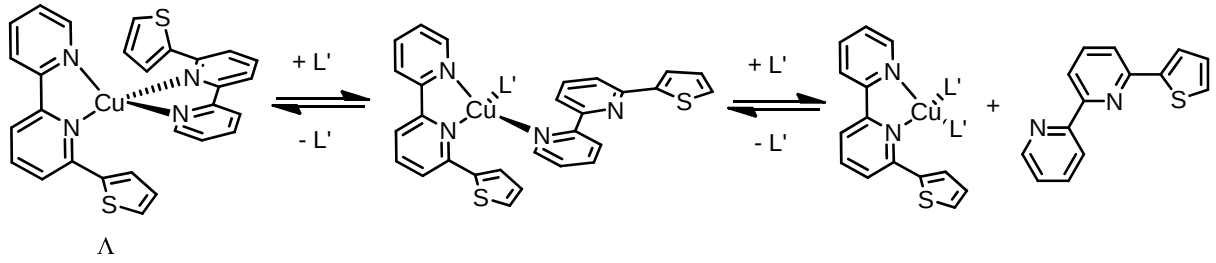


**Scheme 4-5** Proposed dynamic behaviour of copper(I) complexes in solution

It is very likely that the partial or complete dissociation of one ligand is the reason for the broad NMR spectra. In donor solvents, such as acetonitrile or dimethylsulfoxide for example, the broadening can be observed for all complexes independent of the nature of the substituent on the bpy ligands. In less donating solvents (THF, MeOH, $CHCl_3$ or $CH_2Cl_2$) the broadening depends very much on the substituents; smaller substituents show sharp spectra, bulkier and/or (hetero)aromatic substituents on the other hand show slower exchange rates and result in broader signals. Caution is advised when chlorinated solvents are used, due to the presence of HCl which very likely promotes the dynamic processes.

### $^{77}$Se-NMR

As already mentioned in section 3.3.3 metal complexes with the Se containing ligand **4** were prepared and $^{77}$Se-NMR spectra were recorded. Figure 4-58 shows the $^1$H-$^{77}$Se-HMBC spectrum. The observed cross peaks are slightly shifted to higher field ($\delta$ 592 ppm) compared to the free ligand ($\delta$ 603 ppm). In the literature there are not that many examples for coordinated selenophen compounds. The preferred bonding to a metal centre of an unsubstituted selenophen is *via* $\eta^5$ coordination comparable to cyclopentadienyl (Cp). Direct coordination through the Se atom ($\eta^1$) was reported for the first time by CHOI and ANGELICI in 1991 for $[ReCp(CO)_2$(selenophen)] complexes.[113] They observed chemical shifts between 80 and 200 ppm to high field, when the selenium atom was coordinated directly to a metal. Therefore, we can exclude any direct interaction between Se and Ag. A similar chemical shift ($\delta$ 612 ppm) was observed for $[Cu(\mathbf{4})_2][PF_6]$.

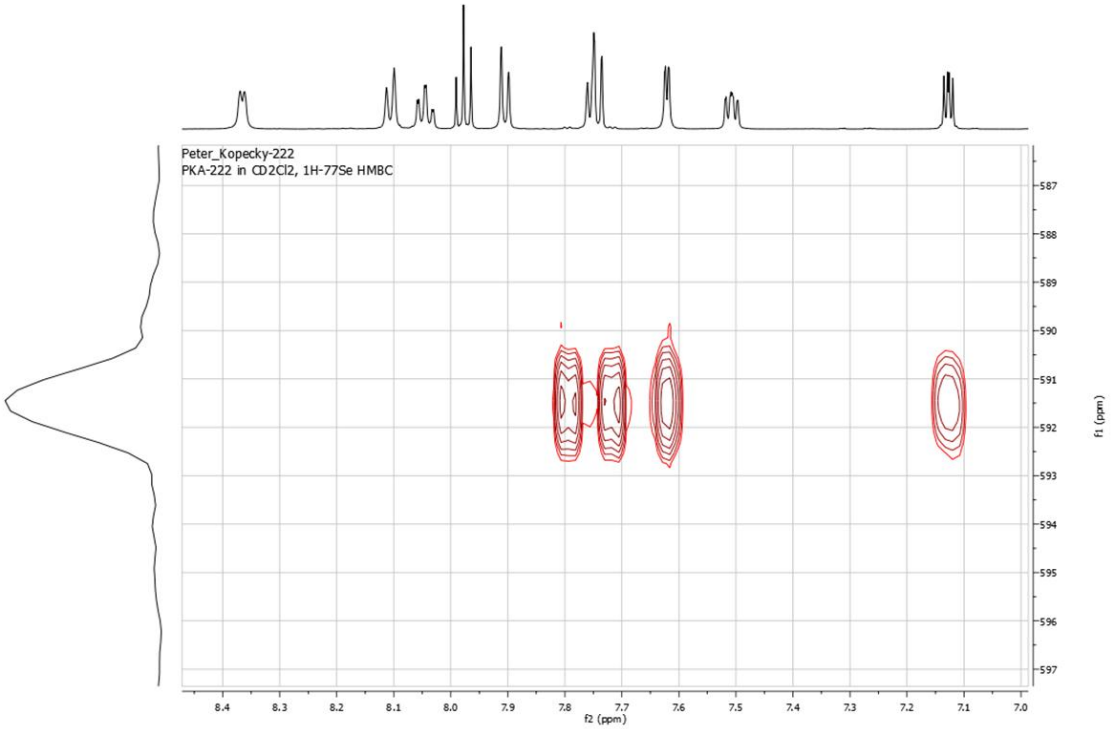


**Figure 4-58** $^{1}$H-$^{77}$Se HMBC NMR of [Ag(**4**)$_2$][PF$_6$].

### 4.1.3 DSCs

As already mentioned in the introduction (see section 1.3.3.7) the recent studies of potential dyes for DSCs in our group have focused on copper(I) complexes incorporating bpy-based and related ligands with carboxylic acid or carboxylate functionalities.[49] While the synthesis of homoleptic complexes of type $[CuL_2]^+$ is straightforward (see section 4.1.1), the requirement to incorporate anchoring groups limits the range of ligands and, therefore, of complexes that can be screened. The efficient preparation of heteroleptic complexes is therefore of importance. We have demonstrated the lability in solution of diimine and phosphane ligands in copper(I) complexes, and the formation of heteroleptic complexes from equilibrium mixtures of two homoleptic species.[51,114] Following these observations, we have adopted a simple strategy for rapid screening of the performance of heteroleptic copper(I) complexes in DSCs. The heteroleptic copper(I) complexes are prepared directly on the $TiO_2$ surface. To achieve this, a common anchoring ligand L' is firstly attached to the semiconductor surface, and this electrode is then immersed into a solution of a homoleptic $[CuL_2]^+$ complexes, where L is a variable ligand. In this work, for the assembly of surface-bound and heteroleptic $[CuLL']^+$, L' is one of the ligands **43**-**46** shown in Figure 4-59, and L = **1**-**6**. Ligands **43**-**45** contain carboxylic acid (carboxylate) anchoring groups, while in **46**, anchoring is established through the phosphonic acid (phosphonate) units. GRÄTZEL has established that absorption of dyes onto $TiO_2$ is enhanced by the presence of phosphonate

groups, which is only reasonable, and can be explained with stronger binding through three Ti…O bonds *vs*. two in carboxylate anchor ligands.[115]

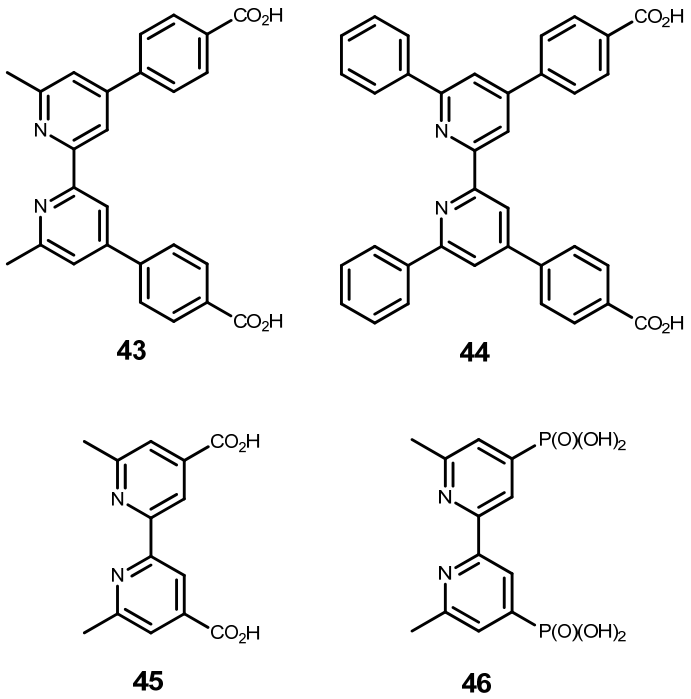


**Figure 4-59** Structures of the anchoring ligands, L', **43**-**46**. The anchoring groups are the carboxylic or phosphonic acids or their conjugate bases.

The preparation of the open cell DSCs is as follows: The anodes were prepared by dipping conducting glass slides with annealed $TiO_2$ (see experimental section) into a DMSO solution of the anchoring ligand L' (**43**-**46**). After washing and drying the slides, they were immersed for 24 hours in ethanol solutions of the homoleptic complexes $[CuL_2][PF_6]$ (L = **1**-**6**), allowing the equilibrium in Scheme 4-6 to be established. The appearance of the slide changed from colourless to red, consistent with the presence of a surface adsorbed copper(I) complex and the red colour persisted after the slide was washed with ethanol.

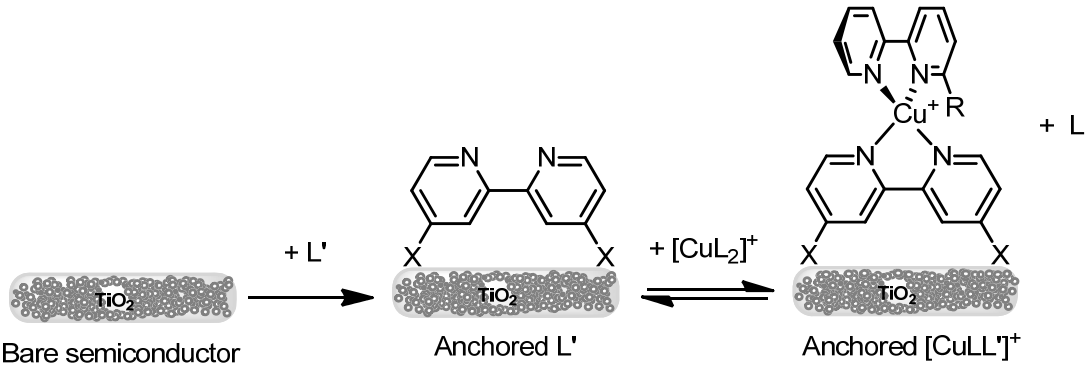


**Scheme 4-6** Sensitizing process: a) adsorption of anchoring ligand; b) ligand exchange leading to surface anchored heteroleptic copper(I) dyes. L = **1**-**6**, L' = **43**-**46**; X = anchoring group (see Figure 4-59).

The characterization of the immobilized, heteroleptic complexes is not trivial. In order to establish the proposed compounds a sample, prepared with L = **4** and L' = **46** was subjected

to MALDI-TOF mass spectrometric analysis. A sample of red-coloured $TiO_2$ was scratched from the surface of the slide and the powder was suspended in dichloromethane and mixed with the MALDI matrix (2,5-dihydroxybenzoic acid). The mass spectrum showed peaks at *m/z* 348.8, 634.7 and 762.7 which were assigned to $[Cu(\mathbf{4})]^+$ (calc. 348.9), $[Cu(\mathbf{4})_2]^+$ (calc. 634.9) and $[Cu(\mathbf{4})(\mathbf{46} - 4H + Et + 2Na)]^+$ (calc. 763.9). Isotope patterns consistent with these ions were observed.

Diffuse reflectance electronic absorption spectra of the surfaces of the slides were also recorded. Figure 4-60 is representative of the results and illustrates the spectra of the $TiO_2$-anchored ligands **43-46** after treatment with $[Cu(\mathbf{1})_2][PF_6]$; corresponding spectra for the remaining 20 devices are given in Figure 4-61. The spectra were compared to that of a $TiO_2$ electrode which had been dipped into a DMSO solution of the homoleptic complex $[Cu(\mathbf{10})_2]Cl$[116] for four hours. The differences between the spectra shown as solid lines in Figure 4-60 provide evidence for the presence of different surface species, and the tail into the visible region is consistent with surface-binding of complexes of copper(I) as opposed to free ligand, the latter being colourless. Although, the spectra for combinations of **43** and $[Cu(\mathbf{1})_2][PF_6]$, and of **46** and $[Cu(\mathbf{1})_2][PF_6]$ look similar, we can rule out the possibility that the spectra arise from different surface coverages of $[Cu(\mathbf{1})_2][PF_6]$ on the basis that ligand **1** has no anchoring groups. Significantly, each of the spectra for the combinations of **43**, **44**, **45** or **46** after treatment with $[Cu(\mathbf{1})_2][PF_6]$ shows a low energy shoulder which coincides with the dominant band in the diffuse reflectance spectrum of $TiO_2$-supported $[Cu(\mathbf{46})_2]^+$. This further supports the presence of the heteroleptic species.

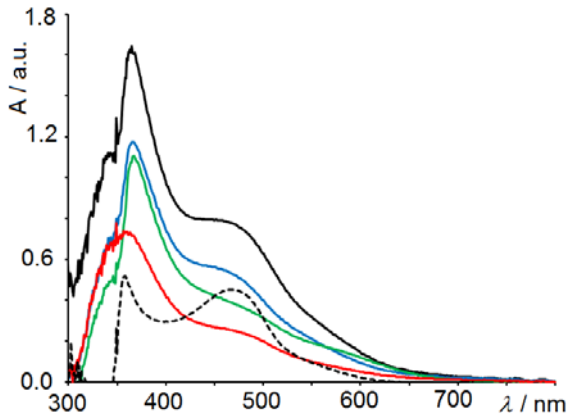


**Figure 4-60** Solid state diffuse reflectance electronic absorption spectra of $TiO_2$-anchored ligands **43** (black), **44** (green), **45** (red) and **46** (blue) after treatment with $[Cu(\mathbf{1})_2][PF_6]$. The hashed line is for $[Cu(\mathbf{46})_2]Cl$.

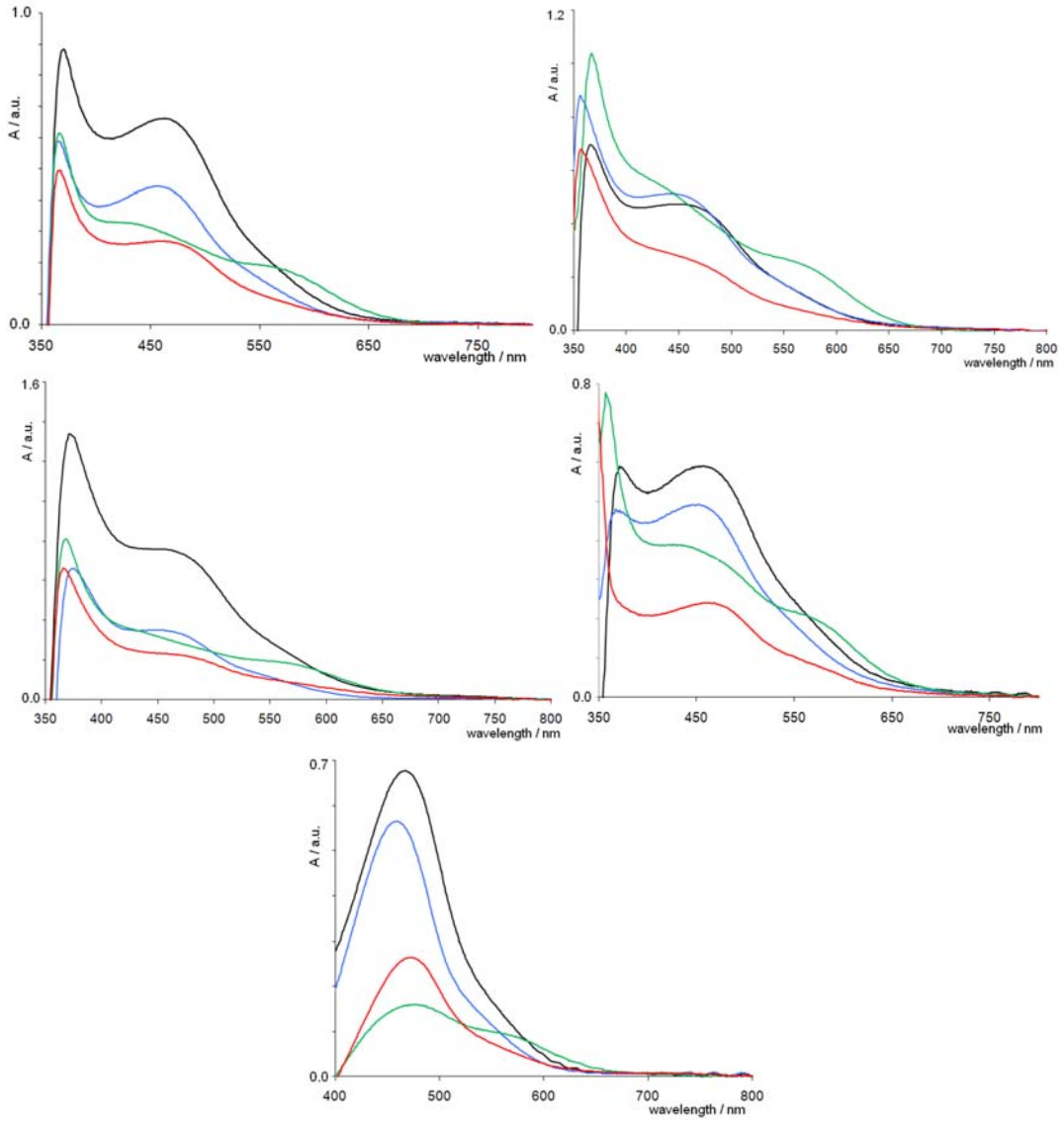


**Figure 4-61** Solid state diffuse reflectance electronic absorption spectra of $TiO_2$-anchored ligands **43** (black), **44** (green), **45** (red) and **46** (blue) after treatment with $[Cu(L)_2][PF_6]$ (L = **2** (top left), **3** (top right), **4** (middle left), **5** (middle right), 6 (bottom).

As far as the solid state diffuse reflectance electronic spectra can be compared, there is a trend to be seen. Devices with anchoring ligand **43** always show the highest absorptivity except for [Cu(**3**)(**43**)]$^+$ followed by devices bearing anchoring ligand **46**. This is somewhat reflected by the measured efficiencies for the DSCs which are always higher for these two anchoring ligands. The devices containing anchoring ligand **44** show a more pronounced lower energy band around 580 nm than with all the others anchoring ligands. This value is somewhat typical for MLCT bands observed for copper(II) polypyridine complexes and could indicate, that due to the phenyl substituents (interligand $\pi$-stacking induces near square planar coordination geometry) the resulting heteroleptic copper complexes are easily oxidized which would also explain the lower intensity of the higher energy band.

Table 4-3 presents the DSC efficiency data for the solar cells and also the data for standard ruthenium dye N719 ($[Ru(4,4'\text{-bis}(CO_2H)bpy)_2(NCS)_2][TBA]_2$) measured under the same

conditions as the copper(I) complexes. The measurements were made in open cells and the configuration is different to optimized cells reporting >10 % efficiency (η) for N719. For a common anchoring ligand L', changing ligand L leads to only small variations in the efficiencies of the solar cells. However, for a common ligand L, the choice of the anchoring ligand has a significant effect on the solar cell efficiency, with ligands **43** and **46** performing the best. When anchoring ligands **43** and **46** are compared the one containing phenyl substituents in the 6,6'-positions (**44**) of the bpy show always lower efficiency. This could be explained with stronger interligand π-interactions (see above) which favour a strongly flattened tetrahedral geometry of the copper metal in the dye molecule, compared to anchoring ligands which have only methyl substituents. This flattening is favourable for $Cu^{2+}$ and makes the regeneration of the dye to $Cu^{+}$ more difficult. Ligands **43** and **45** differ in the spacer between the bpy moiety and the anchoring group. In **45** the carboxy group is attached directly to the bpy and in **43** a phenyl spacer is separating these two. It is not evident why ligand **43** is more efficient but it probably depends on the molecular orbitals levels which would have to be calculated to understand these results better. Anchoring ligands **45** and **46** differ only in the anchoring groups themselves, i.e. $CO_2H$ versus $PO(OH)_2$ (or conjugate bases thereof). A comparison of the data confirms that higher efficiencies are achieved with the phosphonate binding groups which should be considered the anchors of choice for future DSC design.

| $[CuL_2]^+$ | L' | $I_{SC}$ / A cm$^{-2}$ | $V_{OC}$ / V | ff | η / % |
|---|---|---|---|---|---|
| $[Cu(\mathbf{1})_2]^+$ | **43** | 0.005 | 0.524 | 0.45 | 1.21 |
| $[Cu(\mathbf{1})_2]^+$ | **44** | 0.001 | 0.469 | 0.57 | 0.25 |
| $[Cu(\mathbf{1})_2]^+$ | **45** | 0.002 | 0.488 | 0.57 | 0.64 |
| $[Cu(\mathbf{1})_2]^+$ | **46** | 0.004 | 0.579 | 0.57 | 1.34 |
| $[Cu(\mathbf{2})_2]^+$ | **43** | 0.005 | 0.506 | 0.54 | 1.25 |
| $[Cu(\mathbf{2})_2]^+$ | **44** | 0.001 | 0.506 | 0.58 | 0.42 |
| $[Cu(\mathbf{2})_2]^+$ | **45** | 0.001 | 0.451 | 0.62 | 0.40 |
| $[Cu(\mathbf{2})_2]^+$ | **46** | 0.004 | 0.561 | 0.60 | 1.51 |
| $[Cu(\mathbf{3})_2]^+$ | **43** | 0.005 | 0.488 | 0.53 | 1.17 |
| $[Cu(\mathbf{3})_2]^+$ | **44** | 0.001 | 0.414 | 0.62 | 0.22 |
| $[Cu(\mathbf{3})_2]^+$ | **45** | 0.001 | 0.433 | 0.59 | 0.35 |
| $[Cu(\mathbf{2})_2]^+$ | **46** | 0.004 | 0.524 | 0.63 | 1.45 |
| $[Cu(\mathbf{4})_2]^+$ | **43** | 0.005 | 0.488 | 0.57 | 1.31 |
| $[Cu(\mathbf{4})_2]^+$ | **44** | 0.001 | 0.433 | 0.58 | 0.32 |
| $[Cu(\mathbf{4})_2]^+$ | **45** | 0.002 | 0.433 | 0.65 | 0.49 |
| $[Cu(\mathbf{4})_2]^+$ | **46** | 0.004 | 0.543 | 0.63 | 1.31 |
| $[Cu(\mathbf{5})_2]^+$ | **43** | 0.004 | 0.525 | 0.49 | 1.07 |
| $[Cu(\mathbf{5})_2]^+$ | **44** | 0.001 | 0.506 | 0.56 | 0.39 |
| $[Cu(\mathbf{5})_2]^+$ | **45** | 0.002 | 0.451 | 0.60 | 0.48 |
| $[Cu(\mathbf{5})_2]^+$ | **46** | 0.004 | 0.561 | 0.59 | 1.42 |
| $[Cu(\mathbf{6})_2]^+$ | **43** | 0.005 | 0.506 | 0.55 | 1.28 |
| $[Cu(\mathbf{6})_2]^+$ | **44** | 0.001 | 0.487 | 0.56 | 0.31 |
| $[Cu(\mathbf{6})_2]^+$ | **45** | 0.002 | 0.469 | 0.59 | 0.55 |
| $[Cu(\mathbf{6})_2]^+$ | **46** | 0.004 | 0.561 | 0.56 | 1.20 |
| N719 | | 0.015 | 0.715 | 0.43 | 4.50 |

**Table 4-3** DSC efficiency data in comparison to N719 measured under the same conditions (see experimental section). $[CuL_2]^+$ are introduced for surface ligand exchange as hexafluoridophosphate salts.

More device screening using the ligands **10**, **12**, **20**, **30**-**32** and **34** are presently under investigation.

## 4.2 Experimental

### 4.2.1 General method for the synthesis of homoleptic $[Cu(L)_2][PF_6]$

Each synthesis was carried out on a 50 μmol scale unless otherwise stated. $[Cu(NCMe)_4][PF_6]$ (18.6 mg, 50 μmol) was dissolved in MeCN and the ligand (100 μmol) was added. The solution turned deep red immediately. It was stirred for 2 h with TLC monitoring until all free ligand has been consumed. Solvent was removed in *vacuo*, leaving a red or black residue. The product was recrystallized from ethanol when necessary.

### 4.2.2 $[Cu(1)_2][PF_6]$

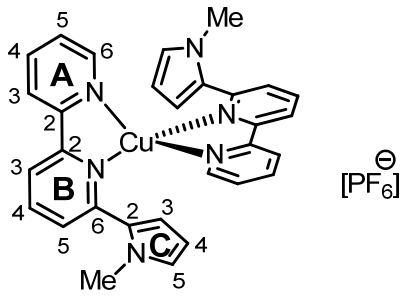


The synthesis was carried out on a 213 mmol scale. $[Cu(\mathbf{1})_2][PF_6]$ was isolated as red crystals (107 mg, 74 %). $^1$H NMR (500 MHz, $CD_2Cl_2$) $\delta$ (ppm) 8.61 (br, 2 H, $H^{6A}$), 8.15 (br, 2 H, $H^{4B}$), 8.08 (br, 2 H, $H^{4A}$), 7.91 (br, 4 H, $H^{3A+B}$), 7.61 (br, 2 H, $H^{5A}$), 7.41 (br, 2 H, $H^{5B}$), 6.10 (br, 2 H, $H^{5C}$), 5.76 (br, 2 H, $H^{3C}$), 5.55 (br, 2 H, $H^{4C}$), 3.28 (s, 6 H, $H^{Me}$); $^{13}C\{^1H\}$ NMR (126 MHz, $CD_2Cl_2$) $\delta$ (ppm) 153.3 ($C^{2A}$), 152.7 ($C^{2B}$), 150.8 ($C^{6B}$), 149.0 ($C^{6A}$), 138.2 ($C^{4A}$), 132.3 ($C^{2C}$), 126.6 ($C^{5A+B}$), 125.3 ($C^{5C}$), 122.7 ($C^{4C}$), 120.3 ($C^{3A+B}$), 111.4 ($C^{3C}$), 108.3 ($C^{4C}$), 35.2 ($C^{Me}$); IR (solid, $\nu$/cm$^{-1}$) 3124 w, 3090 w, 2939 w, 2919 w, 2360 w, 2331 w, 1988 w, 1663 m, 1599 m, 1569 m, 1558 m, 1487 m, 1456 s, 1444 s, 1423 m, 1390 m, 1321 m, 1299 m, 1248 m, 1222 w, 1177 m, 1157 m, 1090 m, 1066 m, 1053 m, 1004 m, 990 w, 914 m, 893 m, 835 s, 833 s, 820 s, 800 s, 770 s, 745 s, 719 s, 678 m, 624 m; UV/vis ($CH_2Cl_2$, 5.0 × 10$^{-5}$ mol dm$^{-3}$) $\lambda_{max}$/nm 242 ($\varepsilon$/dm$^3$ mol$^{-1}$ cm$^{-1}$ 27700), 268 (29700), 297 (27000), sh 330 (17000), 430 (3200), 530 (1800); ESI MS *m/z* 533.0 $[M–PF_6]^+$ (base peak, calc. 533.2); EA: calc. for $C_{30}H_{26}CuF_6N_6P$ C 53.06 %, H 3.86 %, N 12.38%, found C 52.13 %, H 4.01 %, N 12.44 %.

### 4.2.3 [Cu(2)$_2$][PF$_6$]

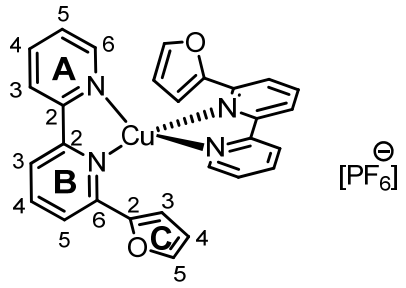

[Cu(**2**)$_2$][PF$_6$] was isolated as red crystals (28 mg, 95 %). $^1$H NMR (500 MHz, $CDCl_3$) $\delta$ (ppm) 8.32 (br, 4 H, $H^{3A+B}$), 8.15 (br, 2 H, $H^{6A}$), 8.07 (br, 4 H, $H^{4A+B}$), 7.86 (br, 2 H, $H^{5B}$), 7.51 (br, 2 H, $H^{5A}$), 7.07 (br, 2 H, $H^{5C}$), 6.85 (br, 4 H, $H^{3C}$), 6.05 (br, 2 H, $H^{4C}$); IR (solid, $\nu$/cm$^{-1}$) 3159 w, 3132 w, 2961 w, 2932 w, 2868 w, 2361 w, 2326 w, 1981 w, 1724 w, 1599 w, 1558 w, 1497 w, 1474 w, 1452 w, 1439 w, 1412 w, 1321 w, 1298 w, 1275 w, 1248 w, 1223 w, 1165 w, 1101 w, 1074 w, 1011 w, 995 w, 914 w, 881 w, 849 s, 825 s, 762 s, 744 s, 731 w, 690 w, 675 w; UV/vis ($CH_2Cl_2$, 1.0 × 10$^{-5}$ mol dm$^{-3}$) $\lambda_{max}$/nm 240 ($\varepsilon$/dm$^3$ mol$^{-1}$ cm$^{-1}$ 26300), 275 (21100), 300 (19000), 328 (23800), 420 (2600), 520 (1900); ESI MS: *m/z* 507.1 [M–PF$_6$]$^+$ (base peak, calc. 507.1); EA: calc. for $C_{28}H_{20}CuF_6N_4O_2P$ C 51.50 %, H 3.09 %, N 8.58 %, found: C 52.30 %, H 3.08 %, N 8.39 %.

### 4.2.4 [Cu(3)$_2$][PF$_6$]

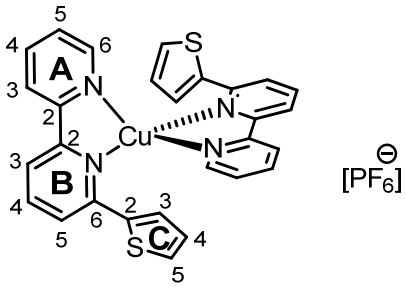

[Cu(**3**)$_2$][PF$_6$] was isolated as red crystals (33 mg, 97 %). $^1$H NMR (500 MHz, $CD_2Cl_2$) $\delta$ (ppm) 8.32 (br, 2 H, $H^{3A}$), 8.22 (br, 2 H, $H^{6A}$), 8.05 (br, 4 H, $H^{4A+B}$), 7.94 (br, 2 H, $H^{4B}$), 7.61 (br, 2 H, $H^{5B}$), 7.51 (br, 2 H, $H^{5A}$), 7.27 (br, 2 H, $H^{5C}$), 6.99 (br, 2 H, $H^{3C}$), 6.61 (br, 2 H, $H^{4C}$); IR (solid, $\nu$/cm$^{-1}$) 3109 w, 2348 w, 1669 w, 1593 m, 1558 m, 1526 w, 1480 w, 1447 s, 1423 m, 1394 m, 1353 w, 1258 m, 1228 m, 1177 m, 1162 m, 1120 w, 1092 w, 1057 w, 1002 w, 825 s, 814 s, 770 s, 740 s, 702 s, 690 s, 655 m, 633 m; UV/vis ($CH_2Cl_2$, 2.1 × 10$^{-5}$ mol dm$^{-3}$) $\lambda_{max}$/nm 242 ($\varepsilon$/dm$^3$ mol$^{-1}$ cm$^{-1}$ 32400), 270 (22600), 320 (22400), 410 (2500), 530 (1600); ESI MS: *m/z* 539.0 [M–PF$_6$]$^+$ (base peak, calc. 539.0). EA: calc. for $C_{28}H_{20}CuF_6N_4PS_2$ C 49.09 %, H 2.94 %, N 8.18 %, found: C 49.12 %, H 2.99 %, N 7.90 %.

### 4.2.5 [Cu(4)$_2$][PF$_6$]

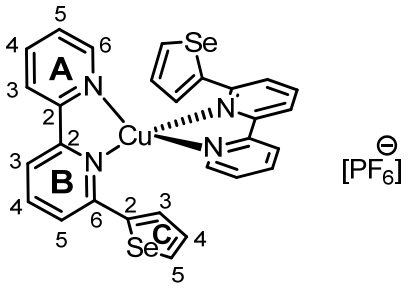


[Cu(**4**)$_2$][PF$_6$] was isolated as red crystals (37 mg, 95 %). $^1$H NMR (500 MHz, $CD_2Cl_2$) $\delta$ (ppm) 8.30 (br, 2 H, H$^{6A}$), 8.23 (br, 2 H, H$^{4B}$), 8.06 (br, 2 H, H$^{3A+B}$), 7.99 (br, 2 H, H$^{4A}$), 7.76 (br, 2 H, H$^{5C}$), 7.67 (br, 2 H, H$^{5B}$), 7.48 (br, 4 H, H$^{3C+5A}$), 6.92 (br, 2 H, H$^{4C}$); IR (solid, $\nu$/cm$^{-1}$) 3115 w, 3101 w, 2926 w, 2854 w, 2361 w, 2338 w, 1724 w, 1653 w, 1593 w, 1558 w, 1539 w, 1481 w, 1448s, 1433 w, 1394 w, 1340 w, 1294 w, 1258 w, 1225 w, 1178 w, 1161 w, 1121 w, 1078 w, 1053 w, 1016 w, 999 w, 972 w, 827s, 768 w, 741 w, 692 w, 677 w, 654 w, 608 w; UV/vis ($CH_2Cl_2$, 1.0×10$^{-5}$ mol dm$^{-3}$) $\lambda_{max}$/nm 247 ($\varepsilon$/dm$^3$ mol$^{-1}$ cm$^{-1}$ 29000), 273 (25300), 322 (22200), 413 (3100), 531 (2300); ESI MS: *m/z* 635.0 [M–PF$_6$]$^+$ (base peak, calc. 634.9). EA: calc. for $C_{28}H_{20}CuF_6N_4PSe_2$, C 43.18 %, H 2.59 %, N 7.19 %, found: C 43.37 %, H 2.73 %, N 6.88 %.

### 4.2.6 [Cu(5)$_2$][PF$_6$]

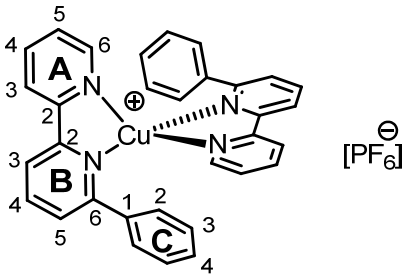


[Cu(**5**)$_2$][PF$_6$] was isolated as red crystals (30 mg, 89 %). $^1$H NMR (500 MHz, $CD_2Cl_2$) $\delta$ (ppm) 8.53 (d, *J* 4.7 Hz, 2 H, H$^{6A}$), 8.16 (d, *J* 8.1 Hz, 2 H, H$^{3A}$), 8.08 (t, *J* 7.7 Hz, 2 H, H$^{4A}$), 7.92 (m, *J* 4.5 Hz, 4 H, H$^{3B+5B}$), 7.57 (m, 2 H, H$^{5A}$), 7.52 (m, 2 H, H$^{4B}$), 7.29 (d, *J* 7.5 Hz, 4 H, H$^{2C}$), 7.02 (t, *J* 7.4 Hz, 2 H, H$^{4C}$), 6.80 (t, *J* 7.6 Hz, 4 H, H$^{3C}$); $^{13}$C{$^1$H} NMR (126 MHz, $CD_2Cl_2$) $\delta$ (ppm) 158.2 (C$^{6B}$), 152.8 (C$^{2A/2B}$), 152.6 (C$^{2A/2B}$), 148.9 (C$^{6A}$), 139.5 (C$^{1C}$), 138.7 (C$^{5B}$), 138.4 (C$^{4A}$), 129.6 (C$^{4C}$), 128.1 (C$^{3C}$), 127.8 (C$^{2C}$), 126.8 (C$^{5A}$), 125.4 (C$^{4B}$), 122.8 (C$^{3A}$), 120.7 (C$^{3B}$); IR (solid, $\nu$/cm$^{-1}$) 3055 w, 2959 w, 2926 w, 2868 w, 2366 w, 2326 w, 1724 w, 1595 w, 1570 w, 1558 w, 1477 w, 1445 s, 1391 w, 1288 w, 1277 w, 1240 w, 1184 w, 1161 w, 1122 w, 1076 w, 1043 w, 1014 w) 1003 w, 928 w, 903 w, 878 w, 831 s, 814 s, 779 s, 754 s, 741 s, 698 s, 636 w; UV/vis ($CH_2Cl_2$, 1.0 × 10$^{-5}$ mol dm$^{-3}$) $\lambda_{max}$/nm 232 ($\varepsilon$/dm$^3$ mol$^{-1}$ cm$^{-1}$ 38100), 263 (28500), 308 (26200), 419 (4400), 526 (3000); ESI MS: *m/z* 527.2 [M–PF$_6$]$^+$ (base peak, calc. 527.1). EA:

calc. for $C_{32}H_{24}CuF_6N_4P{\cdot}EtOH$ C 56.79 %, H 4.20 %, N 7.79%, found C 57.22 %, H 3.95 %, N 7.41 %.

### 4.2.7 [Cu(6)$_2$][PF$_6$]

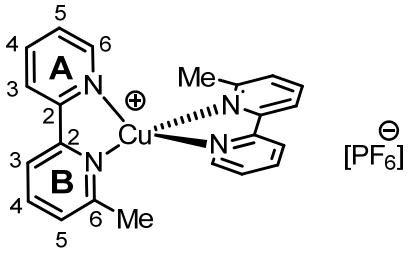


[Cu(**6**)$_2$][PF$_6$] was isolated as red crystals (25 mg, 91 %). $^1$H NMR (500 MHz, $CD_2Cl_2$) $\delta$ (ppm) 8.49 (ddd, *J* 5.0, 1.5, 0.8 Hz, 2 H, H$^{6A}$), 8.34 (d, *J* 8.2 Hz, 2 H, H$^{3A}$), 8.19 (d, *J* 8.0 Hz, 2 H, H$^{3B}$), 8.10 (td, *J* 7.8, 1.6 Hz, 2 H, H$^{4A}$), 8.01 (t, *J* 7.8 Hz, 2 H, H$^{4B}$), 7.55 (ddd, *J* 7.5, 5.1, 1.1 Hz, 2 H, H$^{5A}$), 7.48 (d, *J* 7.7 Hz, 2 H, H$^{5B}$), 2.26 (s, 6 H, H$^{Me}$); $^{13}$C{$^1$H} NMR (126 MHz, $CD_2Cl_2$) $\delta$ (ppm) 158.1 (C$^{6B}$), 152.9 (C$^{2A}$), 151.9 (C$^{2B}$), 149.3 (C$^{6A}$), 138.8 (C$^{4B}$), 138.6 (C$^{4A}$), 126.8 (C$^{5A}$), 126.6 (C$^{5B}$), 122.6 (C$^{3A}$), 119.6 (C$^{3B}$), 25.6 (C$^{Me}$); IR (solid, $\nu$/cm$^{-1}$) 3080 w, 2920 w, 2853 w, 2361 w, 2336 w, 1653 w, 1595 w, 1558 w, 1558 w, 1452 s, 1379 w, 1300 w, 1252 w, 1238 w, 1180 w, 1161 w, 1101 w, 1053 w, 1009 w, 910 w, 876 w, 827 s, 812 s, 766 s, 723 w, 652 w, 631 w; UV/vis ($CH_2Cl_2$, 1.0 × 10$^{-4}$ mol dm$^{-3}$) $\lambda_{max}$/nm 249 ($\varepsilon$/dm$^3$ mol$^{-1}$ cm$^{-1}$ 20000), 265 (25600), 295 (32200), sh 309 (20000), 458 (6400), 530 (1400); ESI MS: *m/z* 403.2 [M–PF$_6$]$^+$ (base peak, calc. 403.1). EA: calc. for $C_{22}H_{20}CuF_6N_4P$ C 48.14 %, H 3.67 %, N 10.21 % found C 48.27 % H 3.81 % N 10.05 %.

### 4.2.8 [Cu(10)$_2$][PF$_6$]

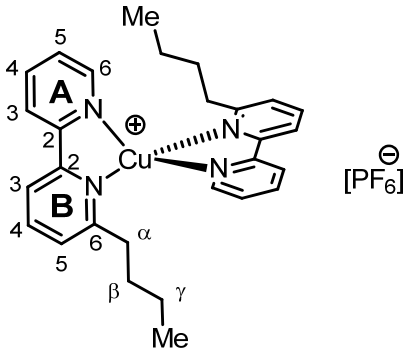


[Cu(**10**)$_2$][PF$_6$] was isolated as bright red crystals (24 mg, 75 %). $^1$H NMR (500 MHz, $CD_2Cl_2$) $\delta$(ppm) 8.53 (dt, *J* 5.1, 1.3 Hz, 2 H, H$^{A6}$), 8.33 (dt, *J* 8.2, 1.1 Hz, 2 H, H$^{3A}$), 8.18 (dd, *J* 8.0, 1.0 Hz, 2 H, H$^{3B}$), 8.10 (ddd, *J* 8.1, 7.7, 7.7, 1.0 Hz, 2 H, H$^{4A}$), 8.03 (t, *J* 7.8 Hz, 2 H, H$^{4B}$), 7.56 (ddd, *J* 7.5, 5.1, 1.1 Hz, 2 H, H$^{5A}$), 7.47 (dd, *J* 7.7, 1.0 Hz, 2 H, H$^{5B}$), 2.52 (q, *J* 8.1 Hz, 4 H, H$^{\alpha}$), 1.36-1.27 (m, 4 H, H$^{\beta}$), 0.93-0.70 (m, 4 H, H$^{\gamma}$), 0.47 (t, *J* 7.4 Hz, 6 H, H$^{Me}$); All other analytical data match those previously reported.[25,41]

### 4.2.9 [Cu(12)$_2$][PF$_6$]

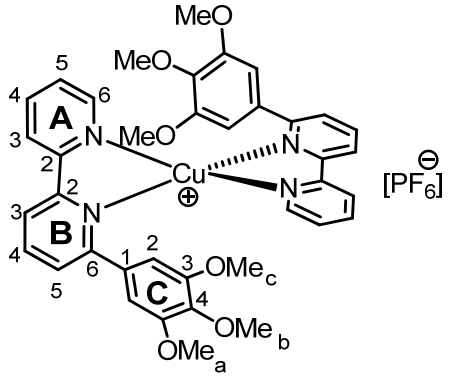


This reaction was carried out on a scale of 31.5 µmol. [Cu(**12**)$_2$][PF$_6$] was isolated as dark red crystals (24 mg, 90 %). $^1$H NMR (400 MHz, $CD_2Cl_2$) $\delta$ (ppm) 8.48 (br s, 2 H, $H^{A6}$), 8.19 (br d, *J* 8.4 Hz, 2 H, $H^{3A}$), 8.08 (br s, 2 H, $H^{3B}$), 8.00 (br s, 4 H, $H^{4A+B}$), 7.57 (br s, 4 H, $H^{5A+B}$), 6.58 (s, 4 H, $H^{2C}$), 3.64 (s, 6 H, $H^{OMe}{}_b$), 3.43 (s, 12 H, $H^{OMe}{}_a$); ESI-MS *m/z*: 707.3 [M-PF$_6$]$^+$ (100 %, calc. 707.2).

### 4.2.10 [Cu(20)$_2$][PF$_6$]

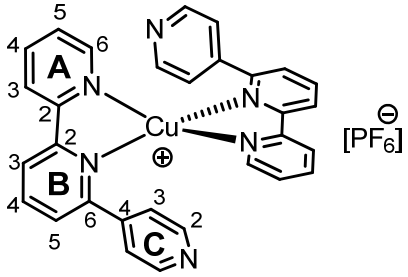


[Cu(**20**)$_2$][PF$_6$] was isolated as red crystals (20 mg, 60 %). $^1$H NMR (500 MHz, $CD_2Cl_2$) $\delta$ (ppm) 8.63 (br s, 2 H, $H^{6A}$), 8.27 (br s, 4 H, $H^{3+4A}$), 8.13 (br s, 4 H, $H^{3+4B}$), 8.04 (br s, 4 H, $H^{2C}$), 7.63 (br s, 4 H, $H^{2C}$), 7.51 (br s, 4 H, $H^{3C}$); ESI-MS *m/z*: 529.2 [M-PF$_6$]$^+$ (100 %, calc. 529.1).

### 4.2.11 [Cu(21)$_2$][PF$_6$]

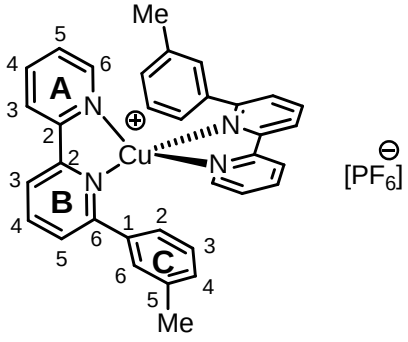


$^1$H NMR (500 MHz, $CD_2Cl_2$) $\delta$ (ppm) 8.56 (br s, 2 H, $H^{6A}$), 8.15 (br s, 2 H, $H^{3A}$), 8.10 (br s, 2 H, $H^{3B}$), 7.89 (br s, 4 H, $H^{3+4B}$), 7.56 (br s, 2 H, $H^{5A}$), 7.51 (br s, 2 H, $H^{5B}$), 7.17 (br s, 2 H, $H^{6C}$), 7.05

(br s, 2 H, $H^{5C}$), 6.85 (s, 2 H, $H^{2C}$), 6.76 (br s, 2 H, $H^{4C}$); ESI-MS *m/z*: 555.3 $[M\text{-}PF_6]^+$ (100 %, calc. 555.2).

### 4.2.12 $[Cu(30)_2][PF_6]$

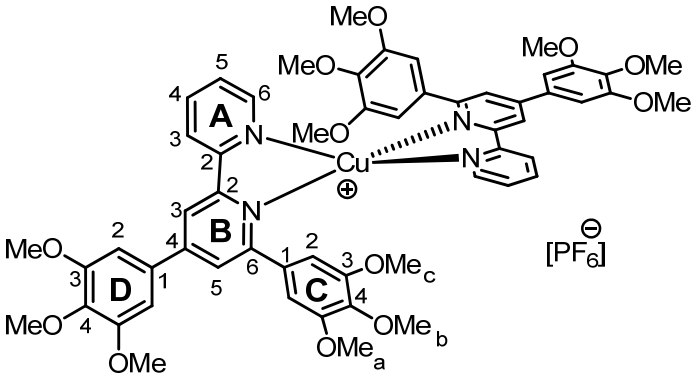


$^1$H NMR (400 MHz, $CD_2Cl_2$) $\delta$ (ppm) 8.77 (br s, 2 H, $H^{6A}$), 8.27 (br d, 2 H, $H^{3A}$), 8.17 (br t, 2 H, $H^{4A}$), 7.97 (br s, 2 H, $H^{3B}$), 7.70 (br t, 2 H, $H^{5A}$), 7.60 (br s, 2 H, $H^{5B}$), 6.93 (s, 4 H, $H^{2D}$), 6.54 (s, 4 H, $H^{2C}$), 3.99 (s, 12 H, $H^{OMe_aC}$), 3.88 (s, 6 H, $H^{OMe_bC}$), 3.66 (s, 6 H, $H^{OMe_bD}$), 3.31 (s, 12 H, $H^{OMe_aD}$); ESI-MS *m/z*: 1039.4 $[M\text{-}PF_6]^+$ (100 %, calc. 1039.3).

### 4.2.13 $[Cu(31)_2][PF_6]$

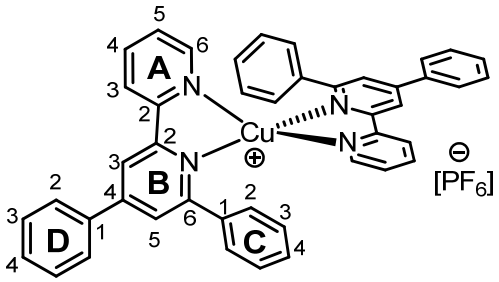


$^1$H NMR (400 MHz, $CD_2Cl_2$) $\delta$ (ppm) 8.65 (br s, 2 H, $H^{6A}$), 8.24 (br s, 2 H, $H^{3A}$), 8.13 (br s, 2 H, $H^{4A}$), 8.03 (br s, 2 H, $H^{3B}$), 7.74 (br s, 6 H, $H^{5A+2C}$), 7.68-7.50 (br m, 8 H, $H^{5B+4C+2C}$), 7.39 (br s, 4 H, $H^{3C}$), 7.06 (br s, 2 H, $H^{4D}$), 6.83 (br s, 4 H, $H^{3D}$); ESI-MS *m/z*: 679.2 $[M\text{-}PF_6]^+$ (100 %, calc. 679.2).

### 4.2.14 $[Cu(32)_2][PF_6]$

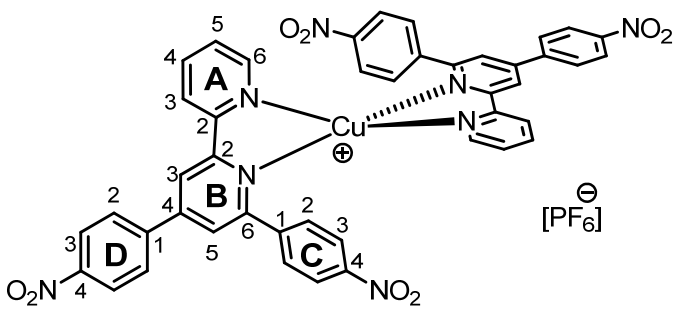

$^1$H NMR (400 MHz, $CD_2Cl_2$) $\delta$ (ppm) 8.68 (d, *J* 4.2 Hz, 2 H, $H^{6A}$), 8.47 (d, *J* 8.4 Hz, 4 H, $H^{3D}$), 8.31 (d, *J* 8.0 Hz, 2 H, $H^{3A}$), 8.21 (t, *J* 7.6 Hz, 2 H, $H^{4A}$), 8.15 (s, 2 H, $H^{3B}$), 8.01 (br s, 2 H, $H^{2C}$), 7.96 (d, *J* 8.4 Hz, 4 H, $H^{2D}$), 7.91 (s, 2 H, $H^{5B}$), 7.73 (t, *J* 6.5 Hz, 2 H, $H^{5A}$), 7.66 (s, 4 H, $H^{3C}$); ESI-MS *m/z*: 859.2 $[M\text{-}PF_6]^+$ (100 %, calc. 859.1).

### 4.2.15 $[Cu(34)_2][PF_6]$

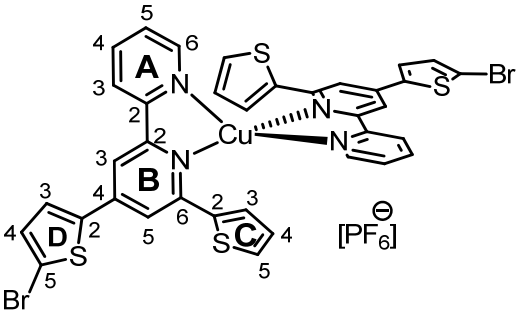

$^1$H NMR (500 MHz, $CD_2Cl_2$, 240 K) $\delta$ (ppm) 8.71 (s, 2 H, $H^{6A}$), 8.28 (d, *J* 6.4 Hz, 2 H, $H^{3A}$), 8.10 (t, *J* 6.4 Hz, 2 H, $H^{4A}$), 8.00 (s, 2 H, $H^{3B}$), 7.64-7.50 (m, 6 H, $H^{5A+B+4D}$), 7.30 (s, 2 H, $H^{5C}$), 7.24 (s, 2 H, $H^{3D}$), 7.00 (s, 2 H, $H^{3C}$), 6.61 (s, 2 H, $H^{4C}$); ESI-MS *m/z*: 858.9 $[M\text{-}PF_6]^+$ (100 %, calc. 858.8).

### 4.2.16 $[Cu(3)_2]$[Δ-TRISPHAT®]

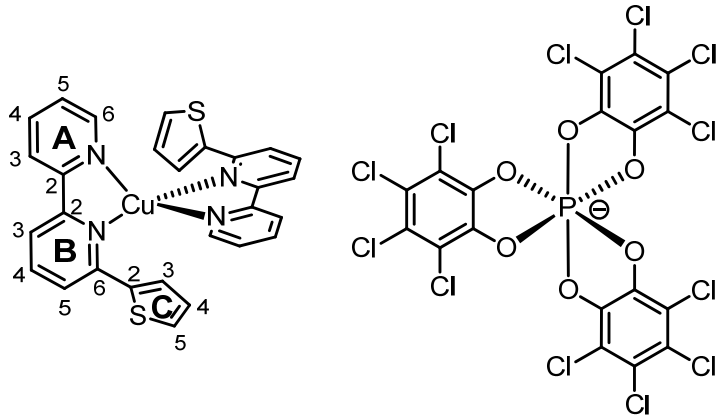

$^1$H NMR (600 MHz, $CD_2Cl_2$) $\delta$ (ppm) 8.32 (br s, 2 H, $H^{6A}$), 8.15 (br d, 2 H, $H^{3A}$), 7.99 (br s, 4 H, $H^{4A+3B}$), 7.92 (br s, 2 H, $H^{4B}$), 7.63 (br s, 2 H, $H^{5A}$), 7.46 (br s, 2 H, $H^{5B}$), 7.28 (s, 2 H, $H^{5C}$), 7.00 (s, 2 H, $H^{3C}$), 6.62 (s, 2 H, $H^{4C}$); ESI-MS *m/z*: 539.1 [M-TRISPHAT]$^+$ (100 %, calc. 539.0).

### 4.2.17 $[Cu(2)_2][PF_6]_2$

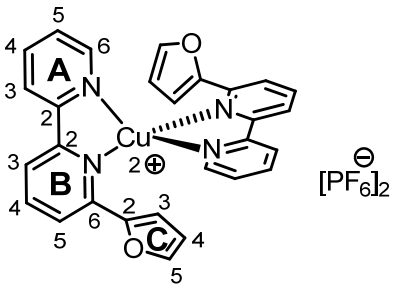

**Method 1**

$CuNO_3$*3 $H_2O$ (7.6 mg, 31.5 µmol) and $NH_4PF_6$ (25.6 mg, 157 µmol) were dissolved in 2 ml $H_2O$ then diluted with 10 ml MeCN. Ligand **2** (14.0 mg, 63.0 µmol) was added in one portion and the pale green solution turned dark green within minutes and a white floccose precipitate formed. This was filtered off and the solution was allowed to slowly evaporate. Over two days green single crystals formed on the upper wall of the vial (lose solvent in air). Upon complete evaporation of the solvents dark red crystals formed. $^1$H NMR (500 MHz, MeCN-$d_3$) $\delta$ (ppm) 10.58 (br s, 6 H), 10.28 (br s, 6 H), 10.00 (br s, 4 H); FAB-MS *m/z*: 301.0 [M-**2**-2$PF_6$]$^+$ (100 %, calc. 301.9), 539.0 [M-2$PF_6$]$^+$ (50 %, calc. 539.0), 683.9 [M-$PF_6$]$^+$ (2 %, calc. 684.0).

**Method 2**

$CuCl_2$*2 $H_2O$ (5.4 mg, 31.5 µmol) and $NH_4PF_6$ (51.3 mg, 315 µmol) were dissolved in 1 ml $H_2O$ then diluted with 10 ml MeCN. Ligand **2** (14.0 mg, 63.0 µmol) was added in one portion and the pale green solution turned dark green within minutes and a white floccose precipitate formed. This was filtered off, the solvent was removed from the filtrate and the dark residue was extracted with MeCN. The evaporation of the solvent yielded dark red crystals. $^1$H NMR (500 MHz, MeCN-$D_3$) $\delta$ (ppm) 11.81 (br s, 2 H), 9.69 (br s, 4 H), 9.21 (br s, 4 H), 8.77 (br s, 6 H), 7.87 (br s, 4 H).

### 4.2.18 $[Cu(3)_2][PF_6]_2$

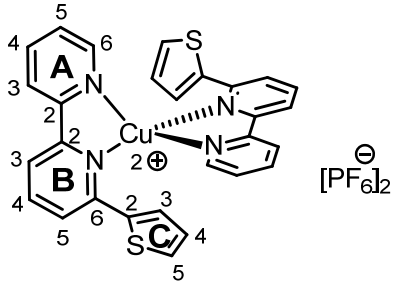


The compounds were prepared following the same procedures as for the previous composite:

**Method 1**

$CuNO_3$*3 $H_2O$ (7.6 mg, 31.5 µmol); (25.6 mg, 157 µmol); ligand **3** (15.0 mg, 63.0 µmol); dark red crystals were obtained. $^1$H NMR (500 MHz, MeCN-$D_3$) $\delta$ (ppm) 8.60 (br s), 7.80 (br s), 7.22 (br s).

**Method 2**

$CuCl_2$*2 $H_2O$ (5.4 mg, 31.5 µmol); (51.3 mg, 315 µmol); ligand **3** (15.0 mg, 63.0 µmol); dark red crystals were obtained. $^1$H NMR (500 MHz, MeCN-$D_3$) $\delta$ (ppm) 8.07 (br s), 7.32 (br s).

### 4.2.19 $[Cu(4)_2][PF_6]_2$

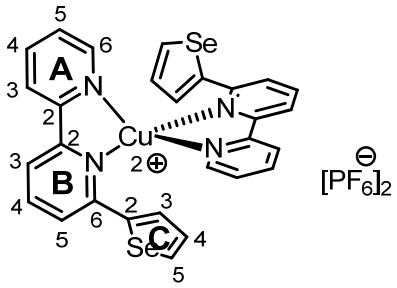

The compounds were prepared following the same procedures as for the previous composite:

**Method 1**

$CuNO_3$*3 $H_2O$ (7.6 mg, 31.5 µmol); (25.6 mg, 157 µmol); ligand **4** (18.0 mg, 63.0 µmol); dark red crystals were obtained. $^1$H NMR (500 MHz, MeCN-$D_3$) $\delta$(ppm) 8.90 (br s), 8.21 (br s), 7.08 (br s).

**Method 2**

$CuCl_2$*2 $H_2O$ (5.4 mg, 31.5 µmol); (51.3 mg, 315 µmol); ligand **3** (15.0 mg, 63.0 µmol); dark red crystals were obtained. $^1$H NMR (500 MHz, MeCN-$D_3$) $\delta$(ppm) 8.89 (br s), 8.20 (br s), 7.08 (br s).

### 4.2.20 $[Ag(2)_2][PF_6]$

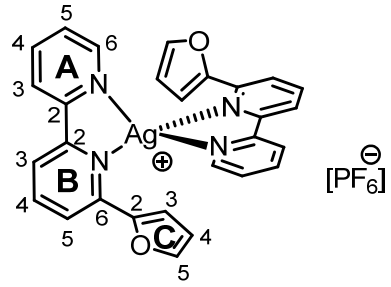

$AgPF_6$ (6.3 mg, 25 µmol) and ligand **2** (11.1 mg, 50 µmol) were dissolved in $CH_2Cl_2$ in the dark. The solution turned slowly yellow and was stirred for 2 h with TLC monitoring until all free ligand has been consumed. The solution was filtered to remove any black precipitate, then the solvent was allowed to evaporate slowly, yielding the desired product as pale yellow single crystals (16.0 mg, 92 %). $^1$H NMR (500 MHz, $CD_2Cl_2$) $\delta$ (ppm) 8.62 (ddd, *J* 5.0, 1.6, 0.9 Hz, 2 H, $H^{6A}$), 8.23 (d, *J* 8.1 Hz, 2 H, $H^{3A}$), 8.10 (td, *J* 8.0, 7.8, 1.7 Hz, 2 H, $H^{4A}$), 8.02-7.96 (m, 4 H, $H^{3+4B}$), 7.76 (dd, *J* 6.6, 2.2 Hz, 2 H, $H^{5B}$), 7.58 (ddd, *J* 7.7, 5.1, 1.2 Hz, 2 H, $H^{5A}$), 7.00 (s, 2 H, $H^{5C}$), 6.98 (d, *J* 3.4 Hz, 2 H, $H^{3C}$), 6.15 (dd, *J* 3.3, 1.7 Hz, 1 H, $H^{4C}$); $^{13}$C NMR (101 MHz, $CD_2Cl_2$) $\delta$ (ppm) 153.35 ($C^{2B}$), 152.03 ($C^{6B}$), 151.30 ($C^{2A}$), 151.27 ($C^{6A}$), 149.63 ($C^{2C}$),

144.35 ($C^{5C}$), 139.95 ($C^{4A}$), 139.70 ($C^{4B}$), 126.12 ($C^{5A}$), 123.83 ($C^{3A}$), 121.75 ($C^{4B}$), 121.54 ($C^{3B}$), 112.56 ($C^{4C}$), 110.65 ($C^{3C}$); FAB-MS *m/z*: 551.2 $[M\text{-}PF_6]^+$ (80 %, calc. 551.0).

### 4.2.21 $[Ag(3)_2][PF_6]$

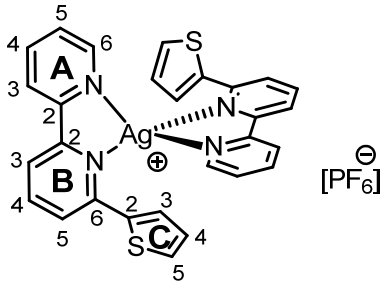

$AgPF_6$ (12.6 mg, 50 μmol) and ligand **3** (23.8 mg, 100 μmol) were dissolved in $CH_2Cl_2$ in the dark. The solution turned slowly yellow and was stirred for 2 h with TLC monitoring until all free ligand has been consumed. The solution was filtered to remove any black precipitate, then the solvent was allowed to evaporate slowly, yielding the desired product as pale yellow single crystals (30.0 mg, 82 %). $^1$H NMR (400 MHz, $CD_2Cl_2$) $\delta$ (ppm) 8.42 (d, *J* 4.6 Hz, 2 H, $H^{6A}$), 8.13 (d, *J* 7.9 Hz, 2 H, $H^{3A}$), 8.06 (td, *J* 9.2, 7.9, 1.4 Hz, 2 H, $H^{4A}$), 7.99 (t, *J* 7.8, 7.8 Hz, 2 H, $H^{4B}$), 7.92 (d, *J* 7.2 Hz, 2 H, $H^{3B}$), 7.74 (dd, *J* 7.7, 1.0 Hz, 2 H, $H^{5B}$), 7.53 (t, *J* 5.2 Hz, 2 H, $H^{5A}$), 7.47 (d, *J* 2.8 Hz, 2 H, $H^{5C}$), 7.04 (d, *J* 4.5 Hz, 2 H, $H^{3C}$), 6.84 (dd, *J* 5.0, 3.7 Hz, 2 H, $H^{4C}$); ESI-MS *m/z*: 583.2 $[M\text{-}PF_6]^+$ (100 %, calc. 583.0).

### 4.2.22 $[Ag(4)_2][PF_6]$

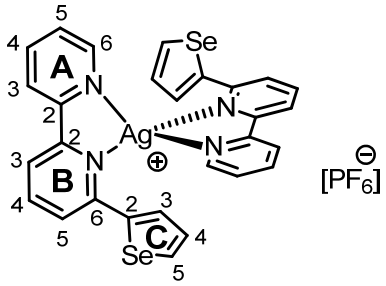

$AgPF_6$ (7.8 mg, 31 μmol) and ligand **4** (17.6 mg, 62 μmol) were dissolved in $CH_2Cl_2$ in the dark. The solution turned slowly yellow and was stirred at room temperature with TLC monitoring until all free ligand has been consumed. The solution was filtered to remove any black precipitate, then the solvent was allowed to evaporate slowly, yielding the desired product as pale yellow single crystals (24.8 mg, 98 %). $^1$H NMR (400 MHz, $CD_2Cl_2$) $\delta$ (ppm) 8.37 (d, *J* 5.0 Hz, 2 H, $H^{6A}$), 8.10 (d, *J* 8.0 Hz, 2 H, $H^{3A}$), 8.04 (td, *J* 7.7, 1.7 Hz, 2 H, $H^{4A}$), 7.98 (t, *J* 7.8 Hz, 2 H, $H^{4B}$), 7.90 (dd, *J* 7.8, 0.9 Hz, 2 H, $H^{3B}$), 7.76-7.72 (m, 4 H, $H^{5C+B}$), 7.62 (dd, *J* 4.0, 1.1 Hz, 2 H, $H^{3C}$), 7.51 (ddd, *J* 7.7, 5.0, 1.1 Hz, 2 H, $H^{5A}$), 7.12 (dd, *J* 5.5, 4.0 Hz, 2 H, $H^{4C}$); $^{13}$C NMR (101 MHz, $CD_2Cl_2$) $\delta$ (ppm) 155.26 ($C^{2B}$), 153.70 ($C^{2A}$), 153.13 ($C^{6B}$), 151.09 ($C^{6A}$), 149.68 ($C^{2C}$), 139.99 ($C^{4B}$), 139.72 ($C^{4A}$), 134.19 ($C^{5C}$), 131.46 ($C^{4C}$), 129.99 ($C^{3C}$), 126.02 ($C^{5A}$),

123.99 ($C^{3A}$), 122.47 ($C^{5B}$), 122.06 ($C^{3B}$); $^{77}$Se NMR (600 MHz, $CD_2Cl_2$) $\delta$ (ppm) 591.49; ESI-MS *m/z*: 678.9 $[M\text{-}PF_6]^+$ (100 %, calc. 678.9).

### 4.2.23 [Ag(3)$_2$][BF$_4$]

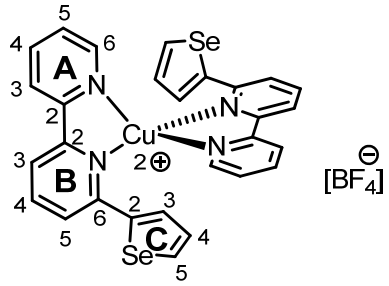


$AgBF_4$ (12.4 mg, 64 μmol) and ligand **4** (36.3 mg, 127 μmol) were dissolved in $CH_2Cl_2$ in the dark. The solution turned slowly yellow and was stirred for 2 h with TLC monitoring until all free ligand has been consumed. The solution was filtered to remove any black precipitate, then the solvent was allowed to evaporate slowly, yielding the desired product as pale yellow single crystals (48.0 mg, 99 %).$^1$H NMR (400 MHz, $CD_2Cl_2$) $\delta$ (ppm) 8.49 (br s, 2 H, $H^{6A}$), 8.24 (br s, 2 H, $H^{3A}$), 8.11-7.98 (m, 4 H, $H^{4A+3B}$), 7.95 (t, *J* 7.7 Hz, 2 H, $H^{4B}$), 7.87 (d, *J* 5.2 Hz, 2 H, $H^{3C}$), 7.76 (d, *J* 7.6 Hz, 2 H, $H^{5B}$), 7.70 (d, *J* 2.5 Hz, 2 H, $H^{5C}$), 7.51 (br s, 2 H, $H^{5A}$), 7.12 (t, *J* 4.3 Hz, 2 H, $H^{4C}$); ESI-MS *m/z*: 678.9 $[M\text{-}BF_4]^+$ (100 %, calc. 678.9).

### 4.2.24 Crystal structure determinations

#### 4.2.24.1 [Cu(1)$_2$][PF$_6$]

$C_{30}H_{26}CuF_6N_6P$, $M$ = 679.08, red block, monoclinic, space group $C2/c$, $a$ = 15.5702(6), $b$ = 12.5528(5), $c$ = 15.1905(6) Å, $\beta$ = 102.575(2)°, $U$ = 2897.8(2) Å$^3$, $Z$ = 4, $D_c$ = 1.556 Mg m$^{-3}$, $\mu$(Mo-K$_\alpha$) = 0.880 mm$^{-1}$, $T$ = 123 K. Total 79592 reflections, 7731 unique, $R_{int}$ = 0.040. Refinement of 6961 reflections (200 parameters) with $I > 2\sigma(I)$ converged at final $R1$ = 0.0319 ($R1$ all data = 0.0345), $wR2$ = 0.0339 ($wR2$ all data = 0.0466), gof = 1.0580.

#### 4.2.24.2 [Cu(2)$_2$][PF$_6$]

$C_{28}H_{20}CuF_6N_4O_2P$, $M$ = 653.00, red plate, monoclinic, space group $P2_1/c$, $a$ = 11.6298(5), $b$ = 8.6881(3), $c$ = 13.7113(6) Å, $\beta$ = 107.915(2)°, $U$ = 1318.23(9) Å$^3$, $Z$ = 2, $D_c$ = 1.645 Mg m$^{-3}$, $\mu$(Mo-K$_\alpha$) = 0.967 mm$^{-1}$, $T$ = 123 K. Total 61626 reflections, 9825 unique, $R_{int}$ = 0.036. Refinement of 8405 reflections (191 parameters) with $I > 2\sigma(I)$ converged at final $R1$ = 0.0394 ($R1$ all data = 0.0470), $wR2$ = 0.0354 ($wR2$ all data = 0.0613), gof = 0.9996.

#### 4.2.24.3 $[Cu(3)_2][PF_6]$

$C_{28}H_{20}CuF_6N_4PS_2$, $M$ = 685.13, red block, triclinic, space group $P$–1, $a$ = 7.1898(2), $b$ = 14.0902(3), $c$ = 14.6598(4) Å, $\alpha$ = 103.270(2), $\beta$ = 99.206(2), $\gamma$ = 98.373(2)°, $U$ = 1400.92(7) Å$^3$, $Z$ = 2, $D_c$ = 1.624 Mg m$^{-3}$, $\mu$(Mo-K$_\alpha$) = 1.053 mm$^{-1}$, $T$ = 123 K. Total 22905 reflections, 7740 unique, $R_{int}$ = 0.046. Refinement of 4821 reflections (114 parameters) with $I$ >2σ ($I$) converged at final $R$1 = 0.0404 ($R$1 all data = 0.0770), $wR$2 = 0.0389 ($wR$2 all data = 0.0696), gof = 1.0610.

#### 4.2.24.4 $[Cu(4)_2][PF_6]$

$C_{28}H_{20}CuF_6N_4PSe_2$, $M$ = 778.91, red block, monoclinic, space group $P2_1/n$, $a$ = 7.8556(16), $b$ = 31.553(6), $c$ = 14.506(3) Å, $\alpha$ = 90.00, $\beta$ = 100.80(3), $\gamma$ = 90.00°, $U$ = 3531.8(12) Å$^3$, $Z$ = 4, $D_c$ = 1.465 Mg m$^{-3}$, $\mu$(Mo-K$_\alpha$) = 2.778 mm$^{-1}$, $T$ = 173 K. Total 58919 reflections, 8135 unique, $R_{int}$ = 0.31. Refinement of 8135 reflections (445 parameters) with $I$ >2σ ($I$) converged at final $R$1 = 0.2453 ($R$1 all data = 0.2659), $wR$2 = 0.5015 ($wR$2 all data = 0.5142), gof = 2.619.

#### 4.2.24.5 $[Cu(5)_2][PF_6]$

$C_{32}H_{24}CuF_6N_4P$, $M$ = 673.07, red plate, monoclinic, space group $C2/c$, $a$ = 8.0516(13), $b$ = 27.170(6), $c$ = 13.159(2) Å, $\beta$ = 96.239(13)°, $U$ = 2861.7(9) Å$^3$, $Z$ = 4, $D_c$ = 1.562 Mg m$^{-3}$, $\mu$(Mo-K$_\alpha$) = 0.889 mm$^{-1}$, $T$ = 173 K. Total 22088 reflections, 3452 unique, $R_{int}$ = 0.0572. Refinement of 3218 reflections (201 parameters) with $I$ >2σ ($I$) converged at final $R$1 = 0.0358 ($R$1 all data = 0.0390), $wR$2 = 0.0944 ($wR$2 all data = 0.0967), gof = 1.073.

#### 4.2.24.6 $[Cu(6)_2][PF_6]$

$C_{22}H_{20}CuF_6N_4P$, $M$ = 548.94, red block, triclinic, space group $P$–1, $a$ = 7.7042(8), $b$ = 10.2596(11), $c$ = 15.3283(14) Å, $\alpha$ = 107.978(8), $\beta$ = 97.393(8), $\gamma$ = 100.067(8)°, $U$ = 1112.90(19) Å$^3$, $Z$ = 2, $D_c$ = 1.638 Mg m$^{-3}$, $\mu$(Mo-K$_\alpha$) = 1.122 mm$^{-1}$, $T$ = 173 K. Total 23465 reflections, 4574 unique, $R_{int}$ = 0.0547. Refinement of 4378 reflections (309 parameters) with $I$ >2σ ($I$) converged at final $R$1 = 0.0414 ($R$1 all data = 0.0428), $wR$2 = 0.1117 ($wR$2 all data = 0.1130), gof = 1.049.

#### 4.2.24.7 $[Cu(12)_2][PF_6]$

$C_{40}H_{39}CuF_6N_5O_6P$, $M$ = 1039.25, black block, monoclinic, space group $Cc$, $a$ = 19.774(5), $b$ = 22.098(5), $c$ = 13.812(4) Å, $\alpha$ = 90.00, $\beta$ = 134.082, $\gamma$ = 90.00°, $U$ = 4335.6(21) Å$^3$, $Z$ = 4, $D_c$ = 1.592 Mg m$^{-3}$, $\mu$(Mo-K$_\alpha$) = 0.682 mm$^{-1}$, $T$ = 173 K. Total 35984 reflections, 9045 unique, $R_{int}$ = 0.0609. Refinement of 9045 reflections (603 parameters) with $I$ >2σ ($I$) converged at final $R$1 = 0.0575 ($R$1 all data = 0.0643), $wR$2 = 0.1478 ($wR$2 all data = 0.1535), gof = 1.064.

#### 4.2.24.8 $[Cu(21)_2][PF_6]$

$C_{41}H_{36}CuF_6N_4P$, $M$ = 793.27, red prism, monoclinic, space group $C2/c$, $a$ = 15.2714(15), $b$ = 23.760(3), $c$ = 10.9568(9) Å, $\alpha$ = 90.00, $\beta$ = 113.100, $\gamma$ = 90.00°, $U$ = 3656.7(6) Å$^3$, $Z$ = 4, $D_c$ = 1.441 Mg m$^{-3}$, $\mu$(Mo-K$_\alpha$) = 0.708 mm$^{-1}$, $T$ = 123 K. Total 164111 reflections, 11054 unique, $R_{int}$ = 0.061. Refinement of 7542 reflections (246 parameters) with $I$ >2σ ($I$) converged at final $R1$ = 0.0370 ($R1$ all data = 0.0541), $wR2$ = 0.0357 ($wR2$ all data = 0.0634), gof = 1.0462.

#### 4.2.24.9 $[Cu(30)_2][PF_6]$

$C_{242}H_{251}Cu_4F_{24}N_{25}O_{48}P_4$, $M$ = 5111. 72, red block, monoclinic, space group $C2/c$, $a$ = 15.8671(10), $b$ = 23.638(2), $c$ = 15.2654(9) Å, $\alpha$ = 90.00, $\beta$ = 95.629, $\gamma$ = 90.00°, $U$ = 5697.9(7) Å$^3$, $Z$ = 1, $D_c$ = 1.490 Mg m$^{-3}$, $\mu$(Mo-K$_\alpha$) = 0.502 mm$^{-1}$, $T$ = 173 K. Total 39681 reflections, 7218 unique, $R_{int}$ = 0.0451. Refinement of 7218 reflections (430 parameters) with $I$ >2σ ($I$) converged at final $R1$ = 0.0388 ($R1$ all data = 0.0427), $wR2$ = 0.1000 ($wR2$ all data = 0.1022), gof = 1.062.

#### 4.2.24.10 $[Cu(32)_2][PF_6]$

$C_{88}H_{100}Cu_2F_8N_{16}O_{20}P_2$, $M$ = 1911.09, red block, monoclinic, space group $P2_1/c$, $a$ = 14.500(10), $b$ = 20.794(4), $c$ = 13.632(3) Å, $\alpha$ = 90.00, $\beta$ = 97.89, $\gamma$ = 90.00°, $U$ = 4071.3(15) Å$^3$, $Z$ = 2, $D_c$ = 1.559 Mg m$^{-3}$, $\mu$(Mo-K$_\alpha$) = 0.646 mm$^{-1}$, $T$ = 173 K. Total 48827 reflections, 7213 unique, $R_{int}$ = 0.2961. Refinement of 7213 reflections (596 parameters) with $I$ >2σ ($I$) converged at final $R1$ = 0.1959 ($R1$ all data = 0.2222), $wR2$ = 0.4426 ($wR2$ all data = 0.4598), gof = 1.082.

#### 4.2.24.11 $[Cu(34)_2][PF_6]$

$C_{74}H_{50}Cu_2F_{12}N_8OP_2S_8$, $M$ = 2060.42, red plate, triclinic, space group $P$-1, $a$ = 10.889(2), $b$ = 13.790(3), $c$ = 14.318(3) Å, $\alpha$ = 85.24(3), $\beta$ = 76.52(3), $\gamma$ = 71.06(3)°, $U$ = 1977.5(7) Å$^3$, $Z$ = 1, $D_c$ = 1.730 Mg m$^{-3}$, $\mu$(Mo-K$_\alpha$) = 2.889 mm$^{-1}$, $T$ = 173 K. Total 31047 reflections, 6965 unique, $R_{int}$ = 0.1202. Refinement of 6965 reflections (545 parameters) with $I$ >2σ ($I$) converged at final $R1$ = 0.0760 ($R1$ all data = 0.0807), $wR2$ = 0.2029 ($wR2$ all data = 0.2078), gof = 1.069.

#### 4.2.24.12 $[Cu(36)_2][PF_6]$

$C_{44}H_{30}Br_2ClCuF_6N_4OP$, $M$ = 1034.42, red plate, orthorhombic, space group $P2_12_12_1$, $a$ = 13.559(3), $b$ = 23.417(5), $c$ = 26.898(5) Å, $\alpha$ = 90.00, $\beta$ = 90.00, $\gamma$ = 90.00°, $U$ = 8540(3) Å$^3$, $Z$ = 1, $D_c$ = 1.609 Mg m$^{-3}$, $\mu$(Mo-K$_\alpha$) = 2.549 mm$^{-1}$, $T$ = 173 K. Total 45600 reflections, 15046 unique, $R_{int}$ = 0.3204. Refinement of 15046 reflections (1109 parameters) with $I$ >2σ ($I$)

converged at final *R*1 = 0.1712 (*R*1 all data = 0.2188), *wR*2 = 0.3756 (*wR*2 all data = 0.4198), gof = 1.807.

#### 4.2.24.13 $[Cu(2)_2][PF_6]_2$

$C_{30}H_{24}Cl_4CuF_{12}N_4O_2P_2$, *M* = 967.82, purple plate, orthorhombic, space group *P*bcn, *a* = 17.628(2), *b* = 13.2011(5), *c* = 15.6874(5) Å, $\alpha$ = 90.00, $\beta$ = 90.00, $\gamma$ = 90.00°, *U* = 3650.6(7) Å$^3$, *Z* = 4, $D_c$ = 1.761 Mg m$^{-3}$, $\mu$(Mo-K$_\alpha$) = 1.077 mm$^{-1}$, *T* = 173 K. Total 24699 reflections, 3401 unique, $R_{int}$ = 0.0861. Refinement of 3041 reflections (249 parameters) with *I* >2σ (*I*) converged at final *R*1 = 0.0517 (*R*1 all data = 0.0594), *wR*2 = 0.1302 (*wR*2 all data = 0.1365), gof = 1.046.

#### 4.2.24.14 $[Cu(3)_2][PF_6]_2$

$C_{32}H_{26}CuF_{12}N_6P_2S_2$, *M* = 912.22, dark red block, orthorhombic, space group *P*bcn, *a* = 16.6355(14), *b* = 13.5604(18), *c* = 16.2253(14) Å, $\alpha$ = 90.00, $\beta$ = 90.00, $\gamma$ = 90.00°, *U* = 3660.2(7) Å$^3$, *Z* = 4, $D_c$ = 1.655 Mg m$^{-3}$, $\mu$(Mo-K$_\alpha$) = 0.894 mm$^{-1}$, *T* = 173 K. Total 74173 reflections, 4308 unique, $R_{int}$ = 0.1156. Refinement of 4308 reflections (297 parameters) with *I* >2σ (*I*) converged at final *R*1 = 0.0498 (*R*1 all data = 0.0579), *wR*2 = 0.1119 (*wR*2 all data = 0.1161), gof = 1.135.

#### 4.2.24.15 $[Cu(4)_2][PF_6]_2$

$C_{32}H_{26}CuF_{12}N_6P_2Se_2$, *M* = 1006.00, dark purple block, orthorhombic, space group *P*bcn, *a* = 16.963(3), *b* = 13.559(2), *c* = 16.548(4) Å, $\alpha$ = 90.00, $\beta$ = 90.00, $\gamma$ = 90.00°, *U* = 3806.1(13) Å$^3$, *Z* = 4, $D_c$ = 1.756 Mg m$^{-3}$, $\mu$(Mo-K$_\alpha$) = 2.663 mm$^{-1}$, *T* = 173 K. Total 41930 reflections, 4023 unique, $R_{int}$ = 0.0812. Refinement of 4023 reflections (370 parameters) with *I* >2σ (*I*) converged at final *R*1 = 0.0577 (*R*1 all data = 0.0660), *wR*2 = 0.1273 (*wR*2 all data = 0.1316), gof = 1.162.

#### 4.2.24.16 $[Cu(3)_2NO_3][PF_6]$

$C_{28}H_{20}CuF_6N_6O_3P_2S_2$, *M* = 846.08, green block, triclinic, space group *P*-1, *a* = 7.6644(15), *b* = 15.599(3), *c* = 15.942(3) Å, $\alpha$ = 113.75(3), $\beta$ = 93.51(3), $\gamma$ = 102.26(3)°, *U* = 1681.6(6) Å$^3$, *Z* = 4, $D_c$ = 1.671 Mg m$^{-3}$, $\mu$(Mo-K$_\alpha$) = 0.967 mm$^{-1}$, *T* = 173 K. Total 22419 reflections, 7296 unique, $R_{int}$ = 0.0615. Refinement of 7296 reflections (595 parameters) with *I* >2σ (*I*) converged at final *R*1 = 0.1003 (*R*1 all data = 0.1063), *wR*2 = 0.3048 (*wR*2 all data = 0.3096), gof = 0.979.

#### 4.2.24.17 $[Cu(4)_2NO_3][PF_6]$

$C_{30}H_{23}CuF_6N_6O_3P_2Se_2$, $M$ = 882.10, green block, triclinic, space group $P$-1, $a$ = 7.767(4), $b$ = 15.599(7), $c$ = 15.760(6) Å, $\alpha$ = 114.16(3), $\beta$ = 100.63(3), $\gamma$ = 91.59(4)°, $U$ = 1700.9(13) Å$^3$, $Z$ = 4, $D_c$ = 1.722 Mg m$^{-3}$, $\mu$(Mo-K$_\alpha$) = 2.904 mm$^{-1}$, $T$ = 173 K. Total 26351 reflections, 6153 unique, $R_{int}$ = 0.2971. Refinement of 6153 reflections (535 parameters) with $I$ >2$\sigma$ ($I$) converged at final $R$1 = 0.0538 ($R$1 all data = 0.0707), $wR$2 = 0.1319 ($wR$2 all data = 0.1459), gof = 1.043.

#### 4.2.24.18 $[Ag(3)_2][PF_6]$

$C_{28}H_{20}AgF_6N_4P_2S_2$, $M$ = 729.44, yellow plates, triclinic, space group $P$-1, $a$ = 7.1835(14), $b$ = 14.358(3), $c$ = 14.663(3) Å, $\alpha$ = 105.69(3), $\beta$ = 96.64(3), $\gamma$ = 97.11(3)°, $U$ = 1427.1(5) Å$^3$, $Z$ = 2, $D_c$ = 1.698 Mg m$^{-3}$, $\mu$(Mo-K$_\alpha$) = 0.975 mm$^{-1}$, $T$ = 173 K. Total 14774 reflections, 5889 unique, $R_{int}$ = 0.1076. Refinement of 5889 reflections (380 parameters) with $I$ >2$\sigma$ ($I$) converged at final $R$1 = 0.1096 ($R$1 all data = 0.1292), $wR$2 = 0.2992 ($wR$2 all data = 0.3188), gof = 1.032.

#### 4.2.24.19 $[Ag(4)_2][PF_6]$

$C_{28}H_{20}AgF_6N_4P_2Se_2$, $M$ = 823.24, colourless block, triclinic, space group $P$-1, $a$ = 10.708(2), $b$ = 12.186(2), $c$ = 12.806(2) Å, $\alpha$ = 65.922(14), $\beta$ = 82.401(16), $\gamma$ = 66.899(3)°, $U$ = 1402.5(5) Å$^3$, $Z$ = 2, $D_c$ = 1.949 Mg m$^{-3}$, $\mu$(Mo-K$_a$) = 3.438 mm$^{-1}$, $T$ = 173 K. Total 20652 reflections, 6007 unique, $R_{int}$ = 0.0854. Refinement of 6007 reflections (379 parameters) with $I$ >2s ($I$) converged at final $R$1 = 0.0450 ($R$1 all data = 0.0557), $wR$2 = 0.1141 ($wR$2 all data = 0.1203), gof = 1.074.

#### 4.2.24.20 $[Ag(4)_2][BF_4]$

$C_{56}H_{42}Ag_2B_2F_8N_8OSe_4$, $M$ = 1548.18, colourless block, triclinic, space group $P$-1, $a$ = 10.5106(12), $b$ = 12.0799(13), $c$ = 12.6586(14) Å, $\alpha$ = 66.199(8), $\beta$ = 82.594(9), $\gamma$ = 67.444(8)°, $U$ = 1357.4(3) Å$^3$, $Z$ = 1, $D_c$ = 1.891 Mg m$^{-3}$, $\mu$(Mo-K$_\alpha$) = 3.480 mm$^{-1}$, $T$ = 173 K. Total 32647 reflections, 7164 unique, $R_{int}$ = 0.0793. Refinement of 7164 reflections (407 parameters) with $I$ >2$\sigma$ ($I$) converged at final $R$1 = 0.0355 ($R$1 all data = 0.0384), $wR$2 = 0.0904 ($wR$2 all data = 0.0923), gof = 1.103.

### 4.2.25 Preparation of solar cells

Nanocrystalline $TiO_2$ electrodes were prepared by doctor blading a colloidal $TiO_2$ paste (Solaronix Nanooxide-T, colloidal anatase) onto a conducting glass slide (F-doped $SnO_2$, Hartford glass company, Tec 8, 8 Ω cm$^{-2}$) to produce a film 6 μm thick. After annealing at 450 °C for 30 min, each slide was cooled to ≈ 80 °C and dipped into a DMSO solution of

ligand **43**, **44**, **45** or **46** (3 mmol $dm^{-3}$) overnight. The colourless slide was then removed from the solution, washed with DMSO, then EtOH, and dried. The functionalized electrode was then dipped into an EtOH solution of $[CuL_2]^+$ (L = **1-6**) (1 mmol $dm^{-3}$) and left to stand for 24 h during which time the slide became red in colour. The slide was removed from the solution, and was washed with EtOH. The solar cells were made using LiI (0.5 mol $dm^{-3}$), $I_2$ (0.05 mol $dm^{-3}$), 1-methylbenzimidazole (0.5 mol $dm^{-3}$) and 1-butyl-3-methylimidazolinium iodide (0.6 mol $dm^{-3}$) in 3-methoxypropionitrile as electrolyte, the latter being chosen to produce the best comparison with the state-of-the-art optimized systems based on N719 (standard dye purchased from Solaronix). Cathodes (size-matched to the anodes) were constructed from FTO glass pieces platinized using $H_2PtCl_6$ (5 mmol $dm^{-3}$) in propan-2-ol, followed by heating to 280 °C for 15 m The anode and cathode were assembled using Surlyn (Dupont) plastic by heating while pressing them together. Measurements were made by irradiating from behind using a light source SolarSim 150 (100 mW $cm^{-2}$ = 1 sun).

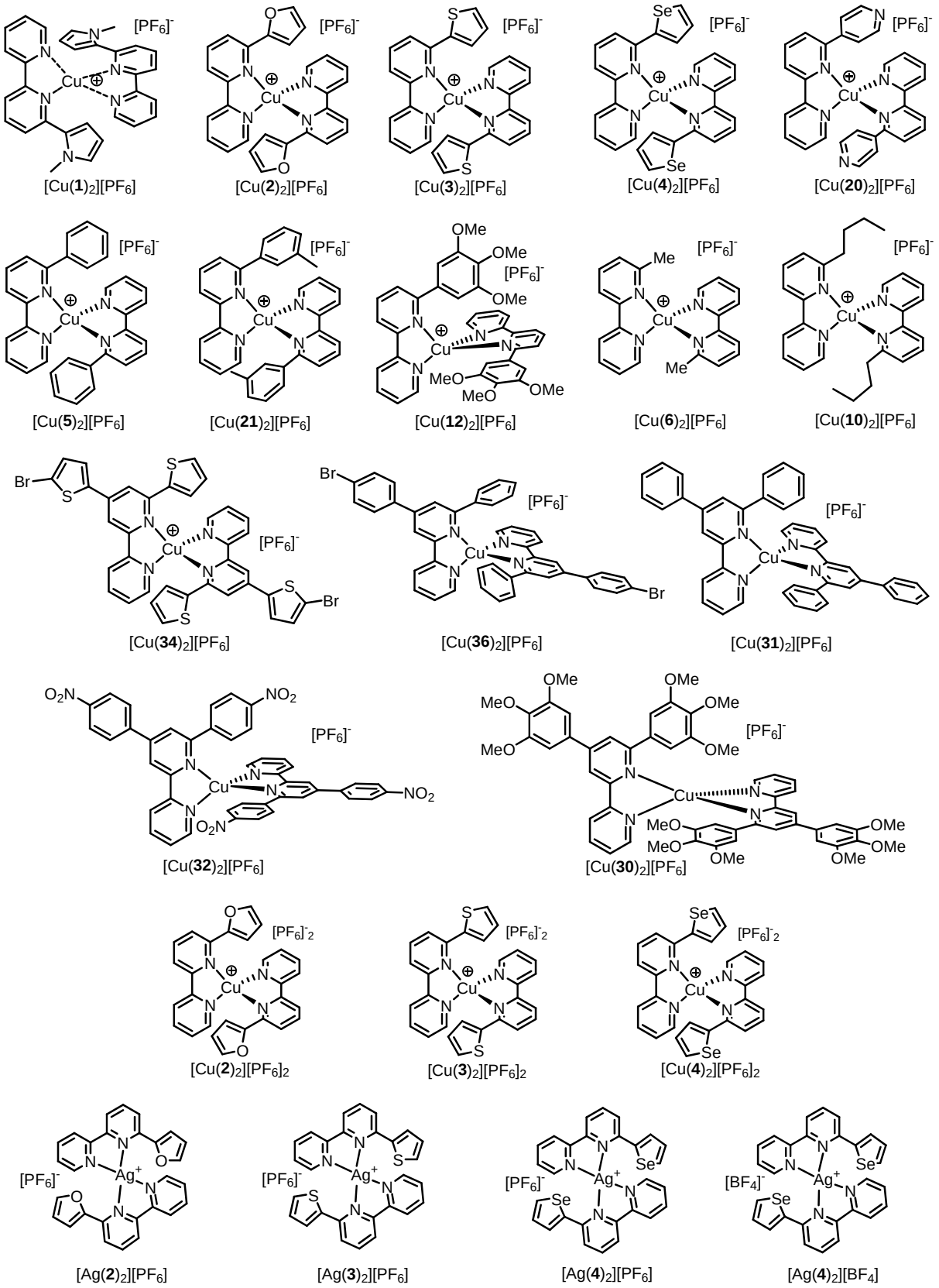


**Figure 4-62** Overview of relevant complexes

# Chapter 5

# 5 Iridium Complexes

## 5.1 Results and Discussion

### 5.1.1 Preparation

The precursor $[Ir(ppy)_2Cl]_2$ was prepared using a standard procedure.[117] The synthesis of the involved ligands was described in chapter 3. All iridium(III) complexes were prepared following a slightly modified standard procedure.[118] Therefore, one equivalent of the iridium precursor was mixed with two equivalents of the appropriate ligand in a microwave vial and suspended in MeOH. This mixture was irradiated for 2 h in a microwave reactor (120 °C, 10-12 bar). The resultant orange solutions were treated with an excess of solid $NH_4PF_6$ to initiate the precipitation of the hexafluoridophosphate salt of the iridium(III) complex. The solvent was removed under reduced pressure; the residue was dissolved in dichloromethane and purified by column chromatography. The products were usually obtained in near quantitative yields.

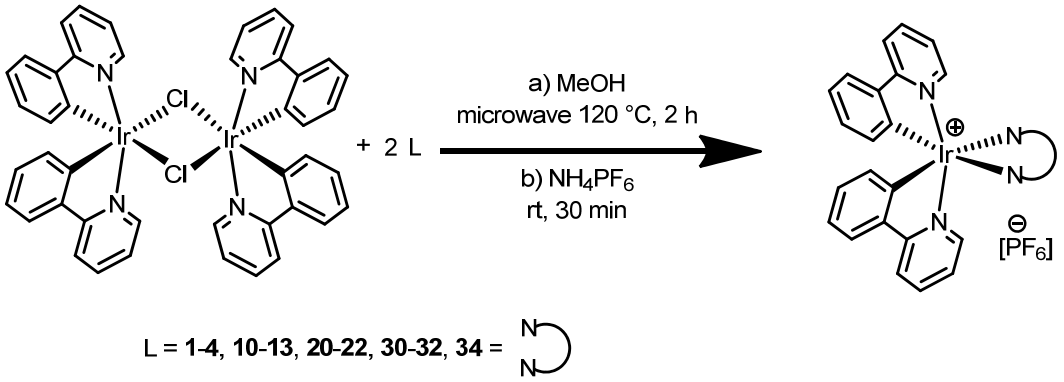


**Scheme 5-1** Synthesis of iridium(III) complexes $[Ir(ppy)_2(L)][PF_6]$.

The main difference to the reported synthesis is the use of a microwave reactor. This results in enormous time saving (2 h instead of 12-24 h with conventional heating), but the yields are also much better. While under reflux conditions the yields never exceeded 90 %, they are almost always nearly quantitative under microwave conditions.

## 5.1.2 Characterization

### 5.1.2.1 Electrospray Mass Spectra

The iridium(III) complexes have been characterized by ESI-MS. All spectra showed only one peak corresponding to the cation without the counter anion $[PF_6]^-$. Figure 5-1 shows a representative mass spectrum of a methanolic solution of $[Ir(ppy)_2(\mathbf{3})][PF_6]$, along with a simulated spectrum showing the expected isotope pattern which is dominant by that of Ir.

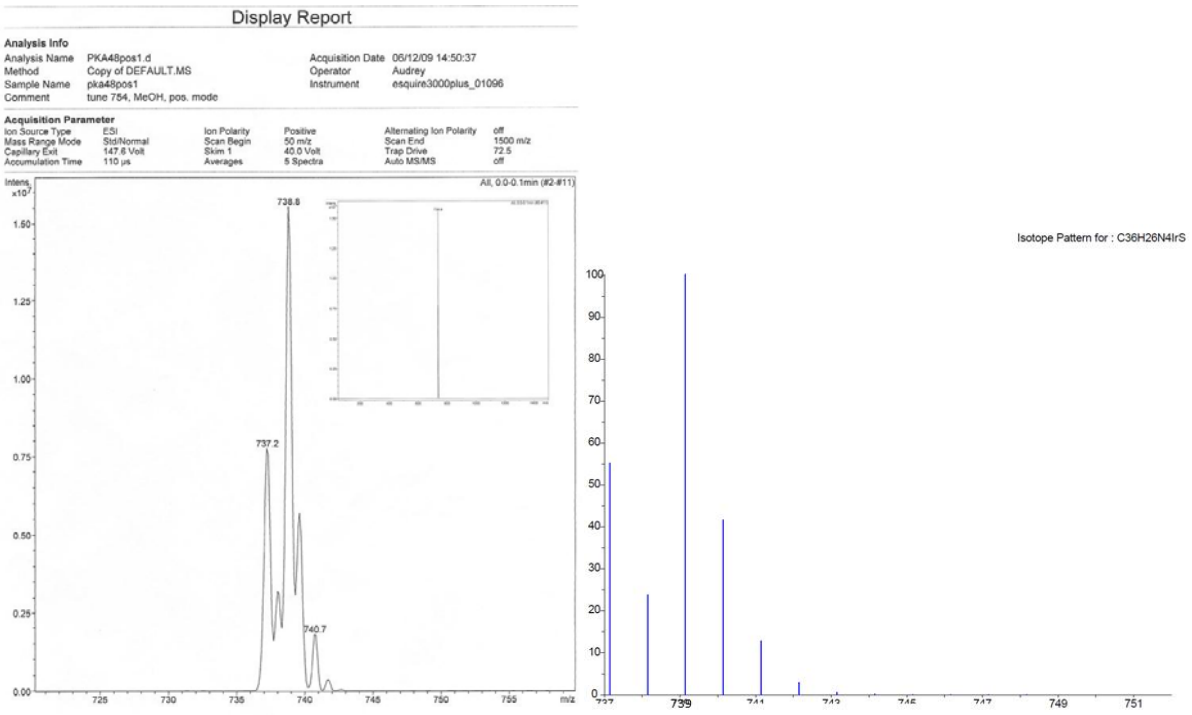


**Figure 5-1** The peak envelope of $[Ir(ppy)_2(\mathbf{3})]^+$ in the ESI-MS of $[Ir(ppy)_2(\mathbf{3})][PF_6]$ (left); simulated spectrum for the same composition (right).

### 5.1.2.2 NMR Spectroscopy

All complexes were characterized by nuclear magnetic resonance spectroscopy. Standard $^1H$ and 2-D experiments, such as COSY, HMQC and HMBC were carried out. The compounds show quite complicated spectra since most protons are not equivalent and are not trivial to assign. The reason for the two phenyl-pyridine ligands being no equivalent is that with the introduction of the asymmetrical bpy-ligand, the cation loses the $C_2$ rotation axis and the symmetry of is lowered to *E* (identity; $C_1$ rotation axis). They show two very similar sets of two four-spin-systems. The unsymmetrical 6'-R-bpy ligands exhibit two three-spin-systems and one four-spin-system. All together a typical $^1H$ NMR spectrum of a $[Ir(ppy)_2(L)][PF_6]$ complex shows 26 proton signals and 36 $^{13}C$-signals. As an example, the $^1H$ NMR spectrum of $[Ir(ppy)_2(\mathbf{3})][PF_6]$ and the assignment of the individual signals is depicted in Figure 5-2.

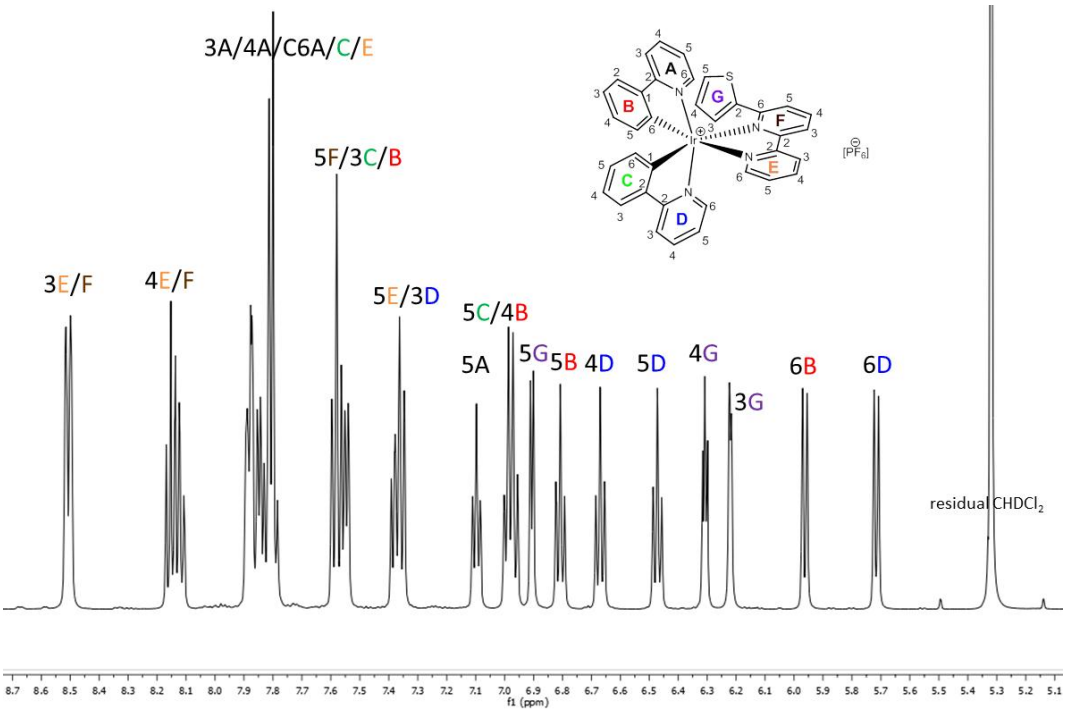


**Figure 5-2** Room temperature 500 MHz $^{1}$H NMR spectrum ($\delta$ 8.7–5.1 ppm) of a $CD_2Cl_2$ solution of [Ir(ppy)$_2$(**3**)][PF$_6$].

Characteristic for all octahedral complexes is the shift of proton 6 on the bpy moieties to higher field, due to shielding effect of an adjacent perpendicular aromatic ring of a second ligand. As an example, Figure 5-3 shows the stacked spectra of free ligand **2** and the iridium(III) complex [Ir(ppy)$_2$(**2**)][PF$_6$].

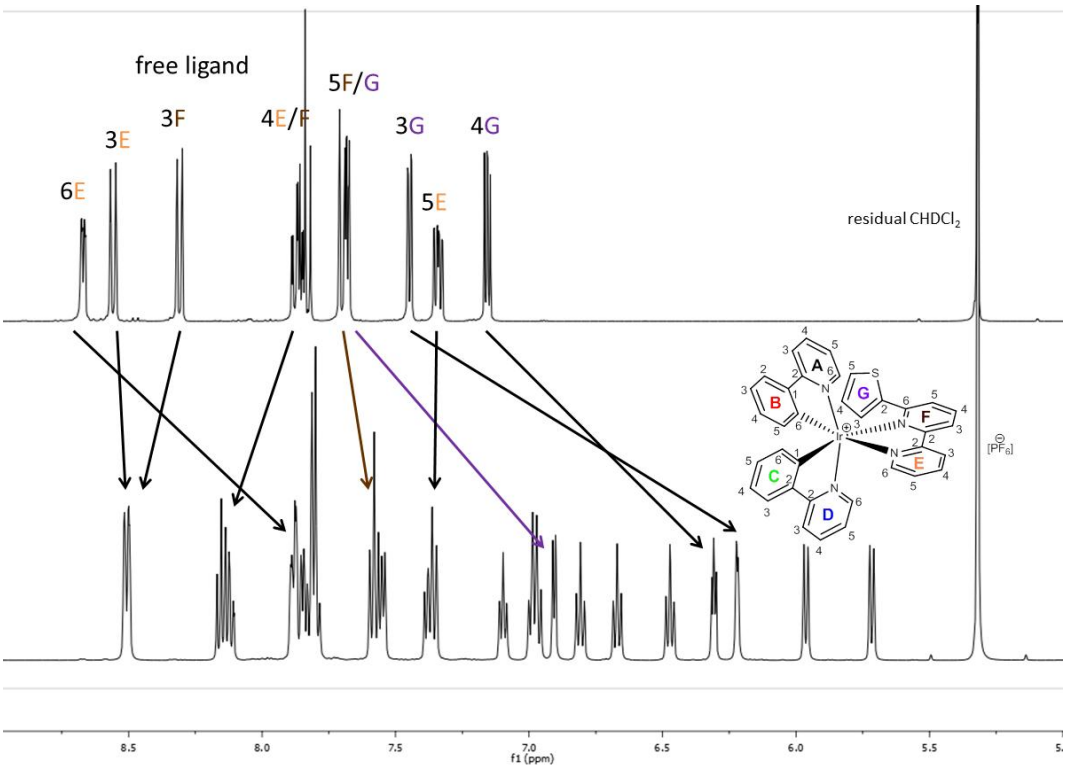


**Figure 5-3** Room temperature 500 MHz $^{1}$H NMR spectra ($\delta$ 8.6–5.4 ppm) of $CD_2Cl_2$ solutions of ligand **3** (up) and [Ir(ppy)$_2$(**2**)][PF$_6$] (bottom), the shift of individual signals upon coordination is indicated with arrows.

The arrows indicate the shift of the corresponding signals. It can be clearly seen, that most of the signals of the pyridine rings do not exhibit big shifts. The 6E proton on the other hand is shifted quite dramatically to higher field with $\Delta\delta$ = 0.85 ppm. This can be explained with the model of electrical ring current in aromatic rings (see Figure 5-4).[119] This model assumes, that the magnetic flux in an aromatic ring induces a ring current which has a shielding effect perpendicular to the plane of the ring and a deshielding effect along the plane.

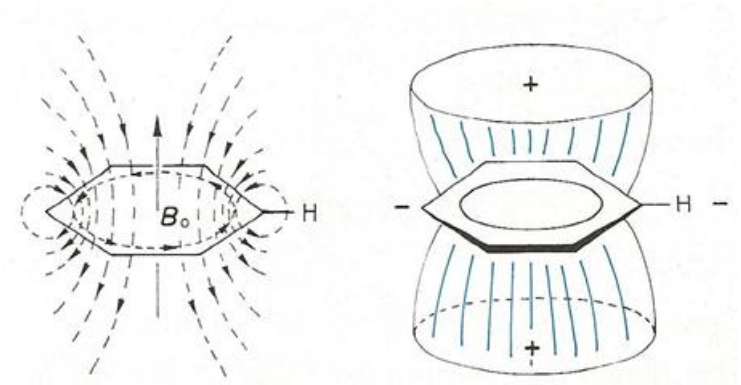


**Figure 5-4** Anisotropic shielding effect of benzene.[119]

When the crystal structure of [Ir(ppy)$_2$(**2**)][PF$_6$] is considered (see page 175), it can be seen that the coordination of the three ligands (two [ppy]$^-$ and ligand **2**) results in an octahedral geometry. This results in all the protons in 6-positions being oriented towards the aromatic ring of an adjacent ligand. Representative examples are shown in Figure 5-5.

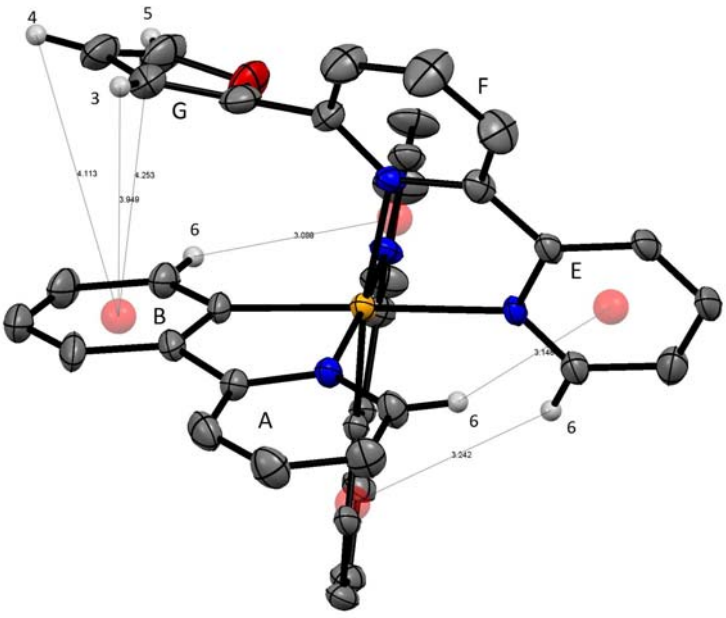


**Figure 5-5** CH-π interactions in [Ir(ppy)$_2$(**2**)][PF$_6$] representative for all iridium(III) complexes (for clarity reasons not all CH-π interactions are shown).

Figuratively, the hydrogen atoms dip into the π-electron cloud of the vicinal aromatic ring and experience a strong shielding which is responsible for the NMR shift of these protons.

Interestingly, the three protons of the furanyl ring also show a similar upfield shift. Again, from the solid state structure of the complex $[Ir(ppy)_2(\mathbf{2})][PF_6]$, it can be seen that the substituent ring is twisted with respect to the bpy ligand and is oriented parallel to the phenyl ring (B) of the $[ppy]^-$ ligand. The distance between the two centroids was measured as 3.5 Å. Similar distances are found between the hydrogen atoms in 6-positions and the centroids of the adjacent rings (3.2-3.7 Å). The same trend was observed for the other iridium(III) complexes as well, which suggests that the structures are comparable for all species.

As a representative $^1$H NMR spectrum of the iridium(III) complexes with 4',6'-substituted bpy ligands, the spectrum of $[Ir(ppy)_2(\mathbf{30})][PF_6]$ is shown in Figure 5-7. The aromatic region is similar to those derivatives without a substituent in 4'-position. The main difference is obviously that the signal for the 4F proton is missing and 3/5F appear as doublets, *J* 1.9 Hz. The protons 2/6H on the substituent in 6'-position (ring G; see Figure 5-7) do not appear as a singlet as one might expect, but as two separate and slightly broadened signals. Compared to the singlet originating from the two 2H protons in the free ligand (**30**), both signals show tremendous shifts to higher field. Again we take the solid state structure to help (Figure 5-6) and we can see that the two protons have quite different surroundings.

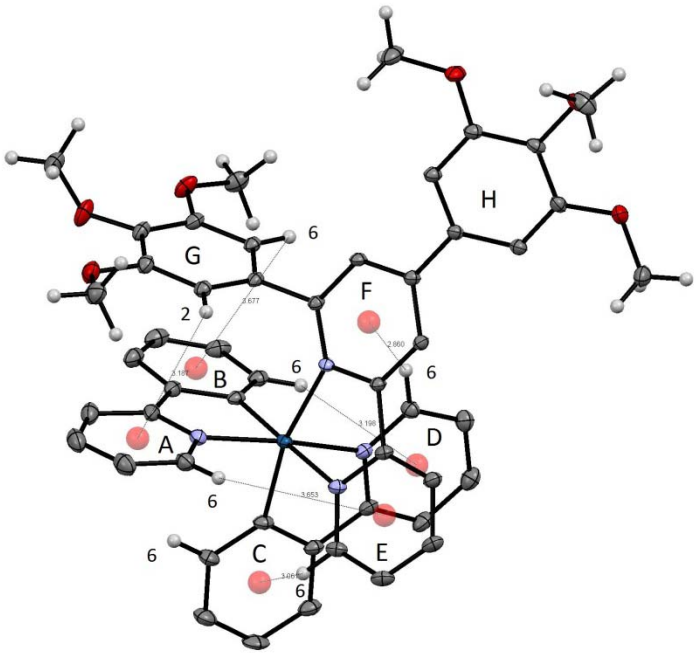


**Figure 5-6** CH-π interactions in $[Ir(ppy)_2(\mathbf{30})][PF_6]$ representative for all iridium(III) complexes (for clarity reasons not all H atoms are shown).

The ring G is twisted with regard to the bpy plane and the angle between the least square planes being 70.0(5)°. This results in distances between the substituent and the vicinal $[ppy]^-$ ligand of 3.5 Å (centroid ring G to centroid phenyl ring of $[ppy]^-$) or 3.2 Å (centroid ring G to plane of $[ppy]^-$). The NMR spectrum suggests that even in solution ring G cannot rotate

freely. Proton 2G lies above the carbon atom 5B the distance being 3.5 Å which is similar to those observed for [Ir(ppy)$_2$(**2**)][PF$_6$] and therefore results in a similar shift of $\Delta\delta$= 0.62 ppm, with regards to the free ligand. The proton 6G exhibits an even bigger shift ($\Delta\delta$= 1.60 ppm) and this can be explained with its position which is directly above the nitrogen atom of ring A, the distance between H$^{6G}$ and the N-atom being 2.985(3) Å. Since there should be more electron density at the nitrogen atom and the proton is even closer to the [ppy]$^-$ plane than H$^{2G}$, the bigger shift becomes obvious. The same is true for the aliphatic region (Figure 5-7; olive box). It shows two sharp signals for the methoxy groups of ring H, the integrals exhibiting the expected 6:3 ratio of integrals. But then it shows three dictinct signals for the methoxy groups on the G ring. This is a similar situation as explained above for the aromatic region. The broadening is the result of hindered rotation of ring G, and they show different shifts to higher field which are also the results of different positions above the adjacent [ppy]$^-$ ligand.

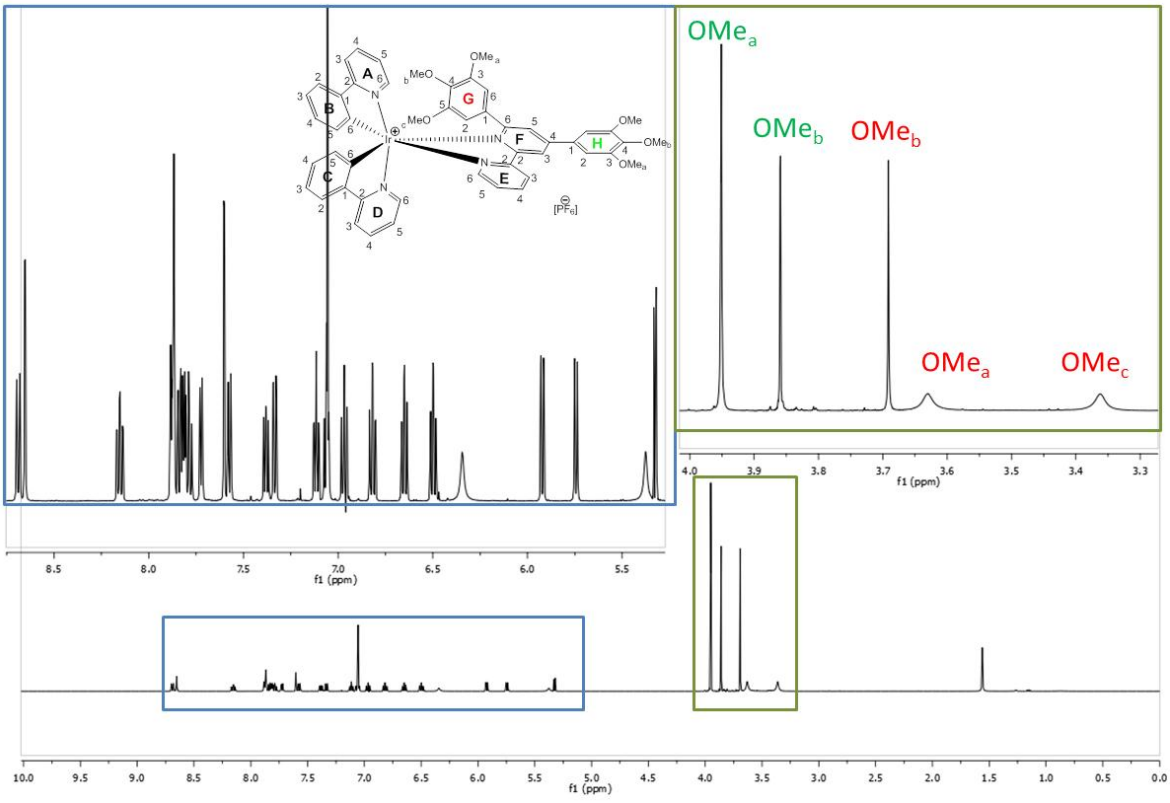


**Figure 5-7** Room temperature 500 MHz $^1$H NMR spectrum ($\delta$ 15.0–(0.0) ppm) of a $CD_2Cl_2$ solution of [Ir(ppy)$_2$(**30**)][PF$_6$] (upper left); blue box, close up of aromatic region; olive box, close up of aliphatic region.

Similar spectra were observed for the remaining iridium(III) complexes bearing 4',6'-R-bpy ligands.

### 5.1.2.3 Solid State Structures

For most of the prepared Ir(III) complexes, it proved to be very difficult to grow single crystals for structure determination. Various crystal growth methods were applied but

yielded only crystals of poor quality. Nevertheless, it was possible to obtain three structures for complexes with ligands **1**, **13** and **30** and a preliminary structure of $[Ir(ppy)_2(\mathbf{2})][PF_6]$.

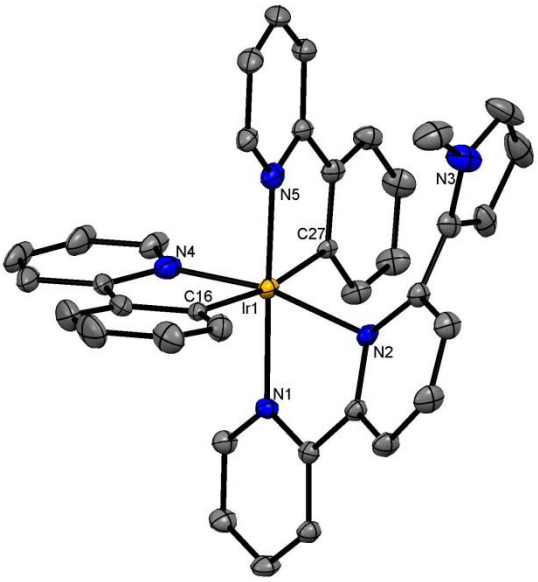


**Figure 5-8** Structure of the $[Ir(ppy)_2(\mathbf{1})]^+$ cation in $[Ir(ppy)_2(\mathbf{1})][PF_6]$ with H atoms omitted (ellipsoids plotted at 25 % probability level). Selected bond parameters: Ir1-N4 1.991(5), Ir1-N5 2.015(5), Ir1-C16 2.035(5), Ir1-C27 2.037(5), Ir1-N1 2.145(4), Ir1-N2 2.193(4) Å, N4-Ir1-N5 87.4(2), N4-Ir1-C16 80.4(2), N5-Ir1-C16 92.2(2), N4-Ir1-C27 92.6(2), N5-Ir1-C27 80.4(2), C16-Ir1-C27 170.13(18), N4-Ir1-N1 94.3(2), N5-Ir1-N1 178.25(18), C16-Ir1-N1 88.24(18), C27-Ir1-N1 99.28(18), N4-Ir1-N2 167.6(2), N5-Ir1-N2 102.73(18), C16-Ir1-N2 91.93(18), C27-Ir1-N2 96.12(17), N1-Ir1-N2 75.56(17)°.

Figure 5-8 shows the molecular structure of $[Ir(ppy)_2(\mathbf{1})][PF_6]$ and the bond parameters of the coordination sphere are listed in the caption. Single crystals were obtained by layering a $CHCl_3$ solution of the compound with toluene, yielding small yellow plates after several weeks. The compound crystallizes in the orthorhombic space group *Pbcn* with solvent molecules which are distorted around a $C_2$ axis. The coordination geometry is a slightly disordered octahedral as expected. The compound is chiral and the displayed cation is the $\Lambda$ isomer, the space group however is achiral and the elemental cell of the crystal structure consists of both symmetry related enantiomers. The Ir…N bond lengths are in the range of 1.99-2.19 Å, with the two Ir…C bonds being 2.035(5) and 2.037(5) Å. The bite angles of the cyclometalating $[ppy]^-$ ligands are 80.4(2)°, i.e. slightly bigger than the one of the bpy ligand (75.56(17)°). A direct result thereof is the non-planarity of the bpy moiety, the least square angles between the two pyridine planes being 21.8°. The *N*-methyl pyrrole substituent on the bpy ligand is twisted with respect to the central pyridine ring of ligand **1**, with an angle between the two planes of pyridine and pyrrole of 66.8°. This allows the pyrrole substituent to undergo $\pi$-$\pi$-interactions with the vicinal, N5 and C27 containing $[ppy]^-$ ligand. The distance between the centroid of the pyrrole substituent and the plane of the $[ppy]^-$ ligand is 3.4 Å, and so is longer than that of the reference compound $[Ir(ppy)_2(\mathbf{5})][PF_6]$ (3.3 Å; see Figure 5-20), which was prepared in a previous work and published elsewhere.[56] The longer

distance is very likely caused by the somewhat bulky methyl substituent on the pyrrole ring which would be supported by the fact that the N... $[ppy]^-$ distance (3.6 Å) is longer than the O…$[ppy]^-$ distance (2.8 Å) in the following compound ($[Ir(ppy)_2(\mathbf{2})][PF_6]$). The packing is dominated by anion-cation interactions, with F…H distances being in the range of 2.4-2.7 Å.

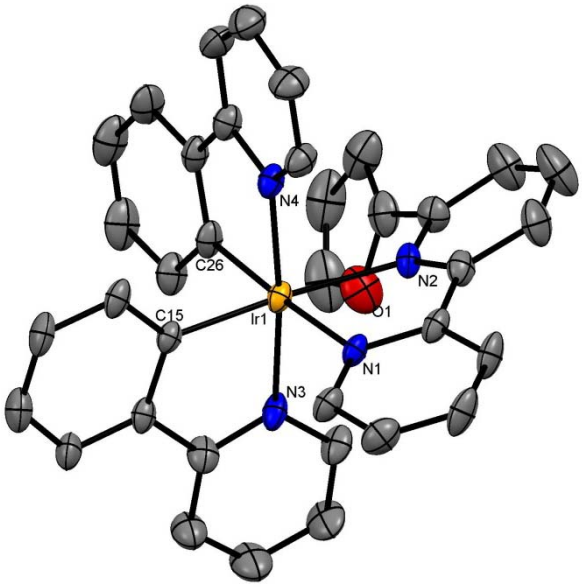


**Figure 5-9** Structure of the $[Ir(ppy)_2(\mathbf{2})]^+$ cation in $[Ir(ppy)_2(\mathbf{2})][PF_6]$ with H atoms omitted (ellipsoids plotted at 25 % probability level). Selected bond parameters: Ir1-C15 2.009(6), Ir1-C26 2.023(6), Ir1-N4 2.038(5), Ir1-N3 2.039(6), Ir1-N1 2.142(5), Ir1-N2 2.213(5) Å, C15-Ir1-C26 84.5(2), C15-Ir1-N4 95.0(2), C26-Ir1-N4 80.2(3), C15-Ir1-N3 80.5(2), C26-Ir1-N3 94.8(3), N4-Ir1-N3 173.69(19), C15-Ir1-N1 96.3(2), C26-Ir1-N1 176.2(2), N4-Ir1-N1 96.0(2), N3-Ir1-N1 89.0(2), C15-Ir1-N2 172.9(2), C26-Ir1-N2 102.6(2), N4-Ir1-N2 85.8(2), N3-Ir1-N2 99.2(2), N1-Ir1-N2 76.5(2)°.

As mentioned above, it was not possible to produce high quality single crystals of $[Ir(ppy)_2(\mathbf{2})][PF_6]$; with the recorded data, only a preliminary structure could be resolved. Nevertheless, it confirms the expected structure and shall be described briefly (Figure 5-9). The compound crystallizes in the monoclinic space group *C*2/*m* with solvents molecules, probably chloroform and acetonitrile. The ligands coordinate in the same manner as in the previous compound and result in a slightly distorted octahedral geometry. Again, the cation shown her has the $\Delta$ configuration but the space group is achiral which means that both enantiomers are present. The intramolecular $\pi$-stacking is more pronounced. The furanyl ring is twisted from the bpy moiety; their planes drawing an angle of 46.6°, which is 20° smaller than for $[Ir(ppy)_2(\mathbf{1})][PF_6]$, but either way results in a nearly parallel orientation to a vicinal $[ppy]^-$ ligand, more precisely the furanyl ring lies above the C26 containing aryl ring. With the furanyl centroid $[ppy]^-$ plane distance being 3.2 Å, this value is even smaller than for the reference compound, the phenyl derivative ($[Ir(ppy)_2(\mathbf{5})][PF_6]$; 3.3 Å). It seems that there are less repulsive $\pi$-$\pi$ interactions compared to the phenyl or pyrrole derivatives, respectively. This would suggest that the steric effect of the methyl group in $[Ir(ppy)_2(\mathbf{1})][PF_6]$ is responsible for longer distance between the two aromatic rings (see

above). The packing also is dictated by anion-cation interactions, with F…H distances being between 2.4 and 2.6 Å.

A representative solid state structure for iridium(III) complexes containing a 4',6'-substituted bpy ligand is shown in Figure 5-10. Suitable single crystals for structure determination were obtained by slow evaporation of a dichloromethane solution of [Ir(ppy)$_2$(**30**)][PF$_6$]. The compound crystallizes in the monoclinic space group $P2_1/n$ without any solvent. The structure is comparable to that of [Ir(ppy)$_2$(**2**)][PF$_6$], the bond parameters are listed in Table 5-1 versus these of [Ir(ppy)$_2$(**32**)][PF$_6$] and will not be described here in detail. The π-stacking and the consequence for the $^1$H NMR spectrum were discussed in section 5.1.2.2.

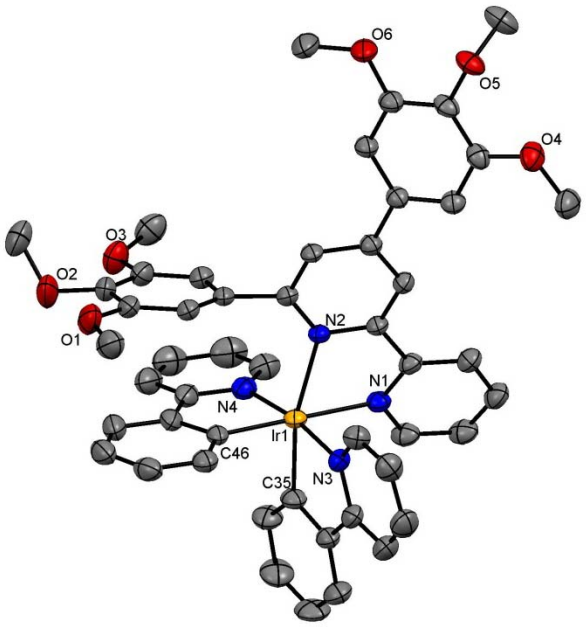


**Figure 5-10** Structure of the [Ir(ppy)$_2$(**30**)]$^+$ cation in [Ir(ppy)$_2$(**30**)][PF$_6$] with H atoms omitted (ellipsoids plotted at 50 % probability level).

The methoxy substituents on the bpy ligand result in intermolecular interactions: hydrogen bonds (2.5-2.8 Å), as well as in CH…π-interactions (2.849(4) Å). Furthermore, there are intermolecular π-π-interactions (3.5 Å) between the phenyl substituents in 4'-positions on the bpy ligands of two distinct cations. However, it is not possible to depict these in one sensible figure and it is therefore not shown here. As always, there are anion-cation interactions with F…H distances being between 2.4 and 2.6 Å.

X-ray quality crystals of [Ir(ppy)$_2$(**32**)][PF$_6$] were grown by slow evaporation of dichloromethane solution of the compound. It crystallises, unlike compound [Ir(ppy)$_2$(**30**)][PF$_6$], in the monoclinic space group *P*-1 with two solvent molecules. The molecular structure of the Λ isomer is depicted in Figure 5-11, this is accompanied by its symmetry related enantiomer, since the space group is achiral. Nevertheless, the molecular

structures of both compounds are very similar and differ only slightly in the bond parameters which are compared in Table 6-1.

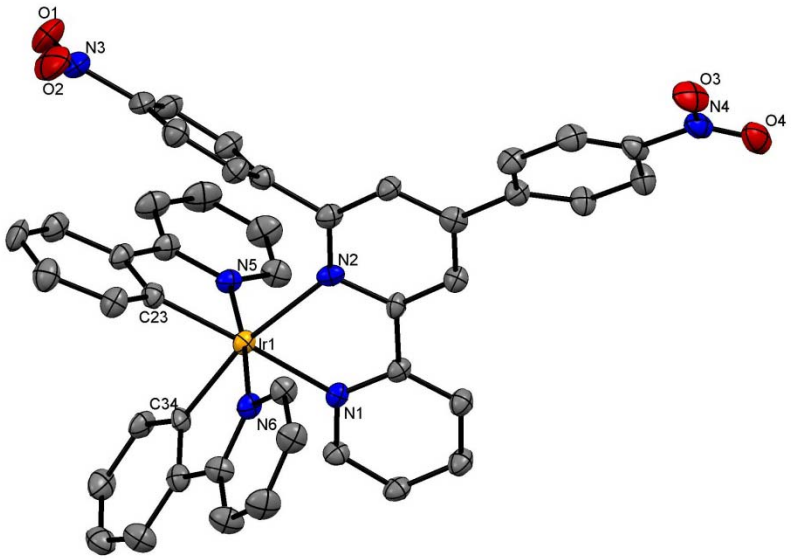


**Figure 5-11** Structure of the $[Ir(ppy)_2(\mathbf{32})]^+$ cation in $[Ir(ppy)_2(\mathbf{32})][PF_6]$ with H atoms omitted (ellipsoids plotted at 30 % probability level).

Similar to compound $[Ir(ppy)_2(\mathbf{30})][PF_6]$ the nitro substituents on the bpy ligands engage in intermolecular hydrogen bonds (2.5-2.7 Å) but no π-π-interactions between the cations can be observed. In addition, there are anion-cation interactions with F…H distances being between 2.4 and 2.6 Å.

| $[Ir(ppy)_2(\mathbf{30})][PF_6]$ | | $[Ir(ppy)_2(\mathbf{32})][PF_6]$ | |
|---|---|---|---|
| | Distance [Å] | | Distance [Å] |
| Ir1-C35 | 2.012(4) | Ir1-C34 | 1.992(6) |
| Ir1-C46 | 2.012(4) | Ir1-C23 | 2.013(8) |
| Ir1-N4 | 2.047(3) | Ir1-N5 | 2.047(6) |
| Ir1-N3 | 2.053(3) | Ir1-N6 | 2.054(6) |
| Ir1-N1 | 2.134(3) | Ir1-N1 | 2.144(6) |
| Ir1-N2 | 2.204(3) | Ir1-N2 | 2.201(6) |
| | Angle [°] | | Angle [°] |
| C35-Ir1-C46 | 87.34(15) | C34-Ir1-C23 | 83.4(3) |
| C35-Ir1-N4 | 91.88(16) | C34-Ir1-N5 | 95.2(3) |
| C46-Ir1-N4 | 80.21(16) | C23-Ir1-N5 | 80.1(3) |
| C35-Ir1-N3 | 81.01(16) | C34-Ir1-N6 | 80.6(3) |
| C46-Ir1-N3 | 94.30(15) | C23-Ir1-N6 | 95.8(3) |
| N4-Ir1-N3 | 171.26(13) | N5-Ir1-N6 | 174.5(2) |
| C35-Ir1-N1 | 92.83(14) | C34-Ir1-N1 | 93.2(2) |
| C46-Ir1-N1 | 178.76(15) | C23-Ir1-N1 | 175.4(2) |
| N4-Ir1-N1 | 101.01(13) | N5-Ir1-N1 | 97.2(2) |
| N3-Ir1-N1 | 84.52(12) | N6-Ir1-N1 | 86.6(2) |
| C35-Ir1-N2 | 166.46(14) | C34-Ir1-N2 | 167.5(2) |
| C46-Ir1-N2 | 104.66(13) | C23-Ir1-N2 | 107.7(2) |
| N4-Ir1-N2 | 96.28(12) | N5-Ir1-N2 | 92.4(2) |
| N3-Ir1-N2 | 91.67(12) | N6-Ir1-N2 | 92.4(2) |
| N1-Ir1-N2 | 75.04(11) | N1-Ir1-N2 | 76.0(2) |

**Table 5-1** Selected bond parameters of $[Ir(ppy)_2(L)][PF_6]$ L = **30** and **32**.

As a test reaction to see whether keto-imine ligands can be used for iridium(III) ligation, the Ir-dimer was reacted with the precursor **13** ((*E*)-1-(pyrid-2-yl)-3-*N*,*N*-dimethylaminoprop-2-ene-1-one). Indeed, the expected compound could be isolated and is surprisingly stable. Suitable single crystals of [Ir(ppy)$_2$(**13**)][PF$_6$] were grown from a $CD_2Cl_2$ solution directly in a NMR tube as red blocks. The compound crystallizes in the monoclinic space group $P2_1/c$ with solvent molecules. The coordination geometry is distorted octahedral, the N…Ir, O…Ir and C…Ir bonds are all in the same range between 1.99 and 2.17 Å. The bite angle of the N,O-ligand (75.40(13)°) is quite similar to that of a bpy ligand. Packing is determined by anion-cation interactions with F…H distances being in the range of 2.9 to 3.0 Å.

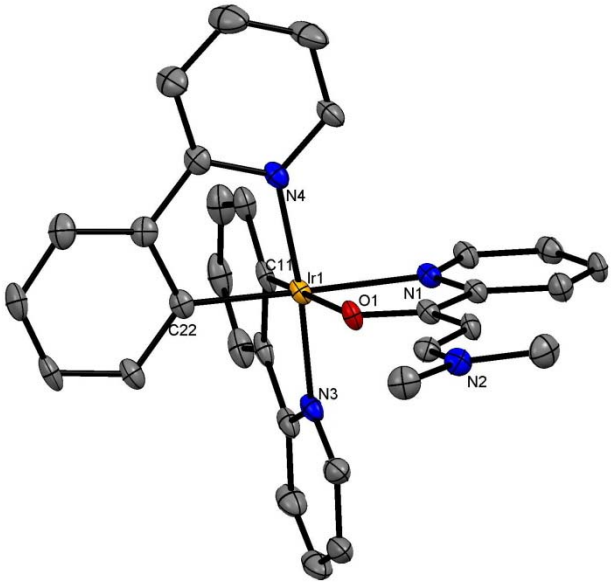


**Figure 5-12** Structure of the [Ir(ppy)$_2$(**13**)]$^+$ cation in [Ir(ppy)$_2$(**13**)][PF$_6$] with H atoms omitted (ellipsoids plotted at 30 % probability level). Selected bond parameters: Ir1-C11 1.987(5), Ir1-C22 2.002(5), Ir1-N3 2.021(4), Ir1-N4 2.033(4), Ir1-N1 2.137(4), Ir1-O1 2.173(3) Å, C11-Ir1-C22 87.19(18), C11-Ir1-N3 80.72(19), C22-Ir1-N3 93.70(18), C11-Ir1-N4 96.11(19), C22-Ir1-N4 80.92(18), N3-Ir1-N4 173.92(16), C11-Ir1-N1 98.69(16), C22-Ir1-N1 173.76(16), N3-Ir1-N1 89.36(15), N4-Ir1-N1 96.26(15), C11-Ir1-O1 172.73(16), C22-Ir1-O1 98.89(15), N3-Ir1-O1 94.84(15), N4-Ir1-O1 88.81(14), N1-Ir1-O1 75.40(13).

#### 5.1.2.4 Electronic Absorption and Emission Spectroscopy

UV-visible absorption spectra were measured in dichlormethane solutions at room temperature (Table 5-2 and Figure 5-13), and they display strong bands in the UV region up to 300 nm attributed to intraligand ($\pi$-$\pi^*$) transitions. Lower-energy absorption bands (300-400 nm) correspond to metal-to-ligand charge transfer (MLCT) transitions. Finally, weak bands with $\varepsilon$ being in the range of 200 to 2000 $M^{-1}\,cm^{-1}$ are observed clearly for all complexes except for [Ir(ppy)$_2$(**4**)][PF$_6$]. These bands are ascribed to spin-forbidden transitions directly to triplet states (460-520 nm).[52,120]

As can be clearly seen, the absorption spectra do not change very much with variation of the substituents on the bpy ligands. Especially, the absorption maxima vary only marginally in

contrast to the intensity. There is no obvious trend in these changes which would be worthy of discussion.

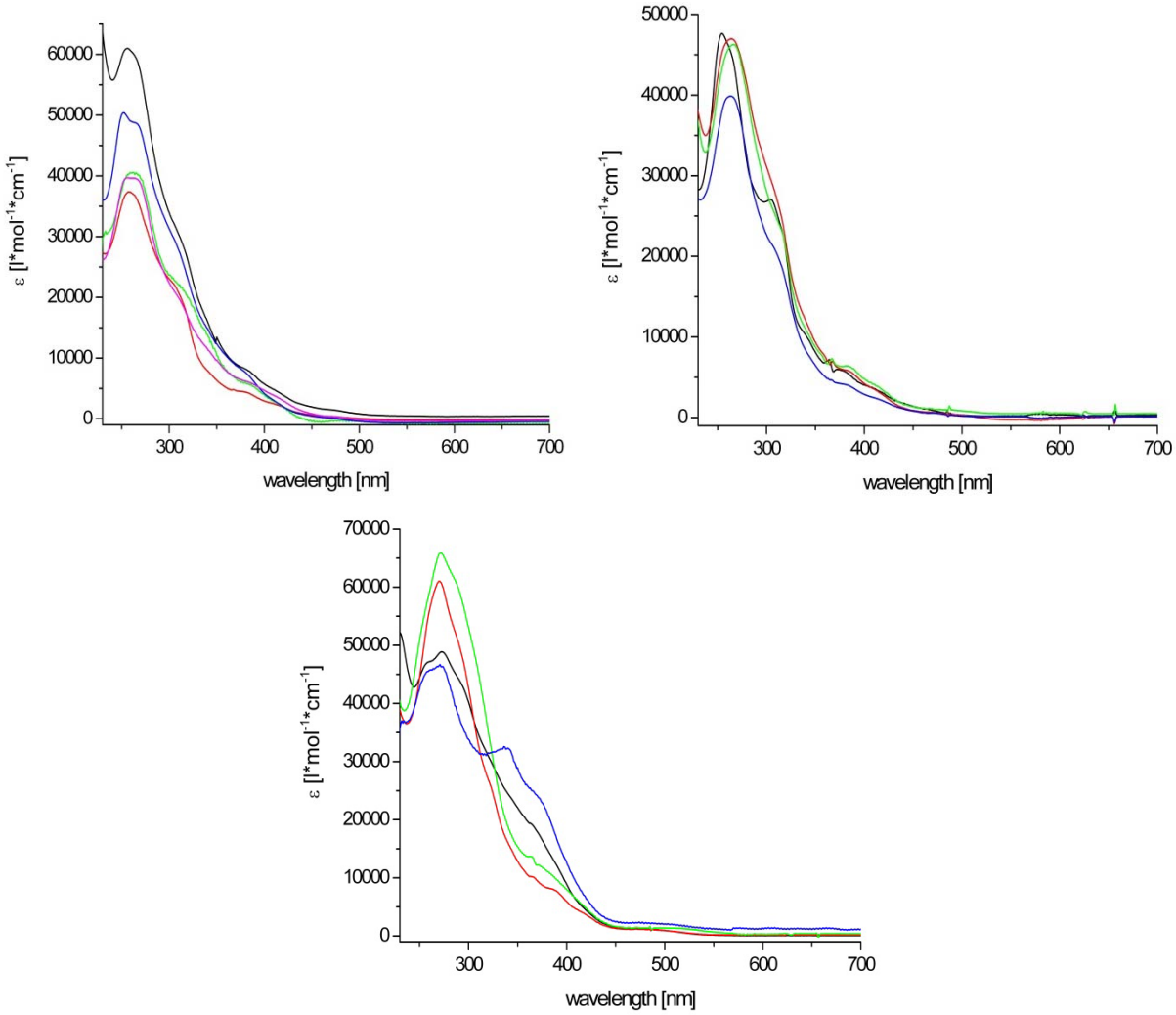


**Figure 5-13** Electronic absorption spectra of $CH_2Cl_2$ solutions of $[Ir(ppy)_2(L)][PF_6]$ for L = **1**-**4** and **20** (top left, key: magenta, L = **1**; blue, L = **2**; black, L = **3**; green, L = **4**; red, L = **20**); for L = **10**-**12** and **21** (top right, key: black, L = **10**; red, L = **12**; green, L = **21**; blue, L = **11**) and for L = **30**-**32** and **34** (bottom, key: black, L = **30**; red, L = **31**; green, L = **32**; blue, L = **34**). See experimental section for solution concentrations.

The photoluminescence on the other hand is more dependent on the nature of the bpy substituents and the emission wavelengths show quite significant shifts upon change of the substituent on the bpy moieties. The measurements were all carried out in aerated dichloromethane solutions at room temperature. Figure 5-14 shows the normalized emission spectra of all (prepared for this thesis) emissive iridium(III) complexes when excited into the MLCT bands (~380 nm). In the upper left graph are depicted the compounds containing a hetero aromatic substituent on the bpy ligand (**1**-**4** and **20**). The unsubstituted reference compound $[Ir(ppy)_2(bpy)][PF_6]$ emits (in aerated dichloromethane) at $\lambda_{em}$ = 582 nm.[121] When the bpy ligand is substituted with a phenyl ring the emission shifts slightly to lower energy (L = **5**, $\lambda_{em}$ = 595 nm). The complexes bearing bpy ligands with hetero aromatic substituent show all emission maxima which exhibit a small bathochromic shift and

the values lie in the range of 601 to 613 nm. Quantum yields and life times were not determined. The next graph (top right) summarizes the complexes with aromatic substituents and *n*-butyl, respectively, on the bpy (**10**-**12** and **21**). $[Ir(ppy)_2(\mathbf{10})][PF_6]$ containing the aliphatic substituent shows an emission at $\lambda_{em}$ = 575 nm, this value is 7 nm lower than for the unsubstituted derivative ($[Ir(ppy)_2(bpy)][PF_6]$). Apparently, the positive inductive effect has a small effect on the LUMO energy, which, from DFT calculations, is believed to be located on the bpy ligand.[122]

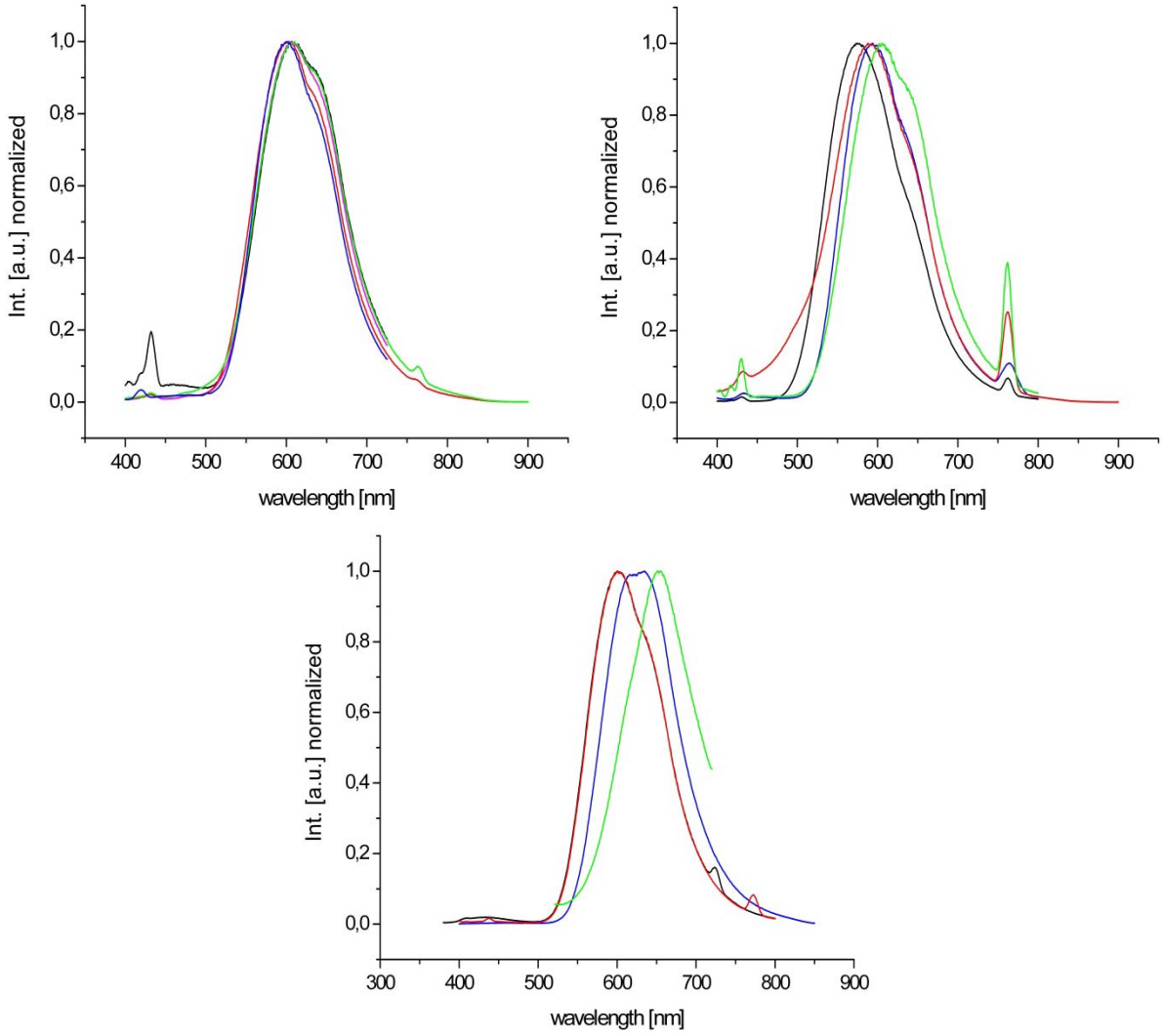


**Figure 5-14** Emission spectra of $CH_2Cl_2$ solutions of $[Ir(ppy)_2(L)][PF_6]$ for L = **1**-**4** and **20** (top left, key: magenta, L = **1**; blue, L = **2**; black, L = **3**; green, L = **4**; red, L = **20**); L = **10**-**12** and **21** (top right, key: black, L = **10**; red, L = **12**; green, L = **21**; blue, L = **11**); for L = **30**-**32** and **34** (bottom, key: black, L = **30**; red, L = **31**; green, L = **32**; blue, L = **34**).

The three complexes with phenyl substituted bpy ligands show that further functionalization has only a small effect. Compounds $[Ir(ppy)_2(\mathbf{11})][PF_6]$ ($\lambda_{em}$ = 594 nm) and $[Ir(ppy)_2(\mathbf{12})][PF_6]$ ($\lambda_{em}$ = 591 nm) are both shifted to lower energy, with respect to the parent compound $[Ir(ppy)_2(\mathbf{5})][PF_6]$, even though the substituents on the phenyl ring have the opposite (strong) inductive effects. For $[Ir(ppy)_2(\mathbf{21})][PF_6]$ on the other hand, where the phenyl ring is

decorated with only one methyl group, a more significant bathochromic shift is observed ($\lambda_{em}$ = 606 nm). The last graph (bottom) in Figure 5-14 shows the emission of the iridium(III) complexes containing a 4',6'-disubstituted bpy ligand. Interestingly, the phenyl derivative ([Ir(ppy)$_2$(**31**)][PF$_6$]) and the one substituted with methoxy groups on the phenyl rings ([Ir(ppy)$_2$(**30**)][PF$_6$]) show the same emission. It seems as if the strong inductive effects of the methoxy groups on the phenyl substituents in the 4'- and the 6'-positions cancel each other out. The nitro derivative [Ir(ppy)$_2$(**32**)][PF$_6$] on the other hand shows quite a significant shift to lower energies ($\lambda_{em}$ = 653 nm). The life times and quantum yields were not determined, but by eye the emission of the last compound seems very weak, and the intensity of it by same opening of the slits in the spectrofluorometer was much lower.

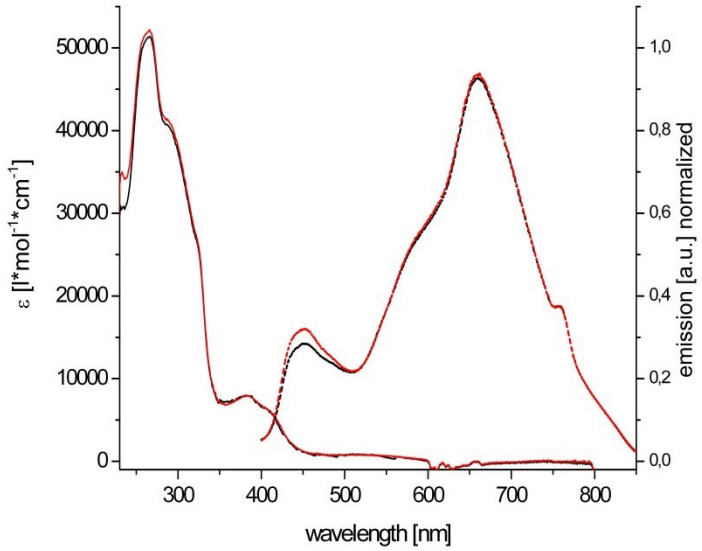


**Figure 5-15** Absorption (solid lines) and emission (hashed lines) spectra of $CH_2Cl_2$ solutions of [Ir(ppy)$_2$(**22**)][PF$_6$] pure (black) and after protonation with TFA (red).

Figure 5-15 shows the absorption and emission spectra of compound [Ir(ppy)$_2$(**22**)][PF$_6$]. Here the bpy ligand carries a substituent in the 5'-position and cannot really be compared to the other complexes. The absorption spectrum shows the expected bands, noteworthy are the MLCT bands ($\lambda_{abs}$ = 380 nm), which are lower in intensity, compared to 6'-substituted bpy ligands ($\varepsilon = 9*10^3$ *vs*. 10-30*10$^3$ M$^{-1}$ cm$^{-1}$). However, the spin forbidden transitions are much more pronounced and show quite high ε values (2200 M$^{-1}$ cm$^{-1}$). The emission is quite red shifted compared to [Ir(ppy)$_2$(bpy)][PF$_6$] and tails off in the near IR region above 800 nm. Since there is a free nitrogen site on the pyridine substituent on the bpy ligand protonation experiments were carried out, similar to those already discussed for the free ligand **22**. But, it can be clearly seen, that after the treatment with TFA neither the absorption spectrum nor the emission change.

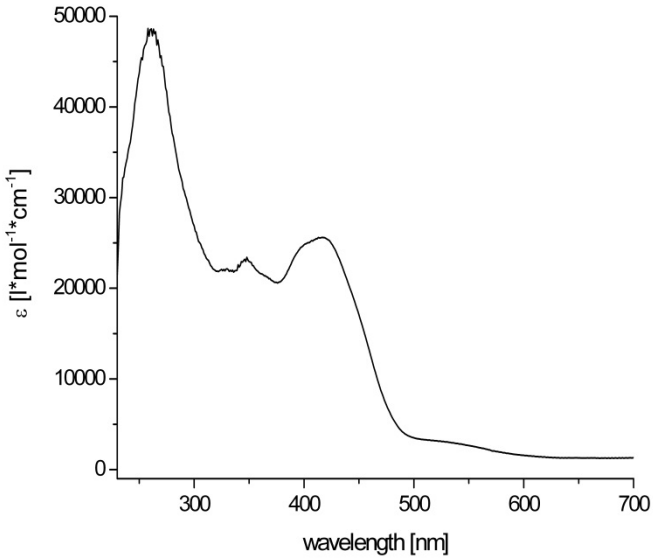


**Figure 5-16** Absorption spectrum of $CH_2Cl_2$ solution of [Ir(ppy)$_2$(**13**)][$PF_6$].

The absorption spectrum of the non-emissive compound [Ir(ppy)$_2$(**13**)][$PF_6$] is depicted in Figure 5-16. This compound contains no bpy ligand but the precursor **13** which acts as a *N,O*-donor-ligand. It shows a LC band at 262 nm, broad MC bands between 300 and 400 nm and a very intense MLCT absorption at 417 nm ($\varepsilon$ = 27500 $M^{-1}$ $cm^{-1}$). The spin forbidden transition is the most intense observed in this work ($\varepsilon$ = 3300 $M^{-1}$ $cm^{-1}$).

The photophysical data for all here discussed iridium(III) complexes are summarized in Table 5-2 below.

| Compound | Absorption in $CH_2Cl_2$ $\lambda_{max}$ [nm] ($\varepsilon$[l*10$^3$/mol*cm]) | | | | | | | Emission $\lambda_{em}$ ($\lambda_{ex}$) [nm] |
|---|---|---|---|---|---|---|---|---|
| [Ir(ppy)$_2$(bpy)][$PF_6$] | 257 (48.0) | | 308 (23.0) | 336 (10.3) | 381 (7.0) | 406 (4.0) | 467 (0.8) | 582 (381) |
| [Ir(ppy)$_2$(**5**)][$PF_6$] | | 267 (44.0) | 311 (23.1) | | 382 (5.5) | 411 (3.4) | 470 (0.8) | 595 (313) |
| [Ir(ppy)$_2$(**1**)][$PF_6$] | 254 (39.8) | 265 (39.8) | 307 (20.7) | | 375 (6.4) | | 467 (0.4) | 611/628 (380) |
| [Ir(ppy)$_2$(**2**)][$PF_6$] | 251 (50.4) | 266 (48.8) | 309 (30.0) | | 372 (8.4) | | 465 (0.2) | 608/636 (380) |
| [Ir(ppy)$_2$(**3**)][$PF_6$] | 255 (61.1) | 265 (60.2) | 309 (32.5) | | 377 (8.5) | | 468 (1.5) | 613/640 (380) |
| [Ir(ppy)$_2$(**4**)][$PF_6$] | | 261 (40.7) | 305 (22.3) | | 383 (5.9) | 414 (2.4) | | 601/633 (380) |
| [Ir(ppy)$_2$(**10**)][$PF_6$] | 253 (47.6) | 263 (45.4) | 303 (27.1) | 338 (10.7) | 375 (5.9) | 404 (3.9) | 464 (1.1) | 575/634 (380) |
| [Ir(ppy)$_2$(**11**)][$PF_6$] | | 263 (39.9) | 305 (21.6) | | 379 (4.1) | 411 (2.4) | 470 (0.6) | 594/631 (380) |
| [Ir(ppy)$_2$(**12**)][$PF_6$] | | 264 (47.0) | 305 (29.4) | | 382 (5.9) | 412 (3.4) | 471 (0.7) | 591/631 (380) |
| [Ir(ppy)$_2$(**13**)][$PF_6$] | | 262 (48.5) | 326 (22.1) | 346 (23.2) | 401 (24.9) | 417 (25.7) | 513 (3.3) | NA |
| [Ir(ppy)$_2$(**20**)][$PF_6$] | 258 (37.4) | 272 (33.7) | 307 (20.6) | | 379 (6.3) | 416 (3.4) | 467 (0.5) | 607/630 (380) |
| [Ir(ppy)$_2$(**21**)][$PF_6$] | | 265 (46.3) | 304 (29.7) | | 383 (6.4) | 408 (4.2) | 487 (1.0) | 606/636 (380) |
| [Ir(ppy)$_2$(**22**)][$PF_6$] | | 263 (51.4) | 287 (40.8) | 322 (26.8) | 382 (7.9) | 409 (6.2) | 519 (0.8) | 450/596/661 (380) |
| [Ir(ppy)$_2$(**30**)][$PF_6$] | 257 (46.9) | 273 (48.9) | | 336 (25.1) | 363 (19.4) | | 464 (1.3) | 603/632 (360) |
| [Ir(ppy)$_2$(**31**)][$PF_6$] | | 270 (61.1) | | 320 (27.3) | 382 (8.2) | | 471 (1.2) | 603/632 (385) |
| [Ir(ppy)$_2$(**32**)][$PF_6$] | | 271 (66.1) | 281 (61.7) | | 374 (11.7) | | 505 (1.3) | 653 (370) |
| [Ir(ppy)$_2$(**34**)][$PF_6$] | 258 (45.5) | 272 (46.5) | | 338 (32.5) | 366 (24.9) | | 480 (2.2) | 616/635 (363) |

**Table 5-2** Electronic absorption and emission data for iridium(III) complexes.

### 5.1.3 Light Emitting Electrochemical Cells (LECs)

Our laboratory does not have the appropriate equipment to prepare LEC-devices and they were therefore prepared in collaboration with the laboratory of H. BOLINK in Valencia, Spain. LECs were prepared from complexes $[Ir(ppy)_2(L)][PF_6]$ (L = **1**, **2** and **3**) using the reported methodology:[56] An indium tin oxide (ITO)-covered substrate was coated with a 0.1-mm spin-coated layer of poly(3,4-ethylenedioxythiophene):poly(styrene sulfonic acid) (PEDOT:PSS) followed by a 90-nm spin-coated layer of a 4:1 molar mixture of the iTMC and the ionic liquid 1-butyl-3-methylimidazolium hexafluoridophosphate and finally an aluminium layer was evaporated as cathode. The ionic liquid is incorporated to improve the turn-on time, the time to reach the maximum luminance ($t_{on}$) of the device.[123] Details concerning the device preparation and characterization can be found in the experimental section. All three devices showed bright orange electroluminescence when biased at 3 V (left graphs in Figure 5-17-Figure 5-19). They show the expected responses of LECs, upon application of low bias to the device a slow increase of the current density and luminance is observed. The turn-on times ($t_{on}$) are very long (33, 21 and 28 h for devices using complexes with bpy ligands **1**, **2** and **3**, respectively) but considerably lower than that observed from the reference device where the active complex $[Ir(ppy)_2(\mathbf{5})][PF_6]$ is used (237 h, Table 5-3). This extremely long $t_{on}$ is not fully understood yet.[56] Possible reasons have been suggested, such as formation of nanometer-sized domains of crystalline complex within the thin film, which would hinder the movement of the counterions. The morphology of thin films of these complexes is not easy to verify, and it has only been analyzed in the case of $[Ru(bpy)_3]^{2+}$, using synchroton X-ray radiation.[124] In that study, it was established that a spin-coated film does consist of nanoscale crystalline domains. Considering that partial crystallization of the complexes takes place, the long $t_{on}$ values can be explained. The lower $t_{on}$ values measured for devices using complexes $[Ir(ppy)_2(L)][PF_6]$ (L = **1**-**3**) suggests a thin film packing of the complex cations that yields more ‘‘free’’ anions. Regardless of the exact origin of the slow responses, the application of short pulses of higher voltages allows for improvement, and it is possible to reach values which are interesting for practical applications.[56,125] For an exact comparison between the devices using the different complexes, this pre-biasing was not applied in this work. Unfortunately, the efficiencies found for the devices using complexes $[Ir(ppy)_2(L)][PF_6]$ (L = **1**-**3**) were lower than those obtained from the devices using complex $[Ir(ppy)_2(\mathbf{5})][PF_6]$ (Table 5-3). This is not necessarily expected in view of the similar values for Photo Luminescence Quantum Efficiency (PLQE) for films of the complexes using the device composition (Table 5-4). It has been established that the External Quantum Efficiencies (EQE) of the LECs are mainly determined by the PLQE values.[122] According to this simple relationship, the EQEs for the devices using complexes $[Ir(ppy)_2(L)][PF_6]$ (L = **1**-**3**) should then

be similar in values (1.30 %). This is not the case and the devices exhibit EQE values in the range of 0.34 to 0.42 %.

The devices with complex $[Ir(ppy)_2(\mathbf{2})][PF_6]$ show unexpectedly high current density up to 1300 $A/m^{-2}$ which is approximately three times higher than those measured for devices using complex $[Ir(ppy)_2(\mathbf{1})][PF_6]$ or $[Ir(ppy)_2(\mathbf{3})][PF_6]$ (Figure 5-17-Figure 5-19) and even ten times higher than those for $[Ir(ppy)_2(\mathbf{5})][PF_6]$. Along with the lower device efficiencies, the maximum luminances obtained for the devices using $[Ir(ppy)_2(L)][PF_6]$ (L = **1**-**3**) are significantly higher than that found for the reference device, reaching only 41, 86 and and 46 $cd/m^2$, respectively, at 3 V bias.

The stability can be expressed as the time to reach half of the maximum brightness (lifetime or $t_{1/2}$), which decreases with faster $t_{on}$. This trend is not fully understood, but has been observed for many LECs.[118,123,126] However, KALYUZHNY *et al*. noticed that $t_{1/2}$ is not a good value to compare the stability of LECs and can only be used when the maximum luminances of the different devices are similar.[127] Furthermore, it is well established that in electroluminescent devices, the time to reach half of the initial luminance depends strongly on the initial luminance chosen. KALYUZHNY *et al*. proposed an alternative method for expressing the stability as the total emitted energy ($E_{tot}$) up to the time the luminance reaches one-fifth of the maximum value ($t_{1/5}$) for a cell area of 3 $mm^2$.[127] The devices described in this work can be compared with both approaches and give always the same result. The devices using $[Ir(ppy)_2(L)][PF_6]$ (L = **1**-**3**) show lower values in $t_{1/2}$ when compared to $[Ir(ppy)_2(\mathbf{5})][PF_6]$ as well as lower values of the total emitted energy (Table 5-3) than the reference device. Hence, it can be stated that the introduction of hetero atoms into the aromatic substituent on the bpy ligand does not have a significant effect on the colour of the emitted light and it rather decreases the device efficiency as well as its stability. Apparently, the hetero atoms make the complexes prone to decomposition.

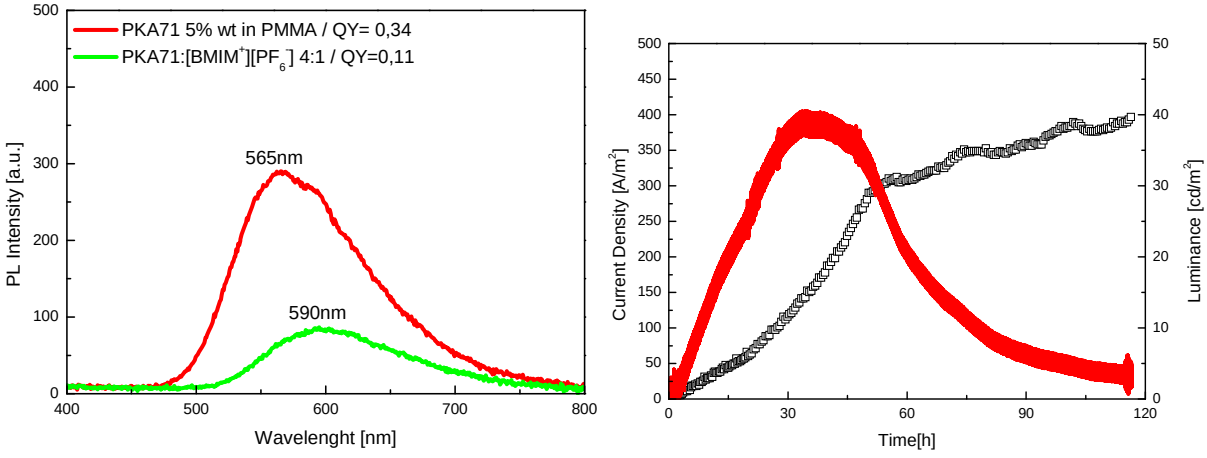


**Figure 5-17** (left) Photoluminescence Spectra of $[Ir(ppy)_2(\mathbf{1})][PF_6]$ in PMMA, red and $[BMIM][PF_6]$, green; (right) performance of a LEC device (ITO2/PEDOT:$PSS_{4083}$/$[Ir(ppy)_2(\mathbf{1})][PF_6]$:$[BMIM][PF_6]$ 4:1 (100 nm)/Al); Luminance (black squares); current density (red).

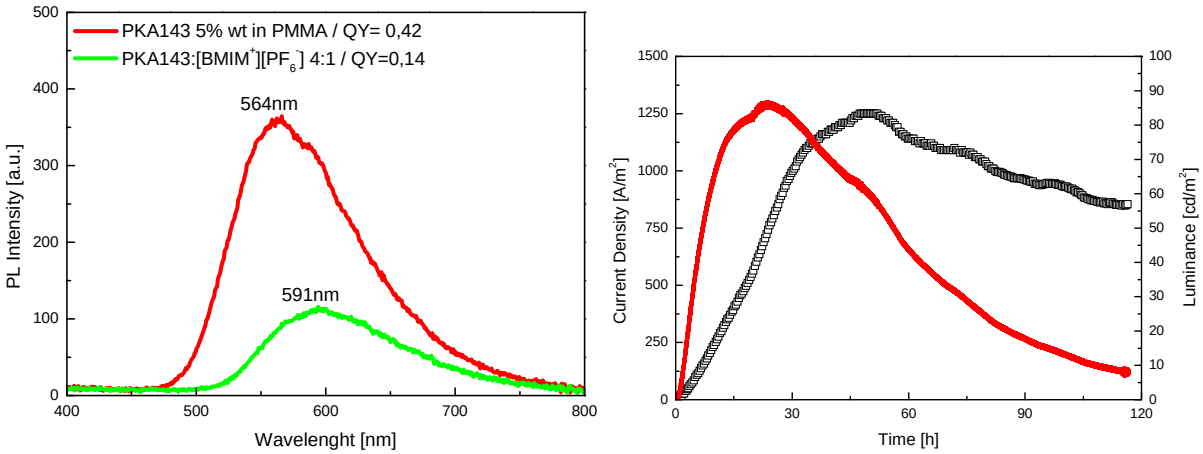


**Figure 5-18** (left) Photoluminescence Spectra of [Ir(ppy)$_2$(**2**)][PF$_6$] in PMMA, red and [BMIM][PF$_6$], green; (right) performance of a LEC device (ITO2/PEDOT:PSS$_{4083}$/[Ir(ppy)$_2$(**2**)][PF$_6$]:[BMIM][PF$_6$] 4:1 (100 nm)/Al); Luminance (black squares); current density (red).

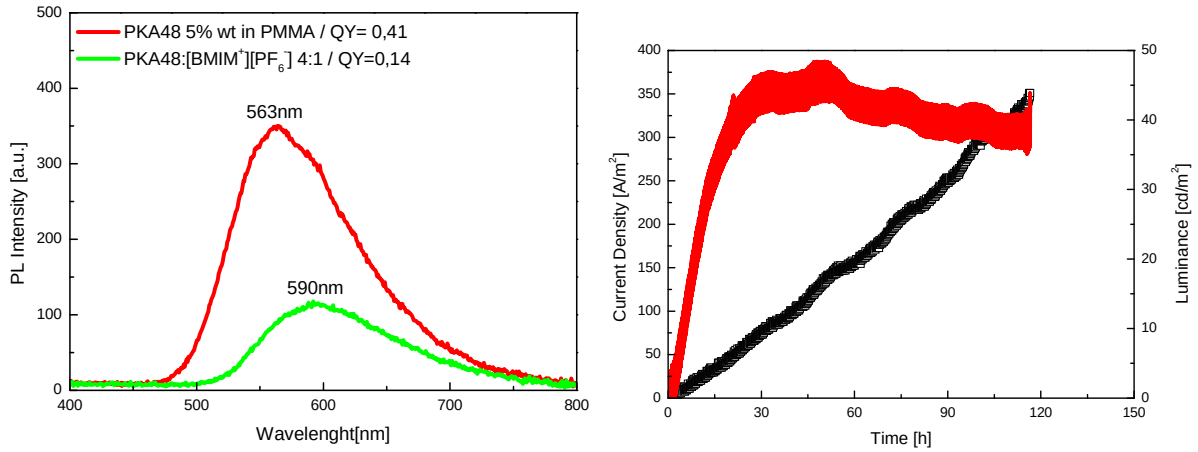


**Figure 5-19** (left) Photoluminescence Spectra of [Ir(ppy)$_2$(**3**)][PF$_6$] in PMMA, red and [BMIM][PF$_6$], green; (right) performance of a LEC device (ITO2/PEDOT:PSS$_{4083}$/[Ir(ppy)$_2$(**3**)][PF$_6$]:[BMIM][PF$_6$] 4:1 (100 nm)/Al); Luminance (black squares); current density (red).

| | $T_{on}$ [h] | $Luminance_{max}$ [cd/m$^2$] | $Efficacy_{max}$ [cd/A] | $T_{1/2}$ [h] | $T_{1/5}$ [h] | E [J] | EQE [%] |
|---|---|---|---|---|---|---|---|
| [Ir(ppy)$_2$(**1**)$_2$][PF$_6$] | 33 | 41 | 1.5 | 61 | 86 | 0.15 | 0.34 |
| [Ir(ppy)$_2$(**2**)$_2$][PF$_6$] | 21 | 86 | 0.4 | 58 | 89 | 0.4 | 0.42 |
| [Ir(ppy)$_2$(**3**)$_2$][PF$_6$] | 28 | 46 | 2.7 | 335 | 540 | 1.22 | 0.41 |
| [Ir(ppy)$_2$(**5**)$_2$][PF$_6$] | 237 | 109 | 3.1 | 1290 | - | 13.6 | 1.3 |

**Table 5-3** Performance of LEC devices at a driving voltage of 3 V.

| | $\lambda_{max}$ [nm] solution | $\lambda_{max}$ [nm] device | $PLQE_{dev}$ | $PLQE_{film}$ |
|---|---|---|---|---|
| [Ir(ppy)$_2$(**1**)$_2$][PF$_6$] | 611 | 590 | 0.11 | 0.34 |
| [Ir(ppy)$_2$(**2**)$_2$][PF$_6$] | 608 | 591 | 0.14 | 0.42 |
| [Ir(ppy)$_2$(**3**)$_2$][PF$_6$] | 613 | 590 | 0.14 | 0.41 |
| [Ir(ppy)$_2$(**5**)$_2$][PF$_6$] | 595 | 595 | 0.21 | 0.37 |

**Table 5-4** Photophysical data for LEC devices.

## 5.2 Experimental

### 5.2.1 $[Ir(ppy)_2(1)][PF_6]$

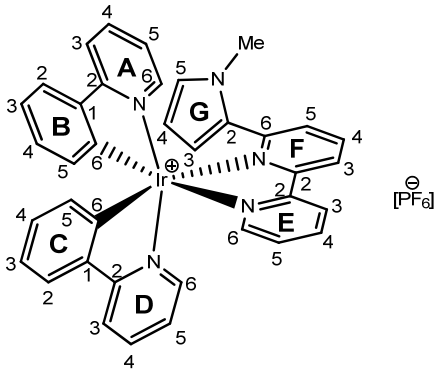


To a 20 ml microwave vial were added ligand **1** (94.5 mg, 402.0 μmol, 2.1 eq) and $[Ir(ppy)_2Cl]_2$ (205.0 mg, 191.0 μmol, 1.0 eq), then suspended in MeOH (10 ml). The mixture was irradiated for 2 h at 120 °C in the microwave reactor. Then the solvent was reduced and the product was precipitated upon addition of $NH_4PF_6$ (250.0 mg, 1.52 mmol, 8.0 eq). The solvent was evaporated and the crude product was passed through a short column ($SiO_2$, $CH_2Cl_2$/MeOH 100:0 to 98:2). The desired product was collected as the second major fraction and dried in a desiccator after solvent removal. It was obtained as an orange powder (320.0mg, 363.7 μmol, 95.2 %). $^1$H NMR (500 MHz, $CD_2Cl_2$) $\delta$ (ppm) 8.47 (d, *J* 8.0 Hz, 1 H, $H^{3F}$), 8.45 (d, *J* ~7.0 Hz, 1 H, $H^{3E}$), 8.18 (t, *J* 7.9 Hz, 1 H, $H^{4F}$), 8.10 (t, *J* 7.9 Hz, 1 H, $H^{4E}$), 7.92 (d, *J* 8.2 Hz, 2 H, $H^{6E+C}$), 7.85 (d, *J* 8.0 Hz, 2 H, $H^{3+6A}$), 7.77 (t, *J* 7.9 Hz, 1 H, $H^{5C}$), 7.71 (br s, 1 H, $H^{5A}$), 7.56 (d, *J* 7.7 Hz, 1 H, $H^{3B}$), 7.48 – 7.41 (m, 3 H, $H^{5G+F,3D}$), 7.38 (dt, *J* 7.5, 1.6 Hz, 1 H, $H^{5E}$), 7.08 (t, *J* 6.6 Hz, 1 H, $H^{4C}$), 7.03 (t, *J* 6.6 Hz, 1 H, $H^{4A}$), 6.96 (t, *J* 7.5 Hz, 1 H, $H^{4B}$), 6.84 (s, *J* 7.5 Hz, 1 H, $H^{5B}$), 6.66 (t, *J* 7.8 Hz, 1 H, $H^{4D}$), 6.56 (t, *J* 7.4 Hz, 1 H, $H^{5D}$), 6.01 (d, *J* 6.3 Hz, 1 H, $H^{6B}$), 5.88 (s, 1 H, $H^{3G}$), 5.82 (d, *J* 7.5 Hz, 1 H, $H^{6D}$), 5.49 (s, 1 H, $H^{4G}$), 3.01 (br s, 3 H, $H^{NMe}$); $^{13}$C NMR (126 MHz, $CD_2Cl_2$) $\delta$ (ppm) 169.68 ($C^{2C}$), 167.80 ($C^{2A}$), 158.01 ($C^{6F}$), 157.84 ($C^{2F}$), 157.57 ($C^{2E}$), 150.81 ($C^{6A}$), 150.21 ($C^{6E}$), 149.32 ($C^{1B}$), 149.22 ($C^{1D}$), 147.32 ($C^{2B}$), 147.31 ($C^{2D}$), 143.64 ($C^{2G}$), 139.74 ($C^{4F}$), 139.59 ($C^{4E}$), 138.76 ($C^{4C}$), 138.51 ($C^{4A}$), 131.33 ($C^{6D}$), 131.25 ($C^{6B}$), 130.94 ($C^{5B}$), 130.60 ($C^{5D}$), 129.87 ($C^{5G}$), 129.34 ($C^{5F}$), 128.19 ($C^{6C}$), 125.48 ($C^{3E}$), 125.15 ($C^{3B}$), 124.94 ($C^{3F}$), 124.02 ($C^{3D}$),123.86 ($C^{5A}$), 123.23 ($C^{5C+E}$), 122.82 ($C^{4B}$), 121.19 ($C^{4D}$), 120.34 ($C^{3A}$), 119.92 ($C^{3C}$), 112.61 ($C^{3G}$), 108.74 ($C^{4G}$), 34.86 ($C^{Me}$); ESI-MS *m/z*: 735.9 $[M\text{-}PF_6]^+$ (100 %, calc. 736.2); IR (solid, $\nu$/cm$^{-1}$) 3130 w, 3063 w, 3042 w, 2350 vw, 2320 vw, 1607 m, 1582 m, 1562 w, 1477 s, 1447 m, 1438 w, 1417 m, 1364 w, 1327 w, 1316 w, 1310 w, 1304 w, 1269 w, 1064 w, 1029 w, 840 vs, 775 w, 757 m, 729 m, 709 m, 690 m; UV/vis ($CH_2Cl_2$, 5.0 x 10$^{-5}$ mol dm$^{-3}$) $\lambda_{max}$/nm 254 ($\varepsilon$/dm$^3$ mol$^{-1}$ cm$^{-1}$ 40000), 265 (39500), 311 (19700), 390 (5700), 465 (400); emission $\lambda_{max}$ ($\lambda_{ex}$) = 601, 624 (303) nm; EA: calc. for $C_{37}H_{29}N_5F_6PIr$, C 50.45 %, H 3.32 %, N 7.95 %, found C 50.12 %, H 3.46 %, N 7.81 %.

### 5.2.2 [Ir(ppy)$_2$(2)][PF$_6$]

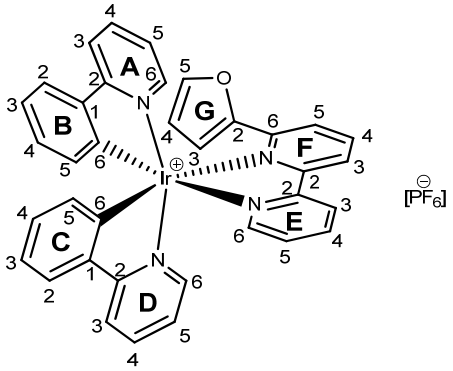


To a 5 ml microwave vial were added ligand **2** (50.0 mg, 225.0 μmol, 2.0 eq) and [Ir(ppy)$_2$Cl]$_2$ (120.5 mg, 112.5 μmol, 1.0 eq), then suspended in MeOH (5 ml). The mixture was irradiated for 45 min at 120 °C in the microwave reactor. Then the solvent was reduced and the product was precipitated upon addition of solid $NH_4PF_6$ (150.0 mg, 0.90 mmol, 8.0 eq). The solvent was evaporated and the crude product was passed through a short column ($SiO_2$, $CH_2Cl_2$/MeOH 100:0-98:2). The desired product was collected as the second major fraction and dried in a desiccator after removal of solvent. It was obtained as an orange powder (200.0 mg, 225.0 μmol, 99.9 %). $^1$H NMR (500 MHz, $CD_2Cl_2$) $\delta$ (ppm) 8.48 (dd, *J* 5.9, 0.6 Hz, 1 H, H$^{3A}$), 8.46 (d, *J* 8.2 Hz, 1 H, H$^{3E}$), 8.39 (dd, *J* 8.9, 0.9 Hz, 1 H, H$^{3F}$), 8.15 (td, *J* 8.0, 1.5 Hz, 1 H, H$^{4E}$), 8.08 (t, *J* 7.9 Hz, 1 H, H$^{4F}$), 7.99 (d, *J* 8.1 Hz, 1 H, H$^{6A}$), 7.87 (td, *J* 8.0, 1.5 Hz, 1 H, H$^{4A}$), 7.82 (dd, *J* 6.0, 0.9 Hz, 1 H, H$^{6E}$), 7.81 (d, *J* 8.2 Hz, 1 H, H$^{3C}$), 7.73 (dt, *J* 7.8, 1.5 Hz, 1 H, H$^{4C}$), 7.70 (dd, *J* 7.9, 0.9 Hz, 1 H, H$^{3B}$), 7.52 (dd, *J* 7.8, 1.0 Hz, 1 H, H$^{5F}$), 7.40 (d, *J* 7.4 Hz, 2 H, H$^{3D+5E}$), 7.37 (d, *J* 4.3 Hz, 1 H, H$^{6C}$), 7.12 (td, *J* 6.6, 1.3 Hz, 1 H, H$^{5A}$), 7.03 – 6.97 (m, 2 H, H$^{5G+4B}$), 6.91 (td, *J* 6.6, 1.3 Hz, 1 H, H$^{5C}$), 6.78 (td, *J* 7.6, 1.3 Hz, 1 H, H$^{5B}$), 6.69 (td, *J* 7.8, 1.0 Hz, 1 H, H$^{4D}$), 6.55 (td, *J* 7.5, 1.2 Hz, 1 H, H$^{5D}$), 6.09 (dd, *J* 3.4, 0.6 Hz, 1 H, H$^{3G}$), 5.98 (d, *J* 7.7 Hz, 1 H, H$^{6B}$), 5.90 (d, *J* 7.6 Hz, 1 H, H$^{6D}$), 5.87 (dd, *J* 3.4, 1.8 Hz, 1 H, H$^{4G}$); $^{13}$C NMR (126 MHz, $CD_2Cl_2$) $\delta$ (ppm) 168.91 (C$^{2C}$), 167.27 (C$^{2A}$), 158.03 (C$^{2F}$), 157.64 (C$^{2E}$), 153.87 (C$^{6F}$), 152.07 (C$^{6A}$), 150.68 (C$^{2G}$), 149.24 (C$^{1D}$), 148.15 (C$^{1B}$), 146.42 (C$^{6E}$), 144.61 (C$^{5G}$), 143.65 (C$^{2B}$), 143.32 (C$^{2D}$), 140.26 (C$^{4F}$), 139.86 (C$^{4E}$), 138.72 (C$^{4C}$), 138.66 (C$^{4A}$), 132.93 (C$^{6D}$), 131.43 (C$^{6B}$), 130.97 (C$^{5B}$), 130.22 (C$^{5D}$), 129.57 (C$^{5F}$), 128.18 (C$^{6C}$), 125.90 (C$^{3E}$), 125.35 (C$^{3B}$), 124.60 (C$^{3F}$), 124.22 (C$^{3D}$), 123.39 (C$^{5A}$), 123.25 (C$^{5C+E}$), 122.93 (C$^{4B}$), 121.67 (C$^{4D}$), 120.16 (C$^{3A}$), 119.75 (C$^{3C}$), 112.57 (C$^{3G}$), 112.08 (C$^{4G}$); ESI-MS *m/z*: 723.1 [M-PF$_6$]$^+$ (100 %, calc. 723.1); IR (solid, $\nu$/cm$^{-1}$) 3124 (w), 3049 (w), 2335 (w), 1607 (m), 1582 (m), 1476 (m), 1437 (m), 1420 (m), 1317 (w), 1270 (w), 1226 (w), 1164 (m), 1125 (w), 1065 (m), 1031 (m), 1014 (m), 920 (w), 885 (w), 831 (s), 821 (s), 796 (m), 754 (s), 728 (s); UV/vis ($CH_2Cl_2$, 5.0 x 10$^{-5}$ mol dm$^{-3}$) $\lambda_{max}$/nm 251 ($\varepsilon$/dm$^3$ mol$^{-1}$ cm$^{-1}$ 50000), 266 (49000), 309 (28000), 372 (8400), 465 (200); emission $\lambda_{max}$ ($\lambda_{ex}$) = 608, 636 (471) nm; EA: calc. for $C_{36}H_{26}N_4OF_6PIr$* ½ $H_2O$, C 49.31 %, H 3.10 %, N 6.39 %, found C 49.23 %, H 3.10 %, N 6.12 %.

### 5.2.3 [Ir(ppy)$_2$(3)][PF$_6$]

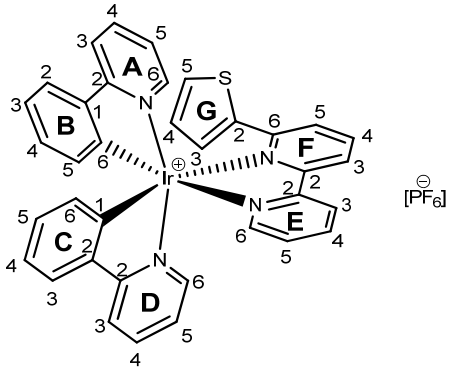

To a 5 ml microwave vial were added ligand **3** (60.0 mg, 250.0 μmol, 2.0 eq) and $[Ir(ppy)_2Cl]_2$ (139.0 mg, 125.0 μmol, 1.0 eq), then suspended in MeOH (5 ml). The mixture was irradiated for 30 min at 110 °C in the microwave reactor. Then the solvent was reduced and the product was precipitated upon addition of solid $NH_4PF_6$ (150.0 mg, 0.90 mmol, 8.0 eq). The solvent was evaporated and the crude product was passed through a short column ($SiO_2$, $CH_2Cl_2$/MeOH 100:0 to 98:2). The desired product was collected as the second major fraction and dried in a desiccator after removal of solvent. It was obtained as an orange powder (224.0 mg, 250.0 μmol, 99.9 %). $^1$H-NMR (500 MHz, $CD_2Cl_2$) $\delta$ (ppm) 8.51 (d, *J* 8.0 Hz, 2 H, $H^{3F+E}$), 8.15 (t, *J* 8.0 Hz, 1 H, $H^{4F}$), 8.13 (dt, *J* 8.0, 2.0 Hz, 1 H, $H^{4E}$), 7.88 (m, 2 H, $H^{6A+C}$), 7.85 (d, *J* 6.0 Hz, 1 H, $H^{6E}$), 7.80 (m, 3 H, $H^{3+3A+4C}$), 7.58 (m, 2 H, $H^{4C+5F}$), 7.54 (d, *J* 6.5 Hz, 1 H, $H^{3B}$), 7.38 (t, *J* 8.0 Hz, 1 H, $H^{5E}$), 7.35 (d, *J* 6.5 Hz, 1 H, $H^{3D}$), 7.10 (t, *J* 6.5 Hz, 1 H, $H^{5A}$), 6.99 (t, *J* 6.5 Hz, 1 H, $H^{5C}$), 6.97 (t, *J* 7.6 Hz, 1 H, $H^{4B}$), 6.90 (s, *J* 5.0 Hz, 1 H, $H^{5G}$), 6.81 (t, *J* 6.3 Hz, 1 H, $H^{5B}$), 6.67 (t, *J* 6.5 Hz, 1 H, $H^{4D}$), 6.47 (t, *J* 6.5 Hz, 1 H, $H^{5D}$), 6.31 (t, *J* 4.4 Hz, 1 H, $H^{4G}$), 6.22 (d, *J* 3.1 Hz, 1 H, $H^{3G}$), 5.96 (d, *J* 7.6 Hz, 1 H, $H^{6B}$), 5.72 (d, *J* 7.6 Hz, 1 H, $H^{6D}$); $^{13}$C NMR (126 MHz, $CD_2Cl_2$) $\delta$ (ppm) 169.28 ($C^{2C}$), 167.49 ($C^{2A}$), 159.02 ($C^{2F}$), 157.64 ($C^{2E}$), 157.41 ($C^{6F}$), 150.86 ($C^{1B}$), 150.82 ($C^{6A}$), 150.44 ($C^{6C}$), 148.88 ($C^{6E}$), 146.56 ($C^{1D}$), 143.50 ($C^{2B}$), 143.19 ($C^{2D}$), 139.99 ($C^{4E}$), 139.86 ($C^{4F}$), 138.78 ($C^{4C}$), 138.70 ($C^{4A}$), 138.60 ($C^{2G}$), 132.57 ($C^{6D}$), 131.45 ($C^{3D}$), 131.22 ($C^{5B}$), 130.94 ($C^{6B}$), 130.14 ($C^{5D}$), 129.79 ($C^{3G}$), 128.30 ($C^{4G}$), 128.04 ($C^{5G}$), 128.01 ($C^{3B}$), 125.79 ($C^{3E}$), 125.21 ($C^{5F}$), 124.70 ($C^{5E}$), 124.51 ($C^{3F}$), 123.76 ($C^{5A}$), 123.31 ($C^{5C}$), 122.93 ($C^{4B}$), 121.32 ($C^{4D}$), 120.33 ($C^{3A}$), 120.19 ($C^{3C}$); EI-MS *m/z*: 739.1 $[M\text{-}PF_6]^+$ (100 %, calc. 739.1); IR (solid, $\nu$/cm$^{-1}$) 3112 (w), 3049 (w), 2628 (w), 2326 (w), 2057 (w), 1982 (w), 1734 (w), 1717 (w), 1684 (m), 1653 (w), 1607 (s), 1583 (s), 1558 (s), 1477 (s), 1456 (s), 1439 (s), 1423 (s), 1419 (s), 1356 (w), 1318 (m), 1268 (m), 1263 (m), 1228 (m), 1164 (m), 1126 (w), 1063 (m), 1030 (m), 1010 (w), 987 (w), 879 (w), 828 (s), 798 (s), 754 (s), 727 (s), 696 (s); UV/vis ($CH_2Cl_2$, 5.0 x 10$^{-5}$ mol dm$^{-3}$) $\lambda_{max}$/nm 255 ($\varepsilon$/dm$^3$ mol$^{-1}$ cm$^{-1}$ 61000), 265 (59000), 309 (31000), 377 (8500), 468 (1500); emission $\lambda_{max}$ ($\lambda_{ex}$) = 613, 640 (384) nm; EA: calc. for $C_{36}H_{26}N_4F_6SPIr*H_2O$, C 47.94 %, H 3.13 %, N 6.21 %, found C 47.87 %, H 3.04 %, N 5.89 .

### 5.2.4 [Ir(ppy)$_2$(4)][PF$_6$]

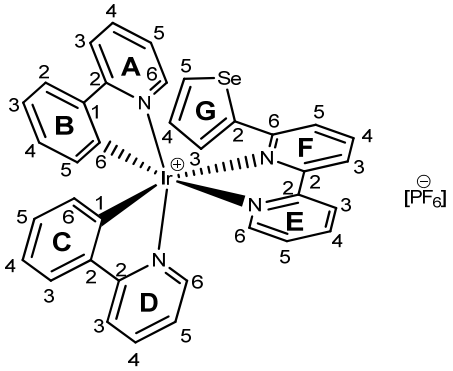


To a 5 ml microwave vial were added ligand **4** (20.0 mg, 69.9 μmol, 2.0 eq) and [Ir(ppy)$_2$Cl]$_2$ (37.4 mg, 34.9 μmol, 1.0 eq), then suspended in MeOH (5 ml). The mixture was irradiated for 45 min at 120 °C in the microwave reactor. Then the solvent was reduced and the product was precipitated upon addition of solid $NH_4PF_6$ (150.0 mg, 0.90 mmol, 16.0 eq). The solvent was evaporated and the crude product was passed through a short column ($SiO_2$, $CH_2Cl_2$/MeOH 100:0-98:2). The desired product was collected as the second major fraction and dried in a desiccator after removal of solvent. It was obtained as an orange powder (62.0 mg, 66.6 μmol, 95.3 %). $^1$H-NMR (500 MHz, $CD_2Cl_2$) $\delta$ (ppm) 8.50 (d, *J* 8.0 Hz, 2 H, $H^{3E+F}$), 8.15 (t, *J* 8.0 Hz, 1 H, $H^{4F}$), 8.17-8.08 (m, 2 H, $H^{4F+E}$), 7.90-7.75 (m, 5 H, $H^{3+4A,3+4C,6E}$), 7.71 (d, *J* 5.8 Hz, 1 H, $H^{6A}$), 7.64 (d, *J* 5.5 Hz, 1 H, $H^{5G}$), 7.63-7.55 (m, 3 H, $H^{3B+5F+6C}$), 7.40-7.33 (m, 2 H, $H^{5E+3D}$), 7.09 (dd, *J* 7.8, 5.8 Hz, 1 H, $H^{5A}$), 7.03-6.95 (m, 2 H, $H^{5C+4B}$), 6.82 (t, *J* 7.5 Hz, 1 H, $H^{5B}$), 6.68 (t, *J* 7.5 Hz, 1 H, $H^{4D}$), 6.51 (dd, *J* 5.5, 3.6 Hz, 1 H, $H^{4G}$), 6.48 (t, *J* 7.5 Hz, 1 H, $H^{5D}$), 6.31 (d, *J* 3.7 Hz, 1 H, $H^{3G}$), 5.97 (d, *J* 7.7 Hz, 1 H, $H^{6B}$), 5.74 (d, *J* 7.7 Hz, 1 H, $H^{6D}$); $^{13}$C NMR (126 MHz, $CD_2Cl_2$) $\delta$ (ppm) 169.36 ($C^{2C}$), 167.55 ($C^{2A}$), 161.13 ($C^{2F}$), 157.51 ($C^{2E}$), 157.40 ($C^{6F}$), 151.34 ($C^{6A}$), 150.84 ($C^{6E}$), 150.24 ($C^{6C}$), 146.66 ($C^{1B+D}$), 144.18 ($C^{2G}$), 143.49 ($C^{2B}$), 143.20 ($C^{2D}$), 139.83 ($C^{4E+F}$), 138.78 ($C^{4A}$), 138.66 ($C^{4C}$), 134.26 ($C^{5G}$), 132.58 ($C^{6D}$), 132.27 ($C^{3G}$), 131.35 ($C^{5F}$), 131.26 ($C^{5B}$), 130.89 ($C^{6B}$), 130.24 ($C^{5D+4G}$), 128.27 ($C^{5E}$), 125.73 ($C^{3E}$), 125.20 ($C^{3B}$), 124.69 ($C^{3F}$), 124.45 ($C^{3D}$), 123.81 ($C^{5A}$), 123.32 ($C^{4B}$), 122.92 ($C^{5C}$), 121.38 ($C^{4D}$), 120.34 ($C^{3A}$), 120.31 ($C^{3C}$); ESI-MS *m/z*: 785.1/787.1 $[M\text{-}PF_6]^+$ (100/97 %, calc. 785.1/787.1); IR (solid, $\nu$/cm$^{-1}$) 3118 (w), 3043 (w), 2924 (w), 2855 (w), 2358 (m), 2340 (m), 2323 (m), 1717 (m), 1684 (m), 1653 (m), 1636 (w), 1607 (m), 1582 (m), 1558 (m), 1539 (m), 1521 (w), 1506 (m), 1476 (s), 1457 (m), 1436 (m), 1420 (m), 1405 (m), 1316 (m), 1306 (m), 1297 (w), 1269 (m), 1260 (m), 1227 (m), 1213 (m), 1165 (m), 1127 (w), 1113 (w), 1063 (m), 1030 (m), 1006 (w), 971 (w), 878 (w), 831 (s), 755 (m), 728 (s), 720 (m), 692 (s), 685 (s), 677 (s), 668 (s), 652 (m), 641 (m); UV/vis ($CH_2Cl_2$, 5.0 x 10$^{-5}$ mol dm$^{-3}$) $\lambda_{max}$/nm 232 ($\varepsilon$/dm$^3$ mol$^{-1}$ cm$^{-1}$ 31200), 258 (41200), 303 (23800), 378 (6800), 468 (200); emission $\lambda_{max}$ ($\lambda_{ex}$) = 603, 640 (300) nm; EA: calc. for $C_{36}H_{26}N_4F_6SePIr$, C 46.46 H 2.82 N 6. 02, found C 46.40 H 2.97 N 5.82.

### 5.2.5 [Ir(ppy)$_2$(20)][PF$_6$]

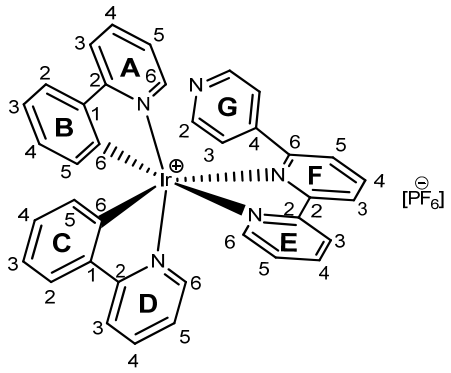

To a 5 ml microwave vial were added ligand **20** (23.3 mg, 100.0 µmol, 2.0 eq) and $[Ir(ppy)_2Cl]_2$ (50.3 mg, 50.0 µmol, 1.0 eq), then suspended in MeOH (5 ml). The mixture was irradiated for 2 h at 120 °C in the microwave reactor. Then the solvent was reduced and the product was precipitated upon addition of solid $NH_4PF_6$ (150.0 mg, 0.90 mmol, 18.0 eq). The solvent was evaporated and the crude product was passed through a short column ($SiO_2$, $CH_2Cl_2$/MeOH 100:0-98:2). The desired product was collected as the second major fraction and dried in a desiccator after removal of solvent. It was obtained as an orange powder (87.0 mg, 100.0 µmol, 99.9 %). $^1$H-NMR (500 MHz, $CD_2Cl_2$) $\delta$ (ppm) 8.62 (dd, *J* 8.2, 1.3 Hz, 1 H, $H^{3F}$), 8.55 (d, *J* 8.4 Hz, 1 H, $H^{3E}$), 8.29 (t, *J* 7.9, 7.9 Hz, 1 H, $H^{4F}$), 8.13 (dt, *J* 8.0, 1.6, 1 H, $H^{4E}$), 8.01 (d, *J* 4.7 Hz, 2 H, $H^{3G}$), 7.91 – 7.86 (m, 3 H, $H^{6E+3+4D}$), 7.84 (ddd, *J* 8.3, 1.4, 0.7 Hz, 1 H, $H^{3A}$), 7.80-7.74 (t, *J* 8.0 Hz, 1 H, $H^{4A}$), 7.68 (dt, *J* 5.8, 1.2, 1.2 Hz, 1 H, $H^{6D}$), 7.55 (dd, *J* 7.8, 1.3 Hz, 1 H, $H^{3B}$), 7.47 – 7.37 (m, 3 H, $H^{6A+5E+F}$), 7.29 (dd, *J* 7.9, 1.3 Hz, 1 H, $H^{3C}$), 7.11 (ddd, *J* 7.5, 5.9, 1.5 Hz, 1 H, $H^{5A}$), 7.06 (ddd, *J* 5.8, 4.9, 4.0 Hz, 1 H, $H^{5D}$), 6.97 (td, *J* 7.7, 1.2 Hz, 1 H, $H^{4B}$), 6.83 (td, *J* 7.5, 1.4 Hz, 1 H, $H^{5B}$), 6.73 (dt, *J* 7.7, 1.2 Hz, 1 H, $H^{4C}$), 6.46 (td, *J* 7.4, 7.4, 1.3 Hz, 1 H, $H^{5C}$), underlying (br s, 2 H, $H^{2G}$), 5.94 (dd, *J* 7.7, 1.1 Hz, 1 H, $H^{6B}$), 5.62 (dd, *J* 7.7, 1.1 Hz, 1 H, $H^{6C}$); $^{13}$C NMR (HMQC/HMBC, 500 MHz, $CD_2Cl_2$) $\delta$ (ppm) 168.90 ($C^{2B+C}$), 168.80 ($C^{2D}$), 167.46 ($C^{2A}$), 163.30 ($C^{2F}$), 157.55 ($C^{6F}$), 156.68 ($C^{2E}$), 150.67 ($C^{6E}$), 149.34 ($C^{6D}$), 149.23 ($C^{2G}$), 149.20 ($C^{6A}$), 144.88 ($C^{4G}$), 143.25 ($C^{1B}$), 143.14 ($C^{1C}$), 140.72 ($C^{4F}$), 139.85 ($C^{4E}$), 138.75 ($C^{4D+A}$), 131.79 ($C^{6C}$), 131.23 ($C^{5B}$), 130.58 ($C^{6B}$), 130.36 ($C^{5C}$), 129.94 ($C^{5F}$), 128.39 ($C^{5E}$), 125.67 ($C^{3E}$), 125.14 ($C^{3B+C}$), 124.80 ($C^{3F}$), 124.04 ($C^{5A}$), 123.36 ($C^{4B}$), 123.06 ($C^{5D}$), 122.60 ($C^{3G}$), 121.73 ($C^{4C}$), 120.52 ($C^{3D}$), 120.33 ($C^{3A}$); ESI-MS *m/z*: 734.2 $[M\text{-}PF_6]^+$ (100 %, calc. 734.2); IR (solid, $\nu$/cm$^{-1}$) 3047 (w), 2930 (w), 2856 (w), 2360 (s), 2356 (m), 2340 (m), 2331 (m), 2319 (m), 2311 (m), 1703 (m), 1699 (m), 1684 (m), 1607 (m), 1594 (m), 1582 (m), 1564 (m), 1558 (m), 1539 (m), 1478 (m), 1447 (m), 1423 (m), 1419 (m), 1405 (m), 1394 (m), 1363 (m), 1316 (w), 1268 (m), 1229 (m), 1217 (m), 1165 (m), 1131 (w), 1110 (w), 1063 (m), 1031 (m), 1008 (m), 877 (m), 832 (s), 801 (m), 755 (m), 736 (m), 729 (m), 717 (m), 692 (m), 668 (s), 653 (m), 639 (m); UV/vis ($CH_2Cl_2$, 5.0 x 10$^{-5}$ mol dm$^{-3}$) $\lambda_{max}$/nm 258 ($\varepsilon$/dm$^3$ mol$^{-1}$ cm$^{-1}$ 36600), 303 (21800), 380 (4600), 409 (2800); emission $\lambda_{max}$ ($\lambda_{ex}$) = 605, 634 (320) nm.

### 5.2.6 [Ir(ppy)$_2$(21)][PF$_6$]

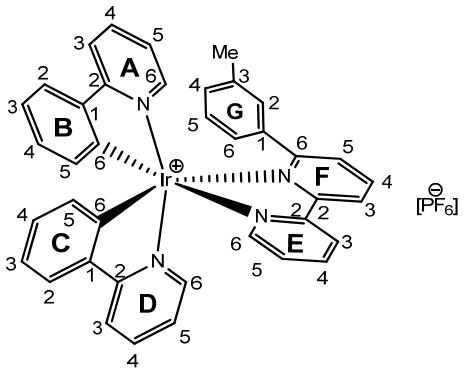


To a 5 ml microwave vial were added ligand **21** (24.6 mg, 100.0 µmol, 2.0 eq) and [Ir(ppy)$_2$Cl]$_2$ (50.3 mg, 50.0 µmol, 1.0 eq), suspended in MeOH (3 ml) and irradiated for 2 h at 120 °C in the microwave reactor. Then the solvent was reduced and the product was precipitated upon addition of solid $NH_4PF_6$ (150.0 mg, 0.90 mmol, 18.0 eq). The solvent was evaporated and the crude product was passed through a short column ($SiO_2$, $CH_2Cl_2$/MeOH 100:0-98:2). The desired product was collected as the second major fraction and dried in a desiccator after removal of solvent and was obtained as an orange powder (89.0 mg, 100.0 µmol, 99.9 %). $^1$H-NMR (500 MHz, $CD_2Cl_2$) (ppm) 8.50 (t, *J* 8.5, 8.5 Hz, 2 H, $H^{3F+E}$), 8.20 (t, *J* 7.9, 7.9 Hz, 1 H, $H^{4F}$), 8.11 (td, *J* 8.2, 8.0, 1.6 Hz, 1 H, $H^{4E}$), 7.89 (ddd, *J* 5.5, 1.6, 0.7 Hz, 1 H, $H^{6E}$), 7.89 – 7.83 (m, 2 H, $H^{3+4D}$), 7.82 (d, *J* 8.0 Hz, 1 H, $H^{3A}$), 7.76 (ddd, *J* 8.2, 7.5, 1.5 Hz, 1 H, $H^{4A}$), 7.70 (d, *J* 5.8 Hz, 1 H, $H^{6D}$), 7.52 (dd, *J* 7.7, 1.2 Hz, 1 H, $H^{3B}$), 7.46 (dd, *J* 7.7, 1.2 Hz, 1 H, $H^{5F}$), 7.38 (ddd, *J* 6.7, 6.1, 1.2 Hz, 2 H, $H^{5E+6A}$), 7.25 (d, *J* 7.5 Hz, 1 H, $H^{3C}$), 7.08 (ddd, *J* 7.4, 5.9, 1.5 Hz, 1 H, $H^{5A}$), 7.04 (td, *J* 6.2, 6.0, 2.4 Hz, 1 H, $H^{5D}$), 6.95 (td, *J* 7.7, 7.7, 1.2 Hz, 1 H, $H^{4B}$), 6.82 (td, *J* 7.5, 7.5, 1.4 Hz, 1 H, $H^{5B}$), 6.72 (d, *J* 7.7 Hz, 1 H, $H^{4G}$), 6.64 (br t, *J* 6.5 Hz, 1 H, $H^{5G}$), 6.58 (td, *J* 7.8, 7.6, 1.2 Hz, 1 H, $H^{5C}$), 6.42 (t, *J* 7.3, 7.3 Hz, 1 H, $H^{5C}$), 6.60-6.00 (br s, 2 H, $H^{2+6G}$), 5.94 (dd, *J* 7.8, 0.9 Hz, 1 H, $H^{6B}$), 5.62 (dd, *J* 7.8, 0.9 Hz, 1 H, $H^{6C}$), 2.00 (s, 3 H, $H^{Me}$); $^{13}$C NMR (HMQC/HMBC, 500 MHz, $CD_2Cl_2$) $\delta$ (ppm) 169.03 ($C^{2D}$), 167.51 ($C^{2A}$), 166.43 ($C^{2F}$), 157.21 ($C^{2E}$), 156.85 ($C^{6F}$), 151.31 ($C^{2C}$), 150.62 ($C^{6E}$), 149.13 ($C^{6D}$), 149.02 ($C^{6A}$), 146.93 ($C^{2B}$), 143.30 ($C^{1G}$), 143.25 ($C^{1B}$), 142.87 ($C^{1C}$), 139.77 ($C^{4F}$), 139.52 ($C^{4E}$), 138.50 ($C^{4A}$), 138.28 ($C^{4D}$), 137.98 ($C^{2G}$), 131.53 ($C^{6C}$), 131.02 ($C^{5B}$), 130.47 ($C^{4G+6B}$), 130.18 ($C^{5F}$), 129.43 ($C^{5C}$), 128.45 ($C^{5G}$), 127.95 ($C^{5E}$), 125.21 ($C^{3E}$), 124.92 ($C^{3B+G}$), 124.80 ($C^{6G}$), 124.31 ($C^{3C}$), 123.73 ($C^{5A}$), 123.66 ($C^{3F}$), 124.04 ($C^{4B}$), 122.62 ($C^{5D}$), 121.01 ($C^{4C}$), 120.10 ($C^{3A+D}$), 168.90 ($C^{Me}$); ESI-MS *m/z*: 747.2 $[M\text{-}PF_6]^+$ (100 %, calc. 747.2); IR (solid, $\nu$/cm$^{-1}$) 3735 (m), 3679 (w), 3634 (w), 3112 (w), 3045 (w), 2930 (w), 2861 (w), 2360 (m), 2356 (m), 2340 (m), 2331 (m), 2311 (m), 1734 (m), 1717 (m), 1684 (m), 1653 (m), 1607 (m), 1583 (m), 1558 (m), 1521 (m), 1478 (m), 1447 (m), 1436 (m), 1419 (m), 1339 (w), 1316 (w), 1297 (w), 1270 (m), 1228 (m), 1165 (m), 1125 (w), 1107 (w), 1064 (m), 1030 (m), 1001 (m), 879 (w), 832 (s), 793 (m), 771 (w), 755 (m), 728 (m), 710 (m), 696 (m), 677 (m), 668 (s), 653 (m), 643 (m); UV/vis ($CH_2Cl_2$, 5.0 x 10$^{-5}$ mol dm$^{-3}$) $\lambda_{max}$/nm

261 (ε/dm$^3$ mol$^{-1}$ cm$^{-1}$ 42000), 307 (23300), 379 (4500), 405 (3100); emission $\lambda_{max}$ ($\lambda_{ex}$) = 607, 637 (308) nm.

### 5.2.7 [Ir(ppy)$_2$(11)][PF$_6$]

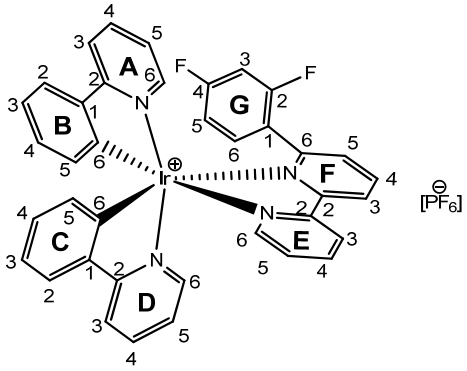


To a 5 ml microwave vial were added ligand **11** (26.8 mg, 100.0 µmol, 2.0 eq) and [Ir(ppy)$_2$Cl]$_2$ (50.3 mg, 50.0 µmol, 1.0 eq), suspended in MeOH (3 ml) and irradiated for 2 h at 120 °C in the microwave reactor. Then the solvent was reduced and the product was precipitated upon addition of solid $NH_4PF_6$ (150.0 mg, 0.90 mmol, 18.0 eq). The solvent was evaporated and the crude product was passed through a short column ($SiO_2$, $CH_2Cl_2$/MeOH 100:0-98:2). The desired product was collected as the second major fraction and dried in a desiccator after removal of solvent. It was obtained as an orange powder (91.0 mg, 99.6 µmol, 99.6 %). $^1$H-NMR (500 MHz, $CD_2Cl_2$) (ppm) 8.62 (dd, *J* 8.2, 1.3 Hz, 1 H, H$^{3F}$), 8.54 (d, *J* 8.2 Hz, 1 H, H$^{3E}$), 8.27 (t, *J* 7.9 Hz, 1 H, H$^{4F}$), 8.11 (t, *J* 7.5 Hz, 1 H, H$^{4E}$), 7.91 – 7.62 (m, 6 H, H$^{6E+3A+D+4A+D+6D}$), 7.55 (d, *J* 7.8 Hz, 1 H, H$^{3B}$), 7.47 (d, *J* 7.8 Hz, 1 H, H$^{5F}$), 7.44 (br s, 1 H, H$^{6A}$), 7.38 (ddd, *J* 7.6, 5.5, 1.2 Hz, 1 H, H$^{5E}$), 7.32 (br s, 1 H, H$^{3C}$), 7.18 – 6.99 (m, 2 H, H$^{5A+D}$), 6.97 (td, *J* 7.7, 1.2 Hz, 1 H, H$^{4B}$), 6.83 (t, *J* 7.5 Hz, 1 H, H$^{5B}$), 6.76 (td, *J* 7.7, 1.2 Hz, 1 H, H$^{4C}$), 6.63-6.36 (br, 2 H, H$^{5C+6G}$), 6.24 (br s, 1 H, H$^{5G}$), 6.13 (br s, 1 H, H$^{3G}$), 5.96 (d, *J* 7.9 Hz, 1 H, H$^{6B}$), 5.86 (br s, 1 H, H$^{6C}$); $^{13}$C-NMR (HMQC/HMBC, 500 MHz, $CD_2Cl_2$) *δ* (ppm) 167.23 (C$^{2D}$), 166.00 (C$^{2A}$), 163.07 (C$^{4G}$), 162.00 (C$^{2G}$), 159.23 (C$^{2F}$), 157.33 (C$^{6F}$), 156.71 (C$^{2E}$), 150.90 (C$^{6E}$), 149.57 (C$^{6A}$), 149.21 (C$^{6D}$), 146.71 (C$^{2B}$), 143.51 (C$^{1B}$), 143.23 (C$^{1C}$), 140.31 (C$^{4F}$), 139.68 (C$^{4E}$), 138.62 (C$^{4A}$), 138.54 (C$^{4D}$), 131.33 (C$^{6B}$), 131.12 (C$^{5B}$), 130.98 (C$^{5F}$), 130.90 (C$^{6G}$), 130.46 (C$^{6C}$), 130.10 (C$^{5C}$), 129.77 (C$^{5E}$), 125.45 (C$^{3E}$), 124.90 (C$^{3B}$), 124.79 (C$^{3F}$), 124.73 (C$^{3C+1G}$), 123.69 (C$^{5D}$), 123.31 (C$^{4B}$), 123.00 (C$^{5A}$), 121.10 (C$^{4C}$), 120.17 (C$^{3A+D}$), 111.55 (C$^{5C}$), 104.19 (C$^{3C}$); ESI-MS *m/z*: 769.2 [M-PF$_6$]$^+$ (100 %, calc. 769.2); IR (solid, ν/cm$^{-1}$) 3115 (w), 3046 (w), 2376 (w), 2324 (w), 1753 (w), 1708 (w), 1622 (w), 1607 (m), 1583 (m), 1564 (m), 1554 (m), 1511 (m), 1478 (s), 1449 (s), 1440 (m), 1422 (m), 1419 (m), 1391 (m), 1317 (w), 1294 (m), 1268 (m), 1228 (m), 1187 (w), 1165 (m), 1140 (m), 1129 (w), 1105 (m), 1093 (m), 1063 (m), 1030 (m), 1007 (w), 964 (m), 879 (w), 833 (s), 752 (s), 729 (s), 702 (m), 669 (m), 653 (m), 641 (m), 627 (m), 611 (m); UV/vis ($CH_2Cl_2$, 5.0 x 10$^{-5}$ mol dm$^{-3}$) $\lambda_{max}$/nm 229 (ε/dm$^3$ mol$^{-1}$ cm$^{-1}$ 36600), 270 (45000), sh 310 (24000), 385 (5500), 419 (2600); emission $\lambda_{max}$ ($\lambda_{ex}$) = 599/634 (275) nm.

### 5.2.8 [Ir(ppy)$_2$(12)][PF$_6$]

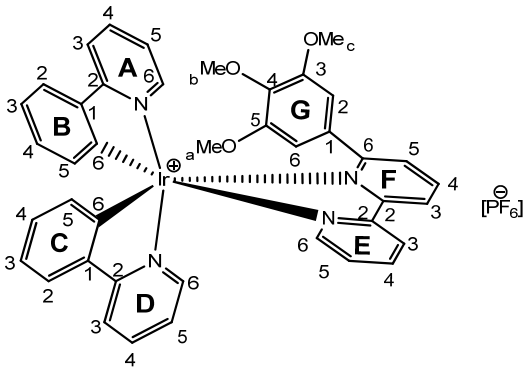


To a 5 ml microwave vial were added ligand **12** (33.3 mg, 31.0 µmol, 2.0 eq) and [Ir(ppy)$_2$Cl]$_2$ (20.3 mg, 62.0 µmol, 1.0 eq), suspended in MeOH (3 ml) and irradiated for 2 h at 120 °C in the microwave reactor. Then the solvent was reduced and the product was precipitated upon addition of solid $NH_4PF_6$ (80.9 mg, 0.50 mmol, 16.0 eq). The solvent was evaporated and the crude product was passed through a short column ($SiO_2$, $CH_2Cl_2$/MeOH 100:0-98:2). The desired product was collected as the second major fraction and dried in a desiccator after removal of solvent and was obtained as an orange powder (59.0 mg, 61.0 µmol, 98.2 %). $^1$H-NMR (500 MHz, $CD_2Cl_2$) (ppm) 8.54 – 8.46 (m, 1 H, $H^{3F+E}$), 8.20 (t, *J* 7.9, 7.9 Hz, 1 H, $H^{4F}$), 8.11 (ddd, *J* 8.2, 7.6, 1.6 Hz, 1 H, $H^{4E}$), 7.89 (ddd, *J* 5.5, 1.6, 0.7 Hz, 1 H, $H^{6E}$), 7.88-7.81 (m, 3 H, $H^{3+4D+3A}$), 7.77 (ddd, *J* 8.2, 7.4, 1.5 Hz, 1 H, $H^{4A}$), 7.70 (ddd, *J* 5.8, 1.5, 0.8 Hz, 1 H, $H^{6D}$), 7.55 (dd, *J* 7.7, 1.4 Hz, 1 H, $H^{3B}$), 7.51 – 7.45 (m, 2 H, $H^{6A+5F}$), 7.38 (ddd, *J* 7.6, 5.5, 1.2 Hz, 1 H, $H^{5E}$), 7.32 (dd, *J* 7.7, 1.3 Hz, 1 H, $H^{3C}$), 7.08 (ddd, *J* 7.4, 5.8, 1.5 Hz, 1 H, $H^{5A}$), 7.04 (ddd, *J* 7.3, 5.8, 1.7 Hz, 1 H, $H^{5D}$), 6.96 (ddd, *J* 7.8, 7.3, 1.2 Hz, 1 H, $H^{4B}$), 6.82 (td, *J* 7.5, 7.4, 1.4 Hz, 1 H, $H^{5B}$), 6.65 (ddd, *J* 7.7, 7.2, 1.2 Hz, 1 H, $H^{4C}$), 6.50 (td, *J* 7.5, 7.5, 1.3 Hz, 1 H, $H^{5C}$), 6.24 (br s, 2 H, $H^{2G}$), 5.89 (ddd, *J* 7.7, 1.2, 0.5 Hz, 1 H, $H^{6B}$), 5.73 (ddd, *J* 7.6, 1.2, 0.5 Hz, 1 H, $H^{6C}$), 3.68 (s, 3 H, $H^{Me}{}_c$), 3.60 (br s, 3 H, $H^{Me}{}_a$), 3.31 (br s, 3 H, $H^{Me}{}_b$); $^{13}$C NMR (HMQC/HMBC, 500 MHz, $CD_2Cl_2$) $\delta$ (ppm) 169.19 ($C^{2D}$), 167.60 ($C^{2A}$), 166.08 ($C^{2F}$), 157.30 ($C^{2E}$), 156.82 ($C^{6F}$), 150.88 ($C^{2B}$), 150.60 ($C^{6E}$), 149.20 ($C^{6A}$), 149.17 ($C^{6D}$), 146.96 ($C^{2C}$), 143.32 ($C^{1B}$), 142.82 ($C^{1C}$), 139.59 ($C^{4F}$), 139.50 ($C^{4E}$), 138.57 ($C^{4A}$), 138.43 ($C^{4D}$), 137.95 ($C^{4G}$), 133.87 ($C^{1G}$), 131.54 ($C^{6C}$), 131.14 ($C^{5B}$), 130.52 ($C^{6B}$), 130.31 ($C^{5F}$), 129.32 ($C^{5C}$), 128.01 ($C^{5E}$), 125.28 ($C^{3E}$), 125.04 ($C^{3B}$), 124.03 ($C^{3C}$), 123.88 ($C^{3F}$), 123.68 ($C^{5A}$), 123.24 ($C^{4B}$), 122.70 ($C^{5D}$), 121.46 ($C^{4C}$), 120.31 ($C^{3A}$), 119.96 ($C^{3D}$), 105.93 ($C^{2G}$), 60.18 ($C^{Me}{}_c$), 55.95 ($C^{Me}{}_a$), 55.64 ($C^{Me}{}_b$); ESI-MS *m/z*: 823.2 $[M\text{-}PF_6]^+$ (40 %, calc. 823.2); UV/vis ($CH_2Cl_2$, 5.0 x $10^{-5}$ mol dm$^{-3}$) $\lambda_{max}$/nm 230 ($\varepsilon$/dm$^3$ mol$^{-1}$ cm$^{-1}$ 37200), 267 (46100), sh 305 (28600), 383 (5000); emission $\lambda_{max}$ ($\lambda_{ex}$) = 600/637 (270) nm.

### 5.2.9 [Ir(ppy)$_2$(10)][PF$_6$]

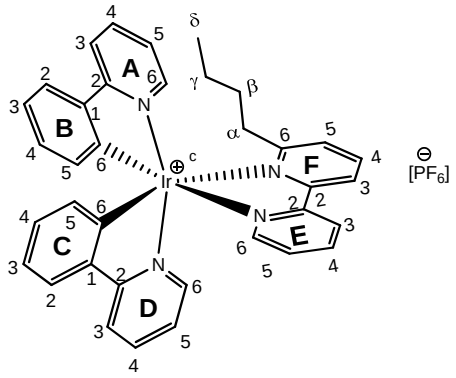


To a 5 ml microwave vial were added ligand **10** (42.4 mg, 200.0 µmol, 2.0 eq) and [Ir(ppy)$_2$Cl]$_2$ (107.1 mg, 100.0 µmol, 1.0 eq), suspended in MeOH (3 ml) and irradiated for 2 h at 120 °C in the microwave reactor. Then the solvent was reduced and the product was precipitated upon addition of solid $NH_4PF_6$ (150.0 mg, 0.90 mmol, 9.0 eq). The solvent was evaporated and the crude product was passed through a short column ($SiO_2$, $CH_2Cl_2$/MeOH 100:0-98:2). The desired product was collected as the second major fraction and dried in a desiccator after removal of solvent. It was obtained as an orange powder (173.6 mg, 100.0 µmol, 99.9 %). $^1$H-NMR (500 MHz, $CD_2Cl_2$) (ppm) 8.46 (d, *J* 8.3 Hz, 1 H, $H^{3E}$), 8.38 (dd, *J* 8.0, 1.0 Hz, 1 H, $H^{3F}$), 8.13 – 8.04 (m, 2 H, $H^{4F+E}$), 7.99 (d, *J* 8.0 Hz, 1 H, $H^{3A}$), 7.95 (dt, *J* 8.2, 1.1 Hz, 1 H, $H^{3D}$), 7.85 (ddd, *J* 5.5, 1.6, 0.7 Hz, 1 H, $H^{6E}$), 7.83 – 7.77 (m, 2 H, $H^{4D+A}$), 7.71 (dd, *J* 7.7, 1.3 Hz, 1 H, $H^{3B}$), 7.70 – 7.63 (m, 2 H, $H^{6D+3C}$), 7.47 (dd, *J* 7.9, 1.2 Hz, 1 H, $H^{5F}$), 7.44 (ddd, *J* 5.9, 1.5, 0.8 Hz, 1 H, $H^{6A}$), 7.35 (ddd, *J* 7.6, 5.6, 1.2 Hz, 1 H, $H^{5E}$), 7.08 – 7.00 (m, 2 H, $H^{4C+5D}$), 7.00 – 6.94 (m, 2 H, $H^{5A+4B}$), 6.89 (td, *J* 7.6, 1.4 Hz, 1 H, $H^{5C}$), 6.84 (td, *J* 7.5, 1.3 Hz, 1 H, $H^{5B}$), 6.26 – 6.20 (dd, *J* 7.7, 0.8 Hz, 1 H, $H^{6B}$), 6.05 (dd, *J* 7.7, 0.8 Hz, 1 H, $H^{6C}$), 2.62 (ddd, *J* 15.2, 11.7, 5.0 Hz, 1 H, $H^{\alpha}$), 2.44 (ddd, *J* 15.2, 11.6, 5.0 Hz, 1 H, $H^{\alpha}$), 1.29 – 1.13 (m, 1 H, $H^{\beta}$), 1.01-0.87 (m, 1 H, $H^{\beta}$), 0.79 – 0.67 (m, 1 H, $H^{\gamma}$), 0.67 – 0.56 (m, 4 H, $H^{\gamma+\delta}$); $^{13}$C NMR (HMQC/HMBC, 500 MHz, $CD_2Cl_2$) $\delta$ (ppm) 168.58 ($C^{2A}$), 168.32 ($C^{2F}$), 167.50 ($C^{2D}$), 157.70 ($C^{2E}$), 156.11 ($C^{6F}$), 151.67 ($C^{2B}$), 150.69 ($C^{6E}$), 149.91 ($C^{6D}$), 148.78 ($C^{6A}$), 147.37 ($C^{2C}$), 143.49 ($C^{1B}$), 143.33 ($C^{1C}$), 140.13 ($C^{4F}$), 139.64 ($C^{4E}$), 138.62 ($C^{4D}$), 138.56 ($C^{4A}$), 132.14 ($C^{6B}$), 131.45 ($C^{5C}$), 130.82 ($C^{5B}$), 130.59 ($C^{6C}$), 127.93 ($C^{5E}$), 127.48 ($C^{5F}$), 125.29 ($C^{3C}$), 125.21 ($C^{3B}$), 125.16 ($C^{3E}$), 123.89 ($C^{5D}$), 123.36 ($C^{4C}$), 123.23 ($C^{5A}$), 122.78 ($C^{3F}$), 122.36 ($C^{4B}$), 120.46 ($C^{3D}$), 120.11 ($C^{3A}$), 40.47 ($C^{\alpha}$), 32.48 ($C^{\beta}$), 22.36 ($C^{\gamma}$), 13.82 ($C^{\delta}$); ESI-MS *m/z*: 713.2 $[M\text{-}PF_6]^+$ (100 %, calc. 713.2); IR (solid, $\nu$/cm$^{-1}$) 3118 (w), 3108 (w), 3043 (w), 2955 (w), 2927 (w), 2869 (w), 2858 (w), 2356 (s), 2340 (s), 2323 (s), 2311 (m), 1945 (w), 1923 (w), 1848 (w), 1829 (w), 1751 (m), 1734 (m), 1706 (m), 1695 (m), 1653 (m), 1636 (m), 1607 (s), 1582 (s), 1558 (s), 1550 (m), 1521 (m), 1506 (m), 1477 (s), 1456 (s), 1450 (s), 1439 (s), 1419 (s), 1405 (m), 1394 (m), 1374 (m), 1317 (m), 1303 (m), 1297 (w), 1269 (m), 1252 (w), 1228 (w), 1186 (w), 1165 (m), 1125 (w), 1099 (w), 1063 (m), 1030 (m), 1004 (w), 938 (w), 878 (m), 830 (s), 793 (s), 755 (s), 736

(s), 729 (s), 711 (m), 694 (m), 668 (s), 655 (w), 643 (m), 626 (m); UV/vis ($CH_2Cl_2$, 5.0 x $10^{-5}$ mol $dm^{-3}$) $\lambda_{max}$/nm 255 ($\varepsilon$/$dm^3$ $mol^{-1}$ $cm^{-1}$ 47300), 304 (26700), 379 (5100), 410 (3500); emission $\lambda_{max}$ ($\lambda_{ex}$) = 574 (322) nm.

### 5.2.10 [Ir(ppy)$_2$(22)][PF$_6$]

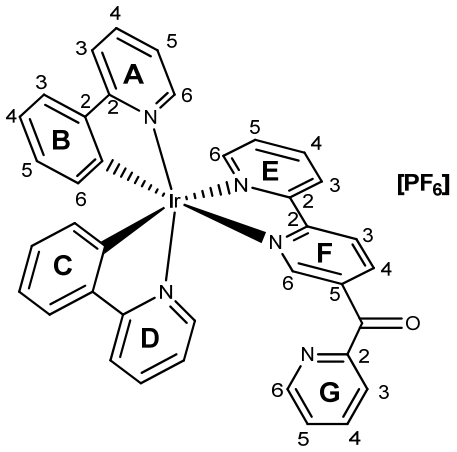


To a 5 ml microwave vial were added ligand **22** (50.0 mg, 191.1 µmol, 2.0 eq) and $[Ir(ppy)_2Cl]_2$ (102.5 mg, 95.7 µmol, 1.0 eq), suspended in MeOH (3 ml) and irradiated for 1 h at 120 °C in the microwave reactor. The resulting mixture contained still starting material and was stirred for a further 15 min at the same conditions in the microwave reactor. TLC then showed 2-acetylpyridine which indicates ligand decomposition and the reaction was stopped. The yellow precipitate (Ir-precursor) was filtered off (38.0 mg, 35.0 µmol). Then the solvent was reduced and the product was precipitated upon addition of solid $NH_4PF_6$ (125.0 mg, 0.77 mmol). The solvent was evaporated and the crude product was passed through a short column ($SiO_2$, $CH_2Cl_2$/MeOH 100:0-98:2). The desired product was collected as the second major fraction and dried in a desiccator after removal of solvent. It was obtained as an red solid (56.0 mg, 61.2 µmol, 32 %). $^1$H-NMR (600 MHz, $CD_2Cl_2$) (ppm) 9.07 (d, *J* 1.8 Hz, 1 H, $H^{6F}$), 8.84 (dd, *J* 8.4, 2.0 Hz, 1 H, $H^{4F}$), 8.62 (d, *J* 8.5 Hz, 1 H, $H^{3F}$), 8.61 (d, *J* 8.3 Hz, 1 H, $H^{3E}$), 8.44 (ddd, *J* 4.7, 1.7, 0.9 Hz, 1 H, $H^{6G}$), 8.19 (td, *J* 8.0, 1.6 Hz, 1 H, $H^{4E}$), 8.12-8.04 (m, 2 H, $H^{6E+3G}$), 7.98 (d, *J* 8.6 Hz, 2 H, $H^{3A+D}$), 7.91 (td, *J* 7.7, 1.7 Hz, 1 H, $H^{4G}$), 7.80 (t, *J* 7.8 Hz, 2 H, $H^{4A+D}$), 7.76 (d, *J* 7.9 Hz, 1 H, $H^{3B}$), 7.73 (d, *J* 7.8 Hz, 1 H, $H^{3C}$), 7.60 (d, *J* 5.6 Hz, 1 H, $H^{6D}$), 7.55 – 7.49 (m, 3 H, $H^{5E+G+6A}$), 7.09 (td, *J* 7.7, 1.2 Hz, 1 H, $H^{4B}$), 7.07 – 6.98 (m, 3 H, $H^{4C+5A+D}$), 6.96 (td, *J* 7.4, 1.3 Hz, 1 H, $H^{5B}$), 6.91 (td, *J* 7.5, 1.3 Hz, 1 H, $H^{5C}$), 6.33 (dd, *J* 7.6, 1.2 Hz, 2 H, $H^{6B+C}$); $^{13}$C NMR (HMQC/HMBC, 500 MHz, $CD_2Cl_2$) $\delta$ (ppm) 188.26 ($C^{C=O}$), 168.00 ($C^{2D}$), 167.89 ($C^{2A}$), 157.91 ($C^{2E}$), 155.05 ($C^{2F}$), 154.21 ($C^{6F}$), 152.69 ($C^{2B/C}$), 151.28 ($C^{6E}$), 149.70 ($C^{6D}$), 149.66 ($C^{6A}$), 149.10 ($C^{6G}$), 148.80 ($C^{2G}$), 143.86 ($C^{1B/C}$), 141.35 ($C^{3F}$), 139.78 ($C^{4E}$), 138.54 ($C^{4A/D}$), 138.10 ($C^{4G}$), 137.82 ($C^{4F}$), 131.83 ($C^{6B/C}$), 131.70 ($C^{5B/C}$), 129.24/127.70 ($C^{5E/G}$), 125.80 ($C^{3E}$), 125.15/125.07 ($C^{3B/C}$), 124.59 ($C^{3G}$), 124.06/123.83 ($C^{5A/D}$), 123.66/123.57 ($C^{4B/C}$), 123.02 ($C^{3F}$), 120.25/120.17 ($C^{3A/D}$); ESI-MS *m/z*: 762.2 $[M\text{-}PF_6]^+$ (100 %, calc. 762.2); IR (solid,

$\nu/cm^{-1}$) 3059 (w), 2920 (m), 2850 (m), 2361 (w), 1717 (m), 1674 (m), 1668 (m), 1662 (m), 1607 (s), 1582 (s), 1563 (m), 1558 (m), 1553 (m), 1478 (s), 1468 (m), 1464 (m), 1436 (m), 1419 (m), 1379 (m), 1360 (m), 1308 (m), 1284 (m), 1270 (m), 1246 (m), 1228 (m), 1165 (m), 1141 (w), 1127 (w), 1114 (w), 1092 (w), 1065 (m), 1032 (m), 996 (m), 947 (m), 878 (m), 830 (s), 801 (s), 795 (s), 750 (s), 738 (s), 730 (s), 719 (s), 698 (s), 678 (s), 662 (m), 619 (m); UV/vis ($CH_2Cl_2$, 1.0 x $10^{-5}$ mol $dm^{-3}$) $\lambda_{max}$/nm 231 ($\varepsilon/dm^3\ mol^{-1}\ cm^{-1}$ 30900), 262 (51000), 288 (40800), sh 321 (27000), 380 (7900), 407 (6400); emission $\lambda_{max}$ ($\lambda_{ex}$) = 587/664 (380) nm.

### 5.2.11 [Ir(ppy)$_2$(30)][PF$_6$]

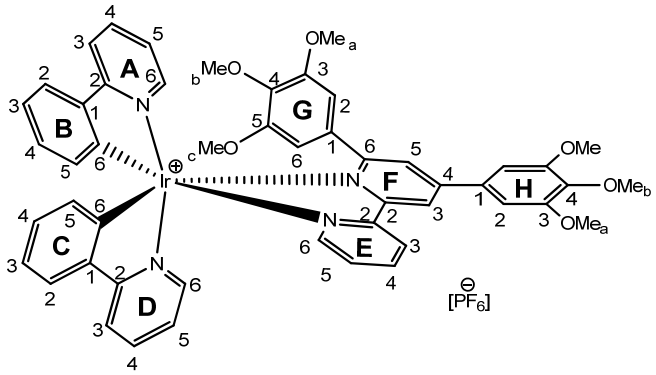


To a 5 ml microwave vial were added ligand **30** (48.9 mg, 100.0 µmol, 2.0 eq) and $[Ir(ppy)_2Cl]_2$ (53.6 mg, 50.0 µmol, 1.0 eq), suspended in MeOH (3 ml) and irradiated for 2 h at 120 °C in the microwave reactor. Then the solvent was reduced and the product was precipitated upon addition of solid $NH_4PF_6$ (130.0 mg, 0.8 mmol, 8.0 eq). The solvent was evaporated and the crude product was passed through a short column ($SiO_2$, $CH_2Cl_2$/MeOH 100:0-98:2). The desired product was collected as the first major fraction and dried in a desiccator after removal of solvent. It was obtained as an orange powder (112.0 mg, 98.8 µmol, 98.8 %). $^1$H-NMR (500 MHz, $CD_2Cl_2$) (ppm) 8.69 (d, *J* 8.3 Hz, 1 H, $H^{3E}$), 8.65 (d, *J* 2.0, 1.0 Hz, 1 H, $H^{3F}$), 8.15 (td, *J* 8.2, 1.6 Hz, 1 H, $H^{4E}$), 7.90 – 7.75 (m, 6 H, $H^{6E+3A+D+4A+D+6A}$), 7.72 (d, *J* 5.2 Hz, 1 H, $H^{6D}$), 7.60 (d, *J* 2.0 Hz, 1 H, $H^{5F}$), 7.57 (d, *J* 6.6 Hz, 1 H, $H^{3B}$), 7.38 (ddd, *J* 7.6, 5.5, 1.1 Hz, 1 H, $H^{5E}$), 7.33 (dd, *J* 7.3, 1.1 Hz, 1 H, $H^{3C}$), 7.12 (ddd, *J* 7.4, 5.8, 1.4 Hz, 2 H, $H^{5D}$), 7.09-7.03 (m, 3 H, $H^{5A+2H}$), 6.97 (ddd, *J* 7.6, 7.2, 1.6 Hz, 1 H, $H^{4B}$), 6.82 (td, *J* 7.6, 1.4 Hz, 1 H, $H^{5B}$), 6.65 (td, *J* 7.8, 1.2 Hz, 1 H, $H^{4C}$), 6.50 (td, *J* 7.5, 1.3 Hz, 1 H, $H^{5C}$), 6.34 (br s, 1 H, $H^{2G}$), 5.92 (dd, *J* 7.7, 0.9 Hz, 1 H, $H^{6B}$), 5.74 (d, *J* 7.6 Hz, 1 H, $H^{6C}$), 5.38 (br s, 1 H, $H^{6G}$), 3.95 (s, 6 H, $H^{OMe_b\ H}$), 3.86 (s, 3 H, $H^{OMe_a\ H}$), 3.69 (s, 3 H, $H^{OMe_b\ G}$), 3.63 (s, 3 H, $H^{OMe_c\ G}$), 3.36 (br s, 2 H, $H^{OMe_a\ G}$); $^{13}$C NMR (HMQC/HMBC, 500 MHz, $CD_2Cl_2$) $\delta$ (ppm) 169.11 ($C^{2A}$), 167.13 ($C^{2D}$), 157.32 ($C^{2F+2E}$), 154.87 ($C^{3H}$), 152.78 ($C^{5G}$), 152.24 ($C^{3G}$), 151.46 ($C^{6F}$), 151.24 ($C^{2C}$), 150.60 ($C^{6E}$), 149.65 ($C^{6A}$), 149.33 ($C^{6D}$), 147.71 ($C^{2B}$), 143.44 ($C^{1B}$), 142.80 ($C^{1C}$), 141.40 ($C^{4H}$), 139.75 ($C^{4E}$), 138.63 ($C^{4A}$), 138.43 ($C^{4D}$), 138.03 ($C^{4G}$), 134.28 ($C^{1G+H}$), 131.64 ($C^{6C}$), 131.18 ($C^{4F}$), 131.07 ($C^{5B}$), 130.64 ($C^{6B}$), 129.33 ($C^{5C}$), 128.10 ($C^{5E}$), 127.43 ($C^{5F}$), 125.82 ($C^{3E}$), 125.10 ($C^{3B}$), 123.97

($C^{3C}$), 123.70 ($C^{5D}$), 123.12 ($C^{4C}$), 122.88 ($C^{5A}$), 121.47 ($C^{3F}$), 121.39 ($C^{4C}$), 120.32 ($C^{3D}$), 120.11 ($C^{3A}$), 106.02 ($C^{2G}$), 105.88 ($C^{6G}$), 105.39 ($C^{2H}$), 61.00 ($C^{OMe_b H}$), 60.17 ($C^{OMe_b G}$), 56.78 ($C^{OMe_a H}$), 55.87 ($C^{OMe_a G}$), 55.82 ($C^{OMe_c G}$); ESI-MS *m/z*: 989.4 $[M\text{-}PF_6]^+$ (100 %, calc. 989.3); IR (solid, $\nu/cm^{-1}$) 3055 (w), 2997 (w), 2935 (w), 2840 (w), 1702 (w), 1606 (m), 1583 (m), 1568 (w), 1564 (w), 1538 (w), 1504 (m), 1477 (m), 1453 (m), 1440 (w), 1393 (m), 1330 (m), 1318 (w), 1306 (w), 1268 (w), 1238 (m), 1164 (w), 1122 (m), 1108 (m), 1101 (m), 1059 (w), 1030 (w), 998 (m), 968 (w), 827 (s), 804 (m), 787 (m), 756 (m), 749 (m), 728 (m), 676 (m), 669 (m), 659 (m), 653 (m), 639 (w); UV/vis ($CH_2Cl_2$, 5.0 x $10^{-5}$ mol $dm^{-3}$) $\lambda_{max}$/nm 232 ($\varepsilon/dm^3\ mol^{-1}\ cm^{-1}$ 51500), 262 (47300), 295 (42000), sh 314 (33100), 366 (18900), 470 (1300); emission $\lambda_{max}$ ($\lambda_{ex}$) = 601/634 (280) nm; EA: calc. for $C_{50}H_{44}N_4O_6F_6PIr$, C 52.92 %, H 3.91 %, N 4.94 %, found C 52.36 %, H 3.92 %, N 4.83 %.

### 5.2.12 [Ir(ppy)$_2$(31)][PF$_6$]

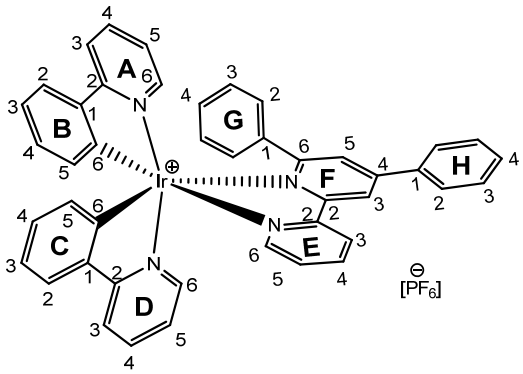


To a 5 ml microwave vial were added ligand **31** (30.8 mg, 100.0 µmol, 2.0 eq) and $[Ir(ppy)_2Cl]_2$ (53.6 mg, 100.0 µmol, 1.0 eq), suspended in MeOH (3 ml) and irradiated for 2 h at 120 °C in the microwave reactor. Then the solvent was reduced and the product was precipitated upon addition of solid $NH_4PF_6$ (130.0 mg, 0.80 mmol, 8.0 eq). The solvent was evaporated and the crude product was passed through a short column ($SiO_2$, $CH_2Cl_2$/MeOH 100:0-98:2). The desired product was collected as the second major fraction and dried in a desiccator after removal of solvent. It was obtained as an orange powder (80.0 mg, 98.9 µmol, 98.9 %). $^1$H-NMR (500 MHz, $CD_2Cl_2$) (ppm) 8.69 (d, *J* 1.9 Hz, 1 H, $H^{3F}$), 8.62 (d, *J* 8.2 Hz, 1 H, $H^{3E}$), 8.14 (td, *J* 8.1, 1.6 Hz, 1 H, $H^{4E}$), 7.94 – 7.80 (m, 6 H, $H^{6E+2H+3D+4H+3A}$), 7.76 (td, *J* 8.2, 1.5 Hz, 1 H, $H^{4A}$), 7.72 – 7.68 (m, 2 H, $H^{6D+5F}$), 7.65 – 7.57 (m, 4 H, $H^{3+4H+6A}$), 7.54 (dd, *J* 7.8, 1.3 Hz,, 1 H, $H^{3B}$), 7.41 (ddd, *J* 7.5, 5.5, 0.9 Hz,1 H, $H^{5E}$), 7.25 (dd, *J* 7.8, 1.1 Hz,1 H, $H^{3C}$), 7.11 – 7.01 (m, 2 H, $H^{5A+D}$), 7.00-6.40 (m, 2 H, $H^{4G+4B}$), 6.83 (td, *J* 7.5, 1.4 Hz,1 H, $H^{5B}$), 6.76 (t, *J* 7.7 Hz, 2 H, $H^{3G}$), 6.62 (dt, *J* 7.6, 1.2 Hz, 1 H, $H^{4C}$), 6.58 (br s, 2 H, $H^{2G}$), 6.40 (td, *J* 7.5, 1.3 Hz, 1H, $H^{5C}$), 5.97 (dd, *J* 7.8, 0.9 Hz, 1 H, $H^{6B}$), 5.60 (dd, *J* 7.8, 0.9 Hz, 1 H, $H^{6C}$); $^{13}$C NMR (HMQC/HMBC, 500 MHz, $CD_2Cl_2$) $\delta$ (ppm) 169.43 ($C^{2D}$), 167.76 ($C^{2A}$), 166.56 ($C^{2F}$), 157.94 ($C^{6F}$), 157.43 ($C^{2E}$), 151.74 ($C^{2C}$), 151.41 ($C^{2B}$), 150.95 ($C^{6E}$), 149.41 ($C^{6A}$), 147.32 ($C^{6D}$), 143.48

($C^{1B}$), 143.23 ($C^{1C}$), 139.78 ($C^{4E}$), 138.66 ($C^{4A}$), 138.46 ($C^{4D}$), 138.24 ($C^{1G}$), 135.62 ($C^{1H}$), 131.91 ($C^{6C}$), 131.71 ($C^{4H}$), 131.65 ($C^{4F}$), 131.33 ($C^{5B}$), 130.74 ($C^{6B}$), 130.24 ($C^{5C}$), 130.10 ($C^{3H}$), 129.57 ($C^{4G}$), 128.41 ($C^{3G}$), 128.33 ($C^{5E}$), 127.94 ($C^{2G}$), 127.80 ($C^{2H}$), 127.74 ($C^{5F}$), 125.49 ($C^{3E}$), 125.17 ($C^{3B}$), 125.03 ($C^{3C}$), 123.88 ($C^{5A}$), 123.34 ($C^{4B}$), 122.92 ($C^{5D}$), 121.40 ($C^{4C}$), 121.32 ($C^{3F}$), 120.40 ($C^{3A}$), 120.34 ($C^{3D}$); ESI-MS *m/z*: 809.2 $[M\text{-}PF_6]^+$ (100 %, calc. 809.2); IR (solid, $\nu/cm^{-1}$) 3118 (w), 3108 (w), 3043 (w), 2955 (w), 2927 (w), 2869 (w), 2858 (w), 2356 (s), 2340 (s), 2323 (s), 2311 (m), 1981 (w), 1607 (m), 1582 (m), 1541 (m), 1533 (w), 1477 (s), 1451 (w), 1439 (m), 1423 (m), 1412 (m), 1397 (m), 1368 (w), 1364 (w), 1316 (w), 1307 (w), 1269 (w), 1243 (w), 1228 (w), 1164 (m), 1126 (w), 1064 (w), 1030 (m), 1021 (w), 1006 (w), 969 (w), 877 (w), 830 (s), 790 (m), 754 (s), 745 (s), 727 (s), 692 (s), 687 (s), 675 (m), 653 (m); UV/vis ($CH_2Cl_2$, 1.0 x $10^{-5}$ mol $dm^{-3}$) $\lambda_{max}$/nm 272 ($\varepsilon/dm^3\ mol^{-1}\ cm^{-1}$ 60800), sh 287 (51900), sh 320 (27000), 390 (7800), br 480 (1100); emission $\lambda_{max}$ ($\lambda_{ex}$) = 602/634 (279) nm; EA: calc. for $C_{44}H_{32}N_4F_6PIr*2\ H_2O$, C 53.38 %, H 3.67 %, N 5.66 %, found C 53.55 %, H 3.47 %, N 5.59 %.

### 5.2.13 [Ir(ppy)$_2$(32)][PF$_6$]

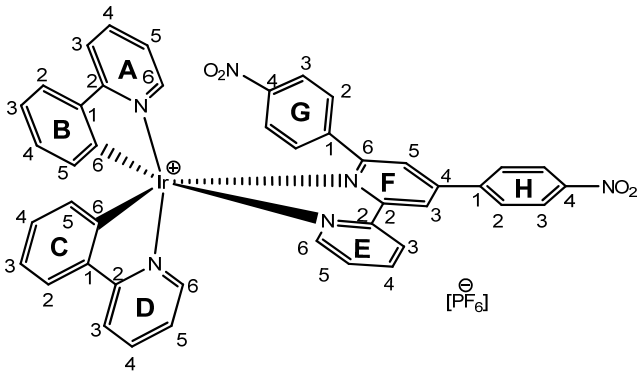


To a 5 ml microwave vial were added ligand **32** (39.8 mg, 100.0 µmol, 2.0 eq) and $[Ir(ppy)_2Cl]_2$ (53.6 mg, 50.0 µmol, 1.0 eq), suspended in MeOH (3 ml) and irradiated for 2 h at 120 °C in the microwave reactor. Then the solvent was reduced and the product was precipitated upon addition of solid $NH_4PF_6$ (130.0 mg, 0.80 mmol, 8.0 eq). The solvent was evaporated and the crude product was passed through a short column ($SiO_2$, $CH_2Cl_2$/MeOH 100:0-98:2). The desired product was collected as the second major fraction and dried in a desiccator after removal of solvent. It was obtained as an orange powder (95.0 mg, 91.0 µmol, 91.0 %). $^1$H-NMR (500 MHz, $CD_2Cl_2$) (ppm) 8.88 (d, *J* 1.8 Hz, 1 H, $H^{3F}$), 8.79 (d, *J* 8.2 Hz, 1 H, $H^{3E}$), 8.42 (d, *J* 8.8 Hz, 2 H, $H^{3H}$), 8.18 (td, *J* 8.1, 8.1, 1.5 Hz, 2 H, $H^{4E}$), 8.10 (d, *J* 8.9 Hz, 2 H, $H^{2H}$), 7.92 – 7.87 (m, 3 H, $H^{6E+3+4D}$), 7.86 (dd, *J* 8.2, 0.9 Hz, 1 H, $H^{3A}$), 7.80 (td, *J* 8.2, 7.8, 1.4 Hz, 1 H, $H^{4A}$), 7.77 (d, *J* 5.8 Hz, 1 H, $H^{6A}$), 7.71 – 7.65 (m, 2 H, $H^{5F+6D}$), 7.60 (br s, 2 H, $H^{3G}$), 7.56 (dd, *J* 7.8, 1.2 Hz, 1 H, $H^{3B}$), 7.42 (ddd, *J* 7.8, 5.6, 0.7 Hz, 1 H, $H^{5E}$), 7.30-6.35 (br s, 2 H, $H^{2G}$)7.25 (dd, *J* 7.8, 1.1 Hz, 2 H, $H^{3C}$), 7.16 (ddd, *J* 7.3, 5.9, 1.5 Hz, 2 H, $H^{5A}$), 7.08 (td, *J* 5.9, 5.9, 2.8 Hz, 1 H, $H^{5D}$), 6.97 (td, *J* 7.7, 7.5, 1.2 Hz, 1 H, $H^{4B}$), 6.82 (td, *J* 7.5, 7.5, 1.4 Hz, 1 H, $H^{5B}$), 6.63 (td, *J* 7.8, 7.6, 1.1 Hz, 1 H, $H^{4C}$), 6.39 (td, *J* 7.4, 7.4, 1.3 Hz, 1 H, $H^{5C}$), 5.92 (dd,

*J* 7.7, 0.9 Hz, 1 H, $H^{6B}$), 5.59 (dd, *J* 7.7, 0.8 Hz, 1 H, $H^{6C}$); $^{13}$C NMR (HMQC/HMBC, 500 MHz, $CD_2Cl_2$) $\delta$ (ppm) 168.36 ($C^{2D}$), 166.97 ($C^{2A}$), 163.53 ($C^{2F}$), 158.11 ($C^{6F}$), 156.13 ($C^{2E}$), 150.73 ($C^{6E}$), 150.55 ($C^{2C}$), 150.49 ($C^{4G}$), 149.76 ($C^{2B}$), 149.40 ($C^{4H}$), 149.21 ($C^{6D}$), 149.10 ($C^{6A}$), 146.08 ($C^{1B}$), 143.00 ($C^{1C}$), 142.88 ($C^{1G}$), 141.15 ($C^{1H+4F}$), 139.63 ($C^{4E}$), 138.59 ($C^{4D}$), 138.51 ($C^{4A}$), 132.08 ($C^{6C}$), 131.00 ($C^{5B}$), 130.11 ($C^{6B}$), 129.81 ($C^{5C}$), 129.99 ($C^{3H}$), 127.34 ($C^{5E}$), 127.10 ($C^{5F}$), 125.97 ($C^{3E}$), 124.80 ($C^{3B+2H}$), 124.38 ($C^{3C}$), 123.88 ($C^{5A}$), 123.44 ($C^{3G}$), 123.33 ($C^{4B}$), 123.20 ($C^{5D}$), 122.98 ($C^{4C}$), 120.08 ($C^{3A}$), 120.04 ($C^{3D}$); ESI-MS *m/z*: 899.3 $[M\text{-}PF_6]^+$ (100 %, calc. 899.2); IR (solid, $\nu$/cm$^{-1}$) 3120 (w), 3108 (w), 3055 (w), 2965 (w), 2937 (w), 2879 (w), 2860 (w), 2356 (s), 2340 (s), 2323 (s), 2311 (m), 1945 (w), 1923 (w), 1848 (w), 1829 (w), 1751 (m), 1734 (m), 1700 (m), 1607 (m), 1583 (m), 1544 (w), 1512 (m), 1506 (m), 1477 (m), 1453 (w), 1438 (w), 1422 (m), 1419 (m), 1395 (w), 1344 (m), 1317 (m), 1309 (w), 1295 (w), 1269 (w), 1228 (w), 1164 (w), 1126 (w), 1108 (w), 1064 (w), 1030 (m), 1014 (w), 1006 (w), 994 (w), 828 (s), 820 (s), 801 (m), 789 (m), 752 (s), 728 (s), 721 (m), 694 (s), 687 (m), 675 (m), 668 (m), 652 (m), 641 (w); UV/vis ($CH_2Cl_2$, 1.0 x 10$^{-5}$ mol dm$^{-3}$) $\lambda_{max}$/nm 274 ($\varepsilon$/dm$^3$ mol$^{-1}$ cm$^{-1}$ 65900), 288 (60500), sh 305 (49400), sh 364 (12500), 485 (1600); emission $\lambda_{max}$ ($\lambda_{ex}$) = 654 (273) nm; EA: calc. for $C_{44}H_{30}N_6O_4F_6PIr$, C 50.62 %, H 2.90 %, N 8.05 %, found C 50.41 %, H 2.96 %, N 8.00 %.

### 5.2.14 [Ir(ppy)$_2$(34)][PF$_6$]

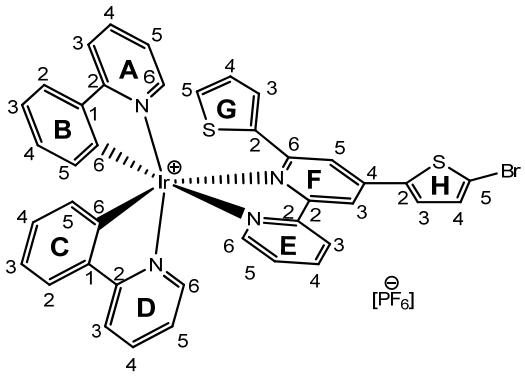


In a 10 ml microwave vial were added ligand **34** (18.0 mg, 45.0 μmol, 2.0 eq) and $[Ir(ppy)_2Cl]_2$ (24.2 mg, 22.5 μmol, 1.0 eq), then suspended in MeOH (10 ml). The mixture was irradiated for 1 h at 120 °C in the microwave reactor. Then the solvent was reduced and the product was precipitated upon addition of $NH_4PF_6$ (250.0 mg, 1.6 mmol). The solvent was evaporated and the crude product was passed through a short column ($SiO_2$, $CH_2Cl_2$/MeOH 100:0-98:2). The desired product was collected as the second major fraction and dried in a desiccator after solvent removal. It was obtained as a dark red powder (41.6 mg, 39.8 μmol, 88 %). $^1$H-NMR (500 MHz, $CD_2Cl_2$) $\delta$ (ppm) 8.64 (d, *J* 8.2 Hz, 1 H, $H^{3E}$), 8.54 (d, *J* 2.0 Hz, 1 H, $H^{3F}$), 8.16 (td, *J* 7.9, 1.7 Hz, 1 H, $H^{4E}$), 7.97 (s, *J* 5.9 Hz, 1 H, $H^{6A}$), 7.89 (td, *J* 7.0, 3.5 Hz, 2 H, $H^{3A+B}$), 7.85 (dd, *J* 5.5, 1.5 Hz, 1 H, $H^{6E}$), 7.81 (t, *J* 8.0 Hz, 2 H, $H^{4A+C}$), 7.71 (d, *J* 4.0 Hz, 1 H, $H^{4H}$), 7.60 (dd,

*J* 7.8, 1.4 Hz, 1 H, $H^{3D}$), 7.56 (d, *J* 1.9 Hz, 1 H, $H^{5F}$), 7.55 (d, *J* 5.8 Hz, 1 H, $H^{6D}$), 7.40 (t, *J* 6.9 Hz, 1 H, $H^{5E}$), 7.36 (t, *J* 7.8 Hz, 1 H, $H^{3C}$), 7.26 (d, *J* 4.0 Hz, 1 H, $H^{3H}$), 7.11 (ddd, *J* 7.4, 5.8, 1.5 Hz, 1 H, $H^{5A}$), 6.99 (m, 2 H, $H^{5D+4B}$), 6.92 (dd, *J* 5.0, 1.3 Hz, 1 H, $H^{5G}$), 6.81 (td, *J* 7.5, 1.4 Hz, 1 H, $H^{5B}$), 6.68 (td, *J* 7.5, 1.2 Hz, 1 H, $H^{4C}$), 6.47 (td, *J* 7.5, 1.4 Hz, 1 H, $H^{5C}$), 6.32 (dd, *J* 5.1, 3.5 Hz, 1 H, $H^{4G}$), 6.26 (dd, *J* 3.6, 1.3 Hz, 1 H, $H^{3G}$), 5.96 (dd, *J* 7.7, 1.2 Hz, 1 H, $H^{6B}$), 5.71 (dd, *J* 7.7, 1.1 Hz, 1 H, $H^{6C}$); $^{13}$C NMR (126 MHz, $CD_2Cl_2$) $\delta$ (ppm) 169.22 ($C^{2D}$), 168.75 ($C^{2F}$), 167.54 ($C^{2A}$), 158.35 ($C^{6F}$), 157.09 ($C^{2E}$), 150.85 ($C^{6E}$), 150.52 ($C^{6A}$), 148.90 ($C^{6D}$), 146.88 ($C^{2B}$), 143.78 ($C^{2C}$), 143.50 ($C^{1B}$), 143.16 ($C^{1C}$), 139.95 ($C^{4E}$), 139.75 ($C^{2H}$), 138.77 ($C^{4A+F}$), 138.69 ($C^{4D}$), 138.35 ($C^{2G}$), 133.16 ($C^{3H}$), 132.59 ($C^{6C}$), 131.24 ($C^{5B}$), 130.96 ($C^{6B}$), 130.20 ($C^{5C}$), 130.17 ($C^{4H}$), 129.85 ($C^{3G}$), 128.49 ($C^{5E}$), 128.07 ($C^{4G}$), 127.95 ($C^{5G}$), 126.18 ($C^{3E}$), 126.06 ($C^{5F}$), 125.23 ($C^{3D}$), 124.47 ($C^{3C}$), 123.75 ($C^{5A}$), 123.31 ($C^{5D}$), 123.02 ($C^{4B}$), 121.32 ($C^{4C}$), 120.35 ($C^{3B}$), 120.16 ($C^{3A}$), 119.61 ($C^{3F}$), 118.66 ($C^{5H}$); ESI-MS *m/z*: 899.4/901.1 $[M\text{-}PF_6]^+$ (100/75 %, calc. 899.4/901.4); IR (solid, $\nu$/cm$^{-1}$) 3099 (w), 3047 (w), 2358 (m), 2337 (w), 1606 (m), 1582 (m), 1559 (m), 1541 (w), 1477 (m), 1464 (w), 1458 (w), 1412 (m), 1339 (w), 1306 (w), 1269 (w), 1231 (w), 1161 (w), 1063 (w), 1030 (w), 1006 (w), 987 (w), 967 (w), 876 (w), 827 (s), 807 (m), 801 (m), 795 (m), 750 (m), 692 (m), 668 (m), 650 (m); UV/vis ($CH_2Cl_2$, 1.0 x 10$^{-6}$ mol dm$^{-3}$) $\lambda_{max}$/nm 232 ($\varepsilon$/dm$^3$ mol$^{-1}$ cm$^{-1}$ 37000), 258 (45500), 269 (46300), 336 (32600), sh 361 (25600), 480 (2300); emission $\lambda_{max}$ ($\lambda_{ex}$) = 622/637 (404) nm.

### 5.2.15 [Ir(ppy)$_2$(13)][PF$_6$]

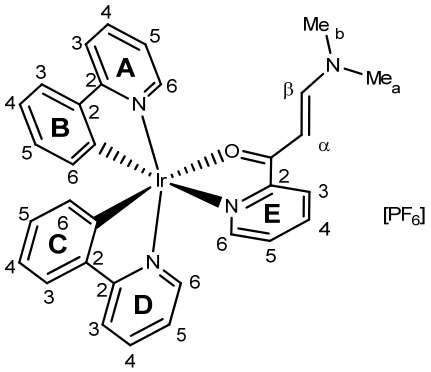


In a 10 ml microwave vial were added ligand **13** (16.4 mg, 93.0 μmol, 2.0 eq) and $[Ir(ppy)_2Cl]_2$ (50.0 mg, 47.0 μmol, 1.0 eq), then suspended in MeOH (10 ml). The mixture was irradiated for 1 h at 120 °C in the microwave reactor. Then the solvent was reduced and the product was precipitated upon addition of $NH_4PF_6$ (70.0 mg, 0.4 mmol, 8.0 eq). The solvent was evaporated and the crude product was passed through a short column ($SiO_2$, $CH_2Cl_2$/MeOH 100:0-98:2). The desired product was collected as the second major fraction and dried in a desiccator after solvent removal. It was obtained as a dark red powder (61.8 mg, 74.4 μmol, 80 %). $^1$H-NMR (500 MHz, $CD_2Cl_2$) $\delta$ (ppm) 8.41 (d, *J* 8.0 Hz,1 H, $H^{3E}$), 8.29 – 8.24 (m, 2 H, $H^{\beta+6D}$), 8.07 (t, *J* 7.7 Hz, 1 H, $H^{4E}$), 8.00-7.94 (m, 2 H, $H^{3A+6E}$), 7.92 (d, *J* 8.1 Hz, 1 H, $H^{3D}$),

7.86-7.75 (m, 2 H, $H^{4A+D}$), 7.69 (d, *J* 8.0 Hz, 1 H, $H^{3C}$), 7.67 (d, *J* 8.0 Hz, 1 H, $H^{3B}$), 7.47 (t, *J* 6.9 Hz, 1 H, $H^{5E}$), 7.44 (d, *J* 5.7 Hz, 1 H, $H^{6A}$), 7.18 (t, *J* 6.5 Hz, 1 H, $H^{5D}$), 7.04 (t, *J* 6.5 Hz, 1 H, $H^{5A}$), 7.02-6.95 (m, 2 H, $H^{4B+C}$), 6.84 (t, *J* 7.4 Hz, 2 H, $H^{5C+B}$), 6.27 (d, *J* 7.6 Hz, 1 H, $H^{6C}$), 6.24-6.16 (m, 2 H, $H^{\alpha+6B}$); $^{13}$C NMR (126 MHz, $CD_2Cl_2$) $\delta$ (ppm) 187.50 ($C^{C=O}$), 168.94 ($C^{2A}$), 167.77 ($C^{2D}$), 159.76 ($C^{\beta}$), 155.50 ($C^{2E}$), 151.39 ($C^{2B}$), 150.64 ($C^{6E}$), 149.07 ($C^{6D}$), 148.91 ($C^{6A}$), 145.09 ($C^{1B}$), 144.83 ($C^{1C}$), 144.16 ($C^{2C}$), 139.20 ($C^{4E}$), 138.61 ($C^{4A}$), 138.44 ($C^{4D}$), 133.09 ($C^{6B}$), 132.36 ($C^{6C}$), 130.90 ($C^{5B}$), 130.37 ($C^{5C}$), 130.03 ($C^{5E}$), 127.52 ($C^{3B}$), 125.34 ($C^{3C}$), 124.91 ($C^{3E}$), 123.48 ($C^{5A}$), 123.37 ($C^{5D}$), 122.78 ($C^{4B}$), 122.46 ($C^{4C}$), 119.95 ($C^{3D}$), 119.86 ($C^{3A}$), 93.66 ($C^{\alpha}$), 47.14 ($C^{Me}$), 39.17 ($C^{Me}$); ESI-MS *m/z*: 677.2 $[M\text{-}PF_6]^+$ (100 %, calc. 677.2); IR (solid, $\nu$/cm$^{-1}$) 3125 (w), 3056 (w), 2931 (w), 2862 (w), 2358 (w), 2329 (w), 1630 (s), 1607 (s), 1600 (m), 1582 (m), 1565 (m), 1517 (s), 1496 (s), 1490 (s), 1475 (s), 1465 (m), 1456 (m), 1439 (m), 1405 (s), 1375 (m), 1363 (m), 1299 (m), 1259 (s), 1252 (s), 1245 (s), 1227 (m), 1161 (m), 1141 (m), 1127 (m), 1119 (m), 1102 (m), 1083 (m), 1062 (m), 1054 (m), 1044 (m), 1031 (m), 1023 (m), 1012 (m), 984 (m), 967 (m), 958 (w), 938 (w), 906 (m), 887 (m), 882 (m), 865 (m), 832 (s), 792 (m), 771 (m), 756 (s), 735 (s), 729 (s), 722 (s), 712 (m), 694 (s), 682 (s), 668 (s), 655 (m), 630 (m); UV/vis ($CH_2Cl_2$, 5.0 x 10$^{-5}$ mol dm$^{-3}$) $\lambda_{max}$/nm 239 ($\varepsilon$/dm$^3$ mol$^{-1}$ cm$^{-1}$ 34300), 267 (47400), 335 (22000), 355 (22100), 408 (25200), 425 (25000), 526 (3000).

## 5.2.16 Crystal structure determinations

### 5.2.16.1 [Ir(ppy)$_2$(1)][PF$_6$]

$C_{81}H_{66}F_{12}N_{10}P_2Ir_2$, *M* = 1853.82, yellow block, orthorhombic, space group *Pbcn*, *a* = 20.941(4), *b* = *20*.129(4), *c* = 16. 916(3) Å, *U* = 7130(2) Å$^3$, *Z* = 4, $D_c$ = 1.727 Mg m$^{-3}$, $\mu$(Mo-K$_\alpha$) = 3.860 mm$^{-1}$, *T* = 173(2) K. Total 123452 reflections, 7385 unique, $R_{int}$ = 0.0734. Refinement of 7385 reflections (529 parameters) with $I>2\sigma(I)$ converged at final *R*1 = 0.0449 (*R*1 all data = 0.0503), *wR*2 = 0.0937 (*wR*2 all data = 0.0960), gof = 1.227.

### 5.2.16.2 [Ir(ppy)$_2$(2)][PF$_6$]

$C_{36}H_{26}ClF_6N_4OPIr$, *M* = 903.23, yellow plates, monoclinic, space group *C*2/*m*, *a* = 18.261(4), *b* = 24.312(5), *c* = 17.281(4) Å, $\beta$ = 95.37(3)°, *U* = 7638(3) Å$^3$, *Z* = 8, $D_c$ = 1.571 Mg m$^{-3}$, $\mu$(Mo-K$_\alpha$) = 3.670 mm$^{-1}$, *T* = 373(2) K. Total 67194 reflections, 10387 unique, $R_{int}$ = 0.1169. Refinement of 10387 reflections (406 parameters) with $I>2\sigma(I)$ converged at final *R*1 = 0.0524 (*R*1 all data = 0.0809), *wR*2 = 0.1311 (*wR*2 all data = 0.1498), gof = 0.880.

### 5.2.16.3 [Ir(ppy)$_2$(13)][PF$_6$]

$C_{65}H_{64}F_{12}N_8O_5P_2Ir_2$, *M* = 1711.59, red block, monoclinic, space group *P*2(1)/*c*, *a* = 16.4951(12), *b* = 13.0662(11), *c* = 16.4258(11) Å, $\beta$ = 113.986(5)°, *U* = 3234.5(4) Å$^3$, *Z* = 2,

$D_c$ = 1.753 Mg m$^{-3}$, $\mu$(Mo-K$_\alpha$) = 4.251 mm$^{-1}$, $T$ = 173(2) K. Total 22644 reflections, 7004 unique, $R_{int}$ = 0.0589. Refinement of 7004 reflections (446 parameters) with $I>2\sigma(I)$ converged at final $R1$ = 0.0357 ($R1$ all data = 0.0387), $wR2$ = 0.0896 ($wR2$ all data = 0.0936), gof = 1.161.

#### 5.2.16.4 [Ir(ppy)$_2$(30)][PF$_6$]

$C_{50}H_{44}F_6N_4O_6PIr$, $M$ = 1134.08, orange block, monoclinic, space group $P2(1)/n$, $a$ = 12.5203(8), $b$ = 18.8096(10), $c$ = 18.9682(13) Å, $\beta$ = 95.328(5)°, $U$ = 2897.8(2) Å$^3$, $Z$ = 4, $D_c$ = 1.694 Mg m$^{-3}$, $\mu$(Mo-K$_\alpha$) = 3.120 mm$^{-1}$, $T$ = 173(2) K. Total 77004 reflections, 10213 unique, $R_{int}$ = 0.0874. Refinement of 10213 reflections (619 parameters) with $I>2\sigma(I)$ converged at final $R1$ = 0.0380 ($R1$ all data = 0.0395), $wR2$ = 0.0937 ($wR2$ all data = 0.0947), gof = 1.095.

#### 5.2.16.5 [Ir(ppy)$_2$(32)][PF$_6$]

$C_{89}H_{70}Cl_2F_{12}N_{12}O_{12}P_2Ir_2$, $M$ = 2244.83, orange plate, triclinic, space group $P$-1, $a$ = 9.776(3), $b$ = 14.684(5), $c$ = 17.409(5) Å, $\alpha$ = 74.15(2), $\beta$ = 76.01(2), $\gamma$ = 72.54(2)°, $U$ = 2258.2(12) Å$^3$, $Z$ = 1, $D_c$ = 1.645 Mg m$^{-3}$, $\mu$(Mo-K$_\alpha$) = 3.130 mm$^{-1}$, $T$ = 173(2) K. Total 30520 reflections, 9370 unique, $R_{int}$ = 0.1209. Refinement of 9370 reflections (622 parameters) with $I>2\sigma(I)$ converged at final $R1$ = 0.0634 ($R1$ all data = 0.0715), $wR2$ = 0.1583 ($wR2$ all data = 0.1650), gof = 1.061.

### 5.2.17 Preparation of LEC devices

These experiments were not conducted in our laboratory but in cooperation with H. J. BOLINK in Spain, Valencia. PEDOT:PSS was purchased from HC-Starck and used solvents were obtained from Aldrich. ITO-coated glass plates (15Ω sq$^{-1}$) were patterned using conventional photolithography (obtained from Naranjosubstrates). The substrates were extensively cleaned using sonification in subsequently water-soap, water, and 2-propanol baths. After drying, the substrates were placed in a UV-ozone cleaner (Jelight 42-220) for 20 min. The electroluminescent devices were prepared as follows. Transparent thin films of complexes [Ir(ppy)$_2$(L)][PF$_6$] (L = **1**-**3**) containing different amounts of the ionic liquid (1-butyl-3-methylimidazolium hexafluorophosphate) were obtained by spinning from acetonitrile solutions using concentrations of 20mg mL$^{-1}$ at 2000 rpm for 40 s, resulting in 80-nm-thick films. Prior to the deposition of the emitting layer, a 100-nm layer of PEDOT:PSS was deposited to increase the device preparation yield. The thickness of the films was determined using an Ambios XP1 profilometer. After spinning the organic layers, the samples were transferred to an inert atmosphere glovebox (< 0.1 ppm $O_2$ and $H_2O$, MBraun) and dried on a hot plate at 80 °C for 1 h. Aluminum metal electrodes (80 nm) were thermally

evaporated using a shadow mask under a vacuum (< $1x10^{-6}$ mbar) using an Edwards Auto500 evaporator integrated into an inert atmosphere glovebox. Current density and luminance versus voltage were measured using a Keithley 2400 source meter and a photodiode coupled to a Keithley 6485 pico-amperometer using a Minolta LS100 to calibrate the photocurrent. EQEs were determined using an integrated sphere coupled to an UDT instruments S370 Optometer. An Avantes luminance spectrometer was used to measure the EL spectrum. Lifetime data were obtained by applying a constant voltage over the device and monitoring the current flow and simultaneously the current generated by a Si-photodiode (Hamamatsu S1336-8BK) calibrated using a Minolta LS100 luminance meter. Custommade equipment consisting of a multichannel rack, from muetta consult, 16 boards with power source, and DAQ (data acquisition)-12 bits ADC (analogue to digital converter) was used to measure the luminance and current density over the time. A custom-designed labview program was used to control the equipment and gather the data on a personal computer. Both the multi-channel rack and the PC are connected via an autonomic power supply unit (SALICRU SLC cube).

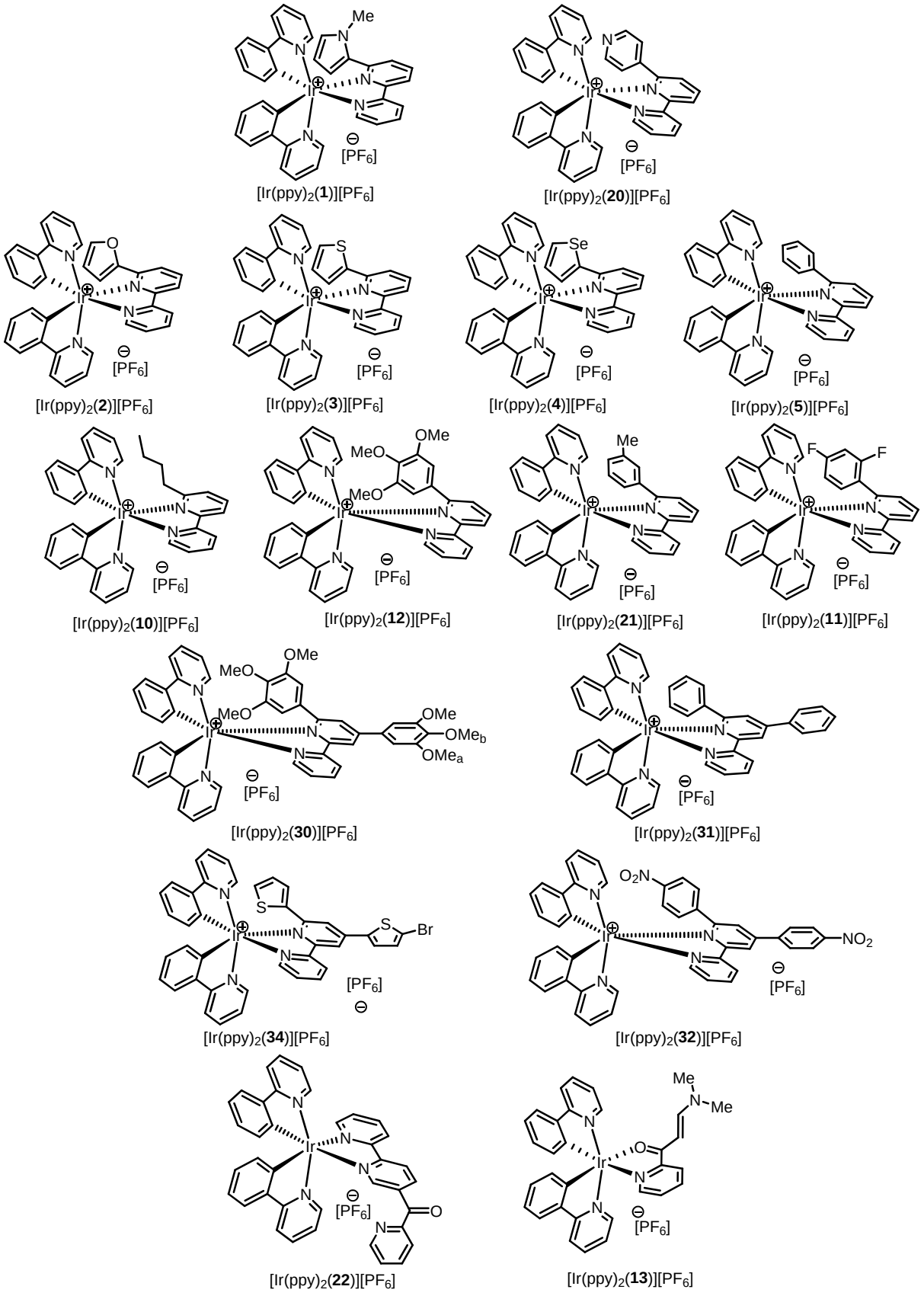


**Figure 5-20** Overview of the iridium(III) complexes

# Chapter 6

# 6 Ruthenium Complexes

## 6.1 Results and Discussion

This chapter focuses on the synthesis of new ruthenium(II) complexes. Two types of ligands were used for their preparation: either entirely new ligands, which were developed for the copper(I) and iridium(III) projects which have been described before, or ligands which although being reported before, their ruthenium(II) complexes were not.

### 6.1.1 Preparation

All complexes have been prepared by standard procedures, commonly used throughout our laboratory with short reaction times and good to excellent yields. Two types of ruthenium(II) complexes were prepared: for one ruthenium tris bpy complexes where one of the ligands carried a substituent mostly in the 6'-position. In addition with the surprisingly new 4'-*tert*butyl-2,2':6',2''-terpyridine ligand diverse octahedral $ML_2$ complexes were prepared (M = Fe, Co, Zn and Ru). An overview of all complexes is given in Figure 6-18.

#### 6.1.1.1 *Tris* bipyridine complexes

The ruthenium(II) tris bpy complexes were prepared by reacting equimolar amounts of the precursor *cis*-$[Ru(bpy)_2Cl_2]*2H_2O$ and the appropriate ligand (L = **1**, **2**, **4**, **10**, **20**-**22** and **34**; Scheme 6-1).

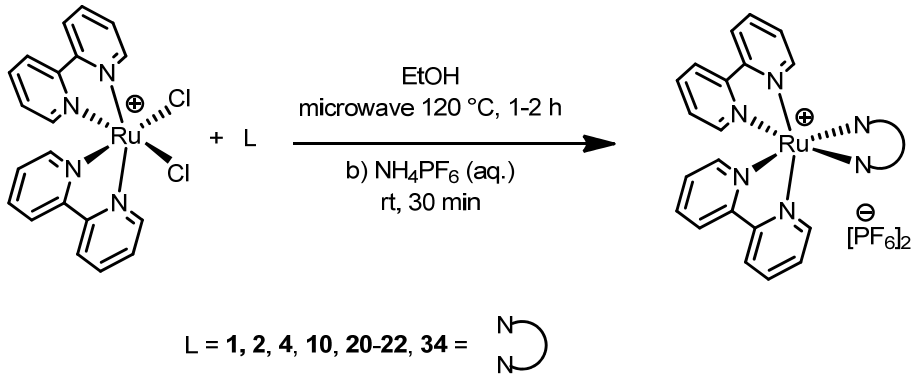


**Scheme 6-1** Synthesis of ruthenium(II) complexes $[Ru(bpy)_2(L)][PF_6]_2$.

The metal precursor was prepared following a literature procedure and the synthesis of the ligands has been described in chapter 3.[128] Both starting materials were suspended in ethanol and stirred at 120 °C for 1 to 2 hours in a microwave reactor. The orange solutions were reduced in volume, and the desired products were precipitated as $[PF_6]^-$ salts by adding aqueous $NH_4PF_6$ solution. Most complexes were sufficiently pure after washing with water and diethyl ether or were purified by PLC if necessary.

### 6.1.1.2 *Bis* terpyridine complexes

To the best of our knowledge ligand **40** had not been reported in the literature before and therefore we decided to prepare several complexes and the results have been reported recently.[75] The very same report describes the homoleptic cobalt(II) and zinc(II) complexes with ligand **40**. These have been prepared by N. HOSTETTLER, and will not be described here. In this work the iron(II) and ruthenium(II) complexes were synthesized. The homoleptic complex $[Fe(\mathbf{40})_2][PF_6]_2$ was prepared by combining two equivalents of **40** with anhydrous $FeCl_2$ in acetonitrile at room temperature. After stirring for 2 h, followed by anion exchange and water induced precipitation, the desired product was obtained in a yield of 87 % (see Scheme 6-2).

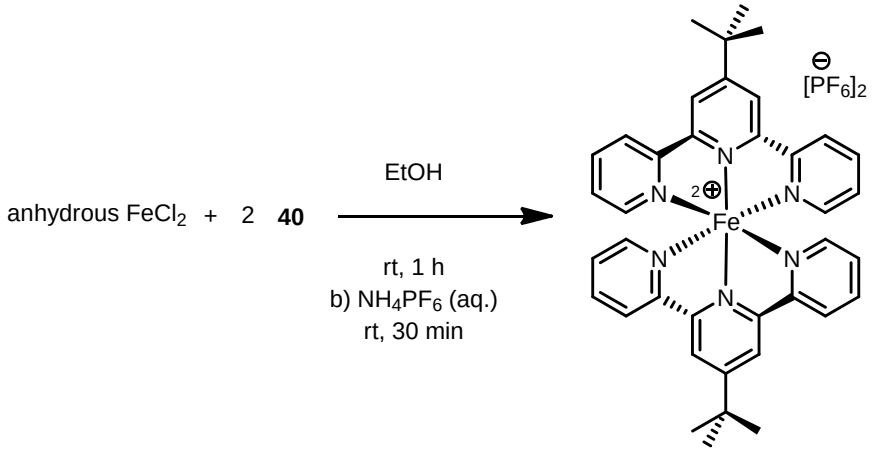


**Scheme 6-2** Synthesis of the iron(II) complex $[Fe(\mathbf{40})_2][PF_6]_2$.

$[Ru(\mathbf{40})_2][PF_6]_2$ was synthesized by first preparing $[Ru(\mathbf{40})Cl_3]$ from $RuCl_3{*}3H_2O$ and ligand **40** in boiling ethanol. This complex was then treated with a second equivalent of **40** in the presence of *N*-ethylmorpholine as reducing agent, and orange $[Ru(\mathbf{40})_2][PF_6]_2$ was isolated in 83 % yield after anion exchange (see Scheme 6-3).

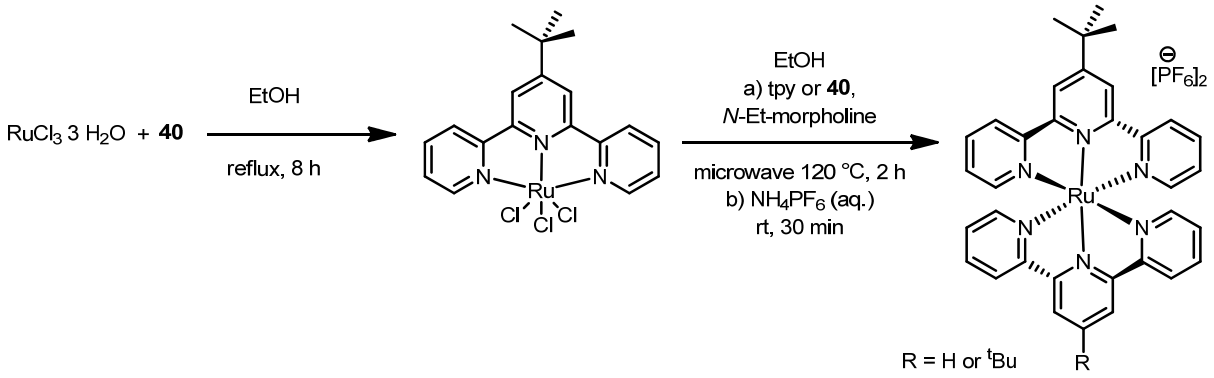


**Scheme 6-3** Synthesis of ruthenium(II) complexes $[Ru(\mathbf{40})(L)][PF_6]_2$, L = tpy or **40**.

The lability of tpy-based ligands in iron(II) systems[129] makes the isolation of heteroleptic complexes relatively difficult. In contrast, ruthenium(II) is kinetically inert and it is well-established that heteroleptic complexes are readily prepared by using an appropriate

[RuLCl$_3$] intermediate.[130] Thus, reaction of [Ru(**40**)Cl$_3$] with an equivalent of tpy followed by anion exchange produced [Ru(tpy)(**40**)][PF$_6$]$_2$ in 76 % yield.

### 6.1.1.3 Test reaction with [Ru(bpy)$_2$(22)][PF$_6$]$_2$

Ligand **22** has an accessible carbonyl group which could undergo further reactions. The initial idea was that the carbonyl group and the free pyridyl ring could simply act as a *N,O*-donor ligand. To prove the concept of *N,O*-donor coordination the two complexes [Ru(bpy)$_2$(**13**)][PF$_6$]$_2$ (see Scheme 6-4) and [Ir(ppy)$_2$(**13**)][PF$_6$] were prepared, the latter being described in chapter 5.

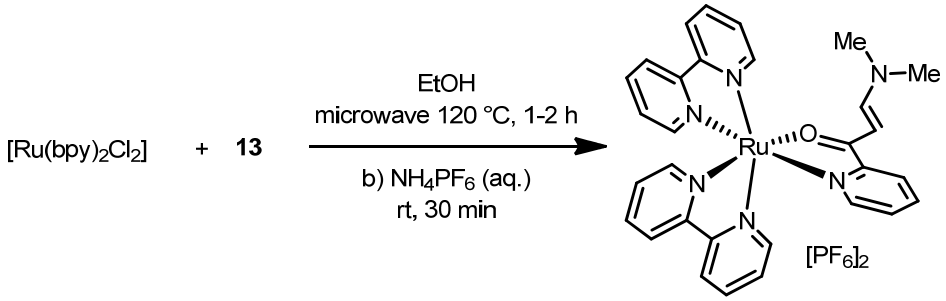


**Scheme 6-4** Test reaction for *N,O*-coordination.

Encouraged by the successful outcome two further test reactions were carried out. In the first instance one equivalent of ligand **22** was reacted with two equivalents of the precursor [Ru(bpy)$_2$Cl$_2$] to see whether it is possible to prepare the dinuclear complex [Ru$_2$(bpy)$_4$(**22**)][PF$_6$]$_4$ (see Scheme 6-5).

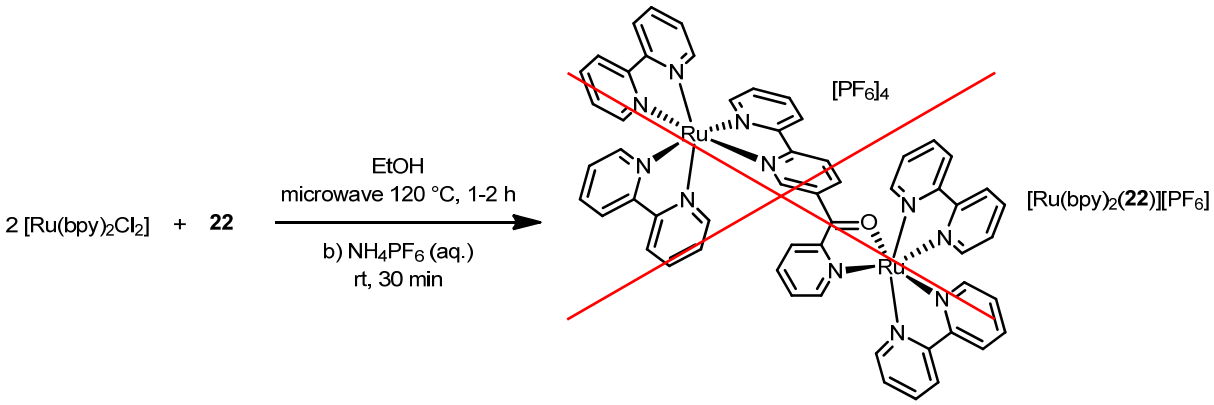


**Scheme 6-5** Attempted one-pot synthesis of a dinuclear ruthenium(II) complex.

The desired compound could not been isolated and the only product observed was the mononuclear complex [Ru(bpy)$_2$(**22**)][PF$_6$]$_2$. Then a two step synthesis was envisioned. The complex [Ru(bpy)$_2$(**22**)][PF$_6$]$_2$ was prepared in a separate reaction (see section 6.1.1.1) and then reacted with [Ru(bpy)$_2$Cl$_2$] or an half equivalent of [Ir(ppy)$_2$Cl]$_2$, respectively. Both reactions did not yield the desired product and only starting material could be recovered (see Scheme 6-6).

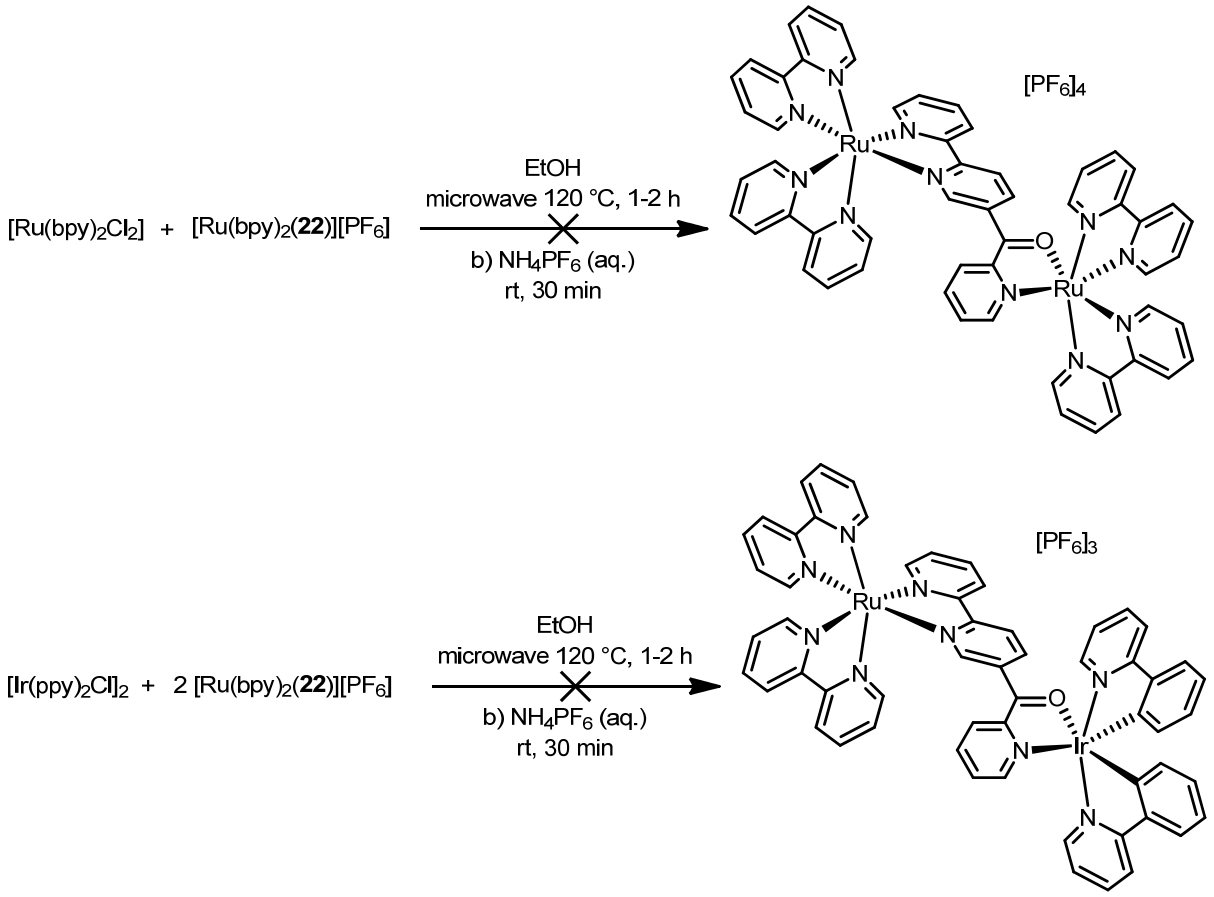


**Scheme 6-6** Attempted synthesis of dinuclear complexes with $[Ru(bpy)_2(\mathbf{22})][PF_6]_2$ as a *N,O*-donor ligand.

This project was started only at the end of the thesis and no further reactions were carried out. Therefore, it is not obvious whether altered reaction conditions would have led to the desired product, or if it cannot be obtained at all.

Eventually, the idea was to engage the complex $[Ru(bpy)_2(\mathbf{22})][PF_6]_2$ in an imine condensation reaction with a diimine (e.g., ethylendiamine (en), see Scheme 6-7) and prepare the dinuclear ruthenium complex which could be used as a ligand with four nitrogen donor atoms. The practical work was carried out by a Wahlpraktikum-student R. WYSS. Following literature procedures, several attempts were carried out reacting two equivalents of complex $[Ru(bpy)_2(\mathbf{22})][PF_6]_2$ with one equivalent of en in ethanol at reflux.[131] While in the literature report the reactions were finished within hours, in our case no reaction could be observed at all. Attempts were undertaken to remove water from the reaction mixture were made by adding $MgSO_4$ as drying agent. A new product was observed but its isolation proved to be difficult. Only in water free conditions was it possible to obtain $^1$H NMR and ESI-MS spectra which were different from the starting material but they suggested that the species was not the desired product. Very likely the en did not act as a reactant but as a base and the starting material reacted with the solvent to form an ethyl diacetal. This result shows that the literature procedures are not reproducible for this system.

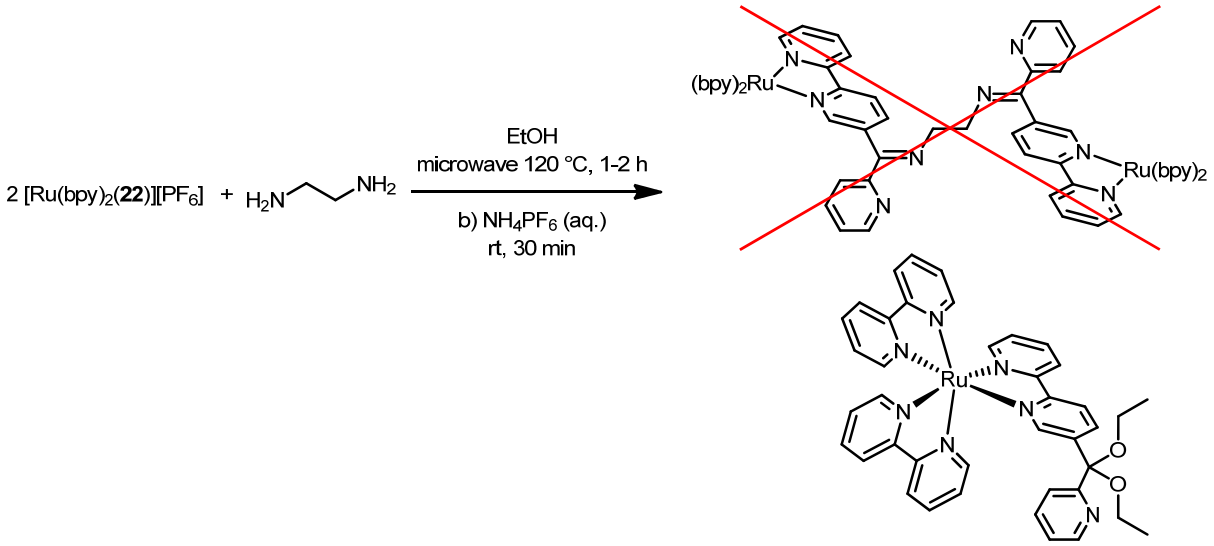


**Scheme 6-7** Attempted imine condensation with 2 equivalents of $[Ru(bpy)_2(22)][PF_6]_2$ and one equivalent of ethylendiamine.

With altered conditions, the desired product could probably be obtained: The solvent should be changed to acetonitrile so that the unwanted side reaction would be avoided. Also, the diimine should be changed, preferably 1,2-diaminobenzene should be used, so that the resulting imine would be more stable (aryl substituted imines are known to be more stable than imines with aliphatic substituents). Unfortunately, there was not enough time to pursue this project further.

### 6.1.2 Characterization

The ruthenium(II) complexes have been characterized by ESI-MS. All spectra showed two major peaks corresponding to the cation without one or two counter anions $[PF_6]^-$, respectively, exhibiting the calculated isotope patterns. Furthermore IR spectra were recorded and if possible the compositions were confirmed by elemental analyses.

#### 6.1.2.1 NMR spectroscopy

All complexes were characterized by nuclear magnetic resonance spectroscopy. Standard $^1H$ and 2-D experiments (COSY, HMQC and HMBC) were carried out. The compounds show quite complicated spectra which are not trivial to assign. The two unsubstituted bipyridine ligands are very similar and give each two sets of four-spin-systems. The unsymmetrical 6'-R-bpy ligands exhibit two three-spin-systems and one four-spin-system. All together a typical $^1H$ NMR spectrum of a $[Ru(bpy)_2(L)][PF_6]_2$ complex shows 26 proton signals and 36 $^{13}C$-signals. As an example, the $^1H$ NMR spectrum of $[Ru(bpy)_2(\mathbf{2})][PF_6]_2$ and the assignment of the individual signals is depicted in Figure 6-1.

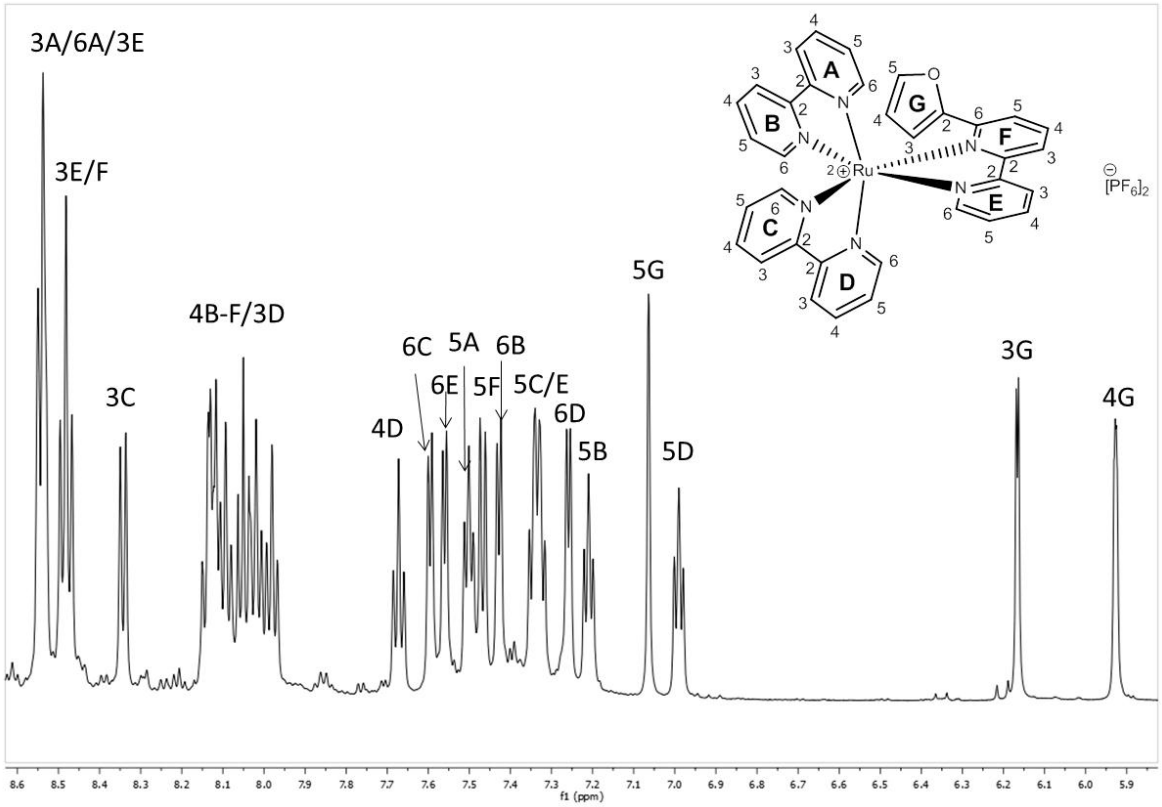


**Figure 6-1** Room temperature 500 MHz $^{1}$H NMR spectrum ($\delta$ 9.0–7.0 ppm) of a MeCN-$d_3$ solution of [Ru(bpy)$_2$(**2**)][PF$_6$]$_2$.

As described for the iridium(III) complexes (see section 5.1.2.2), ruthenium(II) complexes exhibit octahedral coordination geometry, too. The same characteristic high field shift of protons in the 6-positions on the bpy moieties can be observed. In contrast to the iridium compounds, the spectra of the ruthenium complexes are even more difficult to assign due to the fact that many signals do overlap. Therefore, for [Ru(bpy)$_2$(**2**)][PF$_6$]$_2$ additional TOCSY NMR spectra were recorded. TOCSY is the abbreviation for TOtal Correlation SpectroscopY, sometimes it is also referred to as HOHAHA (HOmonuclear HArtmann HAhn). This pulse sequence consists of a 90° pulse followed by the evolution period $t_1$, the magnetization is then spin-locked by a series of 180° pulses. During this mixing time, which is called the spin-lock period, the magnetization exchanges through scalar coupling.

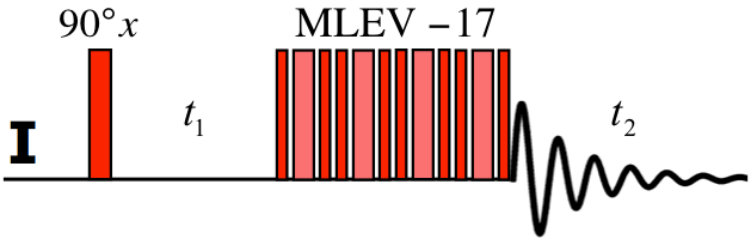


**Figure 6-2** Pulse sequence of a TOCSY NMR experiment

The magnetization transfer is possible between all coupled nuclei in a spin system, even if they are not directly bonded. This allows for separation of the distinct spin systems of each aromatic (pyridyl) ring (see Figure 6-3).

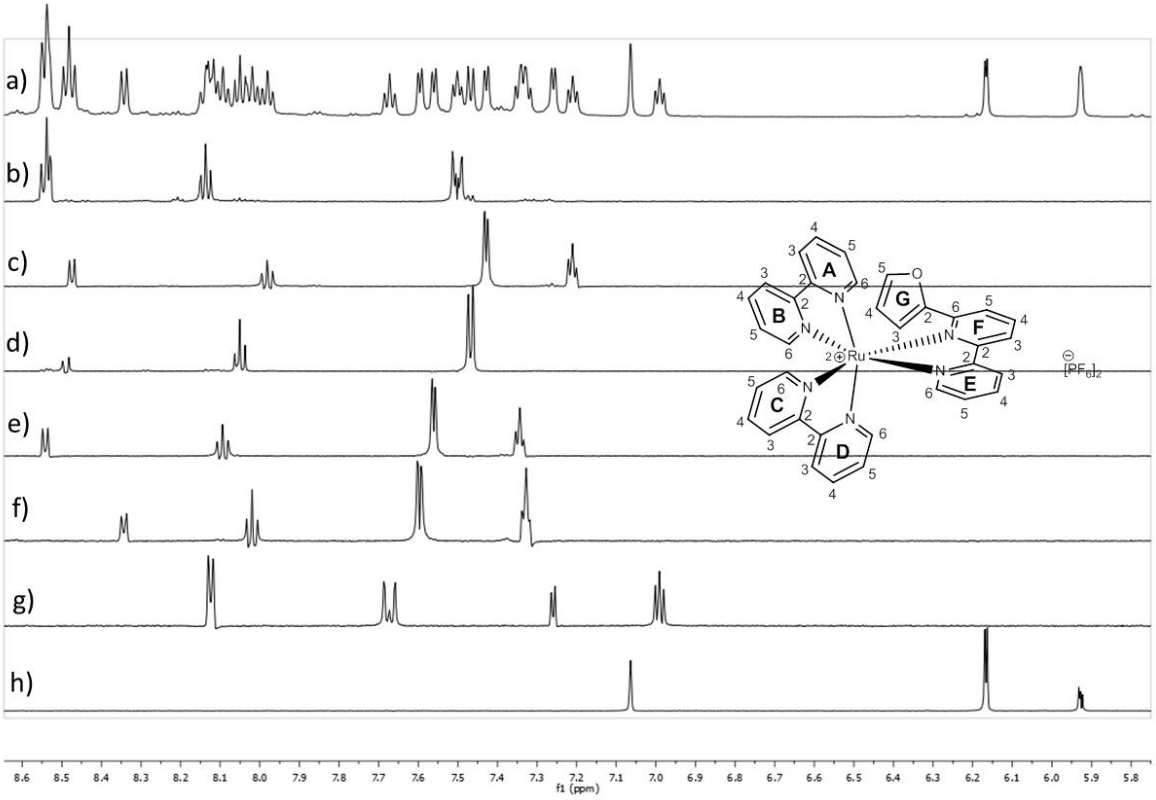


**Figure 6-3** Room temperature 600 MHz $^{1}$H NMR spectrum ($\delta$ 8.6–5.8 ppm) of a MeCN-$d_3$ solution of [Ru(bpy)$_2$(**2**)][PF$_6$]$_2$ and the TOCSY spectra of each spin system of pyridyl rings A-F and furanyl ring G: a) 1H NMR spectrum, b) ring A, c) ring B, d) ring F, e) ring E, f) ring C, g) ring D, h) ring G.

It has to be mentioned, that not all protons in position 6 on the pyridyl rings experience the shielding effect discussed before (see section 5.1.2.2). The signal for proton 6A appears at $\delta$ = 8.53 ppm and is quite similar with regards to the shift in a free bpy ligand. A crystal structure is unfortunately not available for compound [Ru(bpy)$_2$(**2**)][PF$_6$]$_2$ but we might take the structure of complex [Ru(bpy)$_2$(**4**)][PF$_6$]$_2$ as a model compound, which differs only in the hetero atom on the substituent of the asymmetric bpy ligand (see Figure 6-4). If the assumption is right that [Ru(bpy)$_2$(**2**)]$^{2+}$ cation is *iso*-structural with the selenium derivative [Ru(bpy)$_2$(**4**)]$^{2+}$ and the atom distances are similar, the distance between H$^{6A}$ and the oxygen atom of the furanyl substituent would be in the range of a weak hydrogen bond (3.2 Å). Hydrogen bonds are known to have a deshielding effect and to cause a shift of NMR signals to higher field. In the NMR spectrum of [Ru(bpy)$_2$(**4**)][PF$_6$]$_2$ all protons in the 6-positions show a shift to lower field but this is not necessarily in disagreement with the explanation, since selenium should not form strong hydrogen bonds. Further indication that the hydrogen bonding can be responsible for this phenomenon will be explained below for compound [Ru(bpy)$_2$(**22**)][PF$_6$]$_2$. On the other hand, for the iridium(III) compound the low field shift for

proton $H^{6A}$ was not observed, even though the compound exhibits a similar molecular structure.

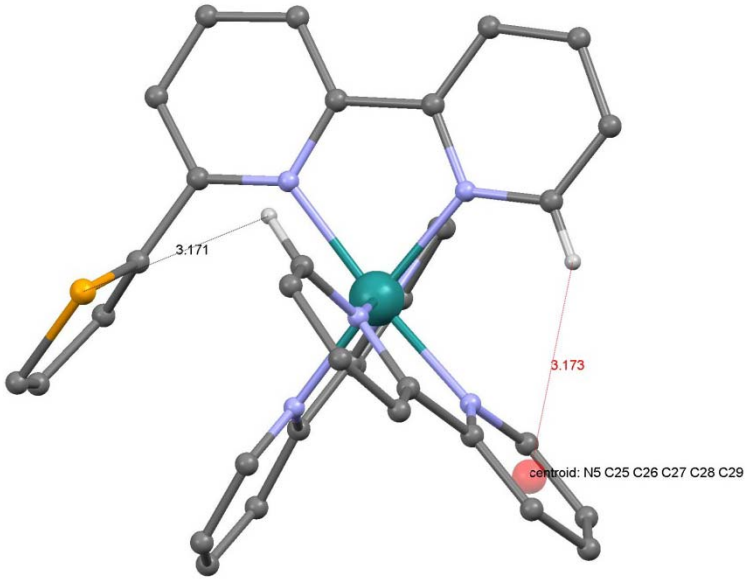


**Figure 6-4** Molecular structure of cation [Ru(bpy)$_2$(**4**)] in [Ru(bpy)$_2$(**4**)][PF$_6$]$_2$, only significant hydrogen atoms are shown (others are omitted) with the following distances: $H^{6A}$…Se 3.1710(9) Å (black), $H^{6E}$…centroid (ring C) 3.2 Å (red).

Other than the fact described above all ruthenium complexes with 6'-R-bpy ligands show similar NMR spectra and were assigned by comparison with the assignment of [Ru(bpy)$_2$(**2**)][PF$_6$]$_2$.

Complex [Ru(bpy)$_2$(**22**)][PF$_6$]$_2$ exhibits similar behaviour as mentioned before. Figure 6-5 depicts the room temperature NMR of the compound and it becomes apparent that protons $H^{4F}$ and $H^{6F}$ are shifted to unusually high values of $\delta$ in ruthenium(II) tris bpy complexes and the signal for $H^{6G}$ is only slightly shifted to higher field compared to the remaining protons in 6-positions. Using the crystal structure (see Figure 6-6) these results can be explained. The pyridoyl substituent on the asymmetric bpy ligand is oriented so that hydrogen atoms $H^{4F}$ and $H^{3G}$ engage in short distances to the oxygen from the carbonyl group (2.433(1)/2.468(1) Å) and form a hydrogen bond. A direct result thereof is a very short distance between $H^{6F}$ and the nitrogen atom of ring G (2.277(1) Å, see Figure 6-6). The signal for $H^{4F}$ is shifted to higher field compared to the remaining protons in 4-position. Surprisingly, the signal of $H^{3G}$ is not affected in the same manner but shows rather an effect of deshielding and the signal appears shifted to higher field. This behaviour is not understood. Even though, proton $H^{6F}$ is oriented towards ring D and exhibits a typical distance to the centroid of the pyridyl ring (3.4 Å), it does not experience a shielding effect of the $\pi$-electrons, but rather a deshielding effect which is caused by the hydrogen bond. The less pronounced shift of proton $H^{6G}$ can be explained by the longer distance to the vicinal

pyridyl ring D (3.6 Å). The remaining peaks in the $^{1}$H NMR spectrum show similar shifts and appear as groups of signals depending on the position of the proton on the pyridyl ring.

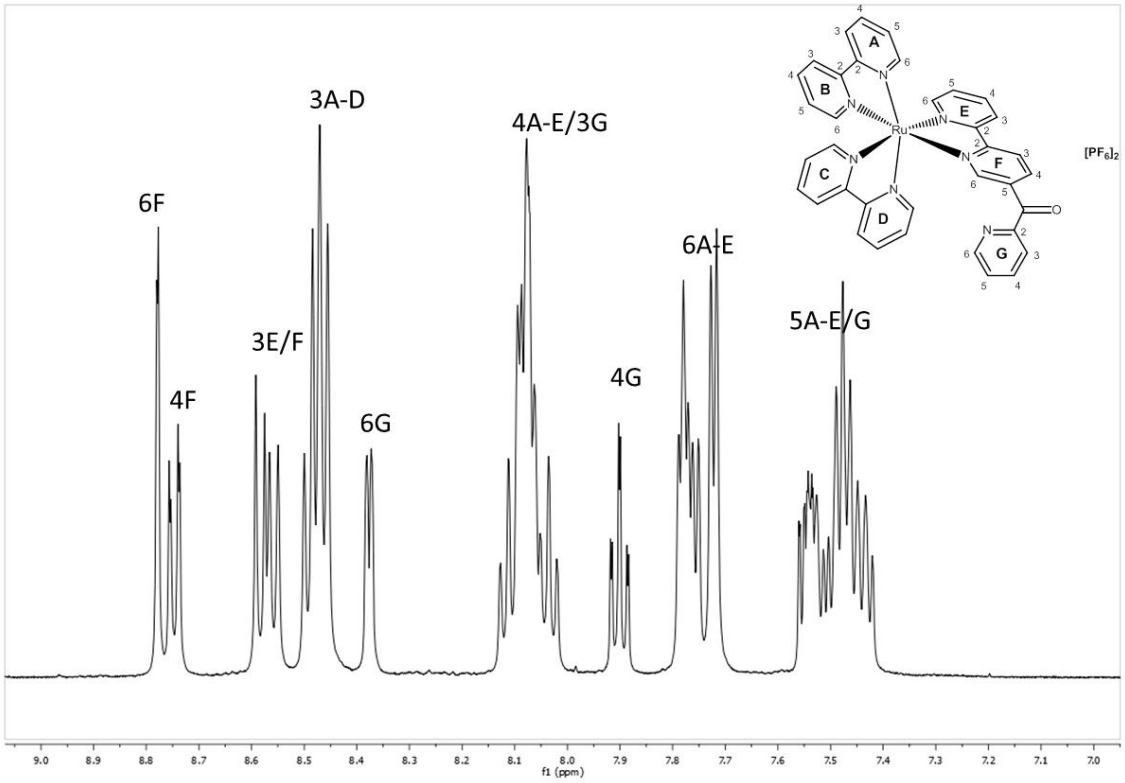


**Figure 6-5** Room temperature 500 MHz $^{1}$H NMR spectrum ($\delta$ 9.0–7.0 ppm) of a $CD_2Cl_2$ solution of $[Ru(bpy)_2(\mathbf{22})][PF_6]_2$.

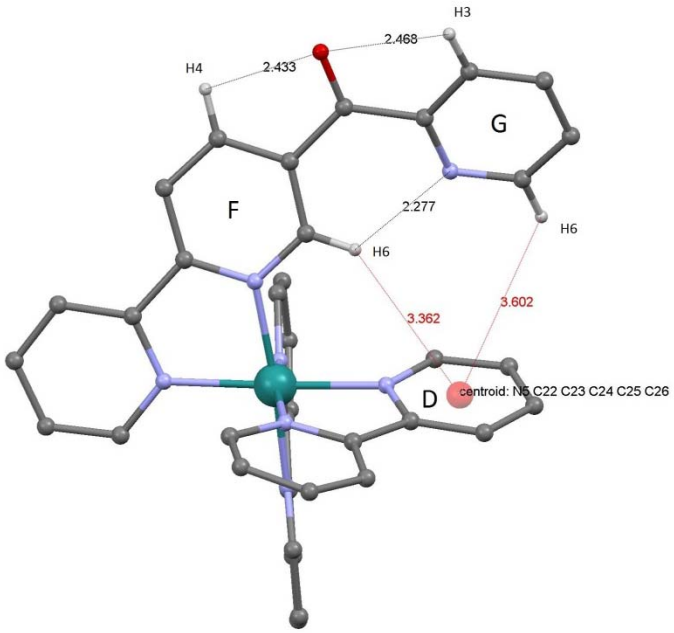


**Figure 6-6** Molecular structure of cation $[Ru(bpy)_2(\mathbf{22})]^{+}$ in $[Ru(bpy)_2(\mathbf{22})][PF_6]_2$, only significant hydrogen atoms are shown (others are omitted) with distances to: $H^{4F}$…O 2.433(1), $H^{3G}$…O 2.468(1), $H^{6F}$…$N^{G}$ 2.277(1) Å (black) $H^{6E}$…centroid (ring D) 3.4 Å and $H^{6F}$…centroid (ring D) 3.6 Å (red).

### 6.1.2.2 Solid State Structures

For some of the ruthenium(II) complexes, it was possible to grow X-ray diffraction quality crystals and their solid state structures could be determined. Single crystals of compound $[Ru(bpy)_2(\mathbf{4})][PF_6]_2$ were grown from a $CD_2Cl_2$ solution by slow evaporation of the solvent. The compound crystalizes in the monoclinic space group $P2_1$ without any solvent. Its molecular structure is shown in Figure 6-7 and selected bond parameters are listed in the caption.

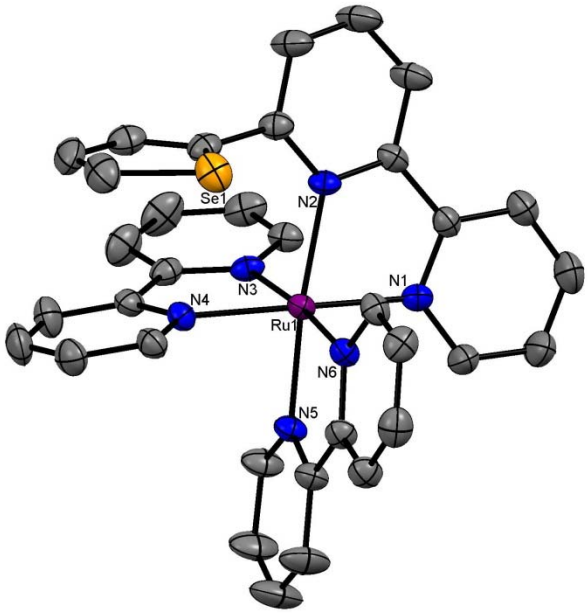


**Figure 6-7** Structure of the $[Ru(bpy)_2(\mathbf{4})]^{2+}$ cation in $[Ru(bpy)_2(\mathbf{4})][PF_6]_2$ with H atoms omitted (ellipsoids plotted at 50 % probability level). Selected bond parameters: Ru1-N6 2.047(4), Ru1-N1 2.049(4), Ru1-N4 2.057(4), Ru1-N3 2.065(4), Ru1-N5 2.066(3), Ru1-N2 2.128(3) Å, N6-Ru1-N1 88.52(14), N6-Ru1-N4 96.75(15), N1-Ru1-N4 174.17(15), N6-Ru1-N3 173.91(15), N1-Ru1-N3 96.49(15), N4-Ru1-N3 78.10(14), N6-Ru1-N5 78.47(15), N1-Ru1-N5 95.88(15), N4-Ru1-N5 82.79(15), N3-Ru1-N5 97.52(14), N6-Ru1-N2 99.39(14), N1-Ru1-N2 78.81(15), N4-Ru1-N2 102.68(14), N3-Ru1-N2 85.01(14), N5-Ru1-N2 174.37(15)°.

As expected, the three bpy ligands ligate the metal forming an octahedral coordination sphere. Five of the Ru…N bond lengths are in the range of 2.047(4)-2.066(3) Å and one bond between Ru and N2 is slightly elongated (2.128 Å, 3-4 % longer compared to the five shorter bonds), N2 being the nitrogen atom adjacent to the selenophenyl substituent. Possibly, this elongation can be associated with the π-stacking of the substituent. In this case the π-π-interactions seem to be more pronounced than in similar iridium(III) complexes (see section 5.1.2.3). The bpy moiety of the asymmetric ligand deviates only marginaly from planarity, the angle between the two planes being 8.4°. The hetero aromatic substituent is twisted from the plane of the central pyridine ring and their planes subtend an angle of 78.2°. This results in a nearly parallel orientation of the selenoyl substituent to the vicinal, N4 containing pyridyl ring, the angle between the two planes being 8.9°. The resulting distance between the centroid of the selenoyl substituent and the plane of the pyridyl ring is 3.2 Å,

and so is relatively short, shorter than in most of corresponding iridium(III) complexes discussed in section 5.1.2.3. The centroid-centroid distance is 3.5 Å and therefore shorter than most centroid distances reported in literature, these being usually between 3.6 and 3.8 Å.[77] Even though, Figure 6-7 might suggest an orientation of the selenium atom toward the metal centre, this is not the case. The selenium atom points rather from the metal centre away, the Se…Ru separation is 4.363(1) Å and therefore it is ~35 % longer than the sum of the van der Waals radii (3.225 Å).[102]

Single crystals of the complex $[Ru(bpy)_2(\mathbf{22})][PF_6]_2$ were grown in an NMR tube by slow evaporation of a $CD_2Cl_2$ solution of the compound. It crystallizes in the triclinic space group *P-1* without solvent molecules. The molecular structure is depicted in Figure 6-8 and the important bond parameters are listed in the caption. The three bpy ligands ligate the metal centre as expected to form octahedral coordination geometry. The bpy moieties deviates only slightly from planarity with angles between the two planes of the pyridyl rings of 4.0 (N1/2), 8.3 (N4/5) and 15.9° (N6/7).

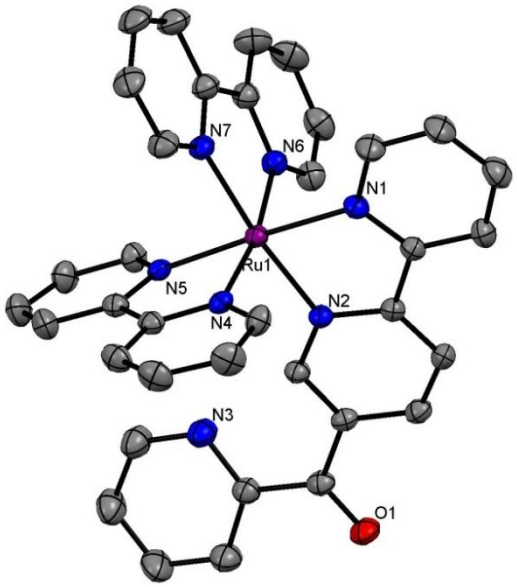


**Figure 6-8** Structure of the $[Ru(bpy)_2(\mathbf{22})]^{2+}$ cation in $[Ru(bpy)_2(\mathbf{22})][PF_6]_2$ with H atoms omitted (ellipsoids plotted at 50 % probability level). Selected bond parameters: Ru1-N5 2.0447(15), Ru1-N2 2.0478(12), Ru1-N7 2.0504(13), Ru1-N6 2.0543(13), Ru1-N1 2.0589(12), Ru1-N4 2.0629(16) Å, N5-Ru1-N2 98.58(6), N5-Ru1-N7 86.46(6), N2-Ru1-N7 173.15(4), N5-Ru1-N6 94.04(6), N2-Ru1-N6 96.13(5), N7-Ru1-N6 78.81(5), N5-Ru1-N1 177.36(6), N2-Ru1-N1 78.92(5), N7-Ru1-N1 96.10(5), N6-Ru1-N1 87.11(5), N5-Ru1-N4 79.20(7), N2-Ru1-N4 91.97(6), N7-Ru1-N4 93.54(6), N6-Ru1-N4 170.16(6), N1-Ru1-N4 99.96(6)°.

The substituent on the asymmetrical bpy ligand is twisted from the plane of the central pyridine ring and their two planes subtend an angle of 25.5°. The orientation of the pyridoyl substituent is dictated by three hydrogen bonds; N3…$H^{6F}$ (2.277(1) Å), O…$H^{4F}$ (2.433(1) Å) and O…$H^{3G}$ (2.468(1) Å; see section 6.1.2.1). The packing is dominated by electrostatic interactions between anions and cations with H…F distances being between 2.5 and 2.7 Å. In addition, there are intermolecular hydrogen bonds between two cations with the distance

O…H35 being 2.375(1) Å and weak intermolecular π-π-interactions between the two N2 containing pyridine rings of two distinct cations. These rings are offset, the distance between the two centroids being 3.9 Å, which seems to be rather week π-π-interaction.[77]

Single crystals of the complex [Ru(bpy)$_2$(**13**)][PF$_6$]$_2$*CH$_2$Cl$_2$ were grown by slow evaporation of a CH$_2$Cl$_2$ solution of the compound. It crystallizes in the monoclinic space group *P2$_1$/n* with a solvent molecule. The molecular structure is depicted in Figure 6-9 and the important bond parameters are listed in Table 6-1. It very much resembles the corresponding iridium(III) complex, differing only slightly in the bond parameters and will not be discussed in detail.

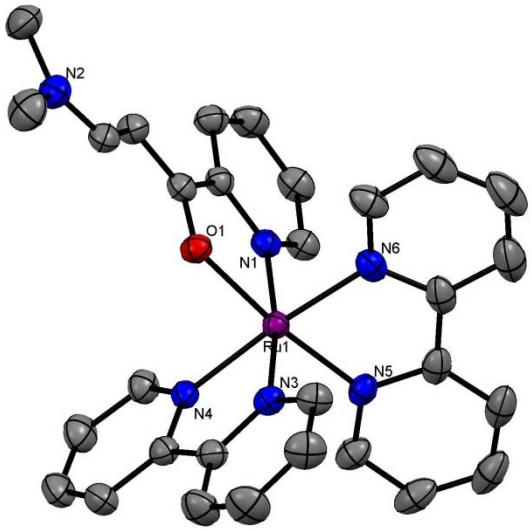


**Figure 6-9** Structure of the [Ru(bpy)$_2$(**13**)]$^{2+}$ cation in [Ru(bpy)$_2$(**13**)][PF$_6$]$_2$*CH$_2$Cl$_2$ with H atoms omitted (ellipsoids plotted at 50 % probability level).

To emphasize the similarity between the two compounds the bond parameters are compared in Table 6-1.

| [Ir(ppy)$_2$(**13**)][PF$_6$]*0.5 CH$_3$OH*H$_2$O | | [Ru(bpy)$_2$(**13**)][PF$_6$]$_2$*CH$_2$Cl$_2$ | |
|---|---|---|---|
| | [Å] | | [Å] |
| Ir1-C11 | 1.987(5) | Ru1-N5 | 2.032(2) |
| Ir1-C22 | 2.002(5) | Ru1-N6 | 2.045(2) |
| Ir1-N3 | 2.021(4) | Ru1-N3 | 2.0535(19) |
| Ir1-N4 | 2.033(4) | Ru1-N4 | 2.0565(19) |
| Ir1-N1 | 2.137(4) | Ru1-N1 | 2.055(2) |
| | [°] | | [°] |
| Ir1-O1 | 2.173(3) | Ru1-O1 | 2.0659(16) |
| C11-Ir1-C22 | 87.19(18) | N6-Ru1-N1 | 87.84(8) |
| C11-Ir1-N3 | 80.72(19) | N3-Ru1-N4 | 79.13(8) |
| C22-Ir1-N3 | 93.70(18) | N6-Ru1-N3 | 96.32(8) |
| C11-Ir1-N4 | 96.11(19) | N5-Ru1-N4 | 97.22(8) |
| C22-Ir1-N4 | 80.92(18) | N5-Ru1-N6 | 79.47(9) |
| N3-Ir1-N4 | 173.92(16) | N5-Ru1-O1 | 173.52(7) |
| C11-Ir1-N1 | 98.69(16) | N5-Ru1-N1 | 98.51(8) |
| C22-Ir1-N1 | 173.76(16) | N6-Ru1-N4 | 174.44(8) |
| N3-Ir1-N1 | 89.36(15) | N5-Ru1-N3 | 90.04(8) |
| N4-Ir1-N1 | 96.26(15) | N1-Ru1-N4 | 97.11(8) |
| C11-Ir1-O1 | 172.73(16) | N3-Ru1-N1 | 171.07(8) |
| C22-Ir1-O1 | 98.89(15) | N6-Ru1-O1 | 94.84(8) |
| N3-Ir1-O1 | 94.84(15) | N3-Ru1-O1 | 93.71(7) |
| N4-Ir1-O1 | 88.81(14) | N4-Ru1-O1 | 88.68(7) |
| N1-Ir1-O1 | 75.40(13) | N1-Ru1-O1 | 78.02(7) |

**Table 6-1** Comparison of bond parameters of [Ir(ppy)$_2$(**13**)][PF$_6$]*0.5 CH$_3$OH*H$_2$O *vs.* [Ru(bpy)$_2$(**13**)][PF$_6$]$_2$*CH$_2$Cl$_2$

X-Ray quality crystals of $[Ru(\mathbf{40})_2][PF_6]_2$ were obtained by slow evaporation of an acetonitrile solution of the compound. The complex crystallizes in the orthorhombic space group *Pbcn*. The structure of the $[Ru(\mathbf{40})_2]^{2+}$ cation is depicted in Figure 6-10 and selected bond parameters are listed in the figure caption or in Table 6-2 *vs.* $[Fe(\mathbf{40})_2][PF_6]_2$. The metal atom resides on the special position ($^1/_2$, *y*, $^3/_4$) on a 2-fold axis. In the $[Ru(\mathbf{40})_2]^{2+}$ cation, the *tert*-butyl substituent is disordered. It has been modelled over two positions with fractional occupancies of 0.71 and 0.29 with a common quaternary atom C16. The $[PF_6]^-$ anion is disordered as well and has been modelled over two positions of 0.51 and 0.49 fractional occupancies. The Ru–N bond distances in $[Ru(\mathbf{40})_2][PF_6]_2$ agree with those found in $[Ru(tpy)_2][PF_6]_2*2MeCN$ (1.974(7)–2.076(6) Å),[132] $[Ru(tpy)_2][PF_6]_2*Me_2CO$ (1.96(1)–2.09(1) Å),[133] $[Ru(tpy)_2][ClO_4]_2*1.1H_2O$ (1.977(6)–2.075(5) Å),[134] $[Ru(tpy)_2]Cl_2*6H_2O$ (1.968(5)–2.074(5) Å),[135] and $[Ru(tpy)_2]Cl_2*4CH_2Cl_2$ (1.969(4)–2.080(4) Å).[136] We note that in $[Ru(tpy)_2][BF_4]_2$, the Ru–N bonds are longer than is typical and lie in the range 2.000(8)–2.102(5) Å.[137,138]

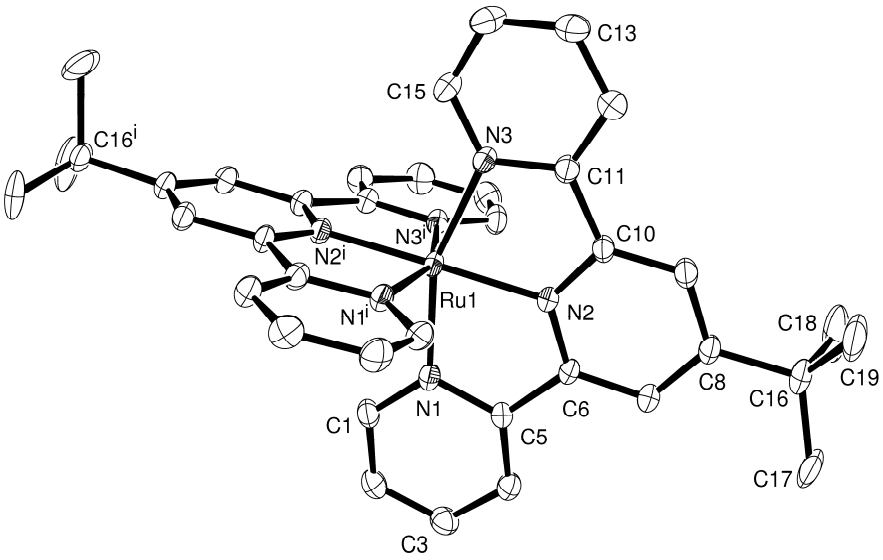


**Figure 6-10** Structure of the $[Ru(\mathbf{40})_2]^+$ cation in $[Ru(\mathbf{40})_2][PF_6]_2$ (ORTEP plot with ellipsoids at the 30 % probability level); H atoms omitted. Symmetry code i = 1 – x, y, 3/2 – z; Selected bond parameters: Ru1-N2 1.986(3), Ru1-N1 2.066(4), Ru1-N3 2.082(4) Å; N2-Ru1-N2$^i$ 179.2(2), N2$^i$-Ru1-N1 100.31(13), N2-Ru1-N1 79.13(13), N1-Ru1-N1$^i$ 94.0(2), N2-Ru1-N3$^i$ 101.89(13), N2-Ru1-N3 78.65(13), N1-Ru1-N3 157.78(13), N1-Ru1-N3$^i$ 89.36(14), N2-Ru1-N3 78.65(13), N2-Ru1-N3$^i$ 101.89(13), N3-Ru1-N3$^i$ 95.8(2)°.

The crystal packing in $[Ru(\mathbf{40})_2][PF_6]_2$ is comparable to similar ruthenium(II) tpy complexes but the *tert*-butyl group has an interesting effect, therefore, this structure will be discussed more in detail. A view along the crystallographic *a*-axis (Figure 6-11a) reveals a grid-like assembly which is a typical and well established packing motif for $\{M(tpy)_2\}$-domains.[139] In the packing diagram in Figure 6-11b, the pyridine ring containing N3 and symmetry related rings are shown in spacefilling representation. Although face-to-face interactions appear to be present, the centrosymmetric pairs of rings are significantly offset with a distance

between the ring centroids of 4.3 Å; this results in only very weak interactions. The {M(tpy)$_2$}-embraces are held at bay by the sterically demanding *tert*-butyl groups, and the dominant attractive packing forces involve CH$_{butyl}$...π contacts. Each *tert*-butyl substituent from one [Ru(**40**)$_2$]$^{2+}$ cation is oriented into a cavity generated by pyridine rings of neighbouring cations (Figure 6-12); the shortest contacts are C18H18C...centroid of ring containing N1$^{iii}$ (3.3 Å) and C17H17B...centroid of ring containing N3$^{iv}$ (3.5 Å), symmetry codes iii = $^3/_2 - x$, $-^1/_2 + y$, $z$ and iv = $^3/_2 - x$, $^1/_2 + y$, $z$. Repulsive H...H contacts between *tert*-butyl groups partly offset the attractive interactions; shortest contact is C17H17C...H17C$^{v}$C17$^{v}$ = 2.52 Å, symmetry code v = $2 - x$, $y$, $^3/_2 - z$. Extensive CH...F contacts contribute to the overall crystal packing.

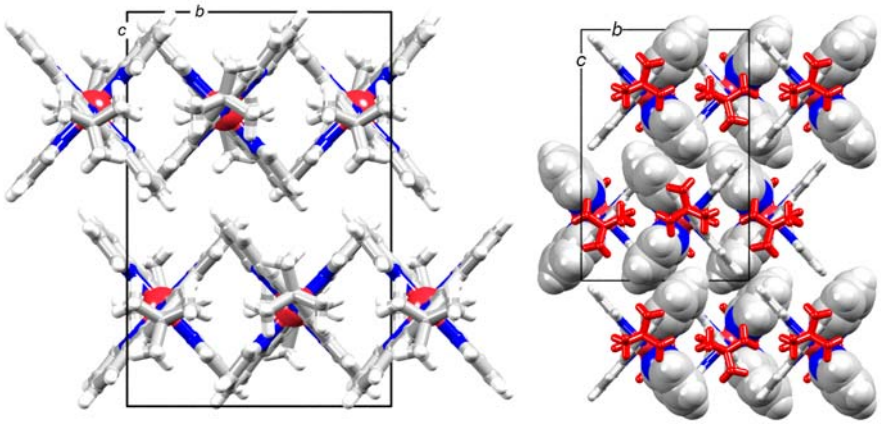


a) b)

**Figure 6-11** Packing of cations in [Ru(**40**)$_2$][PF$_6$]$_2$ with the unit cell viewed down the a-axis:(a) showing the grid-like packing and (b) emphasizing offset face-to-face interactions (*t*-Bu substituents shown in red).

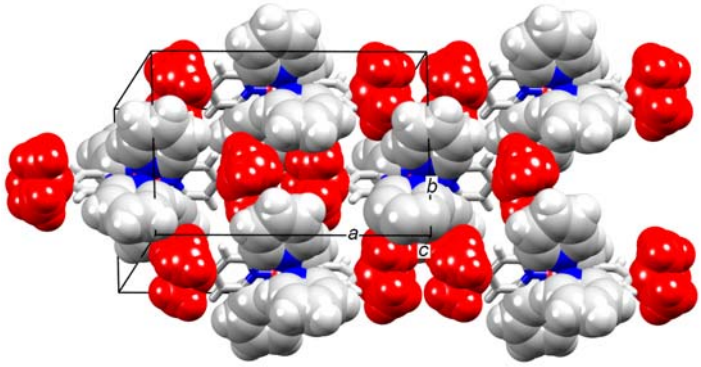


**Figure 6-12** Packing of cations in [Ru(**40**)$_2$][PF$_6$]$_2$ focusing on the CH$_{butyl}$...π interactions (spacefilling representation, *t*-Bu groups shown in red).

Single crystals of complex [Fe(**40**)$_2$][PF$_6$]$_2$ were grown by slow evaporation of a acetonitrile solution of the compound. Although, it crystalizes in a different orthorhombic space group (*Pnna*), it exhibits a very similar molecular structure and similar packing as the above describe complex [Ru(**40**)$_2$][PF$_6$]$_2$, it differs only slightly in the bond parameters of the

coordination geometry. The different space group is very likely due slightly different symmetries withing the elementar cell. Therefore, it will not be described here in detail. The structure is depicted in Figure 6-13 and the bond parameters are listed in Table 6-2 *vs*. the values of $[Ru(\mathbf{40})_2][PF_6]_2$. Furthermore, the bond parameters are comparable to similar $[Fe(4'\text{-R-tpy})_2][PF_6]_2$ compounds: e.g., $[Fe(4'\text{-Cl-tpy})_2][PF_6]_2$,[140] $[Fe(4'\text{-Ph-tpy})_2][PF_6]_2(MeCN)(H_2O)$,[141] or $[Fe(4'\text{-(pyrid-2-yl)-tpy})_2][Cr_2O_7](H_2O)_6$.[142]

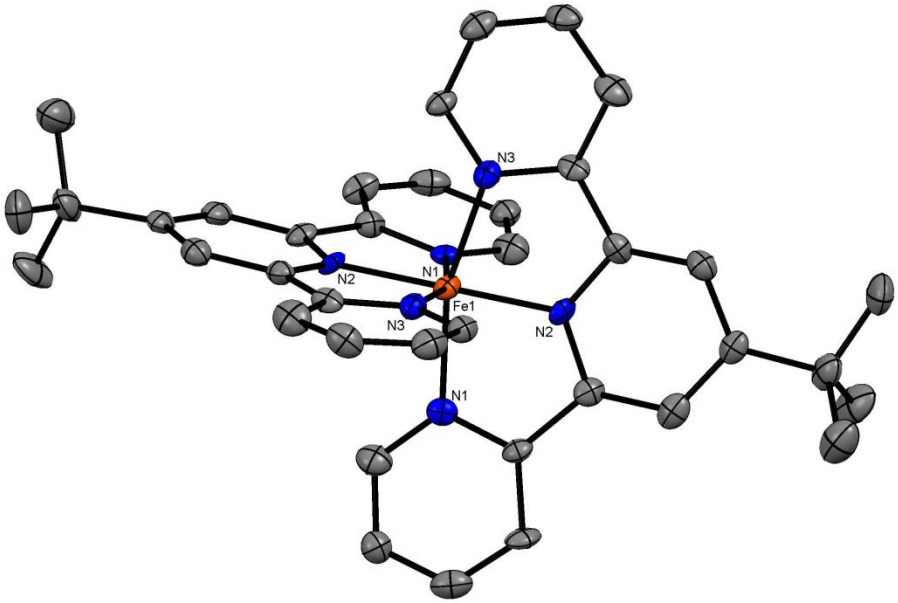


**Figure 6-13** Structure of the $[Fe(\mathbf{40})_2]^+$ cation in $[Fe(\mathbf{40})_2][PF_6]_2$ with H atoms omitted (ellipsoids plotted at 30 % probability level); Symmetry code i = x, 1/2-y, ½-z.

| $[Ru(\mathbf{40})_2][PF_6]_2$ | | $[Fe(\mathbf{40})_2][PF_6]_2$ | |
|---|---|---|---|
| Ru1-N1 | 2.066(4) Å | Fe1-N1 | 1.991(5) Å |
| Ru1-N2 | 1.986(3) Å | Fe1-N3 | 1.946(5) Å |
| Ru1-N3 | 2.082(4) Å | Fe1-N2 | 1.873(4) Å |
| N1-Ru1-N1' | 94.0(2)° | N1-Fe1-N1' | 96.8(3)° |
| N2-Ru1-N2' | 179.2(2)° | N2-Fe1-N2' | 179.9(3)° |
| N3-Ru1-N3' | 95.8(2)° | N3-Fe1-N3' | 91.7(3)° |
| N2-Ru1-N1' | 100.31(13)° | N2-Fe1-N1' | 98.7(2)° |
| N2-Ru1-N1 | 79.13(13)° | N1-Fe1-N2 | 81.3(2)° |
| N2-Ru1-N3' | 101.89(13)° | N3-Fe1-N2' | 98.7(2)° |
| N2-Ru1-N3 | 78.65(13)° | N3-Fe1-N2 | 81.3(2)° |
| N1-Ru1-N3' | 157.78(13)° | N1-Fe1-N3' | 162.42(17)° |
| N1-Ru1-N3 | 89.36(14)° | N3-Fe1-N1 | 88.39(17)° |

**Table 6-2** Selected bond parameters of $[M(\mathbf{40})_2][PF_6]_2$ (M = Fe and Ru).

### 6.1.2.3 Electronic Absorption and Emission Spectroscopy

UV-visible absorption spectra for ruthenium(II) tris bpy complexes were measured in dichloromethane solutions at room temperature (Table 6-3 and Figure 6-14 left side) and they display strong bands in the UV region up to 300 nm attributed to intraligand ($\pi$-$\pi^*$) transitions. Lower-energy absorption bands (300-400 nm) correspond to metal-centred (MC)

transitions, which are lower in intensity (ε between 6000 to 20000 $M^{-1}$ $cm^{-1}$) for compounds where the asymmetric bpy ligand bears only one substituent in the 6'-position. Complex $[Ru(bpy)_2(\mathbf{34})][PF_6]_2$, where the bpy moiety contains an additional substituent in the 4'-position, exhibits a more intense MC transition (ε = 29000 $M^{-1}$ $cm^{-1}$). Finally, the MLCT bands are observed between 400 and 500 nm. As can be clearly seen, the absorption spectra do not change very much with variation of the substituents on the bpy ligands. Especially, the absorption maxima vary only marginally in contrast to the intensity. Noteworthy is the fact that except for $[Ru(bpy)_2(\mathbf{2})][PF_6]_2$ which has similar values for ε compared to the parent compound $[Ru(bpy)_3][PF_6]_2$ (ε = 14000 $M^{-1}$ $cm^{-1}$) and $[Ru(bpy)_2(\mathbf{34})][PF_6]_2$, whose MLCT bands are more intense (ε = 18100 $M^{-1}$ $cm^{-1}$), all the other complexes exhibit MLCT bands which are lower in intensity.

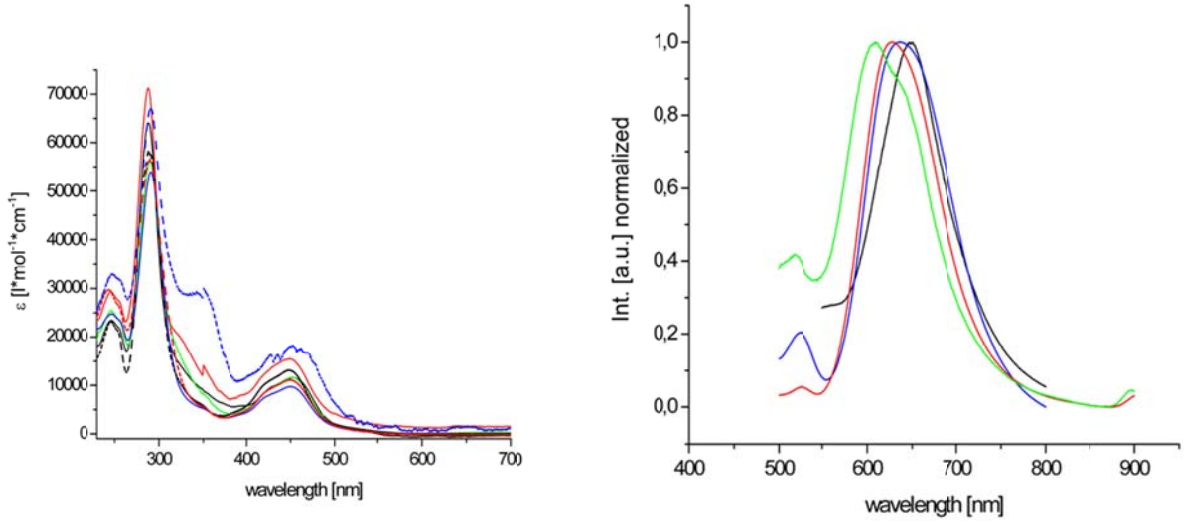


**Figure 6-14** Electronic absorption (left side) spectra of $CH_2Cl_2$ solutions of $[Ru(bpy)_2(L)][PF_6]_2$ for L = **1**, **2**, **4**, **10**, **20** , **21** and **34**; Key: black, L = **1**; red, L = **2**; green, L = **4**; black dashed, L = **10**; blue, L = **20**; red dashed, L = **21**; blue dashed, L = **34** (See experimental section for solution concentrations); and emission spectra (right side, room temperature); Key: green, L = **2**; red, L = **10**; blue, L = **21**; black, L = **34**.

Emission spectra could not be observed for all the ruthenium(II) complexes. The right side of Figure 6-14 depicts the obtained emission spectra for compounds $[Ru(bpy)_2(L)][PF_6]_2$ (L = **2**, **10**, **21** and **34**). The furanyl derivative $[Ru(bpy)_2(\mathbf{2})][PF_6]_2$ a exhibits yellow/orange emission with $\lambda_{max}$ = 608 nm, the *n*butyl derivative (L = **10**) is shifted to lower energy ($\lambda_{max}$ = 627 nm) which is comparable to the parent compound. Compound $[Ru(bpy)_2(\mathbf{21})][PF_6]_2$ shows a bathochromic shift ($\lambda_{max}$ = 636 nm) with respect to $[Ru(bpy)_3][PF_6]_2$ followed by $[Ru(bpy)_2(\mathbf{34})][PF_6]_2$ ($\lambda_{max}$ = 649 nm), which emits orange.

The biggest red shift of the emission was observed for $[Ru(bpy)_2(\mathbf{22})][PF_6]_2$ (Figure 6-15). When excited into the MLCT band, which is higher when compared to the parent compound ($\lambda_{max}$ = 484 *vs* 450 nm), combined with a slightly higher Stokes shift, the emitted light appears red ($\lambda_{max}$ = 673 nm). Again, since ligand **22** has a free nitrogen atom, absorption and

emission spectra were recorded after the solutions were treated with TFA. Yet, as observed for the iridium(III) complex, no change could be observed, except a slight increase in the intensity of the absorption spectrum. So, either the nitrogen atom is not truly free as thought, or the protonation has no effect. In the worst case scenario it is possible that dichloromethane is acidic enough to protonate the complex, which would mean that the observed spectra are both of a protonated species. The experiments should and will be repeated in acetonitrile to exclude or confirm the last possibility.

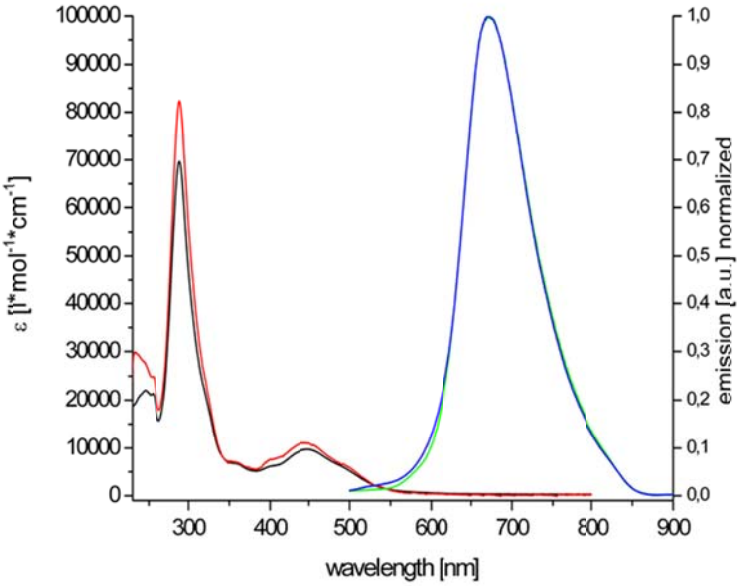


**Figure 6-15** Electronic absorption spectra of $CH_2Cl_2$ solutions of $[Ru(bpy)_2(\mathbf{22})][PF_6]_2$; Key: black, absorption pure; red, absorption protonated (TFA); blue, emission pure; green, emission protonated (TFA).

Compound $[Ru(bpy)_2(\mathbf{13})][PF_6]_2$ shows a similar absorption spectrum to the [Ru(bpy)2(NN)] complexes, even though the *N,O*-donor ligand **13** is coordinated to the ruthenium metal centre (see Figure 6-16).

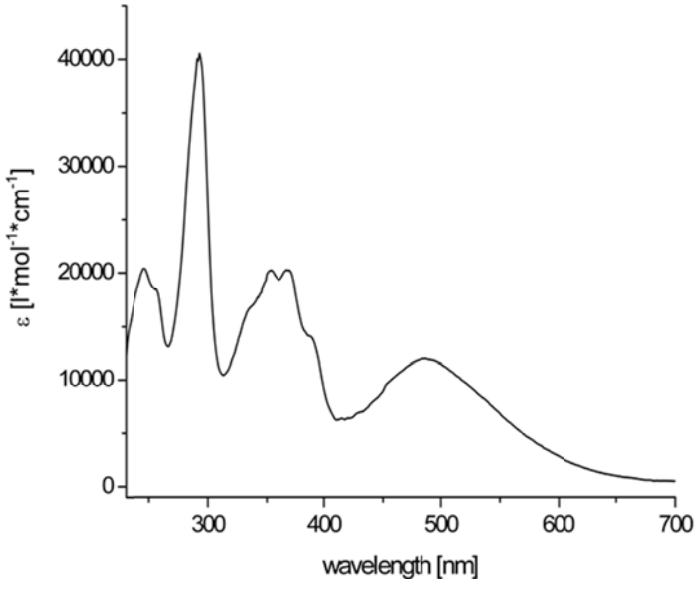


**Figure 6-16** Electronic absorption spectrum of a $CH_2Cl_2$ solution of $[Ru(bpy)_2(\mathbf{13})][PF_6]_2$ ($c = 1*10^{-5}$ mol/L).

The region between 300 and 400 nm shows a fine structure for the MC transition and the MLCT absorption is shifted to lower energies ($\lambda_{max}$ = 486 nm) in contrast to ruthenium trisbpy complexes but similar in intensity. As observed for the corresponding iridium(III) complex [Ir(ppy)$_2$(**13**)][PF$_6$], the ruthenium(II) complex is also not emissive.

The solution electronic absorption spectra of the homoleptic [M(**40**)$_2$][PF$_6$]$_2$ complexes (M = Fe and Ru) are shown in Figure 6-17. The high energy absorptions exhibited by each complex are slightly red-shifted with respect to the free ligand **40** and they arise from $\pi^* \leftarrow \pi$ transitions centred on the tpy domain. The MLCT bands for [Fe(**1**)$_2$][PF$_6$]$_2$ and [Ru(**1**)$_2$][PF$_6$]$_2$ are observed at 554 and 484 nm, showing little change from those exhibited by [Fe(tpy)$_2$][BF$_4$]$_2$ (551 nm) and [Ru(tpy)$_2$][PF$_6$]$_2$ (475 nm).[143] The absorption spectrum of [Ru(tpy)(**40**)][PF$_6$]$_2$ displays similar features to those of [Ru(**40**)$_2$][PF$_6$]$_2$ and [Ru(tpy)$_2$][PF$_6$]$_2$, with the MLCT band appearing at 480 nm.

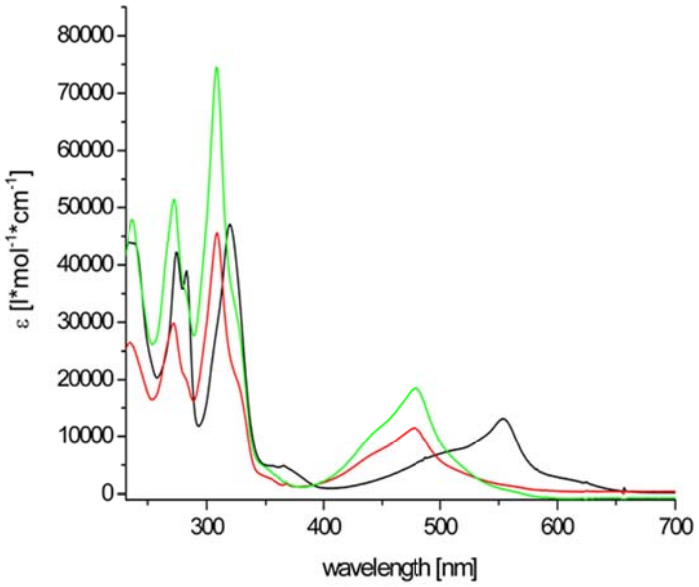


**Figure 6-17** Electronic absorption spectra of $CH_2Cl_2$ solutions of [Fe(**40**)$_2$][PF$_6$]$_2$ (black), [Ru(**40**)$_2$][PF$_6$]$_2$ (red), [Ru(tpy)(**40**)][PF$_6$]$_2$ (green).

| Compound | Absorption in $CH_2Cl_2$ $\lambda_{max}$ [nm] ($\varepsilon$[$10^3$*L*mol$^{-1}$*cm$^{-1}$]) | | | | | | | Emission $\lambda_{em}$ ($\lambda_{ex}$) [nm] |
|---|---|---|---|---|---|---|---|---|
| [Ru(bpy)$_3$][PF$_6$]$_2$ | 244 (16.6) | 253 (14.5) | 286 (52.8) | 350 (9.9) | 358 (8.9) | 442 (12.5) | 450 (14.0) | 620 (450)[a] |
| [Ru(bpy)$_2$(**1**)][PF$_6$]$_2$ | 246 (23.4) | 253 (21.4) | 288 (64.0) | | | 433 (9.9) | 453 (11.6) | - |
| [Ru(bpy)$_2$(**2**)][PF$_6$]$_3$ | 246 (29.5) | 254 (27.6) | 288 (71.1) | | | 433 (14.1) | 449 (15.5) | 608 (448) |
| [Ru(bpy)$_2$(**4**)][PF$_6$]$_4$ | 246 (25.4) | 255 (23.5) | 290 (56.1) | | | 432 (10.0) | 452 (11.6) | - |
| [Ru(bpy)$_2$(**10**)][PF$_6$]$_5$ | 245 (23.4) | 253 (21.4) | 289 (57.7) | | | 429 (11.0) | 448 (13.2) | 627 (448) |
| [Ru(bpy)$_2$(**13**)][PF$_6$]$_6$ | 246 (20.3) | 255 (18.4) | 293 (40.5) | 353 (20.1) | 369 (20.3) | 388 (14.2) | 486 (11.9) | - |
| [Ru(bpy)$_2$(**20**)][PF$_6$]$_7$ | 247 (24.8) | 255 (23.7) | 291 (53.8) | | | 427 (7.9) | 450 (9.7) | - |
| [Ru(bpy)$_2$(**21**)][PF$_6$]$_8$ | 243 (29.6) | 253 (26.6) | 290 (56.7) | | | 429 (9.3) | 450 (11.1) | 636 (449) |
| [Ru(bpy)$_2$(**22**)][PF$_6$]$_9$ | 247 (21.9) | 256 (21.3) | 289 (69.6) | 316 (23.0) | 351 (7.1) | 401 (6.2) | 484 (6.5) | 673 (350) |
| [Ru(bpy)$_2$(**34**)][PF$_6$]$_{10}$ | 246 (33.0) | 257 (31.7) | 291 (66.8) | | 350 (29.1) | 431 (15.5) | 456 (18.0) | 649 (350) |
| [Ru(**40**)$_2$][PF$_6$]$_{11}$ | 235 (26.3) | 272 (29.5) | 279 (21.3) | 309 (45.5) | 323 (21.8) | 452 (8.1) | 478 (11.9) | - |
| [Ru(tpy)(**40**)][PF$_6$]$_{12}$ | 237 (47.7) | 272 (51.6) | 281 (36.3) | 308 (74.4) | 321 (34.9) | 453 (11.9) | 479 (18.6) | - |
| [Fe(**40**)$_2$][PF$_6$]$_{13}$ | 237 (43.9) | 274 (42.1) | 283 (38.9) | 319 (46.9) | 363 (4.9) | 509 (7.8) | 554 (13.3) | - |

**Table 6-3** Electronic absorption and emission data for ruthenium(II) complexes, a) in EtOH[144].

### 6.1.2.4 Electrochemistry of complexes with ligand 40

The free ligand **40** and the metal complexes are redox active, and cyclic voltammetric data are listed in Table 6-4. Processes are reversible unless otherwise stated. The free ligand exhibits one irreversible reduction, while upon coordination, a series of ligand-based reductions is observed, consistent with expectations.[145] The value of $E_{1/2}$ = +0.89 V for [Ru(**40**)$_2$][PF$_6$]$_2$ is at slightly lower potential than $E_{1/2}$ for [Ru(tpy)$_2$][PF$_6$]$_2$ (+0.92 V),[143] indicating that ligand **40** is somewhat electron releasing. For the heteroleptic complex [Ru(tpy)(**40**)][PF$_6$]$_2$, $E_{1/2}$ is the same (within experimental error) as for [Ru(tpy)$_2$][PF$_6$]$_2$. The trend from [Ru(**40**)$_2$][PF$_6$]$_2$ to [Ru(tpy)$_2$][PF$_6$]$_2$ is reinforced by a value of $E_{1/2}$ = +0.67 V for [Fe(**40**)$_2$][PF$_6$]$_2$ compared to +0.74 V for [Fe(tpy)$_2$][PF$_6$]$_2$,[143] and we note that the latter two potentials straddle that observed for [Fe(L)$_2$][PF$_6$]$_2$ ($E_{1/2}$ = +0.71 V) where L is 4'-(4-*t*-BuC$_6$H$_4$)tpy).[146]

| Compound | $E_{ox}$ / V | $E_{red}$ / V | | |
|---|---|---|---|---|
| **40** | | | | –2.60$^{ir}$ |
| [Fe(**40**)$_2$][PF$_6$]$_2$ | +0.70/ +0.63 | –1.71$^{ir}$ | –1.84/ –1.79$^{qr}$ | –2.53/ –2.39$^{qr}$ |
| [Ru(**40**)$_2$][PF$_6$]$_2$ | +0.92/ +0.85 | –1.68$^{ir}$ | –1.92/ –1.82$^{qr}$ | –2.39/ –2.31$^{qr}$ |
| [Ru(tpy)(**40**)][PF$_6$]$_2$ | +0.97/ +0.88 | –1.65$^{ir}$ | –1.91/ –1.79$^{qr}$ | –2.39/ –2.29$^{qr}$ |

**Table 6-4** Redox potentials of ligand **40** and homo- and heteroleptic complexes with respect to Fc/Fc$^+$; MeCN solutions [*t*-Bu$_4$N][PF$_6$] supporting electrolyte, and scan rate of 0.1 V s$^{-1}$ (ir = irreversible; qr = quasi-reversible).

Electrochemical studies on the remaining complexes (Ru as well as Ir) are ongoing.

## 6.2 Experimental

### 6.2.1 [Ru(bpy)$_2$(1)][PF$_6$]$_2$

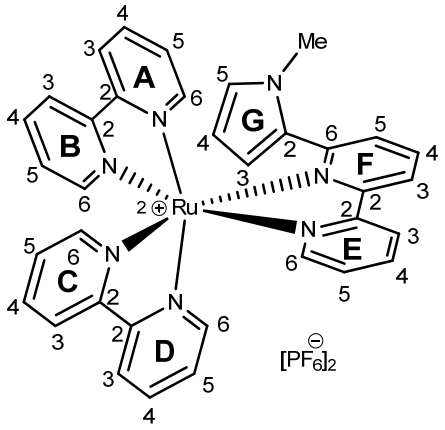


In a 5 ml microwave vial, ligand **1** (30.0 mg, 0.12 mmol, 1.0 eq) and [Ru(bpy)$_2$Cl$_2$] (61.8 mg, 0.12 mmol, 1.0 eq) were suspended in MeOH (4 ml). This mixture was irradiated for 1 h at 110 °C in a microwave reactor. Then solid $NH_4PF_6$ (334 mg, 2.05 mmol, 16.0 eq) was added and the mixture was stirred for a further 45 m The solvent was removed under reduced pressure and the crude product was purified by column chromatography ($SiO_2$,

$CH_2Cl_2$/MeOH 1:0-97:3). The desired product was obtained as the first major fraction as an orange powder (100.0 mg, 0.11 mmol, 84 %). The first minor fraction yielded unreacted ligand (4.0 mg, 0.02 mmol, 13 %). $^1$H NMR (500 MHz, $CD_2Cl_2$) $\delta$ (ppm) 8.48 (d, *J* 8.7 Hz, 2 H), 8.42-8.31 (m, 2 H), 8.28 (d, *J* 8.0 Hz, 1 H), 8.22 (d, *J* 8.7 Hz, 1 H), 8.17-7.91 (m, 5 H), 7.90-7.80 (m, 2 H), 7.63 (d, *J* 4.5 Hz, 1 H), 7.60-7.52 (m, 2 H), 7.49 (t, *J* 5.7 Hz, 1 H), 7.45-7.13 (m, 2 H), 7.08-6.94 (m, 1 H), 6.88 (t, *J* 7.2 Hz, 1 H), 5.90 (m, 1 H), 5.56 (s, 1 H), 5.29 (s, 1 H), 2.42 (s, 3 H); $^{13}$C NMR (500 MHz HMBC/HMQC, $CD_2Cl_2$) $\delta$ (ppm) 155.96, 155.25, 154.62, 154.00, 153.05, 152.42, 151.94, 151.31, 151.04, 150.77, 149.89, 148.75, 146.61, 138.67, 138.56, 136.43, 136.60, 135.37, 133.26, 128.66, 128.05, 127.51, 127.33, 125.63, 125.01, 124.67, 124.38, 124.24, 123.93, 122.39, 121.59, 119.34, 111.59, 109.77, 30.79; ESI-MS *m/z*: 794.2 $[M\text{-}PF_6]^+$ (70 %, calc. 794.1), 324.6 $[M\text{-}2PF_6]^+$ (100 %, calc. 324.6); IR (solid, $\nu$/cm$^{-1}$) 3127 (w), 3111 (w), 3095 (w), 2923 (w), 2855 (w), 2360 (w), 2329 (w), 1700 (m), 1604 (m), 1558 (m), 1465 (m), 1446 (m), 1424 (m), 1418 (m), 1385 (m), 1333 (w), 1307 (w), 1293 (w), 1272 (w), 1243 (m), 1221 (w), 1161 (m), 1125 (w), 1094 (w), 1068 (w), 1026 (w), 877 (m), 825 (s), 807 (s), 799 (s), 757 (m), 752 (m), 739 (m), 717 (m), 712 (m), 694 (m), 685 (m), 660 (m), 648 (m), 624 (w); UV/vis ($CH_2Cl_2$, 1.0 x 10$^{-5}$ mol dm$^{-3}$) $\lambda_{max}$/nm 252 ($\varepsilon$/dm$^3$ mol$^{-1}$ cm$^{-1}$ 22400), 257 (21000), 290 (63200), sh 330 (12900), 435 (10300), 460 (11100); emission $\lambda_{max}$ ($\lambda_{ex}$) = 509, 592, 625 (390) nm; EA: calc. for $C_{35}H_{29}N_7F_{12}P_2Ru$, C 44.79 %, H 3.11 %, N 10.45 %, found C 44.68 %, H 3.22 %, N 10.60 %.

### 6.2.2 $[Ru(bpy)_2(2)][PF_6]_2$

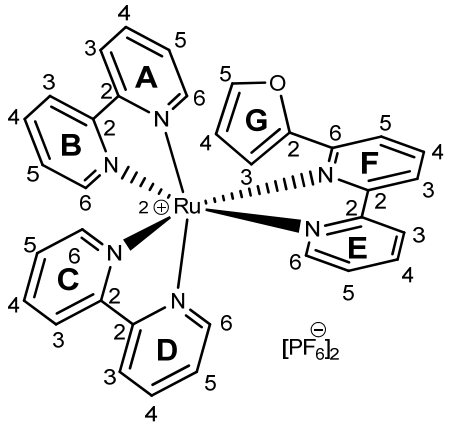


In a 5 ml microwave vial, ligand **2** (13.8 mg, 62.0 mmol, 1.0 eq) and $[Ru(bpy)_2Cl_2]$ (30.0 mg, 62.0 mmol, 1.0 eq) were suspended in MeOH (2 ml). This mixture was irradiated for 1 h at 120 °C in a microwave reactor. The dark red solution was reduced in volume, the product was precipitated upon addition of an aqueous $NH_4PF_6$ solution (~10 ml, ~0.1 M) and stirred for a further 30 m The red solid was filtered off, washed with $H_2O$ and $Et_2O$ then dried in a desiccator. The desired product was obtained as a dark red powder (37.0 mg, 39.0 mmol, 64 %) and required no further purification. The product is slightly water soluble. The

combined filtrates were reduced in volume until the product precipitated. The orange solid was filtered, washed with little $H_2O$ and $Et_2O$ and dried in the dessicator (15.0 mg, 16.0 µmol, 26 %). $^1$H NMR (500 MHz, $CD_3CN$) $\delta$ (ppm) 8.56-8.52 (m, 3 H, $H^{6C+3C+E}$), 8.48 (2d, *J* 7.8 Hz, 2 H, $H^{3F+3D}$), 8.34 (d, *J* 8.1 Hz, 1 H, $H^{3A}$), 8.17-8.11 (m, 2 H, $H^{4C+3D}$), 8.09 (t, *J* 7.9 Hz, 1 H, $H^{4E}$), 8.03 (m, 2 H, $H^{4F+A}$), 7.98 (t, *J* 8.0 Hz, 1 H, $H^{4B}$), 7.67 (t, *J* 7.8 Hz, 1 H, $H^{4D}$), 7.60 (d, *J* 5.4 Hz, 1 H, $H^{6A}$), 7.56 (d, *J* 5.4, Hz, 1 H, $H^{6E}$), 7.50 (t, *J* 6.6 Hz, 2 H, $H^{5C}$), 7.47 (d, *J* 7.7 Hz, 1 H, $H^{5F}$), 7.43 (d, *J* 5.5 Hz, 1 H, $H^{6B}$), 7.34 (2t, *J* 7.5 Hz, 2 H, $H^{5E+A}$), 7.26 (d, *J* 5.3 Hz, 1 H, $H^{6D}$), 7.21 (t, *J* 6.6 Hz, 1 H, $H^{5B}$), 7.07 (s, 1 H, $H^{5G}$), 6.99 (t, *J* 6.6 Hz, 1 H, $H^{5D}$), 6.17 (d, *J* 3.2 Hz, 1 H, $H^{3G}$), 5.94 – 5.91 (m, 1 H, $H^{4G}$); $^{13}$C NMR (126 MHz, $CD_3CN$) $\delta$ (ppm) 159.48 ($C^{2F}$), 159.19 ($C^{2E}$), 158.64 ($C^{2C}$), 158.21 ($C^{2B}$), 157.88 ($C^{2A}$), 157.21 ($C^{2D}$), 155.77 ($C^{6F}$), 155.43 ($C^{6C}$), 152.64 ($C^{6B}$), 152.61 ($C^{6D}$), 151.77 ($C^{6E}$), 151.31 ($C^{6A}$), 145.15 ($C^{2G}$), 139.18 ($C^{4F}$), 138.89 ($C^{4B}$), 138.83 ($C^{4A}$), 138.80 ($C^{4E}$), 138.74 ($C^{4C}$), 137.14 ($C^{4D}$), 130.74 ($C^{5F}$), 128.43 ($C^{5B}$), 128.12 ($C^{5A}$), 128.00 ($C^{5E}$), 127.94 ($C^{5D}$), 127.67 ($C^{5B}$), 126.18 ($C^{3E}$), 125.39 ($C^{3C}$), 125.23 ($C^{3F}$), 124.85 ($C^{3B}$), 124.67 ($C^{3A}$), 123.90 ($C^{3D}$), 112.99 ($C^{4G}$), 112.88 ($C^{3G}$); ESI-MS *m/z*: 781.1 $[M\text{-}PF_6]^+$ (70 %, calc. 781.1), 318.1 $[M\text{-}2PF_6]^+$ (100 %, calc. 318.1); IR (solid, $\nu$/cm$^{-1}$) 3120 (w), 3092 (w), 2363 (w), 2360 (w), 2258 (w), 1710 (w), 1604 (m), 1580 (w), 1466 (m), 1445 (m), 1425 (m), 1390 (w), 1375 (w), 1313 (w), 1275 (w), 1240 (m), 1221 (w), 1161 (m), 1125 (w), 1094 (w), 1067 (w), 1014 (w), 877 (m), 827 (s), 760 (s), 732 (s), 718 (m), 714 (m), 695 (m), 687 (m), 661 (m), 649 (m), 624 (w), 605 (s), 555 (s); UV/vis ($CH_2Cl_2$, 1.0 x 10$^{-5}$ mol dm$^{-3}$) $\lambda_{max}$/nm 250 ($\varepsilon$/dm$^3$ mol$^{-1}$ cm$^{-1}$ 27700), 258 (26000), 289 (71000), sh 326 (19600), 418 (11000), 456 (14800); emission $\lambda_{max}$ ($\lambda_{ex}$) = 504, 592, 635 (425) nm; EA: calc. for $C_{34}H_{26}N_6OF_{12}P_2Ru*1.5\ H_2O$, C 42.87 %, H 3.07 %, N 8.82 %, found C 42.72 %, H 2.94 %, N 8.59 %.

### 6.2.3 $[Ru(bpy)_2(4)][PF_6]_2$

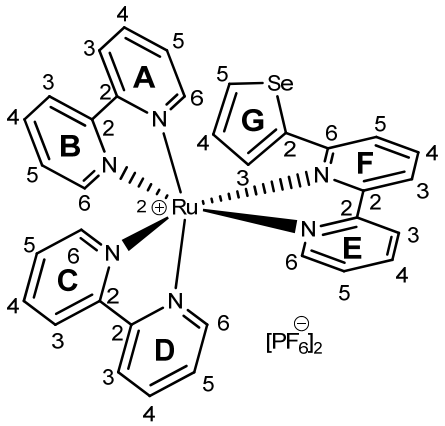


In a 5 ml microwave vial, ligand **4** (20.0 mg, 69.9 µmol, 1.0 eq) and $[Ru(bpy)_2Cl_2]$ (33.8 mg, 69.9 µmol, 1.0 eq) were suspended in MeOH (4 ml). This mixture was irradiated for 1 h at 120 °C in a microwave reactor. The dark red solution was reduced in volume, the product was precipitated upon addition of an aqueous $NH_4PF_6$ solution (~20 ml, ~0.05 M) and stirred

for a further 30 m The red solid was filtered off, washed with $H_2O$ and $Et_2O$, and dried in a desiccator. The desired product was obtained as a dark red powder (44.0 mg, 44.5 µmol, 64 %) and required no further purification. $^1$H NMR (500 MHz, $CD_2Cl_2$) $\delta$ (ppm) 8.54 (2d, *J* 8.2 Hz, 2 H, $H^{3B+E}$), 8.42 (d, *J* 8.2 Hz, 1 H, $H^{3C}$), 8.38 (d, *J* 7.8 Hz, 1 H, $H^{3F}$), 8.32 (d, *J* 8.1 Hz, 1 H, $H^{3D}$), 8.17-8.00 (m, 6 H, $H^{4B+C+E+F+6B+3A}$), 7.94 (t, *J* 7.9 Hz, 1 H, $H^{4D}$), 7.73 (d, *J* 4.3 Hz, 1 H, $H^{5G}$), 7.71 – 7.63 (m, 2 H, $H^{6C+4A}$), 7.57 (t, *J* 6.7 Hz, 1 H, $H^{5B}$), 7.55-7.49 (m, 2 H, $H^{5F+6E}$), 7.47 (t, *J* 6.7 Hz, 1 H, $H^{5C}$), 7.38 (t, *J* 6.7 Hz, 1 H, $H^{5E}$), 7.34 (d, *J* 5.5 Hz, 1 H, $H^{6D}$), 7.29 (t, *J* 6.6 Hz, 1 H, $H^{5D}$), 7.11 (d, *J* 5.6 Hz, 1 H, $H^{6A}$), 6.92 (t, *J* 6.6 Hz, 1 H, $H^{5A}$), 6.63 (br s, 1 H, $H^{4G}$) 6.50-5.75 (br s, 1 H, $H^{3G}$); $^{13}$C NMR (126 MHz, $CD_2Cl_2$) $\delta$ (ppm) 162.61 ($C^{2F}$), 158.21 ($C^{2B}$), 158.06 ($C^{2E}$), 157.37 ($C^{2C}$), 157.36 ($C^{2D}$), 156.44 ($C^{6A}$), 156.32 ($C^{2A}$), 153.27 ($C^{6B}$), 152.18 ($C^{2G}$), 151.78 ($C^{6C}$), 151.49 ($C^{6E}$), 151.19 ($C^{6D}$), 144.88 ($C^{6F}$), 138.90 ($C^{4F}$), 138.84 ($C^{4C}$), 138.77 ($C^{4D}$), 138.55 ($C^{4B}$), 137.79 ($C^{4E}$), 136.84 ($C^{4A}$), 135.27 ($C^{5G}$), 131.53 ($C^{5F}$), 130.41 ($C^{4G}$), 128.78 ($C^{5D}$), 128.41 ($C^{5B}$), 128.19 ($C^{5E}$), 128.04 ($C^{5A}$), 127.45 ($C^{5C}$), 125.68 ($C^{3B}$), 124.98 ($C^{3C}$), 124.82 ($C^{3A}$), 124.62 ($C^{3F}$), 124.30 ($C^{3D}$), 123.49 ($C^{3E}$), 100.54 ($C^{3G}$); ESI-MS *m/z*: 845.5 $[M\text{-}PF_6]^+$ (100 %, calc. 845.0), 350.0 $[M\text{-}2PF_6]^+$ (50 %, calc. 350.0); IR (solid, $\nu$/cm$^{-1}$) 3125 (w), 3093 (w), 2358 (m), 2341 (m), 2322 (w), 1603 (m), 1571 (w), 1558 (m), 1541 (w), 1466 (m), 1459 (m), 1447 (m), 1436 (m), 1427 (m), 1423 (m), 1419 (m), 1387 (m), 1313 (w), 1293 (w), 1271 (w), 1264 (w), 1243 (w), 1213 (w), 1167 (m), 1162 (m), 1125 (w), 891 (m), 879 (m), 831 (s), 809 (s), 801 (s), 759 (s), 741 (s), 729 (s), 705 (s), 687 (s), 668 (s), 645 (m), 640 (m), 624 (m); UV/vis ($CH_2Cl_2$, 1.0 x 10$^{-5}$ mol dm$^{-3}$) $\lambda_{max}$/nm 238 ($\varepsilon$/dm$^3$ mol$^{-1}$ cm$^{-1}$ 22800), 250 (24200), 292 (55300), sh 326 (15500), 428 (9500), 459 (11000); emission $\lambda_{max}$ ($\lambda_{ex}$) = 607, 629 (450) nm.

### 6.2.4 $[Ru(bpy)_2(20)][PF_6]_2$

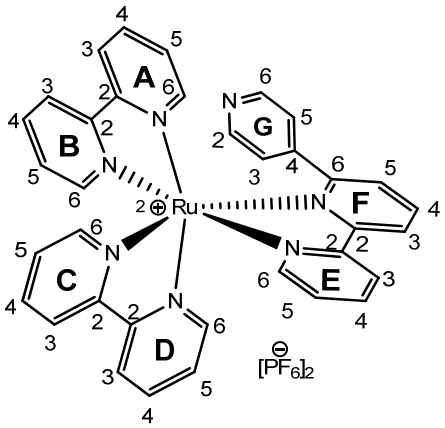


In a 5 ml microwave vial, ligand **20** (23.3 mg, 100.0 µmol, 1.0 eq) and $[Ru(bpy)_2Cl_2]$ (48.4 mg, 100.0 µmol, 1.0 eq) were suspended in MeOH (5 ml). This mixture was irradiated for 1 h at 120 °C in a microwave reactor. The dark red solution was reduced in volume, the product was precipitated upon addition of an aqueous $NH_4PF_6$ solution (~10 ml, ~0.1 M) and stirred

for a further 30 m The orange solid was filtered off, washed with $H_2O$ and $Et_2O$, then dried in a desiccator. The desired product was obtained as an orange powder (62.0 mg, 66.2 µmol, 60 %) and required no further purification. $^1$H NMR (500 MHz, $CD_2Cl_2$) $\delta$ (ppm) 8.80 (m, 1 H, $H^{6G}$), 8.60 (d, *J* 8.2, 1.2 Hz, 1 H, $H^{3F}$), 8.53 (d, *J* 8.3 Hz, 1 H, $H^{3B}$), 8.48 (d, *J* 6.3 Hz, 1 H, $H^{6G}$), 8.37 (d, *J* 8.1 Hz, 1 H, $H^{3D}$), 8.34 (d, *J* 8.1 Hz, 1 H, $H^{3E}$), 8.28 (br s, 1 H, $H^{2G}$), 8.24 (d, *J* 8.2 Hz, 1 H, $H^{3A}$), 8.23 (t, *J* 7.9 Hz, 1 H, $H^{4F}$), 8.37 (d, *J* 7.9, 1.6 Hz, 1 H, $H^{4F}$), 8.12-8.06 (m, 1 H, $H^{4B+E}$), 7.99 (d, *J* 8.1 Hz, 1 H, $H^{3C}$), 7.94 (t, *J* 7.7, 1.8 Hz, 1 H, $H^{4A}$), 7.87 (d, *J* 5.7 Hz, 1 H, $H^{6D}$), 7.80 (d, *J* 5.7 Hz, 1 H, $H^{6E}$), 7.70 (t, *J* 7.9, 1.7 Hz, 1 H, $H^{4C}$), 7.87 (d, *J* 5.7 Hz, 1 H, $H^{6D}$), 7.64 (ddd, *J* 7.6, 5.7, 1.3 Hz, 1 H, $H^{5E}$), 7.60 (ddd, *J* 5.7, 1.5, 0.7 Hz, 1 H, $H^{6B}$), 7.56 (ddd, *J* 7.7, 5.6, 1.3 Hz, 1 H, $H^{5B}$), 7.37 (dd, *J* 7.8, 1.4 Hz, 1 H, $H^{5F}$), 7.35 – 7.30 (m, 2 H, $H^{5+6A}$), 7.24 (br s, 1 H, $H^{3G}$), 7.07 (dd, *J* 5.7, 0.9 Hz, 1 H, $H^{6C}$), 6.95 (ddd, *J* 7.1, 5.6, 1.3, Hz, 1 H, $H^{5C}$), 5.89 (br s, 1 H, $H^{2G}$); $^{13}$C NMR (HMQC/HMBC, 500 MHz, $CD_2Cl_2$) $\delta$ (ppm) 164.49 ($C^{6F}$), 158.29 ($C^{2F}$), 157.80 ($C^{2A}$), 157.73 ($C^{2D}$), 157.58 ($C^{2B}$), 156.93 ($C^{2E}$), 156.30 ($C^{2C}$), 152.47 ($C^{6E}$), 152.16 ($C^{6D}$), 151.71 ($C^{6C}$), 151.65 ($C^{6B}$), 150.94 ($C^{6A}$), 150.58 ($C^{2G}$), 150.15 ($C^{4G}$), 145.18 ($C^{6G}$), 139.41 ($C^{4F}$), 139.05 ($C^{4D}$), 138.90 ($C^{4B+E}$), 138.82 ($C^{4A}$), 137.42 ($C^{4C}$), 130.09 ($C^{5F}$), 128.95 ($C^{5D}$), 128.81 ($C^{5A}$), 128.27 ($C^{5E}$), 128.22 ($C^{5B}$), 127.70 ($C^{5C}$), 125.44 ($C^{3B}$), 124.72 ($C^{3E}$), 124.63 ($C^{3D}$), 124.41 ($C^{3A}$), 124.30 ($C^{3F}$), 123.81 ($C^{3C}$), 122.98 ($C^{5G}$), 122.15 ($C^{3G}$); ESI-MS *m/z*: 792.1 $[M\text{-}PF_6]^+$ (100 %, calc. 792.1), 323.5 $[M\text{-}2PF_6]^+$ (45 %, calc. 323.6); IR (solid, $\nu$/cm$^{-1}$) 3087 (w), 2917 (w), 2356 (s), 2340 (m), 2331 (m), 2311 (m), 2293 (m), 1980 (m), 1869 (m), 1706 (m), 1663 (m), 1653 (m), 1647 (m), 1635 (m), 1603 (m), 1594 (m), 1582 (m), 1558 (m), 1539 (m), 1533 (m), 1506 (m), 1465 (m), 1447 (s), 1429 (m), 1420 (m), 1412 (m), 1387 (m), 1374 (m), 1363 (m), 1355 (m), 1339 (m), 1312 (m), 1272 (m), 1260 (m), 1227 (m), 1222 (m), 1161 (m), 1125 (m), 1104 (m), 1092 (m), 1065 (m), 1048 (m), 1026 (m), 992 (m), 878 (m), 825 (s), 801 (s), 759 (s), 741 (s), 729 (s), 716 (m), 685 (m), 668 (s), 647 (m), 643 (m), 624 (m); UV/vis ($CH_2Cl_2$, 5.0 x 10$^{-5}$ mol dm$^{-3}$) $\lambda_{max}$/nm 246 ($\varepsilon$/dm$^3$ mol$^{-1}$ cm$^{-1}$ 26200), 255 (25200), 291 (61300), 345 (5700), 423 (8200), 451 (10400); emission $\lambda_{max}$ ($\lambda_{ex}$) = 490 + w 590/640 (425), 500 + 600/640 (451) nm.

### 6.2.5 $[Ru(bpy)_2(21)][PF_6]_2$

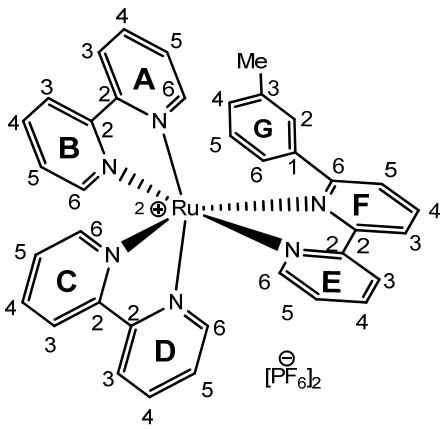

In a 5 ml microwave vial, ligand **21** (12.3 mg, 50.0 µmol, 1.0 eq) and $[Ru(bpy)_2Cl_2]$ (24.2 mg, 50.0 µmol, 1.0 eq) were suspended in MeOH (5 ml). This mixture was irradiated for 1 h at 120 °C in a microwave reactor. The dark red solution was reduced in volume, the product was precipitated upon addition of an aqueous $NH_4PF_6$ solution (~10 ml, ~0.05 M) and stirred for a further 30 m The red solid was filtered off, washed with $H_2O$ and $Et_2O$, then dried in a desiccator. The desired product was obtained as an orange powder (28.2 mg, 29.7 µmol, 59 %) and required no further purification. $^1$H NMR (500 MHz, $CD_2Cl_2$) $\delta$ (ppm) 8.59 (br s, 2 H), 8.39 (br s, 2 H), 8.31 (br s, 3 H), 8.19 (br s, 4 H), 8.10 (br s, 2 H), 7.94 (br s, 2 H), 7.59 (br s, 2 H), 7.37 (br s, 2 H), 6.98 (br s, 3 H), 6.79 (br s, 2 H), 6.58 (br s, 2 H), 2.22 (br s, 2 H), 1.93 (br s, 1 H); $^{13}$C NMR (HMQC/HMBC, 500 MHz, $CD_2Cl_2$) $\delta$ (ppm) 169.45, 158.63, 158.22, 157.34, 157.16, 157.14, 152.83, 151.47, 151.12, 151.05, 151.00, 138.77, 138.35, 138.10, 137.60, 137.35, 137.21, 128.82, 128.33, 128.07, 126.70, 125.07, 124.88, 124.59, 122.28, 110.79, 21.89; ESI-MS *m/z*: 805.2 $[M\text{-}PF_6]^+$ (70 %, calc. 805.1), 330.1 $[M\text{-}2PF_6]^+$ (100 %, calc. 330.1); IR (solid, $\nu$/cm$^{-1}$) 3125 (w), 3095 (w), 2364 (m), 2356 (m), 2340 (m), 2331 (m), 1980 (w), 1848 (w), 1829 (w), 1734 (w), 1717 (w), 1684 (m), 1654 (w), 1603 (m), 1558 (m), 1541 (w), 1521 (w), 1506 (w), 1465 (m), 1447 (m), 1427 (m), 1423 (m), 1419 (m), 1387 (m), 1312 (w), 1272 (w), 1229 (w), 1162 (w), 1070 (w), 1026 (w), 1000 (w), 892 (w), 879 (w), 831 (s), 801 (m), 761 (s), 755 (s), 750 (m), 741 (m), 729 (m), 715 (m), 701 (m), 668 (s), 660 (m), 648 (m); UV/vis ($CH_2Cl_2$, 5.0 x 10$^{-5}$ mol dm$^{-3}$) $\lambda_{max}$/nm 244 ($\varepsilon$/dm$^3$ mol$^{-1}$ cm$^{-1}$ 26300), 256 (22700), 289 (51600), 348 (5200), 428 (8600), 450 (10400); emission $\lambda_{max}$ ($\lambda_{ex}$) = 636 (467) nm.

### 6.2.6 $[Ru(bpy)_2(10)][PF_6]_2$

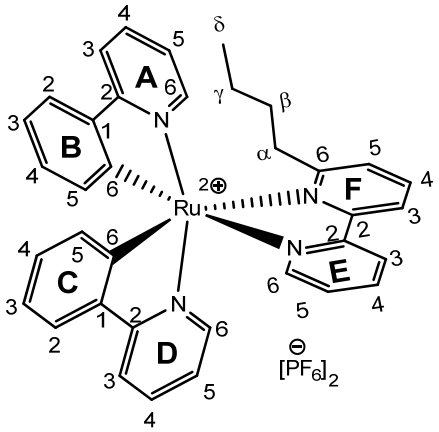


In a 5 ml microwave vial, ligand **10** (10.6 mg, 50.0 µmol, 1.0 eq) and $[Ru(bpy)_2Cl_2]$ (24.2 mg, 50.0 µmol, 1.0 eq) were suspended in MeOH (3 ml). This mixture was irradiated for 1 h at 120 °C in a microwave reactor. The dark red solution was reduced in volume, the product was precipitated upon addition of an aqueous $NH_4PF_6$ solution (~10 ml, ~0.05 M) and stirred for a further 30 m The red solid was filtered off, washed with $H_2O$ and $Et_2O$, then dried in a desiccator. The desired product was obtained as an orange powder (41.0 mg, 44.8 µmol,

90 %) and required no further purification. $^{1}$H NMR (500 MHz, $CD_2Cl_2$) $\delta$ (ppm) 8.48 (d, *J* 8.3 Hz, 2 H, $H^{3A+C}$), 8.46 (d, *J* 8.6 Hz, 1 H, $H^{3E}$), 8.42 (d, *J* 8.1 Hz, 2 H, $H^{3B+D}$), 8.37 (d, *J* 7.9 Hz, 1 H, $H^{3F}$), 8.13-8.00 (m, 5 H, $H^{4A+B+D+E}$), 7.98 (t, *J* 7.5 Hz, 1 H, $H^{4C}$), 7.85 (d, *J* 5.3 Hz, 1 H, $H^{6A}$), 7.72 (d, *J* 5.4 Hz, 1 H, $H^{6B}$), 7.63 (d, *J* 5.3 Hz, 1 H, $H^{6C}$), 7.53-7.41 (m, 5 H, $H^{5A+C+F+6D+E}$), 7.41-7.33 (m, 3 H, $H^{5A-C}$), 2.44 (m, 1 H, $H^{\alpha a}$), 1.85 (m, 1 H, $H^{\alpha b}$), 1.33 (m, 1 H, $H^{\beta a}$), 1.06 (m, 1 H, $H^{\beta b}$), 0.80 (m, 1 H, $H^{\gamma a}$), 0.65 (m, 4 H, $H^{\gamma b+\delta}$); $^{13}$C NMR (HMQC/HMBC, 500 MHz, $CD_2Cl_2$) $\delta$ (ppm) 169.25 ($C^{6F}$), 158.73 ($C^{2B}$), 158.66 ($C^{2E}$), 157.47 ($C^{2A+C}$), 157.34 ($C^{2F}$), 157.14 ($C^{2D}$), 152.75 ($C^{6A}$), 151.54 ($C^{6C}$), 151.48 ($C^{6B}$), 151.46 ($C^{6E}$), 151.18 ($C^{6D}$), 138.82 ($C^{4A}$), 138.77 ($C^{4F}$), 138.73 ($C^{4E}$), 138.60 ($C^{4B}$), 138.35 ($C^{4D}$), 138.21 ($C^{4C}$), 128.82 ($C^{5B}$), 128.41 ($C^{5A+C}$), 128.07 ($C^{5E+D}$), 126.80 ($C^{5F}$), 125.04 ($C^{3E}$), 124.94 ($C^{3A+C}$), 124.69 ($C^{3B+D}$), 122.52 ($C^{3F}$), 38.99 ($C^{\alpha}$), 31.26 ($C^{\beta}$), 22.46 ($C^{\gamma}$), 13.78 ($C^{\delta}$); ESI-MS *m/z*: 771.2 $[M\text{-}PF_6]^+$ (100 %, calc. 771.1), 313.2 $[M\text{-}2PF_6]^+$ (35 %, calc. 313.2); IR (solid, $\nu$/cm$^{-1}$) 3130 (w), 2949 (w), 2875 (w), 2356 (s), 2340 (m), 2331 (m), 2319 (m), 1945 (w), 1922 (w), 1848 (w), 1829 (w), 1772 (w), 1734 (w), 1717 (w), 1700 (m), 1684 (m), 1653 (w), 1603 (w), 1558 (m), 1539 (m), 1521 (w), 1507 (m), 1465 (m), 1456 (m), 1447 (m), 1429 (m), 1420 (m), 1314 (w), 1274 (w), 1245 (w), 1164 (w), 1131 (w), 1065 (w), 1028 (w), 901 (w), 878 (m), 830 (s), 771 (m), 763 (m), 755 (m), 750 (m), 741 (m), 729 (m), 683 (m), 668 (s), 648 (m); UV/vis ($CH_2Cl_2$, 5.0 x 10$^{-5}$ mol dm$^{-3}$) $\lambda_{max}$/nm 246 ($\varepsilon$/dm$^3$ mol$^{-1}$ cm$^{-1}$ 23100), 251 (21900), 289 (58100), 344 (6700), 425 (11000), 450 (13200); emission $\lambda_{max}$ ($\lambda_{ex}$) = 630 (450) nm.

### 6.2.7 $[Ru(bpy)_2(22)][PF_6]_2$

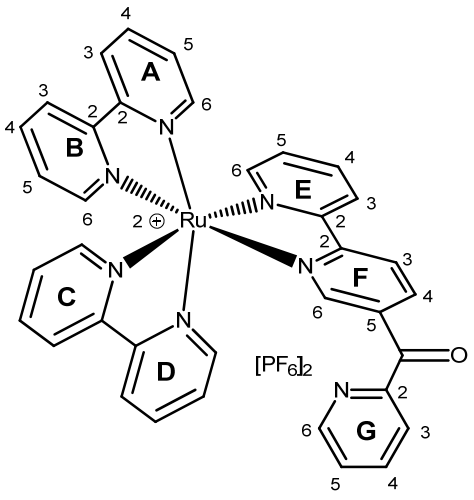


In a 10 ml microwave vial ligand **22** (177.1 mg, 0.68 mmol, 1.0 eq) and $[Ru(bpy)_2Cl_2]$ (328.3 mg, 0.68 mmol, 1.0 eq) were suspended in MeOH (6 ml). This mixture was irradiated for 2 h at 120 °C in a microwave reactor. The dark red solution was reduced in volume, the product was precipitated upon addition of an aqueous $NH_4PF_6$ solution (~20 ml, ~0.1 M) and stirred for a further 30 m The red solid was filtered off, washed with $H_2O$ and $Et_2O$, then dried in a desiccator. The desired product was obtained as a dark red powder (572.0 mg,

0.59 mmol, 87 %) and required no further purification. $^{1}$H NMR (500 MHz, $CD_2Cl_2$) $\delta$ (ppm) 8.78 (d, *J* 1.2 Hz, 1 H, $H^{6F}$), 8.75 (dd, *J* 8.4, 1.6 Hz, 1 H, $H^{4F}$), 8.58 (d, *J* 8.5 Hz, 1 H, $H^{3F}$), 8.56 (d, *J* 8.1 Hz, 1 H, $H^{3E}$), 8.51-8.44 (m, 4 H, $H^{3A-D}$), 8.38 (d, *J* 4.2 Hz, 1 H, $H^{6G}$), 8.14-8.01 (m, 6 H, $H^{3G+4A-E}$), 7.90 (td, *J* 7.8, 1.5 Hz, 1 H, $H^{4G}$), 7.80-7.71 (m, 5 H, $H^{6A-E}$), 7.57-7.41 (m, 6 H, $H^{5A-E+G}$); $^{13}$C NMR (126 MHz, $CD_2Cl_2$) $\delta$ (ppm) 188.10 ($C^{C=O}$), 159.51 ($C^{2F}$), 157.42+157.29+157.21+156.49 ($C^{2A-E}$), 154.68 ($C^{6F}$), 153.08 ($C^{2G}$), 152.16+152.00+151.86 ($C^{6A-D}$), 151.75 ($C^{6E}$), 148.98 ($C^{6G}$), 140.28 ($C^{4F}$), 138.94+138.88+138.82+138.67 ($C^{4A-E}$), 138.32 ($C^{4G}$), 135.38 ($C^{5F}$), 129.44+128.87+128.72+128.50 ($C^{5A-E}$), 128.38 ($C^{5G}$), 126.01 ($C^{3E}$), 125.41 ($C^{3A-D}$), 124.95 ($C^{3G}$), 124.90+124.74 ($C^{3A-D}$), 124.32 ($C^{3F}$); ESI-MS *m/z*: 820.2 $[M\text{-}PF_6]^+$ (100 %, calc. 820.1), 337.6 $[M\text{-}2PF_6]^{2+}$ (75 %, calc 337.6); IR (solid/ $cm^{-1}$) 3122 (w), 3082 (w), 2374 (w), 2345 (w), 1683 (w), 1660 (m), 1652 (m), 1602 (w), 1558 (m), 1500 (w), 1463 (m), 1446 (m), 1434 (m), 1423 (w), 1380 (w), 1308 (m), 1280 (m), 1270 (w), 1246 (m), 1150 (w), 990 (w), 947 (m), 833 (s), 762 (s), 743 (s), 729 (s), 708 (s), 679 (m), 662 (m), 648 (m), 610 (m); UV/vis ($CH_2Cl_2$, 5.0 x $10^{-5}$mol $dm^{-3}$) $\lambda_{max}$/nm 238 ($\varepsilon$/$dm^3$ $mol^{-1}$ $cm^{-1}$ 21100), 247 (21600), 286 (69400), 352 (6800), 441 (9700); emission $\lambda_{max}$ ($\lambda_{ex}$) = 675 (447) nm; EA: calc. for $C_{36}H_{27}N_7OF_{12}P_2Ru*H_2O$, C 44.00 %, H 2.97 %, N 9.98 %, found C 43.92 %, H 2.95 %, N 9.92 %.

### 6.2.8 $[Ru(bpy)_2(34)][PF_6]_2$

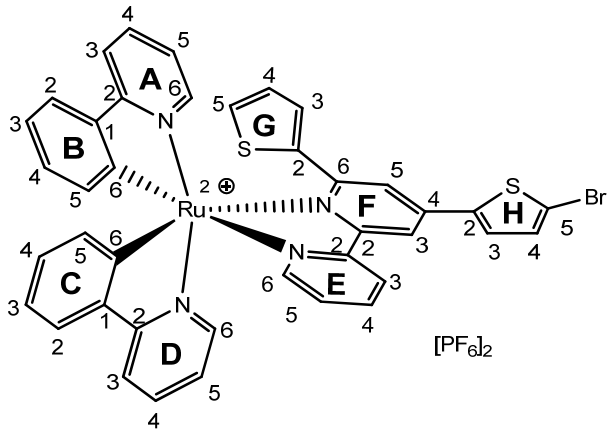


In a 5 ml microwave vial, ligand **34** (20.0 mg, 50.0 μmol, 1.0 eq) and $[Ru(bpy)_2Cl_2]$ (24.3 mg, 50.0 μmol, 1.0 eq) were suspended in MeOH (5 ml). This mixture was irradiated for 1 h at 120 °C in a microwave reactor. TLC control show still free ligand and the mixture was irradiated a second time for 1 h at 120 °C. Then the reaction was stopped due to decomposition (TLC control). The dark red solution was reduced in volume, the product was precipitated upon addition of an aqueous $NH_4PF_6$ solution (~20 ml, ~0.1 M) and stirred for a further 45 m The red solid was filtered off, washed with $H_2O$ and $Et_2O$, then dried in a desiccator. The desired product was obtained as a dark red powder (31.0 mg, 28.1 μmol, 56 %) and required no further purification. $^{1}$H-NMR (500 MHz, $CD_2Cl_2$) $\delta$ (ppm) 8.66 (d, *J* 8.2 Hz, 1 H, $H^{3E}$), 8.57 (s, 1 H, $H^{3F}$), 8.44 (d, *J* 8.1 Hz, 1 H, $H^{3A}$), 8.37 (d, *J* 8.2 Hz, 1 H, $H^{3D}$),

8.34 (d, *J* 8.1 Hz, 1 H, $H^{3B}$), 8.25 (d, *J* 5.3 Hz, 1 H, $H^{6A}$), 8.15-8.07 (m, 3 H, $H^{4A+D+E}$), 8.05 (d, *J* 8.1 Hz, 1 H, $H^{3C}$), 7.95 (t, *J* 7.8 Hz, 1 H, $H^{4B}$), 7.72-7.62 (m, 3 H, $H^{6D+4C+H}$), 7.58 (t, *J* 6.9 Hz, 1 H, $H^{5A}$), 7.51 (d, *J* 5.5 Hz, 1 H, $H^{6E}$), 7.50-7.44 (m, 2 H, $H^{5F+D}$), 7.39 (t, *J* 6.9 Hz, 1 H, $H^{5E}$), 7.34 (d, *J* 5.4 Hz, 1 H, $H^{6B}$), 7.28 (t, *J* 6.9 Hz, 1 H, $H^{5B}$), 7.23 (d, *J* 4.0 Hz, 1 H, $H^{3H}$), 7.05 (d, *J* 5.2 Hz, 1 H, $H^{6C}$), 7.03 (d, *J* 3.9 Hz, 1 H, $H^{5G}$), 6.93 (t, *J* 6.5 Hz, 1 H, $H^{5C}$), 6.45 (s, 1 H, $H^{4G}$), 6.33 (br s, 1 H, $H^{3G}$); $^{13}$C NMR (126 MHz, $CD_2Cl_2$) $\delta$ (ppm) 160.42 ($C^{2G}$), 158.64 ($C^{2E}$), 158.11 ($C^{2A}$), 158.03 ($C^{2F}$), 157.34 ($C^{2B+D}$), 156.41 ($C^{2C}$), 153.45 ($C^{6A+E}$), 151.98 ($C^{6F}$), 151.78 ($C^{6C}$), 151.45 ($C^{6D}$), 151.21 ($C^{6B}$), 142.65 ($C^{2H}$), 139.60 ($C^{4F}$), 138.94 ($C^{4G}$), 138.92 ($C^{4E}$), 138.87 ($C^{4A}$), 138.84 ($C^{4B}$), 138.81 ($C^{4D}$), 136.79 ($C^{4C}$), 133.14 ($C^{3H}$), 130.07 ($C^{4H}$), 129.49 ($C^{3G}$), 128.73 ($C^{5B}$), 128.43 ($C^{5D}$), 128.36 ($C^{5A}$), 128.16 ($C^{5E}$), 127.39 ($C^{00}$), 126.60 ($C^{5F}$), 125.99 ($C^{3E}$), 125.02 ($C^{3B}$), 124.87 ($C^{3D}$), 124.52 ($C^{3C}$), 123.38 ($C^{3C}$), 119.48 ($C^{3F}$), 118.62 ($C^{5H}$); ESI-MS *m/z*: 899.4/901.4 $[M\text{-}PF_6]^+$ (100/80 %, calc. 899.0/901.0); IR (solid, $\nu$/cm$^{-1}$) 3115 (w), 2366 (w), 2330 (w), 1962 (w), 1726 (w), 1606 (m), 1583 (m), 1552 (w), 1466 (m), 1445 (m), 1429 (m), 1414 (m), 1312 (w), 1269 (w), 1235 (m), 1213 (w), 1163 (w), 1090 (w), 1065 (w), 1043 (w), 1007 (w), 966 (w), 878 (m), 832 (s), 801 (s), 784 (s), 761 (s), 749 (s), 741 (s), 729 (s), 716 (s), 710 (s), 690 (s), 685 (m), 671 (s), 661 (m), 639 (m), 624 (m); UV/vis ($CH_2Cl_2$, 7.6 x 10$^{-6}$ mol dm$^{-3}$) $\lambda_{max}$/nm 236 ($\varepsilon$/dm$^3$ mol$^{-1}$ cm$^{-1}$ 28100), 254 (32000), 259 (30600), 293 (66000), 352 (30000), 458 (17200).

### 6.2.9 $[Ru(bpy)_2(13)][PF_6]_2$

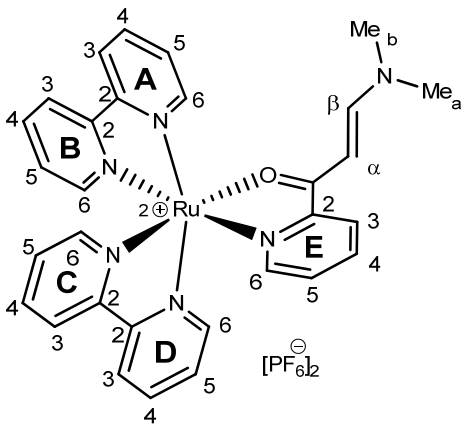


In a 5 ml microwave vial, **13** (8.8 mg, 50.0 μmol, 1.0 eq) and $[Ru(bpy)_2Cl_2]$ (24.2 mg, 50.0 μmol, 1.0 eq) were suspended in MeOH (5 ml). This mixture was irradiated for 1 h at 120 °C in a microwave reactor. The dark red solution was reduced in volume, the product was precipitated upon addition of a solution of aqueous $NH_4PF_6$ solution (~5 ml, ~0.2 M) and stirred for a further 30 m The dark red solid was filtered off, washed with $H_2O$ and $Et_2O$, then dried in a desiccator. The desired product was obtained as a dark red powder (35.0 mg, 39.8 μmol, 80 %) and required no further purification. $^1$H NMR (500 MHz, $CD_2Cl_2$) $\delta$ (ppm) 8.53 (d, *J* 5.5 Hz, 1 H, $H^{6A}$), 8.45 (d, *J* 8.1 Hz, 1 H, $H^{3C}$), 8.42-8.32 (m, 3 H, $H^{3A+B+D}$), 8.30 (d, *J* 8.0 Hz, 1 H, $H^{3E}$), 8.11 (d, *J* 12.0 Hz, 1 H, $H^{\beta}$), 8.10-8.05 (m, 2 H, $H^{4C+A}$), 8.01-7.88 (m, 3 H,

$H^{4E+D+B}$), 7.81 (d, *J* 5.4 Hz, 1 H, $H^{6C}$), 7.72 (d, *J* 5.6 Hz, 1 H, $H^{6B}$), 7.71-7.65 (m, 2 H, $H^{5A+6E}$), 7.63 (d, *J* 5.4 Hz, 1 H, $H^{6D}$), 7.51 (t, *J* 7.0 Hz, 1 H, $H^{5C}$), 7.46 (t, *J* 7.0 Hz, 1 H, $H^{5E}$), 7.36-7.28 (m, 2 H, $H^{5D+B}$), 6.14 (d, *J* 11.6 Hz, 1 H, $H^{\alpha}$), 3.30 (s, 2 H, Me), 3.17 (s, 2 H, Me); $^{13}$C NMR (126 MHz, $CD_2Cl_2$) $\delta$ (ppm) 188.57 ($C^{C=O}$), 159.70 ($C^{\beta}$), 158.96 ($C^{2C}$), 158.21 ($C^{2D}$), 158.06 ($C^{2B}$), 157.49 ($C^{2A}$), 157.31 ($C^{2E}$), 153.29 ($C^{6B}$), 152.34 ($C^{6D}$), 151.81 ($C^{6A}$), 151.68 ($C^{6C}$), 151.59 ($C^{6E}$), 137.98 ($C^{4C}$), 137.94 ($C^{4A}$), 137.90 ($C^{4E}$), 137.50 ($C^{4D}$), 136.81 ($C^{4B}$), 129.95 ($C^{5E}$), 128.30 ($C^{5A}$), 128.12 ($C^{5C}$), 127.84 ($C^{5B}$), 127.31 ($C^{5D}$), 127.14 ($C^{3E}$), 124.55 ($C^{3B}$), 124.12 ($C^{3C}$), 124.08 ($C^{3A}$), 123.93 ($C^{3D}$), 93.66 ($C^{\alpha}$), 47.30 ($C^{Me}$), 39.05 ($C^{Me}$; ESI-MS *m/z*: 721.2 $[M\text{-}PF_6]^+$ (100 %, calc. 721.1), 288.1 $[M\text{-}2PF_6]^{2+}$ (75 %, calc 288.1); IR (solid, $\nu$/cm$^{-1}$) 3089 (w), 2358 (w), 2341 (w), 2331 (w), 1622 (s), 1622 (s), 1616 (s), 1607 (m), 1564 (w), 1506 (m), 1486 (s), 1464 (m), 1447 (m), 1409 (s), 1403 (s), 1393 (m), 1377 (m), 1363 (w), 1301 (m), 1268 (m), 1252 (s), 1245 (m), 1222 (w), 1213 (w), 1165 (w), 1142 (m), 1117 (w), 1078 (w), 1059 (w), 1022 (w), 996 (w), 910 (w), 879 (m), 825 (s), 805 (s), 799 (s), 783 (s), 759 (s), 747 (s), 737 (s), 728 (s), 697 (s), 675 (s), 662 (s), 648 (s), 639 (m); UV/vis ($CH_2Cl_2$, 5.0 x 10$^{-5}$ mol dm$^{-3}$) $\lambda_{max}$/nm 244 ($\varepsilon$/dm$^3$ mol$^{-1}$ cm$^{-1}$ 20000), 254 (18500), 291 (40000), sh 335 (16600), 350 (18900), 368 (21100), 386 (14100), 482 (11900).

### 6.2.10 $[Fe(40)_2][PF_6]_2$

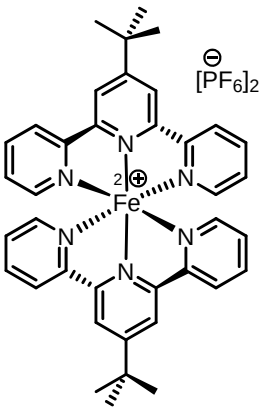


Anhydrous $FeCl_2$ (4.8 mg, 37.5 µmol) and ligand **40** (21.7 mg, 75.0 µmol) were dissolved in EtOH (5 ml), and a dark purple colour was immediately observed. The solution was stirred for 1 h at room temperature. The hexafluoridophosphate salt was precipitated by adding saturated aqueous $NH_4PF_6$. After filtration, the product was washed with EtOH and $Et_2O$, and then dried in a desiccator. $[Fe(\mathbf{40})_2][PF_6]_2$ was isolated as a purple crystalline solid (30.0 mg, 32.4 µmol, 86.5 %). $^1$H NMR (500 MHz, $CD_3CN$) $\delta$ (ppm) 8.88 (s, 4 H, $H^{B3}$), 8.54 (ddd, *J* 8.1, 1.1, 1.1 Hz, 4 H, $H^{3A}$), 7.86 (m, 4 H, $H^{4A}$), 7.05 (m, 8 H, $H^{5+6A}$), 1.77 (s, 18 H, $H^{tBu}$); $^{13}$C NMR (126 MHz, $CD_3CN$) $\delta$ (ppm) 165.3 ($C^{4B}$), 160.5 ($C^{2A}$), 159.1 ($C^{2B}$), 154.0 ($C^{6A}$), 139.5 ($C^{4A}$), 127.9 ($C^{5A}$), 124.4 ($C^{3A}$), 122.3 ($C^{3B}$), 37.4 ($C^{CMe}{}_3$), 31.0 ($C^{CMe}{}_3$). IR (solid, $\nu$/cm$^{-1}$) 3101 w, 2949 w, 2907 w, 2870 w, 1607 m, 1541 w, 1481 m, 1468 m, 1425 m, 1412 m, 1356 w, 1286 m, 1250

m, 1207 w, 1161 w, 1132 m, 1057 w, 883 m, 825 s, 789 s, 754 s, 739 m, 692 m, 654 m, 644 m; UV/vis ($CH_2Cl_2$, 1.0 × $10^{-5}$ mol $dm^{-3}$) $\lambda_{max}$/nm 217 ($\varepsilon$/$dm^3$ $mol^{-1}$ $cm^{-1}$ 37100), 238 (43900), 275 (42200), 283 (39000), 321 (46600), 368 (4700), 502sh (7200), 555 (13200). ESI-MS *m/z* 779.2 $[M\text{-}PF_6]^+$ (base peak, calc. 779.2), 317.1 $[M\text{-}2PF_6]^{2+}$, (calc. 317.1). Found C 49.18, H 4.07, N 9.03; $C_{38}H_{38}F_6FeN_6P_2$ requires C 49.37 H 4.14 N 9.09%.

### 6.2.11 [Ru(40)Cl$_3$]

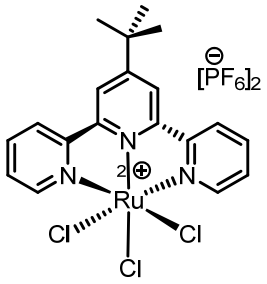


$RuCl_3$∗$3H_2O$ (52 mg, 0.20 mmol) and **40** (72.3 mg, 0.250 mmol) were suspended in EtOH (25 ml), and the mixture was stirred for 8 h under reflux. The red product was collected by filtration, washed with $H_2O$ and $Et_2O$, and dried in a desiccator. Crude [Ru(**40**)$Cl_3$] was obtained as a red powder (80.0 mg) and was used without further characterization.

### 6.2.12 [Ru(40)$_2$][PF$_6$]$_2$

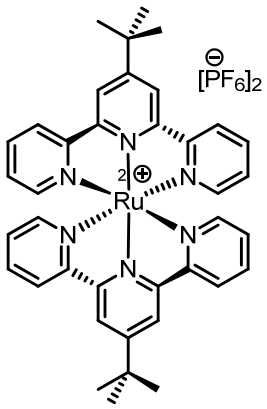


[Ru(**40**)$Cl_3$] (42.1 mg, 84.7 µmol) and ligand **40** (24.5 mg, 84.7 µmol) were combined in EtOH (10 ml) in a microwave vial, and *N*-ethylmorpholine (0.5 ml) was added. The mixture was stirred for 2 h at 120 °C (pressure = 12 bar), after which time the solvent was reduced in volume and the product was precipitated by addition of aqueous $NH_4PF_6$ (163 mg, 20 ml). The orange precipitate was collected by filtration, washed with $H_2O$ and $Et_2O$, then dried in a desiccator. [Ru(**40**)$_2$][$PF_6$]$_2$ was isolated as an orange powder (68.0 mg, 70.1 µmol, 82.8 %). $^1$H NMR (500 MHz, $CD_3CN$) $\delta$ (ppm) 8.71 (s, 4 H, $H^{B3}$), 8.58 (ddd, *J* 8.1, 1.2, 0.8 Hz, 4 H, $H^{A3}$), 7.89 (dt, *J* 7.9, 1.5 Hz, 4 H, $H^{A4}$), 7.30 (ddd, *J* 5.6, 1.4, 0.6, 4 H, $H^{A6}$), 7.13 (m, 4 H, $H^{A5}$), 1.70 (s, 18 H, $H^{tBu}$); $^{13}$C NMR (126 MHz, $CD_3CN$), $\delta$ (ppm) 161.8 ($C^{B4}$), 159.3 ($C^{A2}$), 155.8 ($C^{B2}$), 153.3 ($C^{A6}$), 138.7 ($C^{A4}$), 128.0 ($C^{A5}$), 125.2 ($C^{A3}$), 122.1 ($C^{B3}$), 37.1 ($C^{CMe3}$), 30.9 ($C^{CMe3}$); IR (solid,

$\nu$/cm$^{-1}$) 3117 w, 2947 w, 2910 w, 2874 w, 2361 w, 2334 w, 1684 w, 1647 w, 1605 m, 1558 m, 1537 w, 1506 w, 1477 m, 1464 m, 1423 m, 1404 m, 1364 m, 1348 w, 1288 m, 1250 m, 1165 w, 1132 m, 1034 w, 1022 w, 883 m, 824 s, 802 s, 789 s, 754 s, 737 m, 656 m, 642 s, 615 w; UV/vis (MeCN, $1.0 \times 10^{-5}$ mol dm$^{-3}$) $\lambda_{max}$/nm 238 ($\varepsilon$/dm$^3$ mol$^{-1}$ cm$^{-1}$ 45800), 273 (47500), 309 (64600), 320sh (30500), 439sh (10600), 481 (17700); ESI-MS *m/z*, 825.2 [M-PF$_6$]$^+$ (base peak, calc. 825.2), 340.1 [M-2PF$_6$]$^{2+}$, (calc. 340.1). Found C 46.97 H 3.99 N 8.59; $C_{38}H_{38}F_6N_6P_2Ru$ requires C 47.06, H 3.95 N 8.67%.

### 6.2.13 [Ru(tpy)(40)][PF$_6$]$_2$

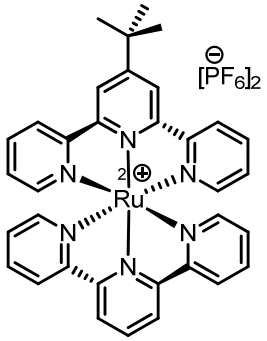


[Ru(tpy)Cl$_3$] was prepared in an analogous manner to [Ru(**40**)Cl$_3$] starting from RuCl$_3$*3H$_2$O (393 mg, 1.5 mmol) and tpy (501 mg, 1.5 mmol). The crude solid was used in the second step. [Ru(tpy)Cl$_3$] (11 mg, 25 µmol) and **40** (7.1 mg, 25 µmol) were combined in EtOH (5 ml) in a microwave vial, and *N*-ethylmorpholine (0.2 ml) was added. Reaction conditions and workup were as for [Ru(**40**)$_2$][PF$_6$]$_2$. [Ru(tpy)(**40**)][PF$_6$]$_2$ was isolated as an orange powder (17 mg, 19 µmol, 76 %). $^1$H NMR (500 MHz, CD$_3$CN) $\delta$ (ppm) 8.73 (overlapping d, 2 H, H$^{D3}$), 8.72 (s, 2 H, H$^{B3}$), 8.58 (d, *J* 8.2 Hz, 2 H, H$^{A3}$), 8.48 (d, *J* 8.0 Hz, 2 H, H$^{C3}$), 8.38 (t, *J* 8.1 Hz, 1 H, H$^{D4}$), 7.91 and 7.89 (overlapping m, 4 H, H$^{C4/A4}$), 7.34 (d, *J* 5.2 Hz, 2 H, H$^{C6}$), 7.29 (d, *J* 5.1 Hz, 2 H, H$^{A6}$), 7.17 (m, 2 H, H$^{C5}$), 7.12 (m, 2 H, H$^{A5}$), 1.70 (s, 9 H, H$^{tBu}$); $^{13}$C NMR (126 MHz, CD$_3$CN) $\delta$ (ppm) 162.2 (C$^{B4}$), 159.2 (C$^{A2}$), 158.8 (C$^{C2}$), 156.5 (C$^{D2}$), 155.6 (C$^{B2}$), 153.5 (C$^{A6}$), 153.3 (C$^{C6}$), 139.0 (C$^{A4+C4}$), 136.5 (C$^{D4}$), 128.4 (C$^{C5}$), 128.2 (C$^{A5}$), 125.2 (C$^{C3}$) 125.2 (C$^{A3}$), 124.6 (C$^{D3}$) 122.2 (C$^{B3}$), 37.2 (C$^{CMe3}$), 31.0 (C$^{CMe3}$). IR (solid, $\nu$/cm$^{-1}$) 3647 m, 3132 w, 2961 w, 2912 w, 2883 w, 2363 m, 2326 w, 1734 w, 1684 m, 1653 m, 1605 m, 1558 s, 1506 m, 1481 m, 1448 m, 1425 m, 1389 m, 1367 m, 1288 m, 1248 m, 1163 w, 1134 m, 1055 w, 1034 w, 895 m, 878 m, 837 s, 827 s, 789 m, 754 m, 735 m, 642 m; UV/vis ($CH_2Cl_2$, $1.0 \times 10^{-5}$ mol dm$^{-3}$) $\lambda_{max}$/nm 237 ($\varepsilon$/dm$^3$ mol$^{-1}$ cm$^{-1}$ 26000), 265sh (24500), 273 (29500), 309 (45700), 430sh (6700), 480 (11600); ESI-MS *m/z* 769.1 [M-PF$_6$]$^+$ (base peak, calc. 769.1), 312.1 [M-2PF$_6$]$^{2+}$ (calc. 312.1). Found C 44.66, H 3.71, N 8.51; $C_{34}H_{30}F_{12}N_6P_2Ru$ requires C 44.70, H 3.31, N 9.20 %.

## 6.2.14 Crystal structure determinations

### 6.2.14.1 $[Ru(bpy)_2(4)][PF_6]_2$

$C_{34}H_{26}F_{12}N_6P_2SeRu$, $M$ = 988.58, red plate, monoclinic, space group $P2_1$, $a$ = 10.821(2), $b$ = 13.342(3), $c$ = 13.616(3) Å, $\beta$ = 112.77(3)°, $U$ = 1812.6(8) Å$^3$, $Z$ = 2, $D_c$ = 1.811 Mg m$^{-3}$, $\mu$(Mo-K$_\alpha$) = 1.623 mm$^{-1}$, $T$ = 173(2) K. Total 26580 reflections, 8149 unique, $R_{int}$ = 0.0648. Refinement of 8149 reflections (560 parameters) with $I > 2\sigma(I)$ converged at final $R1$ = 0.0389 ($R1$ all data = 0.0449), $wR2$ = 0.0828 ($wR2$ all data = 0.0854), gof = 1.070.

### 6.2.14.2 $[Ru(bpy)_2(13)][PF_6]_2$

$C_{31}H_{30}F_{12}N_6OP_2Cl_2Ru$, $M$ = 964.52, red block, monoclinic, space group $P2_1$, $a$ = 11.153(2), $b$ = 20.682(3), $c$ = 16.638(4) Å, $U$ = 3676.7(12) Å$^3$, $Z$ = 4, $D_c$ = 1.742 Mg m$^{-3}$, $\mu$(Mo-K$_\alpha$) = 0.757 mm$^{-1}$, $T$ = 173(2) K. Total 127022 reflections, 8198 unique, $R_{int}$ = 0.0571. Refinement of 8198 reflections (498 parameters) with $I > 2\sigma(I)$ converged at final $R1$ = 0.0367 ($R1$ all data = 0.0377), $wR2$ = 0.0908 ($wR2$ all data = 0.0916), gof = 1.124.

### 6.2.14.3 $[Ru(bpy)_2(22)][PF_6]_2$

$C_{36}H_{27}F_{12}N_7OP_2Ru$, $M$ = 964.66, red block, triclinic, space group $P\text{-}1$, $a$ = 13.044(2), $b$ = 13.552(3), $c$ = 13.756(3) Å, $\alpha$ = 90.976(13), $\beta$ = 114.566(13), $\gamma$ = 118.425(12)°, $U$ = 1873.5(6) Å$^3$, $Z$ = 2, $D_c$ = 1.710 Mg m$^{-3}$, $\mu$(Mo-K$_\alpha$) = 0.606 mm$^{-1}$, $T$ = 173(2) K. Total 35793 reflections, 10931 unique, $R_{int}$ = 0.0513. Refinement of 10931 reflections (705 parameters) with $I > 2\sigma(I)$ converged at final $R1$ = 0.0381 ($R1$ all data = 0.0468), $wR2$ = 0.0888 ($wR2$ all data = 0.0927), gof = 1.060.

### 6.2.14.4 $[Fe(40)_2][PF_6]_2$

$C_{38}H_{38}F_{12}N_6P_2Fe$, $M$ = 924.53, purple needle, orthorhombic, space group $Pnna$, $a$ = 12.422(3), $b$ = 17.804(4), $c$ = 17.978(4) Å, $U$ = 3975.9(14) Å$^3$, $Z$ = 4, $D_c$ = 1.544 Mg m$^{-3}$, $\mu$(Mo-K$_\alpha$) = 0.554 mm$^{-1}$, $T$ = 123 K. Total 25223 reflections, 4561 unique, $R_{int}$ = 0.190. Refinement of 2414 reflections (294 parameters) with $I > 2\sigma(I)$ converged at final $R1$ = 0.1051 ($R1$ all data = 0.2228), $wR2$ = 0.0653 ($wR2$ all data = 0.1121), gof = 1.0746.

### 6.2.14.5 $[Ru(40)_2][PF_6]_2$

$C_{38}H_{38}F_{12}N_6P_2Ru$, $M$ = 969.75, red block, orthorhombic, space group $Pbcn$, $a$ = 18.0899(16), $b$ = 12.209(2), $c$ = 18.3131(19) Å, $U$ = 4044.8(9) Å$^3$, $Z$ = 4, $D_c$ = 1.592 Mg m$^{-3}$, $\mu$(Mo-K$_\alpha$) = 0.559 mm$^{-1}$, $T$ = 173 K. Total 57976 reflections, 4639 unique, $R_{int}$ = 0.1849. Refinement of 4181 reflections (366 parameters) with $I > 2\sigma(I)$ converged at final $R1$ = 0.0695 ($R1$ all data = 0.0753), $wR2$ = 0.1674 ($wR2$ all data = 0.1710), gof = 1.216.

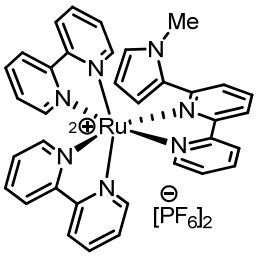


[Ru(bpy)$_2$(**1**)][PF$_6$]$_2$

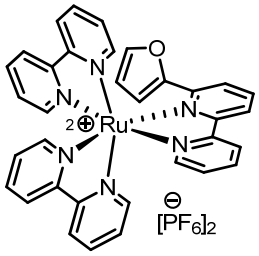


[Ru(bpy)$_2$(**2**)][PF$_6$]$_2$

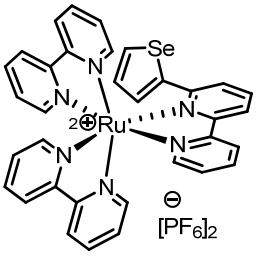


[Ru(bpy)$_2$(**4**)][PF$_6$]$_2$

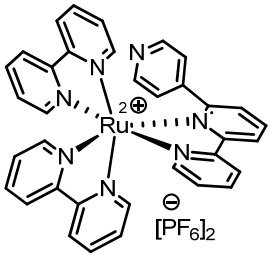


[Ru(bpy)$_2$(**20**)][PF$_6$]$_2$

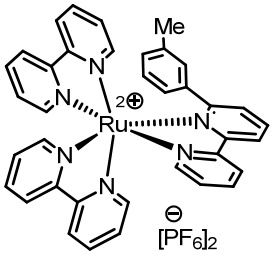


[Ru(bpy)$_2$(**21**)][PF$_6$]$_2$

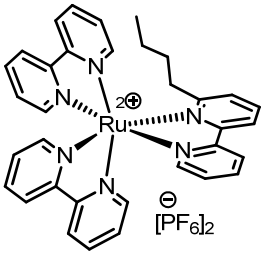


[Ru(bpy)$_2$(**10**)][PF$_6$]$_2$

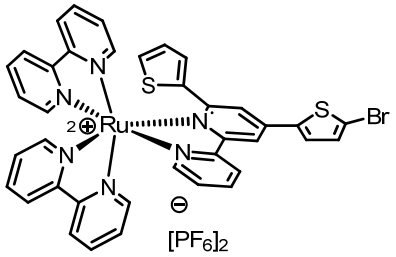


[Ru(bpy)$_2$(**34**)][PF$_6$]$_2$

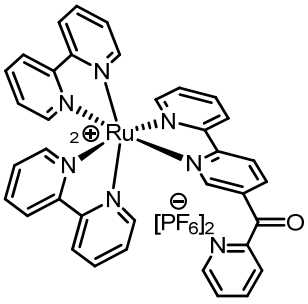


[Ru(bpy)$_2$(**22**)][PF$_6$]$_2$

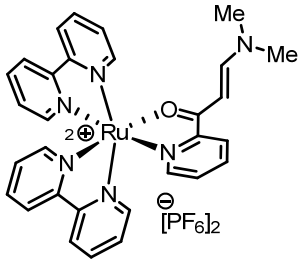


[Ru(bpy)$_2$(**13**)][PF$_6$]$_2$

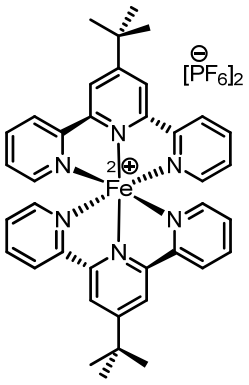


[Fe(**40**)$_2$][PF$_6$]$_2$

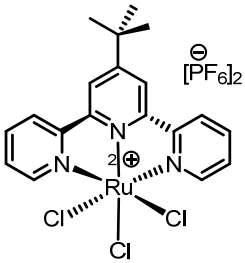


[Ru(**40**)Cl$_3$]

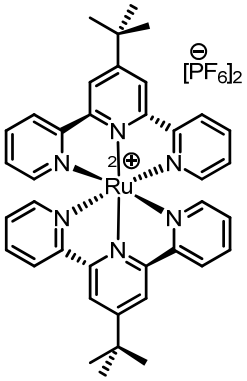


[Ru(**40**)$_2$][PF$_6$]$_2$

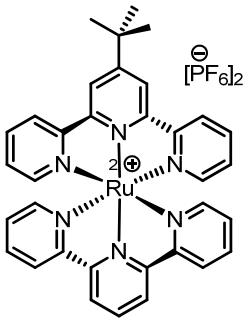


[Ru(tpy)(**40**)][PF$_6$]$_2$

**Figure 6-18** Overview of ruthenium(II) complexes

# Chapter 7

# 7 Conclusions and Outlook

In the PhD thesis presented here, a series of new ligands with bpy and tpy scaffolds were successfully synthesized (Figure 7-1). The new bpy ligands are either decorated only in the 6'-position, or in both 6'- and 4'-positions, and the substituents vary from heteroaromatic ring to aromatic rings with different substitution patterns. Surprisingly, the two tpy ligands which possess a *tert*-butyl group in 4'-position were not, to the best of our knowledge, reported before. The access to these compounds was achieved either by direct lithiation, KRÖHNKE, or JAHNG methods. All ligands were characterized by NMR and mass spectroscopy; in addition X-ray analyses were possible for most of the crystalline compounds.

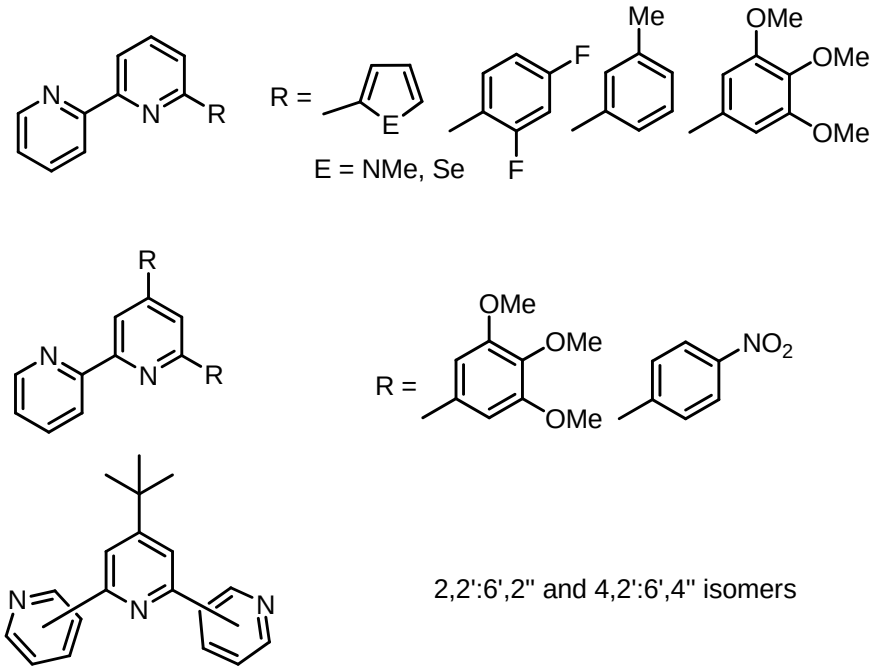


**Figure 7-1** New bpy and tpy ligands.

These new ligands were then used to obtain over 40 equally new metal complexes, predominantly with three metals: copper(I), iridium(III) and ruthenium(II) (Scheme 7-1). The aim of this project was first to characterize the newly synthesized complexes, this was achieved again by NMR and mass spectroscopy, and if possible by X-ray analyses for the crystalline compounds. The copper(I) complexes exhibit interesting dynamic behaviour in solution which causes broadening of the $^{1}$H NMR spectra. The possible mechanism could be established by various low temperature NMR experiments including 2-D spectra such as COSY and EXSY. Furthermore, the need for new ligands evolved which could help to understand the solution behaviour. These were later also used for the preparation of new iridium(III) and ruthenium(II) complexes.

The second focus was on the potential applications of these new compounds: The homoleptic copper(I) complexes were used as precursor for the preparation of heteroleptic

complexes through a ligand exchange reaction directly on the $TiO_2$-surface as sensitizer for photovoltaic devices (DSCs). The iridium(III) complexes have a potential application in LECs, thus, UV/vis absorption and emission were studied for all these complexes in dependence of the substituents on the bpy ligands.

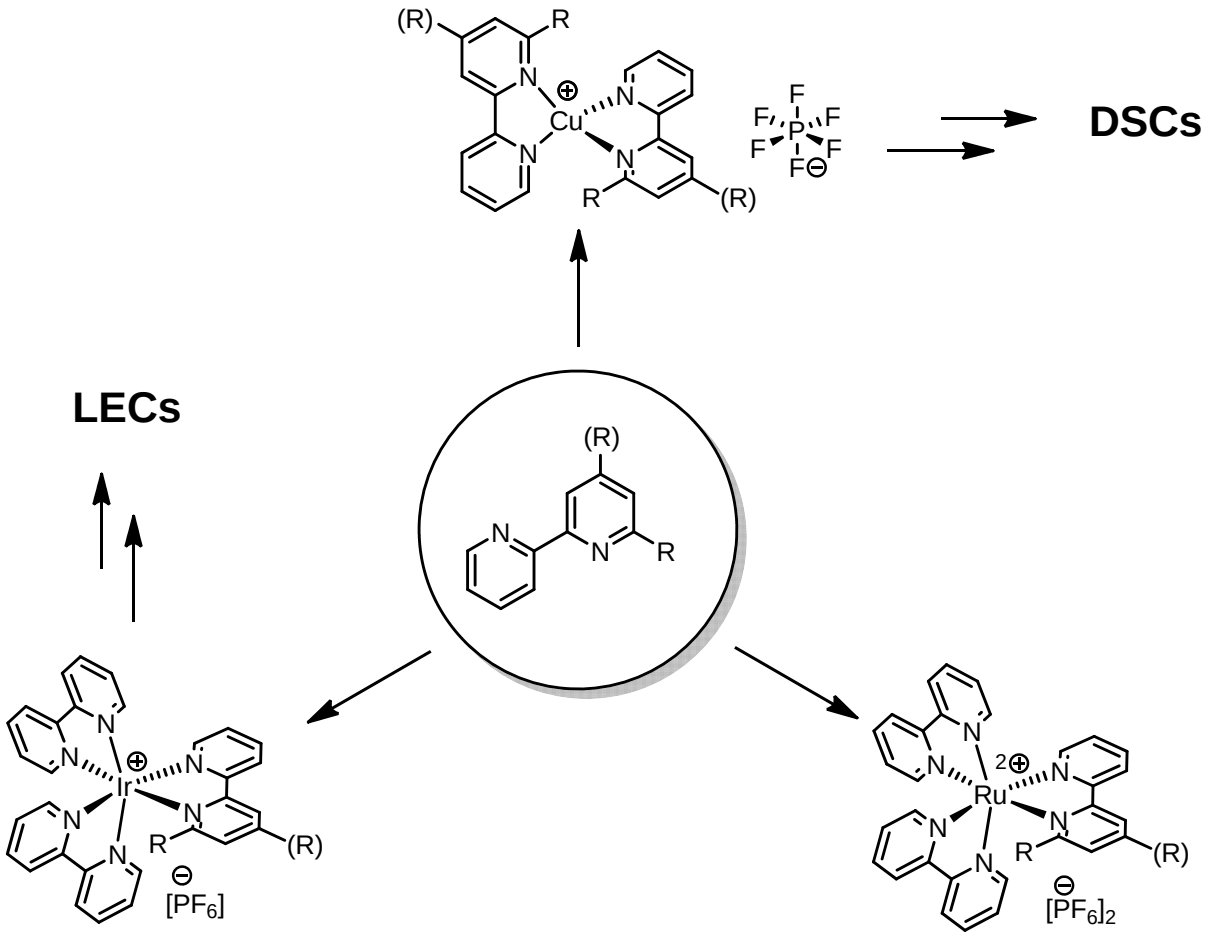


**Scheme 7-1** Preparation of metalorganic complexes and their applications.

In our laboratory 24 different photovoltaic devices were prepared, sensitized with heteroleptic copper(I) complexes. For all of them photocurrents were observed which indicates that only one substituent on the bpy ligand is sufficient to make the resulting complexes stable enough against oxidation of the metal centre. The comparison of the power conversion efficiencies makes clear, that the substituent in the 6' position of a bpy ligand does not have a great influence. Rather more important is the choice of the anchoring ligand. Presently there are more devices under investigation with 4,'6'-substituted bpy derivatives.

In collaboration with a H. BOLINK in Valencia, Spain, three new iridium(III) complexes with hetero aromatic ligands on the bpy ligand were used for the preparation of LECs devices. The results were somewhat disappointing. The incorporation of the hetero atoms in the aryl substituent did not improved the life time of the devices nor hava a great influence on the

emission properties with respect to the reference compound $[Ir(ppy)_2(pbpy)][PF_6]$ (pbpy being 6'-phenyl-2,2'-bipyridine).

In summary, the observed results suggest that the variation of the substituents in 6'-position of the bpy ligands does not influence the photochemical properties of the corresponding metal complexes very much. Further decoration of an aromatic ring, even with substituents with strong electron donating/withdrawing effects did not show a great influence. The biggest effect of substituents could be observed for the electrochemical behaviour of the copper(I) complexes. Further investigation of such ligands for the above mentioned applications is probably not necessary. Nevertheless, the here observed results allowed for the insight into the solid state structures as well as solution behaviour of some complexes.

In near future the few missing experiments, such as electro chemistry and quantum yield determination for the new metal complexes will be conducted.

As far as the DSCs devices are concerned the focous on substituents in 4-positions of the bpy ligands might be reasonable, possibly the use of large chromophores substituents which would create a polarization within the dye molecules. The incorporation of long aliphatic substituents in either 6- or 5-positions of the bpy ligands could prevent the electrolyte ions/molecules to come near enough to the semiconductor and the resulting recombination. These are only two of many ideas which are now pursued in our group.

# *List of references*


[1] Bruker Analytical X-ray Systems, Inc., 2006, APEX2, version 2 User Manual, M86-E01078, Madison, WI.
[2] A. Altomare, G. Cascarano, G. Giacovazzo, A. Guagliardi, M. C. Burla, G. Polidori and M. Camalli, *J. Appl. Cryst.*, 1994, **27**, 435.
[3] P. W. Betteridge, J. R. Carruthers, R. I. Cooper, K. Prout and D. J. Watkin, *J. Appl. Cryst*., 2003, **36**, 1487.
[4] Stoe & Cie, IPDS software v 1.26, Stoe & Cie, Darmstadt, Germany, 1996.
[5] G. M. Sheldrick, Acta Crystallogr., Sect. A, 2008, 64, 112.
[6] L. J. Farrugia, J. Appl. Cryst., 1997, 30, 565.
[7] I. J. Bruno, J. C. Cole, P. R. Edgington, M. K. Kessler, C. F. Macrae, P. McCabe, J. Pearson and R. Taylor, Acta Crystallogr., Sect. B, 2002, 58, 389.
[8] C. F. Macrae, I. J. Bruno, J. A. Chisholm, P. R. Edgington, P. McCabe, E. Pidcock, L. Rodriguez-Monge, R. Taylor, J. van de Streek and P. A. Wood, J. Appl. Cryst., 2008, 41, 466.
[9] F. Blau, *Monatsh. Chem*. **1889**, *1*, 375.
[10] M. Hapke, L. Brandt, A. Lützen, *Chem. Soc. Rev*. **2008**, *37*, 2782.
[11] L.-X. Zhao, J. Sherchan, J. Ki Park, Y. Jahng, B.-S. Jeong, T. Ch. Jeong, Ch.-S. Lee, E.-S. Lee, *Arch. Pharm. Res*. **2006**, *29(12)*, 1091.
[12] D. M. Balitz, J. A. Bush, W. T. Bradner, T. W. Doyle, F. A. O'Herron, D. E. Nettleton, *J. Antibiot.* **1982**, *35*, 259; J.-F- Riou, P. Helissey, L. Grondard, S. Giorgi-Renault, *Mol. Pharmacol.* **1991**, *40*, 699; N. Abe, Y. Nakakita, T. Nakamura, N. Enoki, H. Uchida, T. Takeo, M. Munekata, *J. Antibiot.* **1993**, *46*, 1672.
[13] L. A. Summers, *Adv. Heterocycl. Chem*. **1984**, *35*, 281.
[14] P. J. Steel, *Adv. Heterocycl. Chem*. **1996**, *67*, 1.
[15] E. C. Constable, *Adv. Inorg. Chem*. **1989**, *34*. 1.
[16] A. P. Smith and C. L. Fraser, in Comprehensive Coordination Chemistry II, eds. J. A. McCleverty and T. J. Meyer, Elsevier, Oxford, **2004**, vol. 1, p. 1.
[17] R. O. Steen, L. J. Nurkkala, S. J. Angus-Dunne, C. X. Schmitt, E. C. Constable, M. J. Riley, P. V. Bernhardt, S. J. Dunne, *Eur. J. Inorg. Chem*., **2008**, 1784; L. J. Nurkkala, R. O. Steen, H. K. J. Friberg, J. A. Häggström, P. V. Bernhardt, M. J. Riley and S. J. Dunne, *Eur. J. Inorg. Chem*., **2008**, 4101; I. H. Jenkins, N. G. Rees and P. G. Pickup, *Chem. Mater*., **1997**, *9*, 1213.
[18] e.g., E. C. Constable, S. J. Dunne, D. G. F. Rees, Ch. X. Schmitt, *Chem. Comm*. **1996**, 1169.
[19] E. C. Constable, R. P. G. Henney, P. R. Raithby, L. R. Sousa, *Ang. Chem., Int. Ed*. **1991**, *30(10)*, 1363.
[20] F. Kröhnke, *Synthesis* **1976**, 1.
[21] A. Hantzsch, *Chemische Berichte* **1881**, *14*, 1637; and following reports.
[22] A. Tschitschibabin, *J. Prakt. Chem.* **1924**, *107*, 122; and following reports.
[23] M. Weiss, *J. Am. Chem. Soc*. **1952**, *74(1)*, 200.
[24] e. g., E. C. Constable, C. E. Housecroft, M. Neuburger, I. Poleschak, M. Zehnder, *Polyhedron* **2003**, *22*, 93.
[25] C. O. Dietrich-Buchecker, P. A. Marnot, J. P. Sauvage, *Tetrahedron Lett*. **1982**, *23(50)*, 5291.
[26] B. O'Regan, M. Grätzel, *Nature* **1991**, *353*, 737.
[27] A. Juris, V. Balzani, F. Barigelletti, S. Campagna, P. Belser, A. von Zelewsky, *Coord. Chem. Rev*. **1988**, *84*, 85; S. Campagna, F. Puntoriero, F. Nastasi, G. Bergamini, V. Balzani, *Top. Curr. Chem*. **2007**, *280*, 117.
[28] A. Hagfeldt, G. Boschloo, L. Sun, L. Kloo, H. Pettersson, *Chem. Rev*. **2010**, *110*, 6595.
[29] R. F. Service, *Science* **2005**, *309*, 548; J. Potocnik, *Science* **2007**, *315*, 810.
[30] Q. Schiermeier, J. Tollefson, T. Scully, A. Witze, O. Morton, *Nature* **2008**, *454*, 816.
[31] M. A. Green, K. Emery, D. L. King, Y. Hishikawa, W. Warta, *Progr. Photovolt.: Res. and Appl*. **2006**, *14*, 455.
[32] M. A. Green, *Adv. Mater*. **2001**, *13*, 12.
[33] J. Czochralski, *Zeitschr. phys. Chem.* **1918**, *92*, 219.
[34] H. Gerischer, H. Tributsch, *Ber. Bunsen-Ges. Phys. Chem*. **1968**, *72*, 437; H. Gerischer, M. E. Michel-Beyerle, F. Rebentrost, H. Tributsch, *Electrochim. Acta* **1968**, *13*, 1509.
[35] A. Yella, H-W. Lee, H. N. Tsao, Ch. Yi. A. K. Chandiran, Md. K Nazeeruddin, E. W.-G. Diau, Ch.-Y. Yeh, Sh. M. Zakeerudin, M. Grätzel, *Science* **2011**, *334*, 629.
[36] http://www.finanzen.ch/rohstoffe/kupferpreis?rd=fn; http://minerals.er.usgs.gov/minerals/pubs/commodity/copper/mcs-2012-coppe.pdf
[37] N. Amaroli, G. Accorsi, F. Cardinali, A. Listorti, *Top. Curr. Chem*. **2007**, *280*, 69.
[38] S. Goldstein, G. Czapski, *Inorg. Chem*. **1985**, *24*, 1087.
[39] M. S. Lowry, S. Bernhard, *Chem Eur J* **2006**, *12*, 7970.

[40] N. Armaroli, *Chem. Soc. Rev*. **2001**, *30*, 113.
[41] E.g.; A. K. Ichinaga, J. R. Kirchhoff, D. R. McMillin, C. O. Dietrich-Buchecker, P. A. Marnot, J.-P. Sauvage, *Inorg. Chem*. **1987**, *26*, 4290; C. C. Phifer, D. R. McMillin, *Inorg. Chem*. **1986**, *25*, 1329.
[42] M. T. Miller, T. B. Karpishin, *Inorg. Chem*. **1999**, *38*, 5246; V. Kalsani, M. Schmittel, A. Listorti, G. Accorsi, N. Armaroli, *Inorg. Chem*. **2006**, *45*, 2061.
[43] R. M. Everly, D. R. McMillin, *Photochem. Photobiol*. **1989**, *50*, 711.
[44] L. X. Chen, *Annu. Rev. Phys. Chem*. **2005**, *56*, 221.
[45] M. W. Blaskie, D. R. McMillin, *Inorg. Chem*. **1980**, *19*, 3519.
[46] e. g., R. D. Costa, D. Tordera, E. Orti, H. J. Bolink, J. Schönle, S. Graber, C. E. Housecroft, E. C. Constable, J. A. Zampese, *J. Mat. Chem*. **2011**, *21*, 16108.
[47] M. Schmittel, Ch. Michel, S.-X. Liu, D. Schildbach, D. Fenske, *Eur. J. Inorg. Chem*. **2001**, 1155.
[48] A. Hernandez Redondo, Ph.D. Thesis, University of Basel, **2009**.
[49] T. Bessho, E. C. Constable, M. Grätzel, A. Hernandez Redondo, C. E. Housecroft, W. Kylberg, Md. K. Nazeeruddin, M. Neuburger and S. Schaffner, *Chem. Commun*., **2008**, 3717; B. Bozic-Weber, E. C. Constable, C. E. Houscroft, M. Neuburger, J. R. Price, *Dalton Trans*. **2010**, *39*, 792.
[50] D. V. Scaltrito, D. W. Thompson, J. A. O'Callaghan and G. J. Meyer, *Coord. Chem. Rev*., **2000**, *208*, 243.
[51] A. Hernandez Redondo, E. C. Constable, C. E. Housecroft, *Chimia* **2009**, *63(4)*, 205.
[52] L. Flamigni, A. Barbieri, C. Sabatini, B. Ventura, F. Barigelletti, *Top. Curr. Chem*. **2007**, *281*, 143.
[53] K. Walzer, B. Maennig, M. Pfeiffer, K. Leo, *Chem. Rev*. **2007**, *107*, 1233
[54] T. Hu, L. He, L. Duan, Y. Qiu, *J. Mater. Chem*. **2012**, *22*, 4206.
[55] A. B. Tamayo, S. Garon, T. Sajoto, P. I. Djurovich, I. Tsyba, R. Bau, M. E. Thompson, *Inorg. Chem*. **2005**, *44*, 8723; H. C. Su, C. C. Wu, F. C. Fang, K. T.Wong, *Appl. Phys. Lett*. **2006**, *89*, 261118.
[56] H. J. Bolink, E. Coronado, R. D. Costa, E. Ortí, M. Sessolo, S. Graber, K. Doyle, M. Neuburger, C. E. Housecroft, E. C. Constable, *Adv. Mat*. **2008**, *20*, 3910.
[57] H. J. Bolink, L. Cappelli, E. Coronado, M. Graetzel, E. Ortı´, R. D. Costa, M. Viruela, M. K. Nazeeruddin, *J. Am. Chem. Soc*. **2006**, *128*, 14786.
[58] R. M. Everly, R. Ziessel, J. Suffert, D. R. McMillin, *Inorg. Chem*. **1991**, *30*, 559; E. C. Constable, V. Chaurin, C. E. Housecroft, M. Neuburger, S. Schaffner, *CrystEngComm* **2008**, *10*, 1063.
[59] F. Kröhnke, *Angew. Chem Int. Ed*. **1963**, *2(5)*, 225; G. Ortoleva, *Gazz. chim. ital*. **1899**, *29(1)*, 503; L. C. King, M. McWhirter, *J. Am. Chem. Soc*. **1946**, *68(4)*, 717; L. C. King, *J. Am. Chem. Soc*. **1944**, *66(6)*, 894.
[60] Ligand **6** was prepared and kindly provided by E. Schönhofer.
[61] F. W. Kröck, F. Kröhnke, *Chem. Ber*. **1971**, *104*, 1645.
[62] K. T. Potts, M. J. Cipullo, Ph. Ralli, G. Thodoridis, *J. Org. Chem*. **1982**, *47(16)*, 3027.
[63] D. L. Jameson, L. E. Guise, *Tetrahedron Lett*. **1991**, *32(18)*, 1999.
[64] G. M. Davies, J. C. Jeffery, M. D. Ward, *New J. Chem.* **2003**, *27*, 1550; J.-K. Son, L-X. Zhao, A. Basnet, P. Thapa, R. Karki, Y. Na, Y. Jahng, T. Ch. Jeong, B-S. Jeong, Ch.-S. Lee, E.-S. Lee, *Eur. J. Med. Chem*. **2008**, *43*, 675.
[65] S. Bindal, D. Kumar, D. N. Kommi, S. Bhatiya, A. K. Chakraborti, *Synthesis* **2011**, *12*, 1930.
[66] Y. Jahng, J. G. Park, *Inorg. Chim. Acta* **1998**, *267*, 265; Y. Jahng, J. G. Park, *Bull. Korean Chem. Soc.* **1998**, *19(4)*, 436.
[67] M. M. Abdel-Khalik, M. H. Elnagdi, *Synth. Comm*. **2002**, *32(2)*, 159.
[68] E. C. Constable, B. Kariuki, A. Mahmood, *Polyhedron* **2003**, *22*, 687.
[69] A. Basnet, P. Thapa, R. Karki, Y. Na, Y. Jahng, B.-S. Jeong, T. Ch. Jeong, Ch.-S. Leec, E.-S. Lee, *Bioorg. & Mec. Chem* **2007**, *15*, 4351.
[70] I. Eryazici, Ch. N. Moorefield, S. Durmus, G. R. Newkome, *J. Org. Chem.* **2006**, *71*, 1009.
[71] G. A. Koohmareh, N. Mohammadifard, *J. Polym. Res.* **2011**, *18*, 983.
[72] D. R. Palleros, *J. Chem. Educ*. **2004**, *81(9)*, 1345.
[73] E. C. Constable, C. E. Housecroft, P. Kopecky, M. Neuburger, J. A. Zampese, G. Zhang, *CrystEngComm* **2012**, *14*, 446.
[74] L. Wu, D. Wang, Z. Li, X. Wang and B. Chen, Faming Zhuanli Shenqing, CN 102115461 A 20110706 (patent), **2011**.
[75] E. C. Constable, N. Hostettler, C. E. Housecroft, P. Kopecky, M. Neuburger, J. A. Zampese, *Dalt. Trans*. **2012**, *41*, 2890.
[76] R. A. Jones, B. D. Roney, W. H. F. Sasse, K. O. Wade, *J. Chem. Soc. (B)* **1967**, 106; M. J. Cook, A. R. Katzitzky, S. Nadji, *J. Chem. Soc. Perk. Trans II* **1978**, 1215; D. Cuperly, Ph. Gros, Y. Fort, *J. Org. Chem*. **2002**, *67*, 238.
[77] Ch. Janiak, *Dalt. Trans*. **2000**, 3885.
[78] G. R. Haire, N. E. Leadbeater, J. Lewis, P. R. Raithby, A. J. Edwards and E. C. Constable, *J. Chem. Soc., Dalton*

*Trans.*, **1997**, 2997.
[79] C. Thone, F. Vancea and P.G. Jones, private communication to the Cambridge Structural Database, 2010, refcodes QUWDES, QUWDUI.
[80] D. Das, G.K. Rao and A.K. Singh, *Organometallics*, 2009, **28**, 6054.
[81] G. R. Desiraju, *Acc. Chem. Res*. **1991**, *24(10)*, 291; G. R. Desiraju, *Acc. Chem. Res*. **1996**, *29*, 441; T. Steiner, *ChemComm*. **1997**, 727.
[82] M. Nishio, *CrystEngComm*, **2004**, *6*, 130; M. Nishio, Y. Umezawa, K. Honda, S. Tsuboyama and H. Suezawa, *CrystEngComm*, **2009**, *11*, 1757.
[83] H. Duddek, *Prog. NMR Spec*. **1995**, *27*, 1.
[84] http://chem.ch.huji.ac.il/nmr/techniques/1d/row4/se.html
[85] J. B. Birks, *Rep. Prog. Phys*. **1975**, *38*, 903.
[86] A. Basnet, P. Thapa, R. Karki, Y. Na, Y. Jahng, B.-S. Jeong, T. Ch. Jeong, Ch.-S. Lee, E.-S. Lee, *Bioorg. Med. Chem*. **2007**, *15*, 4351.
[87] A.-K. Pleier, H. Glas, M. Grosche, P. Sirsch, W. R. Thiel, *Synthesis* **2001**, *1*, 55; F. A. Rosa, P. Machado, H. G. Bonacorso, N. Zanatta, M. A. P. Martins, *J. Heterocyclic Chem.* **2008**, *45*, 879.
[88] Ph. Sawle, B. E. Moulton, M. Jarzykowska, C. J. Green, R. Foresti, I. J. S. Fairlamb, R. Motterlini, *Chem. Res. Toxicol*. **2008**, *21(7)*, 1484.
[89] R. Liu, J. Chang, Qi Xiao, Y. Li. H. Chen, H. Zhu, *Dyes and Pigments* **2011**, *88*, 88.
[90] J. G. Cordado, J. K. McCusker, R. G. Bergman, *Chem. Comm*. **2002**, 1496; G. A. Koohmareh, M. Sharifi, *J. Appl. Polym. Sci.* **2010**, *116*, 179.
[91] R. Filler, V. D. Beaucaire, H. H. Kang, *J. Org. Chem.* **1975**, *40(7)*, 935.
[92] L.-X. Zhao, T. Sung Kim, S.-H. Ahn, T.-H. Kim, E.-k Kim, W.-J. Cho, H. Choi, Ch.-S. Lee, J.Ae Kim, T. Ch. Jeong, Ch.-j. Chang, E-S- Lee, *Bioorg. Med. Chem. Lett*. **2001**, *11*, 2659.
[93] H.-K. Fun, Th. Suwunwong, S. Chantrapromma, *Acta Cryst. Sect. E* **2011**, *67(9)*, o2406.
[94] I. Sasaki, L. Vendier, A. Sournia-Saquet, P. G. Lacroix, *Eur. J. Inorg. Chem*. **2006**, 3294.
[95] E. C. Constable, P. R.G. Henney and T.A. Leese, *J. Organomet. Chem*. **1989**, *361*, 277.
[96] R. O. Steen, L. J. Nurkkala, S. J. Angus-Dunne, C. X. Schmitt, E. C. Constable, M. J. Riley, P. V. Bernhardt, S. J. Dunne, *Eur. J. Inorg. Chem*. **2008**, 1784.
[97] D. A. Beauchamp, S. J. Loeb, *Supramolecular Chemistry* **2005**, *17(8)*, 617.
[98] G. W. V. Cave, C. L. Raston, *J. Chem. Soc., Perkin Trans. 1* **2001**, 3258.
[99] D. Qui, J. Wu, Z. Xie, Y. Cheng, L. Wang, *J. Organomet. Chem*. **2009**, *694*, 737.
[100] G. J. Kubas, *Inorg. Synth.*, 1990, **28**, 68.
[101] A. Cinquantini, G. Opromolla, P. Zanello, *J. Chem. Soc. Dalton Trans*. **1991**, 3161.
[102] A. F. Holleman, N Wiberg, *Walter de Gruyter & Co*., Berlin, **1995**, *34. Ed (101)*, p. 1839f.
[103] V. Chaurin, E. C. Constable, C. E. Housecroft, *New J. Chem.* **2006**, *30*, 2337.
[104] M. Munakata, J. Han, A. Nabei, T. Kuroda-Sowa, M. Maekawa, Y. Suenaga, N. Gunjima, *Inorg. Chim. Acta* **2006**, *359*, 4281.
[105] e. g., E. W. Ainscough, E. N. Baker, A. M. Brodie, N. G. Larsen, *J. Chem. Soc., Dalton Trans*. **1981**, 1746.
[106] Ch. O. Dietrich-Buchecker, J.-F. Nierengarten, J.-P. Sauvage, N. Armaroli, V. Balzani, L. De Cola, *J. Am. Chem. Soc*. **1993**, *115*, 11237.
[107] R. M. Williams, L. De Cola, F. Hartl, J.-J. Lagref, J.-M. Planeix, A. De Cian, M. W. Hosseini, *Coord. Chem. Rev*. **2002**, *230*, 253.
[108] e. g., K. Kaneto, K. Yoshino, Y. Inuishi, *Jap. J. Appl. Phys*. **1982**, *21(9)*, L567.
[109] G. M. Chapman, S. P. Stanforth, R. Berridge, C. Pozo-Gonzalo, P. J. Skabara, *J. Mater. Chem*. **2002**, *12*, 2292.
[110] V. Hebbe-Viton, V. Desvergnes, J. J. Jordry, Ch. Dietrich-Buchecker, J-P. Sauvage, J. Lacour, *Dalton Trans*. **2006**, 2058.
[111] Stereochemistry of Coordination Compounds. Von A. von Zelewsky. *John Wiley & Sons*, Chichester, **1996**.
[112] G. C. van Stein, G. van Koten, B. de Bok, L. C. Taylor, K Vrieze, Ch. Brevard, *Inorg. Chim. Acta* **1984**, *89*, 29.
[113] M.-G. Choi, R. J. Angelici, *J. Am. Chem. Soc*. **1991**, *113*, 5651.
[114] E. C. Constable, C. E. Housecroft, P. Kopecky, E. Schönhofer, J. A. Zampese, *CrystEngComm* **2011**, *13*, 2742.
[115] P. Péchy, F. P. Rotzinger, M. K. Nazeeruddin, O. Kohle, S. M. Zakeeruddin, R. Humphry-Baker, M. Grätzel, *J. Chem. Soc., Chem. Comm*. **1995**, 65.
[116] A. Hernández Redondo, Ph.D. Thesis, University of Basel, **2009**.
[117] S. Sprouse, K. A. King, P. J. Spellane, R. J. Watts, *J. Am. Chem. Soc.* **1984**, *106*, 6647.
[118] R. D. Costa, E. Ortí, H. J. Bolink, S. Graber, S. Schaffner, M. Neuburger, C. E. Housecroft, E. C. Constable, *Adv. Funct. Mater*. **2009**, *19*, 3456.

[119] M. Hesse, H. Meier, B. Zeeh, *Spektroskopische Methoden in der organischen Chemie*, Thieme Verlag **2005**, p. 108 ff.
[120] Y. Ohsawa, S. Sprouse, K. A. King, M. K. DeArmond, K. W. Hanck. R. J. Watts, *J. Phys. Chem*. **1987**, *91*, 1054.
[121] S. Graber, Ph.D. Thesis, University of Basel, **2009**.
[122] e. g., R. D. Costa, E. Ortí, H. J. Bolink, S. Graber, C. E. Housecroft, E. C. Constable, *Adv. Funct. Mater*. **2010**, *20*, 1511.
[123] S. T. Parker, J. Slinker, M. S. Lowry, M. P. Cox. S. Bernhard, G. G. Malliaras, *Chem. Mater*. **2005**, *17*, 3187.
[124] D. R. Blasini, J. Rivnay, D. M. Smilgies, J. D. Slinker, S. Flores-Torres, H. D. Abruña, G G. Malliaras, *J. Mater. Chem*. **2007**, *17*, 1458.
[125] E. S. Handy, A. J. Pal, M. F. Rubner, *J. Am. Chem. Soc*. **1999**, *121*, 3525, M. K Nazeeruddin, R. T. Wegh, Z. Zhou, C. Klein, Q. Wang, F. De Angelis, S. Fantacci, M. Graetzel, *Inorg. Chem*. **2006**, *45*, 9245.
[126] J. D. Slinker, J. Rivnay, J. S. Moskowitz, J. B. Parker, S. Bernhard, H. D. Abruña, G. G. Malliaras, *J. Mater. Chem*. **2007**, *17* 2976
[127] G. Kalyuzhny, M. Buda, J. McNeill, P. Barbara, A. J. Bard, *J. Am. Chem. Soc*. **2003**, *125*, 6272.
[128] B. P. Sullivan, D. J. Salmon, T. J. Meyer, *Inorg. Chem*. **1978**, *17*, 3334.
[129] See for example: B. Brisig, E .C. Constable and C. E. Housecroft, *New J. Chem.*, **2007**, 1437; E. C. Constable, K. Harris, C. E. Housecroft, M. Neuburger and J. A. Zampese, *Dalton Trans.*, **2011**, *40*, 11441.
[130] E. C. Constable, A. M. W. Cargill Thompson, D. A. Tocher and M. A. M. Daniels, *New J. Chem.*, **1992**, *16*, 855.
[131] e.g., S. Banerjee, A. Ghosh, B. Wu, P.-G. Lassahn, Ch. Janiak, *Polyhedron*, **2005**, *24*, 593; A. Biswas, M. G. B. Drew, A. Ghosh, *Polyhedron*, **2010**, *29*, 1029.
[132] K. Lashgari, M. Kritikos, R. Norrestam and T. Norrby, *Acta Crystallogr., Sect. C* **1999**, *55*, 64.
[133] S. Pyo, E. Pérez-Cordero, S. G. Bott and L. Echegoyen, *Inorg. Chem*. **1999**, *38*, 3337.
[134] D. C. Craig, M. L. Scudder, W.-A. McHale and H. A. Goodwin, *Aust. J. Chem.* **1998**, *51*, 1131.
[135] M. L. Scudder, D. C. Craig and H. A. Goodwin, *CrystEngComm* **2005**, *7*, 642.
[136] A. G. Walstrom, M. Pink, X. Yang, K. G. Caulton, *Dalton Trans.* **2009**, 6001.
[137] C. A. Tovee, C. A. Kilner, J. A. Thomas and M. A. Halcrow, *CrystEngComm*, **2009**, *11*, 2069.
[138] Bond distances were obtained from the deposited cif file for refcode QUNZAB; CSD version 5.32 updates Nov 2011, see reference 82.
[139] M. L. Scudder, H. A. Goodwin and I. G. Dance, *New J. Chem*. **1999**, *23*, 695; J. McMurtrie and I. Dance, *CrystEngComm* **2005**, *7*, 216; J. McMurtrie and I. Dance, *CrystEngComm* **2005**, *7*, 230; J. McMurtrie and I. Dance, *CrystEngComm* **2010**, *12*, 2700; Z. Yu, A. Nabei, T. Izumi, T. Okubo and T. Kuroda-Sowa, *Acta Crystallogr., Sect. E*. **2008**, *64*, m209.
[140] J. E. Beves, E. C. Constable, C. E. Housecroft, M. Neuburger, S. Schaffner, J. A. Zampese, *Inorg. Chem. Comm*. **2008**, *11*, 1006.
[141] J. McMurtrie, I. Dance, *CrystEngComm* **2009**, *11*, 1141.
[142] S. K. Padhi, R. Sahu, D. Saha, V. Manivannan, *Inorg. Chem. Acta* **2011**, *372*, 383.
[143] E. C. Constable and A. M. W. Cargill Thompson, *J. Chem. Soc., Dalton Trans.* **1994**, 1409.
[144] J. Ferguson, F. Herren, E. R. Krausz, M. Maeder, J. Vrbancich, *Coord. Chem. Rev.* **1985**, *64*, 21.
[145] See for example: E. C. Constable, *Adv. Inorg. Chem.* **1986**, *30*, 69.
[146] E. C. Constable, P. Harveson, D. R. Smith and L. A. Whall, *Tetrahedron* **1994**, *50*, 7799.

## Personal Data


| | |
|---|---|
| Name: | Kopecky |
| First Name: | Peter |
| Date of birth: | 09.12.1978 |
| Place of birth: | Sokolov (Czech Republic) |
| Nationality: | German |
| Marital status: | married |
| Address: | Hans-Holbein-Strasse 28, 89520 Heidenheim, Germany |
| Phone: | 0049175879181 |
| E-mail: | kopecky.peter@gmx.de |


## Education

| | |
|---|---|
| Jul 2012 | PhD, University of Basel |
| Jan 2008 | Chemistry Diploma, University of Karlsruhe |
| Aug 2007-Jan 2008 | Diplomarbeit (equivalent to a master thesis) in inorganic chemistry at the Forschungszentrum Karlsruhe (Institut für Nanotechnologie) |
| 2001-2007 | Studies of Chemistry at the University of Karlsruhe finished with the final diploma exams |
| 1996-1999 | High school, with the Abitur (university entrance qualification) in June 1999, Maria-von-Linden Schule, Heidenheim |
| 1990-1996 | Secondary school with the Mittlere Reife (certificate), Adalbert-Stifter-Realschule, Heidenheim |
| 1985-1990 | Primary school, Sokolov (Czech Republic) |

## Higher Education and Work Experience

| | |
|---|---|
| Feb 2009-Jul 2012 | PhD (Profs. E. C. Constable and C. E. Housecroft), University of Basel, polypyridine transition metal complexes for dye sensitized solar cells and light emitting electrochemical cells |
| Aug – Dec 2008 | LEONARDO DA VINCI-Internship (Dr. B. Louis), Université Louis Pasteur (ULP) Strasbourg, synthesis and catalytic studies of polyoxometalates |
| May – Jul 2008 | Research assistant (Prof. A. Powell), University of Karlsruhe, synthesis of 3d-4f-metal clusters |

| | |
|---|---|
| Feb/ Mar 2008 | Research assistant (Prof. C. von Hänisch), Forschungszentrum Karlsruhe, NMR studies of metalated silylphosphines |
| Aug 2007-Jan 2008 | Diploma student (Prof. C. von Hänisch), Forschungszentrum Karlsruhe, Assays to the reaction characteristics between alkaline earth metal bistrimethylsilylamides and silylphosphines |
| Mar-Jul 2005 | Research assistant (Dr. E. Kervio/ Prof. C. Richert), University of Karlsruhe. Synthesis of thymidine derivatives |
| Mar 2004-Sep 2003 | Truck driver (Gröner Spediton), Söhnstetten, Transport of goods with a 40t truck |
| 1999-2001 | Voluntary draftee (Air force base), Leipheim,<br>Transport of fuel |
| 1996-2005 | Charity work (Arbeiter Wohlfahrt), Heidenheim<br>Annually 4 weeks in the summer break<br>Day care for groups of 20 children; later member in the organization team |

## Scholarship

LEONARDO DA VINCI Scholarship (European Commission) for a 4 months research internship at the ULP Strasbourg

Swiss National Foundation (SNF) Fellowship for a research stay (12 months) at the University of Singapore

## Languages

| | | | |
|---|---|---|---|
| German: | Mother tongue | English: | fluent |
| Czech: | Mother tongue | French: | working knowledge |

## Communications

Paper:


1. P. Kopecky, C. von Hänisch, F. Weigend, A. Kracke, *Eur. J. Inorg. Chem.* **2010**, 258.
2. C. von Hänisch, P. Kopecky, *Z. Allg. Anorg. Chem.* **2010**, *636*, 1522.
3. E. C. Constable, C. E. Housecroft, P. Kopecky, E. Schönhofer, J. A. Zampese, *CrystEngComm* **2011**, *13*, 2742.
4. B. Bozic-Weber, E. C. Constable, C. E. Housecroft, P. Kopecky M. Neuburger, J. A. Zampese, *Dalton Trans.* **2011**, *40(46)*, 12584.
5. E. C. Constable, C. E. Housecroft, P. Kopecky, M. Neuburger, J. A. Zampese, G. Zhang, *CrystEngComm* **2012**, *14(2)*, 446.
6. E. C. Constable, C. E. Housecroft, N. Hostettler, P. Kopecky, M. Neuburger, J. A. Zampese, *Dalton Trans*. **2012**, *41*, 2890.

Poster:

1. Swiss Chemical Society Fall Meeting: 04.09.2009 at EPFL Lausanne “Synthesis of 6-substituted 2,2’-bipyridines and their application in iTCMs for LEECs” E. C. Constable, C. E. Housecroft, P. Kopecky.
2. Swiss Chemical Society Fall Meeting 09.09.2011 at EPFL Lausanne and at IC BIOSOL 12.-17.09.2011, Crete, Greece “Copper-(I)-complexes for Dye Sensitized Solar Cells”; B. Bozic-Weber, E. C. Constable, C. E. Housecroft, P. Kopecky and M. Neuburger.

## Laboratory expertise

Good synthetic skills (incl. Schlenk techniques)

| | |
|---|---|
| Technical knowledge: | Microwave (Biotage); NMR Bruker 250/400/500 (manual mode, VT-NMR, software: ICON-NMR, XWIN-NMR and TOPSpin); UV-Vis (Varian Cary 5000); Fluorescence (Shimadzu 5301PC); IR (Shimadzu FT-IR 8400 S with golden gate ATR); Electro chemistry (CHI 900B). |
| IT-skills: | MS Office (Word, Excell, Powerpoint); Origin, Camebrigde Chemoffice (ChemDraw, 3D); MestReNova, SpinWorks. Basic knowledge in LaTeX. |

## References

1. Prof. E. C. Constable
   Department of Chemistry
   University of Basel
   Spitalstrasse 51
   CH-4056 Basel, Switzerland
   Tel. +41 (0)61 267 10 01
   edwin.constable@unibas.ch
   http://www.chemie.unibas.ch/~constable/

2. PD Dr. Daniel Häussinger
   Department of Chemistry
   University of Basel
   St. Johanns-Ring 19
   CH-4056 Basel, Switzerland
   Tel. +41 (0)61 267 11 59
   Daniel.Haeussinger@unibas.ch